

AN ANALYSIS OF THE PERFORMANCE
CHARACTERISTICS OF CONTINUOUS-WAVE
OPTICAL PARAMETRIC OSCILLATORS

Finlay G. Colville

A Thesis Submitted for the Degree of PhD
at the
University of St Andrews



1995

Full metadata for this item is available in
St Andrews Research Repository
at:

<http://research-repository.st-andrews.ac.uk/>

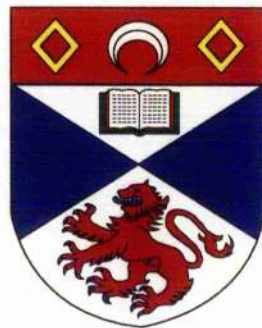
Please use this identifier to cite or link to this item:

<http://hdl.handle.net/10023/14887>

This item is protected by original copyright

*An Analysis of the Performance
Characteristics of Continuous-Wave
Optical Parametric Oscillators.*

F. G. Colville



*J. F. Allen Physics Research Laboratories,
Department of Physics & Astronomy,
University of St. Andrews,
Fife, Scotland.*

*A thesis submitted to the University of St. Andrews
in application for the degree of Doctor of Philosophy,*

September 1994.



ProQuest Number: 10166534

All rights reserved

INFORMATION TO ALL USERS

The quality of this reproduction is dependent upon the quality of the copy submitted.

In the unlikely event that the author did not send a complete manuscript and there are missing pages, these will be noted. Also, if material had to be removed, a note will indicate the deletion.



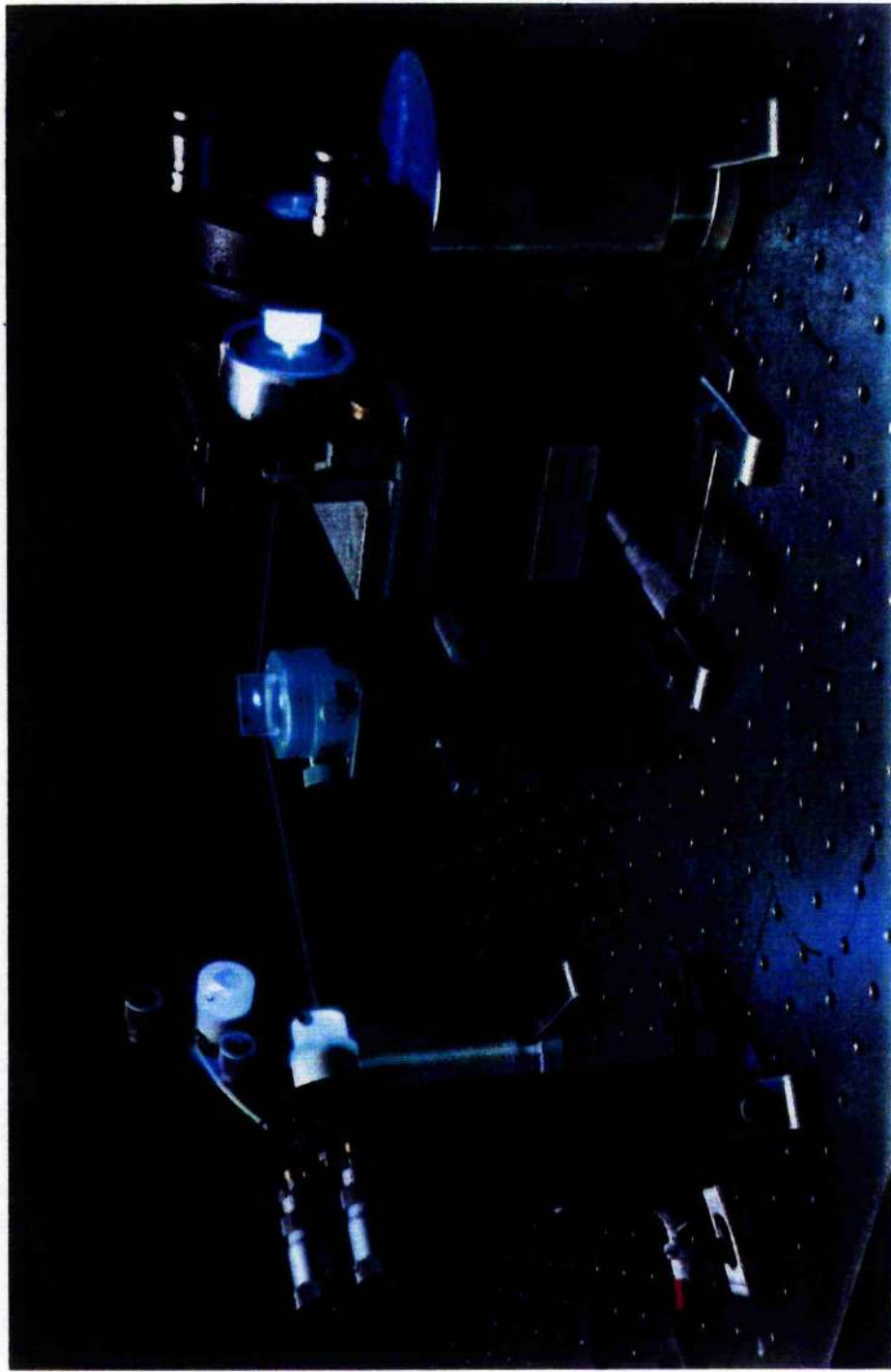
ProQuest 10166534

Published by ProQuest LLC (2017). Copyright of the Dissertation is held by the Author.

All rights reserved.

This work is protected against unauthorized copying under Title 17, United States Code
Microform Edition © ProQuest LLC.

ProQuest LLC.
789 East Eisenhower Parkway
P.O. Box 1346
Ann Arbor, MI 48106 – 1346



Continuous-wave, dual-cavity, doubly-resonant optical parametric oscillator.

Single-frequency pump radiation, at 825 THz, is incident from the right, and down-converts within the nonlinear medium, lithium triborate (second from right) to signal and idler frequencies at ≈ 598 THz (visible) and ≈ 227 THz (infra-red), respectively. The intra-cavity beam-splitter (centre) separates these two frequencies, allowing for independent cavity length control, and smooth, continuous, frequency tuning of the output frequencies.

Declaration.

I hereby certify that this thesis has been composed by myself, that it is a record of my own work, and that it has not been accepted in partial or complete fulfilment of any other degree or professional qualification.

This research was carried out in the J. F. Allen Physics Research Laboratories within the Department of Physics and Astronomy at the University of St. Andrews, under the supervision of M. H. Dunn.

F. G. Colville,
September 1994.

Certificate.

I hereby certify that the candidate has spent nine terms of research work towards the degree of Doctor of Philosophy in the J. F. Allen Physics Research Laboratories within the Department of Physics and Astronomy at the University of St. Andrews, under my supervision, that he has fulfilled the conditions of Ordinance General No. 12 (St. Andrews), and that he is qualified to submit the following thesis in application for the degree of Doctor of Philosophy.

M. H. Dunn,
September 1994.

Abstract.

An analysis of the performance characteristics of continuous-wave optical parametric oscillators.

F. G. Colville

*J. F. Allen Physics Research Laboratories, Department of Physics & Astronomy,
University of St. Andrews, Fife, Scotland.*

This thesis gives a description of studies relating to the development of continuous-wave (cw) optical parametric oscillators (OPOs) and their application to schemes that require high-precision, narrow-linewidth, and frequency-tunable radiation.

There are three separate aims to the work presented within this thesis. First, the requirements on pump sources, nonlinear materials, OPO cavity resonances and phase-matching geometries are analysed with a view to operating cw OPOs with stability above threshold. Second, the results of four distinct experiments are outlined, compared to theory, and discussed within the general context of cw OPO development. Third, this thesis is the first comprehensive review of the above-mentioned performance characteristics of cw OPOs, and focuses on their role as optical frequency dividers within frequency synthesis chains spanning the optical spectrum.

The modelling sections highlight the importance of cavity resonances in cw OPOs when evaluating pump power thresholds, conversion efficiencies, and mode-selection properties. Simultaneous signal and idler cavity resonances are shown to be critical when relying upon cw laser sources to reach OPO threshold powers. Such arrangements require the use of stable pump lasers and servo-locked OPO cavity lengths to maintain this double-resonance condition. There is an in-depth analysis of OPO cavity geometries that can generate frequency-stable and continuously-tunable outputs. The selection of nonlinear materials for cw OPOs is also considered with regard to providing signal and idler frequencies in integral-related frequency ratios, thereby satisfying an important requirement within optical frequency division techniques.

Four specific experiments were designed to address many of the issues raised within the modelling sections. These experiments realized the following novel arrangements: the use of lithium triborate as a gain material

within cw OPOs; a cw OPO which used a pump source operating in the ultra-violet spectral region; the highest frequency output from a cw OPO; a cw OPO which used a tunable pump source operating in the near infra-red spectral region; multiple parameter pump / OPO coarse frequency tuning; a non-degenerate type II cw OPO phase-matching geometry; and a dual-cavity doubly-resonant cw OPO. Other notable features of the experimental designs included stabilized single-frequency output from a single-cavity cw OPO geometry, continuous frequency tuning from a dual-cavity, doubly-resonant OPO resonator, and the general characteristics of low pump power thresholds and moderate conversion efficiencies.

An important feature discussed in detail throughout the thesis is the comparison between type I and type II phase-matching geometries. These two cases give rise to different polarization states for the signal and idler fields within OPO cavities. Type II phase-matching geometries are shown, both in theory and experiments, to be preferable to equivalent type I geometries, when considering stable OPO operation, fine frequency tuning, and multiple cavity oscillators. This is so because type II phase-matching geometries, in general, provide significantly different signal and idler refractive indices which in turn yield a considerable mis-match in the signal and idler free spectral ranges. Subsequently this relaxes the stability requirements within single-cavity doubly-resonant OPOs, and allows for polarization separation to form dual-cavity resonators which are vital to the effective operation of cw OPOs within metrology and spectroscopy.

The work contained in this thesis forms an integral part of current research in cw OPOs, a field presently enjoying its most productive and prosperous period. The potential incorporation of cw OPOs within frequency synthesis chains is shown to be dependent on the further development of pump lasers and nonlinear materials. In the short term, the actual use of cw OPOs is assessed in relation to more convenient and widespread techniques for converting, comparing, and measuring absolute frequencies.

Contents.

	Page.
Chapter I	Introduction.
I. 1	Tunable radiation from optical parametric oscillators. 1
I. 2	Narrow-linewidth and frequency-stable radiation. 4
I. 3	Development of continuous-wave parametric oscillators. 6
I. 4	Present requirements for down-conversion schemes. 18
I. 5	Outline of the work within the thesis. 19
	References. 20
Chapter II	Theoretical background.
II. 1	Introduction. 25
II. 2	Parametric gain analysis. 27
II. 2 (i)	The nonlinear susceptibility. 31
II. 2 (ii)	The coupled amplitude equations for plane waves. 33
II. 2 (iii)	Parametric amplification of focused Gaussian beams. 36
II. 3	Pump power thresholds. 40
II. 3 (i)	Ring cavity resonators. 41
II. 3 (i) (a)	Doubly-resonant oscillator with resonant pump field. 42
II. 3 (i) (b)	Doubly-resonant oscillator with single-pass pump. 53
II. 3 (i) (c)	Singly-resonant oscillator with resonant pump field. 55
II. 3 (i) (d)	Singly-resonant oscillator with single-pass pump. 57
II. 3 (ii)	Ring cavity resonators. 58
II. 3 (ii) (a)	Doubly-resonant oscillator with resonant pump field. 59
II. 3 (ii) (b)	Doubly-resonant oscillator with non-resonant pump field. 63
II. 3 (ii) (c)	Singly-resonant oscillators. 66
II. 3 (iii)	Summary. 68
II. 4	Conversion efficiencies. 70
II. 4 (i)	Doubly-resonant oscillators. 70
II. 4 (ii)	Singly-resonant oscillators. 72
II. 4 (iii)	Gaussian wave modifications. 74
II. 5	Tuning, spectral outputs, and stability requirements. 75
II. 5 (i)	Coarse frequency tuning. 75
II. 5 (ii)	Fine frequency tuning. 75
II. 5 (ii) (a)	Singly-resonant oscillators. 77

II. 5 (ii) (a) (1)	Singly-resonant oscillator with a non-resonant pump field.	78
II. 5 (ii) (a) (2)	Singly-resonant oscillator with a resonant pump field.	80
II. 5 (ii) (a) (3)	Singly-resonant oscillator with a multi-mode pump source.	82
II. 5 (ii) (b)	Doubly-resonant oscillators.	83
II. 5 (ii) (b) (1)	Doubly-resonant oscillator with a non-resonant pump field.	83
II. 5 (ii) (b) (1) (A)	Mode-hopping.	86
II. 5 (ii) (b) (1) (B)	Stability conditions.	87
II. 5 (ii) (b) (1) (C)	Smooth frequency tuning.	91
II. 5 (ii) (b) (2)	Computer model.	93
II. 5 (ii) (b) (3)	Doubly-resonant oscillator with a resonant pump field.	100
II. 5 (iii)	Summary.	101
II. 6	Further properties of the doubly-resonant oscillator.	104
II. 6 (i)	Phase-diffusion linewidths and coherence properties.	104
II. 6 (ii)	Squeezed states of light.	105
II. 6 (iii)	Frequency division and comb generation.	108
II. 7	Mode-matching.	110
II. 8	Conclusions.	114
	References.	116

Chapter III Pump sources and nonlinear materials.

III. 1	Introduction.	123
III. 2	Pump sources.	126
III. 2 (i)	Pump sources in the ultra-violet spectral region.	130
III. 2 (ii)	Pump sources in the visible spectral region.	131
III. 2 (iii)	Pump sources in the near infra-red spectral region.	132
III. 2 (iii) (a)	Diode-laser pumped Nd-based lasers.	133
III. 2 (iii) (b)	Titanium doped sapphire lasers.	133
III. 2 (iii) (c)	Single-frequency diode-lasers.	134
III. 3	Nonlinear materials.	135
III. 3 (i)	Magnesium-oxide doped lithium niobate ($\text{MgO}:\text{LiNbO}_3$).	138
III. 3 (i) (a)	Type I non-critical phase-matching.	139
III. 3 (i) (b)	$\text{MgO}:\text{LiNbO}_3$ phase-matching conclusions.	140
III. 3 (ii)	Potassium niobate (KNbO_3).	141
III. 3 (ii) (a)	Type I non-critical phase-matching; $x-z+z$.	142
III. 3 (ii) (b)	Type I non-critical phase-matching; $x-y+y$.	143
III. 3 (ii) (c)	KNbO_3 phase-matching conclusions.	144
III. 3 (iii)	Potassium titanyl phosphate (KTiOPO_4 : KTP).	146
III. 3 (iii) (a)	Type II non-critical phase-matching.	146

III. 3 (iv)	Potassium titanyl arsenate (KTiOAsO ₄ : KTA).	
	Caesium titanyl arsenate (CsTiOAsO ₄ : CTA).	148
III. 3 (iv) (a)	Type II non-critical phase-matching in KTA.	149
III. 3 (iv) (b)	Type II non-critical phase-matching in CTA.	150
III. 3 (iv) (c)	KTA & CTA phase-matching conclusions.	151
III. 3 (v)	Lithium triborate (LiB ₃ O ₅).	152
III. 3 (v) (a)	Type I non-critical phase-matching.	154
III. 3 (v) (b)	Type II non-critical phase-matching.	157
III. 3 (v) (c)	LBO phase-matching conclusions.	158
III. 3 (vi)	Silver gallium selenide (AgGaSe ₂).	
	Silver thiogallate (AgGaS ₂).	159
III. 3 (vi) (a)	Type I non-critical phase-matching in AgGaSe ₂ .	159
III. 3 (vi) (b)	Type I non-critical phase-matching in AgGaS ₂ .	161
III. 4	Conclusions.	162
III. 5	Outline of experimental work within this thesis.	165
	References.	166

Chapter IV Type I phase-matching in lithium triborate with signal and idler frequencies near frequency-degeneracy.

IV. 1	Introduction.	175
IV. 2	Single-frequency pump source operating at 583 THz.	178
IV. 3	Optical parametric oscillator design.	185
IV. 4	Pump frequency and cavity length requirements.	194
IV. 5	Experimental arrangement.	203
IV. 6	Results and discussion.	206
IV. 7	Conclusions.	212
	References.	215

Chapter V Type II phase-matching in lithium triborate with signal and idler frequencies in a near 3:1 ratio.

V. 1	Introduction.	219
V. 2	Single-frequency pump source operating at 824 THz.	222
V. 3	Optical parametric oscillator design.	226
V. 4	Pump frequency and cavity length requirements.	232
V. 5	Experimental arrangement.	238
V. 6	Results and discussion.	240
V. 7	Conclusions.	248
	References.	250

Chapter VI	Dual-cavity, doubly-resonant oscillator with separate signal and idler cavity length control.	
VI. 1	Introduction.	253
VI. 2	Optical parametric oscillator design.	257
VI. 3	Pump frequency and cavity length requirements.	258
VI. 4	Results and discussion.	260
VI. 5	Conclusions.	267
	References.	270
Chapter VII	Multiple parameter tuning through use of a frequency-tunable titanium-sapphire laser.	
VII. 1	Introduction.	273
VII. 2	Widely-tunable single-frequency pump source.	278
VII. 3	Optical parametric oscillator design.	280
VII. 4	Pump frequency and cavity length requirements.	284
VII. 5	Experimental arrangement.	287
VII. 6	Results and discussion.	288
VII. 7	Conclusions.	290
	References.	293
Chapter VII	Conclusions.	296
Acknowledgements.		
Glossary of symbols.		
Appendix I.	An approximate value to the walk-off allowed in continuous-wave optical parametric oscillators.	
Appendix II.	Listing of mode-selection computer program.	
Appendix III.	Publications & conference proceedings.	

Chapter I.

Introduction.

Contents.		Page.
I. 1	Tunable radiation from optical parametric oscillators.	1
I. 2	Narrow-linewidth and frequency-stable radiation.	4
I. 3	Development of continuous-wave parametric oscillators.	6
I. 4	Present requirements for down-conversion schemes.	18
I. 5	Outline of the work within the thesis.	19
	References.	20

I. 1 Tunable radiation from optical parametric oscillators.

Over the last four decades, the introduction of the laser has prompted significant progress in the fields of optics and spectroscopy. One important attribute of laser sources is their high spectral brightness (flux density per unit solid-angle per unit of frequency interval). This has made possible the study of nonlinear phenomena that are not accessible when using conventional optical sources. While significant advances have been achieved by using lasers as sources of fixed frequency radiation, there has also been considerable interest in developing coherent light sources whose precise operating frequency can be tuned continuously. For example, such tunable sources could be applied within spectroscopy to tune through resonances of interest at any point in the optical spectrum.

The development of tunable oscillators has been problematic since conventional lasers tend to be discrete wavelength devices involving stimulated emission between quantized energy levels in the laser media. Only when these quantized energy levels are tunable, or there are neighbouring energy levels that are sufficiently broadened to merge into each other to form a continuous band, can a continuously tunable laser be built. Even then, the tuning range tends to be limited.

A number of nonlinear techniques are available which allow for frequency shifting the radiation of an input laser beam, while maintaining the coherence of the original laser source. These include stimulated Raman scattering, harmonic generation, and sum and difference frequency mixing. However, in general, to obtain tunable output using these processes, one of the input beams is required to be tunable. Another form of frequency shifting involves the use of optical parametric generation [1].

Optical parametric oscillators (OPOs) are generally powerful solid-state sources of coherent radiation with broad tuning ranges, and they have already been demonstrated to be versatile and practical devices [2]. OPOs are similar to conventional lasers, in both converting energy from a primary source to coherent radiation through light amplification in a resonant cavity.

The optical parametric process is a nonlinear optical process in which a pump photon, propagating in a nonlinear optical crystal, breaks down into two lower-energy photons (termed the signal and the idler), such that the total photon energy is conserved. Radiation is produced simultaneously at these two distinct frequencies which build up from parametric noise: the parametric process relies on the zero point energy (vacuum fluctuations) of one photon per mode as the starting point in the amplitude of the other two waves.

However, the exact frequencies of the two emitted photons cannot be determined uniquely on the basis of energy conservation. For a given pump frequency, there can be a continuous choice of signal and idler frequencies for which energy conservation is satisfied. This forms the basic source of tunability within OPOs. In any given situation, the specific pair of frequencies that will result is dictated by the momentum (phase) conservation condition, or phase-matching condition, that must also be satisfied. Phase-matching dictates that the sum of the wave-vectors of the generated photons is equal to the wave-vector of the pump photon, thus maintaining the relative phase between the waves.

In a normally dispersive and isotropic medium, the material dispersion is such that the momentum or the magnitude of the wave-vector of the pump photon is always too large, due to dispersion, to satisfy the phase-matching condition. To compensate for material dispersion, it must be reduced relative to the sum of those of the emitted photons. The most common approach is to take advantage of the birefringence in an anisotropic

medium (with a non-centrosymmetric symmetry) to compensate for material dispersion. In this way, the signal and idler frequencies can be amplified simultaneously as they propagate through the nonlinear medium in an efficient manner. Gain at the signal and idler frequencies is provided through parametric interaction of the three optical fields with the nonlinear medium. This interaction is a consequence of the nonlinear polarization exhibited by the material.

For a given orientation of the nonlinear crystal with respect to the axis of propagation, conservation of phase-matching will be satisfied for a specific combination of signal and idler frequencies. Therefore, since the refractive indices are dependent on the direction of propagation and on the polarizations of the three waves, the orientation of the nonlinear crystal provides one means for tuning coarsely the output frequencies over a potentially wide spectral bandwidth. In general, the extent of this bandwidth is defined by the optical transparency of the nonlinear material chosen as the gain medium. Another commonly used tuning method involves altering the birefringence through temperature control.

Within experimental OPO configurations, the nonlinear gain element is typically placed within an optical resonator formed by external cavity mirrors, and a pump field is fed into the resonator. At a critical pumping intensity, or pump power threshold, parametric gain causes steady-state oscillation to be set up at either the signal or idler frequency, or at both frequencies, as defined by the level of feedback provided by the cavity mirrors at these two frequencies. The fine output frequencies of the OPO correspond to resonances of the optical structure, or are near such resonances.

To stimulate oscillation within a laser cavity, an incoherent pump source is sufficient as the initial energy source. However, for an OPO, this initial pump source is constrained to be a high intensity source of coherent radiation in its own right. Until recently, the absence of pump sources of high spectral and spatial coherence had delayed widespread interest in the use of OPOs as practical sources of tunable coherent radiation. This requirement is particularly important since the temporal, spatial, and spectral nature of the OPO outputs reflects that of the input pump source.

Therefore, the specific OPO outputs are a combination of three separate effects; phase-matching, pump frequency input (linewidth), and optical cavity resonances. Evidently, to generate narrow-linewidth radiation from an OPO,

the first critical requirement is the use of a narrow-linewidth pump source, and this topic is discussed in the following section.

I. 2 Narrow-linewidth and frequency-stable radiation.

A fundamental limit to the linewidth, or frequency bandwidth, of an optical source is the temporal nature of the source. For example, for radiation derived from a Q-switched laser, with a pulse duration of $\Delta t \approx 10$ nanoseconds, the transform-limited linewidth is $\Delta \nu \approx 50$ MHz, assuming a Gaussian pulse shape. Further, if this pump source operates in the visible spectral region, at a pump wavelength of $\lambda \approx 0.5 \mu\text{m}$, corresponding to a frequency of $\nu \approx 600$ THz, then the fractional stability, or precision, of this frequency is known to within ≈ 1 part in 10^6 . While the precision of such laser radiation represents a considerable improvement over conventional sources of optical radiation, it is not accurate enough to be used within a number of high-precision experiments in quantum optics.

The coherence, phase stability, and narrow spectral width of lasers are of paramount importance within the study of high-resolution spectroscopy [3], optical frequency standards [4], fundamental constant determination [5], space-based measurements [6], metrology [7], coherent communications [6], and gravitational wave detection [8]. Ultra-high resolution intrinsically requires ultra-narrow laser linewidths, as provided specifically from continuous-wave (cw) laser sources. Therefore, to apply an OPO to generate tunable high precision frequency outputs, the OPO should be pumped by a cw laser source, forming a cw OPO device.

In practice, the accuracy of the laser frequency is limited by a number of intrinsic and environmental noise sources; for example, fluctuations in the population inversion, and cavity length perturbations of the optical resonator correspond to mode-broadening in the frequency domain. Short-term laser frequency noise can be reduced by, for example, stabilizing the laser frequency to a transmission fringe of a stable high finesse optical resonator [9]. However, locking the laser frequency to an external cavity does not guarantee an improved long-term absolute stability, since the resonant frequency of the external locking cavity may drift. Long term stability can be achieved by stabilizing the laser frequency to a suitable atomic or molecular transition with high frequency reproducibility / re-settability [10], or by stabilizing a

transmission fringe of a laser reference cavity to the frequency of an auxiliary laser which is then frequency-offset-locked to a stable laser such as an iodine- (I_2) or methane- (CH_4) stabilized He:Ne laser [11].

At present, time and frequency are the most accurately measurable physical quantities [12, 13] and so measurements of other physical quantities, if possible, are reduced to measurements of time and frequency; for example, the definition of the speed of light [14]. The current technique for measuring an optical frequency relative to the primary time standard, the caesium beam standard at $\nu \approx 9.2$ GHz, or some intermediate frequency standard (CO_2 laser or He:Ne laser), utilizes a complex frequency synthesis chain involving harmonics of laser and klystron sources, which typically occupy the physical space of several optical benches [15, 16]. For example, such a method has been extended to the visible spectral region, in which the $\lambda \approx 633$ nm He:Ne laser has been locked to a molecular iodine transition line, with an accuracy of $\approx 10^{-11}$ [16]. In view of the complexity of such optical frequency synthesis techniques, alternative methods have been proposed for measuring and synthesizing new frequencies in terms of low-frequency signals that can be controlled by an atomic clock [17 - 20]. Such devices are often called optical frequency dividers.

Nonlinear frequency conversion processes form an integral part of such optical frequency dividers. For example, consider locking the second harmonic frequency of a Nd:YAG laser to a hyperfine line of iodine [21], as opposed to the example discussed above (He:Ne laser). Through this method, both the fundamental and the second harmonic frequencies are stabilized in frequency to the one optical standard. Indeed, the available power levels of such diode-laser-pumped solid-state lasers are sufficient to generate efficiently, through further nonlinear frequency up-conversion stages, a series of stabilized harmonic frequencies throughout the ultra-violet and near infra-red spectral regions. Therefore, there are potential advantages when locking discrete frequencies that form part of a chain of harmonically related optical frequencies, and when this chain uses laser oscillators only in the visible and near infra-red spectral regions.

The above method involved the application of frequency up-conversion techniques to form new frequencies, higher in frequency than the original laser source. Therefore, in general, it does not allow for lower frequencies that can be referenced to frequency standards in the mid infra-red

and microwave spectral regions. The OPO is ideally suited to provide such frequency down-conversion, when operated with a cw, narrow-linewidth, frequency-stable pump source, and when the outputs of the OPO are determined precisely in relation to the pump frequency [20, 22].

Therefore, cw OPOs are in principle ideal for implementation within frequency chains although the development of such devices has been particularly slow, with relatively few experimental designs compared to their pulsed counterparts. A brief historical perspective of this progress is outlined in the following section.

I. 3 Development of continuous-wave parametric oscillators.

The first demonstrations of OPOs used high peak power pulsed lasers as their pump sources [23]. Shortly after these experiments, considerable attention was directed towards the cw equivalent of these devices, as a source of continuous-wave, narrow-linewidth, and frequency-tunable radiation.

The first cw OPO was reported in May 1968 [24], and used the frequency-doubled multi-longitudinal-mode radiation from a lamp-pumped Nd:YAG laser to pump a doubly-resonant OPO (both signal and idler waves resonant) near frequency degeneracy (signal and idler frequencies approximately equal). From a tuning perspective, visible radiation derived from a fixed frequency cw pump source had been converted efficiently into near infra-red radiation that was tunable over a frequency bandwidth of $\Delta\nu \approx 45$ THz around $\lambda \approx 1 \mu\text{m}$. The success of this experiment prompted a short-lived period of optimism regarding the use of cw OPOs within high precision frequency applications. Consider the editorial comments, taken from the June 1968 issue of *Laser Focus World* [25]:

"Infrared light from a neodymium-doped, yttrium-aluminium-garnet laser (YAG;Nd) has been converted to coherent...light via a tunable, continuously-pumped, parametric oscillator recently described by scientists at Bell Telephone Laboratories (Murray Hill, N. J.). This is the first such system ever built, according to the American Institute of Physics, which further notes that previously the only reported optical parametric, or variable parameter, oscillators were operated with pulsed lasers. In initial experiments, the device was tuned over a range of 9,800 to 11,600 angstroms, but BTL estimates that eventually the practical tunability will be from 6,000 to 40,000

angstroms - that is, from the yellow to the infrared regions of the light spectrum. An oscillator with this tuning range could provide large numbers of carriers for a future optical communication system."

However, the amplitude and frequency stability of the OPO output from this initial device was unsuitable for any further applications, caused primarily by using a multi-mode frequency pump source. Figure I. 1 confirms the undesirable temporal behaviour (output stability) from this first cw OPO, over millisecond timescales [24].

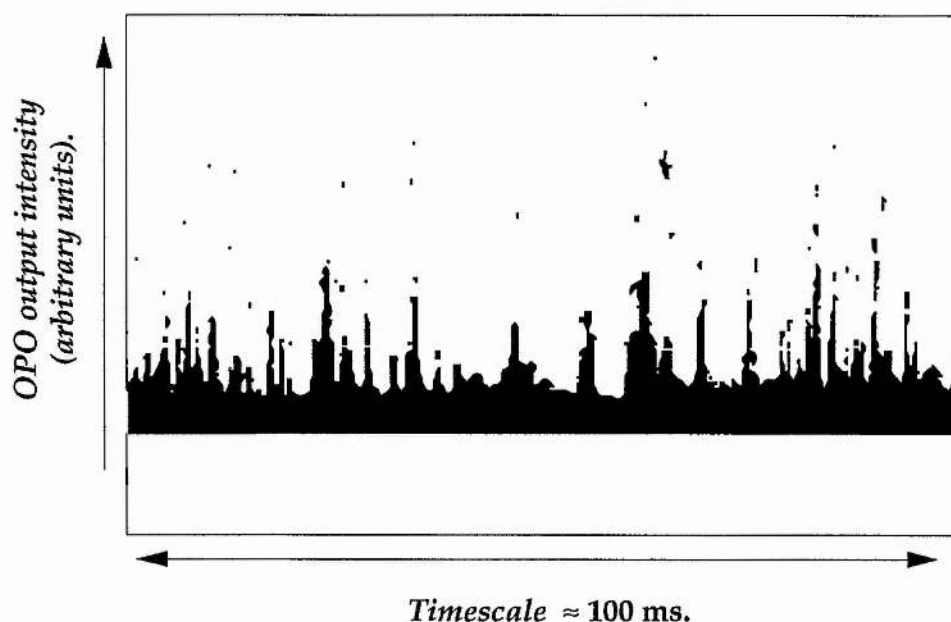


Figure I. 1.
Amplitude fluctuations of the first cw OPO (reference [24]). The width of a typical spike was a few microseconds [24].

Following this experiment, several other groups constructed continuously-pumped OPO devices [26 - 30]. All these experiments utilised high cw power laser sources in the blue / green spectral region, and the nonlinear crystals barium sodium niobate ($\text{Ba}_2\text{NaNb}_5\text{O}_{15}$) or lithium niobate (LiNbO_3) as the OPO gain medium. The outputs from these OPOs were tuned coarsely, by varying the precise phase-matching temperature, around frequency-degeneracy [24, 28, 30] or with signal and idler frequencies in a near 3:1

frequency ratio [26, 27, 29]. The latter geometry, with signal frequency radiation in the red spectral region, was not guided by a sudden requirement to implement OPOs as practical optical frequency dividers operating with high-order integral-related output frequencies, but by a misguided notion that cw OPOs could then provide a practical source of usable cw radiation throughout the visible spectral region. In retrospect, the most noteworthy experimental configuration involved the construction of a ring cavity geometry to eliminate feedback coupling back to the pump source and causing further pump frequency instabilities [27]. This cavity geometry is shown in figure I. 2 [27].

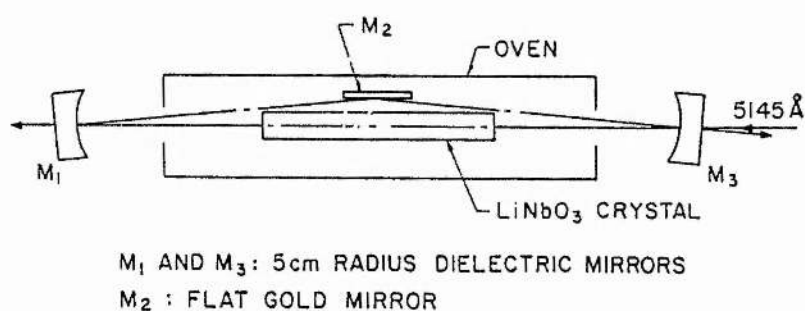


Figure I. 2.

Early cw OPO ring cavity geometry (from reference [27]), reducing feedback to the pump source, and providing increased OPO conversion efficiencies.

In 1969, cw dye lasers were demonstrated and subsequently marketed [31], discouraging even the most ardent supporters of cw OPOs. Dye lasers provided a convenient source of high power, narrow-linewidth, and frequency tunable radiation throughout the visible spectral region.

However, in 1973, a series of pioneering research studies were published [32] which identified the technical difficulties that had been encountered during cw OPO research of the late 1960s / early 1970s, and further, explained why the outputs from these devices had been less than ideal. This re-examination highlighted the potential of cw OPOs when allied

with stable single-frequency pump sources effectively isolated from back reflections and back conversion from the OPO resonator, a requirement which had been initially neglected. When using an isolated and stabilized single-frequency pump source, free-running, amplitude-stable, single-frequency radiation was obtained from a cw OPO, for time periods of a few seconds [32]. Single-frequency operation of this device is displayed in figure I. 3 [32], as viewed on a scanning interferometer.

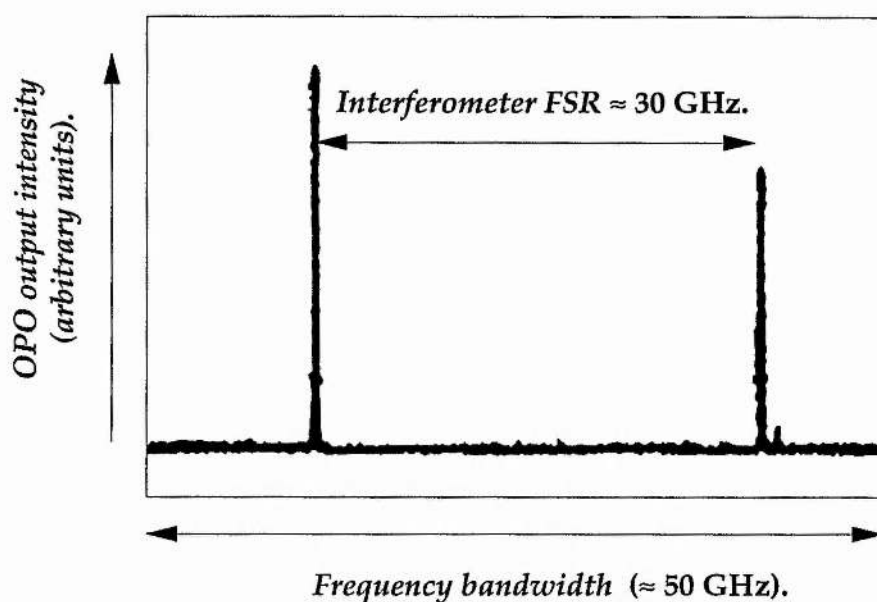


Figure I. 3.

Free-running single frequency operation from a cw OPO (from reference [32]). Only the signal frequency of the signal-idler mode-pair is displayed.

As a final statement, consider the concluding remarks of reference [32], in marked contrast to the initial burst of enthusiasm in cw OPOs.

"...the sensitivity of the device to pump-frequency fluctuations and cavity-length changes requires that the pump be frequency stabilized, an isolator be used, and considerable care be paid to the design of the oscillator cavity. These requirements seem to be entirely feasible. It remains to be determined if practical methods of smoothly tuning the device can be found."

At this time (late 1960s / early 1970s), the emphasis in the design of pulsed OPOs had shifted from the initially unstable, but low threshold, doubly-resonant configurations [23], to OPO cavities in which only one of the signal or idler waves was brought to resonance within the OPO cavity [33]. These singly-resonant oscillators provided tunable radiation that was stable in amplitude and frequency; a consequence of eliminating the requirement of resonating two discrete frequencies within the same OPO cavity. This transition was possible because the peak powers available from pulsed or Q-switched lasers were still well in excess of the higher pump power thresholds required for singly-resonant OPO operation. The low power levels associated with cw laser sources did not allow for this transition in cw OPOs. Combined with the lack of high-precision cw pump frequency sources, this explains why only pulsed OPO configurations were investigated throughout the 1970s and early 1980s.

After the early cw OPO experiments, thirteen years elapsed before any subsequent reports of cw OPOs [34]. Renewed interest was the result of extensive theoretical modelling of the parametric process, which had begun in the earliest days of quantum optics; see reference [34] and references therein. Specifically, it was predicted that cw OPOs could deliver twin outputs whose intensity difference was squeezed below the usual shot noise level that is common to laser radiation in a coherent state. Extensive experimental progress was performed in the field of squeezed light by using cw OPOs, in the late 1980s [34 - 46].

The requirements with regard to frequency stability and tunability were not considered critical when observing reduced quadrature fields in these squeezed states of light experiments. This is because the objective was simply to measure degrees of squeezing below the shot-noise-limit, and not to design usable sources of squeezed light for specific applications. Therefore, experimental designs could employ the established technology of single-frequency argon / krypton-ion lasers or frequency-doubled lamp-pumped Nd:YAG lasers, operating in the green spectral region, as their pump sources. Further, OPO operation near frequency degeneracy was adequate, with signal and idler frequency outputs in the $\lambda \approx 1 \mu\text{m}$ spectral region, where established frequency doubling materials could be used for OPO operation, and where detector efficiencies and optical coatings are of a high quality. Figure I. 4 illustrates a typical arrangement for using cw OPOs to observe squeezed states of light [34].

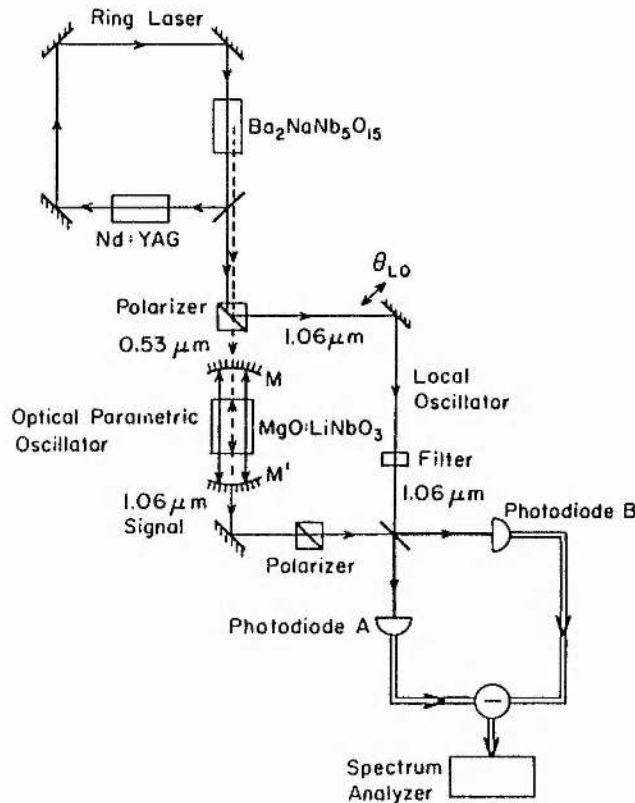


Figure I. 4.
Schematic illustration of the use of cw OPOs for the observation of squeezed states of light (from reference [34]).

With regard to using cw OPOs as high precision sources of frequency-stable and frequency-tunable radiation, the required impetus was provided in the late 1980s. Frequency stable, diode-laser pumped, solid-state laser sources, frequency doubled into the green spectral region, and displaying frequency precision at the kHz-level, were used as the pump sources for compact, monolithic ring cavity, doubly-resonant cw OPOs [47 - 49]. For the first time, cw OPOs delivered amplitude and frequency stable radiation at specific frequencies, as defined by the resonance conditions of the optical cavity [47]. At exact frequency degeneracy, the signal and idler frequencies phase-locked to yield an exact frequency sub-harmonic of the pump frequency, thus providing the first demonstration of optical frequency division through a

down-conversion technique [48]. The monolithic ring cavity OPO is illustrated in figure I. 5 [49].

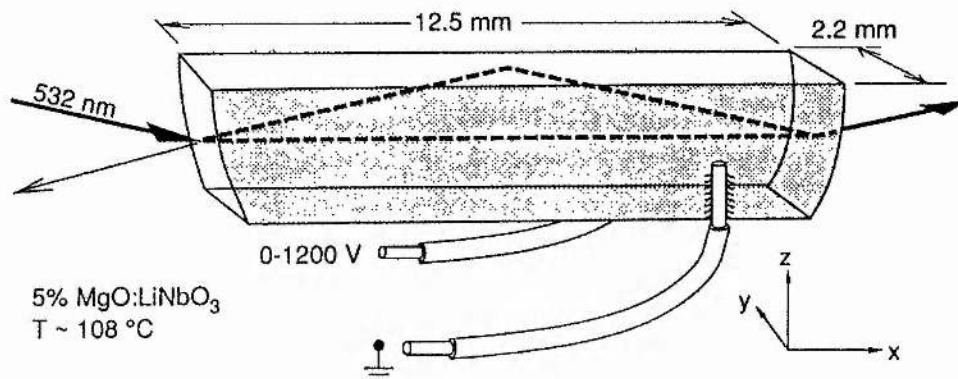


Figure I. 5.

Monolithic cw OPO ring cavity resonator, with high passive stability (from reference [49]). The electric-field applied to the crystal permits fast electro-optic tuning of the refractive indices.

Following such stable and reliable cw OPO operation, their use was proposed as optical frequency dividers within frequency chains spanning the optical spectrum [20, 50 - 51]. Using the technique of offset-locking signal and idler frequencies with a known frequency difference, a highly stable potassium titanyl phosphate (KTP) cw OPO was demonstrated [52], illustrating the potential of using nonlinear materials that could provide type II phase-matching geometries with orthogonally polarized signal and idler fields. Electro-optic tuning and low temperature sensitivity allowed the signal and idler frequency difference to be determined precisely, compared to a known frequency standard, and held stable indefinitely. A schematic of this experimental configuration is illustrated in figure I. 6 [52].

Although this experiment involved the familiar use of a fixed-frequency pump source in the green spectral region, and OPO operation near frequency degeneracy, it illustrated a locking technique that would be required to operate cw OPOs with frequencies that could be referenced to standard

frequency sources. It forms the basis of current research involving cw OPOs, including the work described within this thesis.

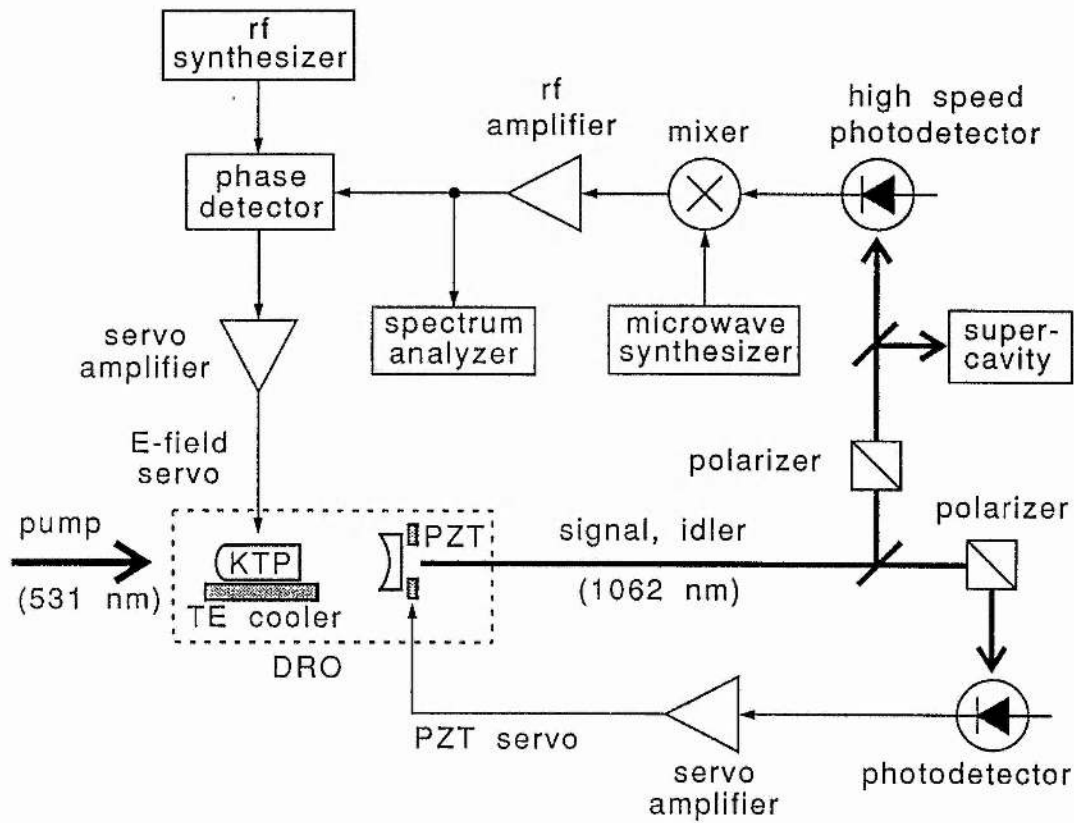


Figure I. 6.

Schematic representation of tunable optical frequency division from a cw OPO, with the signal and idler frequency difference locked to a microwave frequency reference (from reference [52]).

Table I. 1 lists all experimental reports of cw OPOs, from May 1968 to July 1994. (For completeness, the experiments described within this thesis, and those performed by other groups over the course of this work, are included.)

Table I.1. Summary of continuous-wave optical parametric oscillators between 1968 & 1994.

Authors	Ref., date	Pump ν_p	Crystal	OPO ν_s, ν_i	Threshold	Comments
Smith et al.	[24]1968	2 x Nd:YAG 532 nm	$Ba_2NaNb_5O_{15}$	0.98-1.06 μm 1.16-1.06 μm	45 mW	First cw OPO, MLM pump, semi-monolithic design
Byer et al.	[26]1968	Argon-ion 514.5 nm	LiNbO ₃	0.68-0.71 μm 2.11-1.90 μm	410 mW	3:1 frequency coatings, visible signal wave
Byer et al.	[27]1969	Argon-ion 514.5 nm	LiNbO ₃	0.66-0.70 μm 2.33-1.94 μm	150 mW	Ring cavity resonator, high pump depletion
Smith & Parker	[28]1970	2 x Nd:YAG 532 nm	$Ba_2NaNb_5O_{15}$	1.01 μm 1.05 μm	N/A	OPO internal to pump laser cavity
Laurence & Tittel	[29]1971	Argon-ion 488 nm	$Ba_2NaNb_5O_{15}$	0.64-0.66 μm 2.32-1.94 μm	200 mW	3:1 frequency coatings, higher frequency pump
Weller et al.	[30]1972	Argon-ion 514.5 nm	$Ba_2NaNb_5O_{15}$	1.06 μm	N/A	Simultaneous oscillation on multiple clusters
Smith	[32]1973	Argon-ion 514.5 nm	$Ba_2NaNb_5O_{15}$	1.01 μm 1.05 μm	2.8 mW	Stabilized SLM pump, short-term SLM OPO
Wu et al.	[34]1986	2 x Nd:YAG 532 nm	MgO:LiNbO ₃	1.06 μm	25 mW	Triply-resonant OPO, squeezing >50 % < SNL
Wu et al.	[35]1987	2 x Nd:YAG 532 nm	MgO:LiNbO ₃	1.06 μm	25 mW	Triply-resonant OPO, squeezing >60 % < SNL
Reynaud et al.	[36]1987	Argon-ion 528 nm	KTP	1.06 μm	100 mW	KTP as OPO material, first type II geometry

Table I. 1. Cont'd.

Authors	Ref., date	Pump ν_p	Crystal	OPO ν_s, ν_i	Threshold	Comments
Grangier et al.	[37]1987	2 x Nd:YAG 532 nm	KTP	1.06 μm	150 mW	KTP as OPO material, type II phase-matching
Heidmann et al.	[38]1987	Argon-ion 528 nm	KTP	1.05 μm 1.07 μm	80 mW	Actively-stabilized OPO, constant amplitude
Xiao et al.	[39]1988	2 x Nd:YAG 532 nm	MgO:LiNbO ₃	1.06 μm	25 mW	Sub-threshold OPO
Debuisschert et al.	[40]1989	Argon-ion 528 nm	KTP	1.05 μm 1.07 μm	300 mW	Amplitude-stable OPO, squeezing 69 % < SNL
Nabors et al.	[47]1989	2 x Nd:YAG 532 nm	MgO:LiNbO ₃	1.01-1.06 μm 1.06-1.13 μm	12 mW	Monolithic ring OPO, kHz pump, SLM OPO
Nabors et al.	[48]1990	2 x Nd:YAG 532 nm	MgO:LiNbO ₃	1.01-1.06 μm 1.06-1.13 μm	12 mW	Self-phase-locking OPO, coherence properties
Mertz et al.	[41]1990	Argon-ion 528 nm	KTP	1.05 μm 1.07 μm	200 mW	Amplitude-stable OPO, squeezing 24 % < SNL
Nabors & Shelby	[42]1990	2 x Nd:YAG 532 nm	MgO:LiNbO ₃	1.01-1.06 μm 1.06-1.12 μm	12 mW	Free-running SLM OPO, squeezing 53 % < SNL
Leong et al.	[43]1990	Krypton-ion 531 nm	MgO:LiNbO ₃	1.06 μm	40 mW	Amplitude-stable OPO, squeezing < SNL
Eckardt et al.	[49]1991	2 x Nd:YAG 532 nm	MgO:LiNbO ₃	1.01-1.06 μm 1.06-1.13 μm	12 mW	Modelling of type I OPOs, SLM OPO operation

Table I. 1. Cont'd.

Authors	Ref., date	Pump ν_p	Crystal	OPO ν_s, ν_i	Threshold	Comments
Mertz et al.	[44]1991	2 x Nd:YAG 532 nm	KTP	1.06 μm	100 mW	Amplitude-stable OPO, squeezing 86 % < SNL
Polzik et al.	[45]1992	2 x Ti:sapp 428 nm	KNbO ₃	0.86 μm	N/A	Sub-threshold OPO, spectroscopy application
Ou et al.	[46]1992	2 x Nd:YAP 540 nm	KTP	1.08 μm	N/A	Realization of Einstein- Podolsky-Rosen paradox
Lee & Wong	[52]1992	Krypton-ion 531 nm	KTP	1.06 μm	40 mW	Frequency division using a phase-locked OPO
Colville et al.	[53]1993	Argon-ion 514.5 nm	LBO	0.97-1.03 μm 1.03-1.10 μm	50 mW	New nonlinear material, type I LBO
Yang et al.	[54]1993	2 x Nd:YAG 532 nm	KTP	1.04 μm 1.09 μm	1.4 W	First SRO, dble-pass pump, stable OPO, high power
Colville et al.	[55]1993	Argon-ion 363.8 nm	LBO	0.52-0.49 μm 1.32-1.38 μm	115 mW	UV pump, type II LBO, amplitude-stable OPO
Lee & Wong	[56]1993	Krypton-ion 531 nm	KTP	1.06 μm	40 mW	Smooth tuning \approx 0.5 GHz, Amp.frequ. stable OPO
Gerstenberer & Wallace	[57]1993	2 x Nd:YAG 532 nm	MgO:LNbO ₃	0.96-1.06 μm 1.06-1.19 μm	12.9 mW	All-solid-state design, high output powers.
Yang et al.	[58]1993	2 x Nd:YAG 532 nm	KTP	1.04 μm 1.09 μm	1.4 W	Spectral properties of SRO, tuning over 0.6 GHz

Table I. 1. Cont'd.

Authors	Ref., date	Pump ν_p	Crystal	OPO ν_s, ν_i	Threshold	Comments
Schiller & Byer	[59]1993	2 x Nd:YAG 532 nm	MgO:LiNbO ₃	1.00-1.06 μm 1.06-1.14 μm	0.36 mW	Quadruply-resonant, TRO with sub-harmonic
Colville et al.	[60]1994	Argon-ion 363.8 nm	LBO	0.52 μm 1.38 μm	200 mW	Dual-cavity resonator, smooth tuning ≈ 0.4 GHz
Colville et al.	[61]1994	Ti:sapphire 0.78-0.81 μm	LBO	1.49-1.71 μm	360 mW	First tunable pump, multiple parameter tuning
Brothers et al.	[62]1994	Krypton-ion 531 nm	KTP	1.062 μm	40 mW	Comb generation in a resonant modular cavity
Yang et al.	[63]1994	2 x Nd:YAG 532 nm	KTP	1.04 μm 1.09 μm	4.3 W	Singly-resonant OPO, single-pass pump
Lee & Wong	[64]1994	Krypton-ion 531 nm	KTP	1.062 μm	55 mW	Dual-cavity resonator, smooth tuning ≈ 0.9 GHz
Knappe et al.	[65]1994	Ti:sapphire 0.8 μm	KTP	≈ 1.2 μm ≈ 2.6 μm	80 mW	Pump enhanced SRO, direct diode-pumping
Serkland et al.	[66]1994	Nd:YAG 1.064 μm	LiNbO ₃	2.04-2.13 μm 2.13-2.23 μm	130 mW	1 μm pumping, high-finesse DRO
Robertson et al.	[67]1994	Argon-ion 514.5 nm	LBO	0.94-0.93 μm 1.13-1.15 μm	1.0 W	Pump enhanced SRO,
Youn et al.	[68]1994	Argon-ion 514.5 nm	KTP	≈ 1.029 μm	200 mW	Squeezing < SNL

I. 4 Present requirements for down-conversion schemes.

As discussed earlier, recent advances in stable lasers, trapped ions, and atomic fountains offer the possibility of obtaining a precision of 1 part in 10^{15} or better in the next generation of high-resolution optical measurements. To achieve a similar result in accuracy relative to an optical frequency reference, it is necessary to develop the technology that can measure, compare, and synthesize optical frequencies with precision and accuracy. One of the desirable capabilities of such a measurement system is frequency division in the optical domain.

Optical frequency division using OPOs relies upon determining accurately the sum and difference frequencies of the signal and idler outputs. The sum frequency is set by the precision of the pump source, which can be referenced to, for example, an absorption line in the visible spectral region. The difference frequency can take several different forms. If the signal and idler frequencies are close to one another (near frequency degeneracy) then the difference frequency can be referenced to a microwave frequency source. If the signal and idler frequencies are in higher order integral ratios, then up-conversion techniques (e.g. second harmonic generation or sum frequency mixing) can be used to provide exact frequency ratios. This can be obtained by directly comparing one of the pump, signal, or idler frequencies to the new frequency, as generated from the up-conversion scheme, or by taking the difference of these two frequencies and referencing this to a microwave frequency source.

There are a number of immediate requirements that need to be addressed if cw OPOs are to fulfil this role. Pump sources for cw OPOs need to be identified throughout the ultra-violet, visible, and near infra-red spectral regions. In particular, tunable pump sources are required that can allow the signal and idler sum frequency to be selected from extensive frequency bandwidths. Phase-matching geometries in nonlinear materials need to be identified that can produce integral related pump, signal, and idler frequencies. For this, new nonlinear materials must be found that can be implemented into cw phase-matching geometries. Finally, new cw OPO cavity geometries need to be developed that can allow for wide and continuous frequency tuning of the OPO outputs without mode-hopping effects. Specifically, the constraint of resonating two discrete frequencies within the same optical cavity must be eliminated.

I. 5 Outline of the work within the thesis.

The work described in this thesis aims to fulfil two separate requirements; an understanding of the operating conditions necessary to obtain amplitude stable and frequency tunable cw OPO outputs, and the experimental construction of different types of cw OPOs. Therefore, the thesis is divided into two distinct parts.

The theory and modelling of the cw OPOs are included in chapters II and III. Chapter II examines the effects of resonating different optical fields on the pump power required to reach threshold, and on the conversion efficiencies of the output fields, for both linear, standing-wave cavities and ring, travelling-wave cavities. The number of cavity resonances within the OPO gives rise to significantly different mode-selection properties, and these are examined for different cavity arrangements that can allow for multiple parameter control to obtain smooth frequency tuning. Chapter III examines currently available pump sources and nonlinear materials that can be used for implementation within cw OPO schemes. In particular, suitable pump sources are identified that can operate in different spectral regions, and phase-matching geometries in nonlinear crystals are outlined that can allow for the generation of integral-related signal and idler frequencies.

Four distinct experiments are discussed in chapters IV to VII. These involve the use of single-frequency cw pump sources operating in the ultra-violet, visible and near infra-red spectral regions. The pump radiation is derived from both fixed-frequency and widely-tunable laser pump sources. Type I and type II phase-matching geometries are analysed, with respect to coarse and fine frequency tuning, and amplitude-stable OPO operation. Finally, two different types of doubly-resonant optical resonators are constructed that allow for the transition from a single-cavity resonator to a three-mirror dual-cavity resonator that allowed for independent signal and idler cavity length control.

Throughout the text, several different frequency division schemes are discussed using the same nonlinear materials and phase-matching geometries that were realized experimentally. While these schemes are not intended to be the most practical frequency chains, they serve to illustrate the technique of incorporating cw OPOs within the context of frequency metrology. The requirements for cw OPOs as optical frequency dividers form

the basis of this text, and these should be satisfied when considering the most appropriate pump sources, nonlinear materials and detectors.

Chapter VIII provides conclusions to this thesis with regard to the two separate studies, as outlined above. Possible directions for future research involving the use of cw OPOs as optical frequency dividers are discussed in detail. This is related also to the progress that has been made by other groups within the field of cw OPOs during the course of this work.

References.

1. D. L. Weinberg,
"Tunable optical parametric amplifiers and generators,"
in *Laser Focus World*, p35 (April 1969).
R. W. Wallace & S. E. Harris,
"Extending the tunability spectrum,"
in *Laser Focus World*, p42 (November 1970).
2. C. L. Tang, W. R. Bosenberg, T. Ukachi, R. J. Lane, & L. K. Cheng,
"NLO materials display superior performance,"
in *Laser Focus World*, p87 (September 1990).
J. Hecht,
"Tunable mid-infrared sources entice spectroscopists,"
in *Laser Focus World*, p109 (September 1993).
3. See the special issue on ultra sensitive spectroscopy,
J. Opt. Soc. Am. B 2, 1427 (1985).
J. L. Hall *et al.*,
in "Advances in laser spectroscopy," (F. T. Arecchi, F. Strumia, & H. Walther, Eds.),
Plenum, New York, p99 (1983).
4. J. L. Hall, M. Zhu, & P. Buch,
"Prospects for using laser-prepared atomic fountains for optical frequency standards
applications,"
J. Opt. Soc. Am. B 6, 2194 (1989).
L. L. Lewis,
"An introduction to frequency standards,"
Proc. IEEE 79, 927 (1991).
5. P. Zhao, W. Lichten, Z.-X. Zhou, H. P. Layer, & J. C. Berquist,
"Rydberg constant and fundamental atomic physics,"
Phys. Rev. A 39, 2888 (1989).
6. M. Sokolowski & J. Lesh,
in *Proc. Soc. Photo-Opt. Instrum. Eng.* 810, 172 (1987).
7. R. Clark,
"Optical measurement with direct traceability to the primary standards of length and
time...,"
Opt. Eng. 32, 571 (1993).
8. M. M. Davis, J. H. Taylor, J. M. Weisberg, & D. C. Backer,
"High-precision timing observations of the millisecond pulsar PSR1937 & 21,"
Nature (London) 315, 547 (1985).

9. R. L. Barger, M. S. Sorem, & J. L. Hall,
"Frequency standards of a cw dye laser,"
Appl. Phys. Lett. **22**, 573 (1973).
10. F. Y. Wu, R. E. Grove, & S. Ezekiel,
"CW dye laser for ultrahigh-resolution spectroscopy,"
Appl. Phys. Lett. **25**, 73 (1974).
11. J. L. Hall, D. Hils, C. Salomon, & J. M. Chartier,
in "Laser spectroscopy VIII," (W. Persson & S. Svanberg, Eds.), Springer-Verlag, New
York, p376 (1987).
12. J. L. Jespersen, B. E. Blair, & L. E. Gatterer, Eds.,
Special issue on time and frequency,
Proc. IEEE **60**, 476 ff. (1972).
13. J. L. Jespersen & D. W. Hanson, Eds.,
Special issue on time and frequency,
Proc. IEEE **79**, 894 ff. (1991).
14. Comite International des Poids et Mesures, Recommendation 1 (CI-1983),
See "Editor's note," *Metrologia* **19**, 163 (1984).
15. D. A. Jennings, C. R. Pollock, F. R. Peterson, R. E. Drullinger, K. M. Evenson, J. S. Wells,
J. L. Hall, & H. P. Layer,
"Direct frequency measurement of the I₂-stabilized He-Ne 473-THz (633-nm) laser,"
Opt. Lett. **8**, 136 (1983).
16. O. Acef, J. J. Zondy, M. Abed, D. G. Rovera, A. H. Gerard, A. Clairon, Ph. Laurent,
Y. Millerieux, & P. Juncar,
"A CO₂ to visible optical frequency synthesis chain: accurate measurement of the
473 THz HeNe/I₂ laser,"
Opt. Comm. **97**, 29 (1993).
17. D. J. Wineland,
"Laser-to-microwave frequency division using synchrotron radiation,"
J. Appl. Phys. **50**, 2528 (1979).
18. A. E. Kaplan,
"Optical high-order sub-harmonic excitation of free cyclotron electrons,"
Opt. Lett. **12**, 489 (1987).
19. H. R. Telle, D. Meschede, & T. W. Hansch,
"Realization of a new concept for visible frequency division: phase-locking of harmonic
and sum frequencies,"
Opt. Lett. **15**, 532 (1990).
R. Wylands, T. Mukai, & T. W. Hansch,
"Coherent bisection of optical frequency intervals as large as 532 THz,"
Opt. Lett. **17**, 1749 (1992).
20. N. C. Wong,
"Optical frequency division using an optical parametric oscillator,"
Opt. Lett. **15**, 1129 (1990).
21. A. Arie, S. Schiller, E. K. Gustafson, & R. L. Byer,
"Absolute frequency stabilization of diode-laser-pumped Nd:YAG lasers to hyperfine
transitions in molecular iodine,"
Opt. Lett. **17**, 1204 (1992).
22. R. Graham & H. Haken,
"The quantum-fluctuations of the optical parametric oscillator,"
Z. Phys. **210**, 276 (1968).
J. Y. Courtois, A. Smith, C. Fabre, & S. Reynaud,
"Phase diffusion and quantum noise in the optical parametric oscillator: a semi-
classical approach,"
J. Mod. Opt. **38**, 177 (1991).
23. J. A. Giordmaine & R. C. Miller,
"Tunable coherent parametric oscillation in LiNbO₃ at optical frequencies,"
Phys. Rev. Lett. **14**, 973 (1965).

24. R. G. Smith, J. E. Geusic, H. J. Levinstein, J. J. Rubin, S. Singh, & L. G. Van Uitert,
"Continuous optical parametric oscillation in $Ba_2NaNb_5O_{15}$ at optical frequencies,"
Appl. Phys. Lett. **12**, 308 (1968).
25. "Tunable parametric oscillator produces coherent...light from...laser source,"
in *Laser Focus World*, p16 (June 1968).
26. R. L. Byer, M. K. Oshman, J. F. Young, & S. E. Harris,
"Visible cw parametric oscillator,"
Appl. Phys. Lett. **13**, 109 (1968).
27. R. L. Byer, A. Kovrigin, & J. F. Young,
"A cw ring-cavity parametric oscillator,"
Appl. Phys. Lett. **15**, 136 (1969).
28. R. G. Smith & J. V. Parker,
"Experimental observation of and comments on optical parametric oscillation internal
to the laser cavity,"
J. Appl. Phys. **41**, 3401 (1970).
29. C. Laurence & F. Tittel,
"Visible cw parametric oscillator using barium sodium niobate,"
J. Appl. Phys. **42**, 2137 (1971).
30. J. F. Weller, T. G. Giallorenzi, & R. A. Andrews,
"Time-resolved spectral output of a doubly resonant cw optical parametric oscillator,"
J. Appl. Phys. **43**, 4650 (1972).
31. B. B. Snavely,
"Continuous-wave dye lasers,"
in "Dye lasers," (F. P. Schafer, Ed.), Springer-Verlag (1973).
32. R. G. Smith,
"A study of the factors affecting the performance of a continuously pumped doubly
resonant optical parametric oscillator,"
IEEE J. Quant. Electron. **QE-9**, 530 (1973).
33. J. E. Bjorkholm,,
"Efficient optical parametric oscillation using doubly and singly resonant cavities,"
Appl. Phys. Lett. **13**, 53 (1968).
34. L.-A. Wu, H. J. Kimble, J. L. Hall, & H. Wu,
"Generation of squeezed states by parametric down conversion,"
Phys. Rev. Lett. **57**, 2520 (1986).
35. L.-A. Wu, M. Xiao, & H. J. Kimble,
"Squeezed states of light from an optical parametric oscillator,"
J. Opt. Soc. Am. B **4**, 1465 (1987).
36. S. Reynaud, C. Fabre, & E. Giacobino,
"Quantum fluctuations in a two-mode parametric oscillator,"
J. Opt. Soc. Am. B **4**, 1520 (1987).
37. P. Grangier, R. E. Slusher, B. Yurke, & A. LaPorta,
"Squeezed-light-enhanced polarization interferometer,"
Phys. Rev. Lett. **59**, 2153 (1987).
38. A. Heidmann, R. J. Horowicz, S. Reynaud, E. Giacobino, & C. Fabre,
"Observation of quantum noise reduction on twin laser beams,"
Phys. Rev. Lett. **59**, 2555 (1987).
39. M. Xiao, L.-A. Wu, & H. J. Kimble
"Detection of amplitude modulation with squeezed light for sensitivity beyond the
shot-noise limit,"
Opt. Lett. **13**, 476 (1988).
40. T. Debuisschert, S. Reynaud, A. Heidmann, E. Giacobino, & C. Fabre,
"Observation of large quantum noise reduction using an optical parametric oscillator,"
Quant. Opt. **1**, 3 (1989).
41. J. Mertz, A. Heidmann, C. Fabre, E. Giacobino, & S. Reynaud,
"Observation of high-intensity sub-poissonian light using an optical parametric
oscillator,"
Phys. Rev. Lett. **64**, 2897 (1990).

42. C. D. Nabors & R. M. Shelby,
"Two-colour squeezing and sub-shot-noise signal recovery in doubly resonant optical parametric oscillators,"
Phys. Rev. A **42**, 556 (1990).
43. K. W. Leong, N. C. Wong, & J. H. Shapiro,
"Non-classical intensity correlation from a type I phase-matched optical parametric oscillator,"
Opt. Lett. **15**, 1058 (1990).
44. J. Mertz, T. Debuisschert, A. Heidmann, C. Fabre, & E. Giacobino,
"Improvements in the observed intensity correlation of optical parametric oscillator twin beams,"
Opt. Lett. **16**, 1234 (1991).
J. Mertz, A. Heidmann, & C. Fabre,
"Generation of sub-Poissonian light using active control with twin beams,"
Phys. Rev. A **44**, 3229 (1991).
J. G. Rarity, P. R. Tapster, J. A. Levenson, J. C. Garreau, I. Abram, J. Mertz, T. Debuisschert,
A. Heidmann, C. Fabre, & E. Giacobino,
"Quantum correlated twin beams,"
Appl. Phys. B **55**, 250 (1992).
45. E. S. Polzik, J. Carri, & H. J. Kimble,
"Spectroscopy with squeezed light,"
Phys. Rev. Lett. **68**, 3020 (1992).
"Atomic spectroscopy with squeezed light for sensitivity beyond the vacuum-state limit,"
Appl. Phys. B **55**, 279 (1992).
46. Z. Y. Ou, S. F. Pereira, H. J. Kimble, & K. C. Peng,
"Realization of the Einstein-Podolsky-Rosen paradox for continuous variables,"
Phys. Rev. Lett. **68**, 3663 (1992).
"Realization of the Einstein-Podolsky-Rosen paradox for continuous variables in non-degenerate parametric amplification,"
Appl. Phys. B **55**, 265 (1992).
47. C. D. Nabors, R. C. Eckardt, W. J. Kozlovsky, & R. L. Byer,
"Efficient, single-axial-mode operation of a monolithic MgO:LiNbO₃ optical parametric oscillator,"
Opt. Lett. **14**, 1134 (1989).
48. C. D. Nabors, S. T. Yang, T. Day, & R. C. Eckardt,
"Coherence properties of a doubly resonant monolithic optical parametric oscillator,"
J. Opt. Soc. Am. B **7**, 815 (1990).
49. R. C. Eckardt, C. D. Nabors, W. J. Kozlovsky, & R. L. Byer,
"Optical parametric oscillator frequency tuning and control,"
J. Opt. Soc. Am. B **8**, 648 (1991).
50. N. C. Wong,
"Optical frequency counting from the UV to the near IR,"
Opt. Lett. **17**, 1155 (1992).
51. N. C. Wong,
"Proposal for a 10-THz precision optical frequency comb generator,"
IEEE Phot. Tech. Lett. **4**, 1166 (1992).
52. D. Lee & N. C. Wong,
"Tunable optical frequency division using a phase-locked optical parametric oscillator,"
Opt. Lett. **17**, 13 (1992).
53. F. G. Colville, A. J. Henderson, M. J. Padgett, J. Zhang, & M. H. Dunn,
"Continuous-wave parametric oscillation in lithium triborate,"
Opt. Lett. **18**, 205 (1993).
54. S. T. Yang, R. C. Eckardt, & R. L. Byer,
"Continuous-wave singly resonant optical parametric oscillator pumped by a single-frequency resonantly doubled Nd:YAG laser,"
Opt. Lett. **18**, 971 (1993).

55. F. G. Colville, M. J. Padgett, A. J. Henderson, J. Zhang, & M. H. Dunn,
"Continuous-wave parametric oscillator pumped in the ultra-violet,"
Opt. Lett. **19**, 1065 (1993).
56. D. Lee & N. C. Wong,
"Stabilization and tuning of a doubly-resonant optical parametric oscillator,"
J. Opt. Soc. Am. B **10**, 1659 (1993).
57. D. C. Gerstenberger & R. W. Wallace,
"Continuous-wave operation of a doubly resonant lithium niobate optical parametric oscillator system tunable from 966 to 1185 nm,"
J. Opt. Soc. Am. B **10**, 1681 (1993).
58. S. T. Yang, R. C. Eckardt, & R. L. Byer,
"Power and spectral characteristics of continuous-wave parametric oscillators: the doubly to singly resonant transition,"
J. Opt. Soc. Am. B **10**, 1684 (1993).
59. S. Schiller & R. L. Byer,
"Quadruply resonant optical parametric oscillation in a monolithic total-internal-reflection resonator,"
J. Opt. Soc. Am. B **10**, 1696 (1993).
60. F. G. Colville, M. J. Padgett, & M. H. Dunn,
"Continuous-wave, dual-cavity, doubly resonant, optical parametric oscillator,"
Appl. Phys. Lett. **64**, 1490 (1994).
61. F. G. Colville, M. Ebrahinzadeh, W. Sibbett, & M. H. Dunn,
"Continuous-wave LiB_3O_5 optical parametric oscillator pumped by a tunable Ti:sapphire laser,"
Appl. Phys. Lett. **64**, 1765 (1994).
62. L. R. Brothers, D. Lee & N. C. Wong,
"Terahertz optical frequency comb generation and phase locking of an optical parametric oscillator at 665 GHz,"
Opt. Lett. **19**, 245 (1994).
63. S. T. Yang, R. C. Eckardt, & R. L. Byer,
"1.9-W cw ring-cavity KTP singly resonant optical parametric oscillator,"
Opt. Lett. **19**, 475 (1994).
64. D. Lee & N. C. Wong,
"Tuning characteristics of a cw dual-cavity KTP optical parametric oscillator,"
in *Conference on Lasers and Electro-Optics*, Vol. 8 of OSA 1994 Technical Digest Series (Optical Society of America, Washington, D. C., 1994), paper CWE 5.
65. R. Knappe, J. Barschke, C. Becher, B. Beier, M. Scheidt, K.-J. Boller, & R. Wallenstein,
"Injection-locked high power diode arrays and their application as pump sources for blue and green Nd:YAB lasers, monolithic Nd:YAG ring lasers, and cw KTP optical parametric oscillators,"
in *Conference on Lasers and Electro-Optics*, Vol. 8 of OSA 1994 Technical Digest Series (Optical Society of America, Washington, D. C., 1994), paper CThL 4.
66. D. K. Serkland, R. C. Eckardt, & R. L. Byer,
"Continuous-wave total-internal-reflection optical parametric oscillator pumped at 1064 nm,"
Opt. Lett. **19**, 1046 (1994).
67. G. Robertson, M. J. Padgett, & M. H. Dunn,
"Continuous-wave singly resonant pump-enhanced type II LiB_3O_5 optical parametric oscillator,"
Opt. Lett. **19**, 1735 (1994).
68. S.-H. Youn, J.-H. Lee, & J.-S. Chang,
"Quantum-mechanical noise characteristics in a doubly-resonant optical parametric oscillator"
J. Opt. Soc. Am. B **11**, 2282 (1994).

Chapter II.

Theoretical Background.

Contents.	Page.	
II. 1	Introduction.	25
II. 2	Parametric gain analysis.	27
II. 3	Pump power thresholds.	40
II. 4	Conversion efficiencies.	70
II. 5	Tuning, spectral outputs, and stability requirements.	75
II. 6	Further properties of the doubly-resonant oscillator.	104
II. 7	Mode-matching.	110
II. 8	Conclusions.	114
	References.	116

II. 1 Introduction.

This chapter reviews the specific criteria involved when considering the formation of continuous-wave (cw) optical parametric oscillators (OPOs). These criteria are analysed within different sections, each of which describes an important operating condition that must be addressed. The conclusions from each section should be satisfied within the eventual experimental design of a cw OPO.

Before constructing a cw OPO, there are a number of critical assessments that must be performed to establish how the device will operate in practise. These requirements include the following key parameters: incident pump power to reach threshold, optical resonator geometry including material selection, resonance conditions of the cavity, mode-selection properties of the signal and idler frequencies, and effective coupling of the pump radiation into the cavity modes of the signal and idler fields.

In section II. 2, the coupled wave equations of parametric amplification are derived classically. The steady-state equations are presented for the three fields over the length of the gain medium. A nonlinear coupling parameter

is defined in terms of the effective nonlinear coefficient, the phase-synchronism factor, and the spatial overlap of the Gaussian modes over the length of the gain medium. The analysis is valid for the case of small parametric gain, and is restricted to the near field.

Historically, the most important parameter for a cw OPO has been the pump power required to reach threshold, and this is studied in detail in section II. 3. When the pump radiation is derived from a cw laser source, with significantly lower pump powers available, compared to the more familiar pulsed pump sources used for OPOs, then the design of the OPO cavity becomes critical. In particular, within any phase-matching geometry, the resonance conditions must be selected carefully to maximize the gain of the system to reach threshold. Different optical cavities are studied to show the effects on threshold when resonating different fields within the OPO cavity. In addition, the nature of the interaction of the pump field with the signal and idler fields must be examined. In this context, ring-cavities and standing-wave cavities provide significantly different threshold values. When standing-wave cavities are analysed, it is important to consider the relative phasings of the forward and backward travelling waves within the resonator, to reduce the pump power threshold to a minimum.

Once above pump power threshold within an OPO, the conversion efficiency of the pump radiation to signal and idler powers can be considerable. Once again, these conversion efficiencies are dependent on the type of resonator employed (single-pass travelling-wave ring cavity, or double-pass standing-wave linear cavity), and the number of fields that are brought to resonance within the OPO cavity. These different configurations are reviewed in section II. 4.

The most important consideration in the operating characteristics of cw OPOs is the amplitude and frequency stability of the generated signal and idler output frequencies. These are analysed in section II. 5. The resonance properties of the OPO cavity (finesses and free spectral ranges) play the dominant role in determining the fine frequency outputs of an OPO. In general, stable OPO operation becomes more difficult to obtain as the number of resonant fields within the cavity is increased. Cavities that are resonant for both the signal and idler frequencies place stringent requirements on the frequency stability of the pump source, and the mechanical stability of the OPO resonator, to maintain stable OPO operation. The minimum stability

conditions for the pump frequency and the OPO cavity length to obtain stable OPO outputs are examined for different resonator configurations. Further, methods of generating smooth frequency tuning are analysed. Comparisons are made between different cavity designs, and for pump sources that are fixed in frequency or can be tuned smoothly.

Another factor determining the fine frequency properties of the signal and idler frequencies is the linewidth of the usable down-converted outputs. This is shown to be dependent on the frequency stability of the pump source and the noise that is inherent in the generation of the signal and idler frequencies from phase-diffusion in the parametric process. In particular, the production of equal numbers of signal and idler photons in parametric down-conversion makes possible a number of fundamental studies of OPOs in quantum optics. The quadrature amplitudes of the signal and idler beams can be regarded as quantum copies of one another, with almost perfect correlation between the signal and idler photon flux. The significance of these properties is explained in section II. 6, with regard to producing squeezed states of light from cw OPOs, for using cw OPOs within studies of high resolution spectroscopy, and for optical frequency division within optical metrology schemes (frequency chains).

Finally, in section II. 7, there is a brief study of the relevant parameters that must be considered to match the radiation from the pump source to the OPO modes, as defined by the OPO resonator. Useful equations are derived that enable effective mode-matching by transforming the Gaussian parameters of a laser source to provide the required focusing of the pump radiation within the nonlinear gain medium. In addition, formulae are presented to enable calculating the required mirror curvatures within the OPO resonator to provide the desired overlap of the pump, signal, and idler fields over the length of the gain medium.

II. 2 Parametric gain analysis.

When pumped by intense optical radiation at a frequency ν_p , a nonlinear optical material can provide gain at two lower frequencies called the signal frequency, ν_s , and the idler frequency, ν_i . These three frequencies are related by the conservation of energy relation:

$$v_p = v_s + v_i \quad \text{[II. 1]}$$

The parametric interaction is phase-dependent, and proper phasing is required for energy to flow from the pump field to the signal and idler fields. Phase-velocity matching ensures that the relative phase of the three waves does not change with propagation through the nonlinear material. Phase-matching is described by the wave-vector (or phase) mis-match, Δk , which for the case of collinear propagation, can be expressed by the scalar relationship

$$\Delta k = k_p - k_s - k_i = \frac{2\pi(n_p v_p - n_s v_s - n_i v_i)}{c} \quad \text{[II. 2]}$$

where k_p , k_s , and k_i are the wave-vector magnitudes of the pump, signal, and idler waves, respectively, with corresponding indices of refraction given by n_p , n_s , and n_i , and c is the velocity of light. Useful parametric gain exists in the range of signal and idler frequencies for which $|\Delta k| \leq \pi/l$, where l is the length of the nonlinear material [1]. The parametric gain is maximum near $\Delta k = 0$, ensuring that the three waves propagate synchronously with constructive interference. Phase-matching is often achieved by controlling the birefringence of a nonlinear crystal through temperature or angle of propagation.

An OPO requires feedback at either (or both) the signal and idler frequencies. If there is feedback at only one frequency, the device is called a singly resonant oscillator. Doubly-resonant oscillators have feedback simultaneously at the signal and idler frequencies. A further extension to these configurations is to resonate the pump frequency within the OPO cavity. Both singly- and doubly-resonant oscillators can be formed with pump enhanced fields. The doubly-resonant oscillator with a pump enhanced field is often referred to as a triply-resonant oscillator where all three waves are brought to resonance. The number of waves brought to resonance within the OPO cavity affects drastically the operating characteristics of the device. The important differences between the various resonant cavities include the pump power threshold, the conversion efficiencies, and the pump frequency stability requirements.

Typically, feedback is provided by placing the nonlinear material in a cavity formed by external mirrors. This cavity can be formed within the resonator of the pump source, or external to the pump source. In this

chapter, only external resonator designs are considered. Therefore, external cavities are analysed that involve a nonlinear material surrounded by mirrors to provide the desired feedback. However, highly reflecting coatings can be applied directly to the nonlinear material. This allows for the formation of monolithic OPO resonators, and reference to these devices is made frequently throughout the text.

Phase-matching is the major factor in determining the broad (coarse) tuning properties of an OPO, although cavity resonances have the major effect on details of frequency tuning. The conditions $\nu_p = \nu_s + \nu_i$ and $\Delta k = 0$ define the phase-matching curves. The spectral width of the parametric gain is also determined by phase-matching.

Similar to the steady-state analysis of a laser resonator, when the gain exceeds the loss in an OPO, the device reaches threshold and oscillates. At threshold, the output power increases dramatically, similar to the behaviour of a laser. The generated output is coherent and collinear with the pump laser beam. Once above threshold, the parametric oscillator converts efficiently the pump radiation to continuously tunable signal and idler fields, with the gain clamped at its threshold value (similar to the steady-state operation of a laser oscillator). Since the gain is proportional to the pump field, above threshold any additional pump power must be diverted into power at the signal and idler fields.

The first distinction to make is between cw and pulsed operation. In general, these devices have many similarities, when considering the coarse frequency tuning properties of the OPO. However, the most significant difference is the much greater peak pump powers that are available from pulsed laser sources. This allows greater flexibility in the design of the OPO resonator, with regard to cavity resonances, cavity stability, and focusing requirements.

There are many different forms of resonators that have been used to provide cw parametric oscillation. The cavities that are analysed in this chapter are displayed in figure II. 1. Figure II. 1 (a) illustrates parametric amplification over the length of the nonlinear crystal. Figure II. 1 (b) illustrates the ring-cavity oscillator. The ring cavity provides single-pass parametric interaction, and can offer improved OPO conversion efficiency. In addition, this design offers advantages of reduced feedback to the pump source. Figure II. 1 (c) displays the single-cavity, standing-wave OPO where

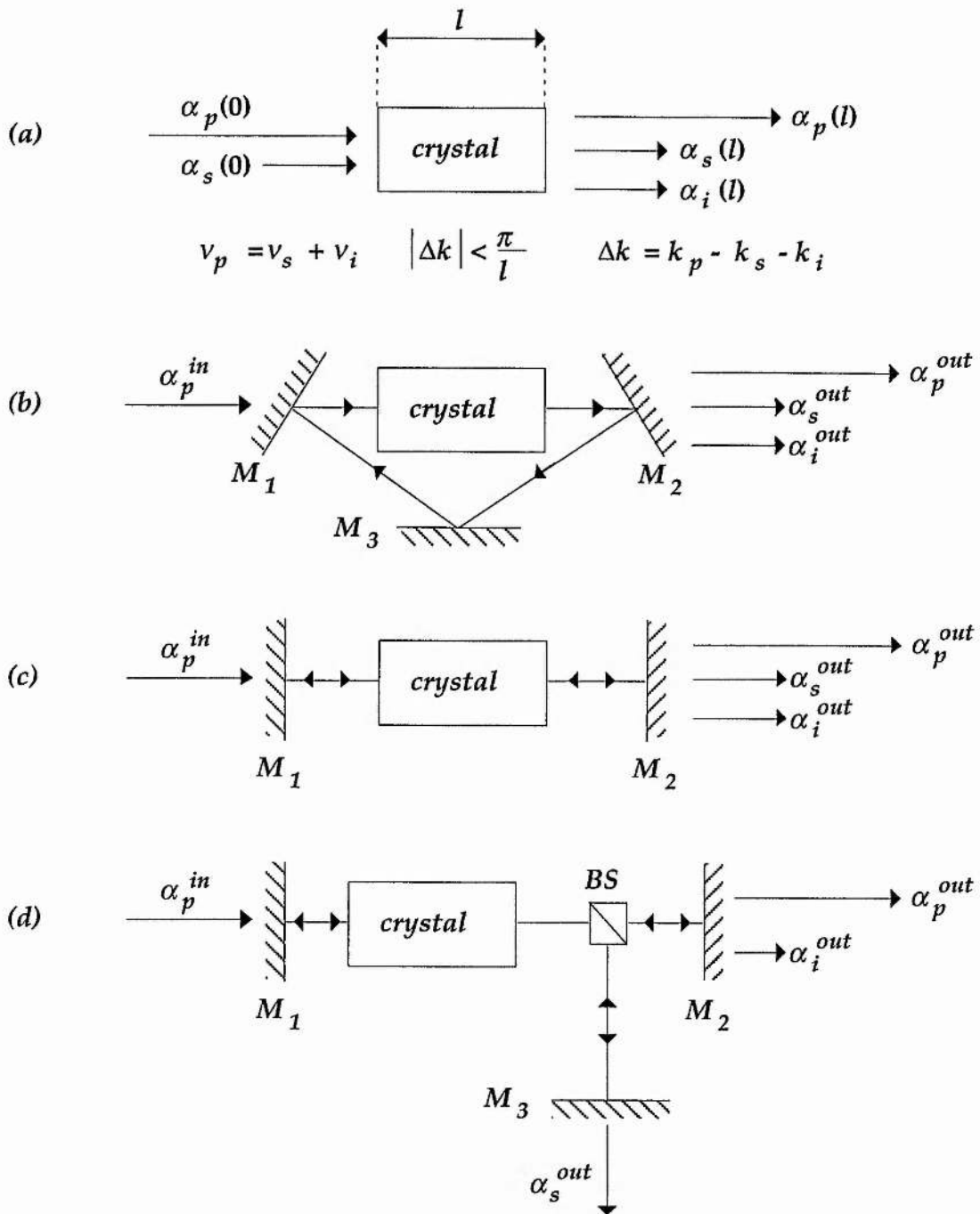


Figure II. 1.

(a) Schematic representation of optical parametric amplification. Optical parametric oscillators are formed by the addition of mirrors that form an optical resonator. (b) Ring-cavity oscillator with travelling-wave fields and a single-pass through the gain medium. (c) Single-cavity oscillator with standing-wave fields. (d) Dual-cavity oscillator with separate optical resonators for different resonant fields; BS: beam-splitter.

the OPO fields are brought to resonance between two common cavity mirrors. Finally, figure II. 1 (d) displays the dual-cavity, standing-wave OPO resonator, which allows separate OPO resonant cavities to be formed with independent cavity length control.

II. 2. (i) The nonlinear susceptibility.

When an electromagnetic wave, E , propagates through a dielectric material, it induces a polarization, P . For most electromagnetic waves, where the electric field is considerably smaller than the intra-atomic field, the response of the induced polarization will be linear in the electric field, and can be expressed as follows:

$$P = \epsilon_0 \chi_s E , \quad [\text{II. 3}]$$

where ϵ_0 is the permittivity of free space, and χ_s is the (linear) electrical susceptibility. The electrical susceptibility is a frequency dependent, complex quantity, of which the real part is related to the refractive index ($|\chi_s| = n^2 - 1$) and is responsible for reflection / refraction, and the imaginary part is related to the absorption properties of the material, and is only significant close to an atomic resonance. Equation II. 3 represents the regime of linear optics.

When the electromagnetic wave has an electric field strength comparable to the intra-atomic field, as provided by the high intensities associated with laser radiation, the response to the field can no longer be described by the linear relation of equation II. 3. Now, it is necessary to expand the induced polarization in powers of E . The relation between the electric field and the polarization can be expressed as the following power series expansion:

$$P = \epsilon_0 \left(\chi_s^{(1)} E + \chi_s^{(2)} E^2 + \chi_s^{(3)} E^3 + \dots \right) , \quad [\text{II. 4}]$$

where $\chi_s^{(1)}$, $\chi_s^{(2)}$, $\chi_s^{(3)}$, etc. are the first, second, third, etc., -order susceptibilities. (The scalar notation in the above equation is used only to simplify the analysis; the susceptibilities are actually tensors.) From equation II. 4, the response of the polarization to the field is no longer linear,

and is referred to simply as nonlinear. By splitting this relation into linear and nonlinear parts (P^{NL}), the polarization can be described as follows:

$$P = \epsilon_0 \chi_s^{(1)} E + P^{NL} . \quad [\text{II. 5}]$$

The nonlinear effects due to the quadratic term (a tensor of rank three) involve the mixing of frequencies in, for example, second harmonic generation, and sum and difference frequency mixing. For the even term to be present, the medium must lack a centre of inversion (non-centrosymmetric). The cubic term gives rise to third harmonic generation, Raman scattering, four wave mixing, and others. The following analysis is restricted to materials which possess a substantial second order nonlinear susceptibility. Terms of higher order, which will be considerably weaker, are neglected.

Following the analysis outlined in reference [2], as extended in reference [3], with the inclusion of the factor ϵ_0 such that the units of $\chi_s^{(2)}$ are in m/V, the second-order nonlinear polarization can be expressed in tensor notation as follows:

$$P^{NL}(v_p) = \epsilon_0 \chi_s^{(2)} : E(v_s) E(v_i) , \quad [\text{II. 6 (a)}]$$

$$P^{NL}(v_s) = \epsilon_0 \chi_s^{(2)} : E^*(v_i) E(v_p) , \quad [\text{II. 6 (b)}]$$

$$P^{NL}(v_i) = \epsilon_0 \chi_s^{(2)} : E^*(v_s) E(v_p) . \quad [\text{II. 6 (c)}]$$

Normally, the measure of nonlinearity is determined by second harmonic generation experiments. Therefore, it is convenient to express the equations in terms of nonlinear coefficients, d_{ijk} , instead of $\chi_s^{(2)}$, such that $\chi_{ijk}^{(2)} = 2d_{ijk}$, where $\chi_{ijk}^{(2)}$ are the components of $\chi_s^{(2)}$. As these d_{ijk} coefficients obey the same crystal symmetry as the piezo-electric coefficients (although different in magnitude), it is also convenient to use the condensed notation [4] that is applied to the piezo-electric coefficients. In this case, the second order nonlinear susceptibilities are specified in the principal axis system (XYZ) of the piezo-electric coefficients. The Z-axis is generally adopted as the polar axis. This condensed notation takes the form

$$d_{ijk} = d_{il(j,k)} , \quad [\text{II. 7}]$$

where

$$l(1,1) = 1, \quad l(2,2) = 2, \quad l(3,3) = 3, \quad l(2,3) = 4, \quad l(1,3) = 5, \quad \text{and} \quad l(1,2) = 6 .$$

and where the subscripts i, j , and k are labelled 1, 2, and 3, respectively. They refer to the axes X, Y , and Z , respectively. The nonlinear polarization equations in terms of the d tensor for the three frequency interactions are given now by [1]

$$P(v_p) = \epsilon_0 2d : E(v_s)E(v_i) , \quad [\text{II. 8 (a)}]$$

$$P(v_s) = \epsilon_0 2d : E^*(v_i)E(v_p) , \quad [\text{II. 8 (b)}]$$

$$P(v_i) = \epsilon_0 2d : E^*(v_s)E(v_p) , \quad [\text{II. 8 (c)}]$$

where the notation implies a vector sum over the axial components. The analysis is simplified further by calculating an effective nonlinear coefficient, d_{eff} , which is the net response of the nonlinearity, taking into account the relation between the E field polarization vectors and the symmetry of the d tensor. The term, d_{eff} , is a measure of the coupling between the three interacting fields, involving projection of all three fields on to the d tensor. The use of d_{eff} allows for scalar notation.

II. 2. (ii) The coupled amplitude equations for plane waves.

The nonlinear polarization allows for the transfer of energy between waves of different frequency. By inserting the nonlinear polarization (equation II. 5) in the Maxwell wave equation allows for the wave equation in a nonlinear medium, as follows:

$$\nabla^2 E = \mu_0 \sigma \frac{\partial E}{\partial t} + \mu_0 \epsilon \frac{\partial^2 E}{\partial t^2} + \mu_0 \frac{\partial^2 P^{NL}}{\partial t^2} , \quad [\text{II. 9}]$$

where μ_0 is the permeability of free space, σ is the coefficient of absorption, and $\epsilon = \epsilon_0 (1 + \chi_s^{(1)})$. The first term on the right hand side allows for

absorption, and the other two are the source terms for wave propagation. Equation II. 9 is a general solution to the problem of waves propagating in a material with quadratic nonlinearity.

The transfer of energy between waves is described by coupled amplitude equations, which give the dependence of the amplitudes of the interacting waves, A_j , on propagation through the nonlinear crystal [5, 6]. These apply only to the case of infinite extent, plane waves. The quadratic nature of the nonlinearity allows for interaction between any three frequencies which satisfy the conservation of energy relation.

The electric field is now assumed to be propagating along a direction, z . The plane wave assumption [1] allows the derivatives with respect to the orthogonal directions, x and y , to be set equal to zero. By applying the slowly varying envelope assumption (the paraxial wave approximation) [2] (i.e. $k\partial E/\partial z \gg \partial^2 E/\partial z^2$), and sorting out the resulting terms into their frequency components, the equations of interest are as follows [2]:

$$\frac{\partial E_p}{\partial z} + \rho_p E_p = i\kappa_p E_s E_i \exp(-i\Delta kz) , \quad [\text{II. 10 (a)}]$$

$$\frac{\partial E_s}{\partial z} + \rho_s E_s = i\kappa_s E_p E_i^* \exp(i\Delta kz) , \quad [\text{II. 10 (b)}]$$

$$\frac{\partial E_i}{\partial z} + \rho_i E_i = i\kappa_i E_p E_s^* \exp(i\Delta kz) , \quad [\text{II. 10 (c)}]$$

where $\rho_j = \mu_0 \sigma_j c / 2$ are the field absorption coefficients, and $\kappa_j = 2\pi \nu_j d_{\text{eff}} / n_j c$ are the coupling (interaction) coefficients.

The coupled differential equations, as given by equation II. 10, connect the three fields via the second order nonlinear susceptibility, and determine the growth of each wave as a function of the other two interacting fields. Within these equations, the initial relative phasing of the waves has been omitted. This relative phasing determines which nonlinear process ensues. The conversion of pump radiation to signal and idler fields is maximum (for $\Delta k = 0$) when the initial relative phasing is equal to $-\pi/2$. If the relative phase term is $+\pi/2$, then the direction of energy flow is reversed, with conversion from signal and idler fields to pump radiation.

Exact solutions to these equations exist [2]. However, a commonly used approximation, which allows solution of the amplitude equations, is to assume that the pump beam is not substantially depleted by conversion to the signal and idler waves ($E_p(z) \equiv E_p(z) \equiv \text{constant}$, $\partial E_p / \partial z = 0$). The undepleted pump approximation reduces the three coupled equations to two simultaneous differential equations (signal and idler terms), allowing solution with appropriate boundary conditions, and is valid where conversion to signal and idler is small. The resulting two amplitude equations have been solved for the general case of input waves at both the signal and idler, where the commonly used simplifying assumption of equal signal and idler absorption has not been made [7]. By using the substitution into a new field variable A_j , proportional to the photon flux, such that

$$A_j(z) = \frac{n_j}{2\pi v_j} E_j(z) , \quad [\text{II. 11}]$$

then the coupled equations for signal and idler, which describe the case of a parametric amplifier with input at both signal and idler, can be written as two coupled linear simultaneous differential equations, describing the exponential growth of the signal and idler fields as they propagate through the nonlinear medium, as follows:

$$\frac{dA_s(z)}{dz} = -i\sqrt{\kappa I_p} A_i^*(z) \exp(-i\Delta kz) , \quad [\text{II. 12 (a)}]$$

$$\frac{dA_i^*(z)}{dz} = i\sqrt{\kappa I_p} A_s(z) \exp(i\Delta kz) , \quad [\text{II. 12 (b)}]$$

where absorption has been neglected, and where

$$\kappa = \frac{8\pi^2 v_s v_i d_{eff}^2}{n_s n_i n_p \epsilon_0 c^3} , \quad [\text{II. 13}]$$

$$I_p = \frac{1}{2} n_p c \epsilon_0 |E_p|^2 . \quad [\text{II. 14}]$$

Further manipulation of these equations allows a general form of solution for the single pass gain to be derived [7].

II. 2. (iii) Parametric amplification of focused Gaussian beams.

The three coupled fields are now assumed to be linearly polarized fundamental Gaussian beams. The length of the interaction is assumed to be smaller than the confocal parameter, so that the expression of the fields, defined along a propagation direction, z , can be given by

$$E_j(z, r, t) = \frac{2\pi\nu_j}{n_j} A_j(z) \exp\left[\frac{-r^2}{W_j^2}\right] \exp[i(2\pi\nu_j t - k_j z)], \quad j = p, s, i. \quad [\text{II. 15}]$$

The radial dependence, r , of the field has a Gaussian shape that is characterized by the beam waist, W_j . In general, if a beam having a Gaussian cross-section is incident on a nonlinear crystal and parametrically amplified, the output beam will no longer be a simple Gaussian. This occurs as a result of Poynting vector walk-off. In general, in an anisotropic medium, the direction of the electric displacement vector and the electric field vector are not in the same direction. Therefore, the wave-vector direction and the direction of energy propagation, as defined by the Poynting vector, are also not in the same direction. When writing equation II. 15, it is assumed that there is no walk-off, which would appear as a translation of the centre of the Gaussian as the beam propagates. The effect of walk-off is to limit the interaction length by reducing the overlap of the three waves. In this case, a more general treatment is necessary. An analysis of this problem, allowing for arbitrarily tight focusing and Poynting vector walk-off, has been given in reference [3]. The analysis considered here is restricted to the important case of near-field focusing and 90° , or non-critical, phase-matching, in which Poynting vector walk-off is absent, and subsequently, there is no limit to the crystal length. An analysis of this case was first given in reference [3].

A near field analysis keeps track of the transverse dependence of the signal, idler and pump modes, but assumes that this transverse dependence does not change over the length of the nonlinear crystal. Therefore, it requires that the confocal parameter of the focus (of all three beams) be as long or longer than the length of the nonlinear crystal.

Inserting the radial dependence of the fields into the coupled equations, the gain for each field depends on the nonlinear polarization, P_j , as given by

$$P_p(r, z) = \frac{8\pi^2 v_s v_i \epsilon_0 d_{eff}}{n_s n_i} A_i(z) A_s(z) \exp\left[\frac{-r^2}{\bar{W}_p^2}\right] \exp[-i\Delta kz] , \quad [\text{II. 16 (a)}]$$

$$P_s(r, z) = \frac{8\pi^2 v_p v_i \epsilon_0 d_{eff}}{n_p n_i} A_p(z) A_i^*(z) \exp\left[\frac{-r^2}{\bar{W}_s^2}\right] \exp[i\Delta kz] , \quad [\text{II. 16 (b)}]$$

$$P_i(r, z) = \frac{8\pi^2 v_p v_s \epsilon_0 d_{eff}}{n_p n_s} A_p(z) A_s^*(z) \exp\left[\frac{-r^2}{\bar{W}_i^2}\right] \exp[i\Delta kz] . \quad [\text{II. 16 (c)}]$$

The strength of the coupling is given by the effective nonlinear coefficient, d_{eff} , obtained by projecting the nonlinear tensor on the polarization direction of the fields. The transverse dependence of the polarization depends on the parameters, \bar{W}_j , which are the beam waist radii ($1/e$ electric field radius), and are defined as

$$\frac{1}{\bar{W}_p^2} = \frac{1}{\bar{W}_s^2} + \frac{1}{\bar{W}_i^2} , \quad [\text{II. 17 (a)}]$$

$$\frac{1}{\bar{W}_s^2} = \frac{1}{\bar{W}_i^2} + \frac{1}{\bar{W}_p^2} , \quad [\text{II. 17 (b)}]$$

$$\frac{1}{\bar{W}_i^2} = \frac{1}{\bar{W}_s^2} + \frac{1}{\bar{W}_p^2} . \quad [\text{II. 17 (c)}]$$

For instance, the idler and the pump mix to yield a polarization at the signal frequency of the form

$$\exp\left(-\frac{r^2}{\bar{W}_s^2}\right) = \exp\left(-\frac{r^2}{\bar{W}_i^2}\right) \exp\left(-\frac{r^2}{\bar{W}_p^2}\right) . \quad [\text{II. 18}]$$

These polarization radii are always smaller than the radius of either of the Gaussian beams which mix to produce them. Overlap integrals must be calculated [9], to compute the coupling between the two normalized modes. This results in a set of coupled wave equations for the fields, as generated by the nonlinear driving polarization:

$$\frac{d\alpha_p}{dz} = -2\kappa\alpha_i(z)\alpha_s(z)\exp[-i\Delta kz] , \quad [\text{II. 19 (a)}]$$

$$\frac{d\alpha_s}{dz} = 2\kappa\alpha_p(z)\alpha_i^*(z)\exp[i\Delta kz] , \quad [\text{II. 19 (b)}]$$

$$\frac{d\alpha_i}{dz} = 2\kappa\alpha_p(z)\alpha_s^*(z)\exp[i\Delta kz] , \quad [\text{II. 19 (c)}]$$

where α_j is defined by

$$\alpha_j(z) = \left(\frac{c\epsilon_0 v_j^2 \pi^3 W_j^2}{h v_j n_j} \right)^{1/2} A_j(z), \quad j = s, i , \quad [\text{II. 20}]$$

$$\alpha_p = i \left(\frac{c\epsilon_0 v_p^2 \pi^3 W_p^2}{h v_p n_p} \right)^{1/2} A_p(z) .$$

and κ is now given by

$$\kappa = d_{eff} M \left(\frac{16\pi h v_p v_s v_i}{\epsilon_0 c^3 n_p n_s n_i} \right)^{1/2} , \quad \text{where} \quad [\text{II. 21}]$$

$$M = \frac{W_p W_s W_i}{W_p^2 W_s^2 + W_p^2 W_i^2 + W_s^2 W_i^2} . \quad [\text{II. 22}]$$

$|\alpha_j|^2$ is normalized to represent the numbers of incident photons per unit time in the mode j ; i.e., to a photon flow. The parameter κ now incorporates the familiar spatial coupling factors [8] which illustrate the failure of the driving polarizations to completely overlap the desired Gaussian modes.

To maximize the coupling factor, M , for fixed signal and idler waists, W_s and W_i , then the pumping beam size should be as follows [8]:

$$\frac{1}{W_p^2} = \frac{1}{W_s^2} + \frac{1}{W_i^2} , \quad [\text{II. 23}]$$

in which case the coupling factor, M , will be

$$M_{max} = \frac{1}{2} \sqrt{\frac{1}{W_s^2 + W_i^2}} . \quad [\text{II. 24}]$$

To maximize the parameter, M , the beam waists, W_s and W_i , should be chosen to be as small as possible. However, since the present analysis is restricted to the near field, the smallest allowed spot sizes are approximately those of the confocal condition; i.e.

$$W_s^2 = \frac{cl}{2\pi n_s v_s} , \quad [\text{II. 25 (a)}]$$

$$W_i^2 = \frac{cl}{2\pi n_i v_i} . \quad [\text{II. 25 (b)}]$$

From equation II. 23, if both the signal and idler are confocally focused, the pump should also be confocally focused [8].

Equations II. 19 can be integrated by developing the expression of the fields in powers of z . As mentioned previously, only the zeroth-order terms in the expression of the gain are considered. Integrating then yields the following expressions for the three fields:

$$\alpha_p(l) = \alpha_p(0) - 2\chi^* \alpha_i(0)\alpha_s(0) , \quad [\text{II. 26 (a)}]$$

$$\alpha_s(l) = \alpha_s(0) + 2\chi\alpha_p(0)\alpha_i^*(0) , \quad [\text{II. 26 (b)}]$$

$$\alpha_i(l) = \alpha_i(0) + 2\chi\alpha_p(0)\alpha_s^*(0) , \quad [\text{II. 26 (c)}]$$

where χ is a function of the nonlinear gain coefficient of the medium, as given by

$$\chi = \kappa l \text{sinc}\left[\frac{\Delta kl}{2}\right] \exp\left[\frac{i\Delta kl}{2}\right] . \quad [\text{II. 27}]$$

Equations II. 26 describe the steady-state equations for the fields propagating through the nonlinear medium. Phase-matching enters into the nonlinear conversion process through the phase-synchronism factor, $\text{sinc}(\Delta kl / 2)$, which

is unity at $\Delta kl = 0$. For $\Delta kl \neq 0$, the efficiency of the device will drop by the factor $\text{sinc}^2(\Delta kl / 2)$.

In the case of confocal focusing that is analysed in this chapter, it is useful to rewrite the expression for the coupling parameter as follows:

$$|\chi|^2 = |d_{\text{eff}}|^2 \frac{\pi^2 l v_p^3 (1 - \delta^2)^2 \text{sinc}^2\left[\frac{\Delta kl}{2}\right]}{2 \epsilon_0 c^4 n_p^2} (h v_p), \quad [\text{II. 28}]$$

where δ is a measure of how far removed from frequency-degeneracy the signal and idler frequencies are phase-matched. It is referred to as the degeneracy factor, such that

$$\delta = \frac{2v_s - v_p}{v_p} = \frac{v_p - 2v_i}{v_p}. \quad [\text{II. 29}]$$

When the signal and idler frequencies are exactly equal, as in the case of exact frequency degeneracy, then the degeneracy factor, $\delta = 0$.

Finally, before starting the analysis of the pump power thresholds, it is useful to express the relation between the photon flows, $|\alpha_j|^2$, and the powers, P_j , as follows:

$$P_j = |\alpha_j|^2 (h v_j). \quad [\text{II. 30}]$$

This expression is used to determine the powers of the three fields entering and leaving the OPO, and in particular the pump power required to reach threshold.

II. 3 Pump power thresholds.

Before radiation can be transferred effectively from the pump field to the signal and idler fields, it is necessary to build up resonant fields within an optical cavity, containing the nonlinear gain medium. This is achieved only when the oscillation thresholds are overcome (i.e. when the round-trip gain exceeds the loss), and steady-state oscillation is provided. In this section, the pump power required to reach threshold is calculated for different cavity

configurations. The study can be divided broadly into two different sections, depending on whether the interaction of the pump field with the nonlinear gain medium takes on the form of travelling waves or standing waves. The ring cavity resonator is used to model the effects of the travelling waves, and the linear cavity resonator models the standing-wave configuration.

For each cavity design, an analysis is given for the general case of the triply-resonant oscillator (or pump-enhanced doubly-resonant oscillator), in which all three waves are strongly resonant within the optical cavity. The pump power thresholds are described conveniently in terms of the cavity finesses and the free spectral ranges of the resonant waves. Other combinations of resonant, non-resonant, and double-pass pump fields are then summarized, and further, compared to the initial triply-resonant oscillator analysis.

II. 3. (i) Ring cavity resonators.

The first geometry described involves the nonlinear crystal located in a ring cavity that is formed by three external mirrors. The ring cavity is the simplest configuration to study since all the fields propagate in one direction and experience the nonlinear interaction only once in each round-trip. (The other geometry analysed involves standing-wave fields, brought to resonance within a linear cavity design.)

The most general case of the ring cavity oscillator is when all three waves are strongly resonant within the cavity. This is the case of the triply-resonant oscillator, or the pump-enhanced doubly-resonant oscillator. In this arrangement, an incoming pump wave is resonated in a low loss, high finesse OPO cavity for the pump frequency. In addition, the two OPO fields (signal and idler) resonate in this same cavity with low losses and high finesses. The optimum operating condition of this OPO configuration is shown to be when the conditions of exact cavity resonance for the pump, signal and idler frequencies are fulfilled. A detuning of any one of these three fields from exact cavity resonance causes an increase in the parametric threshold, and a decrease in the conversion efficiencies of input pump power to external signal and idler output powers.

When the constraint of resonating the pump field is eliminated, and only an input, single-pass, pump field contributes to the parametric gain, then

the doubly-resonant oscillator is formed. This geometry is shown to exhibit an increased pump power threshold compared to the triply-resonant oscillator. However, this geometry displays more freedom over the triply-resonant oscillator in having to satisfy only two conditions of cavity resonance.

Finally, by allowing only one of the generated OPO frequencies to resonate, many of the difficulties associated with the doubly-resonant oscillator, with and without pump field enhancement, can be eliminated. Two different configurations are analysed. These provide for both single-pass and resonant pump fields within the ring-cavity resonator. These designs are compared to both triply-resonant and doubly-resonant oscillators with respect to the aforementioned resonance properties, and further, to the pump powers required to reach threshold.

II. 3. (i) (a) Doubly-resonant oscillator with resonant pump field.

The most common type of resonator used to operate cw OPOs is the doubly-resonant OPO. With the exception of only one experiment [10, 11], all reports of cw OPOs have used this geometry [12]. Many of these devices have involved the use of resonant pump fields to enhance the input pump field within the cavity [13]. The ring-cavity, doubly-resonant oscillator with a pump-enhanced, resonant field, is illustrated schematically in figure II. 2. The OPO cavity is formed by three external mirrors that provide the high finesse cavities for the resonant fields of the OPO.

The length of the nonlinear crystal is denoted by l , and the total length of the cavity in the absence of the crystal is denoted by L_{cav} . Therefore, the empty length of the cavity can be defined as

$$L = L_{cav} - l . \quad [\text{II. 31}]$$

For simplicity, it is assumed that two of the mirrors, M_2 and M_3 in figure II. 2, are perfectly reflecting ($R = 1$), and that the other one, called the coupling mirror, M_1 , has field amplitude reflection and transmission coefficients equal to r_p, r_s, r_i , and t_p, t_s, t_i , respectively. (This approximation is used only to simplify the algebra. It is shown shortly that this analysis is valid for the case of separate coupling mirrors.)

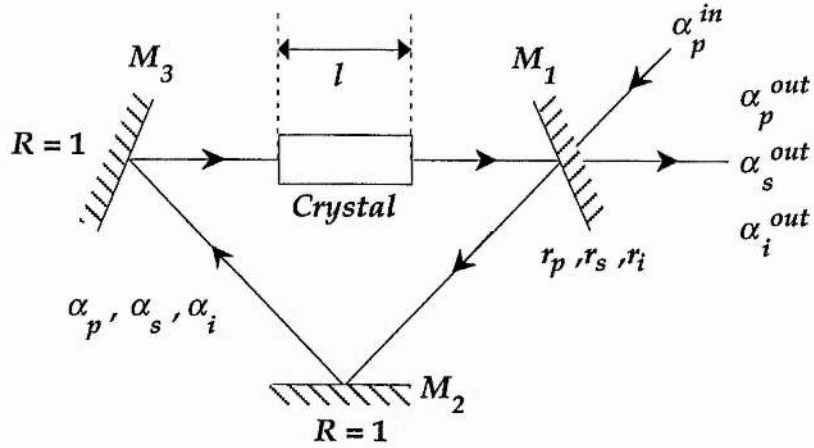


Figure II. 2.

Ring cavity resonator consisting of a crystal of length, l , with a pump-enhanced interaction through the nonlinear medium and doubly-resonant signal and idler frequencies. The incoming pump field, α_p^{in} , produces one output signal field, α_s^{out} , and one idler field, α_i^{out} . A part of the pump field, α_p^{out} , is reflected from the cavity.

When the transmission coefficients of the coupling mirror, γ_j , are small (as in the case of high-finesse, low-loss, optical resonators), the amplitude reflection and transmission coefficients can now be written as

$$r_j = 1 - \gamma_j \quad , \quad \text{[II. 32]}$$

$$t_j = \sqrt{2\gamma_j} \quad , \quad \text{[II. 33]}$$

with $\gamma_j \ll 1$. When the mirrors are free of absorption and scattering, r_j and t_j are related by the following expression:

$$|r_j|^2 + |t_j|^2 = 1 \quad . \quad \text{[II. 34]}$$

Equation II. 34 can be written in terms of the power coefficients of reflection and transmission, R_j and T_j , as follows:

$$R_j = |r_j|^2$$

$$T_j = |t_j|^2$$
[II. 35]

The complex amplitudes of the three interacting fields at an arbitrary position, z , inside the optical cavity are denoted by $\alpha_p(z)$, $\alpha_s(z)$, and $\alpha_i(z)$, for the pump, signal and idler frequencies, respectively. As discussed in section II. 2, they are normalized in such a way that $|\alpha_p|^2$, $|\alpha_s|^2$, and $|\alpha_i|^2$ are in units of photon flow. (Within parametric down-conversion, the signal and idler photons are created in equal photon numbers. Therefore, it is intuitive to express the field relations in terms of their photon flows.) They are expressed in terms of the electric-field envelopes, A_j , by the use of equation II. 20, defined in the previous section. The waves entering into the cavity are denoted by α_p^{in} , α_i^{in} , and α_s^{in} , and the waves leaving the cavity are given by α_p^{out} , α_i^{out} , and α_s^{out} .

To determine the equations for the field amplitudes, it is necessary to take into account the gain and losses experienced by the various fields when they propagate inside the cavity. In the steady-state regime, the parametric gain on one round-trip must match the losses. Consider first the coupling of the fields at the coupling mirror, as illustrated by figure II. 3

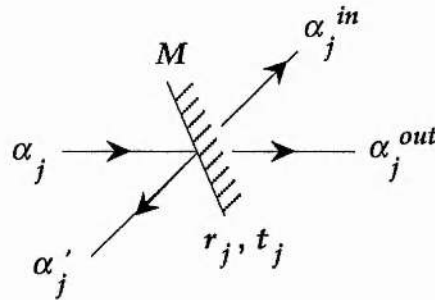


Figure II. 3.
The coupling of the fields entering and leaving the resonator at the partially reflecting cavity mirror.

The intra-cavity fields, α_j and α_j' in figure II. 3, are related to the fields entering, α_j^{in} , and leaving, α_j^{out} , the cavity by the following relations:

$$\begin{aligned}\alpha'_j &= r_j \alpha_j + t_j \alpha_j^{in} \\ \alpha_j^{out} &= t_j \alpha_j - r_j \alpha_j^{in} \end{aligned} \quad [\text{II. 35}]$$

where r_j and t_j are the coefficients of reflection and transmission for the electric fields.

In a round-trip of the ring-cavity, each field experiences a linear phase shift, φ_j , as given by

$$\varphi_j = \frac{2\pi\nu_j}{c}(n_j l + L) . \quad [\text{II. 36}]$$

In this section, the effects of the phase shifts resulting from the reflection on the cavity mirrors are not taken into account. Their effect is important only in the case of a linear standing-wave cavity with forward and backward travelling waves, and is studied in section II. 3 (ii).

Equating gain and losses in one round-trip, the equations governing the three fields in the steady-state regime are

$$\alpha_p [1 - r_p \exp(i\varphi_p)] = -2\chi^* \alpha_s \alpha_i r_p \exp(i\varphi_p) + t_p \alpha_p^{in} , \quad [\text{II. 37 (a)}]$$

$$\alpha_s [1 - r_s \exp(i\varphi_s)] = 2\chi \alpha_p \alpha_i^* r_s \exp(i\varphi_s) , \quad [\text{II. 37 (b)}]$$

$$\alpha_i [1 - r_i \exp(i\varphi_i)] = 2\chi \alpha_p \alpha_s^* r_i \exp(i\varphi_i) , \quad [\text{II. 37 (c)}]$$

where α_p^{in} denotes the input pump field. No input signal and idler modes are considered in this analysis, although their effect on the performance of doubly-resonant oscillators has been considered [14]. Note that the signal and idler fields are symmetric under interchange of indices.

The phase detunings, $\delta\varphi_j$, of the fields from the exact cavity resonances are defined such that

$$\varphi_j = 2p_j\pi + \delta\varphi_j , \quad [\text{II. 38}]$$

where p_j is an integer. It is assumed that these detunings are small, and such that

$$|\delta\phi_j| \ll 2\pi . \quad [\text{II. 39}]$$

It is useful for future calculations to express the phase detunings, $\delta\phi_j$, in terms of the cavity frequency detunings, $\Delta\nu_j$, and the free spectral ranges of the optical cavity, FSR_j . Allowing for dispersion in the nonlinear medium, the free spectral ranges, FSR_j , within the ring-cavity, are defined by

$$FSR_j = \left(\frac{c}{n_j l + L} \right) \cdot \left(1 + \frac{\frac{dn_j}{d\nu_j} l \nu_j}{n_j l + L} \right) . \quad [\text{II. 40}]$$

When the effects of dispersion are neglected, this expression reduces to the more familiar relation for the free spectral range in terms of the optical length of the cavity. Therefore, the free spectral ranges, FSR_j , in the absence of dispersion, are defined by

$$FSR_j = \frac{c}{n_j l + L} . \quad [\text{II. 41}]$$

As discussed previously, doubly-resonant oscillation of the signal and idler frequencies requires the simultaneous resonance of these two fields. However, as shown in equation II. 40, the effects of birefringence within the nonlinear medium causes different free spectral ranges, or axial-mode spacings, for the two waves. Therefore, the simultaneous resonance condition occurs only at discrete intervals in frequency (or cavity length), when the two axial modes are in coincidence.

A useful device for understanding the requirement for simultaneous cavity resonances is a type of diagram used first in reference [16], and more recently in reference [17]. The cavity resonances of the signal and idler frequencies are plotted as a function of the respective frequencies, as shown schematically in figure II. 4. The difference between the signal and idler axial mode spacings, or free spectral ranges, FSR_s and FSR_i , respectively, is exaggerated in this figure for the purpose of illustration. One frequency, here the signal, increases from left to right. The other frequency scale, the idler, is

determined by the first scale and the conservation of energy condition in such a way that any vertical line drawn through the diagram will give signal and idler frequencies that satisfy the conservation of energy relation. If a signal and idler resonance pair lies on a vertical line, it satisfies the simultaneous resonance condition. If the birefringence of the nonlinear medium changes, the position of the resonances will advance along the scales, one to the left and one to the right, at slightly different rates because of dispersion, but the scales will not change. If the pump frequency changes, the frequencies of the cavity resonances will not change, but one of the scales will be displaced with respect to the other, and the respective resonances will move with that scale.

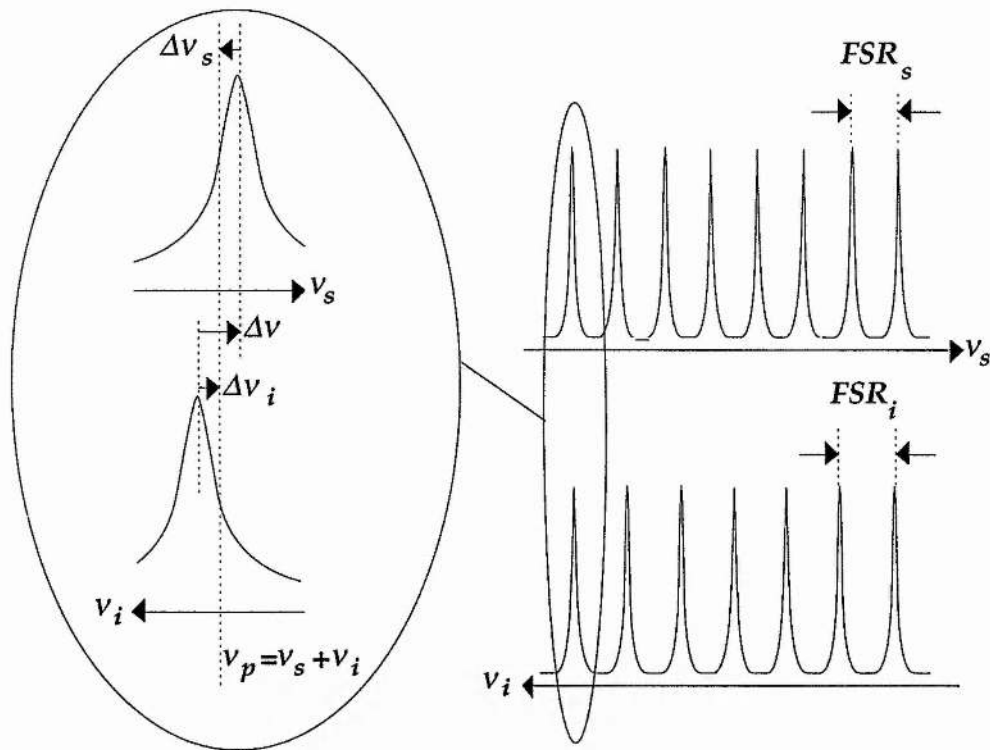


Figure II. 4.

Diagram that shows the relationship between the doubly-resonant oscillator signal and idler resonance frequencies and the conservation of energy condition. A signal-idler mode-pair that has both resonances centred on a vertical line is in coincidence, satisfying conservation of energy. Dispersion is exaggerated in this schematic representation.

Simultaneous resonance of signal and idler mode-pairs occurs as a tuning parameter is adjusted continuously. However, in general, the coincidence is not perfect, and oscillation of a particular mode-pair depends on the degree of frequency matching and phase-matching. Typically, there is a mis-match in the frequencies of the signal and idler waves from exact cavity resonances. The frequency mis-match, $\Delta\nu$, of a signal and idler mode-pair is defined as the shift in frequency that is required of either the signal or the idler in order to bring the two resonances into coincidence to satisfy equation II. 1. This frequency mis-match plays a significant role in the mode-selection and tuning properties of the output frequencies, and is discussed in detail in section II. 5. The frequency mis-match of the signal and idler frequencies from perfect resonance is expressed as the sum of two frequency components as follows:

$$\Delta\nu = \Delta\nu_s + \Delta\nu_i . \quad [\text{II. 42}]$$

Here, $\Delta\nu_s$ is the frequency shift from the peak of the signal resonance (exact cavity resonance) to the signal frequency that is most favourable for oscillation of that mode-pair (as defined by a vertical line in figure II. 4). Correspondingly, $\Delta\nu_i$ is the frequency shift from the peak of the idler resonance to the idler frequency that is most favourable for oscillation. The signal component is measured on the signal frequency scale, and the idler component is measured on the idler frequency scale. The direction of these scales are opposite. One increases from left to right, and the other is reversed, increasing from right to left. Therefore, $\Delta\nu_s$ and $\Delta\nu_i$ appear in opposite directions even though they have the same sign.

The phase-detunings (ring/linear cavities) can be expressed as follows:

$$\delta\phi_j = \frac{2\pi\Delta\nu_j}{FSR_j} . \quad [\text{II. 43}]$$

In addition to the losses resulting from the transmission of the coupling mirror, spurious losses may occur because of absorption in the nonlinear crystal, or scattering on the optical interfaces. The spurious energy loss coefficient for each field is denoted by $2\mu_j$, assumed small. Equations II. 37, when only the terms of the lowest order in γ_j , μ_j , $\delta\phi_j$, and χ are retained, become

$$\alpha_p(\gamma'_p - i\delta\phi_p) = -2\chi^* \alpha_s \alpha_i + \sqrt{2\gamma_p} \alpha_p^{in} , \quad [\text{II. 44 (a)}]$$

$$\alpha_s(\gamma'_s - i\delta\phi_s) = 2\chi \alpha_p \alpha_i^* , \quad [\text{II. 44 (b)}]$$

$$\alpha_i(\gamma'_i - i\delta\phi_i) = 2\chi \alpha_p \alpha_s^* , \quad [\text{II. 44 (c)}]$$

where

$$\gamma'_i = \gamma_i + \mu_j . \quad [\text{II. 45}]$$

The parameter, γ'_j , is simply the sum of the total electric field losses, as experienced on a round-trip. It is convenient to express the phase-shifts and the losses on a round-trip as the relative detunings, Δ_j . These are defined by:

$$\Delta_j = \frac{\delta\phi_j}{\gamma'_j} . \quad [\text{II. 46}]$$

The steady-state equations of the triply-resonant oscillator now become

$$\alpha_p \gamma'_p (1 - i\Delta_p) = -2\chi^* \alpha_s \alpha_i + \sqrt{2\gamma_p} \alpha_p^{in} , \quad [\text{II. 47 (a)}]$$

$$\alpha_s \gamma'_s (1 - i\Delta_s) = 2\chi \alpha_p \alpha_i^* , \quad [\text{II. 47 (b)}]$$

$$\alpha_i \gamma'_i (1 - i\Delta_i) = 2\chi \alpha_p \alpha_s^* . \quad [\text{II. 47 (c)}]$$

Therefore, the parametric gain, experienced over the length of the nonlinear medium, must compensate both for a decrease in amplitude and for a phase change that is due to propagation in the cavity.

Equations II. 47 (b) and II. 47 (c) can be used to determine the oscillation conditions of the triply-resonant oscillator. This is achieved by multiplying equation II. 47 (b) by the complex conjugate of equation II. 47 (c), and this yields the following expression for the pump field intensity in terms of the signal and idler losses and detunings:

$$\gamma'_s \gamma'_i (1 - i\Delta_s)(1 - i\Delta_i) = 4|\chi|^2 |\alpha_p|^2 . \quad [\text{II. 48}]$$

This equation can be split up into its real and imaginary terms. Each term relates to important operating characteristics of the oscillator. The imaginary part of equation II. 48 provides the following expression:

$$\Delta_s = \Delta_i = \Delta . \quad [\text{II. 49}]$$

Equation II. 49 illustrates that the ratio between the detunings and the total losses must be identical for the two fields, α_s and α_i . If this condition is not fulfilled, then oscillation cannot occur. To understand this, consider the outgoing fields of the oscillator: i.e., the number of photons emerging from the cavity modes, $j = s, i$, per unit time. The outgoing fields of the oscillator are given by

$$|\alpha_j^{out}|^2 = 2\gamma_j' |\alpha_j|^2 . \quad [\text{II. 50}]$$

Equation II. 50 represents the useful output coupling of the intra-cavity electric field intensity. By multiplying equation II. 47 (b) by α_i^* , and equation II. 47 (c) by α_s^* , the outgoing signal and idler fields can be related by

$$|\alpha_s^{out}|^2 (1 - i\Delta_s) = |\alpha_i^{out}|^2 (1 - i\Delta_i) . \quad [\text{II. 51}]$$

This expression shows that, when equation II. 49 is verified, and when the system operates in the steady-state condition, the total number of photons emerging from the cavity (including spurious losses) is the same for the two fields. This condition must be strictly fulfilled since the photons are produced at the same rate in the crystal for each of the signal and idler fields.

Consider the number of photons that are transmitted through the coupling mirror. Their flows are given by

$$I_j = |\alpha_j^{out}|^2 = 2\gamma_j |\alpha_j|^2 . \quad [\text{II. 52}]$$

The ratio between the two flows is given by

$$\frac{I_s}{I_i} = \frac{\gamma_s |\alpha_s|^2}{\gamma_i |\alpha_i|^2} = \frac{\gamma_s \gamma_i'}{\gamma_i \gamma_s'} . \quad [\text{II. 53}]$$

In general, this ratio is not unity. This implies that spurious losses introduce an imbalance between the beams emerging from the cavity at frequencies ν_s and ν_i . When the predominant source of loss is from the useful output coupling, and therefore $\gamma_j \approx \gamma'_j$, then the ratio between the two flows approaches unity, i.e. $I_s / I_i \approx 1$.

The previous analysis resulted from isolating the imaginary part of equation II. 48. Consider now the real part of equation II. 48, as given by

$$|\alpha_p|^2 = \frac{\gamma'_s \gamma'_i (1 + \Delta^2)}{4|\chi|^2} . \quad \text{[II. 54]}$$

This relation shows that the pump field inside the cavity is constant above threshold (neglecting a second-order term in χ in the limit of the approximation). To calculate the threshold pump field required, the signal and idler fields, α_s and α_i , are set to zero in equation II. 47 (a). This provides the following expression that relates the incoming pump intensity at threshold to the intra-cavity pump field:

$$(\gamma'_p)^2 |\alpha_p|^2 (1 + \Delta_p^2) = 2\gamma_p |\alpha_p^{in}|_{th}^2 . \quad \text{[II. 55]}$$

Therefore, the incoming pump intensity necessary to reach threshold is

$$|\alpha_p^{in}|_{th}^2 = \frac{(\gamma'_p)^2 \gamma'_s \gamma'_i}{8|\chi|^2 \gamma_p} (1 + \Delta^2) (1 + \Delta_p^2) . \quad \text{[II. 56]}$$

The minimum value is obtained for zero detunings. This corresponds to the situation in which all three waves are on exact cavity resonances within the oscillator. Exact pump resonance provides the maximum intra-cavity pump field, and exact and simultaneous signal and idler resonances provide perfect overlap of these two fields.

The above relations can be written in a more convenient manner, by expressing them in terms of the cavity finesses, F_j , and the free spectral ranges, FSR_j . (In practise, it is often easier to measure the ratio of the resonance width to axial-mode spacing than it is to measure losses directly.)

For small losses, the amplitude loss coefficients, γ'_j , can be related to the cavity finesses, F_j , by

$$F_j \approx \frac{\pi}{\gamma'_j} . \quad [\text{II. 57}]$$

The relative detunings of the waves from perfect resonance can now be expressed as

$$\Delta_j = \frac{2\Delta\nu_j F_j}{FSR_j} \quad [\text{II. 58}]$$

Therefore, the expression for the intra-cavity pump field, as given by equation II. 54, can be rewritten as

$$|\alpha_p|^2 = \frac{\pi^2}{4|\chi|^2 F_s F_i} \left[1 + \left(\frac{2\Delta\nu_s F_s F_i}{F_s FSR_i + FSR_i F_s} \right)^2 \right] \quad [\text{II. 59}]$$

The input pump intensity at threshold can be expressed as

$$|\alpha_p^{in}|_{th}^2 = \frac{\pi^2}{4|\chi|^2 F_s F_i} \left[1 + \left(\frac{2\Delta\nu_s F_s F_i}{F_s FSR_i + F_i FSR_s} \right)^2 \right] \frac{\pi^2}{2\gamma_p F_p^2} \left[1 + \left(\frac{2\Delta\nu_p F_p}{FSR_p} \right)^2 \right] . \quad [\text{II. 60}]$$

The maximum enhancement of the pump field inside the cavity occurs for zero detuning of the pump field from exact pump resonance, $\Delta\nu_p = 0$, and can be written in the limit of low losses as [18]

$$E_{p-max} = \frac{2\gamma_p F_p^2}{\pi^2} . \quad [\text{II. 61}]$$

Substituting equation II. 61 in equation II. 60 provides a useful expression for the incident pump intensity to reach threshold, in terms of the three frequency detunings and the pump field enhancement on resonance:

$$|\alpha_p^{in}|_{th}^2 = \frac{\pi^2}{4|\chi|^2 F_s F_i} \left[1 + \left(\frac{2\Delta\nu F_s F_i}{F_i FSR_s + F_s FSR_i} \right)^2 \right] \frac{1}{E_{p-max}} \left[1 + \left(\frac{2\Delta\nu_p F_p}{FSR_p} \right)^2 \right]. \quad [\text{II. 62}]$$

Again, the minimum pump threshold is obtained by setting the detunings to zero. Therefore, in terms of the signal and idler finesses and the pump field enhancement on resonance, the minimum pump power threshold reduces to

$$|\alpha_p^{in}|_{th-min}^2 = \frac{\pi^2}{4|\chi|^2 F_s F_i E_{p-max}}. \quad [\text{II. 63}]$$

To obtain an expression for the incident pump power required to reach threshold, the focusing and coupling of the pump field to the cavity modes must be considered. However, it is important to realise that the derivation above is adequate to model the effects of detunings on the threshold, and will be used to examine these effects in section II. 5, with respect to mode-selection and fine frequency control.

II. 3. (i) (b) Doubly-resonant oscillator with single-pass pump.

In the previous section, the oscillating conditions were derived for the case of the doubly-resonant oscillator with a resonant pump field. The effects of the pump resonance were shown to contribute to an additional detuning constraint on the threshold. The effects of pump resonance can be eliminated by allowing for single-pass, non-resonant pump field interaction in the nonlinear gain medium. This is the case of the doubly-resonant oscillator with a single-pass, non-resonant pump field.

In this configuration, the pump field incident on the OPO cavity is set equal to the pump field incident on the nonlinear crystal. The OPO cavity is formed again by three external mirrors that provide high finesse cavities for the signal and idler frequencies. The mirrors that constitute the cavity are assumed to be perfectly reflecting for the three waves, except for the coupling mirror, which has amplitude transmission and reflection coefficients equal to r_s and r_i , and t_s and t_i , for the signal and idler fields, respectively. However, the coupling mirror, M_1 in figure II. 2, is assumed to be perfectly transmitting for the pump field; i.e.

$$\begin{aligned} r_p &= 0 \\ t_p &= 1 \end{aligned} \quad \text{[II. 64]}$$

This allows for single-pass, non-resonant pump field interaction with the optical cavity.

The threshold analysis of the doubly-resonant oscillator with a single-pass pump field follows closely the analysis of the triply-resonant oscillator, but with the above correction for the coupling mirror. Therefore, using the same approximations for low-loss cavities for the resonant signal and idler fields, and small phase-detunings of the resonant fields from exact cavity resonances, the threshold equation can be expressed as follows:

$$\left| \alpha_p^{in} \right|_{th}^2 = \frac{\pi^2}{4|\chi|^2 F_s F_i} \left[1 + \left(\frac{2\Delta\nu F_s F_i}{F_i FSR_s + F_s FSR_i} \right)^2 \right]. \quad \text{[II. 65]}$$

The minimum value of equation II. 65 is obtained for zero detuning of the signal and idler fields from perfect coincidence. As expected, this value is equal to the minimum intra-cavity pump intensity for the triply-resonant oscillator. When the resonances of the signal and idler frequencies overlap perfectly, as in the case of zero detuning ($\Delta\nu=0$), the minimum pump threshold can be expressed as follows:

$$\left| \alpha_p^{in} \right|_{th-min}^2 = \frac{\pi^2}{4|\chi|^2 F_s F_i}. \quad \text{[II. 66]}$$

The minimum threshold intensity for the single-pass pump, doubly-resonant oscillator can be equated to the equivalent value for the pump resonant, doubly-resonant oscillator, by the pump enhancement factor, E_{p-max} :

$$\left| \alpha_p^{in} \right|_{th-min}^2 (DRO) = E_{p-max} \times \left| \alpha_p^{in} \right|_{th-min}^2 (TRO) \quad \text{[II. 67]}$$

Therefore, as expected, the threshold conditions for the single-pass doubly-resonant oscillator are identical to the pump-enhanced doubly-resonant oscillator, when the pump field enhancement is taken into consideration. When the conditions for perfect resonance are satisfied, the threshold of the triply-resonant oscillator is reduced by a factor equal to the cavity

enhancement of the pump field, compared to the equivalent single-pass pump device.

II. 3. (i) (c) Singly-resonant oscillator with resonant pump field.

In this configuration, only one of the generated OPO fields is brought to resonance, in addition to the resonance of the pump field. In this analysis, it is assumed that the idler frequency is brought to resonance and that the signal frequency is completely non-resonant. The mirrors that constitute the cavity are assumed to be perfectly reflecting except for the coupling mirror, M_1 in figure II. 2, which has amplitude reflection and transmission coefficients equal to r_p and r_i , and t_p and t_i , for the pump and the idler frequencies, respectively. The coupling mirror is assumed to be perfectly transmitting for the signal frequency; i.e.

$$\begin{aligned} r_s &= 0 \\ t_s &= 1 \end{aligned} \quad [11. 68]$$

The threshold analysis of the singly-resonant oscillator with a field-enhanced pump interaction follows closely the analysis of the triply-resonant oscillator, but with the above correction for the coupling mirror. The Gaussian beam analysis of the doubly-resonant oscillator is maintained such that the signal, idler and pump waves can be described by well defined spatial variations, as defined by the modes of the resonator. It should be noted that this is not necessarily correct for singly resonant oscillators, where the non-resonant wave can propagate freely with the radial variation of the driving polarization. The assumption of equal confocal parameters in the following analysis is made primarily to enable a direct comparison with the doubly-resonant oscillators. For an exact derivation of the threshold, the analysis of reference [19] should be consulted.

Therefore, using the same approximations for low-loss cavities for the resonant pump and idler fields, and small phase-detunings of the resonant fields from exact cavity resonances, the threshold can be written as follows:

$$|\alpha_p|^2 = \frac{\gamma_i'}{4|\chi|^2} \quad [II. 69]$$

This relation shows that the internal pump field above threshold is constant, and does not depend on the exact resonant cavity frequency. This is a consequence of singly-resonant operation. The following expression relates the incoming pump intensity to the intra-cavity pump field:

$$(\gamma'_p)^2 |\alpha_p|^2 (1 + \Delta_p^2) = 2\gamma_p |\alpha_p^{in}|_{th}^2 . \quad [\text{II. 70}]$$

Therefore, the incoming pump intensity to reach threshold is given by

$$|\alpha_p^{in}|_{th}^2 = \frac{(\gamma'_p)^2 \gamma'_i}{8|\chi|^2 \gamma_p} (1 + \Delta_p^2) . \quad [\text{II. 71}]$$

The minimum value is obtained for zero detuning of the pump frequency from exact cavity resonance. Only the pump detuning plays a role in the threshold of the pump-enhanced singly-resonant oscillator. This is related to the amount of pump radiation that is coupled effectively into the resonator, and the degree of pump enhancement within the cavity.

When written in terms of the cavity finesses and the free spectral ranges, equation II. 69 reduces to

$$|\alpha_p|^2 = \frac{\pi}{4|\chi|^2 F_i} . \quad [\text{II. 72}]$$

The input pump intensity can be expressed as

$$|\alpha_p^{in}|_{th}^2 = \frac{\pi}{4|\chi|^2 F_i} \times \frac{\pi^2}{2\gamma_p F_p^2} \left[1 + \left(\frac{2\Delta\nu_p F_p}{FSR_p} \right)^2 \right] . \quad [\text{II. 73}]$$

For the minimum pump threshold, the detuning of the pump field is zero, and the above expression becomes

$$|\alpha_p^{in}|_{th-min}^2 = \frac{\pi}{4|\chi|^2 F_i E_{p-max}} . \quad [\text{II. 74}]$$

It is interesting to compare the relative thresholds of the pump-enhanced doubly-resonant oscillator and the pump-enhanced singly-resonant oscillator. The ratio of these can be written as

$$\left| \alpha_p^{in} \right|_{th-min}^2 (DRO) = \left| \alpha_p^{in} \right|_{th-min}^2 (SRO) \times \left(\frac{\pi}{F_s} \right). \quad [\text{II. 75}]$$

Therefore, the threshold of the doubly-resonant oscillator is shown to be significantly lower than the equivalent singly-resonant oscillator. For example, for a signal cavity with a finesse of $F_s \approx 300$, the threshold is reduced by two orders of magnitude when compared to the singly-resonant oscillator. However, the disadvantage of an increased pump power threshold for the singly-resonant oscillator is partially offset by the relaxed resonance requirements. Mode-selection from these different cavities is directly related to these resonance conditions, and is discussed in more detail in section II. 5.

II. 3. (i) (d) Singly-resonant oscillator with single-pass pump.

The final ring cavity configuration to be studied is for the case when only one of the generated OPO fields is brought to resonance within the cavity, and when the pump field makes a single-pass through the gain medium. This is the singly-resonant oscillator with a single-pass pump field. The OPO cavity is formed by three external mirrors that provide a high finesse cavity for the resonant idler frequency only. It is assumed that the mirrors that constitute the cavity are perfectly reflecting except the coupling mirror, which has amplitude reflection and transmission coefficients for the idler frequency equal to r_i and t_i , respectively. To ensure single-pass pump interaction and a non-resonant signal frequency, the coupling mirror is assumed to be perfectly transmitting for the pump and signal frequencies; i.e.

$$\begin{aligned} r_s = r_p &= 0 \\ t_s = t_p &= 1 \end{aligned} \quad [\text{11. 76}]$$

This allows for only one resonant field in the cavity. The singly-resonant oscillator with arbitrary feedback at the signal frequency has been analysed recently in reference [11].

The threshold analysis of the singly-resonant oscillator with a single-pass pump field follows closely the analysis of the singly-resonant oscillator with an enhanced pump field, but with the above correction for the coupling mirror. Therefore, using the same approximations for low-loss cavities for the resonant idler field, and small phase-detunings of the resonant field from exact cavity resonance, the threshold is

$$|\alpha_p^{in}|_{th-min}^2 = \frac{\pi}{4|\chi|^2 F_i} . \quad [\text{II. 77}]$$

Therefore, the pump intensity to reach threshold is independent of the relative dephasings of any of the three frequencies. The requirement on the pump frequency detuning has been eliminated by removing the resonance condition for the pump frequency within the resonator. The idler frequency is simply set by the cavity resonance frequency, and the signal frequency takes on that frequency which satisfies the conservation of energy relation.

A comparison of the minimum pump intensities for the singly-resonant oscillator, with and without a resonant pump field, confirm that the threshold of the pump enhanced system can be lowered by the factor E_{p-max} , when the pump field is exactly on resonance.

II. 3. (ii) Linear cavity resonators.

In section II. 3 (i), the simple case of the ring cavity resonator was studied. In this section, the linear cavity resonator is analysed. The linear cavity resonator has been extensively utilized for cw OPO experiments. In particular, all the experimental OPO configurations that are described in this thesis (chapters IV to VII), involve the use of linear, standing-wave cavity resonators.

The most important difference in standing-wave oscillators, compared to travelling-wave oscillators, is the existence of both forward and backward travelling waves over the length of the gain medium. Subsequently, the linear cavity resonator and the ring cavity resonator have different values for the pump threshold intensity (and for the signal and idler conversion efficiencies) when the reflection phase shifts on the cavity mirrors for the different interacting waves are taken into consideration.

II. 3. (ii) (a) Doubly-resonant oscillator with resonant pump field.

The first linear-cavity to be analysed is the standing-wave, doubly-resonant oscillator, with a strongly-resonant pump field. This type of oscillator is illustrated schematically in figure II. 5. The OPO cavity is formed by one external mirror, M' , and one mirror coated directly on one end of the crystal, M . This represents a semi-monolithic cavity design that provides the high finesse cavities for the three resonant fields. The threshold and conversion efficiency analyses are identical to a linear, standing-wave cavity design with two discrete cavity mirrors, external to the crystal. The semi-monolithic device is analysed only to simplify the algebra.

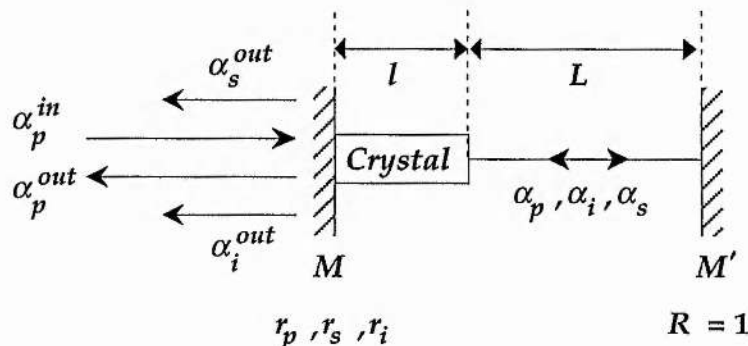


Figure II. 5.

Sketch of a semi-monolithic linear-cavity doubly-resonant oscillator with a resonant pump field. The crystal length is l , and the cavity length is $l + L$. Mirror M is coated directly on one end of the crystal.

The length of the nonlinear crystal is denoted by l , and the distance separating the crystal from the external mirror is denoted by L . The external mirror, M' , is assumed to be perfectly reflecting for the three resonant fields. The other mirror, M , has amplitude reflection and transmission coefficients equal to r_p, r_s, r_i , and t_p, t_s, t_i , respectively.

The reflection phase-shifts on mirrors M and M' are denoted by δ_j and δ'_j , respectively. The main difference between the ring cavity OPO and the standing-wave, linear cavity OPO is that the three waves interact only once per round trip in the ring cavity and twice in the linear cavity case, with

a specific phase shift accumulated during the propagation between the two parametric interactions.

The equations relating the three interacting waves in the cavity on mirror M , at lowest order in the parametric interaction parameter, χ , are as follows [20]:

$$\alpha_p [1 - r_p \exp(i\varphi_p)] = -2\chi^* \alpha_s \alpha_i \exp(i\varphi_p) [r_p + r_s r_i \exp(i\theta' - i\Delta kl)] + t_p \alpha_p^{in} , \quad [\text{II. 78 (a)}]$$

$$\alpha_s [1 - r_s \exp(i\varphi_s)] = 2\chi \alpha_p \alpha_i^* \exp(i\varphi_s) [r_s + r_p r_i \exp(-i\theta' + i\Delta kl)] , \quad [\text{II. 78 (b)}]$$

$$\alpha_i [1 - r_i \exp(i\varphi_i)] = 2\chi \alpha_p \alpha_s^* \exp(i\varphi_i) [r_i + r_p r_s \exp(-i\theta' + i\Delta kl)] , \quad [\text{II. 78 (c)}]$$

where θ' is the accumulated cavity round-trip phase shift for the three waves, such that

$$\theta' = \delta'_s + \delta'_i - \delta'_p . \quad [\text{II. 79}]$$

In the simple case of small reflection losses, where $r_j = 1 - \gamma_j \approx 1$, and quasi-resonant fields, where $\varphi_j = 2p_j\pi + \delta\varphi_j$, with $\delta\varphi_j \ll 2\pi$, the steady-state equations become

$$\alpha_p (\gamma'_p - i\delta\varphi_p) = -2\chi^* \alpha_s \alpha_i [1 + \exp(i\theta' - i\Delta kl)] + \sqrt{2\gamma_p} \alpha_p^{in} , \quad [\text{II. 80 (a)}]$$

$$\alpha_s (\gamma'_s - i\delta\varphi_s) = 2\chi \alpha_p \alpha_i^* [1 + \exp(-i\theta' + i\Delta kl)] , \quad [\text{II. 80 (b)}]$$

$$\alpha_i (\gamma'_i - i\delta\varphi_i) = 2\chi \alpha_p \alpha_s^* [1 + \exp(-i\theta' + i\Delta kl)] . \quad [\text{II. 80 (c)}]$$

Equations II. 80 coincide with equations II. 47, written in the same conditions for the ring cavity OPO, provided that the coupling coefficient, χ , is replaced by the quantity

$$\chi' = \chi [1 + \exp(-i\theta' + i\Delta kl)] , \quad [\text{II. 81}]$$

or, as a function of the crystal effective nonlinear coefficient, κ , by

$$\chi' = \kappa l \operatorname{sinc}\left(\frac{\Delta kl}{2}\right) \exp\left(i\frac{\Delta kl}{2}\right) [1 + \exp(i\Delta kl - i\theta')] . \quad [\text{II. 82}]$$

Therefore, the discussion for the ring cavity is valid in this new configuration, but with a slightly changed form of the phase-matching function. This is because standing waves, and not travelling waves as in the ring case, must be matched for optimum coupling in the crystal. The phase-matching now depends on the mirror phase shifts, which determine the relative position of the nodes and antinodes of the three interacting standing waves and the value of their overlap. Following the same steps, as outlined for the ring oscillators in section II. 3 (i), the oscillation threshold can be expressed as follows [20]:

$$|\alpha_p^{in}|_{th}^2 = \frac{(\gamma_p')^2 \gamma_s' \gamma_i'}{32 \kappa^2 l^2 \gamma_p} (1 + \Delta^2) (1 + \Delta_p^2) \frac{\left(\frac{\Delta kl}{2}\right)^2}{\sin^2\left(\frac{\Delta kl}{2}\right) \cos^2\left(\frac{\Delta kl}{2} - \frac{\theta'}{2}\right)} . \quad [\text{II. 83}]$$

For cavity length values in which the pump, signal and idler modes are exactly resonant, the threshold for OPO oscillation is given now by

$$|\alpha_p^{in}|_{th}^2 = \frac{(\gamma_p')^2 \gamma_s' \gamma_i'}{32 \kappa^2 l^2 \gamma_p} \frac{\left(\frac{\Delta kl}{2}\right)^2}{\sin^2\left(\frac{\Delta kl}{2}\right) \cos^2\left(\frac{\Delta kl}{2} - \frac{\theta'}{2}\right)} . \quad [\text{II. 84}]$$

A function, $F(\Delta kl, \theta')$, is defined as the reduction factor for linear-cavity, triply resonant oscillators with three high finesse fields, as follows

$$F(\Delta kl, \theta') = \frac{\left(\frac{\Delta kl}{2}\right)^2}{\sin^2\left(\frac{\Delta kl}{2}\right) \cos^2\left(\frac{\Delta kl}{2} - \frac{\theta'}{2}\right)} . \quad [\text{II. 85}]$$

Figure II. 6 shows how this quantity varies as a function of $\Delta kl / 2$ when θ' is altered (assuming that θ' is positive). The individual parabolas describe an envelope for the threshold minima, with the actual threshold curve consisting of very narrow dips tangent to this curve for specific values of the parameters given by the resonance conditions. A non-zero value of θ'

induces a shift of the curve minimum to non-zero positive values of Δk . When θ' reaches the value of $\theta' = \pi$, the curve has two minima of equal value, centred at $\Delta kl \approx \pm 2.33$, and then the absolute minimum jumps to negative values of Δk , and again reaches the ring cavity value of zero when $\theta' = 2\pi$. At low pump intensities, the OPO will work only near these threshold minima, and therefore, a linear OPO will generate signal and idler frequencies that are different from those of a ring cavity OPO. Figure II. 6 shows also that the minimum threshold is achieved when $\theta' = 0$ (it is then equal to the ring cavity OPO threshold divided by four, as could be expected in a system in which the crystal is used twice per round trip), and increases only by a factor of 1.92 when $\theta' = \pi$.

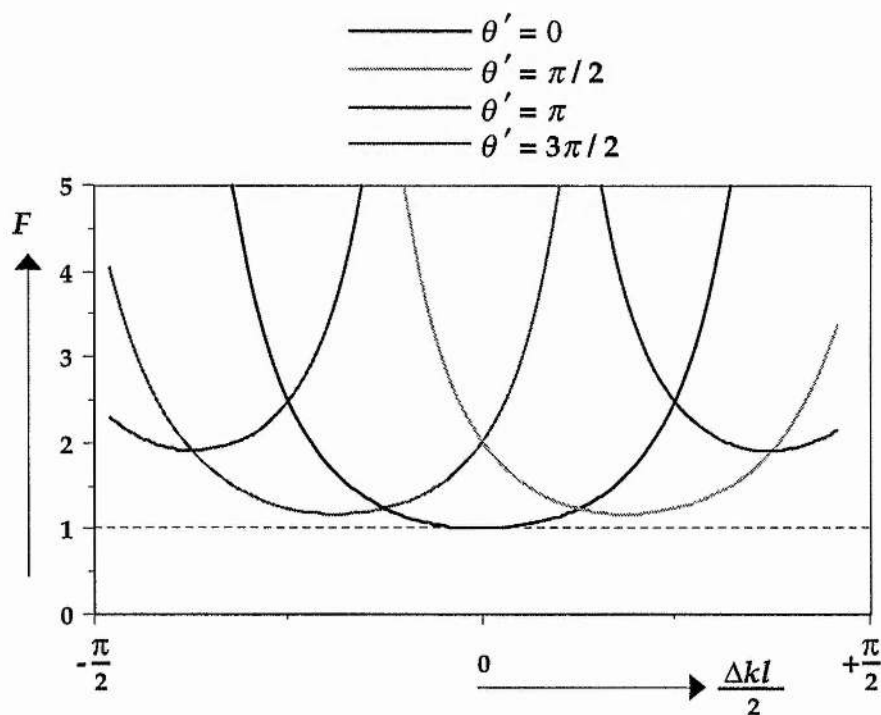


Figure II. 6.
Variation of the threshold reduction factor as a function of the phase-matching coefficient, $\Delta kl/2$, for different values of the mirror phase-shift parameter, θ' .

Therefore, for the standing-wave doubly-resonant oscillator with a resonant pump field, the minimum pump intensity required to reach threshold can be expressed as follows:

$$|\alpha_p^{in}|_{th-min}^2 = \frac{\pi^2}{16\kappa^2 l^2 F_s F_i E_{p-max}} \quad \text{[II. 86]}$$

II. 3. (ii) (b) Doubly-resonant oscillator with non-resonant pump field.

The next linear-cavity configuration to be analysed is the standing-wave, doubly-resonant oscillator, with a non-resonant pump field. The OPO cavity is formed again by one external mirror, M' , and one mirror directly coated on one end of the crystal, M . This cavity design provides for high finesse cavities for the signal and idler resonant fields, and suppresses the resonance for the pump field. There are two different variations of this cavity design; the single pass pump and the double pass pump.

The first configuration studied is for the single-pass pump field. The phase-shift upon reflection for the pump-reflecting mirror, M' , is defined as θ' , and such that

$$\theta' = \delta'_s + \delta'_i - \delta'_p \quad \text{[II. 87]}$$

This system has been discussed in reference [21]. The threshold can be written as

$$|\alpha_p^{in}|_{th}^2 = \frac{\gamma'_s \gamma'_i}{4\kappa^2 l^2} \frac{\left(\frac{\Delta kl}{2}\right)^2}{\sin^2\left(\frac{\Delta kl}{2}\right) \left[1 + |r_p|^2 + 2|r_p| \cos(\Delta kl - \theta')\right]} \quad \text{[II. 88]}$$

For $r_p = 0$, this equation reduces, as expected, to the expression for a doubly-resonant oscillator with a single-pass pump field. Therefore, the threshold for this configuration is

$$|\alpha_p^{in}|_{th}^2 = \frac{\gamma'_s \gamma'_i}{4\kappa^2 l^2 \text{sinc}^2\left(\frac{\Delta kl}{2}\right)} \quad \text{[II. 89]}$$

The threshold reaches a minimum value for $\Delta kl = 0$. The minimum threshold for the single-pass pump doubly-resonant oscillator is now written as follows:

$$\left| \alpha_p^{in} \right|_{th-min}^2 = \frac{\pi^2}{4\kappa^2 l^2 F_s F_i} \quad [\text{II. 90}]$$

As expected, this expression is the same as the doubly-resonant ring-cavity oscillator with a single-pass pump field.

For finite values of r_p , the threshold depends upon both θ' and Δkl . Again, a function $F(\Delta kl, \theta')$, is defined as the reduction factor for doubly-resonant oscillators with a finite pump reflectivity, as follows

$$F(\Delta kl, \theta') = \frac{\left(\frac{\Delta kl}{2} \right)^2}{\sin^2 \left(\frac{\Delta kl}{2} \right) \left[1 + |r_p|^2 + 2|r_p| \cos(\Delta kl - \theta') \right]} \quad [\text{II. 91}]$$

This function is plotted in figure II. 7 for different values of the electric field pump reflectivity, r_p . The threshold always depends on θ' and Δkl . However, for values of $|r_p| > 0.35$, the double-pass doubly-resonant oscillator always has a lower threshold than the single-pass oscillator [21]. For the ideal case of $|r_p| = 1$ and $\theta' = 0$, then $F(\Delta kl, \theta') = 1/4$, and the threshold is reduced by a factor of four, and can be expressed as follows:

$$\left| \alpha_p^{in} \right|_{th-min}^2 = \frac{\pi^2}{16\kappa^2 l^2 F_s F_i} \quad [\text{II. 92}]$$

For this specific example, the maximum gain in the forward direction is obtained when the phase of the pump wave leads the phase of the sum of the signal and idler waves by $\pi/2$. If this phase-relation is maintained upon reflection, the interaction length is $2l$, and the round-trip gain is four times the forward gain; the threshold intensity is a quarter of that for single-pass. For this case of $|r_p| = 1$, the threshold is considerably lower than the single-pass threshold, regardless of θ' . In addition, the gain curve for $|r_p| = 1$ is about half as wide as for the single-pass case. Conversely, if the relative phase changes by π upon reflection, the round-trip gain is zero for $\Delta k = 0$. However, for other values of Δk , the round-trip gain is not zero, and the device operates at the particular value of Δk providing the lowest threshold: figure II. 7. As the pump reflectivity approaches unity, maximum reductions in threshold are provided irrespective of the phase change on reflection, as implied by the depth of the minima of figure II. 7 (c).

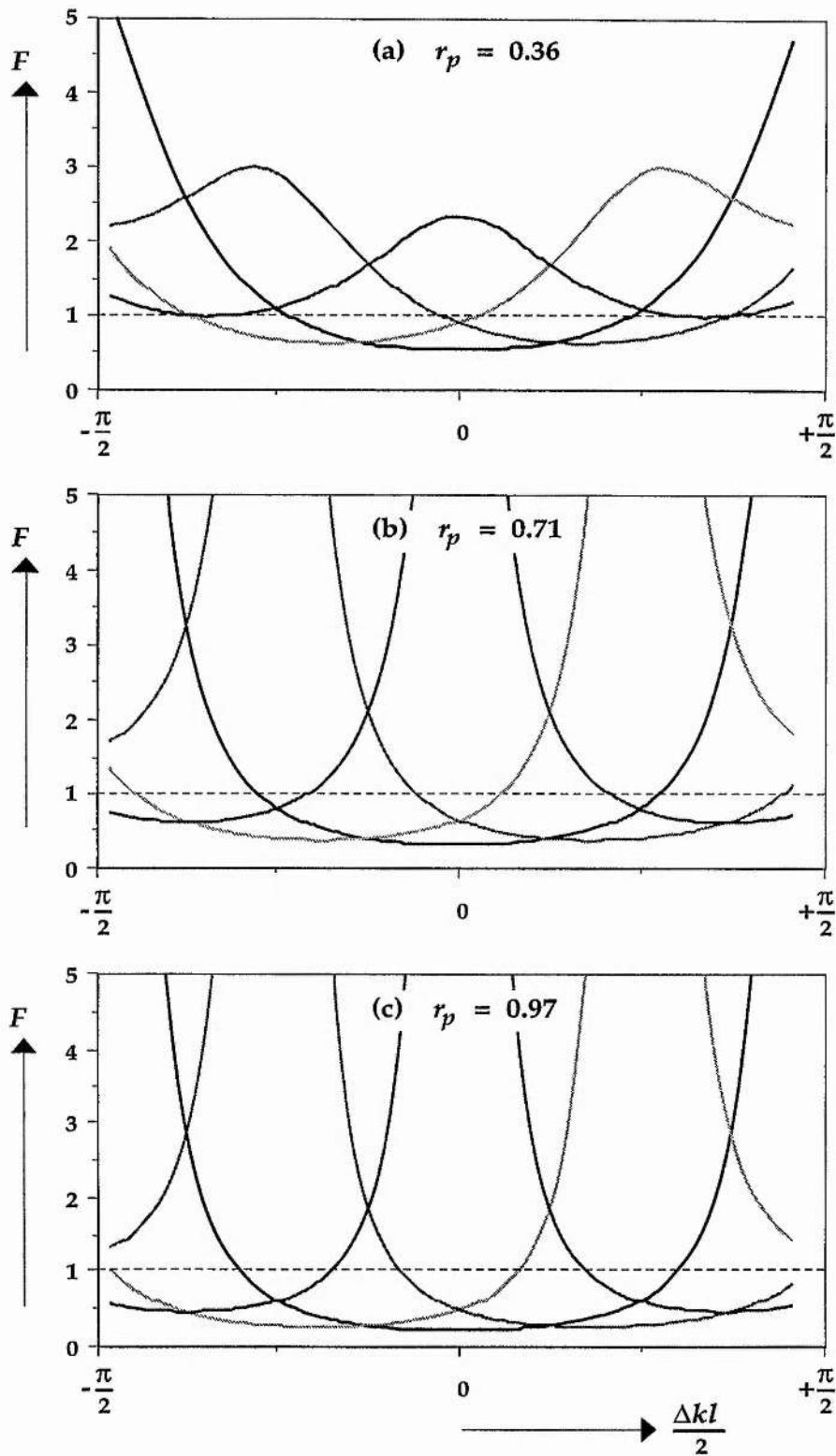


Figure II. 7.
 Variation of the threshold reduction factor for different values of the external mirror pump reflectivity. Shadings as indicated in figure II. 6.

II. 3. (ii) (c) Singly-resonant oscillators.

The final linear-cavity configuration to be analysed is the standing-wave, singly-resonant oscillator. Once again, the resonant wave is taken to be the idler frequency. The most simple geometry involves a resonant idler wave, with single-pass pump and idler fields. Extensions to this involve double passing the pump wave or both the pump and the non-resonant signal frequency waves. Finally, the effects of pump resonance, with and without a double-pass non-resonant wave, are considered.

In the first case, the idler frequency is brought to resonance, with the pump and the signal frequencies passing once through the gain medium. This is the linear cavity singly-resonant oscillator. The pump power threshold for this geometry is identical to that of the ring-cavity resonator with a non-resonant pump field. Therefore, the pump field can be expressed as follows:

$$\left| \alpha_p^{in} \right|_{th-min}^2 = \frac{\pi}{4\kappa^2 l^2 F_i} \frac{1}{\text{sinc}^2\left(\frac{\Delta kl}{2}\right)}. \quad [\text{II. 93}]$$

As expected, the threshold is independent of the phase-detuning of the resonant idler frequency. The threshold takes on its minimum value at line centre, where $\Delta kl = 0$.

When the pump wave is reflected by the external cavity mirror, this forms the singly-resonant oscillator with a double-pass pump field. In this case, the non-resonant wave is assumed to remain single-pass. The threshold can be expressed as follows [21]:

$$\left| \alpha_p^{in} \right|_{th-min}^2 = \frac{\pi}{4\kappa^2 l^2 F_i} \frac{1}{\left(1 + |r_p|^2\right)} \frac{1}{\text{sinc}^2\left(\frac{\Delta kl}{2}\right)}. \quad [\text{II. 94}]$$

The phases of the forward-going pump wave and the resonant idler wave at $z = 0$, and of the backward-going pump and resonant idler wave at $z = l$ are unimportant provided that both the cavity mirrors are completely transmitting for the non-resonant signal wave. Thus any changes upon reflection at $z = l$ are not of consequence, and maximum gain for the resonant idler wave occurs for $\Delta k = 0$. (Note that this was not true for the double-pass,

doubly-resonant oscillator.) For the ideal case of $|r_p|=1$, the threshold is a factor of two lower than the single pass singly-resonant oscillator.

The singly-resonant oscillator with double-passed signal and pump frequencies (or the round-trip singly-resonant oscillator) has been considered in reference [11]. Similar to the doubly-resonant oscillator examples, the threshold is dependent on the relative phase of the reflected waves. The reduction is identical to that obtained from double-passing the pump field in the analysis of the doubly-resonant oscillator. Therefore, the pump power threshold can be expressed as follows:

$$|\alpha_p^{in}|_{th}^2 = \frac{\pi}{4\kappa^2 l^2 F_i} \frac{\left(\frac{\Delta kl}{2}\right)^2}{\sin^2\left(\frac{\Delta kl}{2}\right) \left[1 + |r_p|^2 + 2|r_p| \cos(\Delta kl - \theta')\right]} \quad [\text{II. 95}]$$

For $r_p=0$, this equation reduces to the expression for a singly-resonant oscillator with a single-pass pump field. For the ideal case of $|r_p|=1$, the threshold is a factor of four lower than for the single-pass singly-resonant oscillator.

The effects of pump resonance are now incorporated into the above analysis. The first case considered is for a singly-resonant idler frequency, a single-pass signal field, and a strongly resonant pump field. This configuration can be considered to be identical to the double-pass pump configuration, with the addition of a resonant pump field. Therefore, assuming that the pump field is exactly on resonance, the minimum pump power threshold can be expressed as follows:

$$|\alpha_p^{in}|_{th-min}^2 = \frac{\pi}{8\kappa^2 l^2 F_i} \frac{1}{E_{p-max}} \frac{1}{\text{sinc}^2\left(\frac{\Delta kl}{2}\right)} \quad [\text{II. 96}]$$

The final cavity configuration involves strongly-resonant idler and pump fields, and a double-passed non-resonant signal field. The threshold for this can be expressed as follows:

$$\left| \alpha_p^{in} \right|_{th}^2 = \frac{\pi}{16\kappa^2 l^2 F_i} \frac{1}{E_{p-max}} \frac{\left(\frac{\Delta kl}{2} \right)^2}{\sin^2 \left(\frac{\Delta kl}{2} \right) \cos^2 \left(\frac{\Delta kl}{2} - \frac{\theta'}{2} \right)}. \quad [\text{II. 97}]$$

Similar to the doubly-resonant oscillator configurations with a double-pass pump field, the relative dephasings must be considered.

II. 3. (iii) Summary.

The threshold intensities for different cavity configurations have been analysed, in the limit of small parametric gain and high finesse cavities for the resonant fields.

First, the ring-cavity resonator was analysed, with travelling waves and a single-pass parametric interaction. The lowest threshold was obtained when all three waves were exactly on resonance within the cavity. However, removing any one of the three resonant fields off exact cavity resonance has the effect of increasing the threshold. This requirement is studied in more detail in section II. 5, with regard to the amplitude and frequency stability of the signal and idler outputs from this OPO. The highest threshold was obtained for the singly-resonant oscillator with a non-resonant, single-pass pump interaction. However, the threshold for this configuration was, as expected, shown to be independent of the dephasing of all three frequencies. This will be shown to allow for greater ease in controlling the amplitude and frequency stability of the output from this OPO configuration, and is discussed also in section II. 5.

The linear-cavity resonators were analysed to study the effect of parametric gain in two directions through the nonlinear medium. The threshold intensities were identical to the ring-cavity when the pump passed through the crystal in one direction only. However, when double-passing was allowed for, significant reductions in the threshold were shown to be possible. The same conditions with respect to amplitude and frequency stability apply to the linear-cavity geometry, depending on the number of fields that are required to be brought to resonance simultaneously.

The results of this section are summarized in table II. 1. The minimum pump power thresholds (in units of Watts) are evaluated

assuming confocal focusing and optimum dephasings where appropriate. The terms within the coupling factor are as defined in section II. 2.

Table II. 1.
Pump power thresholds for cw OPOs.

<i>Configuration</i>	<i>Ring - cavity</i>	<i>Linear - cavity</i>
<i>Doubly-resonant</i>		
<i>Resonant pump</i>	$K \frac{\pi^2}{F_s F_i E_{p-max}}$	$K \frac{\pi^2}{4 F_s F_i E_{p-max}}$
<i>Non-resonant single-pass pump</i>	$K \frac{\pi^2}{F_s F_i}$	$K \frac{\pi^2}{F_s F_i}$
<i>Non-resonant double-pass pump</i>		$K \frac{\pi^2}{4 F_s F_i}$
<i>Singly-resonant</i>		
<i>Resonant pump, single-pass signal</i>	$K \frac{\pi}{F_i E_{p-max}}$	$K \frac{\pi}{2 F_i E_{p-max}}$
<i>Resonant pump, double-pass signal</i>		$K \frac{\pi}{4 F_i E_{p-max}}$
<i>Non-resonant single-pass pump</i>	$K \frac{\pi}{F_i}$	$K \frac{\pi}{F_i}$
<i>Non-resonant double-pass pump</i>		$K \frac{\pi}{2 F_i}$
<i>Non-resonant double-pass p, s</i>		$K \frac{\pi}{4 F_i}$

$$K = \frac{n_p^2 \epsilon_0 c^4}{2 \pi^2 l |d_{eff}|^2 (1 - \delta^2)^2 v_p^3}$$

II. 4 Conversion efficiencies.

Optical parametric oscillators have been demonstrated to be highly efficient devices for converting fixed frequency pump radiation to tunable signal and idler frequency outputs. In this section, there is an analysis of the conversion efficiencies from these devices. Again, the analysis is divided into two subsections, depending on the nature of the fields within the OPO resonator. In this respect, the cases of the doubly-resonant and singly-resonant oscillators provide significantly different values for the external conversion efficiencies.

II. 4 (i) Doubly-resonant oscillators.

This section analyses the external conversion efficiencies of the doubly-resonant oscillator, both with and without pump field enhancement. First, a dimensionless parameter, σ , is defined as follows:

$$\sigma = \frac{|\alpha_p^{in}|^2}{|\alpha_p^{in}|_{th-min}^2} , \quad [\text{II. 98}]$$

such that σ can be regarded as the pumping level, or how far above threshold the OPO operates. The external conversion efficiency can be expressed as the ratio of the sum of the signal and idler output intensities to the input pump intensity. This is defined by the parameter, η_{ext} , such that

$$\eta_{ext} = \frac{2(\gamma_s |\alpha_s|^2 + \gamma_i |\alpha_i|^2)}{|\alpha_p^{in}|^2} = \frac{I_s + I_i}{|\alpha_p^{in}|^2} . \quad [\text{II. 99}]$$

The doubly-resonant, ring-cavity oscillator with a single-pass pump interaction has been analysed in reference [22], and this analysis is equally valid with a pump-enhanced field. The external conversion efficiency can be expressed as follows [22]:

$$\eta_{ext} = \frac{2}{\sigma} \left(\frac{F_s \gamma_s + F_i \gamma_i}{\pi} \right) (\sqrt{\sigma} - 1) . \quad [\text{II. 100}]$$

This value reaches a maximum value when $\sigma = 4$; i.e., when pumping at four times above threshold. The maximum efficiency can now be expressed as follows:

$$\eta_{ext} = \frac{F_s \gamma_s + F_i \gamma_i}{2\pi} . \quad [\text{II. 101}]$$

When the only sources of loss are those of useful output coupling, the finesses can be expressed as $F_j = \pi / \gamma_j$, and the conversion efficiency can attain a maximum theoretical value of $\eta_{ext} = 100 \%$, when pumping at four times above threshold. (However, for cw OPOs, parasitic losses generally constitute the majority of the signal and idler round-trip losses, and in practise, the conversion efficiencies are reduced significantly from the theoretical maximum value.)

The conversion efficiencies in the linear-cavity, doubly-resonant oscillator with a single-pass pump interaction were first treated in reference [23]. The external conversion efficiency can be expressed as follows [23]:

$$\eta_{ext} = \frac{1}{\sigma} \left(\frac{F_s \gamma_s + F_i \gamma_i}{\pi} \right) (\sqrt{\sigma} - 1) , \quad [\text{II. 102}]$$

which takes on a maximum value of $\eta_{ext} = 50 \%$, when pumping, again, at four times above threshold. The transmitted (forward) pump power limits at the threshold power which forms the basis for the optical limiter proposed in reference [23]. The linear cavity involves signal and idler waves travelling in the forward and backward directions. The reflected (backward) pump intensity can be expressed as follows [23]

$$|\alpha_p^{out}|^2 = |\alpha_p^{in}|_{th}^2 (\sqrt{\sigma} - 1)^2 . \quad [\text{II. 103}]$$

This reflected pump power is not truly reflected, but is generated by sum generation of the back-travelling signal and idler waves. The back generated pump acts to reduce the signal and idler powers, and can simultaneously feed power back into the pumping laser which can induce pump laser frequency and power instabilities.

The case of a double-pass pump, doubly-resonant, linear-cavity geometry has been analysed in reference [21]. This analysis is equally valid for the case of the pump-enhanced, doubly-resonant configuration. The external conversion efficiencies can be written as follows [21]:

$$\eta_{ext} = \frac{1}{\sigma} \left(\frac{1 + |r_p|^2 + 2|r_p| \cos(\Delta kl - \theta')}{1 + |r_p| \cos(\Delta kl - \theta')} \right) \left(\frac{F_s \gamma_s + F_i \gamma_i}{\pi} \right) (\sqrt{\sigma} - 1) . \quad [\text{II. 104}]$$

Therefore, the conversion efficiencies, similar to the threshold pump powers, can be increased by double-passing the pump field. The conversion efficiency depends on the relative dephasing of the backward generated waves. When the relative dephasing of the backward travelling wave is at its optimum value, the conversion efficiency is identical to that of the ring-cavity oscillators.

II. 4 (ii) Singly-resonant oscillators.

For the singly-resonant oscillator, the external conversion efficiencies of the resonant and non-resonant waves are significantly different. It is assumed again that the idler frequency is resonant and that the signal frequency is completely non-resonant. Further, the case of singly-resonant operation at line centre is studied.

The following analysis is valid for all of the singly-resonant devices with no reflectivity at the cavity mirrors for the non-resonant signal frequency. The effect of a double-pass pump interaction is incorporated in the factor $|r_p|$. By setting this factor to zero, the analysis reduces to that of the singly-resonant devices with a single-pass pump interaction (either in the form of a resonant or non-resonant ring cavity, or a non-resonant, single-pass linear cavity). For these configurations, the fields for the non-resonant wave are calculated in the two possible directions of photon flow. The output intensities can be expressed as follows [1]:

$$|\alpha_i^{out}|^2 = |\alpha_p^{in}|^2 \left(\frac{F_i \gamma_i}{2\pi} \right) \left[1 - \cos^2 \beta \left(|r_p| \cos^2 \beta + 1 - |r_p| \right) \right] , \quad [\text{II. 105 (a)}]$$

$$|\alpha_s^{out}|_+^2 = |\alpha_p^{in}|^2 \frac{\sin^2 \beta}{2} , \quad [\text{II. 105 (b)}]$$

$$|\alpha_s^{out}|_-^2 = |\alpha_p^{in}|^2 \frac{\sin^2 \beta \cos^2 \beta}{2} , \text{ where} \quad [\text{II. 105 (c)}]$$

$$\beta^2 = \frac{|\alpha_i^{out}|^2}{|\alpha_p^{in}|^2} \frac{\sigma}{(1+|r_p|)} . \quad [\text{II. 105 (d)}]$$

In the above expressions, the subscripts (+) and (-) refer to the fields in the forward and backward directions, respectively.

Equations II. 105 must be solved by numerical analysis [24]. The maximum external conversion efficiency is found to be produced when [24]

$$\sigma = \left(\frac{\pi}{2}\right)^2 . \quad [\text{II. 106}]$$

Consider the ideal case of $|r_p| = 0$, and $F_i = \gamma_i / \pi$, when the pump is travelling in one direction, and the losses of the resonant field are the sum of useful output couplings. The signal and idler intensities become

$$|\alpha_i^{out}|^2 = \frac{1}{2} |\alpha_p^{in}|^2 (1 - \cos^2 \beta) , \quad [\text{II. 107 (a)}]$$

$$|\alpha_s^{out}|^2 = \frac{1}{2} |\alpha_p^{in}|^2 \sin^2 \beta . \quad [\text{II. 107 (b)}]$$

For maximum conversion, $\beta = \sqrt{\sigma} = \pi / 2$, and equations II. 107 reduce, as expected, to the following:

$$|\alpha_i^{out}|_{max}^2 = |\alpha_s^{out}|_{max}^2 = \frac{1}{2} |\alpha_p^{in}|^2 . \quad [\text{II. 108}]$$

Equation II. 108 illustrates that, under optimum conditions, all the pump photons are converted into signal and idler photons, and further, all of these photons are transmitted out of the OPO cavity in the form of useful OPO outputs. The equal numbers of signal and idler photons is consistent with

the conservation of energy relation. Further, the efficiency of the resonant wave is close to 100 % over the wide range $2.5 \leq \sigma \leq 8.5$ [24].

II. 4 (iii) Gaussian wave modifications.

The above analyses were confined to the general case of plane waves. Early comparisons of experimental results to the calculated efficiencies and pump depletions did not show close agreement, and the plane-wave analyses were replaced by beams with Gaussian intensity profiles [25]. The mode considers a plane-wave pump beam with a Gaussian intensity profile:

$$I(r) = I_p \exp\left(-\frac{2r^2}{W_p^2}\right), \quad [\text{II. 109}]$$

where W_p is the beam radius, incident on the parametric oscillator. Following the analysis of reference [25], and by integrating over the Gaussian profile treating the above-threshold and below-threshold regions independently, the conversion efficiency of the single-pass pump standing-wave resonator can be expressed as follows:

$$\eta_{ext} = \frac{1}{\sigma} \left(\frac{F_s \gamma_s + F_i \gamma_i}{\pi} \right) (\sqrt{\sigma} - 1 - \ln \sqrt{\sigma}) . \quad [\text{II. 110}]$$

Compared to the plane-wave case, the doubly-resonant oscillator with a Gaussian intensity does not show power limiting, and reaches a maximum efficiency of only 41 %, at a pumping level of $\sigma = 12.5$. Similarly, for the ring resonator, the efficiency is only 82 %, at $\sigma = 12.5$, instead of 100 % as in the plane-wave analysis [25].

The singly-resonant oscillator can be treated in a similar manner. In this case, the solution remains in an integral form [25]. The maximum efficiency is found to be 71 % at 6.5 times above threshold [25].

II. 5 Tuning, spectral output, and stability requirements.

The spectral characteristics of an optical parametric oscillator include the tuning range and method of tuning, the gain bandwidth, and the detailed spectral structure within the gain bandwidth determined by the resonance properties of the optical cavity. The tuning behaviour can be separated broadly into two different areas. First, the coarse frequency outputs of the signal and idler frequencies are determined by the phase-matching condition of the nonlinear material for a given pump frequency. Unlike the laser, the parametric oscillator does not depend on resonant transitions and consequently can be tuned over wide frequency bandwidths. Second, the fine frequency content of the outputs, for a given phase-matching geometry, determines the linewidths of the signal and idler output frequencies. Whereas coarse frequency tuning defines a broad spectral region over which the signal and idler frequencies are phase-matched, the fine tuning properties are the critical requirement in providing narrow-linewidth, amplitude-stable, and continuously-tunable radiation from OPOs.

II. 5 (i) Coarse frequency tuning.

The parametric gain linewidth is determined by satisfying the conservation of energy relation and the wave-vector condition:

$$\nu_p = \nu_s + \nu_i , \quad [\text{II. 111}]$$

$$k_p = k_s + k_i + \Delta k . \quad [\text{II. 112}]$$

where Δk is the momentum mis-match. The centre of the gain linewidth occurs at $\Delta k = 0$.

With a fixed source of pump frequency, any process which changes the refractive indices at the signal, idler or pump frequencies will tune the outputs of the oscillator. Tuning methods include the following: temperature [26], angular variation of the extra-ordinary refractive index [27], or electro-optic variation of the refractive indices [28]. In general, temperature and angular tuning have been used to tune OPOs over broad, coarse ranges, with fast electro-optic tuning restricted for fine frequency control [29]. However, for stable operation of OPOs, it is highly appropriate to use

nonlinear materials which exhibit a low sensitivity to temperature. In this respect, temperature tuning can be applied as a further method for smooth frequency tuning [29, 30].

Assuming a fixed source of pump frequency (and collinear phase-matching), the rate of tuning can be expressed as follows:

$$\Delta k = -\frac{\partial k_s}{\partial \nu_s} \Delta \nu_s - \frac{\partial k_i}{\partial \nu_i} \Delta \nu_i . \quad [\text{II. 113}]$$

The dispersive constant, b , is defined as

$$b = \frac{\partial k_i}{\partial \nu_i} - \frac{\partial k_s}{\partial \nu_s} . \quad [\text{II. 114}]$$

From conservation of energy, the change in the idler frequency is equal in magnitude, and opposite in sign, to the change in the signal frequency; i.e., $\Delta \nu = \Delta \nu_i = -\Delta \nu_s$. Therefore, equation [II. 113] can be re-written as

$$\frac{\Delta k l}{2} = b \frac{\Delta \nu l}{2} . \quad [\text{II. 115}]$$

As discussed previously, the half-power gain linewidth is determined approximately by the condition $\Delta k l / 2 \approx \pi$. Therefore, the tuning range can be expressed as follows:

$$\Delta \nu \approx \frac{2\pi}{bl} , \quad [\text{II. 116}]$$

which also describes the phase-matching bandwidth contribution to the OPO linewidth. In general, materials that possess a small dispersive constant give rise to large tuning rates.

Tuning curves for parametric oscillators are determined by solving the phase-matching equations for the signal and idler frequencies, for a given pump frequency, as a function of the tuning variable. The indices of refraction are given by an analytical expression in the form of a Sellmeier equation [31, 32]. The tuning curves for a variety of nonlinear materials, appropriate for use within cw OPO arrangements, are discussed fully in chapter III.

II. 5 (ii) Fine frequency tuning.

The fine frequency output properties of the generated signal and idler frequencies in an OPO are highly dependent on the resonance conditions of the OPO cavity [8, 11, 16, 17, 20, 33 - 36]. In general, the mode selection of the output frequencies becomes more complicated as the number of resonant waves within the OPO cavity is increased [36]. As expected, the spectral properties of the singly-resonant OPO, with a non-resonant pump field [11], are the least complicated. The addition of extra cavity resonances serves only to complicate further the tuning properties of these devices. The most intricate cavity design involves a single-cavity OPO with all three frequencies brought to resonance simultaneously between two common cavity mirrors, as occurs in a doubly-resonant oscillator with a pump-enhanced field [20].

These tuning difficulties are transferred directly into practical difficulties associated with constructing amplitude and frequency stable OPO cavities. Therefore, it is important to consider first why additional resonances complicate the output properties of an OPO, the requirements on the stability of the pump source and the OPO cavity length, to maintain stable OPO operation, and, further, steps that can be taken to introduce additional tuning parameters by altering the design of the OPO cavities that have been discussed to date.

This section analyses the amplitude and frequency stability of the outputs of the different types of linear cavity OPOs that were studied in section II. 3. The section is divided into two sub-sections, outlining the properties of singly-resonant and doubly-resonant OPO cavity designs, with and without resonant pump fields. In both sub-sections, simple expressions are derived to predict the level of stability required from the pump source and the OPO cavity length to maintain amplitude and frequency stable OPO operation. In addition, methods of smooth frequency tuning are presented, with emphasis on the design of a dual-cavity oscillator, which permits separate resonant cavities to be formed within a single OPO configuration.

II. 5 (ii) (a) Singly-resonant oscillators.

When deriving the threshold conditions for the singly-resonant oscillator, it was assumed that one of the generated OPO frequencies, in this case the idler frequency, was resonant in the OPO cavity. The signal frequency was

assumed to be completely non-resonant, such that this frequency was independent of any cavity resonance constraints. For the analysis of tuning, these resonance conditions are maintained. Two different regimes are examined depending upon the interaction of the pump frequency in the cavity. In section II. 5 (i) (a) (1), the singly-resonant oscillator with a non-resonant pump frequency is considered. In section II. 5 (i) (b) (2), pump-resonance effects are incorporated.

II. 5 (ii) (a) (1) Singly-resonant oscillator with a non-resonant pump field.

With regard to fine frequency tuning, the most simple cavity to consider is the singly-resonant oscillator with a non-resonant pump field [11]. In section II. 3, the threshold for this cavity configuration was shown to be as follows:

$$|\alpha_p^{in}|_{th}^2 \propto \frac{1}{\text{sinc}^2\left(\frac{\Delta kl}{2}\right)}. \quad [\text{II. 117}]$$

Therefore, the threshold pump power is independent of the relative detunings of the three frequencies, and the output amplitudes of the signal and idler waves should remain constant [11].

Single-resonance dictates that the resonant idler frequency is set simply by the cavity length constraint and the phase-matching condition. Within a standing-wave linear cavity, the coincidence with a cavity mode requires that

$$v_i = \frac{m_i c}{2(n_i l + L_i)}, \quad [\text{II. 118}]$$

where m_i is the longitudinal mode number of the idler frequency. The signal frequency simply takes on the value that satisfies the conservation of energy relation, and such that

$$v_s = v_p - v_i. \quad [\text{II. 119}]$$

With a fixed frequency pump source, the effects of perturbations and detuning of the cavity length can be evaluated. Instabilities in the cavity

length are manifested as instabilities in the idler frequency. For a cavity length perturbation of ΔL_i , the corresponding frequency shift of the resonant idler frequency is given by Δv_i , and such that

$$\Delta v_i = -\frac{v_i}{n_i l + L_i} \Delta L_i . \quad [\text{II. 120}]$$

For a fixed source of pump frequency, the frequency output of the signal frequency will show the same level of frequency stability as the idler frequency, such that

$$v_s \pm \Delta v_s = v_p - (v_i \pm \Delta v_i) . \quad [\text{II. 121}]$$

The allowable frequency excursion, or smooth frequency tuning, of the OPO output frequencies, for a fixed frequency pump source, is one half of the cavity free spectral range either side of the peak of the phase-matching gain bandwidth curve [11]. This is because singly-resonant oscillation occurs on the cavity mode nearest parametric gain centre. Therefore, the range of smooth frequency tuning from a singly-resonant oscillator with a fixed pump frequency is given by

$$|\Delta v_{i-max}| = |\Delta v_{s-max}| = FSR_i . \quad [\text{II. 122}]$$

When the cavity length is fixed, the idler frequency will be fixed. Now the pump frequency can be considered as a free tuning parameter. Changes in the pump frequency, either from frequency jitter, or controlled frequency detuning, will be taken up by the signal frequency, required by the conservation of energy relation. Therefore, for a fixed resonant idler frequency, the non-resonant signal frequency is given simply by

$$v_s \pm \Delta v_s = (v_p \pm \Delta v_p) - v_i . \quad [\text{II. 123}]$$

Increased tuning bandwidths are now possible by holding the idler frequency constant while detuning the pump frequency. In this manner, the maximum range of smooth frequency tuning of the non-resonant signal frequency is limited by the range of smooth frequency tuning possible from the pump source. The pump frequency change required for the parametric gain peak to be shifted by one half of the free spectral range either side of the gain peak

from the idler cavity resonance is given by the stability factor, defined in reference [37] as:

$$\Delta v_{p-max} = \Delta v_{s-max} = \frac{\left. \frac{\partial k_s}{\partial v_s} \right|_{v_s(o)} - \left. \frac{\partial k_i}{\partial v_i} \right|_{v_i(o)}}{\left. \frac{\partial k_p}{\partial v_p} \right|_{v_p(o)} - \left. \frac{\partial k_s}{\partial v_s} \right|_{v_s(o)}} FSR_i . \quad [II. 124]$$

where the subscripts of the index derivatives represent the values at parametric gain centre.

It has been shown that the singly-resonant oscillator with a non-resonant pump field should display high degrees of amplitude and frequency stability. Furthermore, the single resonance condition allows for smooth frequency tuning without the need for complicated servo-control of the pump frequency or the OPO cavity length [10].

II. 5 (ii) (a) (2) Singly-resonant oscillator with a resonant pump field.

The above analysis is now extended to include the effects of pump frequency resonance within the OPO cavity. This configuration represents the case of the singly-resonant oscillator with a pump enhanced resonant field. Therefore, the OPO cavity must satisfy simultaneously the resonant idler and pump frequency conditions. The threshold for this cavity design was shown to be as follows

$$\left| \alpha_p^{in} \right|_{th}^2 \propto \frac{1}{\text{sinc}^2\left(\frac{\Delta kl}{2}\right)} (1 + \Delta_p^2) . \quad [II. 125]$$

Therefore, the threshold pump intensity is proportional to the detuning of the pump frequency. As the cavity length changes, the intra-cavity pump field will come on and off resonance, and the input threshold intensity will vary accordingly. When exactly off pump resonance, no pump radiation can be coupled into the resonator and the OPO cannot oscillate.

The cavity length over which the pump-enhanced singly-resonant oscillator operates can be estimated by considering the optical bandwidth of

the resonant pump field, defined by a unity relative detuning parameter: i.e. $\Delta_p = 1$. (Note that, despite the factor of two difference in the ring and linear cavity definitions of the free spectral ranges and the phase-detunings, these factors are cancelled out by the relative detuning parameter.) The pump resonance effects are illustrated in figure II. 8.

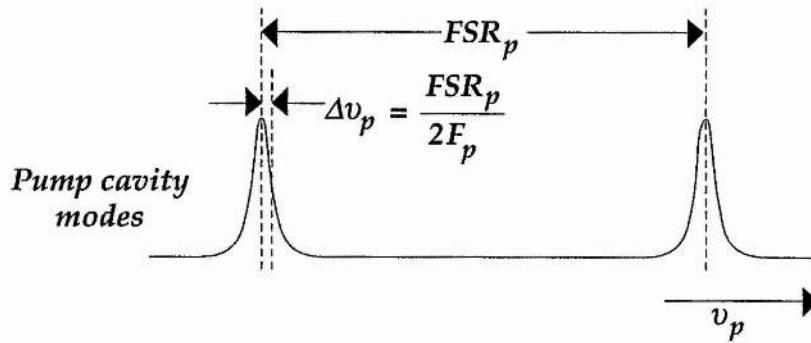


Figure II. 8.

Optical bandwidth of the pump frequency in a pump enhanced OPO, as a function of the free spectral range and the cavity finesse.

The total cavity length over which the OPO can operate is taken as the total cavity bandwidth, defined as follows:

$$\Delta L = \frac{c}{2\nu_p F_p} \quad . \quad [\text{II. 126}]$$

Therefore, the maximum smooth tuning of the idler frequency can be expressed as

$$|\Delta\nu_{i-max}| = |\Delta\nu_{s-max}| = \frac{FSR_i}{F_p} \frac{\nu_i}{\nu_p} \quad . \quad [\text{II. 127}]$$

For a comprehensive analysis of the single-cavity, pump-enhanced, singly-resonant oscillator, it would be necessary to calculate the exact intra-cavity pump intensity when operating at cavity lengths detuned from exact cavity resonance. In addition, when the conversion efficiencies of the OPOs are appreciable, then the generated signal and idler fields would cause the

impedance matching of the pump source into the resonator to change significantly.

In conclusion, there are additional tuning complexities involved when resonating the pump field within a singly-resonant OPO cavity. These considerations must be balanced against the requirements for threshold of an equivalent single-pass-pump singly-resonant oscillator, or indeed the single-pass-pump doubly-resonant oscillator. A practical solution could involve servo-locking the pump frequency to the OPO cavity length, or to an external cavity formed by separating internally the pump and resonant OPO fields. With the recent demonstration of highly compact, monolithic OPO resonators [38 - 41], such a technique could prove particularly effective. Here, the pump frequency could be locked to the monolithic resonator, and one of the OPO fields resonated via an external cavity mirror.

II. 5 (ii) (a) (3) Singly-resonant oscillator with a multi-mode pump source.

One interesting feature, not yet demonstrated experimentally, is the use of a multi-longitudinal-mode laser to pump a cw singly-resonant oscillator. In this case the linewidth of the pump wave would be typically at the GHz-level, comprising a number of cavity modes with random amplitude and phase distribution. The non-resonant wave would take on a correspondingly large frequency linewidth. This method has been proposed [42], but demonstrated only with pulsed pump sources [43].

Within the equivalent cw singly-resonant configuration, the noisy non-resonant wave would be discarded, and the usable output would be the leakage field of the narrow-linewidth, high-finesse, resonant wave. This differs from the pulsed configurations, in which the more powerful non-resonant field is considered often as the usable frequency output. In this device, the pump wave could not be resonated, since this would impose frequency selection of the multi-mode input pump field. However, the pump field could be double-passed to lower the threshold, without affecting the frequency stability of the resonant OPO field.

II. 5 (ii) (b) Doubly-resonant oscillators.

The doubly-resonant OPO is configured routinely in experimental demonstrations of cw OPOs [12]. The double-resonance condition results in significantly lower pump power thresholds compared to singly resonant OPOs, and lowers the linewidth of the resonant outputs [44]. (This latter topic is discussed further in section II. 6.) However, the tuning properties are constrained by having to satisfy simultaneously four conditions; energy conservation, phase-matching, and cavity resonances for the signal and idler frequencies. This results in complicated mode selection properties as the pump frequency or the OPO cavity length is detuned from a perfect overlap of the signal and idler cavity resonances [33 - 35]. There has been substantial theoretical modelling of the causes of these frequency instabilities, and on methods of overcoming these constraints.

In this section, mode selection in doubly resonant OPOs is examined. This involves a study of the doubly-resonant OPO with a non-resonant pump field, and the more complicated triply-resonant OPO. For each configuration, the effects of cavity length and pump frequency detunings on the outputs of the OPO are considered in detail.

II. 5 (ii) (b) (1) Doubly-resonant oscillator with a non-resonant pump field.

In this section, two different cavity configurations are analysed; the single- and dual-cavity doubly-resonant OPOs. Figure II. 9 (a) illustrates the conventional single-cavity doubly-resonant oscillator, in which two mirrors are coated to be highly-reflecting at both the signal and idler frequencies. The dual-cavity doubly-resonant OPO is shown schematically in figure II. 9 (b), in which an additional optical component separates spatially the signal and idler fields and a third cavity mirror forms a second optical resonator [45 - 48].

The conditions for resonance of the signal and idler frequencies in a doubly-resonant OPO are given by

$$\nu_s = \frac{m_s c}{2(n_s l + L_s)} \quad , \quad \text{[II. 128 (a)]}$$

$$\nu_i = \frac{m_i c}{2(n_i l + L_i)} \quad , \quad \text{[II. 128 (b)]}$$

where m_s and m_i are the longitudinal mode numbers of the signal and idler frequencies, respectively. The empty cavity lengths are denoted by L_s and L_i for the signal and idler frequencies, respectively.

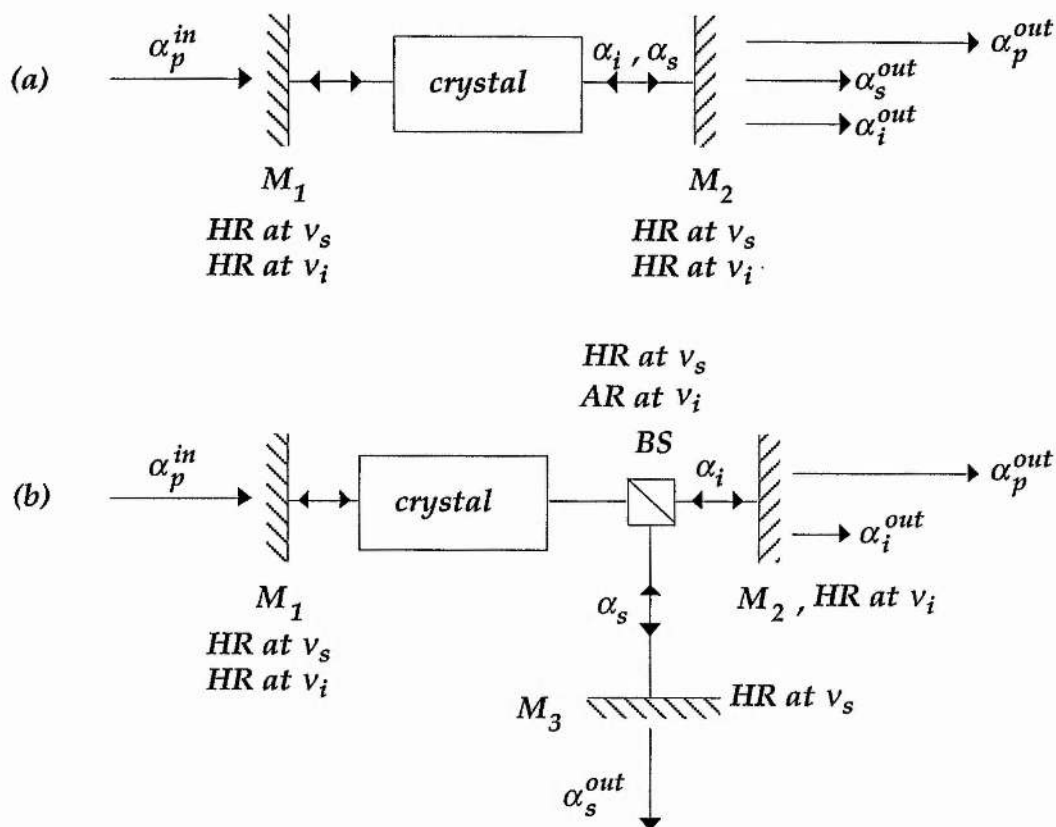


Figure II. 9.

Schematic representation of doubly-resonant oscillator cavity designs. In (a), the single-cavity oscillator employs two mirrors, both highly-reflecting (HR) at the signal and idler frequencies. In (b), an intra-cavity beam-splitter (BS) separates the signal and idler fields into different resonators to allow for independent cavity length control. The beam-splitter is highly-reflecting for one frequency, and anti-reflecting (AR) for the other frequency.

It is necessary to make an important distinction in the theoretical approach adopted when modelling the frequency properties of doubly-resonant oscillators. This involves the effects of dispersion within the nonlinear medium, and their effect on the respective optical cavity lengths of the signal

and idler fields. When the optical lengths, or free spectral ranges, of the signal and idler cavities are approximately equal, then the effects of dispersion become critical [17, 34]. This is particularly true for single-cavity type I phase-matching geometries operating near frequency degeneracy [49 - 52]. In this geometry, the nearly-equal signal and idler frequencies are polarized along the same crystal axis and have almost identical free spectral ranges.

When the tuning properties of the type I phase-matching geometry near frequency-degeneracy are analysed, it is imperative to account for the dispersive properties of the nonlinear medium. This topic has been considered uniquely in reference [17]. The analysis is complicated and requires considerable numerical modelling. This specific geometry is not studied analytically within this thesis. However, comparison is made to the results of reference [17], with regard to a computer program that was developed to model mode-selection in doubly-resonant oscillators [35], and which is discussed later.

The following analysis is specific to the case when the dispersion terms used within the definition of the free spectral ranges are small with respect to other tuning parameters, and can be neglected. In particular, this applies to type I phase-matching geometries significantly removed from frequency-degeneracy [54 - 56], and to type II phase-matching geometries [57 - 59]. The case of the type II phase-matching geometry is important because the signal and idler frequencies are polarized along orthogonal axes of the birefringent nonlinear medium. Therefore, the free spectral ranges of the signal and idler fields are necessarily different, even when operating at the exact frequency-degeneracy point within a single-cavity resonator arrangement.

Changes in the optical lengths of the signal and idler cavities of ΔL_s and ΔL_i cause the resonant frequencies of the signal and idler fields to alter by Δv_s and Δv_i , respectively, and such that

$$\Delta v_s = \frac{-\Delta L_s v_s}{(n_s l + L_s)} , \quad \text{[II. 129 (a)]}$$

$$\Delta v_i = \frac{-\Delta L_i v_i}{(n_i l + L_i)} . \quad \text{[II. 129 (b)]}$$

The remainder of the analysis is presented in terms of the free spectral ranges, FSR_j , and the finesses, F_j , of the cavities. Therefore, the above expressions can be rewritten as

$$\Delta v_s = \frac{-2\Delta L_s v_s FSR_s}{c}, \quad [\text{II. 130 (a)}]$$

$$\Delta v_i = \frac{-2\Delta L_i v_i FSR_i}{c}. \quad [\text{II. 130 (b)}]$$

The mis-match in the free spectral ranges is defined as ΔFSR , such that

$$\Delta FSR = FSR_s - FSR_i \approx \frac{c\Delta n}{(\bar{n}l + \bar{L})^2}. \quad [\text{II. 131}]$$

where Δn is the difference of the refractive indices of the signal and idler frequencies within the nonlinear medium, such that $\Delta n = |n_s - n_i|$, \bar{n} is the average refractive index, given by $\bar{n} = (n_s + n_i)/2$, and \bar{L} is the average (empty) optical cavity length.

II. 5 (ii) (b) (1) (A) Mode-hopping.

In general, the signal and idler output frequencies are determined as a compromise between the optimum phase-matching condition and the requirement that both frequencies lie close to longitudinal mode frequencies of the resonating cavities. Pairs of signal and idler modes that come close to satisfying the requirement for conservation of energy are termed signal and idler mode-pairs. Within the phase-matching bandwidth, there are usually a number of different signal and idler frequency mode-pairs for which the loss is low enough for the OPO to oscillate. Comparatively small changes in either of the cavity mode frequencies or the pump frequency may lead to the OPO output switching from one mode-pair to another. Depending on the degree of mis-match in the free spectral ranges and in their finesses, the new mode-pair is either adjacent to the original (termed a mode-hop) or many mode-pairs removed (termed a cluster-hop). This mode- and cluster-hopping behaviour has been discussed by a number of authors [16, 17].

The mis-match in the FSR s of the signal and idler cavities dictates the level of cavity length or pump frequency detuning required to cause the output of the OPO to hop to an adjacent signal and idler mode-pair [17]. Assuming that the original mode-pair is exactly on resonance, then by changing the cavity mode frequencies by a total amount equal to the mis-match in the FSR s, a mode-hop will occur. Therefore, the condition for a mode-hop is given by

$$|\Delta\nu_s| + |\Delta\nu_i| = \frac{2(\Delta L_s \nu_s FSR_s + \Delta L_i \nu_i FSR_i)}{c} = \Delta FSR . \quad [\text{II. 132}]$$

In the single-cavity OPO, it is assumed that the cavity length detunings and the FSR s of the signal and idler frequencies are approximately equal; i.e. $\Delta L_s = \Delta L_i = \Delta L$ and $FSR_s = FSR_i = FSR$. Therefore, the cavity length detuning required to cause a mode-hop is provided by substituting $\Delta L = \Delta L_{hop}$ in equation II. 132 to yield

$$\Delta L_{hop} = \frac{c}{2\nu_p} \frac{\Delta FSR}{FSR} . \quad [\text{II. 133}]$$

Substituting for the refractive indices and cavity lengths, as given by equation II. 131, in the above expression, the common cavity length detuning required for the output of the OPO to hop to an adjacent signal and idler frequency mode-pair is given by

$$\Delta L_{hop} = \frac{c}{2\nu_p} \frac{\Delta n l}{(\bar{n}l + \bar{L})} . \quad [\text{II. 134}]$$

Alternatively, the pump frequency detuning required to cause a mode-hop is given by

$$\Delta\nu_{p-hop} = \Delta FSR . \quad [\text{II. 135}]$$

II. 5 (ii) (b) (1) (B) Stability conditions.

To evaluate the stability requirements on the pump frequency and the cavity length, it is necessary to examine the range over which the available pump power is sufficient to maintain oscillation on a single signal and idler

frequency mode-pair. Consider figure II. 10, which illustrates the signal and idler frequencies.

Any vertical cursor line drawn through both scales corresponds to values of the signal and idler frequencies that satisfy the conservation of energy relation. A change in cavity length is modelled by shifting the resonance peaks higher or lower in frequency. A change in the pump frequency is modelled by rotating the cursor line slightly away from the vertical. In both cases, the operating condition of the OPO can be predicted by shifting horizontally the line until a resonance condition for the signal and idler fields can be accessed simultaneously. This figure can be used to derive expressions to predict the tolerance to the fluctuations in the cavity length or the pump frequency regarding operation of the OPO on the same signal and idler frequency mode-pair.

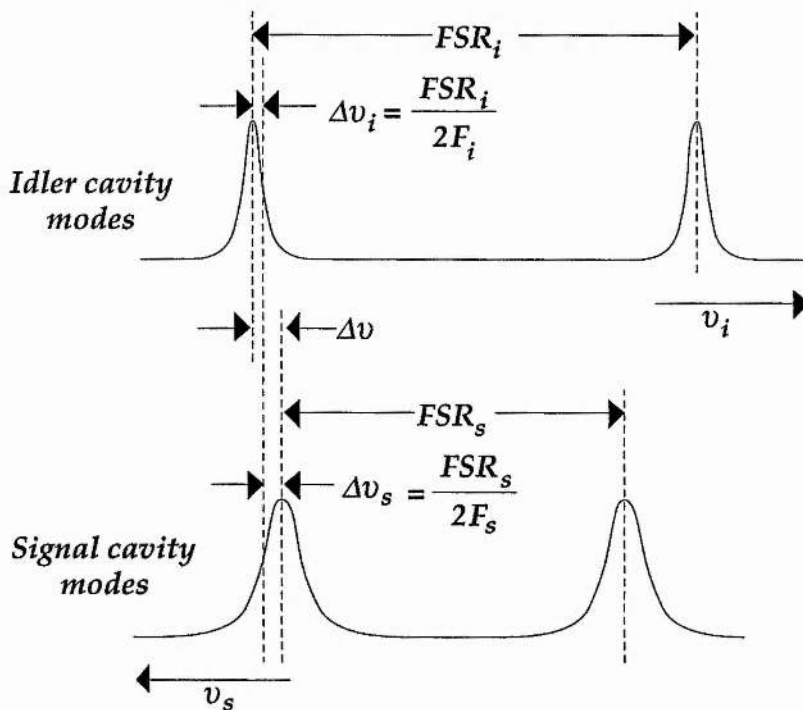


Figure II. 10

Signal-idler resonance diagram similar to figure II. 4, expanded in detail. The doubly-resonant oscillating frequencies divide the frequency mis-match, $\Delta\nu$, into the components, $\Delta\nu_s$ and $\Delta\nu_i$.

From figure II. 10, the maximum detuning allowed, $\Delta\nu$, while retaining operation on a single signal and idler frequency mode-pair, is given approximately by

$$\Delta\nu = \Delta\nu_s + \Delta\nu_i \leq \frac{FSR_s}{2F_s} + \frac{FSR_i}{2F_i} . \quad [\text{II. 136}]$$

This relation can be compared to equation II. 65 in section II. 2, which represents the threshold parameter, $|\alpha_p^{in}|_{th}^2$, for a single-pass pump doubly-resonant oscillator. This threshold parameter was shown to be

$$|\alpha_p^{in}|_{th}^2 \propto \left[1 + \left(\frac{2\Delta\nu F_s F_i}{F_s FSR_i + F_i FSR_s} \right)^2 \right] . \quad [\text{II. 137}]$$

Therefore, equation II. 136 is related to the second term of equation II. 137, and corresponds to the detuning required to double the value of $|\alpha_p^{in}|_{th}^2$. Equation II. 136 is used directly to derive the stability requirements on the cavity length to maintain the OPO above threshold, and operating on the same signal and idler frequency mode-pair. Within this section, the point at which the threshold parameter, $|\alpha_p^{in}|_{th}^2$, doubles is taken as the range over which the OPO remains operational. By substituting equation II. 130 for the change in the signal and idler frequencies, equation II. 136 becomes

$$\left| \frac{4}{c} (\Delta L_s \nu_s FSR_s + \Delta L_i \nu_i FSR_i) \right| \leq \frac{FSR_s}{F_s} + \frac{FSR_i}{F_i} . \quad [\text{II. 138}]$$

In the simple case of a single-cavity OPO, with approximately equal finesses for the signal and idler fields, then $FSR_s \approx FSR_i$, $F_s \approx F_i \approx F$, and $\Delta L_s = \Delta L_i = \Delta L$. Therefore, the cavity length stability, ΔL_{stab} , required to maintain the OPO above threshold is given by

$$\Delta L_{stab} \approx \pm \frac{c}{2\nu_p F} . \quad [\text{II. 139}]$$

For a single-cavity OPO with significantly different finesses for the signal and idler fields, equation II. 138 is dominated by the lower cavity finesse, F_{min} . The corresponding requirement on the cavity length is now given by

$$\Delta L_{stab} \approx \pm \frac{c}{4\nu_p F_{min}} . \quad [\text{II. 140}]$$

For the dual-cavity OPO configuration, the FSR_s of the signal and idler fields may be significantly different. In this case, and assuming that both cavities are subject to the same change in cavity length and have comparable cavity finesses, the stability requirements become

$$\Delta L_{stab} \approx \pm \frac{c}{4\nu_i F_i} \quad \text{for } FSR_s \ll FSR_i , \text{ and} \quad [\text{II. 141 (a)}]$$

$$\Delta L_{stab} \approx \pm \frac{c}{4\nu_s F_s} \quad \text{for } FSR_s \gg FSR_i . \quad [\text{II. 141 (b)}]$$

Therefore, for a dual-cavity OPO, the length stability requirements are dominated by the finesse of the shorter of the two cavities. Therefore, the pump power threshold can be reduced by increasing the finesse of the longer cavity length without any significant decrease in the stability requirements.

The stability conditions for the pump frequency are now considered. For fixed cavity lengths, which are initially in perfect resonance for both the signal and idler waves, the influence of pump frequency detuning, $\Delta\nu_p$, can also be obtained directly from equation II. 136. Similar to the cavity length detuning analysis, an indication as to the pump frequency detuning over which the OPO remains on a single signal and idler frequency mode-pair, is given by

$$|\Delta\nu_p| \leq \frac{FSR_s}{2F_s} + \frac{FSR_i}{2F_i} . \quad [\text{II. 142}]$$

For a single cavity OPO with approximately equal finesses for the signal and idler fields, the required stability of the pump frequency, $\Delta\nu_{p-stab}$, is given by

$$\Delta\nu_{p-stab} \approx \pm \frac{FSR}{F} , \quad [\text{II. 143}]$$

where $FSR_s \approx FSR_i \approx FSR$, and $F_s \approx F_i \approx F$.

For a single-cavity OPO with significantly different finesses for the signal and idler fields, equation II. 142 is dominated by the smaller of the two

finesses. Therefore, in this case, the stability requirement for the pump frequency becomes

$$\Delta v_{p-stab} \approx \pm \frac{FSR}{2F_{min}} , \quad [\text{II. 144}]$$

where F_{min} is the smaller of the two cavity finesses.

As with the cavity length stability requirements, the finesse of the high finesse cavity can be increased without affecting the pump frequency stability requirements. Note that, unlike cavity length stability, the requirements on the pump frequency stability become more stringent as the cavity length is increased.

Similar to the expressions for the cavity length stability, the pump frequency stability requirements can be re-written for the case of a dual-cavity oscillator, in which the FSR s and the finesses of the signal and idler cavities may differ significantly. For the case of unequal finesses and unequal FSR s, the pump frequency stability requirements are given by

$$\Delta v_{p-stab} \approx \pm \frac{FSR_i}{2F_i} \quad \text{for } FSR_s \ll FSR_i , \quad [\text{II. 145 (a)}]$$

$$\Delta v_{p-stab} \approx \pm \frac{FSR_s}{2F_s} \quad \text{for } FSR_s \gg FSR_i . \quad [\text{II. 145 (b)}]$$

Therefore, in general, a short, low-finesse cavity for either the signal or idler field can reduce the demands on the pump frequency stability.

II. 5 (ii) (b) (1) (C) Smooth frequency tuning.

To date, the requirements on the stability of the cavity length and the pump frequency have been studied with a view to maintaining the double-resonance condition within single- and dual-cavity resonators. Multiple parameter tuning is now introduced to illustrate that some of the above requirements can be relaxed, opening up the possibility for extensive smooth frequency tuning of the OPO outputs.

From equation II. 136, the relationship between the pump frequency detuning and the cavity length detuning required to maintain the double resonance condition can be expressed as

$$\Delta v_p = \Delta v_s + \Delta v_i \approx -\frac{2\Delta L_s v_s FSR_s}{c} - \frac{2\Delta L_i v_i FSR_i}{c} . \quad [\text{II. 146}]$$

This equation illustrates that even when using a somewhat unstable pump source, the double-resonance condition for the signal and idler fields can be maintained by suitable control of the length of the signal and / or idler cavity.

For a single-cavity oscillator, equation II. 146 reduces to

$$\Delta v_p = -\Delta L \left(\frac{2v_p FSR}{c} \right) . \quad [\text{II. 147}]$$

Smooth and continuous tuning of the signal and idler frequencies can now be obtained by changing the cavity length while controlling simultaneously the pump frequency to maintain the double-resonance condition.

In general, for a fixed pump frequency and by simply changing the common cavity length, a single-cavity oscillator cannot be used to tune continuously the signal and idler outputs while maintaining both the signal and idler fields on resonance. To achieve significant degrees of continuous tuning with a fixed frequency pump source, it is essential to have independent control of the signal and idler cavity lengths.

Given a fixed, non-tunable pump frequency, the change in the signal frequency is equal in magnitude, and opposite in sign, to the change in the idler frequency; i.e.

$$\Delta v_s = -\Delta v_i . \quad [\text{II. 148}]$$

The relation between ΔL_s and ΔL_i to provide smooth frequency tuning from the dual-cavity oscillator can be expressed as

$$\Delta L_s = -\Delta L_i \frac{v_i FSR_i}{v_s FSR_s} . \quad [\text{II. 149}]$$

Therefore, in addition to allowing for relaxed stability requirements on the pump frequency and the OPO cavity length, dual-cavity oscillators offer the possibility for continuous frequency tuning of the OPO outputs. This may be provided by holding the pump frequency fixed, and altering the two cavity lengths to satisfy equation II. 149.

Alternatively, one of the cavity lengths (frequencies) can be fixed. In this case, detuning the pump frequency can be compensated by controlling the optical length of the other OPO cavity. For a fixed signal frequency cavity length, the relation between ΔL_i and $\Delta \nu_p$ to provide smooth frequency tuning can be expressed as

$$\Delta L_i = -\Delta \nu_p \frac{c}{2\nu_i FSR_i} \quad \text{[II. 150]}$$

In summary, dual-cavity oscillators are ideally suited for providing highly stable OPO radiation. Having eliminated the constraints of mode / cluster hopping, signal and idler frequencies can be tuned over frequency regions that can approach the entire phase-matching bandwidth of the OPO ($\Delta \nu \approx 10$ s GHz), when pumped with a fixed / known pump frequency.

II. 5 (ii) (b) (2) Computer model.

A computer model was developed to study further the mode-selection properties of single-cavity doubly-resonant oscillators [35]. Consider equation II. 68, which describes the threshold for each signal and idler mode-pair. This equation can be re-written as the product of three separate terms; i.e.

$$|\alpha_p^{in}|_{th}^2 \propto \left(\frac{\pi^2}{F_s F_i} \right) \times \left(\frac{1}{\text{sinc}^2(\Delta k l / 2)} \right) \times \left[1 + \left(\frac{2\Delta \nu F_s F_i}{F_s FSR_i + F_i FSR_s} \right)^2 \right] \quad \text{[II. 151]}$$

The first term describes the reduction in threshold achieved by forming a doubly-resonant OPO. This quantity is equivalent to the number of round cavity trips made by the signal frequency multiplied by the number of round cavity trips made by the idler frequency. The second term describes the increase in threshold due to non-perfect phase-matching in the crystal. The

third term describes the increase in threshold when the signal and idler frequencies do not match exactly the cavity mode frequencies.

The computer model used the above expression to calculate directly the threshold of every possible signal and idler mode-pair within the phase-matching bandwidth of the OPO: see appendix II. For given values of the pump frequency, the OPO cavity length, and the crystal temperature, the signal and idler mode-pairs with the lowest thresholds can be identified and the actual values of the signal and idler frequencies can be calculated. Subsequently, by varying one of the input parameters, the tuning behaviour of the OPO can be predicted.

Before studying the results of the computer model in detail, the general principles governing the selection of the lowest signal and idler mode-pairs are considered. For cavity lengths above a few 10s millimetres, many possible modes fall within the phase-matching bandwidth, and the threshold of a mode-pair is dominated by the degree of overlap between the signal and idler modes. A range of mode-pairs over which the overlap is good form a mode-cluster [16]. The number of signal modes between each cluster, M_{cl} , can be expressed as [34]

$$M_{cl} = \frac{FSR}{\Delta FSR} . \quad [\text{II. 152}]$$

Several mode-clusters fall within the phase-matching bandwidth. The number of modes within each cluster, N_{cl} , is a function of the finesses of the cavity at the signal and idler frequencies. From equation II. 152, the number of mode-pairs within a cluster, for which the threshold is within a factor of five of its minimum value, is given approximately by

$$N_{cl} = M_{cl} \left(\frac{1}{F_s} + \frac{1}{F_i} \right) . \quad [\text{II. 153}]$$

When $FSR_s \approx FSR_i$, each cluster comprises many mode-pairs and the central mode-pair will always have a good overlap, such that

$$\Delta v_{cluster \text{ centre}} \ll \frac{FSR_s}{F_s} + \frac{FSR_i}{F_i} . \quad [\text{II. 154}]$$

In this case, the lowest threshold mode-pair will lie at the centre of the cluster that is itself closest to the phase-matching condition, i.e. $\Delta k \approx 0$.

When the FSRs are significantly different, it can no longer be assumed that the central mode-pair within any particular cluster will show good overlap. The cluster closest to the phase-matching condition may not necessarily contain the mode-pair with the best overlap and the lowest threshold mode-pair may lie in a neighbouring cluster.

The nonlinear medium chosen for the computer modelling was lithium triborate (LBO) [60]. At the moment, the actual material used is not important. The critical parameter that was studied was the effect on the output frequencies caused by different mis-matches in the free spectral ranges of the signal and idler optical cavities, as discussed above. For this, it was necessary to know the refractive indices, their change with temperature and the thermal expansion of the chosen crystal. To calculate the refractive indices, the Sellmeier equations with coefficients as given in reference [61] were used. The temperature dependence of the refractive indices was based on the results as presented in reference [62]. This data is valid only near room temperature, but in the absence of more accurate coefficients, they have been used over the entire temperature range of interest. The thermal expansion data for LBO have also been published [63].

Two different configurations were analysed, corresponding to different mis-matches in the free spectral ranges of the signal and idler cavities. The first configuration examines the type I phase-matching geometry near frequency-degeneracy; case (a). As discussed previously, in this phase-matching geometry, the free spectral ranges of the signal and idler frequencies are similar. In this configuration, the mis-match in the free spectral ranges was set to $\Delta FSR \approx 0.16\%$. The second configuration examines the type II phase-matching geometry near frequency-degeneracy; case (b). Although the frequencies of the three waves were identical to the former type I phase-matching case, the mis-match in the free spectral ranges is significantly higher due to the type II phase-matching geometry. In this case, $\Delta FSR \approx 1.24\%$.

In each configuration, the cavity mirror separation was set to $L_m \approx 33$ mm and the finesses of the resonant signal and idler fields were $F_s \approx F_i \approx 300$. In addition, the pump frequency was set to $\nu_p = 583$ THz. (This specific frequency corresponds to a high gain transition line from an argon-

ion gas laser, operating in the visible spectral region, and corresponds to a free space pump wavelength of $\lambda_p = 514.5$ nm).

*Table II. 2.
Modelling of type I and type II
phase-matching.*

	(a) Type I	(b) Type II
<i>Pump frequency</i>	583 THz	583 THz
<i>Signal frequency</i>	317 THz	317 THz
<i>Idler frequency</i>	267 THz	267 THz
<i>Temperature</i>	173.4°C	20.0°C
<i>Signal/idler finesse</i>	300	300
n_p	1.6054	1.5797
n_s	1.6070	1.5924
n_i	1.6035	1.5647
$\Delta n = n_s - n_i $	0.22 %	1.75 %
L_m	33 mm	33 mm
l	20 mm	20 mm
ΔFSR	0.16 %	1.24 %

Therefore, since all the other parameters are equal except for the mis-match in the free spectral ranges, the differences in the outputs of the OPO can be attributed entirely to the mis-match in the free spectral ranges of the signal and idler fields. This explains why the nonlinear material LBO was selected for the analysis. For the chosen pump frequency, both type I and type II phase-matching geometries can be selected to give the same signal and idler output frequencies. The input parameters for the computer model are summarized in table II. 2.

In each case, as described above, graphs were produced to display the influence of the pump frequency, the OPO cavity length, and the crystal temperature, on the selection of the lowest threshold mode-pair. In each case, the threshold is plotted against detuning for the five lowest threshold modes. The graphs do not show the exact frequencies of the signal and idler waves, but the mode number of the oscillating modes. The numbers shown on the graph correspond to the mode number of the signal field.

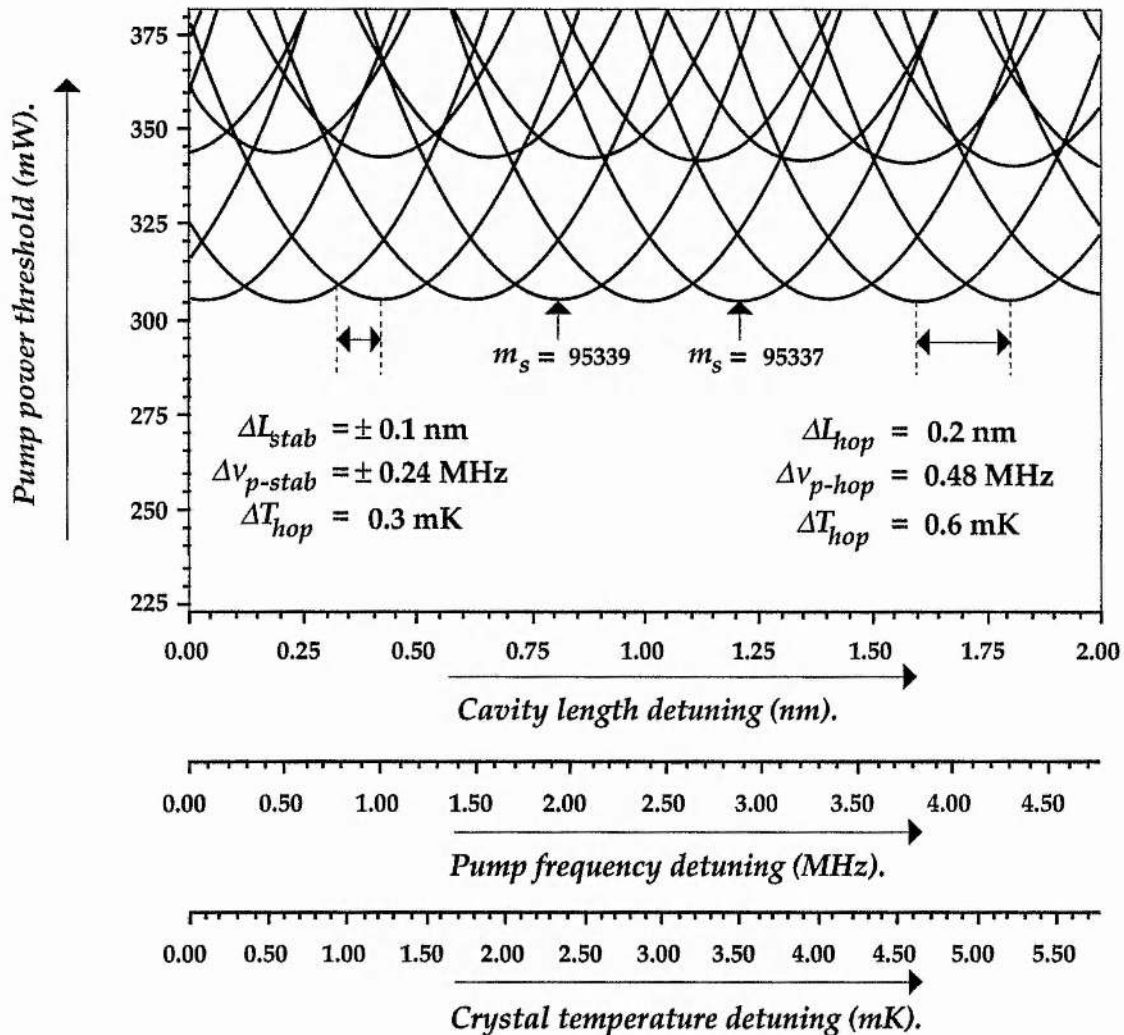


Figure II. 11.

The effects of detunings in the cavity length, the pump frequency, and the crystal temperature on the selection of the lowest threshold signal and idler mode-pairs, for the case of the type I phase-matching geometry near frequency-degeneracy.

For case (a) (type I phase-matching near degeneracy) the mode-selection properties are displayed in figure II. 11. Under sufficient detuning, the lowest threshold mode-pair hops by one mode to the adjacent mode-pair in the same cluster (mode-hop). This phase-matching geometry has approximately equal free spectral ranges, and the change in frequency between adjacent mode-pairs is small. Therefore, a mode-pair possessing good overlap is always present within the cluster closest to the perfect phase-matching condition, and the lowest threshold mode-pair always lies in the central mode cluster.

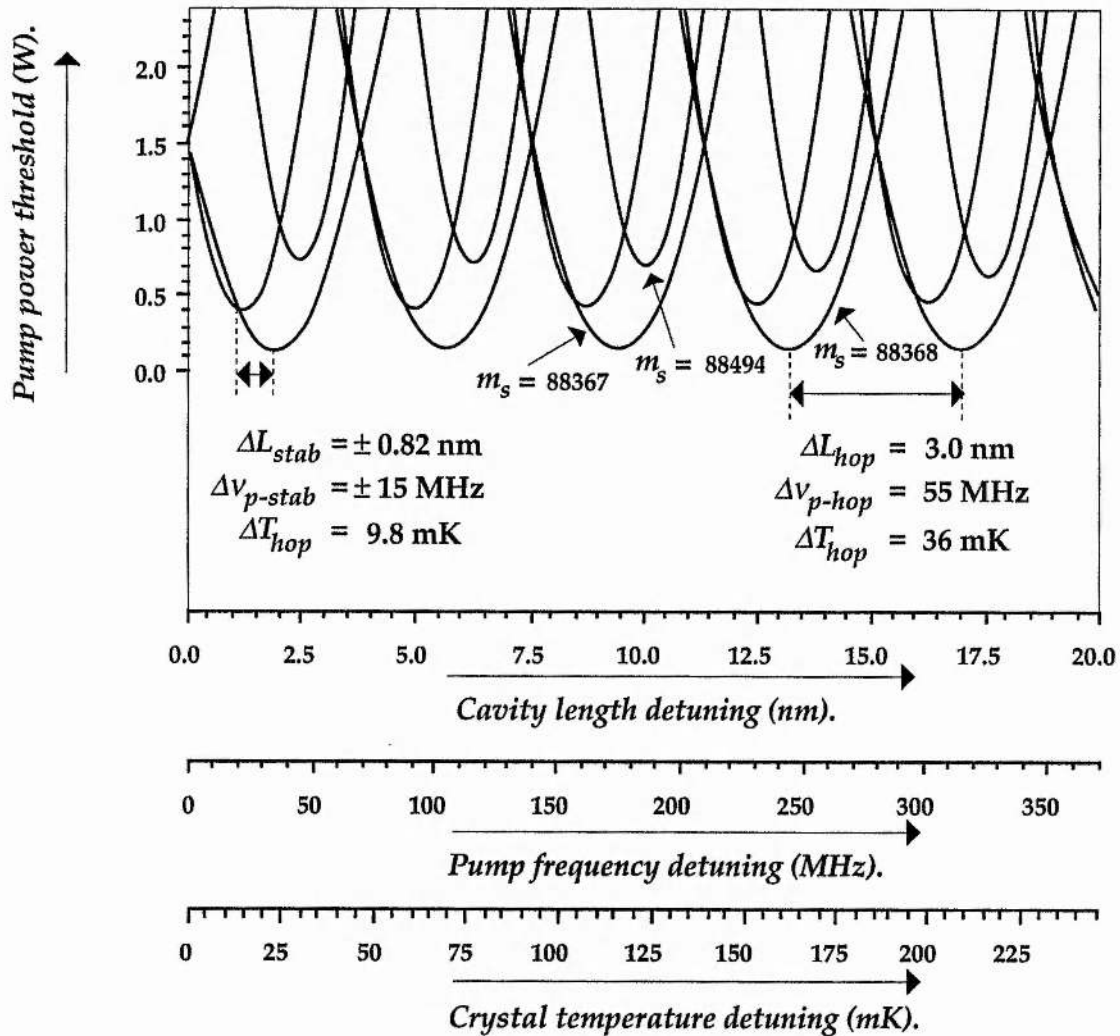


Figure II. 12.

The effects of detunings in the cavity length, the pump frequency, and the crystal temperature on the selection of the lowest threshold signal and idler mode-pairs, for the case of the type II phase-matching geometry near frequency-degeneracy.

For case (b) (type II phase-matching), the mode-selection properties are displayed in figure II. 12, where the mis-match in the free spectral ranges is significantly different to the type I geometry. Therefore, this system may exhibit cluster-hops. Any particular mode cluster is not guaranteed to have a mode-pair with good overlap, and the lowest threshold mode-pair may fall in a cluster away from perfect phase-matching. Tuning is characterized by the lowest threshold mode-pair hopping to a mode-pair in a neighbouring cluster, away from perfect phase-matching. After several cluster hops, the lowest threshold mode jumps back to an adjacent mode within the original cluster. It is revealing to contrast the thresholds between the mode-pairs in adjacent clusters with the mode-pairs in the central cluster. In general, the threshold for a signal/idler mode-pair in an adjacent cluster is significantly greater than those in the central cluster. Therefore, for pump powers close to threshold, the tuning of the OPO will be characterized by mode-hopping to an adjacent mode-pair within the same cluster. However, in contrast with type I phase-matching, the OPO will operate only for discrete values of the pump frequency and the OPO cavity length, near to mode-pair coincidences. This behaviour points towards stable operation on single signal and idler mode-pairs with sufficient control of the three tuning parameters.

The stability requirements for the two different configurations are displayed in table II. 3. The stringent temperature requirements are a consequence of the thermal expansion of the nonlinear material and at this level do not affect the phase-matching. Therefore, the temperature drift could be compensated by accurate, closed-loop control of the cavity lengths.

*Table II. 3.
Stability requirements to hold operation on a
single signal and idler frequency mode-pair in
a single-cavity, doubly-resonant OPO.*

	<i>Type I</i>	<i>Type II</i>
<i>Pump frequency</i>	± 0.24 MHz	± 15 MHz
<i>OPO cavity length</i>	± 0.1 nm	± 0.8 nm
<i>Crystal temperature</i>	± 0.3 mK	± 9.8 mK

A further comparison can be made between the modelling of the type II phase-matching geometry and equations II. 139 and II. 143, derived in the previous section for such an OPO configuration. Equations II. 139 and II. 143 predict cavity length and pump frequency stability requirements of $\Delta L_{stab} \approx \pm 0.86$ nm and $\Delta \nu_{p-stab} \approx \pm 12$ MHz, respectively, in good agreement with case (b) above. Further, equations II. 134 and II. 135 predict hopping between adjacent mode-pairs for cavity length and pump frequency shifts of $\Delta L_{hop} \approx \pm 3.2$ nm and $\Delta \nu_{p-hop} \approx \pm 42$ MHz, respectively.

In conclusion, type II phase-matching geometries offer significant advantages over type I geometries, given the same values of pump, signal, and idler frequencies. When type I phase-matched geometries are operated with signal and idler frequencies significantly removed from frequency degeneracy, then the mis-match in the signal and idler frequencies increases, and the mode-selection characteristics become similar to the type II geometry, analysed above.

Therefore, the critical parameter is the mis-match in the free spectral ranges of the signal and idler fields, regardless of the phase-matching geometry. However, the orthogonal signal and idler polarizations of type II phase-matching allow for further advantages in the frequency control of the OPO outputs, by assisting the formation of dual-cavity oscillators. (This topic is discussed further in chapter VI.)

II. 5 (ii) (b) (3) Doubly-resonant oscillator with a resonant pump field.

When the cavity is resonant also at the pump frequency, then the mode-selection properties of the doubly-resonant oscillator are further complicated. Similar to the effects of pump resonance on the outputs from the singly-resonant oscillator, the cavity length must satisfy first the requirement for pump resonance in order to reach oscillation threshold.

For most cavity configurations, the pump resonance condition will not alter significantly the mode-selection properties of the doubly-resonant oscillator. This is because the stability requirements to maintain operation on a single-frequency signal and idler mode-pair are generally more stringent than the requirements to maintain the pump frequency on resonance within the optical cavity. The mode-selection properties of the single-cavity doubly-

resonant oscillator with a pump enhanced field have been studied in detail in reference [20].

When the dual cavity configuration is employed, pump resonance conditions in either of the optical cavities will affect the range of smooth frequency tuning that can be provided from the dual-cavity resonator. The following analysis assumes again that the OPO operates with an intra-cavity pump field at twice the threshold intensity. For a resonant pump field within the idler cavity, the range over which the idler cavity can be scanned, while maintaining an OPO output, is given approximately by

$$\Delta L_i = \frac{c}{2\nu_p F_p} , \quad [\text{II. 155}]$$

where F_p is the finesse of the idler cavity for the pump field. This places an upper limit on the length over which the cavities can be scanned and therefore, a limit on the smooth tuning range of the dual-cavity OPO. The maximum tuning range can be expressed as follows:

$$|\Delta\nu_{i-max}| = |\Delta\nu_{s-max}| = \frac{FSR_i}{F_p} \frac{\nu_i}{\nu_p} . \quad [\text{II. 156}]$$

Similarly, if the pump frequency is resonant within the signal cavity, then the range of smooth frequency tuning becomes

$$|\Delta\nu_{s-max}| = |\Delta\nu_{i-max}| = \frac{FSR_s}{F_p} \frac{\nu_s}{\nu_p} . \quad [\text{II. 157}]$$

where F_p is the finesse of the signal cavity for the pump field.

II. 4 (iii) Summary.

The key equations governing the mode-selection within doubly-resonant OPOs are summarized in table II. 4.

Table II. 4.
Key stability and tuning expressions for
doubly-resonant optical parametric oscillators.

	<i>Single-cavity</i> $FSR_s \approx FSR_i \approx FSR$ $F_s \approx F_i \approx F$	<i>Dual-cavity</i> $FSR_s \gg FSR_i$
$\Delta L_{hop} \approx$	$\frac{c}{2v_p} \frac{\Delta n l}{(\bar{n}l + L)}$	
$\Delta v_{p-hop} \approx$	ΔFSR	
$\Delta L_{stab} \approx$	$\pm \frac{c}{2v_p F}$	$\pm \frac{c}{4v_s F_s}$
$\Delta v_{p-stab} \approx$	$\pm \frac{FSR}{F}$	$\pm \frac{FSR_s}{2F_s}$
<i>OPO tuning with a fixed pump frequency</i>		$\Delta L_s = -\Delta L_i \frac{v_s}{v_i} \frac{FSR_i}{FSR_s}$
<i>OPO tuning with a tunable pump frequency</i>	$\Delta L = -\Delta v_p \frac{c}{2v_p FSR}$	* $\Delta L_i = -\Delta v_p \frac{c}{2v_i FSR_i}$
<i>OPO tuning with a resonant pump field</i>		** $\Delta v_{s,i} \approx \frac{FSR_i}{F_p} \frac{v_i}{v_p}$

* Fixed signal cavity length.

** Pump resonant in idler cavity.

Although the analysis of this chapter has treated only linear cavity designs, the same conditions hold for ring cavity oscillators, with the appropriate modifications to the free spectral ranges. However, the transition from single- to dual-cavity oscillator is more complicated, as illustrated in figure II. 13.

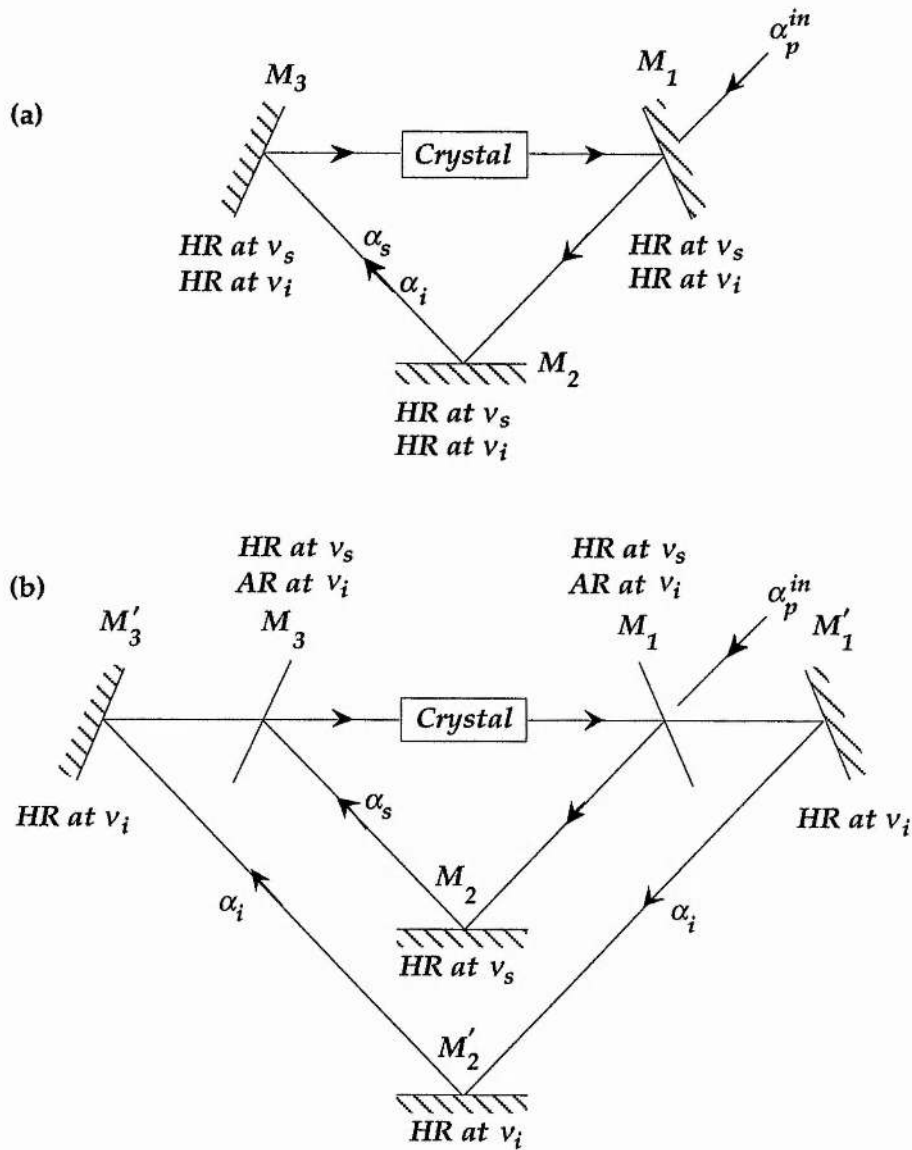


Figure II. 13.
The transition from (a) single-cavity to (b) dual-cavity oscillator,
for the case of ring cavity oscillators.

To operate a dual-cavity oscillator within a ring cavity configuration would require the use of two intra-cavity beamsplitters, as shown in figure II. 13. (Similar to the ring cavities described earlier, the ring cavity of figure II. 13 neglects the effects of astigmatism, caused by the intra-cavity fields interacting with the confining cavity mirrors at oblique angles. However, astigmatism is not an issue that affects OPO tuning characteristics, and further, can be compensated for easily by standard techniques.)

II. 6 Further properties of the doubly-resonant oscillator.

II. 6 (i) Phase-diffusion linewidths and coherence properties.

Of fundamental importance in the application of optical parametric oscillators to schemes that require high precision frequency outputs are the linewidths of the signal and idler frequencies and their difference frequency. In a theoretical study of the parametric oscillator [44], it was concluded that the signal-idler phase sum follows the pump phase, and that the phase difference undergoes phase diffusion. Therefore, the linewidths of the signal and idler frequencies have two noise sources: the fluctuation of the input pump source and the diffusion of the phase difference. This linewidth (half-width, half-maximum), for the case of a single-cavity resonator, is given by [44, 64]

$$\Delta\nu_{s,i} = \frac{F_{i,s}^2}{(F_s + F_i)^2} \Delta\nu_p + \frac{h\nu_{s,i}\pi^2}{P_{s,i}} \left(\frac{FSR^2}{(F_s + F_i)^2} + \frac{\Delta\nu^2}{4} \right) (\bar{n}_s + \bar{n}_i + 1) , \quad [\text{II. 158}]$$

where the terms have their usual meanings, \bar{n} is the average thermal photon number (analogous to the effects of spontaneous emission within laser oscillation), and single-cavity OPO operation is assumed with nearly-equal FSRs.

For nearly degenerate OPO operation ($F_s = F_i$), exact cavity resonances, and for optical frequencies ($\bar{n}_s = \bar{n}_i \ll 1$), equation II. 158 can now be reduced to

$$\Delta\nu_i = \Delta\nu_s = \frac{1}{4} \Delta\nu_p + \frac{h\nu_s\pi^2 FSR^2}{4P_s F_s^2} . \quad [\text{II. 159}]$$

The first term is due to the pump linewidth, and the second term is the quantum phase diffusion term, similar to the usual Schawlow-Townes laser linewidth [65], in which the amplification of spontaneous emission creates random phase fluctuations in the laser output.

The pump term of equation II. 159 indicates an output fractional stability of $1/2(\Delta\nu_p / \nu_p)$; a factor of two better than the pump source. To assess the effect of the phase-diffusion term, consider the example of a signal output with a frequency of $\nu_s = 3 \times 10^{14}$ Hz, an output power of $P_s = 10$ mW,

and a cavity spectral linewidth of $FSR/F = 1.5 \times 10^7 \text{ sec}^{-1}$. The phase diffusion linewidth is then $\approx 1 \text{ mHz}$, yielding a diffusion-limited fractional stability of 3 parts in 10^{18} . The difference frequency, δ , which is limited by phase diffusion, is therefore stable and can be easily phase-locked to a reference source.

When the signal and idler frequencies are removed from frequency degeneracy, then this allows for the interesting possibility of generating tunable radiation with ultra-narrow linewidths, as discussed in reference [64]. In a non-degenerate OPO with unequal finesses, $F_s \gg F_i$, the linewidth of the higher finesse signal wave can be significantly smaller than either the pump or idler linewidth. For example, consider a pump linewidth of $\Delta\nu_p \approx 10 \text{ kHz}$ and a 1:10 ratio in the signal and idler output coupling ($F_i = 0.1F_s$). Equation II. 158 predicts a pump induced signal frequency linewidth of $\Delta\nu_s \approx 90 \text{ Hz}$, compared with a linewidth of $\Delta\nu_s \approx 2.5 \text{ kHz}$ if the finesses are equal. The signal frequency can be determined by locking it to a reference atomic transition. Therefore, a signal frequency can be generated that is much more stable than the pump laser. This could provide an efficient and convenient way to generate tunable sources with extremely narrow linewidths for ultrahigh-resolution applications.

Experimental coherence studies of doubly-resonant OPOs have been limited by their extreme sensitivity to cavity stability and pump fluctuations. Recently, by using an all-solid-state pump source stabilized at the kHz-level, and a monolithic ring OPO resonator, pump / OPO phase-locking at degeneracy, pump / OPO phase correlations, signal-idler heterodyne measurements, and pump / OPO phase transmodulation, have been demonstrated [66]. To determine the OPO linewidth, a heterodyne beat-note measurement of the signal frequency from the OPO and an independent ring laser was performed. This showed that the OPO did in fact reproduce the linewidth of the pump laser. The OPO operated reliably at frequency degeneracy without any form of injection locking, and was a phase-locked sub-harmonic of the pump [66].

II. 6 (ii) Squeezed states of light.

Another application that takes advantage of the unique coherence properties of OPOs is squeezed light. The quantum fluctuations in the fields emitted by

optical parametric amplifiers (OPAs) and OPOs have been studied in great detail during the past few years [67]. The degenerate OPO and OPA have shown both in theory and in practice to produce non-classical light; i.e. quadrature-phase squeezed light.

The limits on the detection of small changes in amplitude of the electromagnetic field is of fundamental and practical importance in optical physics. While a variety of noise sources of technical origin often limit sensitivity, the fundamental limit on the detection of a small absorption of loss, μ , has been the so-called shot-noise limit, which sets a lower bound on the minimum detectable change δA of the coherent amplitude A of the field given by $\mu \cong \delta A/A \cong 1/\sqrt{N}$, where N is the number of photons from the input beam detected during the chosen integration time of the measurement. With conventional laser light in a coherent state, it is not possible to proceed further to a sensitivity greater than that specified by the shot-noise limit. Improvements in precision beyond the shot-noise limit can be realised by employing squeezed states of light. A squeezed state is characterized by a phase-dependent redistribution of quantum fluctuations such that the variance of one of two quadrature components of the field is reduced below that of the vacuum state [68].

In a non-degenerate OPA / OPO, there is almost perfect correlation between the signal and idler photon flux. This correlation can be used to generate photon states with substantially reduced photon-number variance. The correlation between the signal and idler fields can be accounted for only by a quantum treatment since the unexcited modes gain excitation by way of spontaneous parametric fluorescence.

The initial squeezed-state experiments used cw lasers to generate squeezing of the electro-magnetic field, either by four-wave mixing or by parametric amplification [69]. Because the nonlinear susceptibilities available for both these systems are small, it was necessary to enhance both the pump and the squeezed field within high-finesse cavities to obtain large degrees of squeezing.

In OPO photon counting experiments, the signal and idler channels are considered. The quantum parametric amplifier emits one photon into the idler channel for each photon which it adds to the signal channel, making it possible to observe non-classical photon correlations between the twin beams. In such an experiment, the photon noise is suppressed in the difference

between the intensities, $\Delta I = I_s - I_i$. Therefore, it is the signal-idler intensity difference that is squeezed, while the anti-squeezed variable is the phase-difference of the signal and idler frequencies.

When taken individually, the signal and idler beams show no such non-classical behaviour. In fact, either beam on its own should have statistics indistinguishable from narrow-band thermal light. On the other hand, these excess fluctuations are strongly correlated such that, for large gain in a lossless system, the quadrature amplitudes of the signal and idler beams become quantum copies of each other over a bandwidth set by the OPO linewidth.

In the OPO, one can expect an important quantum noise reduction for the following reasons: (i) It is based on a second order nonlinear process using a nonlinear crystal very far from its absorption band, having a very weak residual linear absorption. This device turns out to be almost free of excess noise sources; (ii) In the OPO, the ultimate quantum noise reduction factor, R , in the intensity difference, ΔI , between the twin beams is equal to

$$R = \left(\frac{\gamma' - \gamma}{\gamma'} \right)^2, \quad [\text{II. 160}]$$

or the ratio of useful to total round-trip losses in the resonator. This efficiency can be viewed as the ratio of the number of photons emitted from the OPO to the number that are created within the nonlinear medium. Therefore, the noise reduction factor, R , can be reduced by increasing the output coupling. However, the drawback to this is an increase in the pump power threshold. To allow for this, the use of the triply resonant oscillator is often applied; (iii) The noise reduction is particularly insensitive to changes in various parameters characterizing the system. These include pump field intensity, provided that the OPO is properly balanced (the mirror transmissions and the losses are the same for the signal and idler fields), and cavity detunings from the resonant fields. The noise reduction factor produced in experiments can be close to the value predicted by equation II. 160. In addition to intra-cavity loss mechanisms, the other limiting factor in squeezed state experiments is the imperfect quantum efficiencies of the detectors used to monitor the signal and idler channels, and the effect of slightly unbalanced detection channels for non-degenerate OPO frequencies.

Such experiments have all utilized single-frequency, cw pump sources in the green spectral region [13, 50, 52, 57, 58, 70, 71]. These sources have been either gas lasers operating at lasing transitions of $\nu_p \approx 600$ THz, or frequency-doubled near infra-red Nd:YAG lasers. The OPOs have been phase-matched to provide signal and idler frequencies close to frequency-degeneracy, with, in general, all three waves resonant within the OPO cavities. Both type I and type II phase-matched nonlinear materials have been used. In particular, when type II phase-matching is employed, this enables a convenient way to separate and monitor externally the intensities of the twin beams, and their noise spectrum. When the pump source is derived from a Nd:YAG laser fundamental, then this source can act as a local-oscillator frequency or phase-reference, against which the squeezed light can be compared [13]. It is possible to generate squeezed states from a sub-threshold, multi-mode OPO [50] (one pump mode, but a multitude of pairs of cavity modes for the signal and idler fields that satisfy both the cavity resonance conditions and the phase-matching requirements). This allows for the construction of a low-loss, single-port cavity without requiring frequency selectivity to enforce degenerate operation, and without the technical difficulties that accompany stable operation above threshold.

Substantial noise reductions below the shot-noise limit have been observed by a number of workers, with reduction factors in excess of $R \approx 50$ % reported. Potentially, the use of squeezed light affords a better performance than coherent-state light in high-sensitivity measurements, such as gravity-wave interferometry and spectroscopy.

II. 6. (iii) Frequency division and comb generation.

The most demanding application currently being proposed for cw OPOs is as optical frequency dividers [64]. As discussed earlier, a number of precision measurements are currently limited by the resolution of interferometric measurements to approximately 1 part in 10^{10} [72]. The capability of making precise frequency comparison and calibration will also be important to the areas of optical frequency standards and coherent communications.

In general, interferometric wavelength comparisons are limited by the uncertainties in the mirror phase-shifts. In order to meet future requirements of 10^{-15} or better resolution, non-interferometric direct

frequency measurements are necessary. Frequency synthesis chains have been constructed [73] involving harmonics of laser and klystron sources to compare, for example, the I₂-stabilized 633-nm He:Ne laser to the 9.2 GHz caesium clock.

A new technique of frequency division has been proposed recently [64], based on coherent down-conversion in an OPO. An OPO satisfies all the fundamental requirements of a frequency measurement and synthesis system: high efficiency, resolution, and precision, with frequency uncertainties that are limited by the inputs and not by the apparatus. A measurement of the output difference frequency of a nearly-degenerate OPO, $\delta = \nu_s - \nu_i$, in conjunction with the conservation of energy relation, $\nu_p = \nu_s + \nu_i$, determines precisely the signal and idler frequencies. Such a frequency divider is illustrated schematically in figure II. 14.

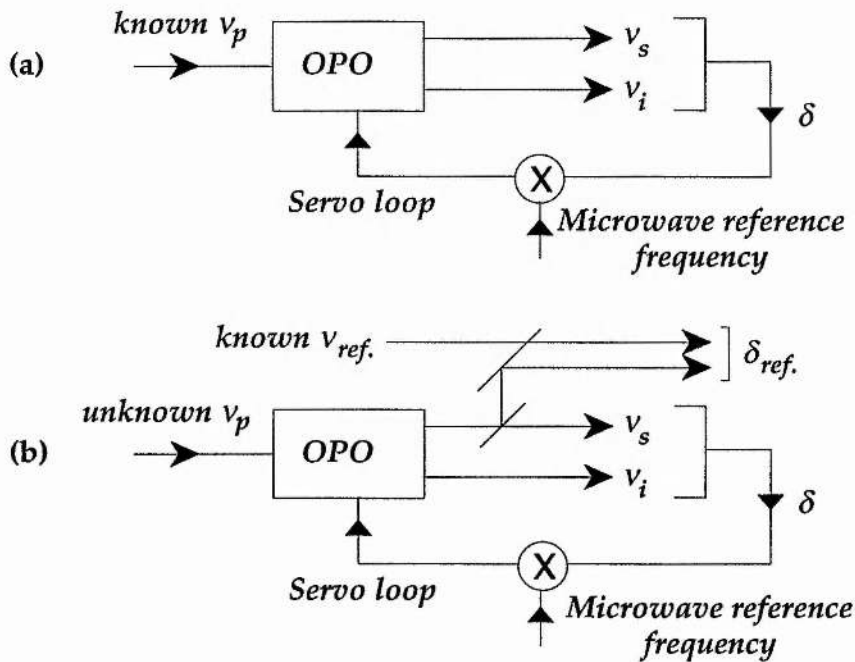


Figure II. 14.

Schematic configurations of an OPO divider for (a) synthesizing new frequencies, and (b) for measuring an unknown input frequency (from reference [64]).

As a frequency divider, the difference frequency can be phase-locked to a reference frequency source, such that the known input frequency is divided into two precisely known frequencies. Since δ is adjustable, the divider can operate as a frequency synthesizer. The frequency divider can be used also to measure accurately an unknown input frequency. Here δ is locked to the microwave reference and the signal frequency is measured by beating it with a reference optical frequency. The special case of exact division by two has been demonstrated [66], with self-phase locking at degeneracy. The outputs from a near degenerate KTP OPO have been offset-locked, using the above technique, resulting in a beat-note linewidth at the Hz-level [29, 30].

Extensions to this scheme involve cascading the frequency dividers in serial and parallel configurations to measure, synthesize and compare frequencies [74 - 76]. The parallel configuration could be adapted as a precision optical frequency comb generator over THz frequency bandwidths [75]. A single laser could act as the pump source for a set of OPOs whose evenly spaced outputs form the major frequency markers of the comb. The OPO outputs could then be externally modulated [77] to generate nearly overlapping combs of modulation sidebands that could serve as minor frequency markers and facilitate the phase locking of the OPOs.

Absolute frequency reference of the signal, idler and pump frequencies can be provided in frequency dividers by locking one of the three frequencies to an atomic or molecular resonance with kHz frequency precision. This technique is significant for metrology and spectroscopy, for which frequency chains are required across a variety of spectral bands, and for this, higher order phase-locked frequency dividers (3:1, 4:1,...) than the 2:1 frequency degenerate OPOs discussed above, are currently required.

II. 7 Mode-matching.

It was discussed in section II. 2 that the nonlinear coupling within the gain medium was dependent on the exact spatial overlap between the three fields. To obtain maximum benefit from the nonlinear interaction, the beams should be focused to small spot sizes within the nonlinear material to obtain high power densities.

In phase-matching geometries where propagation is significantly removed from a principal crystal axis, the effects of Poynting-vector walk-off

can present a limit to the size of the focused spots desired within the optical cavity. It is then necessary to compare the reduction in threshold from tight focusing, due to the high power densities, with the possible increase in loss due to walk-off caused by the tight spot sizes. These considerations are addressed regularly when operating pulsed OPOs in critical phase-matched geometries.

As discussed earlier, the low pump powers associated with cw lasers require that the effects due to Poynting-vector walk-off over the length of the gain region should be eliminated, or at a level that does not cause a large increase in the threshold of the OPO; see appendix I. It is reasonable to suggest that cw OPOs can only be operated above threshold by focusing the input pump radiation to small spot sizes to obtain high power densities. It was assumed that the optimum focusing of the fields in cw OPOs can be approximated by the analysis of section II. 2, in which the confocal parameters of the three waves were set equal to the length of the nonlinear crystal.

This section summarizes the basic equations that are relevant to the focusing requirements of cw OPOs. The beams considered are assumed to be lowest order fundamental fields (confined most strongly near the optical axis) with a Gaussian radial intensity distribution. In general, higher order transverse modes are suppressed in cw OPOs due to the magnitude of the gains involved compared to the diffraction losses experienced by higher order modes.

The most important mode-matching consideration involves matching the beam parameters of the input pump source to those desired within the OPO cavity for optimum coupling. These matching requirements become more stringent when the OPO cavity is designed to enhance the circulating pump field, in for example the triply-resonant oscillator. In this case, deviations from the conditions of exact mode-matching can result in decreased coupling of the input pump field into the OPO cavity.

Consider a nonlinear crystal of interaction length, l , situated within a linear, standing-wave, two-mirror, optical cavity with an empty (free-space) cavity length, L . The confocal parameter is defined by b and such that

$$b = 2z_R = 2 \left(\frac{\text{beam area}}{\lambda} \right) = \frac{2\pi n_j W_j^2}{\lambda_j} . \quad [\text{II. 161}]$$

where z_R is the Rayleigh range.

Setting the confocal parameter equal to the length of the crystal provides the optimum spot sizes for the three waves. This is because the region from $-z_R$ to $+z_R$ can be regarded as the focal zone, or the approximate-collimated region. Therefore, in this region (crystal), beam diffraction has less of an effect on the overlap of the three interacting waves over the length of the gain medium. The spot size of the waist ($1/e$ electric field radius) at the centre of the nonlinear crystal is then defined as follows:

$$W_j^2 = \frac{l\lambda_j}{2\pi n_j} . \quad [\text{II. 162}]$$

The spacing of the mirrors must provide these spot sizes, while simultaneously satisfying cavity stability for the resonator. In most cases, this is conveniently provided by placing two curved mirror surfaces either side of the crystal, equidistant from the crystal faces. While this provides a reliable method of satisfying the optimum focusing conditions, other possibilities must be considered. These include direct fabrication of the dielectric reflecting coatings on spherically curved crystal faces, thus forming compact and mechanically stable monolithic resonator configurations. However, this requires accurate polishing of the surfaces and cannot always be provided with given crystal growth procedures. Another variation involves asymmetric resonator designs with one extended optical mirror spacing that allows for the incorporation of intra-cavity components (e.g. within the dual-cavity resonator). For the remainder of this analysis, the resonators are assumed to be concave symmetric designs, but the method of analysis is valid for the other cavity configurations described above.

The most convenient procedure for location of the cavity mirrors is to propagate the desired Gaussian beam from the waist size at the centre of the nonlinear crystal, over a free-space distance, until the radius of curvature of the beam matches that of the chosen curved mirror surface. The spacing of the mirrors must then satisfy the following relation [78]:

$$R = \frac{2\pi^2 W_j^4}{\lambda_j^2 L'} + \frac{L'}{2} , \quad [\text{II. 163}]$$

where L' is the effective length of the cavity, as defined by

$$L' = L + (l/n_j) . \quad [\text{II. 164}]$$

Therefore, the cavity geometry, as dictated by the mirror curvatures, defines confocal focusing. Further, cavity stability is necessarily achieved since the wavefront curvatures match the mirror curvatures, thereby retracing the same (stable) pattern each time across the cavity. The next step involves ensuring that the pump source is properly mode-matched into this resonator. To provide this, the curvature / spot size of the incident pump beam (as characterized by the complex q -beam parameter [78]) is matched to that required in the OPO cavity.

Mode-matching can be accomplished by selecting the appropriate lens (or lenses) to transform the input pump beam accordingly. Given the sizes, $W_{p,laser}$ and $W_{p,OPO}$, of the input pump waist and the OPO cavity waist, respectively, and a lens of focal length, f , the position of this lens to match the two beams can be found by specifying the distances, d_{laser} and d_{OPO} , of the two waists, either side of the focusing lens, such that [78]

$$d_{laser} = f + \left(\frac{W_{p,laser}}{W_{p,OPO}} \sqrt{f^2 - f_c^2} \right) , \quad [\text{II. 165 (a)}]$$

$$d_{OPO} = f + \left(\frac{W_{p,OPO}}{W_{p,laser}} \sqrt{f^2 - f_c^2} \right) , \quad [\text{II. 165 (b)}]$$

where f_c is the minimum, or characteristic, focal length that can be used, and is given by [78]

$$f_c = \frac{\pi W_{p,OPO} W_{p,laser}}{\lambda_p} . \quad [\text{II. 166}]$$

Therefore, suitable mode-matching lenses can be selected if the waist sizes and their relative locations are known, either side of the focusing lens.

The above equations can be greatly simplified by assuming that the pump beam is being focused at a point in the far field of the beam divergence profile (i.e. at locations $\gg |z_R|$). Therefore, assuming that the focusing power

of the lens dominates over the initial divergence, the new waist (W_2) is located near to the focal point of the lens, and is of the size

$$W_2 = \frac{\lambda_p f}{\pi W_1} , \quad \text{[II. 167]}$$

where W_1 is the spot size at the lens.

Finally, note that equations [II. 165 (a)] and [II. 165 (b)] reduce to the classical Newton object/image expression if $f_c = 0$; i.e. the spot sizes are reduced to zero.

II. 8 Conclusions.

This chapter has outlined the theory required to model the performance of cw-pumped OPOs. It has focused on two main aspects: pump power thresholds and tuning characteristics. Both of these depend critically on the number of resonant fields within the OPO cavity, and the subsequent constraints placed on the cavity mirrors of the resonator.

Since the nature of these studies is three-wave mixing, then up to three fields can be brought to resonance within the OPO cavity. Their first effect is on the pump power threshold. As expected, increasing the number of resonant fields within the OPO results in lower pump power thresholds. Predictably, full benefit is achieved only when all the resonant fields satisfy simultaneously exact cavity resonances.

The detuning of resonant fields also plays an important role in the tuning characteristics of cw OPOs. To obtain smooth frequency tuning from cw OPOs, the fields that are subject to resonance conditions must be tuned together so that the energy conservation relation is always satisfied. There are several different methods for continuously tuning cw OPOs. The first consideration is whether or not the pump can be considered as a tuning parameter. This depends ultimately on the desired application. In any application that requires precisely determined, absolute frequencies, it is highly unlikely that the pump frequency can be considered to be tunable. For less demanding applications (e.g. spectroscopy), a tunable pump source may be tolerated.

When the pump frequency is tunable, then single-cavity, singly-resonant and doubly-resonant OPOs allow for multiple parameter tuning. For the singly-resonant device, the resonant OPO field can remain fixed or be scanned with the pump frequency. Either way, both sum and difference frequency selection arises. In the doubly-resonant OPO, tuning the pump frequency must be matched by both the signal and idler resonance conditions. The addition of pump resonance effects to lower the pump power thresholds can only be decoupled from the tuning characteristics by resonating the pump field in a separately formed build-up cavity that does not affect directly the signal and/or idler resonance conditions.

When using a fixed pump frequency, only truly singly-resonant OPOs allow for difference frequency control in a simplified, free-running manner. If doubly-resonant OPOs are to match this performance, they must be formed with independent cavity length control via dual-cavity resonators. Dual-cavity, doubly-resonant OPOs allow for pump power thresholds at the mW-level, smooth frequency tuning from either a fixed frequency pump source or a tunable pump source, and a convenient method of controlling independently the finesses and free spectral ranges of the signal and idler fields. The dual-cavity, doubly-resonant OPO can be regarded as the ideal OPO configuration for high precision frequency applications. Only when other applications are targeted in which the specifications are considerably relaxed (or when multi-watt, kHz, single-frequency lasers are available at any frequency from the ultra-violet to the mid-infra-red spectral regions) can other types of cw OPOs be considered.

This chapter also discussed conversion efficiencies in cw OPOs, mode-matching, and coherence properties of cw OPOs.

The internal conversion efficiencies of OPOs, irrespective of the fields resonated, are considerable. This is because, once above threshold, additional pump power is diverted directly to signal and idler photons. The main differences arise in the external conversion efficiencies, dictated by the resonance conditions of the OPOs. When the signal or idler fields are constrained to high finesse cavities, then, as expected, the ratio of useful to parasitic losses governs the external conversion efficiency. The most practical method of providing high external conversion efficiencies is to eliminate the resonance condition for either the signal or idler field, as in a singly-resonant oscillator. However, as with any optical resonator, high external conversion

efficiencies can always be obtained by operating well above threshold, and adjusting the output coupling such that this value is significantly above the other (parasitic) cavity losses. In general, the extreme dependence of the pump power threshold on cavity finesses does not allow for such flexibility in experimental designs.

The mode-matching of the three fields over the length of the gain medium can be achieved by setting the cavity mirror spacings/curvatures to fix the resonant transverse beam dimensions, and focusing the pump field to optimize the three wave interaction. The degree of overlap between the three fields is optimized when all the fields are approximately collimated (low diffraction effects) in the focal zone of the gaussian beam profile. Perhaps the most important case to consider is when the input pump field is itself resonant in the OPO cavity. In this case, the pump enhancement factor depends upon the precise spatial mode overlap between the intra- and extra-cavity pump fields.

While, in most cases, the stability of the OPO outputs is dictated by the pump frequency stability, the limit to the signal and idler frequency is determined by phase-diffusion effects. Whereas the sum of the signal and idler phases remains fixed, the phase-difference diffuses randomly, similar to the effects of spontaneous emission on the coherence of a laser oscillator.

References.

1. See the following review papers:
 - R. L. Byer,
in "Treatise in Quantum Electronics," (H. Rabin & C. L. Tang, Eds.), Academic Press, New York (1973).
 - R. G. Smith,
"Optical parametric oscillators,"
in "Lasers: a series of advances," vol. 4, (A. K. Levine & A. J. DeMaria Eds.) Marcel Dekker, New York, 189 (1976).
 - A. Yariv,
"Theory of the optical parametric oscillator,"
IEEE J. Quant. Electron. QE-2, 418 (1966).
 - V. W. Brunner, H. Paul, & A. Bandilla,
"The optical parametric oscillator. 1,"
Annalen der Physik. 7, 69 (1971).
2. J. A. Armstrong, N. Bloembergen, J. Ducuing, & P. S. Pershan,
"Interactions between light waves in a nonlinear dielectric,"
Phys. Rev. 127, 1918 (1962).

3. G. D. Boyd & D. A. Kleinman,
"Parametric interaction of focused Gaussian light beams,"
J. Appl. Phys. **39**, 3597 (1968).
4. J. F. Nye,
"Physical properties of crystals," Oxford University Press (1976).
5. F. Zernike & J. E. Midwinter,
"Applied nonlinear optics," Wiley Series in Pure & Applied Optics (S. S. Ballard Ed.)
John Wiley, New York (1973).
6. A. Yariv,
"Quantum electronics," 3rd Edn., John Wiley, Singapore (1989).
7. M. Zahler & Y. Ben-Aryeh,
"Loss effects in classical non-degenerate parametric amplifier,"
Opt. Comm. **79**, 361 (1990).
8. G. D. Boyd & A. Ashkin,
"Theory of parametric oscillator threshold with single-mode optical masers and
observation of amplification in LiNbO₃,"
Phys. Rev. **146**, 187 (1966).
9. W. Brunner & H. Paul,
in "Progress in Optics," (E. Wolf, Ed.), North-Holland, Amsterdam, p15 (1977).
10. S. T. Yang, R. C. Eckardt, & R. L. Byer,
"Continuous-wave singly resonant optical parametric oscillator pumped by a single-
frequency resonantly doubled Nd:YAG laser,"
Opt. Lett. **18**, 971 (1993).
"1.9-W cw ring-cavity KTP singly resonant optical parametric oscillator,"
Opt. Lett. **19**, 475 (1994).
11. S. T. Yang, R. C. Eckardt, & R. L. Byer,
"Power and spectral characteristics of continuous wave parametric oscillators: the
doubly to singly resonant transition,"
J. Opt. Soc. Am. B **10**, 1684 (1993).
12. See table I. 1 in chapter I of this thesis, and references therein.
13. L.-A. Wu, H. J. Kimble, J. L. Hall, & H. Wu,
"Generation of squeezed states by parametric down conversion,"
Phys. Rev. Lett. **57**, 2520 (1986).
14. M. J. Collett & D. F. Walls,
"Quantum limits to light amplifiers,"
Phys. Rev. Lett. **61**, 2442 (1988).
S. Reynaud & A. Heidmann,
"A semi-classical linear input output transformation for quantum fluctuations,"
Opt. Comm. **71**, 209 (1989).
N. C. Wong,
"Squeezed amplification in a non-degenerate parametric amplifier,"
Opt. Lett. **16**, 1698 (1991).
15. E. Hecht & A. Zojak,
in "Optics," Addison-Wesley, chapter 9 (1974).
16. J. A. Giordmaine & R. C. Miller,
"Tunable coherent parametric oscillation in LiNbO₃ at optical frequencies,"
Phys. Rev. Lett. **14**, 973 (1965).
"Optical parametric oscillation in LiNbO₃,"
in "Physics of Quantum Electronics," (P. L. Kelly, B. Lax, & P. E. Tannenwald Eds.),
McGraw-Hill, New York (1966).
17. R. C. Eckardt, C. D. Nabors, W. J. Kozlovsky, & R. L. Byer,
"Optical parametric oscillator frequency tuning and control,"
J. Opt. Soc. Am. B **8**, 648 (1991).
18. A. E. Siegman,
"Lasers," University Science Books (1986).
19. S. Guha, F.-J. Wu, & J. Falk,
"The effects of focusing on parametric oscillation,"
IEEE J. Quant. Electron. QE-18, 907 (1982).

- R. Fischer, C. Tran-ba, & L. W. Wiczorek,
"Optimal focusing in a singly resonant optical parametric oscillator,"
Sov. J. Quant. Electron. 7, 1455 (1978).
20. T. Debuisschert, A. Sizmann, E. Giacobino, & C. Fabre,
"Type-II continuous-wave optical parametric oscillators: oscillation and frequency-tuning characteristics,"
J. Opt. Soc. Am. B 10, 1668 (1993).
21. J. E. Bjorkholm,
"Analysis of the doubly resonant optical parametric oscillator without power-dependent reflections,"
IEEE J. Quant. Electron. QE-5, 293 (1969).
J. E. Bjorkholm, A. Ashkin, & R. G. Smith,
"Improvement of optical parametric oscillators by non-resonant pump reflection,"
IEEE J. Quant. Electron. QE-6, 797 (1970).
22. R. Fischer,
Exp. Technik der Physik XIX, 193 (1971).
23. A. E. Siegman,
"Nonlinear optical effects: an optical power limiter,"
Appl. Opt. 1, 739 (1962).
24. S. E. Harris,
"Tunable optical parametric oscillators,"
Proc. IEEE 57, 2096 (1969).
25. P. P. Bey & C. L. Tang,
"Plane-wave theory of parametric oscillator and coupled oscillator-upconverter,"
IEEE J. Quant. Electron. QE-8, 361 (1972).
26. M. Ebrahimzadeh, G. P. A. Malcolm, & A. I. Ferguson,
"Continuous-wave mode-locked optical parametric oscillator synchronously pumped by a diode-laser-pumped solid-state laser,"
Opt. Lett. 17, 183 (1992).
F. G. Colville, M. Ebrahimzadeh, W. Sibbett, & M. H. Dunn,
"Continuous-wave LiB_3O_5 optical parametric oscillator pumped by a tunable Ti:sapphire laser,"
Appl. Phys. Lett. 64, 1765 (1994).
27. R. L. Byer, R. L. Herbst, & R. N. Fleming,
"A broadly tunable IR source,"
in "Laser spectroscopy," (S. Haroche, J. C. Peabay-Peyroula, T. W. Hansch, & S. E. Harris Eds.), Springer-Verlag, Berlin, 207 (1975).
28. N. I. Adams III & J. J. Barrett,
"Electric field control of 90° phase-matching in KDP,"
IEEE J. Quant. Electron. QE-2, 430 (1966).
L. B. Kreuzer,
"Ruby-laser-pumped optical parametric oscillator with electro-optic effect tuning,"
Appl. Phys. Lett. 10, 336 (1967).
29. D. Lee & N. C. Wong,
"Tunable optical frequency division using a phase-locked optical parametric oscillator,"
Opt. Lett. 17, 13 (1992).
30. D. Lee & N. C. Wong,
"Stabilization and tuning of a doubly-resonant optical parametric oscillator,"
J. Opt. Soc. Am. B 10, 1659 (1993).
31. B. Tatian,
"Fitting refractive-index data with the Sellmeier dispersion formula,"
Appl. Opt. 23, 4477 (1984).
32. O. N. Stavroudis & L. E. Sutton,
"Rapid method for interpolating refractive index measurements,"
J. Opt. Soc. Am. 51, 368 (1961).

33. J. Falk,
"Instabilities in the doubly resonant parametric oscillator: a theoretical analysis,"
IEEE J. Quant. Electron. QE-7, 230 (1971).
34. R. G. Smith,
"A study of factors affecting the performance of a continuously pumped doubly resonant optical parametric oscillator,"
IEEE J. Quant. Electron. QE-9, 530 (1973).
35. M. J. Padgett, F. G. Colville, & M. H. Dunn,
"Mode selection in doubly-resonant optical parametric oscillators,"
In press, IEEE J. Quant. Electron..
36. S. Schiller & R. L. Byer,
"Quadruply resonant optical parametric oscillation in a monolithic total-internal-reflection resonator,"
J. Opt. Soc. Am. B 10, 1696 (1993).
37. A. I. Kovrigin & R. L. Byer,
"Stability factor for optical parametric oscillators,"
IEEE J. Quant. Electron. QE-5, 384 (1969).
38. C. D. Nabors, R. C. Eckardt, W. J. Kozlovsky, & R. L. Byer,
"Efficient, single-axial-mode operation of a monolithic MgO:LiNbO₃ optical parametric oscillator,"
Opt. Lett. 14, 1134 (1989).
39. W. J. Kozlovsky, C. D. Nabors, R. C. Eckardt, & R. L. Byer,
"Monolithic MgO:LiNbO₃ doubly resonant optical parametric oscillator pumped by a frequency-doubled diode-laser-pumped Nd:YAG laser,"
Opt. Lett. 14, 66 (1989).
40. W. J. Kozlovsky, C. D. Nabors, & R. L. Byer,
"Second-harmonic generation of a continuous-wave diode-pumped Nd:YAG laser using an externally resonant cavity,"
Opt. Lett. 12, 1014 (1987).
41. T. J. Kane & R. L. Byer,
"Monolithic, unidirectional single-mode Nd:YAG ring laser,"
Opt. Lett. 10, 65 (1985).
42. S. E. Harris,
"Threshold of multimode parametric oscillators,"
IEEE J. Quant. Electron. QE-2, 701 (1966).
43. J. E. Bjorkholm,
"Some properties of doubly and singly resonant optical parametric oscillators,"
Appl. Phys. Lett. 13, 399 (1968).
44. R. Graham & H. Haken,
"The quantum-fluctuations of the optical parametric oscillator,"
Z. Phys. 210, 276 (1968).
45. F. G. Colville, M. J. Padgett, & M. H. Dunn,
"Continuous-wave, dual-cavity, doubly-resonant, optical parametric oscillator,"
Appl. Phys. Lett. 64, 1490 (1994).
46. F. G. Colville, M. J. Padgett, & M. H. Dunn,
"Continuous-wave, dual-cavity, doubly-resonant, optical parametric oscillator,"
in *Digest of Topical Meeting on Advanced Solid-State Lasers*, paper AWA3 (1994).
F. G. Colville, M. J. Padgett, & M. H. Dunn,
"Smooth frequency tuning from optical parametric oscillators: the transition from single- to dual-cavity oscillators,"
in *Proceedings of Topical Meeting on Advanced Solid-State Lasers*, (1994).
47. D. Lee & N. C. Wong,
"Tuning characteristics of a cw dual-cavity KTP optical parametric oscillator,"
in *Conference on Lasers and Electro-Optics*, Vol. 8 of OSA 1994 Technical Digest Series (Optical Society of America, Washington, D. C., 1994), paper CWE 5.
48. N. C. Wong,
"Gravity-wave detection via an optical parametric oscillator,"
Phys. Rev. A 45, 3176 (1992).

49. R. G. Smith, J. E. Geusic, H. J. Levinstein, J. J. Rubin, S. Singh, & L. G. Van Uitert,
"Continuous optical parametric oscillation in $Ba_2NaNb_5O_{15}$,"
Appl. Phys. Lett. **12**, 308 (1968).
50. L.-A. Wu, M. Xiao, & H. J. Kimble,
"Squeezed states of light from an optical parametric oscillator,"
J. Opt. Soc. Am. B **4**, 1465 (1987).
51. F. G. Colville, A. J. Henderson, J. Zhang, M. J. Padgett, & M. H. Dunn,
"Continuous-wave parametric oscillation in lithium triborate,"
Opt. Lett. **18**, 205 (1993).
52. E. S. Polzik, J. Carri, & H. J. Kimble,
"Spectroscopy with squeezed light,"
Phys. Rev. Lett. **68**, 3020 (1992).
53. R. G. Smith & J. V. Parker,
"Experimental observation of and comments on optical parametric oscillation internal
to the laser cavity,"
J. Appl. Phys. **41**, 3401 (1970).
54. R. L. Byer, M. K. Oshman, J. F. Young, & S. E. Harris,
"Visible cw parametric oscillator,"
Appl. Phys. Lett. **13**, 109 (1968).
55. R. L. Byer, A. Kovrigin, & J. F. Young,
"A cw ring-cavity parametric oscillator,"
Appl. Phys. Lett. **15**, 136 (1969).
56. C. Laurence & F. Tittel,
"Visible cw parametric oscillator using barium sodium niobate,"
J. Appl. Phys. **42**, 2137 (1971).
57. T. Debuisschert, S. Reynaud, A. Heidmann, E. Giacobino, & C. Fabre,
"Observation of large quantum noise reduction using an optical parametric oscillator,"
Quant. Opt. **1**, 3 (1989).
S. Reynaud, C. Fabre, & E. Giacobino,
"Quantum fluctuations in a two-mode parametric oscillator,"
J. Opt. Soc. Am B **4**, 1520 (1987).
A. Heidmann, R. J. Horowicz, S. Reynaud, E. Giacobino, & C. Fabre,
"Observation of quantum noise reduction on twin laser beams,"
Phys. Rev. Lett. **59**, 2555 (1987).
58. P. Grangier, R. E. Slusher, B. Yurke, & A. LaPorta,
"Squeezed-light-enhanced polarization interferometer,"
Phys. Rev. Lett. **59**, 2153 (1987).
59. F. G. Colville, M. J. Padgett, A. J. Henderson, J. Zhang, & M. H. Dunn,
"Continuous-wave parametric oscillator pumped in the ultra-violet,"
Opt. Lett. **18**, 1065 (1993).
60. C. Chen, Y. Wu, A. Jiang, B. Wu, G. You, R. Li, & S. Lin,
"New nonlinear-optical crystal: LiB_3O_5 ,"
J. Opt. Soc. Am. B **6**, 616 (1969).
Laser focus world,
"Chinese lab grows new nonlinear borate crystals,"
p129, November 1989.
61. S. Lin, J. Y. Huang, J. Ling, C. Chen, & Y. Shen,
"Optical parametric amplification in a lithium triborate crystal tunable from 0.65 to
2.5 μm ,"
Appl. Phys. Lett. **59**, 1541 (1991).
62. S. Velsko, M. Webb, L. Davis, & C. Huang,
"Phase-matched harmonic generation in lithium triborate (LBO),"
IEEE J. Quant. Electron. **QE-27**, 2182 (1991).
63. L. Wei, D. Guiging, H. Qingzhen, Z. An, & L. Jingkui,
"Anisotropic thermal expansion of LiB_3O_5 ,"
J. Phys. D **23**, 1073 (1990).

64. N. C. Wong,
"Optical frequency division using an optical parametric oscillator,"
Opt. Lett. **15**, 1129 (1990).
65. A. L. Schawlow & C. H. Townes,
"Infrared and optical masers,"
Phys. Rev. **112**, 1940 (1958).
66. C. D. Nabors, S. T. Yang, T. Day, & R. L. Byer,
"Coherence properties of a doubly-resonant monolithic optical parametric oscillator,"
J. Opt. Soc. Am. B **7**, 815 (1990).
67. See, e.g. the feature issue on squeezed states of the electromagnetic field,
J. Opt. Soc. Am. B **4**, (H. J. Kimble & D. F. Walls, Eds.), 1450-1741 (1987).
68. See the following review papers:
L. Mandel,
"Fluctuations of light beams,"
in "Progress in Optics," (E. Wolf, Ed.), North-Holland, Amsterdam, p181 (1963).
M. C. Teich & B. E. A. Saleh,
"Photon bunching and antibunching,"
in "Progress in Optics," (E. Wolf, Ed.), North-Holland, Amsterdam, p1 (1988).
D. F. Walls,
"Squeezed states of light,"
Nature **306**, 141 (1983).
"Light gets a quantum squeeze,"
New Scientist **19**, 41 (1991).
C. Fabre, E. Giacobino, & P. Grangier,
"Quand l'OPO fait mieux que le laser,"
La Recherche **198**, 540 (Vol. 19, 1988).
M. C. Teich & B. E. A. Saleh,
"Squeezed and antibunched light,"
Physics Today, 26 (June, 1990).
69. C. M. Savage & D. F. Walls,
"Squeezing by parametric oscillation and intracavity four-wave mixing,"
J. Opt. Soc. Am. B **4**, 1514 (1987).
B. Yurke & R. E. Slusher,
in "Quantum Optics IV," (J. D. Harvey & D. F. Walls, Eds.), Springer-Verlag, New York (1986).
R. M. Shelby, M. D. Levenson, S. H. Perlmutter, R. G. DeVoe, & D. F. Walls,
"Broad-band parametric deamplification of quantum noise in an optical fibre,"
Phys. Rev. Lett. **57**, 691 (1986).
70. C. D. Nabors & R. Shelby,
"Two-colour squeezing and sub-shot-noise signal recovery in doubly resonant optical parametric oscillators,"
Phys. Rev. A **42**, 556 (1990).
71. K. W. Leong, N. C. Wong, & J. M. Shapiro,
"Nonclassical intensity correlation from a type I phase-matched optical parametric oscillator,"
Opt. Lett. **15**, 1058 (1990).
72. P. Zhao, W. Lichten, Z.-X. Zhou, H. P. Layer, & J. Bergquist,
"Rydberg constant and fundamental atomic physics,"
Phys. Rev. A **39**, 2888 (1989).
E. A. Hildum, U. Boesl, D. H. McIntyre, R. G. Beausoleil, & T. W. Hansch,
"Measurement of the 1S-2S frequency in atomic hydrogen,"
Phys. Rev. Lett. **56**, 576 (1986).
J. R. M. Barr, J. M. Girkin, J. M. Tolchard, & A. I. Ferguson,
"Interferometric measurement of the $1S_{1/2}$ - $2S_{1/2}$ transition frequency in atomic hydrogen,"
Phys. Rev. Lett. **56**, 580 (1986).

73. D. A. Jennings, C. R. Pollock, F. R. Petersen, K. M. Evenson, J. S. Wells, J. L. Hall, & H. P. Layer,
 "Direct frequency measurement of the I₂-stabilized He-Ne 473-THz (633-nm) laser,"
Opt. Lett. **8**, 136 (1983).
- O. Acef, J. J. Zondy, M. Abed, D. G. Rovera, A. H. Gerard, A. Clairon, Ph. Laurent, Y. Millerioux, & P. Juncar,
 "A CO₂ to visible optical frequency synthesis chain: accurate measurement of the 473 THz HeNe/I₂ laser,"
Opt. Comm. **97**, 29 (1993).
74. K. Nakagawa, M. Kourogi, & M. Ohtsu,
 "Proposal of a frequency-synthesis chain between the microwave and optical frequencies of the Ca intercombination line at 657 nm using diode lasers,"
Appl. Phys. B **57**, 425 (1993).
75. N. C. Wong,
 "Optical frequency counting from the UV to the near IR,"
Opt. Lett. **17**, 1155 (1992).
76. N. C. Wong,
 "Proposal for a 10 THz precision optical frequency comb generator,"
IEEE Phot. Tech. Lett. **4**, 1166 (1992).
- W. Wang & M. Ohtsu,
 "Continuous-wave optical parametric amplifier that uses a diode laser for a wideband coherent optical frequency sweep generator,"
Opt. Lett. **18**, 876 (1993).
- K.-P. Ho & J. Kahn,
 "Optical frequency comb generator using phase modulation in amplified circulating loop,"
IEEE Phot. Tech. Lett. **5**, 721 (1993).
- M. Kourogi, K. Nakagawa, & M. Ohtsu,
 "Wide-span optical frequency comb generator for accurate optical frequency difference measurement,"
IEEE J. Quant. Electron. **QE-29**, 2693 (1993).
77. L. R. Brothers, D. Lee, & N. C. Wong,
 "Terahertz optical frequency comb generation and phase locking of an optical parametric oscillator at 665 GHz,"
Opt. Lett. **19**, 245 (1994).
- H. R. Telle, D. Meschede, & T. W. Hansch,
 "Realization of a new concept for visible frequency division: phase locking of harmonic and sum frequencies,"
Opt. Lett. **15**, 532 (1990).
78. H. Kogelnik & T. Li,
 "Laser beams and resonators,"
Appl. Opt. **5**, 1550 (1966).
- A. G. Fox & T. Li,
 "Resonant modes in a maser interferometer,"
Bell Sys. Tech. J. **40**, 498 (1961).

Chapter III.

Pump sources and nonlinear materials.

Contents.	Page.
III. 1 Introduction.	123
III. 2 Pump sources.	126
III. 3 Nonlinear materials.	135
III. 4 Conclusions.	162
III. 5 Outline of experimental work described in this thesis.	165
References.	166

III. 1 Introduction.

In general, the steady development of optical parametric oscillators (OPOs) has relied upon the widespread availability of high power, narrow-linewidth pump lasers, and high quality nonlinear optical materials. This has been especially true for continuous-wave (cw) OPOs, where the pump source and nonlinear material specifications are at their most stringent. This chapter examines the properties of currently available pump sources and nonlinear materials that can be considered for use within cw OPO systems. The pump threshold and stability requirements are compared when using pump sources operating in different spectral regions, and when resonating various fields within the OPO cavities. The phase-matching configurations of the different nonlinear media are discussed, with the emphasis on generating amplitude and frequency stable outputs.

Following the initial demonstrations of cw OPOs [1, 2], their reliable operation was hampered mainly by a lack of suitable pump sources and nonlinear optical materials. In the late 1960s, the highest power single-frequency radiation in the visible spectral region was obtained from argon-ion lasers [3 - 5]. In general, these gas lasers are inefficient, difficult to stabilize in frequency, and can be tuned in frequency over a narrow spectral region, as defined by the gain-bandwidths of the lasing transitions. As pump sources for cw OPOs, argon-ion lasers are of limited use, other than to investigate the

frequency properties of specific OPO configurations / phase-matching geometries. These initial cw OPOs operated with multi-longitudinal-mode pump sources. As expected, the spectral outputs from these devices were unsatisfactory, caused by the random phase and amplitude distribution associated with multi-mode operation of the pump sources, and their corresponding effect on the frequency mode selection from the OPOs.

The first demonstration of frequency stability in the output of a cw OPO was reported in 1973 in reference [6], which compared the use of argon-ion lasers and frequency-doubled Nd:YAG lasers as the pump source for an OPO with signal and idler frequencies near degeneracy. The OPO cavity finesses were altered to provide increased output power levels when operating significantly above threshold. When the pump source was isolated effectively, and was actively stabilized on a single-frequency, the output of the OPO maintained some degree of stability on single-frequency mode-pairs, although only for time periods of a few seconds [6].

The most positive conclusion that can be drawn from the early research into cw OPOs was that these devices could operate consistently above threshold with pump power thresholds at the mW-level if the pump beam was focused to provide optimum spatial overlap with doubly-resonant, high finesse, signal and idler fields. Pump sources operating only in the green spectral region, and OPO operation with signal and idler frequencies near frequency degeneracy [1, 7, 8] or in a near 3:1 frequency ratio [2, 9, 10], had been demonstrated in these initial designs. This limited range of output frequencies was due to the lack of available cw pump sources in other spectral regions, and a lack of high quality nonlinear materials that could provide suitable phase-matching geometries for these pump frequencies. These early cw OPOs had used the nonlinear materials lithium niobate (LiNbO_3) [2, 9], and barium sodium niobate ($\text{BaNaNb}_5\text{O}_{15}$) [1, 6 - 8, 10] in temperature-tuned, type I non-critical phase-matching geometries. These materials had been selected for use within cw OPOs due to information that had been obtained from their more regular application as second-harmonic frequency converters of near infra-red laser sources [11 - 13], and in particular for converting the radiation from Nd:YAG lasers to the visible spectral region.

The more general conclusion from this early research was that cw OPOs displayed erratic and unstable behaviour, and would require a level of pump frequency stability that was not then available. In addition, nonlinear

materials were yet to be developed that could prevent the familiar problems of crystal damage, caused by tightly focused pump spot sizes and high intra-cavity circulating fields.

Given the emergence of dye laser technology throughout the 1970s, it was hardly surprising that reports of cw OPOs were confined only to brief mentions within the summaries of OPO work during this period [14 - 16]. Dye lasers were marketed shortly after their initial demonstrations [17], and cw devices could be tuned over extensive frequency bandwidths in the visible and near infra-red spectral regions [18]. Their wide tunability was only one advantage: more specifically, dye lasers could be pumped by the standard multi-line output from ion lasers, could operate with cw powers at the Watt-level [19], could easily attain single-frequency operation [20], and could be actively stabilized to kHz-frequency precision [21]. Therefore, some of the most desirable attributes of a workable cw OPO based system could be obtained from a commercially-available product.

Despite the obvious advantages of dye lasers over cw OPOs in the visible spectral region for smooth / coarse, narrow-linewidth, frequency tuning, research involving cw OPOs was re-examined in the early 1980s. Their use was not then for widely tunable radiation from a single pump / crystal geometry, but rather, within high precision applications that utilized some of the unique properties of cw OPOs, as discussed in section II. 6.

The development of compact, efficient, narrow-linewidth, and frequency-stable, all-solid-state, diode-laser-pumped Nd-based lasers [22], and the introduction of new high-quality nonlinear optical materials [23], allowed for this renewed interest in cw OPOs. Nonlinear materials include magnesium oxide doped lithium niobate ($\text{MgO}:\text{LiNbO}_3$) [24], potassium titanyl phosphate (KTP) [23], lithium triborate (LBO) [24] and potassium niobate (KNbO_3) [25]. This has allowed for the application of cw OPOs to produce squeezed states of light, with signal - idler intensity correlations below the shot-noise level [28, 29]. The materials used within this context were KTP [29, 30, 31], $\text{MgO}:\text{LiNbO}_3$ [32, 33], and KNbO_3 [34]. The pump sources were either frequency stabilized argon / krypton-ion lasers [30, 31] or frequency-doubled Nd:YAG lasers [32, 33]. To date, this area of research constitutes the only application that has been able to utilize the properties of cw OPOs. (Other less researched applications include high-resolution

spectroscopy [34], optical frequency division [35], and optical frequency comb generation [36 - 38].)

At present, the emphasis of the research involving cw OPO development is not concerned with the coarse frequency tuning properties available from these devices, or their immediate packaging through a commercial product, but is geared towards the new challenges within applications that require high-precision, frequency-stable outputs [39 - 43]. These are the schemes involving cw OPOs as optical frequency dividers within frequency chains spanning the optical spectrum [35 - 38].

The pump sources required for optical frequency division techniques should be frequency-tunable, narrow-linewidth, and high-power single-frequency lasers, or their frequency harmonics. Pump frequency tuning is essential to operate the frequency divider with specific frequency ratios, allowed from the freedom in selecting both the sum and difference frequencies of the OPO outputs [44], and these can be referenced to known and / or unknown frequency sources. Without any frequency reference markers, the cw OPO remains simply an interesting frequency down-converter of visible laser radiation.

One of the most urgent requirements for such optical frequency division schemes is to demonstrate stable cw OPOs that can use tunable lasers (or their frequency harmonics) in different spectral regions, as their pump sources. For this, phase-matching geometries that can deliver desired integral ratios of signal:idler frequency outputs (1:1 [39, 41], 2:1, 3:1, etc.), and can be tuned smoothly in frequency over \approx GHz-bandwidths [41, 43] around a reference frequency marker need be identified.

III. 2 Pump sources.

This section considers the requirements on the pump sources for cw OPOs. The equations are recalled from chapter II for the pump power thresholds, and for the pump frequency stability to maintain amplitude and frequency stable operation of the cw OPO on single-frequency signal and idler mode-pairs. Typical values are calculated, and compared directly to the pump sources that are currently available for use. Finally, there is a discussion of the pump sources that are most likely to emerge within the next few years that will be suitable for incorporation within cw OPO applications.

The first critical requirement for the pump source is the pump power required to reach threshold for the OPO. Recall that there are several different cavity variations available, which are outlined in chapter II, and that these provide different expressions for the pump power threshold of the OPO. These cavity designs can be divided broadly into three categories; singly, doubly, and triply-resonant oscillators. The pump power thresholds for these systems were summarized in section II. 3. The equations for the minimum pump power thresholds (in units of Watts) for the three above-mentioned configurations are as follows:

$$\text{Singly-resonant : } \left(P_p^{in} \right)_{th-min} = \frac{n_p^2 \epsilon_0 c^4}{2\pi^2 l |d_{eff}|^2 v_p^3} \times \frac{\pi}{F_i} , \quad [\text{III. 1}]$$

$$\text{Doubly-resonant : } \left(P_p^{in} \right)_{th-min} = \frac{n_p^2 \epsilon_0 c^4}{2\pi^2 l |d_{eff}|^2 v_p^3} \times \frac{\pi^2}{F_s F_i} , \quad [\text{III. 2}]$$

$$\text{Triply-resonant : } \left(P_p^{in} \right)_{th-min} = \frac{n_p^2 \epsilon_0 c^4}{2\pi^2 l |d_{eff}|^2 v_p^3} \times \frac{\pi^2}{4F_s F_i E_{p-max}} , \quad [\text{III. 3}]$$

where it is assumed that the signal and idler frequencies are approximately equal, and that there are no additional double-pass pump conditions, as discussed in chapter II. (Operation away from frequency-degeneracy requires simply an additional multiplicative factor to the following analysis. In addition, these minimum pump power thresholds assume that the resonant waves satisfy exact cavity resonances.)

To obtain realistic experimental pump power values, the following typical values are inserted into the above equations:

$$l = 20 \text{ mm}, \quad d_{eff} = 3 \text{ pm/V}, \quad n_p = 1.6 . \quad [\text{III. 4}]$$

For resonant OPO fields, the signal and idler finesses are assumed to be $F_s \approx F_i \approx 300$, and for resonant pump fields, the maximum pump field enhancement is assumed to be $E_{p-max} \approx 10$.

Threshold values are calculated now for pump sources operating in different spectral regions (ultra-violet, visible, and near infra-red),

corresponding to frequencies (wavelengths) of $\nu_p = 1000$ THz ($\lambda_p = 300$ nm : ultra-violet), $\nu_p = 500$ THz ($\lambda_p = 600$ nm : visible) and $\nu_p = 250$ THz ($\lambda_p = 1.2$ μm : infra-red). The results are displayed in table III. 1.

Table III. 1.
Pump power thresholds.

	Pump frequency, ν_p Pump wavelength, λ_p		
	1000 THz 0.3 μm	500 THz 0.6 μm	250 THz 1.2 μm
<i>Singly resonant oscillator</i> (Watts)	0.54	4.32	34.6
<i>Doubly resonant oscillator</i> (mW)	5.66	45.3	362
<i>Triply resonant oscillator</i> (mW)	0.14	0.57	2.27

There are two important distinctions that can be interpreted from the above analysis. First, due to the dependence of the pump power threshold with the inverse of the third power of the pump frequency, significant reductions in pump power threshold can be obtained by using the higher energy photons associated with short-wavelength, ultra-violet pump sources [45]. Second, as expected, the pump power thresholds for singly-resonant oscillators are significantly higher than those of the other cavity geometries [46]. The lowest thresholds ($P_{p-th}^{in} \approx \mu\text{W}$) are obtained when all three waves are resonant, as in the case of the triply-resonant oscillator [30 - 32].

These figures can be related to those values of pump power threshold that have been reported from experimental cw OPO configurations. The only singly-resonant oscillator reported to date has operated, as expected, with a threshold at the Watt-level, for a pump source in the visible spectral region [46, 47]. Doubly- and triply-resonant oscillators have operated consistently with pump power thresholds at the mW-level for pump sources operating in each of the three spectral regions studied (ultra-violet [45], visible [6], and near infra-red [44]). The lowest threshold from a cw OPO

($P_{p-th}^{in} \approx 0.4$ mW) has been obtained from the extension of a triply-resonant oscillator to a quadruply-resonant oscillator. This requires simultaneous resonance for the signal, idler, and pump frequencies, in addition to the sub-harmonic frequency of the pump. Such a cavity geometry is analysed explicitly in reference [48]. (It is significant that all the experimental designs have employed confocal focusing geometries, combined with phase-matching geometries contributing negligible losses from the effects of Poynting vector walk-off, and in particular, non-critical phase-matching; see appendix I.)

The pump frequency stability requirements are now reviewed. The following analysis is specific to cavities in which the signal and idler frequencies are resonant, and consequently, low pump power levels are required to reach OPO threshold. The modelling in chapter II illustrated that the pump frequency should be a single-frequency source, stabilized, in general, at the MHz-level, to maintain OPO operation on a single signal and idler frequency mode-pair. Recall the pump frequency requirements for single- and dual-cavity resonators, as derived in chapter II:

$$\text{Single-cavity} \quad \Delta v_{p-stab} \approx \pm \frac{FSR}{F} , \quad [\text{III. 4}]$$

$$\text{Dual-cavity} \quad \Delta v_{p-stab} \approx \pm \frac{FSR_s}{2F_s} , \quad [\text{III. 5}]$$

where it is assumed that, within the single-cavity oscillator, the finesses of the signal and idler fields are similar (i.e. $F_s \approx F_i \approx F$), and within the dual-cavity oscillator, the free spectral range of the signal field is significantly greater than the idler field (i.e. $FSR_s \gg FSR_i$). When the signal and idler free spectral ranges are similar within the dual-cavity oscillator, then the analysis of the single-cavity oscillator is approximately valid.

For a single-cavity resonator, with signal and idler finesses of $F_s \approx F_i \approx 300$, corresponding to round-trip power losses of ≈ 2.1 %, and free spectral ranges of $FSR_s \approx FSR_i \approx 4$ GHz, corresponding to standing-wave optical cavity lengths of ≈ 37.5 mm, then the pump frequency stability, as given by equation III. 4, is $\Delta v_{p-stab} \approx 13.3$ MHz. The desire to increase the cavity finesses to lower the threshold has the undesirable effect of increasing the level of pump frequency stability required for stable OPO operation. Therefore, the selection of cavity finesses must be considered carefully in the

design of a cw OPO, as explained specifically in reference [40]. For the single-cavity oscillator, short cavity lengths should be employed (with correspondingly large free spectral ranges).

For a dual-cavity oscillator with significantly different free spectral ranges for the signal and idler fields, the threshold and stability requirements can be partially decoupled. In this respect, a short, low finesse cavity for either the signal or idler frequency can reduce the requirements on the pump source. Low pump power thresholds can now be maintained by increasing the finesse of the longer cavity length without affecting the pump frequency requirements. Again, the advantages of the dual-cavity oscillator over the single-cavity oscillator, are evident. (The dual-cavity oscillator is discussed in detail in chapter VI, which includes the first experimental realization of such a device.)

While frequency stability at the MHz-level is adequate to prevent hopping to adjacent mode-pairs, it is unsuitable for high precision frequency applications. Such schemes require pump sources stabilized to sub-kHz levels [49 - 52] to allow for accessible signal and idler frequencies displaying this level of frequency stability. Frequency stabilization at the kHz-level should be seen as acceptable for pump sources within the context of OPO frequency division schemes.

These two requirements (power and stability) are discussed in the section III. 2 (i), which analyses pump sources that operate in the three spectral regions, as defined earlier.

III. 2 (i) Pump sources in the ultra-violet spectral region.

In the ultra-violet spectral region (in general, $\nu_p \geq 750$ THz), there is a lack of appropriate lasing transitions that can combine the properties of high cw power, and narrow-linewidth frequency output. Presently, the highest cw powers in this spectral region are generated from transition lines of argon-ion lasers, which can operate with single-frequency stability at the MHz-level [53]. More accessible pumping radiation in the ultra-violet spectral region is likely to become available soon from all-solid-state, diode-laser-based sources (either as the pump source for an all-solid-state laser, or as the actual narrow-linewidth source), frequency up-converted to the ultra-violet spectral region. Such schemes may include frequency doubling Ti:sapphire lasers, whose

frequency tunability offers a significant advantage over fixed frequency laser sources [54, 55]. (Ti:sapphire lasers are discussed further in section III. 2 (iii).)

The literature within the field of harmonic generation has focused primarily on experiments concerning the second-harmonic generation of all-solid-state laser sources [56 - 59], while the techniques of frequency tripling / quadrupling remain largely unexplored. It is likely that the generation of large cw powers at the fourth frequency harmonics of solid-state lasers will precede third harmonic generation techniques. From a practical viewpoint, it is easier to resonantly-double a single frequency source externally [57 - 60], than to combine a laser fundamental with its second harmonic frequency in a cw doubly-resonant external geometry, to generate efficiently the third harmonic frequency.

To date, the only reported cw OPO experiment to utilize a pump source operating in the ultra-violet spectral region has involved the use of an argon-ion laser, operating at a fixed frequency of $\nu_p = 824$ THz ($\lambda_p = 363.8$ nm) [45]. (This experiment is discussed specifically in chapter V of the thesis which includes a further discussion on the selection of pump sources in the ultra-violet spectral region.)

III. 2 (ii) Pump sources in the visible spectral region.

In the visible spectral region (defined here as $420 \geq \nu_p \geq 750$ THz), current pump sources include high power, narrow-linewidth, single-frequency gas lasers (argon-ion or krypton-ion), diode-laser-pumped, frequency up-converted Nd-based laser sources, and dye lasers. Indeed, many of these sources have been used within the past few years as the pump sources for cw doubly-resonant oscillators. (An argon-ion laser operating in the visible spectral region is used as the pump source for the OPO described in chapter IV of the thesis [61].)

The above-mentioned laser sources have frequency outputs that are confined by the gain-bandwidths of the lasing transitions. For example, an argon-ion laser has a typical gain-bandwidth of $\Delta\nu_{g-b} \approx 6$ GHz [62], whereas a frequency-doubled Nd-based solid-state laser has a gain-bandwidth of $\Delta\nu_{g-b} \approx 200$ GHz [63].

Despite having a limited frequency output range, diode-laser-pumped, all-solid-state, Nd-based lasers, frequency up-converted to the visible spectral region, are highly appropriate as the pump sources for cw OPOs. Recently, such sources have been locked in frequency to absorption lines of iodine, with frequency precisions of a few parts in 10^{11} [64]. This level of stability is suitable for frequency division schemes, when combined with high cw power radiation to pump serial or parallel OPO configurations [36, 37]. High power levels at the second frequency harmonic can be generated efficiently by placing the doubling crystal within the laser cavity [56], or in an external cavity in which the fundamental laser power is considerably enhanced [57 - 60]. (Direct OPO pumping with Nd-based laser sources is discussed in the following section.)

It is reasonable to predict that, within the next few years, cw diode-lasers will become available at higher frequencies and with higher single-frequency power levels; a persistent trend over the past decade [65]. When they become available, they will provide the ideal source of visible pump radiation for cw OPOs. (The use of diode-lasers, and other tunable sources that extend into the visible spectral region, but which operate with higher powers in the near infra-red spectral region, are discussed in the following section.)

In the meantime, dye lasers could be used effectively as pump sources for cw OPOs. Such experiments would serve to illustrate the potential of using pump sources of widely-tunable visible radiation with widely tunable cw OPOs operating in the near infra-red spectral region [44]. Phase-matching geometries and nonlinear material specifications could be established that would enable the transfer of the pump source to, for example, diode lasers, when they become available with higher powers at higher frequencies.

III. 2 (iii) Pump sources in the near infra-red spectral region.

In the near infra-red spectral region, there are a number of sources that can be considered for pumping directly cw OPOs further into the infra-red spectral region. These include Nd-based lasers, Ti:sapphire lasers, and phase-locked diode-laser arrays. Each of these laser sources is now considered separately.

III. 2 (iii) (a) Diode-laser pumped Nd-based lasers.

The diode-laser-pumped Nd-based laser system (e.g. Nd:YAG or Nd:YLF) is one of the most efficient and reliable ways of generating coherent radiation in the near infra-red spectral region [22]. The current generation of multi-Watt diode lasers offer operating lifetimes of thousands of hours, high electrical-to-optical conversion efficiencies, and have good spectral overlap with the pump bands of solid-state lasers [65]. The output powers of all-solid-state lasers have gradually been increased over the past decade, driven by the desire to generate multi-Watt outputs at frequency harmonics, and for applications such as gravitational-wave detection [66, 67].

High-power performance can be obtained by side-pumping a slab laser with direct contact cooling [66, 67]. Multiple fibre-coupling of the pumping diodes offers flexibility, since the pump source and the laser head can be designed almost independently [66]. Frequency stability at high powers can be obtained by injection seeding a low power output laser to control the properties of the high-power oscillator [66 - 68]. Such all-solid-state sources can deliver multi-Watt output powers in a single-frequency with short-term linewidths of tens of kHz [66, 67].

However, these near infra-red laser sources, with output frequencies at $\nu_p \approx 300$ THz, have not been used directly as the pump sources for cw OPOs. This is partly due to the increase in threshold when using the lower energy photons associated with infra-red laser sources, and more specifically, to a lack of suitable nonlinear materials offering low threshold phase-matching geometries for cw OPO operation. When appropriate nonlinear materials become available, a Nd-based laser / cw OPO arrangement will allow for the generation of high power and high spectral quality radiation in the mid infra-red spectral region, in the same manner that up-conversion techniques have been utilized so effectively in the past decade for generating visible and ultra-violet frequency harmonics [56, 59]. (Newly developed nonlinear materials that may provide such radiation are discussed in section III. 3.)

III. 2 (iii) (b) Titanium-doped sapphire lasers.

The Ti:sapphire laser ($\text{Ti:Al}_2\text{O}_3$) was reported first in the early 1980s, and has since been the subject of extensive investigation [69]. The Ti:sapphire laser is a broadly tunable solid-state laser with emission from $\nu_p \approx 450$ to 270 THz

($\lambda_p \approx 0.67$ to $1.1 \mu\text{m}$). Single-frequency Ti:sapphire lasers have excellent passive stability, and with active stabilization techniques, linewidths of $\Delta\nu_{p\text{-stab}} \leq 10$ kHz can be obtained readily [70]. The broad tunability, high output powers in excess of $P_p \geq 2$ W, and the possibility of narrow-linewidth operation, makes the Ti:sapphire laser an excellent source for a number of diverse applications, including high resolution spectroscopy [71] and as a pump source for cw OPOs [44].

Frequency doubling of Ti:sapphire lasers can generate radiation tunable from $\nu_p \approx 900$ to 540 THz ($\lambda_p \approx 335$ to 550 nm) [54]. Of particular interest is the ultra-violet end of this range where, as discussed earlier, other laser sources are relatively inefficient and difficult to operate.

The peak absorption of the Ti:sapphire laser is in the region of ≈ 600 THz (500 nm), allowing it to be pumped by the frequency-doubled output of diode-laser pumped Nd-based lasers [72]. However, the more recently developed chromium-doped vibronic solid-state laser gain media may soon offer an alternative to Ti:sapphire lasers (e.g. $\text{Cr}^{3+}:\text{LiSrAlF}_6$ [73]) as they have strong absorption bands that directly overlap the radiation from high power diode-lasers, and can exhibit low pump power thresholds. Other more traditional chromium-doped vibronic solid-state gain media (e.g. $\text{Cr}^{3+}:\text{BeCaAl}_2\text{O}_3$; alexandrite [74]) are also benefiting from the availability of high power diode-laser pump sources, and have also displayed low pump power thresholds in end-pumped configurations [75]. Even so, Ti:sapphire lasers currently represent the most attractive source for pumping cw OPOs, either directly, or via their frequency harmonics. This is due to their widespread availability combined with their potential to be converted efficiently to lower and higher frequencies, through frequency up- / down-conversion techniques.

To date, there has only been one report of a cw OPO that has operated with a Ti:sapphire laser as the pump source [44], and this experiment is outlined in chapter VII of the thesis, which discusses further applications that combine the use of Ti:sapphire lasers and cw OPOs.

II. 2 (iii) (c) Single-frequency diode-lasers.

While the properties of vibronic-based solid-state lasers make them highly appropriate as the pump sources for cw OPOs, in the longer term, they are

likely to be replaced by high-power phase-locked diode-laser arrays [76]. The recent developments in semiconductor diode-laser technology [65] must be considered with respect to the proposed use of cw OPOs [36, 37] operating in different spectral regions. This can be viewed from two standpoints: first, as alternatives to cw OPOs as high-precision, frequency-tunable devices; second, as the pump sources for cw OPOs to down-convert diode-laser radiation to spectral regions where diode-lasers do not exist, or cannot be operated with high power and narrow-linewidth outputs.

Scalable, high power output has been obtained by the coherent addition of injection-locked high-power diode lasers [77], and by the recent development of monolithic integration of a master oscillator diode-laser and a power amplifier, which delivers multi-watt, single-frequency output powers [65, 78].

Current research in diode-laser technology in the near infra-red spectral region offers significant practical advantages over the use of cw OPOs, regarding continuous frequency tuning over distinct spectral bandwidths. However, by combining tunable diode-lasers with nonlinear techniques involving both frequency up-conversion and down-conversion, there are a number of interesting applications for cw OPOs. In particular, cw OPOs have been considered as integral parts of several optical diode-laser based frequency chains [38, 79].

III. 3 Nonlinear materials.

This section analyses the criteria for selecting nonlinear materials for use within cw OPO configurations. Currently available materials are reviewed with regard to non-critical phase-matching geometries, coarse and fine frequency tuning properties, material fabrication, and optical damage threshold limitations. (This section does not include an analysis of phase-matching in nonlinear media that can be found in a number of general review papers on nonlinear optics [14 - 16, 23, 80].)

It was discussed in chapter II that, to allow for cw parametric oscillation, it was necessary to focus pump beams to minimum spot sizes within the nonlinear materials, and that high finesse cavities were required for the resonant fields of the OPO. This dictates that the nonlinear material must withstand high cw power intensities, and have negligible scattering and

absorption losses for the resonant fields. When these two specifications are considered, many nonlinear materials fail to satisfy cw OPO requirements.

Taking the pump power threshold values, as calculated in section III. 2, and applying the conditions of confocal focusing, then the power intensities of the focused spot sizes within the crystals at threshold are 1.3 MW/cm^2 (singly-resonant oscillator), 14 kW/cm^2 (doubly-resonant oscillator), and 170 W/cm^2 (triply-resonant oscillator). These significantly different power intensities highlight further the difficulties in forming singly-resonant oscillators [47]. Further, to maintain a finesse of $F \approx 300$ in a standing-wave optical cavity, the round-trip power losses must be less than $\beta_{r-t} \leq 2\%$. In such a standing-wave resonator, the fields propagate in forward and backward directions through the nonlinear material. Therefore, in general, nonlinear materials for cw OPOs must contribute low absorption losses for all resonant fields.

Another important consideration when aiming to maximise the parametric gain over the whole gain element is to minimize the effects of Poynting vector walk-off, due to propagation away from principal optical axes. This implies that non-critical phase-matching geometries are preferable for cw OPO use. However, this does not exclude critical phase-matched geometries. Within any phase-matched geometry, the walk-off should be evaluated. It is assumed at this stage that non-critical phase-matched geometries are essential for cw OPO operation. The incorporation of critical phase-matching geometries with low walk-off is considered in appendix I.

Of particular importance within OPO designs is the general feature of tuning. However, as discussed in chapter II, this can be sub-divided into coarse and fine frequency tuning. Coarse frequency tuning has long been the favourable property of OPOs that operate with pulsed pump sources, with the ability of a single pump source / nonlinear crystal arrangement to generate extensive frequency bandwidths [14]. In general, for a fixed frequency pump source, large degrees of coarse frequency tuning are possible through rotation of the crystal axes, or by changing the phase-matching temperature. However, neither temperature nor angle tuning offers a convenient method for fine frequency control of the outputs from cw OPOs. The most appropriate method of controlling the fine frequency properties of an OPO is through piezo-electric tuning of the nonlinear medium [39, 41, 42], or by independent

cavity length control of external cavity mirrors within a dual-cavity oscillator [43, 81].

Another important property of material selection involves the fabrication of nonlinear crystals. This topic can also be divided into two categories: monolithic crystal configurations and optical coatings. One method of reducing cavity losses to a minimum is to deposit dielectric coatings directly on the crystal surfaces. In addition, by curving the ends of the crystal, the requirement for external cavity mirrors can be eliminated. This has profound effects on the pump power threshold, but more importantly, on the mechanical rigidity and inherent stability of the OPO resonator [39, 40].

When external mirrors are required, the faces of the nonlinear crystal should contribute negligible losses to the system. In principle, this can be achieved by Brewster-cut nonlinear crystals, optical contacting mirror substrates directly on the crystal faces, or by applying anti-reflection coatings to the faces of the nonlinear material. Brewster cuts are usually discarded within cw OPOs due to differences in the frequencies and polarizations of the resonant fields. Optical contacting would require an index matching fluid with very high specifications with regard to power densities and transmission for discrete, and perhaps widely-spaced, frequencies. Therefore, anti-reflection coatings are the obvious choice, and are commonly used. However, when specifications are for triple anti-reflection coatings, high power densities, and elevated temperature operation, the match of the coating and crystal materials must be examined closely.

Historically, the subject of material selection for cw OPOs has followed closely that of second-harmonic generation experiments. The selection of nonlinear materials for cw frequency-doubling is almost identical to that of cw OPOs; i.e. non-critical phase-matching geometries, moderate effective nonlinear coefficients, low absorption losses, high damage thresholds, and relative ease of crystal fabrication.

Several different nonlinear materials are now reviewed, each of which has properties that makes it suitable for incorporation within cw OPO designs, following successful use within cw frequency up-conversion schemes, and in particular, second harmonic generation. For each material, the crystal properties are reviewed and tuning curves are presented for non-critical phase-matching geometries. (The axes labelling systems adopted within this

chapter are specific to the particular materials, and conform to the conventions that are commonly applied to within their respective literatures.) Finally, within each phase-matching geometry, fine frequency tuning methods are discussed with a view to obtaining frequency stable and frequency tunable signal and idler radiation.

In contrast to more traditional methods of comparing nonlinear materials, the suitability of the materials is not evaluated simply from transparency ranges and figures of merit based on effective nonlinear coefficients. Specifically, the properties of each material relevant to the generation of frequency stable / tunable OPO radiation are presented.

III. 3 (i) Magnesium oxide doped lithium niobate (MgO:LiNbO₃) [24, 40, 82].

Lithium niobate (LiNbO₃) is well known as a technologically important optical material, which finds wide use in Q-switch applications and as a substrate for integrated optic devices. Historically, its use in the near infra-red and visible spectral regions has been limited by photo-refractive induced damage. Magnesium oxide doped lithium niobate (MgO:LiNbO₃) has been developed to eliminate some of the problems associated with pure LiNbO₃, with regard to optically induced damage and phase-matching temperatures for second harmonic generation. Specifically, at the standard doping level of 5 % MgO, the phase-matching temperatures for second harmonic generation of Nd-based lasers are increased from below room-temperature (for pure LiNbO₃) to $T_{xtal} \approx 100$ °C [82].

MgO:LiNbO₃ has a transmission range that extends from $\lambda \approx 0.4$ to 5 μm . The absorption coefficients are typically < 0.1 % / cm and ≈ 2 % / cm at wavelengths of $\lambda \approx 1.064$ and 0.532 μm , respectively. The low absorption loss at $\lambda \approx 1$ μm has enabled its successful implementation within cw intra-cavity frequency doubling schemes, and within ultra-high finesse external cavity designs. In particular, MgO:LiNbO₃ can be fabricated and coated easily to form external monolithic resonators. Such designs have been utilized as cw OPO cavities, with pump sources operating at $\lambda \approx 0.53$ μm , and OPO operation around frequency degeneracy. However, a wider range of pump sources and OPO outputs are possible within this phase-matching geometry, and these are discussed within this section.

III. 3 (i) (a) Type I non-critical phase-matching.

Similar to the phase-matching properties of pure LiNbO_3 , only type I non-critical phase-matching can be considered when using $\text{MgO}:\text{LiNbO}_3$ as the nonlinear material within OPO applications. The effects of temperature tuning for fixed frequency pump sources, under the conditions of non-critical phase-matching, are displayed in figure III. 1. In this phase-matching geometry, the pump field is polarized along the z principal optical axis, and the signal and idler fields are polarized along the y axis, with propagation along the x axis ($\theta=90^\circ, \phi=0^\circ; e \rightarrow o + o; d_{\text{eff}} \approx 5.95 \text{ pm/V}$).

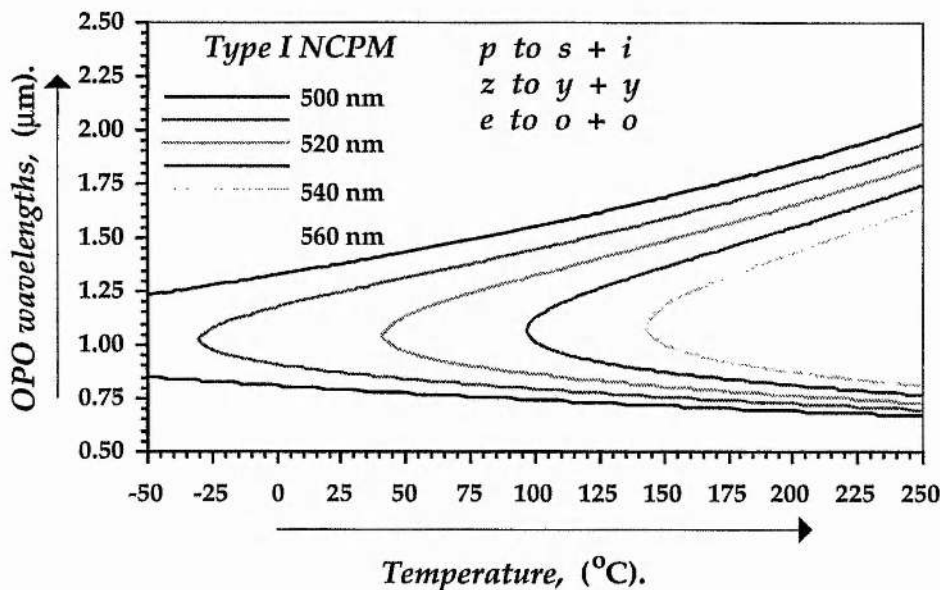


Figure III. 1.

Calculated type I non-critical phase-matching in $\text{MgO}:\text{LiNbO}_3$, with fixed frequency pump sources in the visible spectral region, and temperature tuning.

Figure III. 1 illustrates that type I non-critical phase-matching is available when using pump sources operating in the visible spectral region between $0.5 < \lambda_p < 0.56 \mu\text{m}$. The outputs from these OPOs involve signal and idler frequencies tunable around frequency degeneracy, including, in general, 2:1 signal:idler frequency ratios. Consider now holding the crystal temperature fixed, and varying the phase-matching temperature under non-critical phase-matching. The calculated phase-matching curves are displayed in figure III. 2.

Figure III. 2 illustrates further the possibility of using MgO:LiNbO₃ for cw OPO applications with pump sources operating in the green / yellow spectral region, and with OPO outputs tunable around frequency degeneracy. Note that the range of signal and idler frequencies is limited by the elevated phase-matching temperatures, and not by the transmission range of the material, which extends out to $\lambda \approx 4 \mu\text{m}$.

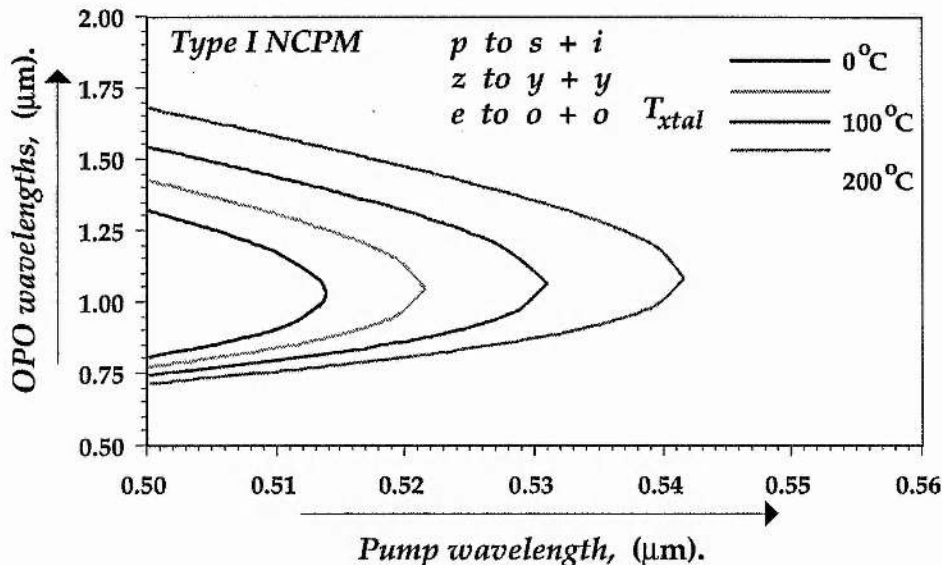


Figure III. 2.
Calculated type I phase-matching curves for MgO:LiNbO₃, with pump frequency tuning and fixed phase-matching temperatures

III. 3 (i) (b) MgO:LiNbO₃ phase-matching conclusions.

The non-critical phase-matching curves for MgO:LiNbO₃ have been presented for pump frequency tuning with a fixed phase-matched temperature, and for temperature tuning with a fixed pump frequency. In both geometries, wide (coarse) frequency tuning of the OPO outputs around frequency degeneracy is possible. The range of available signal and idler frequencies is limited by increased operating temperatures. In particular, high temperature operation ($T_{xtal} \approx 250 \text{ }^\circ\text{C}$) requires an oxygen bleed to eliminate oxygen out-diffusion, and subsequent browning of the crystal.

The low damage threshold of MgO:LiNbO₃ for cw operation represents a further limit to the input pump power that can be focused within the material. Optically induced damage is at its most critical for radiation in the green spectral region, where the pump sources for these non-critical phase-matching geometries exist. Recent experiments have shown that, for cw operation at $\lambda \approx 532$ nm, damage occurs at power intensities of ≈ 0.8 MW/cm².

The high effective nonlinear coefficients, the possibility of fabricating the material to form monolithic ultra-high finesse resonators, and the electro-optic tuning capability of MgO:LiNbO₃, have been critical to its application within cw OPO designs. The lack of non-critical phase-matching geometries for pump frequencies in different spectral regions, the type I phase-matching geometry with parallel polarized signal and idler fields, and the high temperature dependence of the refractive indices, indicate that MgO:LiNbO₃ has limited use for fine frequency control within cw based optical frequency division techniques. However, as shown in references [39] and [40], highly stable fixed frequency OPO outputs can be provided, when this material is used within cw OPOs, and combined with a frequency stable pump source at the kHz-level.

III. 3 (ii) Potassium niobate (KNbO₃) [27, 83].

Potassium niobate (KNbO₃) has received considerable attention in recent years due to its high effective nonlinear coefficients, its high electro-optic coefficients, and its capability to generate the second harmonic frequencies of dye lasers, AlGaAs diode lasers, and Ti:sapphire lasers, in non-critical phase-matching geometries near room-temperature. In general, KNbO₃ has been used for frequency doubling radiation from $\lambda \approx 0.85$ to 1 μ m into the blue / green spectral region, and is the material of choice for doubling low-power laser diodes operating at $\lambda \approx 0.86$ μ m.

The transparency range of KNbO₃ is from $\lambda \approx 0.3$ to ≈ 4 μ m. Two distinct type I non-critical phase-matching geometries have been utilized for second harmonic generation. These geometries are now studied with respect to using KNbO₃ for temperature-tuned cw OPO applications. The principal optical axes x , y , and z correspond to the crystallographic axes c , a , and b , respectively. For KNbO₃, the effective nonlinear optical coefficients vanish

for type II non-critical phase-matching. The material is stable over the temperature range from $T_{xtal} \approx -50$ to 223 °C

III. 3 (ii) (a) Type I non-critical phase-matching; $x \rightarrow z + z$.

The first type I non-critical phase-matched geometry in KNbO_3 involves propagation along the crystal y axis, with the pump field polarized along the x axis and the parallel polarized OPO fields polarized along the z axis ($\theta = 90^\circ, \varphi = 0^\circ$; $e \rightarrow o + o$; $d_{eff} \approx 18$ pm/V). The temperature-tuned non-critical phase-matching curves for fixed pump frequencies operating in the blue spectral region, are displayed in figure III. 3.

Figure III. 3 illustrates the potential for using pump sources operating in the blue spectral region for cw OPO applications. Temperature tuning for a fixed frequency pump source is rapid, and would require a high degree of precision in the exact phase-matching temperature. When this crystal temperature is held fixed, then the pump frequency could be varied. This behaviour is illustrated in figure III. 4.

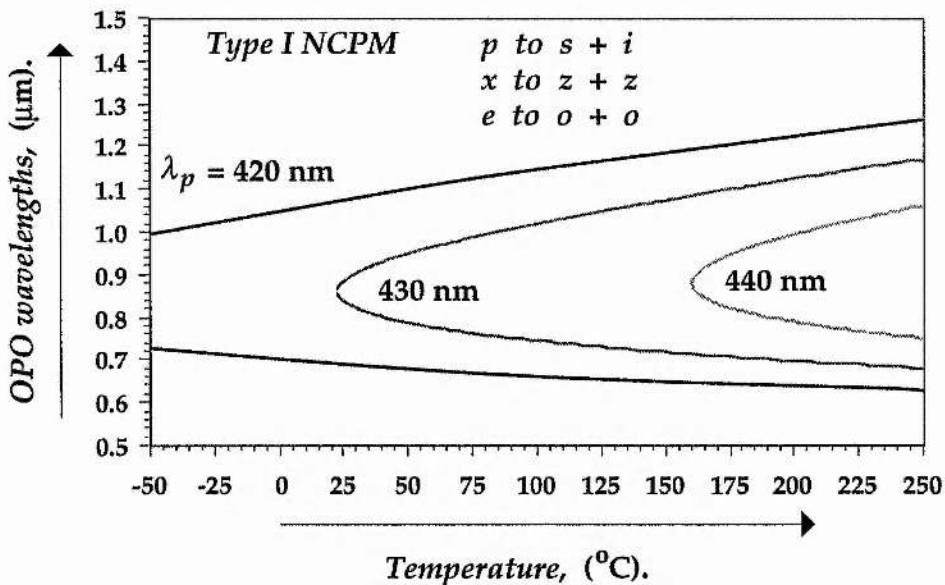


Figure III. 3.

Calculated type I non-critical phase-matching in KNbO_3 , with the pump and OPO fields polarized along the x and z principal optical axes, respectively, and for tuning of the phase-matching temperature.

Figure III. 4 is significant because it represents the range of signal and idler frequencies that could be generated by using the second harmonic frequency of a diode laser or a Ti:sapphire laser, as the pump source for a cw OPO. Again, this phase-matching geometry would require accurate control of the fixed crystal temperatures.

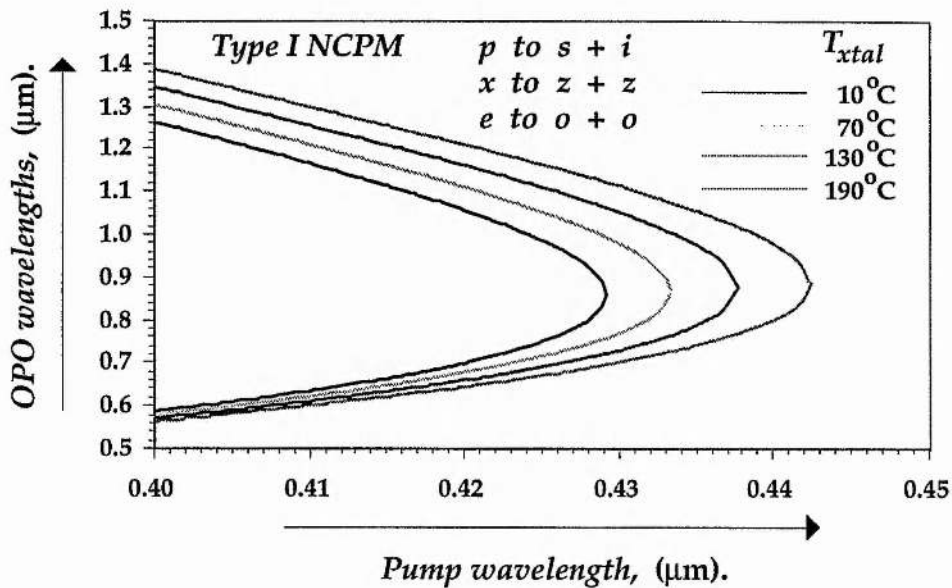


Figure III. 4. Calculated type I non-critical phase-matching in KNbO_3 , with the pump and OPO fields polarized along the x and z principal optical axes, respectively, and for tuning of the pump frequency.

III. 3 (ii) (b) Type I non-critical phase-matching; $x \rightarrow y + y$.

The second type I non-critical phase-matched geometry in KNbO_3 involves propagation along the crystal z axis, with the pump field polarized along the x axis and the parallel polarized OPO fields polarized along the y axis ($\theta = 90^\circ, \varphi = 90^\circ$; $e \rightarrow o + o$; $d_{\text{eff}} \approx 16 \text{ pm/V}$). The temperature-tuned non-critical phase-matching curves are displayed in figure III. 5.

Similar to the previous type I phase-matching geometry in KNbO_3 , temperature tuning around frequency degeneracy is possible when using fixed frequency pump sources. However, figure III. 5 illustrates that pump sources in the blue / green spectral region could be used as the pump source

for a cw KNbO₃ OPO. This encompasses the second harmonic frequencies of Nd-based laser sources. The effects of pump frequency tuning for fixed phase-matching temperatures are considered in figure III. 6.

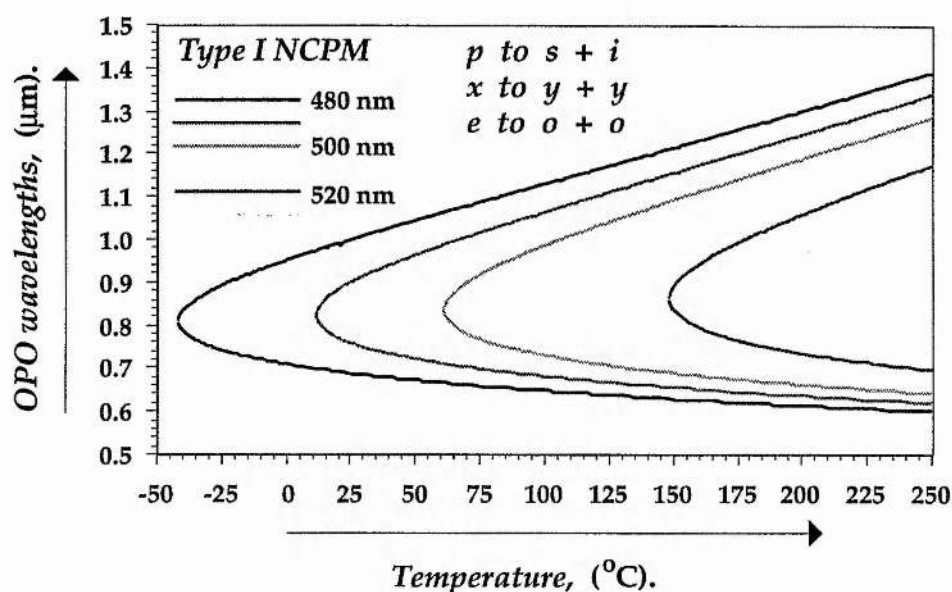


Figure III. 5.

Calculated type I non-critical phase-matching in KNbO₃, with the pump and OPO fields polarized along the x and y principal optical axes, respectively, and for tuning of the pump frequency.

III. 3 (ii) (c) KNbO₃ phase-matching conclusions

The above analyses have highlighted the possibility of using KNbO₃ in temperature tuned type I non-critical phase-matched geometries, when using pump sources that operate in the visible (blue / green) spectral region. The signal and idler frequencies would be tunable around frequency degeneracy, and, in general, could provide signal:idler frequencies in the ratio 2:1.

Despite its high effective nonlinear coefficients, the pump power levels must be considered due to the presence of optically induced damage mechanisms inherent within KNbO₃. In addition to the high temperature sensitivity, above temperatures of $T_{xtal} \approx 40$ °C, there is a thermally induced depoling in single domain KNbO₃. Therefore, reliable heating and cooling of the crystal requires an applied electric field across the crystal. Further, the

absorption in the blue spectral region is significant ($> 5\%$ / cm at $\lambda = 420$ nm), and can cause local heating of the crystal by a focused laser beam, altering phase-matching conditions, and reducing conversion efficiencies. Similar to MgO:LiNbO₃, the range of signal and idler outputs would be limited by the phase-matching temperature range accessible, and not by the transparency of the material.

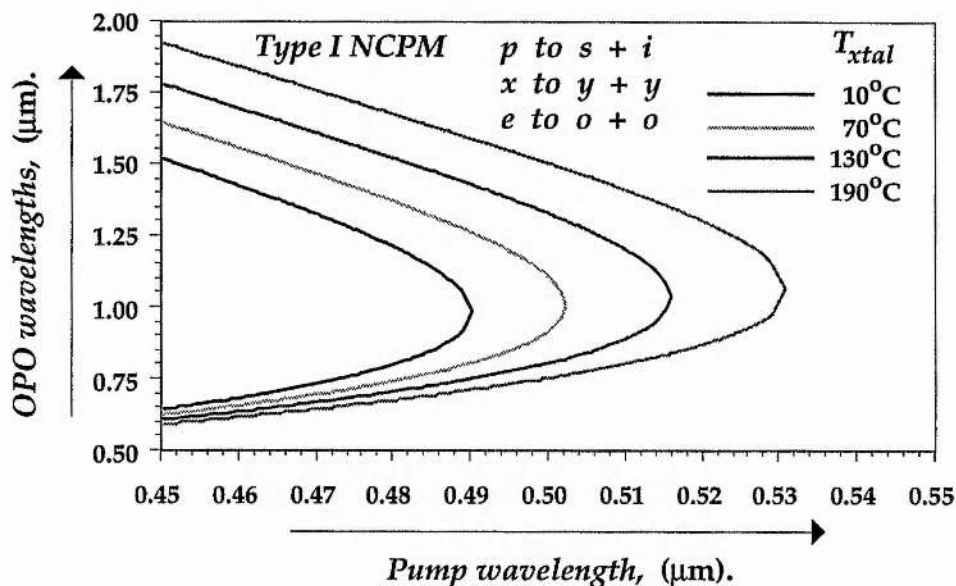


Figure III. 6.

Calculated type I non-critical phase-matching in KNbO₃, with the pump and OPO fields polarized along the x and y principal optical axes, respectively, and for tuning of the phase-matching temperature.

Therefore, KNbO₃ may prove to be a useful material for cw OPO applications, when the pump source is derived from a tunable near infra-red source, such as the frequency doubled radiation from a single frequency diode laser, a tunable Ti:sapphire laser, or a Nd-based laser. The high temperature sensitivity in the type I phase-matching geometry would require high precision temperature control combined with frequency stable pump sources operating at the kHz-level. Smooth frequency tuning with a fixed frequency pump source would demand dual cavity length control of the signal and idler frequencies.

III. 3 (iii) Potassium titanyl phosphate (KTiOPO₄; KTP) [25, 84].

Potassium titanyl phosphate (KTiOPO₄; KTP) is a relatively new nonlinear material that has been shown to have excellent properties for several nonlinear optical applications and, in particular, for frequency doubling the $\lambda \approx 1 \mu\text{m}$ radiation of Nd-based lasers. Its high effective nonlinear coefficients, high damage threshold, wide acceptance angles, and thermally stable phase-matching properties, make it useful for this purpose. Its large electro-optic coefficients and low dielectric constants make it attractive for various electro-optic applications, such as modulators and Q-switches. KTP is highly suitable for frequency up-conversion techniques, offering high conversion efficiency when frequency doubling, or when generating sum and difference frequencies. KTP has been used to mix the radiation from Nd:YAG lasers and diode lasers operating at $\lambda \approx 0.8 \mu\text{m}$, to provide radiation in the blue spectral region.

KTP has a transparency range from $\lambda \approx 0.35$ to $4.5 \mu\text{m}$, with measurable absorption beyond $\lambda \approx 2.8 \mu\text{m}$. However, single crystals of KTP reveal some absorption over the region $\lambda \approx 2.5$ to $4.5 \mu\text{m}$. The absorption loss at $\lambda \approx 1.06 \mu\text{m}$ is $\approx 1\%$ / cm and a few % at $\lambda \approx 0.53 \mu\text{m}$. KTP offers type II non-critical phase-matching. (The principal axes x , y , and z , correspond to the crystallographic axes a , b , and c , respectively.)

III. 3 (iii) (a) Type II non-critical phase-matching.

Type II critical phase-matching is used regularly for second harmonic generation of near infra-red lasers, and for OPO use when pumped with sources operating between $\lambda \approx 0.5$ to $1.1 \mu\text{m}$. When using pump sources operating in the near infra-red spectral region (specifically Ti:sapphire and Nd-based lasers), KTP OPOs have been operated with an idler frequency output in the $\lambda \approx 3$ to $4 \mu\text{m}$ spectral region. However, this has only been possible when using cw mode-locked and Q-switched lasers, where singly-resonant OPO geometries have been employed. For cw operation, the absorption, as discussed above, prevents doubly-resonant, high-finesse cavities when using these lasers as the pump sources.

Two type II non-critical phase-matching geometries are analysed, each of which has a moderate effective nonlinear coefficient. Figure III. 7 displays the signal and idler outputs for room-temperature operation, with the pump

and signal fields polarized along the y -optical axis, and the idler field orthogonal, along the z -axis ($o \rightarrow o + e$: $\theta = 90^\circ$, $\phi = 0^\circ$: $d_{\text{eff}} \approx 3.2 \text{ pm/V}$). Only room-temperature operation is considered for KTP since the thermal dependence of the refractive indices is small. While this prevents wide (coarse) frequency tuning, as illustrated with the type I materials previously, low temperature sensitivity now becomes a particularly effective method for controlling the fine frequency properties of the signal and idler output frequencies.

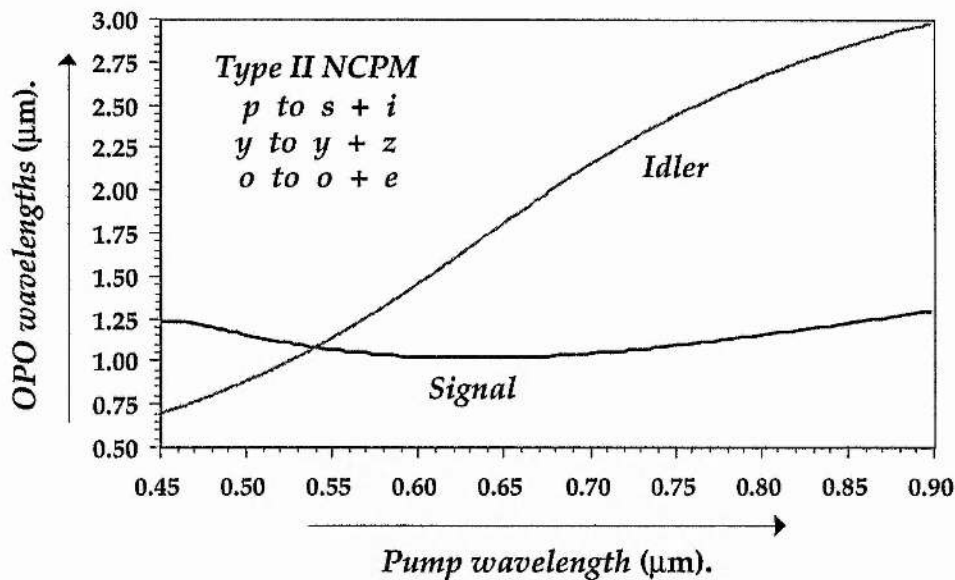


Figure III. 7.

Type II non-critical phase matching in KTP ($o \rightarrow o + e$: $\theta = 90^\circ$, $\phi = 0^\circ$).

Figure III. 8 displays signal and idler outputs for room-temperature operation, with the pump and signal fields polarized along the x -optical axis, and the idler field orthogonal, along the z -axis ($\theta = 90^\circ$, $\phi = 90^\circ$: $d_{\text{eff}} \approx 1.9 \text{ pm/V}$).

When using pump sources in the green spectral region, KTP has been shown to be the material of choice for cw OPO operation near frequency-degeneracy. The high effective nonlinear coefficient ($d_{\text{eff}} \approx 3.2 \text{ pm/V}$), the low temperature sensitivity, the high damage threshold, and the type II phase-matching geometry, have allowed for frequency stable signal and idler radiation from such OPOs.

The low walk-off angles in critically phase-matched geometries have extended its operation in the cw regime beyond that of non-critical phase-matching. As displayed in figures III. 7 and III. 8, and when operating with pump sources in the region $\lambda \approx 0.7$ to $0.8 \mu\text{m}$, signal and idler frequencies in 2:1 frequency ratios could be generated. Therefore, KTP is an attractive material for use with Ti:sapphire lasers operating at wavelengths shorter than $\lambda \approx 0.8$.

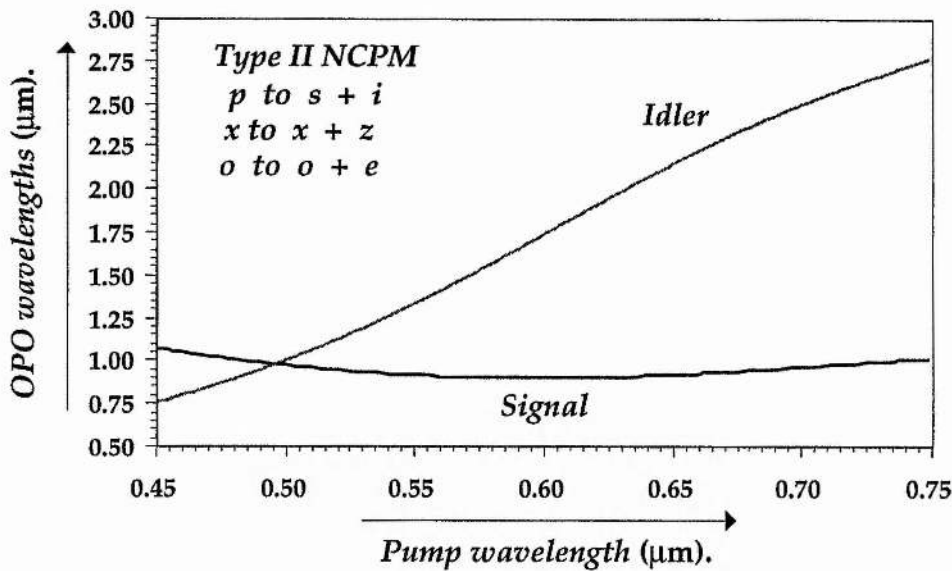


Figure III. 8.

Type II non-critical phase matching in KTP ($o \rightarrow o + e; \theta = 90^\circ, \phi = 90^\circ$).

III. 3 (iv) Potassium titanyl arsenate (KTiOAsO₄; KTA) [85];

Caesium titanyl arsenate (CsTiOAsO₄; CTA) [86].

KTP is just one member of the isomorphic family of nonlinear optical materials with the generic composition $MTiOXO_4$ where M is K, Rb, Tl, NH_4 , or Cs, and X is P or As. Some of these other materials have more advantageous nonlinear optical characteristics than KTP. In particular, the materials KTA and CTA have recently become viable alternatives to KTP, and offer improved performance for specific applications.

KTA and CTA are similar to KTP, but with one important difference; As discussed previously, KTP has a strong absorption band near $\lambda \approx 3.5 \mu\text{m}$

due to the orthophosphate overtone. KTA and CTA have no significant absorptions out to $\lambda \approx 3.7 \mu\text{m}$, making them the preferred materials for constructing OPOs to operate in the mid infra-red spectral region, with the potential for tuning to wavelengths that are inaccessible with KTP. Further, high finesse resonant idler fields can now be considered in the $\lambda \approx 2 - 3 \mu\text{m}$ spectral region, opening up the possibility of longer wavelength pump sources for doubly-resonant (cw) OPOs.

III. 3 (iv) (a) Type II non-critical phase-matching in KTA.

As with KTP, the effective nonlinear coefficient in KTA is maximised for the type II interaction ($\theta = 90^\circ$, $\phi = 0^\circ$; $o \rightarrow o + e$; $y \rightarrow y + z$), with $d_{\text{eff}} \approx 20\%$ larger than KTP. Non-critical phase-matching is also possible with a slightly reduced effective nonlinear coefficient: ($\theta = 90^\circ$, $\phi = 90^\circ$; $o \rightarrow o + e$; $x \rightarrow x + z$). The transparency of KTA has been measured to be from $\lambda \approx 0.35$ to $5 \mu\text{m}$, with negligible absorption out to $\lambda \approx 3.7 \mu\text{m}$. Non-critical phase-matched OPO outputs are shown in figures III. 9 and III. 10. Similar to KTP, only room-temperature operation is analysed.

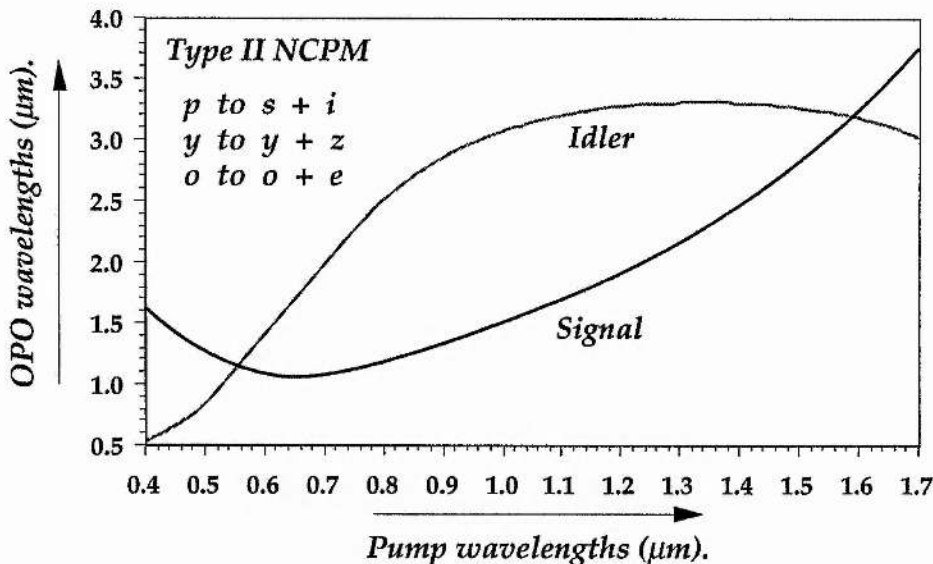


Figure III. 9.

Type II non-critical phase matching in KTA ($o \rightarrow o + e$; $\theta = 90^\circ$, $\phi = 0^\circ$).

The extended infra-red transparency allows for the use of pump sources operating anywhere between $\lambda \approx 0.4$ and $1.7 \mu\text{m}$. In particular, this includes the use of Ti:sapphire lasers and the fundamental wavelengths of Nd-based lasers. Near-degenerate OPOs can be formed when using pump sources at either $\lambda \approx 0.55 \mu\text{m}$ (similar to KTP) or $\lambda \approx 1.6 \mu\text{m}$. With pump sources operating at $\lambda \approx 1 \mu\text{m}$, the signal and idler frequencies are in near 2:1 frequency ratios. In particular, this latter phase-matching geometry could form part of a Nd-based frequency chain, offering integral related down-converted frequencies, whose fractional stability could be determined by locking the second harmonic frequency of the Nd-based laser to a molecular iodine transition.

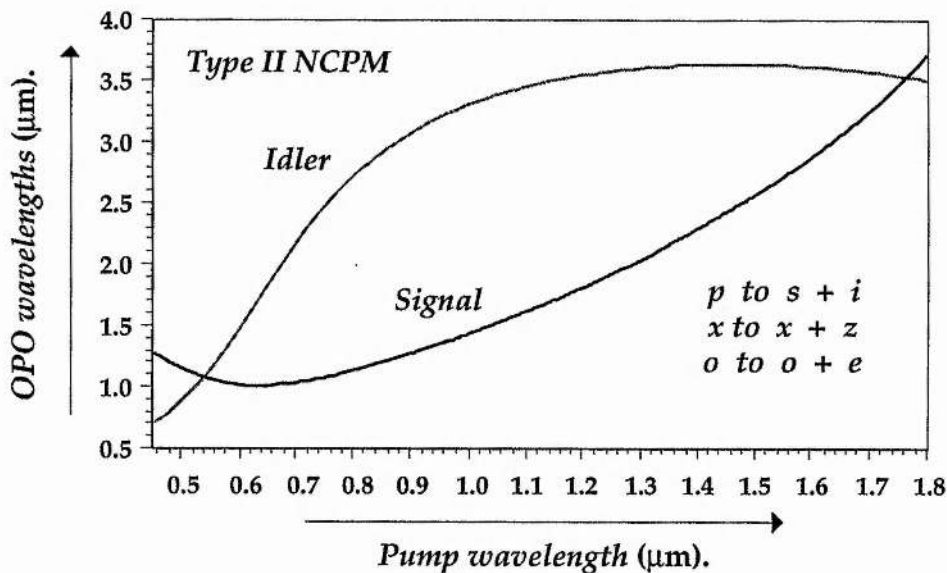


Figure III. 10.

Type II non-critical phase matching in KTA ($o \rightarrow o + e; \theta = 90^\circ, \phi = 90^\circ$).

III. 3 (iv) (b) Type II non-critical phase-matching in CTA.

CTA has nearly the same transparency range as KTA and a nonlinearity of the order of KTP. However, the tuning characteristics of CTA are quite different from those of KTP and KTA. CTA first received considerable attention as a second harmonic generator of Nd-based lasers operating at $\lambda \approx 1.3 \mu\text{m}$. However, the phase-matching properties of CTA for OPO operation are

particularly interesting. Figure III. 11 displays type II non-critical phase-matching ($\theta = 90^\circ$, $\phi = 0^\circ$; $o \rightarrow o+e$; $y \rightarrow y+z$). Figure III. 12 displays the other type II phase-matching geometry ($\theta = 90^\circ$, $\phi = 90^\circ$; $o \rightarrow o+e$; $x \rightarrow x+z$).

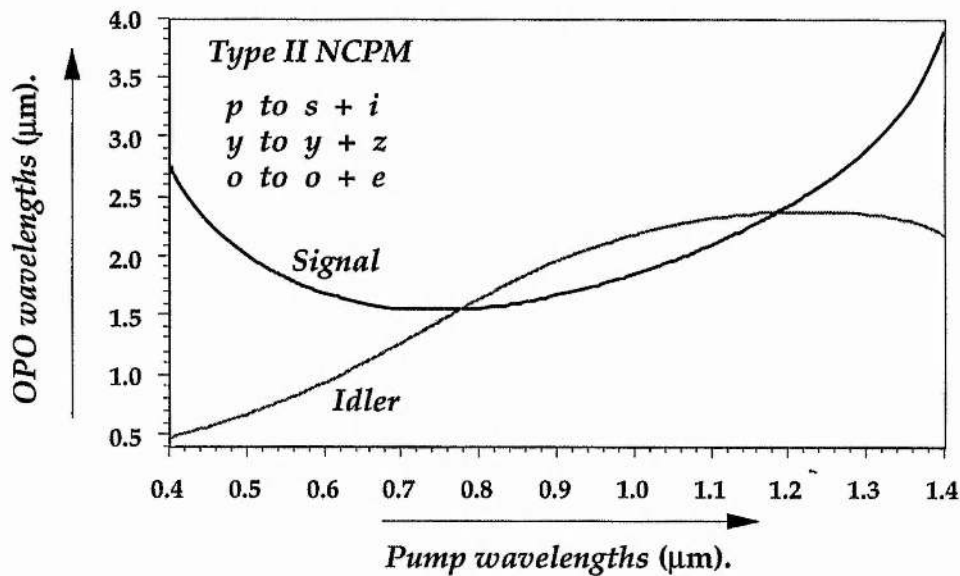


Figure III. 11.

Type II non-critical phase matching in CTA ($o \rightarrow o+e$; $\theta = 90^\circ$, $\phi = 0^\circ$).

For CTA, the range of OPO pump wavelengths is from $\lambda \approx 0.4$ to $1.4 \mu\text{m}$, assuming negligible absorption out to $\lambda \approx 3.7 \mu\text{m}$. For pump sources at $\lambda \approx 0.5 \mu\text{m}$, OPO outputs could be generated in a near 3:1 frequency ratio (figure III. 11) or in a near 2:1 frequency ratio (figure III. 12). For pump wavelengths between $\lambda \approx 0.7$ and $1.2 \mu\text{m}$, OPOs could operate near frequency degeneracy. Of particular interest with CTA is the possibility of generating radiation around $\lambda \approx 2 \mu\text{m}$, from either a $\lambda \approx 1 \mu\text{m}$ or $0.5 \mu\text{m}$ pump source.

III. 3 (iv) (c) KTA & CTA phase-matching conclusions.

Both KTA and CTA are only beginning to emerge as viable OPO materials. Presently, the possibility of crystal imperfections is relatively high, as they are relatively new crystals and their growth technology is still being perfected. In particular, single domain crystals have been difficult to reproduce in large

quantities, and impurities have been reported in growth methods that can alter phase-matching conditions.

However, KTA and CTA share many of the advantageous properties of KTP, allowing for the use of preferred type II phase-matching geometries with low temperature sensitivity and significant electro-optic coefficients of the same magnitude as KTP. Furthermore, both KTA and CTA should also allow for critical phase-matched geometries, important to alter the signal and idler frequencies into exact integral frequency ratios of the pump source within frequency division schemes.

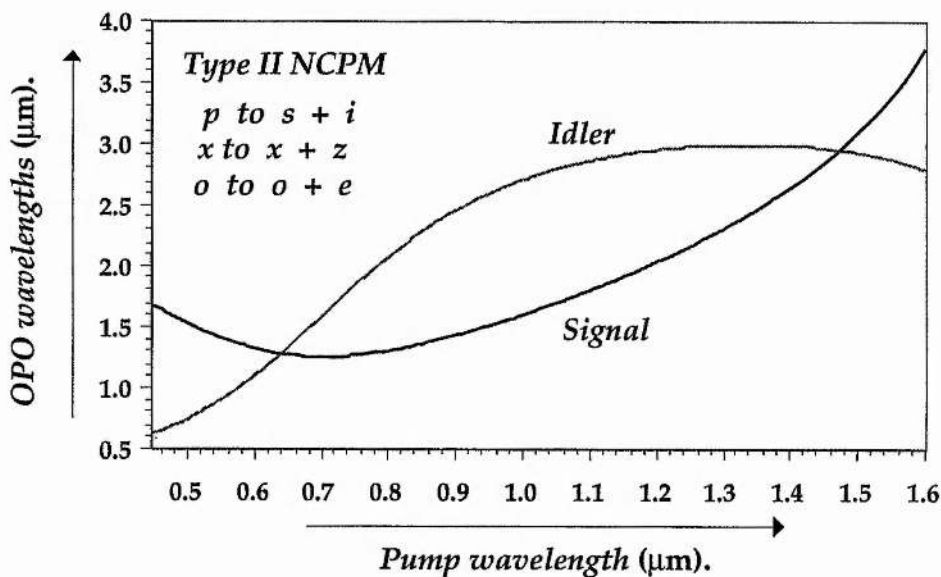


Figure III. 12.

Type II non-critical phase matching in CTA ($o \rightarrow o + e; \theta = 90^\circ, \phi = 90^\circ$).

III. 3 (v) Lithium triborate (LiB_3O_5 ; LBO) [26, 87].

Lithium triborate (LBO) is a recently developed nonlinear optical material that displays many excellent optical properties, such as high transparency in the near infra-red, visible and ultra-violet spectral regions, high optical damage thresholds, and moderate nonlinear coefficients. This material also has the ability to provide non-critical phase-matched geometries for pump sources operating in different spectral regions. Accordingly, the optical

characteristics of LBO are, at present, the subject of considerable interest, and this section discusses specifically the properties of LBO that are relevant to its implementation within cw OPO schemes.

The transmission range of LBO extends from $\lambda \approx 160$ nm in the ultra-violet spectral region to $\lambda \approx 2.6$ μm in the near infra-red spectral region, with negligible absorption losses above $\lambda \approx 280$ nm. Typical absorption coefficients are ≈ 0.035 % / cm and ≈ 0.31 % / cm at wavelengths of $\lambda = 1.064$ μm and $\lambda = 351$ nm / 364 nm, respectively. In particular, the extended ultra-violet transmission has opened up prospects for the development of highly efficient solid-state sources of coherent radiation, by using LBO as an efficient frequency up-converter. LBO has allowed for highly efficient third harmonic generation of Nd-based lasers.

The birefringence of LBO has a high thermal dependence, which makes it particularly sensitive to environmental temperature and laser induced heating. This feature can be used effectively to allow for coarse frequency temperature tuning, especially under the conditions of non-critical phase-matching, but must be examined closely with regard to fine frequency tuning. (In the absence of ideal temperature data for LBO, those provided in reference [87], valid from $T_{xtal} \approx 20$ to 65 $^{\circ}\text{C}$, are assumed to be valid over the temperature range from $T_{xtal} \approx 20$ to 200 $^{\circ}\text{C}$.)

There have been no specific values for optical damage when using LBO in cw experiments. While this prevents an exact figure, it implies that LBO can withstand the very high power levels that have been focused into the crystals (see reference [57], and the discussion of second harmonic generation within reference [41]). In particular, LBO probably has the highest cw surface damage threshold of all commonly used inorganic nonlinear optical crystals.

Crystal growth lengths of useful size ($l_{xtal} \approx 20$ to 30 mm) and optical quality are readily available. However, the strongly anisotropic thermal expansion of the crystal (with contraction along the y optical axis) places constraints on the choice of dielectric coating materials that can be applied to the crystal faces (e.g. complicated triple anti-reflection coatings combined with operation at elevated temperatures). When coating materials can be found that are more sympathetic with the thermal expansion effects of LBO, then the range of available coatings for this crystal will increase substantially.

III. 3 (v) (a) Type I non-critical phase-matching.

LBO can be temperature tuned in the type I non-critical phase-matching geometry ($\theta = 90^\circ$, $\phi = 0^\circ$; $e \rightarrow o + o$; $d_{eff} \approx 1.2 \text{ pm/V}$), with the pump field polarized along the y principal optical axis, and the generated signal and idler fields polarized along the z axis, and with propagation along the x axis (see reference [87] for a definition of the optic axes. The principal optical axes x , y , and z are parallel to the crystallographic axes a , c , and b , respectively.)

This non-critical phase-matching geometry is used regularly in LBO for generating the second frequency harmonics of near infra-red laser sources. In particular, between room temperature and $T_{xtal} \approx 300^\circ\text{C}$, this geometry can be used for frequency doubling sources between $0.9 < \lambda_{fund} < 1.7 \mu\text{m}$. The combination of moderate nonlinear coefficients ($d_{eff} \approx 1 \text{ pm/V}$), and a high damage threshold, make LBO the doubling crystal of choice for high power density laser beams. (For low to middle power densities, and within selective phase-matching geometries, KTP can offer an advantage with increased effective nonlinear coefficients.) Therefore, this opens up the possibility of OPO operation under non-critical phase-matching when using pump sources in the region $0.45 < \lambda_p < 0.85 \mu\text{m}$.

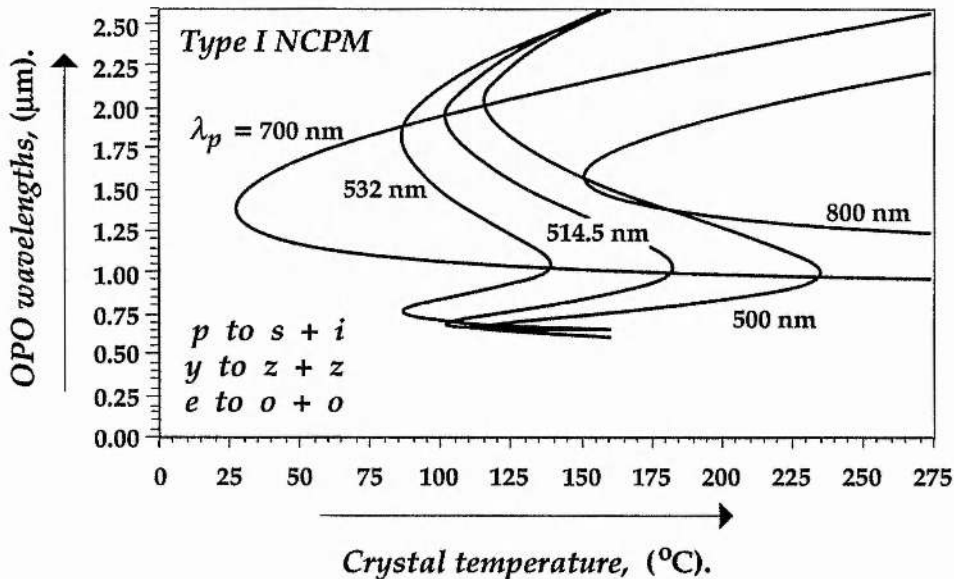


Figure III. 13

Calculated temperature tuning under the conditions of type I non-critical phase-matching in LBO, for fixed wavelength pump sources.

Type I non-critical phase-matching curves, for a selection of widely spaced cw pump wavelengths, are displayed in figure III. 13, revealing some interesting features. As discussed above, non-critical phase-matching geometries are available for pump sources operating throughout the visible and near infrared spectral regions. The phase-matching temperatures required for each arrangement can be accessed conveniently in experimental designs. OPO outputs are available over the entire transmission range of LBO (with an idler wavelength cut-off at $\lambda_i \approx 2.6 \mu\text{m}$). This indicates that LBO is an excellent nonlinear crystal for generating a widely tunable wavelength range from a fixed pump wavelength source.

For pump sources in the green spectral region, LBO exhibits doubled-value retracing behaviour, opening up the possibility of generating high-order integral ratios of signal and idler frequencies. Retracing here means that the phase-matching signal frequency is not a monotonically increasing or decreasing function of the crystal orientation angle or temperature. This feature offers possibilities within the context of using cw OPOs as optical frequency dividers. Such a technique is illustrated explicitly in figure III. 14, for the visible pump wavelength of $\lambda_p = 514.5 \text{ nm}$.

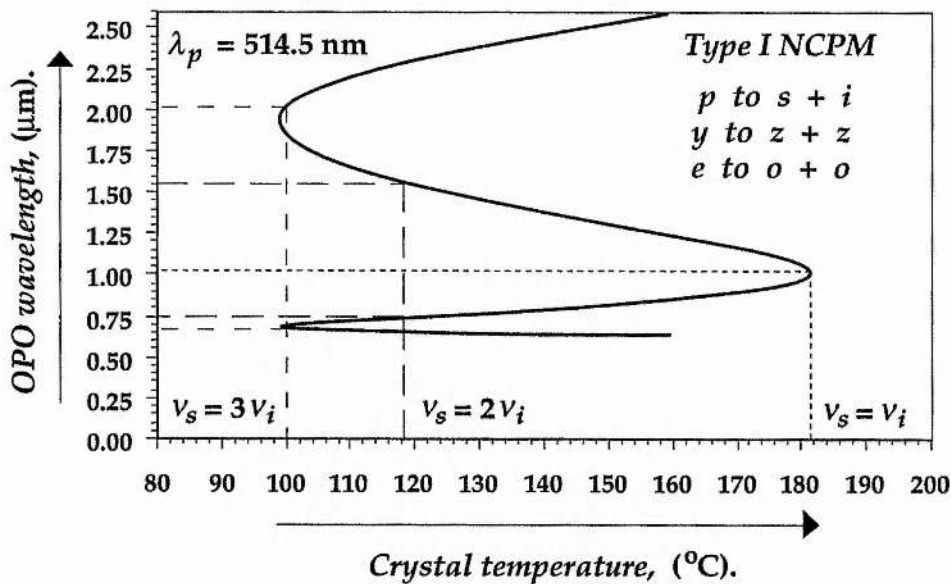


Figure III. 14.

Calculated type I non-critical phase-matching in LBO, for a fixed frequency pump source in the green spectral region, illustrating its potential for generating integral ratios of signal and idler frequencies.

From figure III. 14, signal:idler frequencies in integral ratios of 1:1, 2:1, and 3:1 can be accessed within this phase-matching configuration. The exact location of these frequencies would require a high precision in the temperature of the crystal, in addition to OPO geometries that would allow for smooth frequency tuning. As discussed in chapter II, the type I phase-matching geometry, with parallel polarized signal and idler fields, dictates that dual-cavity resonators are essential to obtain independent cavity length control. Such resonators would require dichroic coating separation or prism separation to split the intra-cavity signal and idler fields, and open up the possibility for smooth frequency tuning at the GHz-level.

A further possibility within the type I geometry is to hold the crystal temperature fixed, and to use a tunable pump source to access new combinations of signal and idler frequencies. This method of multiple parameter tuning is illustrated in figure III. 15.

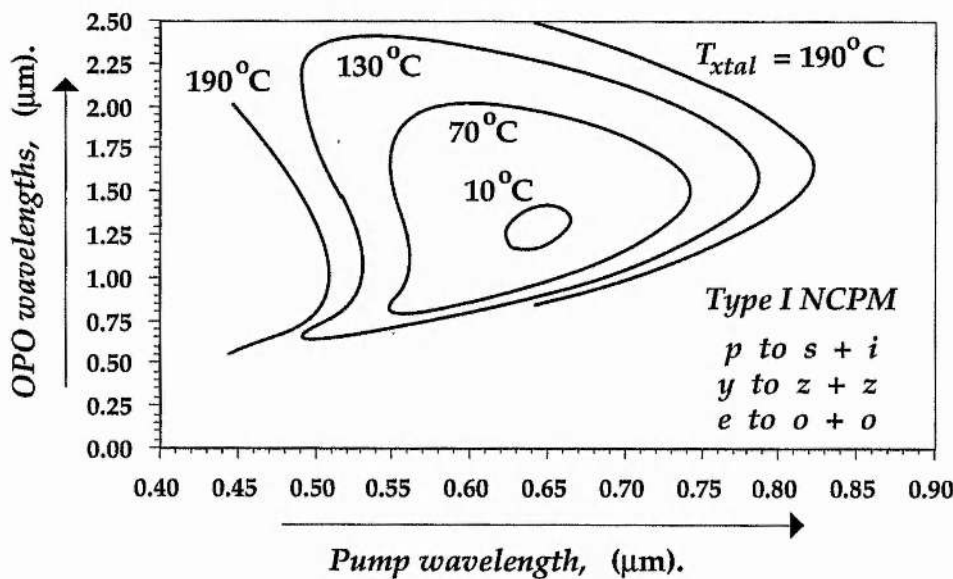


Figure III. 15.

Calculated type I non-critical phase-matching in LBO, for fixed crystal temperatures and tunable pump sources.

Again, a number of options exist within this type I phase-matching geometry. In particular, tunable pump sources, such as Ti:sapphire lasers, diode-lasers, or their second frequency harmonics, could be used as the pump sources for

cw OPOs. Another possible pump source is a visible dye laser. For example, consider the combination of a rhodamine 6G dye laser and type I non-critically phase-matched, temperature-tuned LBO. By tuning the wavelength of the pump source from $\lambda_p \approx 0.56$ to $0.62 \mu\text{m}$, and heating the LBO crystal between $T_{xtal} \approx 10$ to 190°C , coarse cw radiation from the pump wavelength range through to $\lambda \approx 2.6 \mu\text{m}$ could be generated, if such a requirement arose.

The ability to tune both the pump source and the crystal temperature, under the conditions of non-critical phase-matching, allows for coarse and fine multiple parameter selection of the signal and idler frequency outputs. As discussed throughout the text, such a tuning method is essential to the implementation of cw OPOs within optical frequency metrology schemes, and is considered in detail in chapter VII, which describes the use of a tunable Ti:sapphire laser as the pump source for a LBO cw OPO operating in the temperature-tuned type I non-critical phase-matching geometry.

III. 3 (v) (b) Type II non-critical phase-matching.

In addition to the phase-matching geometries outlined above, there is also the possibility of type II non-critical phase-matching within LBO. However, in this case, the temperature dependence of the refractive indices is reduced significantly. While this excludes the wide (coarse) frequency tuning characteristics of the type I phase-matching geometry, it reduces the rapid temperature effects which can prove undesirable within the context of fine frequency control.

Within the type II phase-matching geometry, the pump and idler fields are polarized along the y principal optical axis, and the signal field is polarized along the x axis, with the propagation direction along the z axis ($\theta = 0^\circ$, $\phi = 90^\circ$; $o \rightarrow e+o$; $d_{eff} \approx 1 \text{ pm/V}$). The calculated phase-matching curves for temperature operation from $T_{xtal} = 20^\circ\text{C}$ to 200°C are illustrated in figure III. 16. This graph illustrates that pump sources in the ultra-violet, visible, and near infra-red spectral regions can be used with type II non-critically phase-matched LBO. For pump sources in the ultra-violet spectral region, widely-spaced signal and idler frequencies can be generated, with the possibility of signal frequency tuning in the near ultra-violet. In particular, type II non-critical phase-matching is possible when using the fourth

frequency harmonic of a Nd-based laser, in addition to the fundamental and second harmonic frequencies of a tunable Ti:sapphire laser.

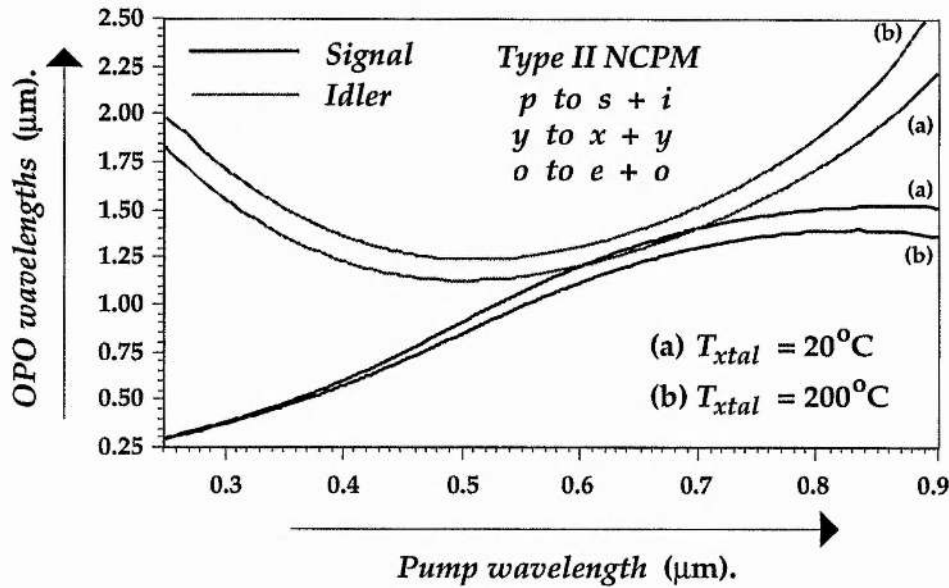


Figure III. 16.
 Calculated phase-matching for type II non-critical phase-matching in LBO, when tuning the pump frequency and the phase-matching temperature.

As with KTP, KTA, and CTA, the orthogonal signal and idler polarizations of the type II phase-matching geometry are ideally suited for separating the intra-cavity fields to form a dual-cavity resonator. This topic is discussed specifically in chapter VI of the thesis, when using LBO in the type II phase-matching geometry.

III. 3 (v) (c) LBO phase-matching conclusions.

The calculated phase-matching curves for both type I and type II non-critical phase-matching indicate that LBO is a candidate for use as the nonlinear material within cw OPO designs. A wide range of pump sources can be used to provide widely spaced signal and idler frequencies. The extended transparency of LBO into the ultra-violet spectral region places it in a unique position when using high frequency cw pump sources.

Within any particular phase-matching geometry, mK temperature effects must be considered carefully, when aiming to provide frequency stable and frequency tunable OPO outputs. In particular, these effects are most critical in the type I phase-matching geometry near frequency degeneracy, and at the retracing turning points. The exact temperature dependence of the refractive indices can affect the centre of the phase-matching gain bandwidth and the optical cavity length through thermal expansion effects. In this respect, the type II phase-matching geometry is more appropriate for frequency stable OPO operation. The temperature effects of the type II geometry are evaluated in the experimental arrangement outlined in chapter V of the thesis.

III. 3 (vi) Silver gallium selenide (AgGaSe_2) [88].

Silver thiogallate (AgGaS_2) [89].

In the mid-infra-red spectral region, the number of crystals suitable for parametric generation is small due, in general, to the limited transparency of dielectric materials at long wavelengths. To date, all the materials studied in this chapter have allowed for phase-matching geometries in which the pump wavelengths were located in the visible spectral region, and the OPO outputs were confined to wavelengths shorter than $\lambda \approx 4 \mu\text{m}$. A class of promising materials for the mid-infra-red spectral region are the ternary (semiconductor) chalcopyrite crystals, AgGaSe_2 and AgGaS_2 , which combine large transparency ranges with favourable birefringence and high nonlinear optical nonlinearity.

III. 3 (vi) (a) Type I non-critical phase-matching in AgGaSe_2 .

The use of AgGaSe_2 for nonlinear infra-red applications was proposed in the early 1970s. However, at this time, growth related problems made it difficult to obtain high quality crystals of adequate size. In particular, it was beset with two difficulties associated with crystal growth: crystals tended to crack during the growth process, and grown crystals tended to display high loss in the near infra-red. In recent years, improved quality boules have been grown, and this has allowed for OPOs to be formed with AgGaSe_2 . The transparency of AgGaSe_2 extends out to $\lambda \approx 13 \mu\text{m}$.

To date, only pulsed near infra-red laser sources have been used AgGaSe₂. Originally, critical phase-matched geometries were used with $\lambda \approx 2 \mu\text{m}$ holmium-based laser pump sources. However, thermal lensing difficulties with the $\lambda \approx 2 \mu\text{m}$ pump source cause damage site formation. The use of shorter wavelength pump sources can prevent this problem.

The type I non-critical phase-matching geometry in AgGaSe₂ takes advantage of these shorter wavelength pump sources. For type I phase-matching, there are two separate branches: one for pump wavelengths in the short wavelength (band-gap) dispersive region, and the other for pump wavelengths in the long wavelength (reststrahl) dispersive region. The former of these is displayed in figure III. 17.

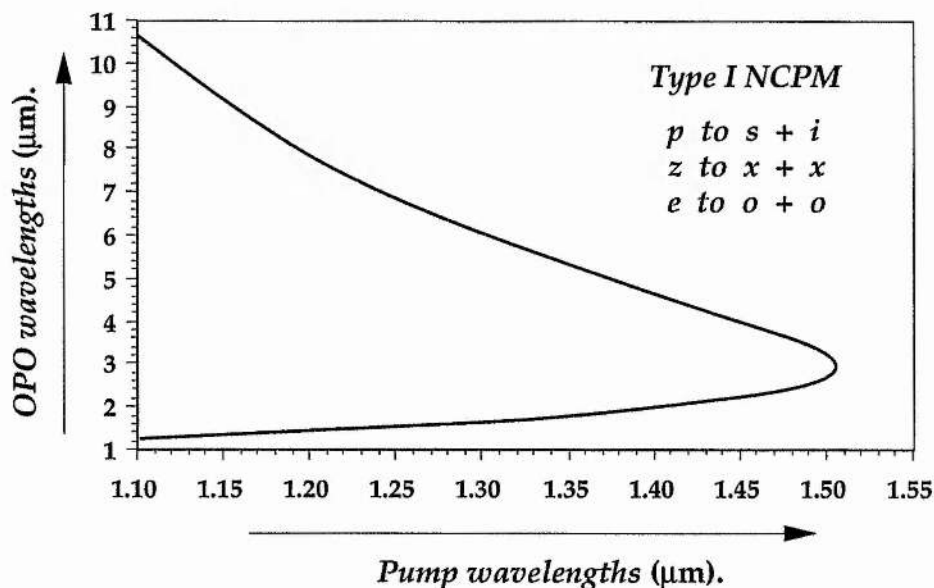


Figure III. 17.

Type I non-critical phase matching in AgGaSe₂, with pump wavelength tuning and operation at room-temperature.

Only room-temperature operation is considered. Temperature tuning is neglected only because of the uncertainties in the precise values of the refractive indices above room-temperature. However, even if the thermal dependence of the refractive indices are an order of magnitude lower than LiNbO₃, as inferred in reference [88], then temperature tuning could be considered. This would be important to increase the range of possible pump

sources for OPO operation, and in particular, to allow for shorter wavelength pump source (e.g. Nd-based lasers or Ti:sapphire lasers).

III. 3 (vi) (b) Type I non-critical phase-matching in AgGaS₂.

The development of AgGaS₂ has been driven by the desire to produce a convenient laser-based source for high-resolution spectroscopy applications in the $\lambda \approx 2$ to 20 μm wavelength region, where virtually all fundamental vibrational modes of molecules and molecular ions exist. AgGaS₂ is similar to AgGaSe₂ except that regions of transmission and phase-matching are shifted to shorter wavelengths, and it has a lower nonlinear coefficient.

AgGaS₂ is transparent from $\lambda \approx 0.53$ to 12 μm (typical absorption coefficients $\approx 0.04 \text{ cm}^{-1}$), and crystals of high optical quality in large dimensions ($> 45 \text{ mm}$) have been used for infra-red generation by mixing, up-conversion into the visible spectral region, and for second harmonic generation of CO₂ lasers. (Note that an intrinsic three-phonon absorption of 0.6 cm^{-1} , near $\lambda \approx 10 \mu\text{m}$, limits its use for second harmonic generation of CO₂ lasers.) In particular, the use of AgGaS₂ for cw difference frequency generation in the mid-infra-red region is important for high resolution spectroscopy, when using pump and signal laser sources in the visible spectral region (e. g. dye, Ti:sapphire, and diode lasers).

AgGaS₂ has adequate birefringence to phase-match for both type I and type II interactions. For non-critical phase-matching, only the type I phase-matching geometry has a non-zero effective nonlinear coefficient ($d_{\text{eff}} \approx 30 \text{ pm/V}$). Similar to AgGaSe₂, room-temperature phase-matching in the short wavelength (band-gap) dispersive region is considered for AgGaS₂; see figure III. 18. This figure illustrates the possibility of using pump sources in the visible and near infra-red spectral regions to generate idler frequency radiation in the mid-infra-red region, out to the transparency cut-off.

However, before being used for cw OPO applications, a number of factors must be addressed. These include the mechanisms responsible for optically induced damage, the temperature dependence of the refractive indices, and the magnitude of the effective nonlinear coefficients. Further, index of refraction measurements need to be made on currently available high optical quality crystals to improve the accuracy of the dispersion equations.

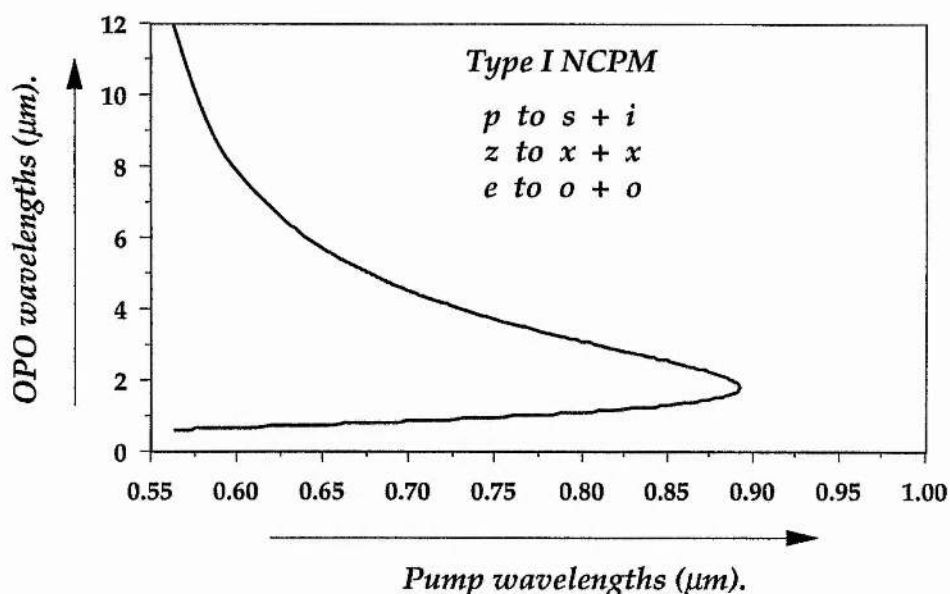


Figure III. 18.

Type I non-critical phase matching in AgGaS_2 , with pump wavelength tuning and operation at room-temperature.

III. 4 Conclusions.

This chapter has analysed the two critical requirements for the construction of low threshold cw OPOs that can deliver frequency stable / tunable signal and idler outputs; pump sources and nonlinear materials.

In general, pump sources should be single frequency lasers, or their frequency harmonics, providing high power, narrow-linewidth, frequency-stable, and frequency tunable radiation. Nonlinear materials should possess moderate effective nonlinear coefficients, have high optical damage thresholds, low temperature sensitivities, and should be easily fabricated.

Diode-laser based sources were considered ideal as the pump sources for cw OPOs. These lasers can deliver high spectral quality optical radiation, either for direct pumping of OPOs, or as the pump source for another solid-state gain medium that in turn can act as the pump source for the OPO. Of particular importance for cw OPO schemes are pump sources whose output can be selected from over a large frequency bandwidth. In this respect, diode lasers and vibronic-based gain media are particularly attractive.

Nonlinear materials that can be phase-matched in type II non-critical geometries, with low temperature sensitivities, are ideal for OPO applications. Such phase-matching geometries are available when using LBO, KTP, KTA, and CTA. For KTP, KTA, and CTA, the low walk-off in critically phase-matched geometries may allow for further signal and idler frequency selection. The use of KTA and CTA with a Nd-based laser as the pump source can allow for cw frequency tunable radiation in the $\lambda \approx 2$ to $4 \mu\text{m}$ spectral region.

The important characteristics of the different nonlinear optical materials studied in this chapter are displayed in table III. 2.

Table III. 2.
 Nonlinear materials for cw OPO use: non-critical phase-matching geometries.

Material	MgO:LiNbO ₃	KNbO ₃	KTP	KTA	CTA	LBO	AgGaSe ₂	AgGaS ₂
Type I / II NCPM	I	I (a), I (b)	II (a, b)	II (a, b)	II (a, b)	I, II	I	I
Transparency (μm)	0.4 to 5	0.3 to 4	0.35 to 2.8	0.35 to 5	0.35 to 5	0.16 to 2.6	≈ 0.8 to ≈ 16	≈ 0.5 to ≈ 12
d_{eff} (pm/V)	6	18, 16	3.2	≈ 3	≈ 3	≈ 1, ≈ 1	≈ 30	≈ 30
I_{dam} (MW/cm ²)	≈ 0.8	≈ 0.1	≈ 2	N/A	N/A	> 25	N/A	N/A
Pump $\Delta\lambda$ (μm)	0.5 to 0.56	0.4 to 0.45 to 0.44 0.53	0.45 to 0.85	0.45 to 1.7	0.45 to 1.6	0.5 to 0.25 to 0.8 0.9	1.10 to 1.5	0.55 to 0.9
OPO $\Delta\lambda$ (μm)	0.6 to 2	0.6 to 0.6 to 1.25 1.25	0.7 to 2.8	0.6 to 3.7	0.5 to 3.7	0.7 to 0.3 to 2.6 2.6	1.3 to 10.6	0.7 to 12
Comments	high e-o cfmt low 1 μm loss	depoling & thermal effects	critical tune, low dn / dT	as per KTP IR trans.	IR trans., new sig./idler	high dn / dT, retracing effect	IR pumps, growth concern	visible pumps, DFM use

III. 5 Outline of experimental work described in the thesis.

The experimental work described within the thesis involves the use of single frequency pump sources operating in the ultra-violet, visible, and near infra-red spectral regions, as the pump sources for different cw OPO configurations. The pump source radiation is derived from fixed frequency laser sources (ultra-violet and visible regions), and a widely tunable near infra-red laser source.

The nonlinear material for each of the devices was LBO, operating in both the type I and type II non-critical phase-matching geometries, outlined within this chapter. The type I phase-matching geometries were operated at elevated temperatures and near frequency degeneracy; the type II phase-matching geometry was operated near room temperature and with signal and idler frequencies in a near 3:1 frequency ratio. In total, the signal and idler frequencies were tuned over selected frequency bandwidths between $\lambda \approx 0.49$ and $1.71 \mu\text{m}$, limited by the bandwidth of the optical coatings applied to the resonator components. When the tunable pump source was used, a wide range of signal and idler frequencies was obtained by tuning both the pump frequency and the phase-matching temperature.

*Table III. 3.
Outline of experimental work.*

	<i>Pump source</i>	<i>Nonlinear material</i>	<i>OPO outputs</i>	<i>Single/ Dual-cavity</i>
<i>Chapter IV</i>	<i>Argon ion 514.5 nm</i>	<i>LBO, Type I NCPM</i>	<i>\approx Degeneracy</i>	<i>Single</i>
<i>Chapter V</i>	<i>Argon ion 363.8 nm</i>	<i>LBO, Type II NCPM</i>	<i>\approx 3:1</i>	<i>Single</i>
<i>Chapter VI</i>	<i>Argon ion 363.8 nm</i>	<i>LBO, Type II NCPM</i>	<i>\approx 3:1</i>	<i>Dual</i>
<i>Chapter VII</i>	<i>Ti:sapphire 780 - 810 nm</i>	<i>LBO, Type I NCPM</i>	<i>\approx Degeneracy</i>	<i>Single</i>

Single-cavity resonator geometries were constructed that allowed for amplitude stable operation on single signal and idler frequency mode-pairs. Dual-cavity resonators allowed for smooth frequency tuning of the OPO

outputs with a fixed frequency pump source. Temperature effects were analysed with respect to the range of smooth frequency tuning possible from these devices. These configurations are summarized in table III. 3.

References.

1. R. G. Smith, J. E. Geusic, H. J. Levinstein, J. J. Rubin, S. Singh, & L. G. Van Uitert, "Continuous optical parametric oscillation in $Ba_2NaNb_5O_{15}$," *Appl. Phys. Lett.* **12**, 308 (1968).
2. R. L. Byer, M. K. Oshman, J. F. Young, & S. E. Harris, "Visible cw parametric oscillator," *Appl. Phys. Lett.* **13**, 109 (1968).
3. M. Hercher, "Tunable single mode operation of gas lasers using intracavity tilted etalons," *Appl. Opt.* **8**, 1103 (1969).
4. J. P. Hohimer, R. C. Kelly, & F. K. Tittel, "Frequency stabilization of a high power argon laser," *Appl. Opt.* **11**, 626 (1972).
5. J. R. Fendley, "Continuous UV lasers," *IEEE J. Quant. Electron.* **QE-4**, 627 (1968).
6. R. G. Smith, "A study of factors affecting the performance of a continuously pumped doubly resonant optical parametric oscillator," *IEEE J. Quant. Electron.* **QE-9**, 530 (1973).
7. R. G. Smith & J. V. Parker, "Experimental observation of and comments on optical parametric oscillation internal to the laser cavity," *J. Appl. Phys.* **41**, 3401 (1970).
8. J. F. Weller, T. G. Giallorenzi, & R. A. Andrews, "Time-resolved spectral output of a doubly resonant cw optical parametric oscillator," *J. Appl. Phys.* **43**, 4651 (1972).
9. R. L. Byer, A. Kovrigin, & J. F. Young, "A cw ring-cavity parametric oscillator," *Appl. Phys. Lett.* **15**, 136 (1969).
10. C. Laurence & F. Tittel, "Visible cw parametric oscillator using barium sodium niobate," *J. Appl. Phys.* **42**, 2137 (1971).
11. R. G. Smith, K. Nassau, & M. F. Galvin, "Efficient continuous optical second-harmonic generation," *Appl. Phys. Lett.* **7**, 256 (1965).
12. J. E. Geusic, H. J. Levinstein, S. Singh, R. G. Smith, & L. G. Van Uitert, "Continuous $0.532\text{-}\mu$ solid-state source using $Ba_2NaNb_5O_{15}$," *Appl. Phys. Lett.* **12**, 306 (1968).
13. R. B. Chesler, M. A. Karr, & J. E. Geusic, "Repetitively Q-switched Nd:YAIG-LiIO₃ $0.53\text{-}\mu$ harmonic source," *J. Appl. Phys.* **41**, 4125 (1970).
14. R. L. Byer, in "Treatise in Quantum Electronics," (H. Rabin & C. L. Tang, Eds.), Academic Press, New York (1973).

15. R. G. Smith,
"Optical parametric oscillators,"
in "Lasers: a series of advances," vol. 4, (A. K. Levine & A. J. DeMaria Eds.) Marcel
Dekker, New York, 189 (1976).
16. R. Fischer & L. A. Kulevskii,
"Optical parametric oscillators (review),"
Sov. J. Quant. Electron. 7, 135 (1977).
17. O. G. Peterson, S. A. Tuccio, & B. B. Snavely,
"CW operation of an organic dye solution laser,"
Appl. Phys. Lett. 17, 245 (1970).
Scientific American,
"Organic lasers,"
Vol. 220, 2, 30 (1969).
18. M. Hercher & H. A. Pike,
"Continuous dye-laser emission from 5220 to 6570 Å,"
IEEE J. Quant. Electron. QE-7, 473 (1971).
19. S. A. Tuccio & F. C. Strome, Jr,
"Design and operation of a tunable continuous dye laser,"
Appl. Opt. 11, 64 (1972).
20. R. L. Barger, M. S. Sorem, & J. L. Hall,
"Frequency stabilization of a cw dye laser,"
Appl. Phys. Lett. 22, 573 (1973).
21. R. L. Barger, J. B. West, & T. C. English,
"Fast frequency stabilization of a cw dye laser,"
Appl. Phys. Lett. 27, 31 (1975).
22. T. J. Kane & R. L. Byer,
"Monolithic, unidirectional single-mode Nd:YAG ring laser,"
Opt. Lett. 10, 65 (1985).
R. L. Byer,
"Diode laser-pumped solid-state lasers,"
Science 23, 742 (1988).
23. J. T. Lin,
"Nonlinear crystals for tunable coherent sources,"
Opt. & Quant. Electron. 22, 283 (1990).
D. N. Nikogosyan & G. G. Gurzadyan,
"Crystals for nonlinear optics,"
Sov. J. Quant. Electron. 17, 970 (1987).
24. D. A. Bryan, R. Gerson, & H. E. Tomaschke,
"Increased optical damage resistance in lithium niobate,"
Appl. Phys. Lett. 44, 847 (1984).
25. J. D. Bierlein & H. Vanherzeele,
"Potassium titanyl phosphate: properties and new applications,"
J. Opt. Soc. Am. B 6, 622 (1989).
26. C. Chen, Y. Wu, A. Jiang, B. Wu, G. You, R. Li, & S. Lin,
"New nonlinear-optical crystal: LiB₃O₅,"
J. Opt. Soc. Am. B 6, 616 (1969).
27. Y. Uematsu,
"Nonlinear optical properties of KNbO₃ single crystal in the orthorhombic phase,"
Japan J. Appl. Phys. 11, 163 (1972).
28. L.-A. Wu, M. Xiao, & H. J. Kimble,
"Squeezed states of light from an optical parametric oscillator,"
J. Opt. Soc. Am. B 4, 1465 (1987).
29. P. Grangier, R. E. Slusher, B. Yurke, & A. LaPorta,
"Squeezed-light-enhanced polarization interferometer,"
Phys. Rev. Lett. 59, 2153 (1987).
30. T. Debuisschert, S. Reynaud, A. Heidmann, E. Giacobino, & C. Fabre,
"Observation of large quantum noise reduction using an optical parametric oscillator,"
Quant. Opt. 1, 3 (1989).

- S. Reynaud, C. Fabre, & E. Giacobino,
 "Quantum fluctuations in a two-mode parametric oscillator,"
J. Opt. Soc. Am B **4**, 1520 (1987).
- A. Heidmann, R. J. Horowicz, S. Reynaud, E. Giacobino, & C. Fabre,
 "Observation of quantum noise reduction on twin laser beams,"
Phys. Rev. Lett. **59**, 2555 (1987).
31. K. W. Leong, N. C. Wong, & J. M. Shapiro,
 "Nonclassical intensity correlation from a type I phase-matched optical parametric oscillator,"
Opt. Lett. **15**, 1058 (1990).
32. L.-A. Wu, H. J. Kimble, J. L. Hall, & H. Wu,
 "Generation of squeezed states by parametric down conversion,"
Phys. Rev. Lett. **57**, 2520 (1986).
33. C. D. Nabors & R. Shelby,
 "Two-colour squeezing and sub-shot-noise signal recovery in doubly resonant optical parametric oscillators,"
Phys. Rev. A **42**, 556 (1990).
34. E. S. Polzik, J. Carri, & H. J. Kimble,
 "Spectroscopy with squeezed light,"
Phys. Rev. Lett. **68**, 3020 (1992).
35. N. C. Wong,
 "Optical frequency division using an optical parametric oscillator,"
Opt. Lett. **15**, 1129 (1990).
36. N. C. Wong,
 "Optical frequency counting from the UV to the near IR,"
Opt. Lett. **17**, 1155 (1992).
37. L. R. Brothers, D. Lee, & N. C. Wong,
 "Terahertz optical frequency comb generation and phase locking of an optical parametric oscillator at 665 GHz,"
Opt. Lett. **19**, 245 (1994).
- N. C. Wong,
 "Proposal for a 10 THz precision optical frequency comb generator,"
IEEE Phot. Tech. Lett. **4**, 1166 (1992).
38. W. Wang & M. Ohtsu,
 "Continuous-wave optical parametric amplifier that uses a diode laser for a wideband coherent optical frequency sweep generator,"
Opt. Lett. **18**, 876 (1993).
- M. Kourogi, K. Nakagawa, & M. Ohtsu,
 "Wide-span optical frequency comb generator for accurate optical frequency difference measurement,"
IEEE J. Quant. Electron. **QE-29**, 2693 (1993).
39. C. D. Nabors, S. T. Yang, T. Day, & R. L. Byer,
 "Coherence properties of a doubly-resonant monolithic optical parametric oscillator,"
J. Opt. Soc. Am. B **7**, 815 (1990).
40. R. C. Eckardt, C. D. Nabors, W. J. Kozlovsky, & R. L. Byer,
 "Optical parametric oscillator frequency tuning and control,"
J. Opt. Soc. Am. B **8**, 648 (1991).
41. D. Lee & N. C. Wong,
 "Tunable optical frequency division using a phase-locked optical parametric oscillator,"
Opt. Lett. **17**, 13 (1992).
42. D. Lee & N. C. Wong,
 "Stabilization and tuning of a doubly-resonant optical parametric oscillator,"
J. Opt. Soc. Am. B **10**, 1659 (1993).
43. F. G. Colville, M. J. Padgett, & M. H. Dunn,
 "Continuous-wave, dual-cavity, doubly-resonant, optical parametric oscillator,"
Appl. Phys. Lett. **64**, 1490 (1994).

44. F. G. Colville, M. Ebrahimzadeh, W. Sibbett, & M. H. Dunn,
"Continuous-wave LiB_3O_5 optical parametric oscillator pumped by a tunable Ti:sapphire laser,"
Appl. Phys. Lett. **64**, 1765 (1994).
45. F. G. Colville, M. J. Padgett, A. J. Henderson, J. Zhang, & M. H. Dunn,
"Continuous-wave parametric oscillator pumped in the ultra-violet,"
Opt. Lett. **18**, 1065 (1993).
46. S. T. Yang, R. C. Eckardt, & R. L. Byer,
"Continuous-wave singly resonant optical parametric oscillator pumped by a single-frequency resonantly doubled Nd:YAG laser,"
Opt. Lett. **18**, 971 (1993).
"1.9-W cw ring-cavity KTP singly resonant optical parametric oscillator,"
Opt. Lett. **19**, 475 (1994).
47. S. T. Yang, R. C. Eckardt, & R. L. Byer,
"Power and spectral characteristics of continuous wave parametric oscillators: the doubly to singly resonant transition,"
J. Opt. Soc. Am. B **10**, 1684 (1993).
48. S. Schiller & R. L. Byer,
"Quadruply resonant optical parametric oscillation in a monolithic total-internal-reflection resonator,"
J. Opt. Soc. Am. B **10**, 1696 (1993).
49. W. R. C. Rowley & D. C. Wilson,
"Wave-length stabilization of an optical maser,"
Nature, Vol. **200**, Nov., 746 (1963).
50. B. Zhou, T. J. Kane, G. J. Dixon, & R. L. Byer,
"Efficient, frequency-stable laser-diode-pumped Nd:YAG laser,"
Opt. Lett. **10**, 62 (1985).
51. Ch. Salomon, D. Hils, & J. L. Hall,
"Laser stabilization at the millihertz level,"
J. Opt. Soc. Am. B **5**, 1576 (1988).
52. D. Shoemaker, A. Brillat, C. Nary Man, O. Cregut, & G. Kerr,
"Frequency-stabilized laser-diode-pumped Nd:YAG laser,"
Opt. Lett. **14**, 609 (1989).
53. K. Banse, G. Herziger, G. Schafer, & W. Seelig,
"Continuous UV-laser power in the watt range,"
Phys. Lett. **27A**, 682 (1968).
54. Da-Wun Chen & J. T. Lin,
"Temperature-tuned phase-matching properties of LiB_3O_5 for Ti:sapphire laser frequency doubling,"
IEEE J. Quant. Electron. **QE-29**, 307 (1993).
55. G. A. Skripko, S. G. Bartoshevich, I. V. Mikhnyuk, & I. G. Tarazevich,
" LiB_3O_5 : a highly efficient frequency converter for Ti:sapphire lasers,"
Opt. Lett. **16**, 1726 (1991).
C. S. Adams & A. I. Ferguson,
"Tunable narrow linewidth ultra-violet light generation by frequency doubling of a ring Ti:sapphire laser using lithium tri-borate in an external enhancement cavity,"
Opt. Comm. **90**, 89 (1992).
56. L. Y. Liu, M. Oka, W. Wiechmann, & S. Kubota,
"Longitudinally diode-pumped continuous-wave 3.5-W green laser,"
Opt. Lett. **19**, 189 (1994).
57. S. T. Yang, C. C. Pohalski, E. K. Gustafson, R. L. Byer, R. S. Feigelson, R. J. Raymakers, & R. K. Route,
"6.5-W, 532-nm radiation by cw resonant external-cavity second-harmonic generation of an 18-W Nd:YAG laser in LiB_3O_5 ,"
Opt. Lett. **16**, 1493 (1991).
58. E. S. Polzik & H. J. Kimble,
"Frequency doubling with KNbO_3 in an external cavity,"
Opt. Lett. **16**, 1400 (1991).

59. G. Hall & A. I. Ferguson,
"Generation of single-frequency radiation at 1064, 1319, and 659.5 nm with an all-solid-state, out of plane Nd:YAG laser,"
Opt. Lett. **19**, 557 (1994).
60. Y. Taira,
"Continuous 6-watt coherent deep UV generation using a resonant doubling technique,"
in *Conference on Lasers and Electro-Optics*, Vol. 10 of OSA 1993 Technical Digest Series (Optical Society of America, Washington, D. C., 1993), paper CFL 3.
61. F. G. Colville, A. J. Henderson, J. Zhang, M. J. Padgett, & M. H. Dunn,
"Continuous-wave parametric oscillation in lithium triborate,"
Opt. Lett. **18**, 205 (1993).
62. I. Gorog, & F. W. Spong,
"An approximate linewidth determination method and the magnetic-field-tunable stable spectrum of the argon laser,"
IEEE J. Quant. Electron. **QE-3**, 691 (1967).
63. W. Koehner,
in "Solid-state laser engineering," Springer-Verlag (1988).
64. A. Arie, S. Schiller, E. K. Gustafson, & R. L. Byer,
"Absolute frequency stabilization of diode-laser-pumped Nd:YAG lasers to hyperfine transitions in molecular iodine,"
Opt. Lett. **17**, 1204 (1992).
65. G. T. Forrest,
"Diode-laser arrays achieve increased power and brightness,"
in *Laser Focus World*, p59 (August 1988).
66. A. D. Farinas, E. K. Gustafson, & R. L. Byer,
"Design and characterization of a 5.5-W, cw, injection-locked, fibre-coupled, laser-diode-pumped Nd:YAG miniature-slab laser,"
Opt. Lett. **19**, 114 (1994).
67. D. Golla, I. Freitag, H. Zellmer, W. Schone, I. Kropke, & H. Welling,
"15 W single-frequency operation of a cw, diode laser-pumped Nd:YAG ring laser,"
Opt. Comm. **98**, 86 (1993).
68. C. D. Nabors, A. D. Farinas, T. Day, S. T. Yang, E. K. Gustafson, & R. L. Byer,
"Injection locking of a 13-W cw Nd:YAG laser,"
Opt. Lett. **14**, 1189 (1989).
69. P. F. Moulton,
"Spectroscopic and laser characteristics of Ti:Al₂O₃,"
J. Opt. Soc. Am. B **3**, 125 (1986).
70. T. L. Boyd & H. J. Kimble,
"Frequency stabilization of a continuous-wave Ti:sapphire laser,"
Opt. Lett. **16**, 808 (1991).
71. K. F. Wall & A. Sanchez,
"Titanium sapphire lasers,"
Lincoln Lab. J. **3**, 447 (1990).
72. J. Harrison, A. Finch, D. M. Rines, G. A. Rines, & P. F. Moulton,
"Low-threshold, cw, all-solid-state Ti:Al₂O₃ laser,"
Opt. Lett. **16**, 581 (1991).
73. M. D. Perry, S. A. Payne, T. Ditmire, R. Beach, G. J. Quarles, W. Ignatuk, R. Olson, & J. Weston,
"Better materials trigger Cr:LiSAF laser development,"
in *Laser Focus World*, p85 (September 1993).
R. S. Geels, D. F. Welch, D. R. Scifres, D. P. Bour, D. W. Treat, & R. D. Bringans,
"20-W cw monolithic visible diode array,"
in *Conference on Lasers and Electro-Optics*, Vol. 12 of OSA 1993 Technical Digest Series (Optical Society of America, Washington, D. C., 1993), paper CThQ 3.
74. J. C. Walling, D. F. Heller, H. Samelson, D. J. Harter, J. A. Pete, & R. C. Morris,
"Tunable alexandrite lasers: development and performance,"
IEEE J. Quant. Electron. **QE-21**, 1568 (1985).

75. R. Scheps, B. M. Gately, J. F. Myers, J. S. Krasinski, & D. F. Heller,
"Alexandrite laser pumped by semiconductor lasers,"
Appl. Phys. Lett. **56**, 2288 (1990).
76. R. Knappe, J. Barschke, C. Becher, B. Beier, M. Scheidt, K.-J. Boller, & R. Wallenstein,
"Injection-locked high power diode arrays and their application as pump sources for
blue and green Nd:YAB lasers, monolithic Nd:YAG ring lasers, and cw KTP optical
parametric oscillators,"
in *Conference on Lasers and Electro-Optics*, Vol. 8 of OSA 1994 Technical Digest Series
(Optical Society of America, Washington, D. C., 1994), paper CThL 4.
77. W. Wang, K. Nakagawa, S. Sayama, & M. Ohtsu,
"Coherent addition of injection-locked high-power AlGaAs diode lasers,"
Opt. Lett. **17**, 1593 (1992).
78. "New dawn beckons for semiconductor laser,"
in *Physics World*, p35, February 1994.
R. S. Geels, D. W. Nam, D. P. Bour, D. W. Treat, D. F. Welch, & D. R. Scifres,
"Low threshold high-power single-mode visible laser diodes,"
in *Conference on Lasers and Electro-Optics*, Vol. 10 of OSA 1992 Technical Digest Series
(Optical Society of America, Washington, D. C., 1992), paper CMA 4.
79. K. Nakagawa, M. Kourogi, & M. Ohtsu,
"Proposal of a frequency-synthesis chain between the microwave and optical
frequencies of the Ca intercombination line at 657 nm using diode lasers,"
Appl. Phys. B **57**, 425 (1993).
80. B. S. Wherrett,
"An introduction to nonlinear optics,"
in *Proceedings of Sixteenth Scottish Summer School in Physics*, (P. G. Harper &
B. S. Wherrett, Eds.), Academic Press, p1 (1975).
81. D. Lee & N. C. Wong,
"Tuning characteristics of a cw dual-cavity KTP optical parametric oscillator,"
in *Conference on Lasers and Electro-Optics*, Vol. 8 of OSA 1994 Technical Digest Series
(Optical Society of America, Washington, D. C., 1994), paper CWE 5.
82. See the following review papers on LiNbO₃ (and MgO:LiNbO₃) and references therein:
J. A. Armstrong, N. Bloembergen, J. Ducuing, & P. S. Pershan,
"Interactions between light waves in a nonlinear dielectric,"
Phys. Rev. **127**, 1918 (1962).
A. Ashkin, G. B. Boyd, J. M. Dziedzic, R. G. Smith, A. A. Ballman, J. J. Levinstein, &
K. Nassau,
"Optically-induced refractive index inhomogeneities in LiNbO₃ and LiTaO₃,"
Appl. Phys. Lett. **9**, 72 (1966).
G. J. Edwards & M. Lawrence,
"A temperature-dependent dispersion equation for congruently grown lithium niobate,"
Opt. & Quant. Electron. **16**, 373 (1984).
D. F. Nelson & R. M. Mikulyak,
"Refractive indices of congruently melting lithium niobate,"
J. Appl. Phys. **45**, 3688 (1974).
D. S. Smith, H. D. Riccius, & R. P. Edwin,
"Refractive indices of lithium niobate,"
Opt. Comm. **17**, 332 (1976).
83. See the following review papers on KNbO₃ and references therein:
Y. Uematsu & T. Fukuda,
"Characteristics and performance of KNbO₃ - YAIG/Nd intracavity second harmonic
generation,"
Japan. J. Appl. Phys. **12**, 841 (1973).
B. Zysset, I. Biaggio, & P. Gunter,
"Refractive indices of orthorhombic KNbO₃. I. Dispersion and temperature
dependence,"
J. Opt. Soc. Am. B **9**, 380 (1992).

- I. Biaggio, P. Kerkoc, L.-S. Wu, P. Gunter, & B. Zysset,
 "Refractive indices of orthorhombic KNbO_3 . II. Phase-matching configurations for nonlinear-optical interactions,"
J. Opt. Soc. Am. B **9**, 507 (1992).
- J.-C. Baumert, J. Hoffnagle, & P. Gunter,
 "Nonlinear optical effects in KNbO_3 crystals at $\text{Al}_x\text{Ga}_{1-x}\text{As}$, dye, ruby, and Nd:YAG laser wavelengths,"
Proc. SPIE **492**, 374 (1984).
- K. Kato,
 "High-efficiency high-power parametric oscillation in KNbO_3 ,"
IEEE J. Quant. Electron. **QE-18**, 451 (1982).
84. See the following review papers on KTP and references therein:
 H. Vanherzeele & J. D. Bierlein,
 "Magnitude of the nonlinear-optical coefficients of KTiOPO_4 ,"
Opt. Lett. **17**, 982 (1992).
 R. F. Belt, G. Gashurov, & Y. S. Liu,
 "KTP as a harmonic generator for Nd:YAG lasers,"
Laser Focus World, 110 (Oct. 1985).
 W. Wang, K. Nakagawa, Y. Toda, & M. Ohtsu,
 "1.5 μm diode laser-based nonlinear frequency conversions by using potassium titanyl phosphate,"
Appl. Phys. Lett. **61**, 1886 (1992).
85. See the following review papers on KTA and references therein:
 J. D. Bierlein, H. Vanherzeele, & A. A. Ballman,
 "Linear and nonlinear optical properties of flux-grown KTiOAsO_4 ,"
Appl. Phys. Lett. **54**, 783 (1989).
 M. G. Jani, J. T. Murray, R. R. Petrin, R. C. Powell, D. N. Loiacono, & G. M. Loiacono,
 "Pump wavelength tuning of optical parametric oscillations and frequency mixing in KTiOAsO_4 ,"
Appl. Phys. Lett. **60**, 2327 (1992).
 G. M. Loiacono, D. N. Loiacono, J. J. Zola, R. A. Stolzenberger, T. McGee, & R. G. Norwood,
 "Optical properties and ionic conductivity of KTiOAsO_4 crystals,"
Appl. Phys. Lett. **61**, 895 (1992).
 L. K. Cheng, L.-T. Cheng, J. D. Bierlein, F. C. Zumsteg, & A. A. Ballman,
 "Properties of doped and undoped crystals of single domain KTiOAsO_4 ,"
Appl. Phys. Lett. **62**, 346 (1993).
 P. E. Powers, S. Ramakrishna, C. L. Tang, & L. K. Cheng,
 "Optical parametric oscillation with KTiOAsO_4 ,"
Opt. Lett. **18**, 1171 (1993).
86. See the following review papers on CTA and references therein:
 L. T. Cheng, L. K. Cheng, J. D. Bierlein, & F. C. Zumsteg,
 "Nonlinear optical and electro-optical properties of single crystal CsTiOAsO_4 ,"
Appl. Phys. Lett. **63**, 2618 (1993).
 P. E. Powers, C. L. Tang, & L. K. Cheng,
 "High-repetition-rate femtosecond optical parametric oscillator based on CsTiOAsO_4 ,"
Opt. Lett. **19**, 37 (1994).
 L. K. Cheng, L. T. Cheng, J. D. Bierlein, & J. Parise,
 "Phase-matching property optimization using birefringence tuning in solid solutions of KTiOAsO_4 isomorphs,"
Appl. Phys. Lett. **64**, 1321 (1994).
 C. L. Tang, P. E. Powers, & R. J. Ellingson,
 "Optical parametric processes and broadly tunable femtosecond sources,"
Appl. Phys. B **58**, 243 (1994).
87. See the following review papers on LBO and references therein:
 S. Lin, Z. Sun, B. Wu, & C. Chen,
 "The nonlinear optical characteristics of a LiB_3O_5 crystal,"
J. Appl. Phys. **67**, 634 (1990).

- T. Ukachi, R. J. Lane, W. R. Bosenberg, & C. L. Tang,
 "Measurements of non-critically phase-matched second-harmonic generation in a LiB_3O_5 crystal,"
Appl. Phys. Lett. **57**, 980 (1990).
- L. Wei, D. Guiqing, H. Qingzhen, Z. An, & L. Jingkui,
 "Anisotropic thermal expansion of LiB_3O_5 ,"
J. Phys. D **23**, 1073 (1990).
- F. Xie, B. Wu, G. You, & C. Chen,
 "Characterization of LiB_3O_5 crystal for second-harmonic generation,"
Opt. Lett. **16**, 1237 (1991).
- S. Lin, B. Wu, F. Xie, & C. Chen,
 "Phase-matching retracing behaviour: New features in LiB_3O_5 ,"
Appl. Phys. Lett. **59**, 1541 (1991).
- S. P. Velsko, M. Webb, L. Davis, & C. Huang,
 "Phase-matched harmonic generation in lithium triborate (LBO),"
IEEE J. Quant. Electron. **QE-27**, 2182 (1991).
- G. A. Skripko, S. G. Bartoshevich, I. V. Mikhnyuk, & I. G. Tarazevich,
 " LiB_3O_5 : a highly efficient frequency converter for Ti:sapphire lasers,"
Opt. Lett. **16**, 1726 (1991).
- D. N. Nikogosyan,
 "Lithium triborate (LBO): A review of its properties and applications,"
Appl. Phys. A **58**, 181 (1994).
88. See the following review papers on AgGaSe_2 and references therein:
 G. D. Boyd, H. M. Kasper, J. H. McFee, & F. G. Storz,
 "Linear and nonlinear optical properties of some ternary selenides,"
IEEE J. Quant. Electron. **QE-8**, 900 (1972).
- R. C. Eckardt, Y. X. Fan, R. L. Byer, R. K. Route, R. S. Feigelson, & J. van der Laan,
 "Efficient second harmonic generation of 10- μm radiation in AgGaSe_2 ,"
Appl. Phys. Lett. **47**, 786 (1985).
- R. C. Eckardt, Y. X. Fan, R. L. Byer, C. L. Marquardt, M. E. Storm, & L. Esterowitz,
 "Broadly tunable infrared parametric oscillator using AgGaSe_2 ,"
Appl. Phys. Lett. **49**, 608 (1986).
- N. P. Barnes, D. J. Gettemy, J. R. Hietanen, & R. A. Iannini,
 "Parametric amplification in AgGaSe_2 ,"
Appl. Opt. **28**, 5162 (1989).
- P. A. Budni, M. G. Knights, E. P. Chicklis, & K. L. Schepler,
 "Kilohertz AgGaSe_2 optical parametric oscillator pumped at 2 μm ,"
Opt. Lett. **18**, 1068 (1993).
89. See the following review papers on AgGaS_2 and references therein:
 G. D. Boyd, H. M. Kasper, & J. H. McFee,
 "Linear and nonlinear optical properties of AgGaS_2 , CuGaS_2 , and CuInS_2 , and theory of the wedge technique for the measurement of nonlinear coefficients,"
IEEE J. Quant. Electron. **QE-7**, 563 (1971).
- P. J. Kupecek, C. A. Schwartz, & D. S. Chemla,
 "Silver thiogallate (AgGaS_2) - Part I: Nonlinear optical properties,"
IEEE J. Quant. Electron. **QE-10**, 540 (1974).
- G. C. Bhar & R. C. Smith,
 "Silver thiogallate (AgGaS_2) - Part II: Linear optical properties,"
IEEE J. Quant. Electron. **QE-10**, 546 (1974).
- T. Elsaesser, A. Seilmeier, W. Kaiser, P. Koidl, & G. Brandt,
 "Parametric generation of tunable picosecond pulses in the medium infrared using AgGaS_2 crystals,"
Appl. Phys. Lett. **44**, 383 (1984).
- Y. X. Fan, R. C. Eckardt, R. L. Byer, R. K. Route, & R. S. Feigelson,
 " AgGaS_2 infrared parametric oscillator,"
Appl. Phys. Lett. **45**, 313 (1984).

- A. H. Hielscher, C. E. Miller, D. C. Bayard, U. Simon, K. P. Smolka, R. F. Curl, & F. K. Tittel,
"Optimization of a midinfrared high-resolution difference-frequency laser spectrometer,"
J. Opt. Soc. Am. B 9, 1962 (1992).
- U. Simon, C. E. Miller, C. C. Bradley, R. G. Hulet, R. F. Curl, & F. K. Tittel,
"Difference frequency generation in AgGaS₂ by use of single-mode diode-laser pump sources,"
Opt. Lett. 18, 1062 (1993).

Chapter IV.

Type I Phase-Matching in Lithium Triborate with Signal and Idler Frequencies near Frequency-Degeneracy.

Contents.	Page.	
IV. 1	Introduction.	175
IV. 2	Single-frequency pump source operating at 583 THz.	178
IV. 3	Optical parametric oscillator design.	185
IV. 4	Pump frequency and cavity length requirements.	194
IV. 5	Experimental arrangement.	203
IV. 6	Results and discussion.	206
IV. 7	Conclusions.	212
	References.	215

IV. 1 Introduction.

This chapter is the first of four experimental chapters. It describes the operating characteristics of the first continuous-wave (cw) optical parametric oscillator (OPO) that used the nonlinear material lithium triborate (LBO) as the gain medium [1]. The study of cw OPOs in the previous three chapters has been concerned solely with modelling the performance of these devices. As expected, within experimental arrangements, there are additional (hitherto unknown) factors that need to be addressed. This chapter examines in detail all the steps considered within the laboratory when building a cw OPO, and how some of the specific modelling of the previous chapters needs to be modified within the experimental (non-ideal) situation.

The OPO was optically pumped by a cw argon-ion laser that was configured to deliver single-frequency radiation in the visible spectral region, with an operating frequency of $\nu_p = 583$ THz, and corresponding to a free-space pump wavelength of $\lambda_p = 514.5$ nm. The LBO crystal was cut for propagation along the x principal optical axis and heated to temperatures of $T_{xtal} \approx 183$ °C to satisfy the conditions of type I non-critical phase-matching. The design of the linear, standing-wave, single-cavity, doubly-resonant OPO

resonator was chosen to allow down-conversion of pump source radiation into near infra-red OPO radiation, which could be tuned coarsely around the frequency-degeneracy point at $\nu_s \approx \nu_i \approx \nu_p / 2 \approx 292$ THz.

The characteristics of the pump source for the OPO are outlined in section IV. 2. The argon-ion laser was selected as a convenient source of high-power radiation with narrow-linewidth, single-frequency, output powers at the Watt-level. High power levels were available from several visible lasing lines of the argon-ion laser in the blue / green spectral region. The argon-ion laser was configured to operate free-running on a single transition line, at the familiar wavelength of $\lambda_p = 514.5$ nm, by using an intra-cavity prism for spatial frequency selection. An etalon was then placed within the linear, standing-wave laser resonator to provide a stable and reliable output, with power levels in excess of $P_p \geq 5$ W radiation in a single-frequency at $\nu_p = 583$ THz. The short-term ($\Delta t \approx 1$ second) frequency jitter of the free-running pump source (FWHM) was measured at $\Delta\nu_{p-stab} \approx \pm 10$ MHz.

The choice of the nonlinear material, the phase-matching geometry, and the coatings applied to the OPO resonator components, are explained in detail in section IV. 3. The nonlinear material LBO was selected primarily to assess its performance as a gain medium within this, and, more importantly, further cw-pumped OPO configurations [2, 3]. The phase-matching geometry was guided by the requirements for minimum pump power operation of a LBO cw OPO above threshold. The optical coatings, the resonator geometry, and the phase-matching temperatures were selected specifically to provide double-resonance at the signal and idler frequencies at, and around, the frequency-degeneracy point. The two-mirror OPO cavity formed a high finesse resonator ($F_s \approx F_i \approx 600$) for both the signal and idler fields by ensuring low round-trip cavity losses at, and around, frequency-degeneracy, corresponding to a centre wavelength of $2\lambda_p = 1.029$ μm . The optical qualities of the OPO components were assessed by calculating the finesse of the OPO resonator for incident radiation from a single-frequency Nd:YAG laser, which operated within $\Delta\nu \approx 10$ THz of the OPO frequency-degeneracy point, at a frequency of $\nu = 282$ THz, corresponding to a wavelength of $\lambda = 1.064$ μm . In addition, the precise phase-matching temperatures of the OPO around frequency-degeneracy were estimated by extrapolating from published temperature data on the frequency up-conversion of near infra-red laser sources which had used LBO in the type I non-critical phase-matching geometry. The phase-matching temperature and the temperature acceptance

bandwidth for second-harmonic generation, when using the LBO crystal in this phase-matching geometry, were assessed by performing a single-pass frequency-doubling experiment with the aforementioned Nd:YAG laser as the source of near infra-red input radiation.

The expected mode selection properties of the output frequencies of this OPO are discussed in section IV. 4. The consequences of operating the single-cavity doubly-resonant OPO under type I phase-matching and with signal and idler frequencies close to the frequency-degeneracy point, are explained. In particular, the use of a single-cavity OPO resonator design for this phase-matching geometry placed the most stringent requirements on the stability of the pump frequency and the OPO cavity length to provide amplitude and frequency stable OPO outputs. The computer program, discussed in chapter II, was used again to examine the effects of detunings / perturbations in the pump frequency, and the OPO cavity length, on the output of the OPO. The requirement on the frequency stability of the pump source was estimated to be $\Delta\nu_{p-stab} \approx \pm 170$ kHz, and this limiting factor is discussed further in relation to the argon-ion laser, selected as the pump source for the OPO. Further pump source requirements were considered with a view to providing the minimum OPO pump power threshold, and, in addition, to the case when the signal and idler finesses of the OPO cavity were relaxed to increase the ratio of useful output coupling to parasitic losses, and therefore to provide increased external conversion efficiencies from the OPO when operating with input pump powers significantly above threshold.

The experimental arrangement is described in section IV. 5. The free-running single-frequency operation of the argon-ion laser was monitored on a scanning confocal *Fabry-Perot* interferometer with a free spectral range of $FSR_{int} = 2$ GHz. The pump mode was matched into the OPO resonator by using a single lens of focal length $f = 250$ mm, which provided near-optimum spatial overlap between the pump, signal and idler waves within the gain medium. The free-running single-frequency operation of the pump laser was isolated from back-reflections and back-conversion from the linear, standing-wave, on-axis OPO resonator, by using a *Faraday* isolator that provided greater than ≈ 30 dB attenuation. The OPO output was separated from the pump radiation by filters and polarizers, and monitored separately on a fast photo-diode and a scanning confocal *Fabry-Perot* interferometer.

The results of the argon-ion pumped cw OPO are presented in section IV. 6. The OPO operated with a minimum pump power threshold of $P_p^{th} \approx 50$ mW. By altering the precise phase-matching temperature of the LBO crystal between $T_{xtal} \approx 183$ and 180 °C, the output frequencies of the OPO could be tuned coarsely, under temperature-tuned type I non-critical phase-matching, over a frequency bandwidth of $\Delta\nu_s + \Delta\nu_i \approx 40$ THz, centred at frequency-degeneracy, and corresponding to wavelengths from $\lambda_s \approx 0.96$ to 1.03 μm and from $\lambda_i \approx 1.03$ to 1.11 μm , for the signal and idler outputs respectively. When the cavity mirrors were changed to provide higher values of output coupling for the signal and idler fields, the ratio of useful to parasitic losses within the OPO resonator was increased. This had the effect of increasing the pump power threshold to $P_p^{th} \approx 250$ mW, while providing significant external optical conversion efficiencies that approached $\eta_{ext} \approx 10$ %, when operating at approximately four times above threshold.

Finally, in section IV. 7, emphasis is directed towards providing improvements in the amplitude and frequency stability of the outputs of a doubly-resonant OPO, operating with type I phase-matching and with signal and idler outputs near frequency-degeneracy. In particular, improvements in the frequency stability of the pump source, the phase-matching geometry employed, the ratio of the signal to idler frequencies, and the OPO resonator design, are considered in detail. The conclusions of this chapter helped to serve as guidelines for the design of amplitude-stable and frequency-tunable cw OPOs that are outlined in chapters V and VI of this thesis.

IV. 2 Single-frequency pump source operating at 583 THz.

In this section, the operating characteristics of the source of pump frequency for the OPO are considered in detail. This involves a description of the argon-ion laser, and the properties that make it suitable for use as a source of input radiation for the OPO. The steps taken to provide narrow-linewidth output radiation from the argon-ion laser are outlined, and the resulting frequency jitter / linewidth of the pump source is measured and discussed.

The pump source for the OPO described in this chapter was selected to fulfil several criteria, as discussed in more general terms in chapter III. The specific characteristics of the pump source for this cw OPO included continuous-wave output, single longitudinal mode operation, high power

output, and operation in the visible spectral region, at a frequency near to $\nu_p \approx 600$ THz, and corresponding to a free-space pump wavelength near to $\lambda_p \approx 0.5 \mu\text{m}$.

Single longitudinal mode operation was required to allow for the possibility of efficient and stable operation of the OPO outputs. High power radiation with single-frequency output at the Watt-level was required to operate a doubly-resonant LBO OPO reliably and consistently above threshold. Frequency operation near to $\nu_p \approx 600$ THz was required to operate the OPO with signal and idler frequency outputs in the near infra-red spectral region, and close to a frequency-degeneracy point in the near infra-red with $\nu_s \approx \nu_i \approx \nu_p / 2 \approx 300$ THz (i.e. $2\lambda_p \approx 1 \mu\text{m}$). In recent years, the near infra-red spectral region ($\lambda \approx 1$ to $2 \mu\text{m}$) has been the subject of considerable research. Consequently, the quality of optical coatings and nonlinear materials in this spectral region is well documented. This reduces substantially the level of uncertainty with regard to forming a low loss resonator for the proposed frequency-degenerate OPO.

As discussed in chapter II, when the signal and idler frequencies of an OPO are equal, as occurs at the point of exact frequency-degeneracy, the OPO frequency down-conversion process, or energy transfer, is the exact opposite of second harmonic generation. To summarize, a nonlinear material that can be phase-matched to frequency-double a source operating at a frequency of ν_p , to provide its second harmonic at a frequency of $2\nu_p$, is a prime candidate for a frequency-degenerate OPO. In the equivalent OPO configuration, the pump source operates at a frequency of $2\nu_p$ and the OPO operates at, and around, frequency degeneracy at ν_p , given the same nonlinear material and phase-matching arrangement. Owing to the substantial work reported for the second harmonic generation of near infra-red solid-state lasers operating at frequencies of $\nu_p \approx 300$ THz [4 - 6], it was decided to operate the OPO under phase-matching conditions that were similar to these frequency-doubling processes. In particular, there has been substantial progress recently when frequency-doubling the radiation from diode-laser-pumped Nd-based lasers (e.g. Nd:YAG and Nd:YLF). This has been due to the excellent spatial and spectral properties that can be provided from these all-solid-state laser sources operating in the near infra-red spectral region [7 - 9], and the desire to produce efficiently harmonics of these frequencies in different spectral regions (e.g. visible and ultra-violet) where such high quality optical radiation is difficult to produce, or does not exist [4, 10].

Therefore, the requirement was for a pump source that operated at a frequency near to $\nu_p \approx 600$ THz. Such sources emit radiation in the blue / green spectral region, and operate with wavelengths near to $\lambda_p \approx 0.5$ μm . Taking into consideration the requirements of the pump source with respect to the efficient and reliable operation of a frequency and amplitude stable cw OPO, there are a limited number of laser pump sources that can be considered as the pump source for such an OPO. These include gas lasers that can be forced to operate on single transition lines, or near infrared solid-state lasers, when frequency up-converted to the green spectral region. Suitable gas lasers include argon-ion [11, 12] and krypton-ion lasers [13, 14]. Argon-ion lasers have a number of transition lines in the blue / green spectral region, with the highest gains at frequencies (wavelengths) of 615 THz (488 nm), 583 THz (514.5 nm) and 568 THz (528 nm). Krypton-ion lasers have a strong lasing line at 565 THz (531 nm). Suitable solid-state pump sources include diode-laser-pumped Nd:YAG [8] and Nd:YLF [15] lasers, frequency-doubled with crystals of LBO [6], KTP [5], or MgO:LiNbO₃ [4], and operating at frequencies (wavelengths) of 564 THz (532 nm) and 574 THz (523 nm), respectively.

The pump source that was selected for the OPO was an argon-ion laser operating at a frequency of $\nu_p \approx 583$ THz. It was chosen as a convenient source of high power, narrow-linewidth, single-frequency radiation when operating at a pump frequency of $\nu_p \approx 600$ THz. (Specifically, the argon-ion laser was the only source available to work with in the laboratory when this experiment was performed.) Therefore, the argon-ion laser was suitable as a pump source for this OPO arrangement when operating in the green spectral region. Moreover, this particular laser source could also be operated efficiently and reliably with high cw output power levels at higher frequencies, in the ultra-violet spectral region, where $\nu_p \approx 900$ THz. One of these higher frequencies would be used as the pump source for further cw OPO work; see chapters V and VI. The argon-ion laser used was a modified, commercial laser product that was manufactured by *Spectra-Physics* (model 2045-E).

The *Spectra-Physics* model 2045-E argon-ion laser (hereafter referred to as the pump source) was configured as a linear, standing-wave resonator. The cavity mirrors were highly-reflecting over a broadband range ($\Delta\lambda \approx 70$ nm [16]) that encompassed several of the blue / green transition lines. Through the use of an intra-cavity dispersing prism, the argon-ion

laser operated on just one transition line, corresponding to a wavelength of $\lambda_p = 514.5$ nm. (Dispersion within the prism allows only one line to be perfectly aligned with the high-reflector.) Figure IV.1 displays a schematic representation of the laser source.

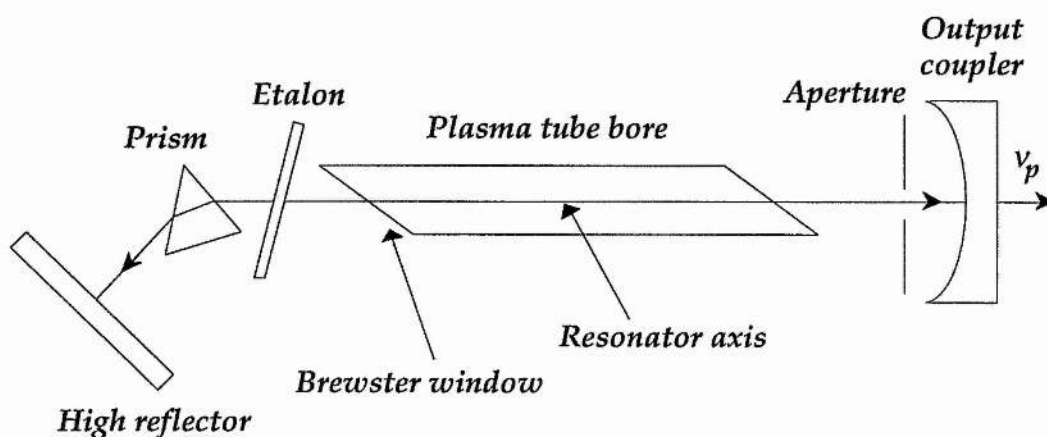


Figure IV. 1.

Schematic representation of the argon-ion laser resonator, used as the source of input pump frequency for the OPO. The intra-cavity prism ensures single-line emission, and the intra-cavity etalon provides single longitudinal mode output.

In general, the gain-bandwidths of gas lasers exhibit significant broadening due to the effects of homogeneous and inhomogeneous broadening [17]. For an argon-ion laser, operating on a single transition line at a frequency of $\nu_p = 583$ THz, or a wavelength of $\lambda_p = 514.5$ nm, the frequency gain-bandwidth is $\Delta\nu_{g-b} \approx 6$ GHz [17], due primarily to the effects of inhomogeneous broadening: Doppler broadening of spectral lines due to high plasma temperatures, magnetic fields via the Zeeman effect, and pressure and radiation broadening.

Therefore, for such a linear, standing-wave optical resonator, with a cavity length of $L \approx 1.78$ m, corresponding to an axial mode spacing, or free spectral range of $FSR \approx 84$ MHz, then without any intra-cavity frequency selective elements, the output consisted of a number of longitudinal modes. (Only if the optical length, L , of the cavity is made sufficiently short, where $c / 2L > \Delta\nu_{g-b}$, or $L < 25$ mm, will this laser oscillate on a single frequency.)

However, in general, longer lengths of laser gain media are employed in commercial argon-ion lasers to obtain greater output powers.

Therefore, the spectral output was found to be a rapidly fluctuating function of time, consisting of a number of longitudinal modes with random amplitude and phase. To be suitable for use as a pump source for the cw OPO, it was necessary to reduce the linewidth of the output, by suppressing the unwanted longitudinal resonances to obtain single frequency output. This was achieved simply by placing a tilted etalon within the resonator, to select one of the axial modes under the gain profile. The air-spaced etalon used was 11 mm in thickness and consisted of two thin, fused-silica, dielectric-coated windows separated by a hollow, low-expansion tube made also of fused-silica [16]: $FSR_{etalon} \approx 14\text{GHz} > \Delta\nu_{g-b}$. Single-frequency operation was obtained by tilting the etalon slightly off the axis of the resonator. The use of an intra-cavity etalon has the advantages of simplicity of fabrication, relative insensitivity to vibration, and a low insertion loss resulting in a high efficiency. If the etalon is positioned so that the loss generated by the etalon is a minimum in the centre of the gain curve, the modes that can oscillate are reduced to those where the gain exceeds the combination of etalon loss and output coupling loss, or about $\approx \pm 2\text{GHz}$, as displayed in figure IV. 2.

In addition to the etalon, there is another mechanism that further reduces the number of modes which oscillate. The unsaturated gain curve applies only when the laser first begins to lase. As the laser oscillation builds, it reaches intensities which significantly reduce the population difference between the upper and lower laser states, with the result that the gain at the frequency of oscillation is reduced, or saturates, to a level that matches the losses that occur: hole-burning.

Longitudinal modes are close enough in frequency that, in a fully operating laser, adjacent modes will compete with one another. This mode competition arises from the fact that a given excited ion, which nominally will be stimulated at a specific frequency (related to its energy, relative velocity and any Zeeman effects) can undergo stimulated emission over a narrow range of frequencies that covers several longitudinal modes. Any mode within this range which is slightly favoured over the others will essentially use all the gain available and the other neighbouring modes will disappear. Therefore, the etalon finesse is chosen to provide a broad-band

intra-cavity filter to allow for power to be transferred from adjacent modes near line-centre into the most-favoured mode.

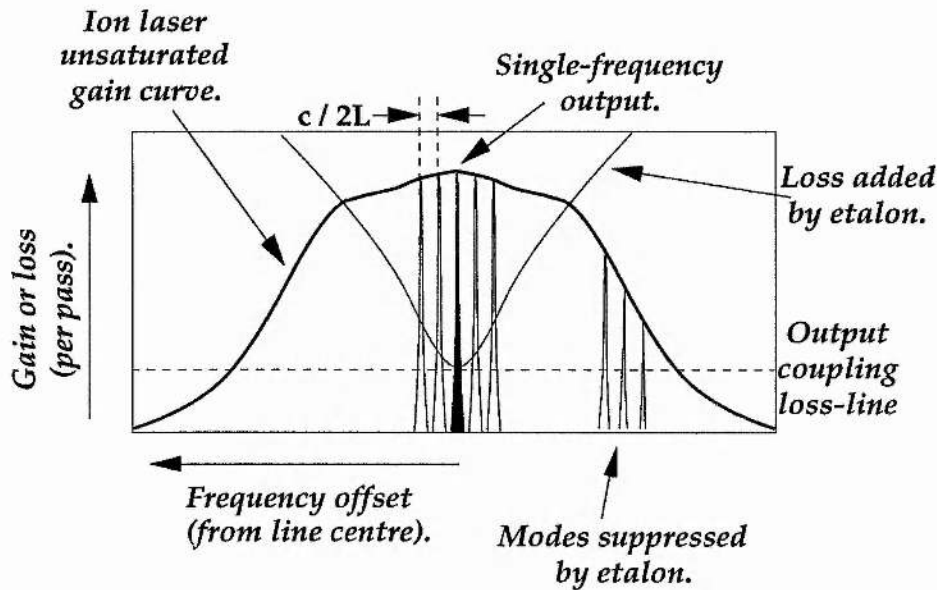


Figure IV. 2
Single-frequency selection using an etalon for the 514.5 nm line.

Single-frequency operation was monitored on a scanning confocal interferometer ($FSR_{int} = 2$ GHz). Free-running, single-frequency operation of the laser is shown in figure IV. 3. Typically, single-frequency power levels in excess of $P_p \approx 5$ W could be achieved in this manner, representing a conversion efficiency of $\approx 50\%$ from multi-mode to single-mode operation.

As explained in chapter II, it is important to evaluate the exact linewidth, or frequency stability, $\Delta\nu_{p-stab}$, of the pump laser since this plays a significant role in the amplitude and frequency stability of the signal and idler outputs. Therefore, it is worthwhile considering the principal causes of laser frequency instability in such large-frame argon-ion lasers. The laser frequency stability depends almost entirely on the stability of the cavity resonance [11, 18]. (Frequency variations due to fluctuations in refractive index of the inverted population are not usually observed unless the discharge is electrically noisy [11, 18]. At line centre, fluctuations in inverted population have a negligible effect on the cavity resonance [11, 18].)

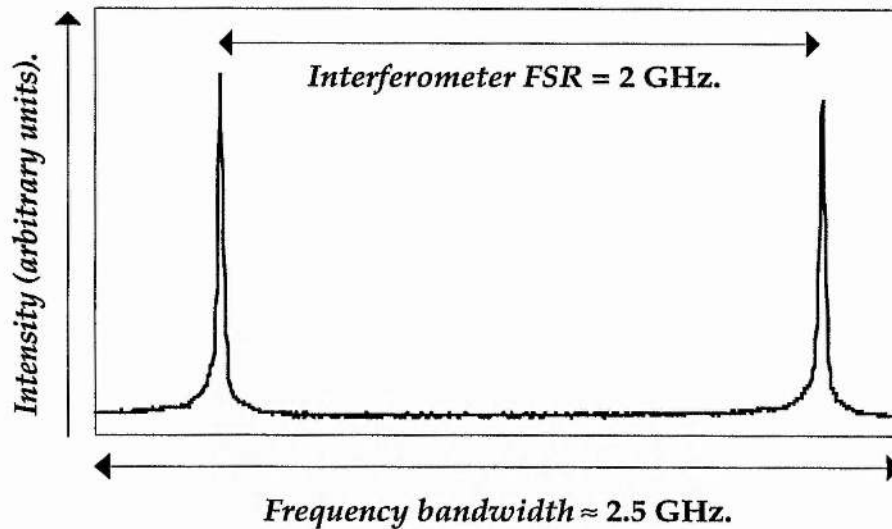


Figure IV. 3.

Single-frequency operation at a frequency of $\nu_p = 583$ THz.

Changes in the ambient temperature and pressure are responsible for most of the long term drift in cavity resonance due to the cavity length and the intra-cavity etalon thermal expansions. Much more serious are mechanical vibrations/resonances of the cavity and / or the optical bench generated by airborne sound waves. The short-term frequency jitter was determined primarily by cavity vibrations induced by water flow in the laser head. The frequency range was in the low- to mid-audio region (≈ 20 to 500 Hz) with mechanically-enhanced resonances dominating [16]. The short-term ($\Delta t \approx 1$ second) frequency-jitter was measured to be $\Delta \nu_{p-stab} \approx \pm 10$ MHz (half-width at half-maximum), by observing the fluctuations in the intensity transmitted through the invar-based, stable monitoring external etalon.

Table IV. 1
Characteristics of the input pump frequency.

Pump source		Argon-ion laser
Frequency	ν_p	583 THz
Wavelength	λ_p	514.5 nm
Jitter (≈ 1 second)	$\Delta \nu_{p-stab}$	$\approx \pm 10$ MHz
Power	P_p^{in}	≈ 5 W

In chapter II, it was shown that the important requirement for the pump source of a cw OPO was the short term frequency jitter. To recap, linewidths at the \approx MHz-level are usually marginal for stable OPO operation. The consequence of operating the argon-ion laser with a short-term frequency jitter at the 10 MHz-level is, as expected critical, and the effects of this are discussed further in section IV. 5. The important characteristics of the argon-ion laser, used as the source of input pump frequency for the cw OPO, are summarized in table IV. 1.

IV. 3 Optical parametric oscillator design.

This section describes in detail the design of the OPO resonator. In particular, the crystal properties are examined that would allow for the generation of tunable, near infra-red, optical radiation around the frequency-degeneracy point, when using the argon-ion laser as the pump source operating at a frequency of $\nu_p = 583$ THz, and an OPO containing the nonlinear material LBO. The resonator components are analysed with a view to obtaining low pump power thresholds, wide (coarse) frequency tuning, amplitude-stable OPO operation, and significant values for the external conversion efficiency.

The nonlinear material chosen for the OPO was lithium triborate (LiB_3O_5 ; LBO) [19]. Prior to this experiment, only $\text{Ba}_2\text{NaNb}_5\text{O}_{15}$ [20], LiNbO_3 [21] (or $\text{MgO}:\text{LiNbO}_3$ [22]), KTP [23] and KNbO_3 [24] had been used as the nonlinear materials within cw OPOs. LBO was selected for its low absorption and scattering losses at both the pump frequency and around frequency-degeneracy [6], non-critical phase-matching for pump sources operating at frequencies of $\nu_p \approx 600$ THz [25], moderate nonlinear coefficients ($d_{\text{eff}} \approx 1$ pm/V [19]), and its high optical damage threshold ($I_{\text{dam}} \geq 20$ GW/cm² [6]). Such properties suggest the suitability of LBO as the gain medium within cw OPO applications. The only desirable property that cannot be accessed when using LBO is electro-optic tuning. The electro-optic coefficients of LBO have gone unreported in press, but preliminary investigations have suggested that they are not at a level that could enable useful electro-optic tuning [26, 27].

As discussed in chapter II, nonlinear materials that possess significant electro-optic tuning properties, and can be fabricated to form monolithic / semi-monolithic OPO resonators, are highly suitable for use

within cw OPO configurations [28, 29]. Indeed, other workers have highlighted the benefits of using such nonlinear materials, when operating with pump sources in the green spectral region, and OPOs operating in the near infra-red spectral region around frequency degeneracy [22, 23, 28, 29]. When the benefits of electro-optic tuning and monolithic fabrication are combined with room-temperature operation and type II phase-matching, the nonlinear material KTP is the crystal of choice [29]. For pump sources in the green spectral region, KTP is a prime candidate for degenerate and near degenerate OPO operation. However, it is the coarse frequency tuning properties of LBO under non-critical phase-matching that make this a worthwhile system to study, with the possibility of generating large frequency differences between the signal and idler outputs in phase-matching geometries that are unique to LBO [3, 30], and cannot be generated when using either KTP or MgO:LiNbO₃ (the two main contenders).

As discussed in chapter III, both type I and type II phase-matching geometries are available from LBO, when using pump sources that operate at frequencies around $\nu_p \approx 600$ THz. However, in general, for non-critical phase-matching at frequency-degeneracy, only type I phase-matching can be employed. This phase-matching geometry in LBO is used regularly to obtain the second frequency harmonic of laser sources operating in the near infra-red spectral region [6, 31]. In particular, LBO is the crystal of choice for frequency-doubling cw lasers when the power intensities within the nonlinear materials are at a level that excludes the use of KTP and LiNbO₃ [6], whose effective nonlinear coefficients are superior to LBO, and which can be used more efficiently at low power levels where power intensities are reduced and optical induced damage is prevented [4, 5].

When pumped at frequencies near to $\nu_p \approx 600$ THz, LBO can be temperature-tuned under type I non-critical phase-matching, with $\theta = 90^\circ$, and $\phi = 0^\circ$ [25, 32]. The crystal for this experiment was cut for propagation along the x-axis. In this phase-matching geometry, the pump field was polarized along the crystal y-axis and the generated signal and idler frequencies were polarized along the crystal z-axis: $e \rightarrow o+o$.

The dimensions of the crystal were specified to be 3, 3, and 20 mm along the y, z, and x principal optical axes, respectively. (At this time, 20 mm represented the longest growth of the crystal.) The crystal cut and the polarizations of the pump, signal and idler fields are displayed in figure IV. 4.

The crystal was cut with plane-parallel, polished input and output faces. These faces were coated to be anti-reflecting at both the pump frequency and around the frequency-degeneracy point. The critical value is at frequency-degeneracy, since the signal and idler frequencies require high finesse cavities to ensure double-resonance with a low pump power threshold.

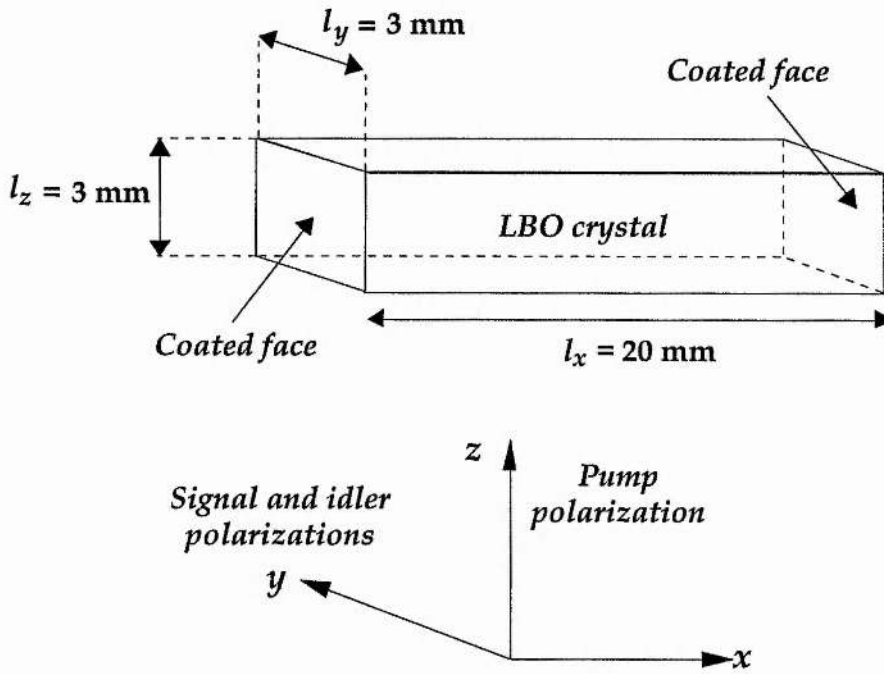


Figure IV. 4.
Schematic representation of the LBO crystal, cut for propagation along the x -axis, to satisfy type I non-critical phase-matching.

The single-pass transmission losses, incorporating reflection losses from the dual anti-reflection coatings and absorption / scattering in the material, were specified to be $\beta_{s,s-p} \approx \beta_{i,s-p} < 0.25\%$ around 292 THz (OPO frequencies) and $\beta_{p,s-p} < 2\%$ at 583 THz (pump frequency).

The crystal was placed within a temperature-controlled oven, heated to achieve the desired phase-matching temperatures, and surrounded by two cavity mirrors to form a low loss resonator for the signal and idler fields. In addition, mirror curvatures and spacings were selected to satisfy cavity stability and confocal focusing of the three waves within the gain medium.

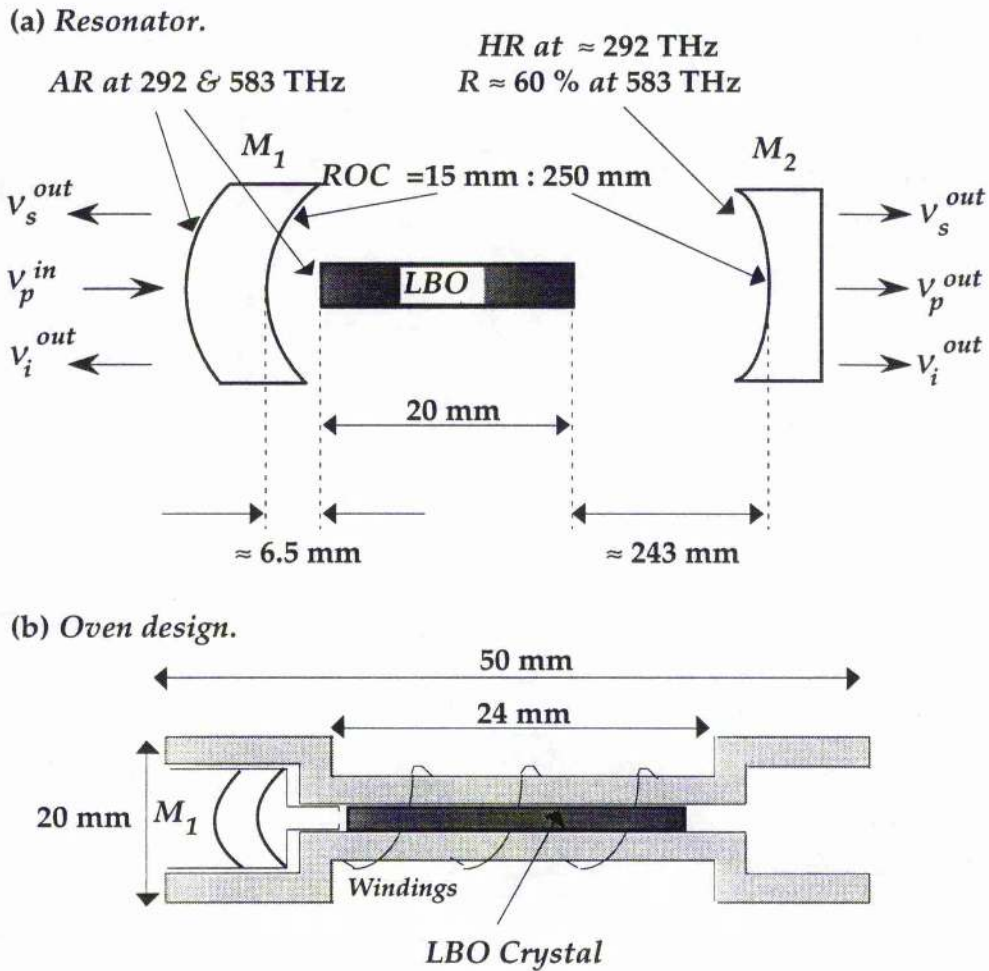


Figure IV. 5.

(a) Schematic representation of the standing-wave, single-cavity, resonator geometry used for the OPO. The nonlinear material was located within a temperature-stabilized oven (b), and heated to temperatures of $T_{xtal} \approx 183$ °C to satisfy the conditions of non-critical phase-matching. HR: high-reflecting; AR: anti-reflecting; ROC: radius-of-curvature.

As discussed in chapter II, to satisfy confocal focusing requirements within the nonlinear material of length, $l = 20$ mm, the resonator must provide spot sizes of $W_p \approx 31.9$ μm and $W_s \approx W_i \approx 45.2$ μm for the pump and signal / idler fields, respectively, and these should be located at the centre of the nonlinear crystal (see equations II. 161 and II. 162). To provide for this, and taking into consideration the design restrictions of using an oven to enclose the crystal, a resonator geometry was selected that incorporated one cavity mirror, M_1 in

figure IV. 5 (a), fixed in position within the oven (15 mm radius-of-curvature), and the other cavity mirror, M_2 , located external to the oven with its location determined by fine piezo-electric control on the mirror position (250 mm radius-of-curvature).

The temperature of the crystal was reached by passing a current of $I \approx 15$ A along a 4.5 m length of nichrome wire of resistivity $\rho \approx 25 \Omega/\text{m}$. The temperature was monitored by feedback to a temperature control unit which could maintain the crystal temperature to within $\Delta T_{xtal} \approx \pm 0.1$ °C. This cavity geometry is illustrated schematically in figure IV. 5 (b).

The cavity mirrors were coated to provide high-reflectivity at around frequency-degeneracy ($R_s \approx R_i > 99.7$ %) and partial reflectivity at the pump frequency ($R_p \approx 60$ %). The coatings were selected primarily to provide a high finesse resonator for the signal and idler fields. The effects of the pump reflectivity, and the corresponding finesse of the OPO cavity at the pump frequency, are considered in detail in section IV. 4. To assess the optical quality of the OPO mirrors / nonlinear crystal, the following experiment was performed to estimate the cavity finesse near degeneracy; figure IV. 6.

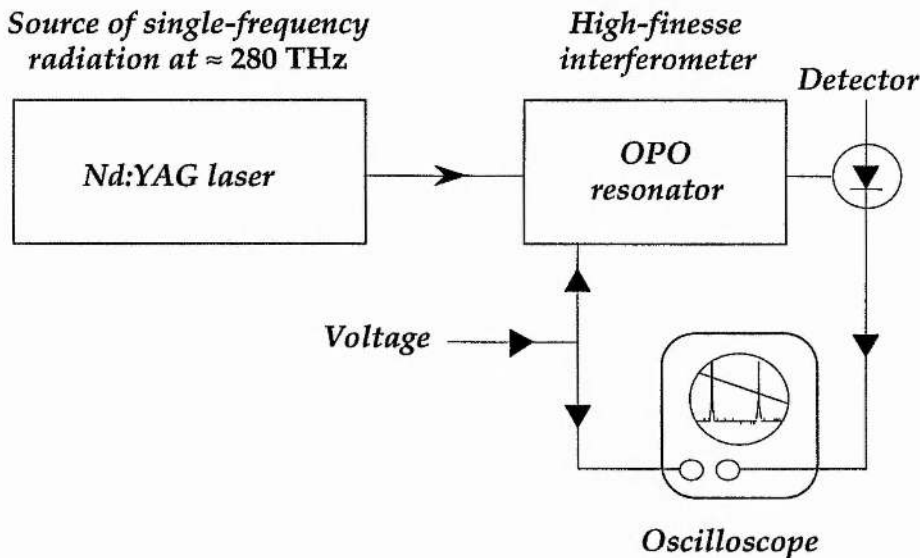


Figure IV. 6.

Experimental arrangement to assess the cavity finesse for frequencies near OPO frequency-degeneracy. The output from a single-frequency, linearly-polarized, Nd:YAG laser is incident on the OPO cavity, which acts as a high-finesse filter for the incident radiation.

The OPO resonator was used as an interferometer to analyse the radiation from a diode-laser-pumped Nd:YAG laser, which operated on a single-frequency at $\nu = 282$ THz, corresponding to a wavelength of $\lambda = 1.064$ μm . By measuring the finesse of this interferometer, an indication as to the parasitic loss of the OPO resonator at $\nu = 282$ THz could be made. Given the proximity of this frequency to the frequency-degenerate point of the proposed argon-ion pumped OPO (within $\Delta\nu \approx 10$ THz), and the assumption that the optical quality of the coatings was comparable for these two frequencies, the loss of the OPO resonator for the signal and idler frequencies could be estimated. By scanning the OPO cavity length by applying a ramp voltage to one cavity mirror that was mounted on a piezo-electric element, and monitoring the intensity of the transmitted output, the finesse of the cavity at the frequency $\nu = 282$ THz was calculated by examining the resonance peaks of figure IV. 7.

Two different sets of finesse peaks are shown in figure IV. 7. (a). These correspond to the two orthogonal polarization components within the LBO crystal, resolved along different crystal axes of the resonator. (Within the resolution of the apparatus used, the two free spectral ranges appear equal, although dispersion within the birefringent LBO crystal causes unequal free spectral ranges.) The resonance peaks of higher intensity corresponded to radiation at $\nu = 282$ THz polarized along the y -axis of the LBO crystal, and simulated the finesse that would be provided by an idler frequency of the argon-ion pumped OPO, detuned by $\Delta\nu \approx 10$ THz from the exact frequency-degeneracy point. The finesse of these peaks was examined in more detail in figure IV. 7. (b).

From figure IV. 7, the finesse of the cavity can be calculated by using the following expression that relates the cavity finesse (F_c) to the cavity free spectral range (FSR_c) and full-width power at half-maximum ($FWHM$) of the resonance peaks [33]; i.e.

$$F_c = \frac{FSR_c}{FWHM} \quad \text{[IV. 1]}$$

The round-trip cavity loss, $\beta_{c,r-t}$, can be expressed as a function of the cavity finesse, in the case of low loss resonators, as follows [33]:

$$\beta_{c,r-t} \approx \frac{2\pi}{F_c} \quad \text{[IV. 2]}$$

Therefore, by combining the above two expressions, the round-trip cavity power loss can be written approximately as follows:

$$\beta_{c,r-t} \approx 2\pi \frac{FWHM}{FSR_c} \quad [IV.3]$$

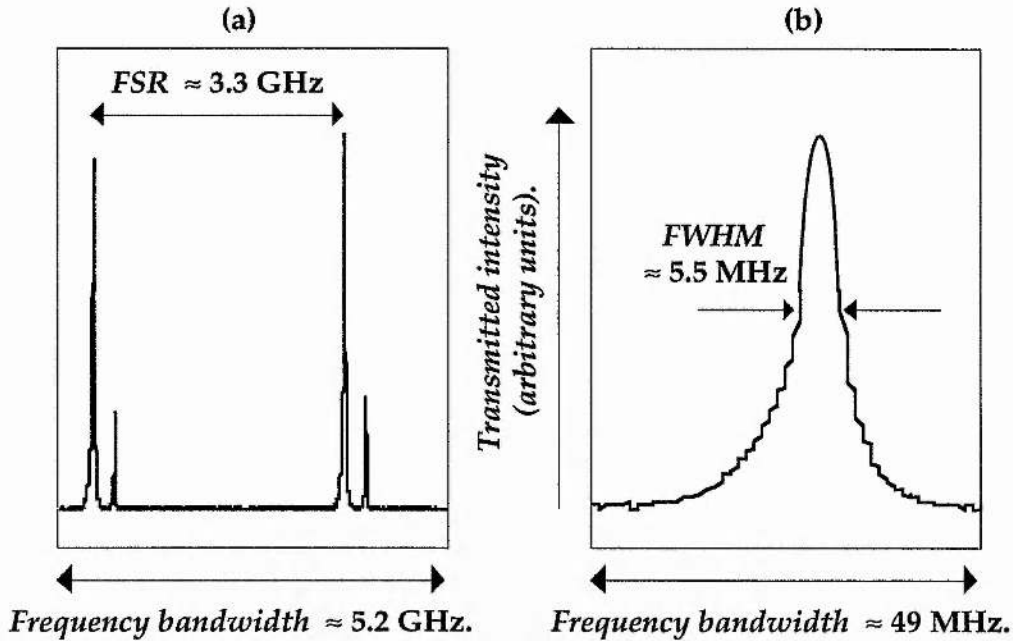


Figure IV. 7.

Finesse peaks of the OPO resonator for an input frequency at $\nu = 282$ THz, and within $\Delta\nu = 10$ THz of the proposed degenerate signal and idler OPO frequencies. In figure IV. 6 (a), the two sets of peaks correspond to linearly-polarized input radiation polarized along orthogonal axes of the LBO crystal. In figure IV. 6 (b), the resonance peak from the higher intensity polarization component along the y principal LBO axis, is expanded to evaluate the *FWHM*.

Hence, from figure IV. 7, and for a frequency of $\nu = 282$ THz, the finesse is calculated to be $F \approx 600$, and the round-trip cavity power loss is estimated to be $\beta_{c,r-t}(\nu = 282 \text{ THz}) \approx 1.0\%$. This latter value is now taken as an approximation as to the signal and idler round-trip power losses in the OPO.

Another critical parameter in the successful operation of the OPO is the exact phase-matching temperature of the nonlinear crystal for this specific

phase-matching geometry. For most commonly used nonlinear materials, this can be calculated readily from data on the temperature dependence of the refractive indices that can be found in literature. However, for LBO, the published data at this time was valid only near room-temperature [34]. Therefore, another method was required to predict the temperature of the phase-matching process in the OPO. This was obtained by extrapolating from temperature data reported for second-harmonic generation experiments using LBO in the type I non-critical phase-matching geometry [35 - 37].

There is substantial information on the phase-matching temperatures for second harmonic generation of near infra-red laser sources into the visible (blue / green spectral region), using type I non-critically phase-matched LBO [6, 31, 35, 36]. As discussed, the phase-matching geometry and temperature for second harmonic generation are identical to that of a frequency-degenerate OPO, but with the opposite direction of energy transfer.

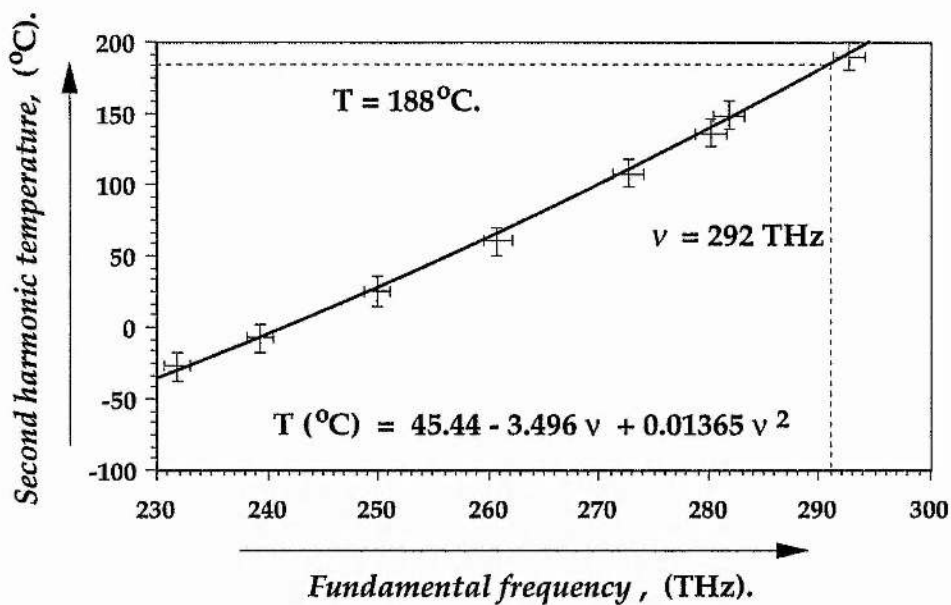


Figure IV. 8.
Non-critical phase-matching temperatures for second harmonic generation of near infra-red sources using type I non-critically phase-matched LBO. (From references [35 - 37].)

Therefore, although there are no specific laser sources available at $\nu = 292$ THz, by extrapolating from other near infra-red frequency doubling processes, the operating temperature of an argon-ion pumped frequency-degenerate OPO could be predicted. These temperatures are shown plotted in figure IV. 8, and from this, a temperature of $T_{xtal} \approx 188$ °C is predicted for the point of exact frequency-degeneracy for the OPO.

To confirm some of the temperature phase-matching properties of the LBO crystal, it was used to generate the second harmonic frequency of a Nd:YAG laser which operated at a frequency of $\nu = 282$ THz, in an external single-pass arrangement. Figure IV. 9 confirms the phase-matching temperature for this frequency conversion process. The phase-matching temperature for second harmonic generation was measured to be $T_{xtal} \approx 149$ °C, and the full-width at half maximum (FWHM) was measured to be $\Delta T \approx 1.6$ °C, indicating a temperature acceptance bandwidth of 3.2 °C cm, a factor of ≈ 20 % lower than other reports of this phase-matching configuration [6, 31], suggesting a temperature gradient along the oven.

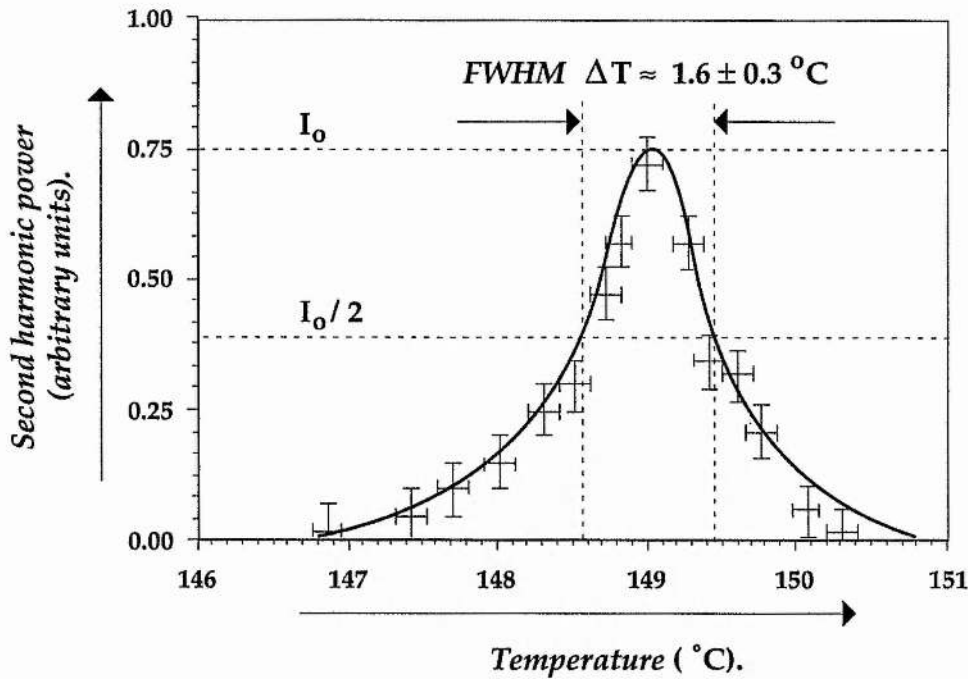


Figure IV. 9.
Phase-matching temperature and temperature acceptance bandwidth for the LBO crystal, when used to generate the second harmonic frequency of a Nd:YAG laser operating at a frequency of $\nu = 282$ THz.

In summary, useful information regarding the cavity losses for the resonant sub-harmonic frequencies and the phase-matching temperatures for operation of the OPO near frequency-degeneracy, has been obtained. This guided the design of the experimental arrangement. In particular, the finesse measurements were used to predict the power levels that would be required from the argon-ion laser.

IV. 4 Pump frequency and cavity length requirements.

In this section, there is an analysis of the power and stability requirements of the pump frequency and the OPO cavity length to maintain stable OPO operation on a single signal and idler frequency mode-pair. With the information gained regarding the OPO cavity finesses, a value for the pump power threshold was estimated. Additional parameters that affected the operation of the OPO were examined, including, in particular, the effects caused by partial resonance of the pump field within the OPO cavity.

The requirements on the stability of the pump frequency and the OPO cavity length in a type I phase-matching geometry near frequency-degeneracy were analysed in detail in chapter II. To recap, this phase-matching geometry was shown to be the most demanding of all possible phase-matching configurations, to maintain single signal and idler frequency mode-pair operation from a single-cavity OPO. This was because the signal and idler frequencies are approximately equal and are polarized along the same crystal axis. Subsequently, the cavity free spectral ranges are approximately equal. It was predicted that pump frequency perturbations of $\Delta\nu_{p-stab} < \text{MHz}$ or cavity length detunings of $\Delta L_{stab} < \text{nm}$ would cause the output of the OPO to hop from one mode-pair to another (see section II. 4 (ii) (b) (1)).

The computer program [38], discussed in chapter II, was used to predict the tolerance of the OPO output to perturbations / detunings in the pump frequency and the OPO cavity length. The input data used for the following graphs is collected in table IV. 2, and is specific to the argon-ion pumped near-degenerate LBO OPO that was to be constructed. Two different experimental situations were modelled, depending on whether the OPO was operated close to frequency-degeneracy, or detuned coarsely by changing the precise phase-matching temperature of the crystal. The finesses and the cavity lengths were

set equal to the experimental values, and differ from those that were used within the more general modelling of chapter II.

Table IV. 2
Input data used for the computer model.

<i>Phase-matching</i>		<i>Type I (a, b)</i>
<i>Pump frequency</i>	ν_p	583 THz
<i>Signal frequency</i>	ν_s	(294, 308 THz)
<i>Idler frequency</i>	ν_i	(289, 275 THz)
<i>Frequency mis-match</i>	$\Delta\nu$	(5, 33 THz)
<i>Temperature</i>	T_{xtal}	(177.8, 176°C)
<i>Crystal length</i>	l	20 mm
<i>OPO finesses</i>	F_s, F_i	600
<i>Mirror separation</i>	L	269 mm
<i>FSR mis-match</i>	ΔFSR	(0.003, 0.02 %)

Two different phase-matching temperatures were studied to yield signal and idler frequency mis-matches of $\Delta\nu = 5$ and 33 THz, for the near-degenerate, (a), and non-degenerate, (b), cases, respectively. (Note that the phase-matching temperatures differ slightly from those predicted from the analysis of section IV. 3. This is because the computer model assumes that the reported data for the temperature dependence of the refractive indices [34] are valid up to these higher phase-matching temperatures) The different frequency mis-matches correspond to mis-matches in the free spectral ranges of $\Delta FSR = 0.003$ and 0.02 %, respectively. As expected for the type I phase-matching geometry, the mis-match in the free spectral ranges approach zero as the signal and idler frequencies approach the exact point of frequency-degeneracy.

The effects of detuning on the output of the near-degenerate, single-cavity OPO, case (a), are illustrated in figure IV. 9. For the type I phase-matching geometry near frequency-degeneracy, the output of the OPO hops between adjacent mode-pairs for comparatively small detunings in the pump frequency or the OPO cavity length.

The overlap of the threshold minima of successive mode-pair parabolas ensures that, for most pumping rates above threshold, the OPO will remain operational. Therefore, between successive mode-hops, the OPO will be subject to an amplitude modulation which is dependent on the width of the minima curves (as defined by the cavity finesses) and the proximity of these curves (as defined by the free spectral ranges). Figure IV. 10 illustrates that the pump frequency must be stable to within $\Delta\nu_{p-stab} \approx \pm 100$ kHz to maintain operation on a single signal and idler frequency mode-pair. In addition, the common signal and idler cavity length of the single-cavity OPO must be stable to within $\Delta L_{stab} \approx \pm 5$ pm. The expected amplitude modulation is shown by horizontal markers that define the difference in threshold between the lowest threshold mode-pairs.

The more stringent requirements predicted here, compared to the modelling of chapter II, are due mainly to two reasons. First, the finesses are significantly higher ($\approx 50\%$ greater) than used before; this decreases the width of the threshold minima. Second, the cavity length of the single cavity OPO is significantly longer than before (a factor of ≈ 8), and this further decreases the mis-match in the free spectral ranges of the signal and idler fields since the length of the crystal represents a smaller fraction of the total cavity lengths.

As discussed in chapter III, cavity length control, for a fixed frequency pump source, can generally be provided by servo-control feedback. Therefore, the main requirement was on the stability of the pump frequency. Given that the frequency stability of the argon-ion laser was almost two orders of magnitude worse than the minimum pump frequency stability requirements for the OPO, as predicted above, it was anticipated that the OPO would not operate in a stable manner on a single signal and idler frequency mode-pair. This would have required a pump source that was actively stabilized at the kHz-level.

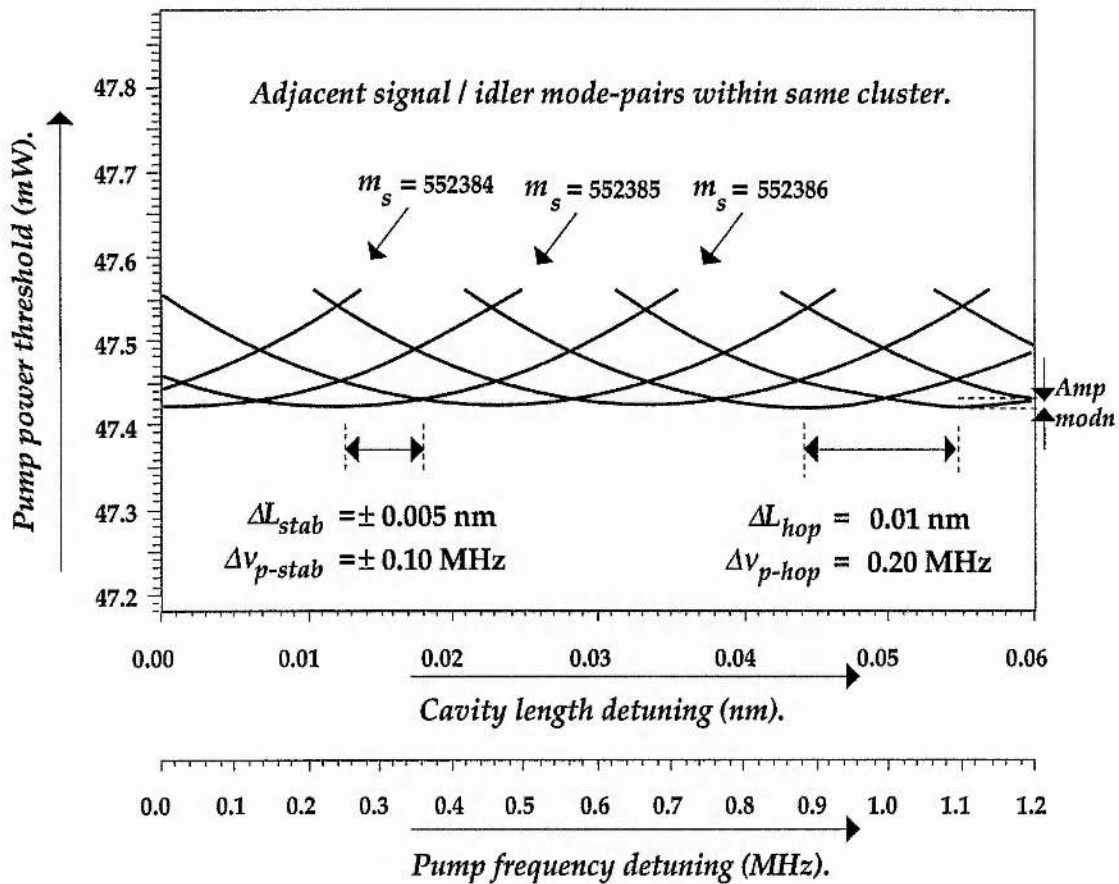


Figure IV. 10.

The effect on the mode selection of the output of the near-degenerate OPO for a pump frequency detuning of $\Delta v_p = 1.2 \text{ MHz}$, and a cavity length detuning of $\Delta L = 0.06 \text{ nm}$; case (a).

Similar predictions were then made by removing the frequencies further from degeneracy (now $\Delta v = 33 \text{ THz}$), and evaluating the equivalent pump frequency and cavity length stability requirements; case (b). Figure IV. 11 shows that the pump frequency must now be held stable to within $\Delta v_{p-stab} \approx \pm 170 \text{ kHz}$, and that the OPO cavity length must be held stable to within $\Delta L_{stab} \approx \pm 10 \text{ pm}$, to maintain operation on a single signal and idler frequency mode-pair. The threshold parabola for separate mode-pairs are of the same form as case (a), due to the equivalent cavity finesses, but the larger mis-match in the free spectral ranges effectively pushes these curves further apart, and relaxes the tolerance to pump frequency and cavity length detunings to maintain single mode-pair operation. Consequently, the

amplitude modulation is expected to increase as the OPO is removed further from degeneracy.

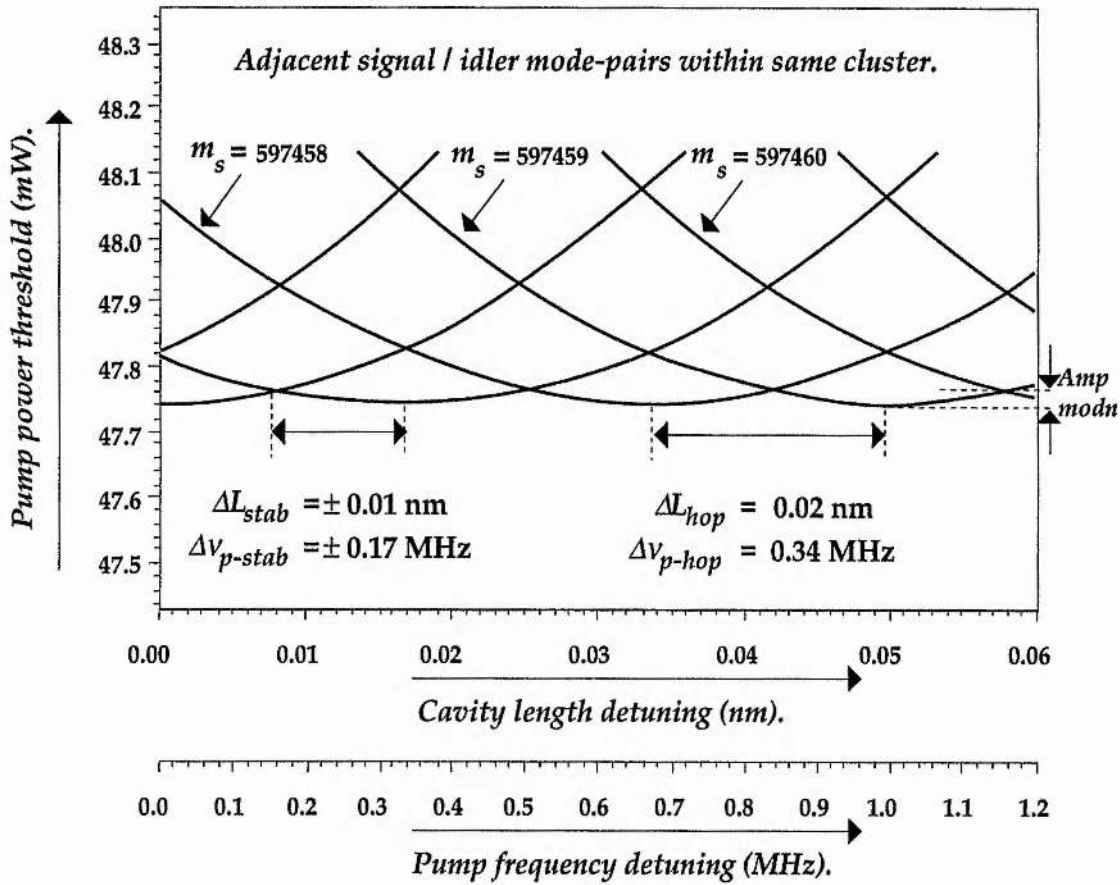


Figure IV. 11

The effect on the mode selection of the output of the non-degenerate OPO for a pump frequency detuning of $\Delta v_p = 1.2 \text{ MHz}$, and for a cavity length detuning of $\Delta L = 0.06 \text{ nm}$; case (b).

In the design of the OPO resonator, there was an additional factor that complicated the tuning characteristics of the OPO outputs. Besides satisfying near perfect resonance for the signal and idler frequencies, pump resonance effects had to be evaluated within the OPO cavity. The reflectivity of the OPO cavity mirrors at the pump frequency was specified to be $R_p \approx 60 \%$. This was chosen to assist alignment of the OPO cavity (by aligning the cavity mirrors to resonate the pump field, the OPO resonator was necessarily aligned), to provide a method of determining the quality of the mode-matching, and to

reduce further the threshold of the OPO. As discussed in chapter II, by resonating the pump frequency in the OPO cavity, reductions in the threshold over equivalent single-pass, non-resonant pump arrangements, can be obtained as a result of both double-pass pump interaction [29] and pump field enhancement [39]. (This is true as long as the pump frequency is held on resonance within the cavity.) However, it was this pump resonance condition that further complicated the requirements for stable OPO operation.

To predict the pump power threshold of the OPO, we used the expression derived for a pump-enhanced doubly-resonant OPO, with the pump held on resonance and the optimum phase-relationship between the pump, signal and idler waves being maintained on the return pass through the nonlinear crystal. This expression was derived in chapter II, and is as follows:

$$\left(P_p^{in}\right)_{th-min} = \frac{n_p^2 \epsilon_0 c^4}{8F_s F_i E_{p-max} |d_{eff}|^2 (1-\delta^2)^2 v_p^3} \quad [IV. 4]$$

Table IV. 3 lists the values that were used within the above threshold equation. The different finesse values correspond to the case of the OPO cavity formed by two high-reflectors (finesse ≈ 600 for a 1.0 % round-trip power loss), and when one of the high-reflectors is replaced by an output coupler of specified output coupling of ≈ 0.5 % (finesse ≈ 400 for a 1.5 % round-trip power loss).

From these values, equation IV. 4 predicts a pump power threshold of $P_{p-min}^{th} = 9.15$ mW (20.5 mW), for the case of signal / idler finesse of $F_s \approx F_i = 600$ (400), respectively (assuming optimum mode-matching and confocal focusing).

While the above threshold analysis follows the most appropriate equation derived in chapter II, it was not necessarily the most accurate expression to use to predict the pump power threshold of this OPO. The partial reflectivity of the cavity mirrors at the pump frequency implied that the pump field losses were significant and not at the level that allowed for the assumption of a high finesse, low-loss resonator for the pump field. Therefore, it was not strictly correct to use the threshold equation for the triply-resonant oscillator with three low-loss fields on resonance. However, it was equally incorrect to assume the straight-forward double-resonance

analysis because there were two equal, enhanced pump fields, counter-propagating within the OPO cavity.

Table IV. 3
Parameter values for threshold analysis.

<i>Pump frequency</i>	ν_p	583 THz
<i>Pump ref. index</i>	n_p	1.61
<i>Crystal length</i>	l	20 mm
<i>Nonlinear coefficient</i>	d_{eff}	≈ 0.84 pm/V
<i>Degeneracy factor</i>	δ	≈ 1
<i>Signal/idler finesse</i>	F_s, F_i	600 (400)
<i>Pump enhancement</i>	E_{p-max}	2.5

To account for this, a combination of the two is now adopted that involves directly incorporating double-pass and field enhancement terms within the standard doubly-resonant OPO analysis. By comparing equations II. 85, and II. 87, the following expression can be formed:

$$\left(P_p^{in}\right)_{th-min} = \frac{n_p^2 \epsilon_0 c^4}{2F_s F_i E_p (1 + |r_p|)^2 |d_{eff}|^2 (1 - \delta^2)^2 \nu_p^3} , \quad [IV. 5]$$

where E_p is the measured pump field enhancement on resonance in the absence of OPO conversion (i.e. sub-threshold operation), and r_p is the electric-field reflectivity of the output cavity mirror at the pump frequency (a value of $r_p = 0.77$ for $R_p = 60\%$). As r_p approaches unity, the factor is four is returned to the analysis, and the triply-resonant OPO equation is formed (equation IV. 4).

The pump enhancement on resonance was measured to be $E_p \approx 1.8$, which is lower than the value, as predicted by the resonance conditions of the

cavity, and was attributed to imperfect mode-matching of the pump source into the OPO cavity. When using this value for the pump field enhancement, the threshold values are now $P_{p-min}^{th} = 16.1$ mW and 36.2 mW, a factor of approximately two higher than the previous predictions, but still well within the power available from the argon-ion laser.

The resonance effects of (partial) pump reflectivity are now considered. For matched mirror reflectivities of $R_p \approx 60\%$ at the pump frequency, the effects of OPO cavity length and pump frequency detuning on the intra-cavity pump field enhancement factor, E_p , can be modelled by the following relationship [33]:

$$E_p(\nu_p, L_c) = \frac{P_p^{circ.}}{P_p^{in}} = \frac{T_p}{1 - 2 \cos(4\pi\nu_p L_c / c) R_p \exp(-\beta_p) + R_p^2 \exp(-2\beta_p)}, \quad [IV. 6]$$

where β_p is the intra-cavity, round-trip, parasitic power loss at the pump frequency (assumed to be $\approx 5\%$), $P_p^{circ.}$ is the circulating pump field inside the resonator, and L_c is the optical length of the OPO cavity.

The intra-cavity power loss only becomes critical when the reflectivity of the cavity mirrors for the pump frequency are high. In this case, the field enhancement on resonance can be reduced significantly, but the reflectivities of the separate input and output coupling mirrors must be chosen carefully to ensure that the cavity is correctly impedance-matched. Within this experiment, parasitic power losses of sub - 10 % do not significantly degrade the pump field enhancement factor. (See reference [33] for a more rigorous explanation.)

It is useful to show graphically the expected variation of the pump field within the OPO resonator, as defined by equation IV. 6, for both cavity length and pump frequency detunings, which affect the intra-cavity pump field. These effects are depicted in figure IV. 12, in which the effects of efficient OPO conversion (pump depletion) have been neglected. As mentioned earlier, these effects contribute to a form of intra-cavity parasitic loss for the enhanced field, and will decrease the enhancement factor. Therefore, this graph models the sub-threshold case.

Table IV. 4

Requirements on pump frequency and cavity length.

Signal and idler frequency double-resonance.

<i>Pump frequency</i>	$\Delta\nu_{p-stab}$	$\approx \pm 170$ kHz
<i>Cavity length</i>	ΔL_{stab}	$\approx \pm 10$ μm

Pump frequency resonance.

<i>Pump frequency</i>	$\Delta\nu_{p-stab}$	$\approx \pm 0.1$ GHz
<i>Cavity length</i>	ΔL_{stab}	$\approx \pm 0.05$ μm

Pump power threshold.

<i>High finesse</i>	P_{p-th}^{in}	16.1 mW
<i>Low finesse</i>		36.2 mW

To summarize, the threshold requirement is well within the available power level from the argon-ion laser. However, the pump frequency stability is only good enough to maintain the pump frequency near resonance within the OPO cavity. It is far from adequate to maintain a particular mode-pair of the signal and idler fields on resonance simultaneously. Therefore, the OPO is expected to display mode-hopping frequency characteristics, while the pump field is at, or close to, exact pump field resonance.

IV. 5 Experimental arrangement.

This section describes the apparatus that was used to provide reliable and efficient operation of the doubly-resonant OPO above threshold. In particular, two aspects of the experimental arrangement are considered in detail. These are the mode-matching of the pump beam into the OPO resonator, and the isolation of the pump source from back-reflections and

back-conversion from the OPO resonator. The experimental arrangement is illustrated in figure IV. 13.

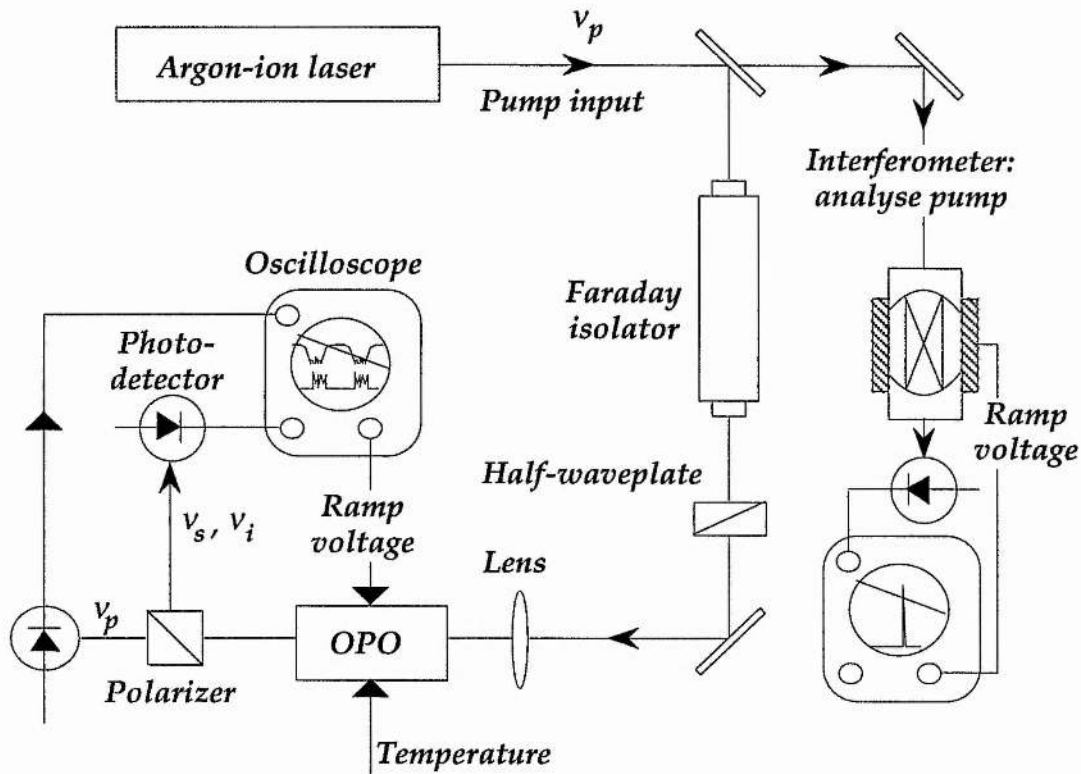


Figure IV. 13.

Layout of the apparatus used to operate the cw OPO. A *Faraday* isolator prevents feedback into the pump laser, and a single focusing lens matches the pump radiation into the OPO cavity.

It was necessary to isolate the single-frequency pump source from two separate causes. First, since the OPO cavity had significant resonance effects for the pump frequency, back-reflections would be present if the OPO cavity was not perfectly impedance-matched for the input radiation. Second, backward-travelling signal and idler fields generate pump radiation that can also feedback to the laser source. To provide isolation of the single-frequency pump source, a *Faraday* isolator was employed, and this arrangement provided ≈ 30 dB attenuation. (Note that the use of a ring-cavity OPO would reduce the effects of pump feedback.)

The second important design consideration was the mode-matching of the pump beam into the OPO resonator. The argon-ion output beam had to be transformed by at least one lens to fulfil the required beam parameters at the input mirror of the OPO, and therefore achieve the desired focusing the pump wave. This analysis follows the equations derived in chapter II. The argon-ion laser output had the following beam parameters [16]; full-angle divergence at $1/e^2$ power points:

$$2\theta_p = \frac{2\lambda_p}{n\pi W_{p,laser}} = 0.5 \text{ mrad.} \quad [\text{IV. 7}]$$

This implied an effective waist size for the pump source of $W_{p,laser} = 655 \mu\text{m}$, located near the plane high-reflector in the argon-ion laser cavity (see figure IV. 1), where the lens effect of the output-coupler has been accounted for. Figure IV. 14 displays a theoretical graph of focal length plotted against the distances from the lenses for different focal length lenses, to match the pump Gaussian profile to that required throughout the length of the gain medium for confocal focusing requirements, where $W_{p,OPO} \approx 31.9 \mu\text{m}$.

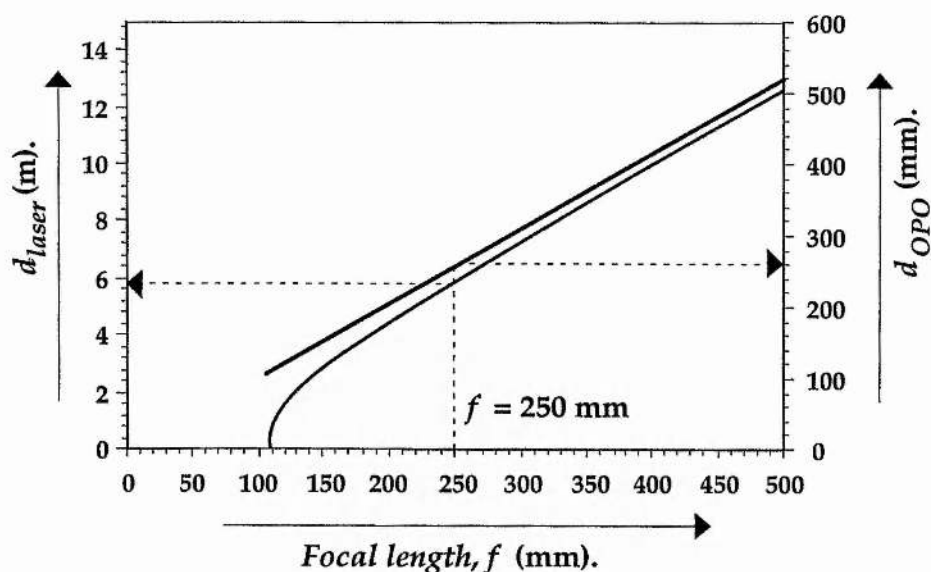


Figure IV. 14.

Theoretical locations of the pump and focused OPO waists for different values of the focal length of the single lens, to match the argon-ion beam to the mode defined by the OPO resonator.

From figure IV. 14, a number of different focal length lenses could be used to obtain the desired focusing. In practice, the choice of lens was dictated by the physical length of the argon-ion laser (recall that the beam waist in the argon-ion laser was located near the plane high-reflector, and therefore is situated at ≈ 2 m from the actual output of the laser). Taking into consideration the free-space propagation over the length of the optical bench, and the optical lengths of the auxiliary optical components, a lens of focal length $f = 250$ mm was selected.

An important consideration of the experimental design was the use of a meniscus input coupling lens (mirror) that was fabricated to reduce the effects of focusing of the pump mode. The rear surface of this mirror was curved specifically to a value of $ROC_{in}(15 \text{ mm}) + d_{substrate}(5 \text{ mm}) = 20 \text{ mm}$. This reduced the effects of de-focusing the beam that would have otherwise been present in a plano-concave substrate. While it is not possible to eliminate completely the effect of the input substrate (due to the propagation of the Gaussian beam within the dense substrate, with refractive index ≈ 1.54), the tolerance on the position of the actual focusing lens, with the focused spot size and location, was relaxed considerably.

IV. 6 Results and discussion.

In this section, the results of the argon-ion pumped cw OPO operating near frequency-degeneracy are presented. Two different resonator configurations were examined that provided for the minimum pump power thresholds (high finesse cavity) and for significant external conversion efficiencies (low finesse cavity). The frequency properties of the OPO output are discussed in view of the previous analyses. In particular, by studying the effects of cavity length detunings over nanometre ranges, the stringent pump and OPO resonance requirements, as presented in section IV. 4, are illustrated. Finally, the frequency tuning range, as permitted by the bandwidth of the optical coatings within the OPO resonator, is reported.

First, the OPO was arranged with two highly-reflecting OPO cavity-mirrors, forming the high-finesse resonator for the signal and idler frequencies. This OPO operated with a minimum pump power threshold of $P_{p-min}^{th} \approx 50$ mW. This represented the power, as measured incident on the OPO resonator, and equated to $P_p \approx 80$ mW of actual argon-ion power.

(Approximately 70 % of the laser output could be focused on the OPO cavity, caused mainly by transmission losses due to uncoated isolator components.)

The power characteristics of the OPO are displayed in figure IV. 15. The OPO power levels were measured by calibrating the peak intensity levels of the OPO outputs on a fast photo-diode. The power levels measured were due to the combined output power of the signal and idler fields. The power outputs from the two exit ports of the OPO cavity (assumed equal) were taken into account to yield a final value for the external OPO power generated.

The experimental threshold value was significantly higher than that predicted from equation IV. 5 ($P_{p-min}^{th} \approx 16$ mW). This was attributed to the imperfect mode-coupling of the pump beam into the resonator, as implied by the lower value of the field enhancement factor, and the temperature gradient within the oven. In addition, the choice of the mirror curvatures and their locations (one internal to the oven, one external), and subsequent asymmetry of the resonator constructed, placed a high level of precision on the exact positions of the two cavity mirrors to obtain the optimum focusing.

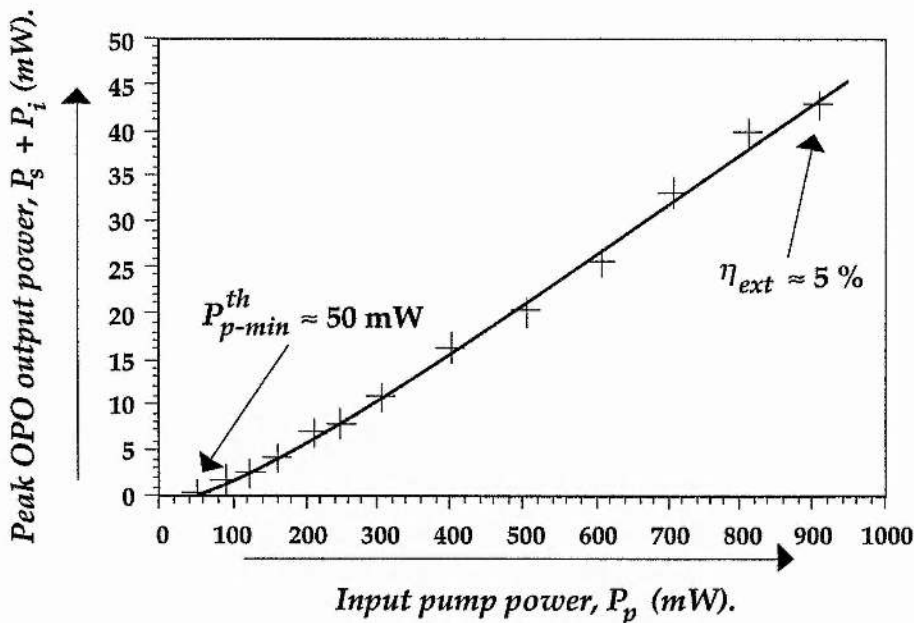


Figure IV. 15.

Input and output powers for the high-finesse ($F \approx 600$) OPO cavity, showing a minimum pump power threshold of $P_{p-min}^{th} \approx 50$ mW and a maximum external conversion efficiency of $\eta_{ext} \approx 5\%$.

When the ratio of useful to parasitic losses was increased by using the 0.5 % output coupler in place of one of the high-reflectors, increased external conversion efficiencies were obtained. However, since the cavity finesse were lower (≈ 400), due to higher cavity losses, the OPO operated with an increased threshold, as displayed in figure IV. 16. When operating at approximately four times the pump threshold of $P_p^{in-th} \approx 250$ mW, corresponding to an incident pump power of $P_p^{in} \approx 1$ W, the external conversion efficiencies were measured to be $\eta_{ext} \approx 10$ %.

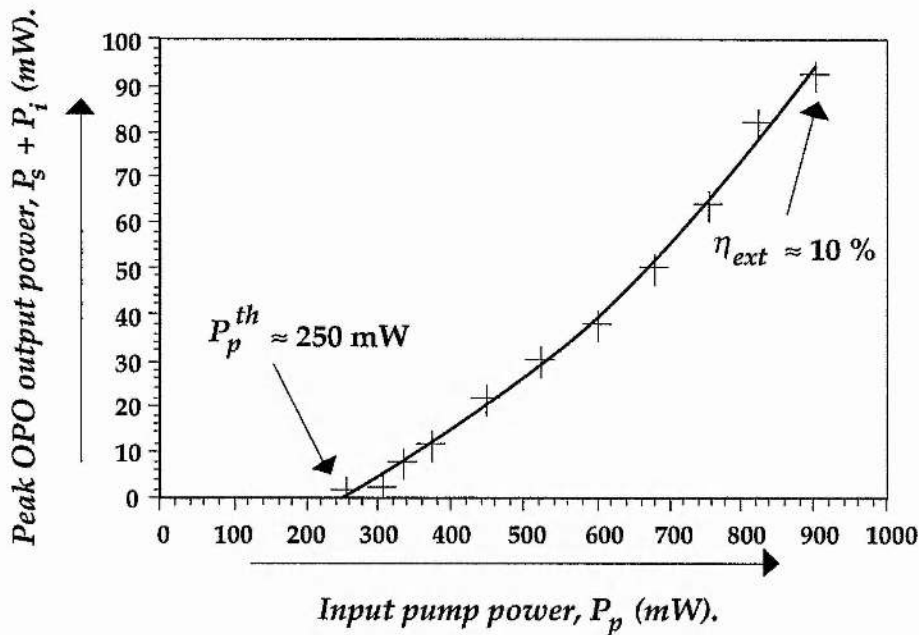


Figure IV. 16.

Input and output powers for the lower-finesse ($F \approx 400$) OPO cavity, showing a pump power threshold of $P_p^{th} \approx 250$ mW, and a maximum external conversion efficiency of $\eta_{ext} \approx 10$ %.

To assess the performance of the OPO with respect to amplitude and frequency stability, the cavity length was ramped over nanometre ranges, by applying a voltage to a piezo-electric element that controlled the position of one of the cavity mirrors (in this case, the output coupler). Both pump and OPO resonance conditions could be evaluated using this technique. The effects on the pump field due to detuning off exact pump field resonance, and from the effects of depletion due to OPO operation, were evaluated by

monitoring the variations in the transmitted pump wave, or the reflected pump wave, through pump resonance. The intensity variations of the transmitted pump field, along with the OPO output, are displayed in figure IV. 17.

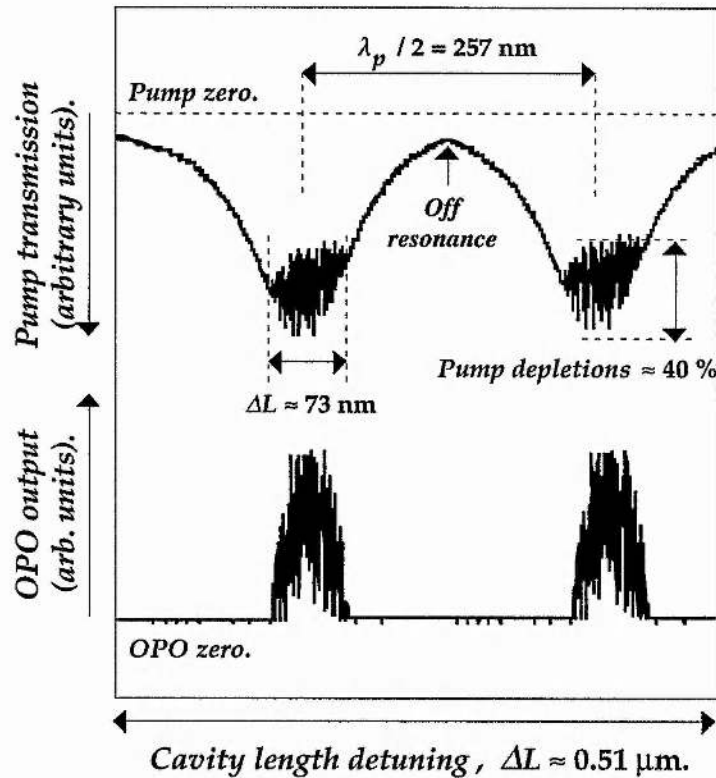


Figure IV. 17.

Variations in the intensity of the transmitted pump field, and the OPO output, as the cavity length is detuned through $\Delta L \approx 0.51 \mu\text{m}$.

This figure displays the expected effects due to the partial pump resonance nature of the OPO cavity. The OPO operated only when the intra-cavity pump field was sufficient to overcome threshold, and this happens for a finite region near exact pump resonance, corresponding to a cavity length detuning of $\Delta L \approx 73 \text{ nm}$, in good agreement with figure IV. 12. Moreover, when there is sufficient gain within the resonator, the conversion of the OPO acts as a source of internal pump field depletion, or loss. This is displayed in the upper trace of figure IV. 17. Depletion in the transmitted pump field

implies OPO operation, and this is shown to follow exactly the variations in the detected pump field.

When the cavity operated sufficiently close to exact pump field resonance, the OPO was observed to remain on constantly until the pump field dropped below the threshold value. This implied that for every cavity length position, there existed a signal and idler mode-pair that could overcome threshold. This confirms the analysis of figure IV.10, in section IV.6, which predicted that the OPO would remain oscillating, as long as the pump field was above threshold.

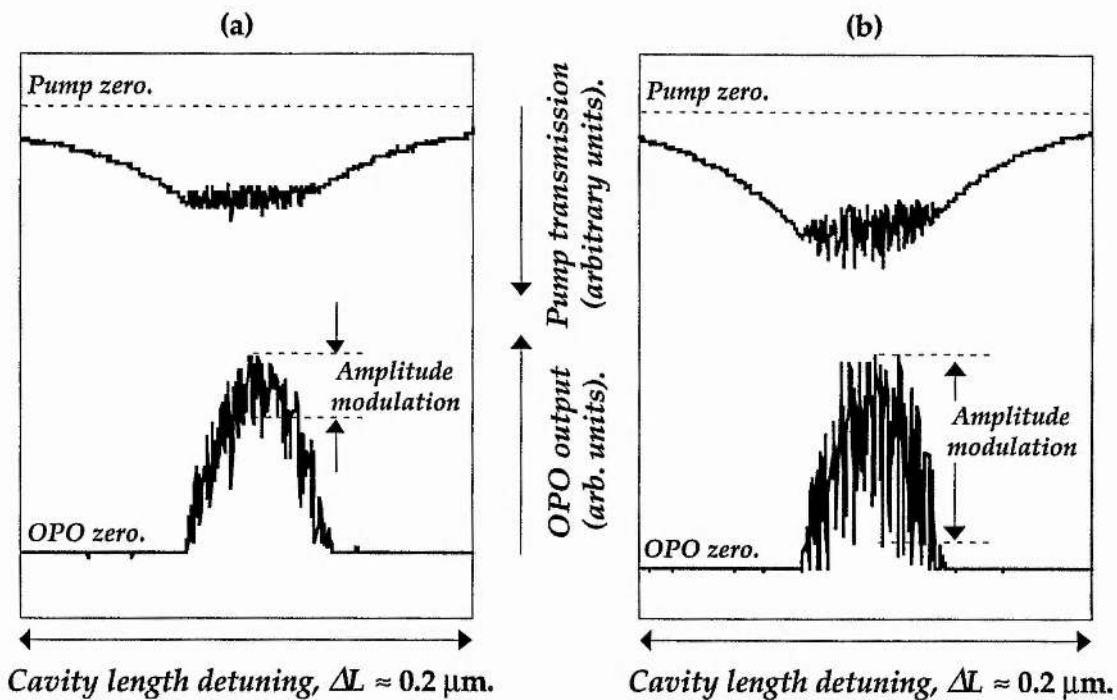


Figure IV. 18.

Transmitted pump field and OPO output for near-degenerate (a) and non-degenerate (b) signal and idler frequencies, for cavity length detunings of $\Delta L \approx 0.2 \mu\text{m}$.

The influence of cavity length detuning was examined near frequency-degeneracy when the signal and idler frequencies were separated by $\Delta\nu \approx 5 \text{ THz}$, and when operating with signal and idler frequencies significantly removed from frequency-degeneracy where $\Delta\nu \approx 33 \text{ THz}$. As

predicted in section IV. 6, this should result in an increased level of amplitude modulation in the output of the OPO, due to the increased mismatch in the free spectral ranges of the signal and idler fields. This behaviour is displayed in figure IV. 18.

Again, good agreement is displayed between experiment and modelling. When the frequency mis-match is increased, as in case (b), the amplitude modulation of the OPO output is greater, due to the larger mismatch in the free spectral ranges. The sharp peaks / dips in figure IV. 18 (b) correspond to discrete signal and idler frequency mode-pairs. It is useful to consider the changes that would be displayed if the frequencies were removed further from degeneracy. This would eventually have the effect of increasing the amplitude modulation to 100 %, and would provide discrete signal and idler frequency mode-pairs. (This type of behaviour is illustrated in the type II phase-matched OPO that is outlined in chapter V.)

Table IV. 5
Operating characteristics of the cw OPO.

<i>Pump power threshold</i>	P_p^{th}	$\approx 50 \text{ mW (high-finesse)}$
		$\approx 250 \text{ mW (low-finesse)}$
<i>External efficiency</i>	η_{ext}	$\approx 5 \% \text{ (high-finesse)}$
		$\approx 10 \% \text{ (low-finesse)}$
<i>Signal frequency tuning</i>	$\Delta\nu_s$	292 - 313 THz
<i>Idler frequency tuning</i>	$\Delta\nu_i$	292 - 271 THz

The output frequencies of the OPO were varied coarsely by changing the precise phase-matching temperature of the LBO crystal. Frequency-degeneracy occurred at a temperature of $T_{xtal} \approx 183 \text{ }^\circ\text{C}$, close to the value as extrapolated in section IV. 6. By varying the temperature between $T_{xtal} \approx 183$ and $\approx 180 \text{ }^\circ\text{C}$, the signal and idler frequencies could each be detuned by $\Delta\nu_s = \Delta\nu_i \approx 21 \text{ THz}$ from frequency-degeneracy. Therefore, the OPO covered a

total frequency bandwidth of $\Delta\nu = \Delta\nu_s + \Delta\nu_i \approx 42$ THz, corresponding to signal and idler frequencies from $\nu_s \approx 292$ to 313 THz and from $\nu_i \approx 292$ to 271 THz, respectively. The frequency range is determined in this case by the bandwidth of the optical coatings, and the corresponding range over which these coatings can maintain high-finesse, double-resonance, for non-degenerate signal and idler frequency mode-pairs.

The experimental results are summarized in table IV. 5, and are discussed in more general terms, with respect to further OPO operation using LBO, operating in different phase-matching geometries, in the following section.

IV. 7 Conclusions.

The performance of the argon-ion laser pumped near frequency-degenerate type I phase-matched cw OPO has displayed many of the characteristics that were predicted from theory and modelling [1]. The requirements on the stability of the pump frequency and the OPO cavity length are at their most stringent when operating doubly-resonant OPOs near frequency-degeneracy and under the conditions of type I phase-matching [40].

The decision to construct the LBO OPO within a linear, standing-wave, single-cavity resonator was chosen simply to provide the lowest possible pump power threshold from a LBO cw OPO. This information was required to implement the design of further cw OPOs that could utilise this nonlinear gain material. The consequence of this did yield sub-100 mW pump power thresholds, and the external efficiencies were of an order that could be used within several of the proposed applications of cw OPOs. However, a more conclusive study of this OPO was at the same time hampered by this cavity design.

By operating the OPO near frequency-degeneracy and under the conditions of type I phase-matching, the mis-match in the free spectral ranges was not at the level that could permit stable single-frequency signal and idler mode-pairs to be maintained. Since methods of discriminating between the OPO frequencies were difficult to implement efficiently, there was limited prospect for decoupling the optical paths of the signal and idler fields within the resonator, and thus opening up the possibility of independent cavity length control from a dual-cavity geometry [41].

Although the cavity length requirement to hold single-frequency mode-pairs is within the level that can be provided by servo-loop control, the minimum pump frequency requirement is two orders of magnitude within the best performance that could be obtained from the free-running argon-ion laser. Therefore, the pump frequency stability was always the limiting factor in providing a stable output from this frequency conversion process.

When type I phase-matching is the only option for doubly-resonant OPOs operating near-frequency degeneracy, useful outputs can only be obtained by using pump sources that are stabilized at the kHz-level [22, 28]. If an alternative material can be found that can operate under the conditions of type II phase-matching, then this crystal will always be used in preference, if the device can be operated above threshold [23, 29].

The above-mentioned conclusions were used to model the design of the next cw OPO, which operated under the conditions of type II phase-matching and with signal and idler frequencies significantly removed from frequency-degeneracy [2]. The results of this experiment are presented in the next chapter.

Two further extensions to this phase-matching geometry in LBO are now examined. First, consider using a pump source in the green spectral region and signal and idler OPO frequencies that are significantly removed from frequency-degeneracy. It was discussed in chapter III that, for pump sources in the green spectral region, any signal and idler frequency pair between 0.65 and 2.5 μm can be generated from temperature-tuned, type I, non-critically phase-matched, LBO [25]. Consequently, within the context of frequency metrology, high integer ratios of signal and idler frequencies could be theoretically obtained, as discussed in chapter III. Consider one particular phase-matched integer ratio, in which a pump source in the green spectral region is used to generate signal and idler frequencies in a 3:1 frequency ratio. Such an arrangement is illustrated in figure IV. 18.

If the pump source is derived from a near infra-red laser source, then the exact location of the 3:1 frequencies could be found by frequency-doubling the idler frequency radiation, and comparing this to the initial 1 μm source, as shown in figure IV. 19. In this geometry, the signal frequency could be used to drive, for example, the $^2S_{1/2} - ^2D_{5/2}$ 674 nm electric quadrupole 'clock' transition of the strontium ion [42], which has a natural width of ≈ 0.4 Hz [42].

Therefore, such an OPO has the potential to act as a frequency divider, linking a visible optical frequency standard with mid infra-red laser sources [43].

Second, the pump frequency could be replaced by a lower frequency source, allowing for radiation in the 1 to 2 μm spectral region to be provided from the LBO OPO. In this case, the pump frequency could be tuned coarsely, allowing the OPO to be maintained near to frequency degeneracy, if required. This type of geometry is outlined in the experiment that is discussed in chapter VII of this thesis [3].

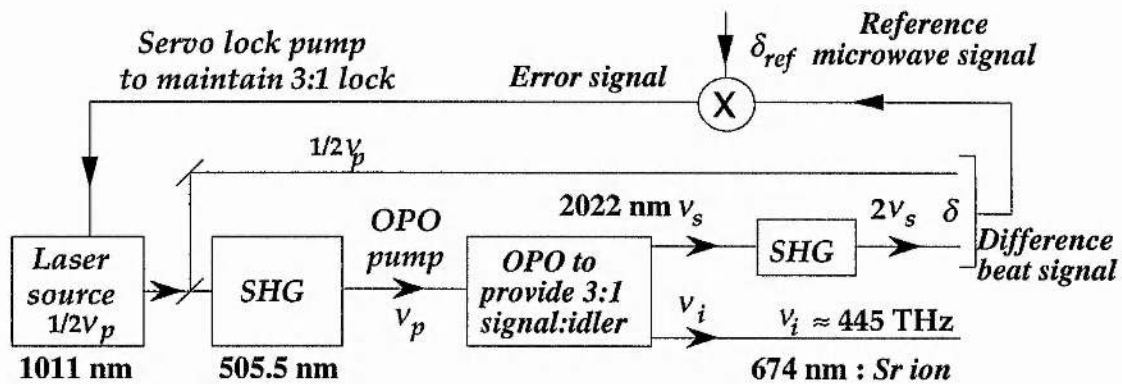


Figure IV. 19.

Proposed experiment combining a single-frequency pump source in the green spectral region with temperature-tuned, type I non-critically phase-matched LBO OPO. In this arrangement, signal and idler frequencies in a 3:1 ratio could be used to provide a link between the 'clock' transition of a strontium ion and a holmium-based laser operating at $\approx 2\ \mu\text{m}$. SHG; second harmonic generation; δ ; frequency difference.

However, the main conclusion that can be taken from this experiment is that, to obtain useful outputs from doubly-resonant cw OPOs operating near frequency-degeneracy in the type I phase-matched geometry, the pump source must be stable to kHz-levels. This confirms the problems experienced by other workers, using type I nonlinear materials, combined with relatively unstable pump sources [20, 21]. It further confirms the advantages of using a pump source with inherent frequency stability [22, 28, 40]. If the requirement is for frequency stable, fixed frequency, signal and idler frequency mode-pairs,

then this arrangement could fulfil such a role. However, if smooth frequency tuning is also required from the OPO, then further modifications must be applied. In particular, a dual-cavity design would be particularly effective in this respect [41]. To date, smooth frequency tuning has not been demonstrated from any cw OPO, in which a type I phase-matched nonlinear material has been used.

References.

1. F. G. Colville, A. J. Henderson, J. Zhang, M. J. Padgett, & M. H. Dunn, "Continuous-wave parametric oscillation in lithium triborate," *Opt. Lett.* **18**, 205 (1993).
2. F. G. Colville, M. J. Padgett, A. J. Henderson, J. Zhang, & M. H. Dunn, "Continuous-wave parametric oscillator pumped in the ultra-violet," *Opt. Lett.* **18**, 1065 (1993).
3. F. G. Colville, M. Ebrahimzadeh, W. Sibbett, & M. H. Dunn, "Continuous-wave LiB_3O_5 optical parametric oscillator pumped by a tunable Ti:sapphire laser," *Appl. Phys. Lett.* **64**, 1765 (1994).
4. W. J. Kozlovsky, C. D. Nabors, & R. L. Byer, "Second-harmonic generation of a continuous-wave diode-pumped Nd:YAG laser using an externally resonant cavity," *Opt. Lett.* **12**, 1014 (1987).
5. W. Wang, K. Nakagawa, Y. Toda, & M. Ohtsu, "1.5 μm diode laser-based nonlinear frequency conversions by using potassium titanyl phosphate," *Appl. Phys. Lett.* **61**, 1886 (1992).
6. S. T. Yang, C. C. Pohalski, E. K. Gustafson, R. L. Byer, R. S. Feigelson, R. J. Raymakers, & R. K. Route, "6.5-W, 532-nm radiation by cw resonant external-cavity second-harmonic generation of an 18-W Nd:YAG laser in LiB_3O_5 ," *Opt. Lett.* **16**, 1493 (1991).
7. T. J. Kane & R. L. Byer, "Monolithic, unidirectional single-mode Nd:YAG ring laser," *Opt. Lett.* **10**, 65 (1985).
R. L. Byer, "Diode laser-pumped solid-state lasers," *Science* **23**, 742 (1988).
8. A. D. Farinas, E. K. Gustafson, & R. L. Byer, "Design and characterization of a 5.5-W, cw, injection-locked, fibre-coupled, laser-diode-pumped Nd:YAG miniature-slab laser," *Opt. Lett.* **19**, 114 (1994).
9. D. Golla, I. Freitag, H. Zellmer, W. Schone, I. Kropke, & H. Welling, "15 W single-frequency operation of a cw, diode laser-pumped Nd:YAG ring laser," *Opt. Comm.* **98**, 86 (1993).
10. L. Y. Liu, M. Oka, W. Wiechmann, & S. Kubota, "Longitudinally diode-pumped continuous-wave 3.5-W green laser," *Opt. Lett.* **19**, 189 (1994).

11. J. P. Hohimer, R. C. Kelly, & F. K. Tittel,
"Frequency stabilization of a high power argon laser,"
Appl. Opt. **11**, 626 (1972).
12. N. A. Robertson, S. Hoggan, J. B. Mangan, & J. Hough,
"Intensity stabilisation of an argon laser using an electro-optic modulator - performance and limitations,"
Appl. Phys. B **39**, 149 (1986).
13. W. B. Bridges,
"Laser action in singly ionized krypton and xenon,"
Proc. IEEE **52**, 843 (1964).
14. H. R. Luthi, W. Seelig, & J. Steinger,
"Continuous visible laser action in singly ionized argon, krypton, and xenon,"
Appl. Phys. Lett. **4**, 178 (1964).
15. T. Y. Fan, G. J. Dixon, & R. L. Byer,
"Efficient GaAlAs diode-laser-pumped operation of Nd:YLF at 1.047 μm with intracavity doubling to 523.6 μm ,"
Opt. Lett. **11**, 204 (1986).
- T. M. Baer, D. F. Head, P. Gooding, G. J. Kintz, & S. Hutchison,
"Performance of diode-pumped Nd:YAG and Nd:YLF lasers in a tightly folded resonator configuration,"
IEEE J. Quant. Electron. **QE-28**, 1131 (1992).
16. Model 2040E and 2045E; High power ion laser,
Spectra-Physics laser products division, CA 94039-7013, USA.
Instruction manual, part no. 0000-210A, Rev. A, October 1990.
- J. Eckstrand, S. C. Guggenheimer, & D. L. Wright,
"Active single-frequency stabilization of an argon-ion laser,"
in *Conference on Lasers and Electro-Optics*, Vol. 9 of OSA 1992 Technical Digest Series (Optical Society of America, Washington, D. C., 1992), paper CPC 4.
17. M. Hercher,
"Tunable single mode operation of gas lasers using intracavity tilted etalons,"
Appl. Opt. **8**, 1103 (1969).
18. *Laser focus world*,
"Stabilizing a high-power single-frequency argon-laser,"
p21, January 1968.
"Ion lasers deliver power at visible and UV wavelengths,"
p97, December 1992.
19. C. Chen, Y. Wu, A. Jiang, B. Wu, G. You, R. Li, & S. Lin,
"New nonlinear-optical crystal: LiB_3O_5 ,"
J. Opt. Soc. Am. B **6**, 616 (1969).
- Laser focus world*,
"Chinese lab grows new nonlinear borate crystals,"
p129, November 1989.
20. R. G. Smith, J. E. Geusic, H. J. Levinstein, J. J. Rubin, S. Singh, & L. G. Van Uitert,
"Continuous optical parametric oscillation in $\text{Ba}_2\text{NaNb}_5\text{O}_{15}$,"
Appl. Phys. Lett. **12**, 308 (1968).
21. R. L. Byer, M. K. Oshman, J. F. Young, & S. E. Harris,
"Visible cw parametric oscillator,"
Appl. Phys. Lett. **13**, 109 (1968).
22. C. D. Nabors, R. C. Eckardt, W. J. Kozlovsky, & R. L. Byer,
"Efficient, single-axial-mode operation of a monolithic $\text{MgO}:\text{LiNbO}_3$ optical parametric oscillator,"
Opt. Lett. **14**, 1134 (1989).
23. S. Reynaud, C. Fabre, & E. Giacobino,
"Quantum fluctuations in a two-mode parametric oscillator,"
J. Opt. Soc. Am. B **4**, 1520 (1987).
24. E. S. Polzik, J. Carri, & H. J. Kimble,
"Spectroscopy with squeezed light,"
Phys. Rev. Lett. **68**, 3020 (1992).

25. S. Lin, J. Y. Huang, J. Ling, C. Chen, & Y. R. Shen,
"Optical parametric amplification in a lithium triborate crystal tunable from 0.65 to 2.5 μm ,"
Appl. Phys. Lett. **59**, 2805 (1991).
- M. Ebrahimzadeh, G. J. Hall, & A. I. Ferguson,
"Singly resonant, all-solid-state, mode-locked LiB_3O_5 optical parametric oscillator tunable from 652 nm to 2.65 μm ,"
Opt. Lett. **17**, 652 (1992).
26. C. Chen,
Private communication.
27. Unpublished results.
Several kV was applied across the axes of various LBO crystals, placed within one arm of a *Michelson* interferometer, and with no detectable change in the optical path length.
28. C. D. Nabors, S. T. Yang, T. Day, & R. L. Byer,
"Coherence properties of a doubly-resonant monolithic optical parametric oscillator,"
J. Opt. Soc. Am. B **7**, 815 (1990).
29. D. Lee & N. C. Wong,
"Tunable optical frequency division using a phase-locked optical parametric oscillator,"
Opt. Lett. **17**, 13 (1992).
30. F. Hanson & D. Dick,
"Blue parametric generation from temperature-tuned LiB_3O_5 ,"
Opt. Lett. **16**, 205 (1991).
31. J. Y. Huang, Y. R. Shen, C. Chen, & B. Wu,
"Noncritically phase-matched second-harmonic generation and optical parametric amplification in a lithium triborate crystal,"
Appl. Phys. Lett. **58**, 1579 (1991).
32. M. Ebrahimzadeh, G. P. A. Malcolm, & A. I. Ferguson,
"Continuous-wave mode-locked optical parametric oscillator synchronously pumped by a diode-laser-pumped solid-state laser,"
Opt. Lett. **17**, 183 (1992).
33. A. E. Siegman,
in *Lasers*, University Science Books, CA, USA, 1986, chapter 11.
34. S. Velsko, M. Webb, L. Davis, & C. Huang,
"Phase-matched harmonic generation in lithium triborate (LBO),"
IEEE J. Quant. Electron. **QE-27**, 2182 (1991).
35. T. Ukachi, R. J. Lane, W. R. Bosenberg, & C. L. Tang,
"Measurements of noncritically phase-matched second-harmonic generation in a Li_3BO_5 crystal,"
Appl. Phys. Lett. **57**, 980 (1990).
36. F. Xie, B. Wu, G. You, & C. Chen,
"Characterization of Li_3BO_5 crystal for second-harmonic generation,"
Opt. Lett. **16**, 1237 (1991).
37. FC Castech product literature (and references therein),
Lithium triborate (Li_3BO_5).
38. M. J. Padgett, F. G. Colville, & M. H. Dunn,
"Mode selection in doubly-resonant optical parametric oscillators,"
In press, *IEEE J. Quant. Electron.*
39. S. Schiller & R. L. Byer,
"Quadruply resonant optical parametric oscillation in a monolithic total-internal-reflection resonator,"
J. Opt. Soc. Am. **10**, 1696 (1993).
40. R. C. Eckardt, C. D. Nabors, W. J. Kozlovsky, & R. L. Byer,
"Optical parametric oscillator frequency tuning and control,"
J. Opt. Soc. Am. B **8**, 648 (1991).

41. F. G. Colville, M. J. Padgett, & M. H. Dunn,
"Continuous-wave, dual-cavity, doubly-resonant, optical parametric oscillator,"
Appl. Phys. Lett. **64**, 1490 (1994).
42. G. P. Barwood, C. S. Edwards, P. Gill, H. A. Klein, & W. R. C. Rowley,
"Observation of the $5s^2S_{1/2}$ - $4d^2D_{5/2}$ transition in a single laser-cooled trapped Sr ion
by using an all-solid-state system of lasers,"
Opt. Lett. **18**, 732 (1993).
43. N. C. Wong,
"Optical frequency division using an optical parametric oscillator,"
Opt. Lett. **15**, 1129 (1990).

Chapter V.

Type II Phase-Matching in Lithium Triborate with Signal and Idler Frequencies in a near 3:1 Ratio.

Contents.	Page.	
V. 1	Introduction.	219
V. 2	Single-frequency pump source operating at 824 THz.	222
V. 3	Optical parametric oscillator design.	228
V. 4	Pump frequency and cavity length requirements.	232
V. 5	Experimental arrangement.	238
V. 6	Results and discussion.	240
V. 7	Conclusions.	248
	References.	250

V. 1 Introduction.

This chapter describes the operating characteristics of a continuous-wave (cw) optical parametric oscillator (OPO) that operated at room-temperature, exploited the type II non-critical phase-matching geometry in lithium triborate (LBO), and generated signal and idler frequency outputs in a near 3:1 frequency ratio [1]. The OPO was pumped by the same commercial, large-frame argon-ion laser that was described in chapter IV [2]. However, for this cw OPO arrangement, the argon-ion laser was configured specifically to deliver single-frequency, narrow-linewidth and frequency-stabilized radiation in the ultra-violet spectral region at a frequency of $\nu_p = 824$ THz, and corresponding to a wavelength of $\lambda_p = 363.8$ nm. The nonlinear material LBO was cut for propagation along the z principal optical axis, and operated near room-temperature to satisfy the conditions of type II non-critical phase-matching [3 - 5]. The design of the linear, standing-wave, single-cavity, doubly-resonant OPO resonator was chosen to convert fixed frequency pump source radiation into tunable OPO outputs in the green ($\nu_s \approx 600$ THz) and near infra-red ($\nu_i \approx 220$ THz) spectral regions, for the signal and idler frequencies respectively.

The characteristics of the pump source for the OPO are outlined in detail in section V. 2. The argon-ion laser was selected as a convenient source of high-power radiation with narrow-linewidth, single-frequency output powers at the Watt-level available in the ultra-violet spectral region. The argon-ion laser was configured to oscillate on a single transition line, at a wavelength of $\lambda_p = 363.8$ nm, by using wavelength selective optics to suppress other nearby lasing transitions. A solid-etalon placed within the linear, standing-wave laser resonator provided a stable and reliable output with power levels in excess of $P_p \approx 1$ W radiation in a single-frequency at $\nu_p = 824$ THz. The short-term frequency stability was determined by servo-locking the laser cavity length to a stable external confocal etalon of free spectral range $FSR = 8$ GHz, and with a finesse of $F \approx 150$, by the side-of-fringe locking technique. This resulted in a short-term ($\Delta t \approx 1$ second) frequency jitter (FWHM) of $\Delta\nu_{p-stab} \approx \pm 3$ MHz.

The choice of the nonlinear material, the phase-matching geometry, and the coatings applied to the resonator components, are explained in detail in section V. 3. The nonlinear material LBO was chosen to provide a type II phase-matching geometry at room-temperature, and with signal and idler frequencies widely-removed from the frequency-degeneracy point. The optical coatings deposited on the intra-cavity surfaces, and the resonator geometry, were selected specifically to provide double-resonance for both the signal and idler frequencies at room-temperature. The OPO cavity formed a high finesse single-cavity resonator ($F_s \approx F_i \approx 400$) for both the signal and idler frequencies.

The expected mode-selection properties of the output frequencies of this OPO are discussed in section V. 4. Type II phase-matching geometries have been discussed frequently throughout the text, in the context of providing more relaxed requirements on the stability of the pump frequency and the OPO cavity length than type I geometries, to maintain operation on a single signal and idler frequency mode-pair [6 - 9]. To recap, this is because the signal and idler frequencies in type II phase-matching are polarized along orthogonal axes of the OPO resonator, and experience significantly different optical paths due to the presence of the birefringent nonlinear medium. This can provide a significant mis-match in the free spectral ranges of the signal and idler fields (in this case $\Delta FSR \approx 2.1$ %) even within a single-cavity OPO arrangement.

The computer program [9], discussed in chapter II, was used again to examine the effects of detunings / perturbations in the pump frequency and the OPO cavity length. The requirement on the stability of the pump frequency was calculated to be $\Delta\nu_{p-stab} \approx \pm 16$ MHz, nearly two orders of magnitude higher than the requirements on the type I phase-matched, near frequency-degenerate OPO, described in chapter IV. In particular, the stability level of the frequency-stabilized pump source was within these requirements, as predicted by the computer model. In addition, pump source requirements were considered with respect to providing the minimum OPO pump power threshold.

The experimental arrangement is described in section V. 5. The pump mode was matched into the OPO resonator by using a single lens of focal length $f = 250$ mm, which provided for near optimum spatial overlap between the pump, signal and idler waves within the gain medium. The frequency-stabilized single-frequency operation of the pump laser was isolated from back-reflections and back-conversion from the linear, standing-wave OPO resonator, by using an acousto-optic modulator that frequency-shifted the pump radiation by $\Delta\nu = 70$ MHz. The OPO outputs were separated from the pump radiation by the use of filters and polarizers, and each was monitored separately.

The experimental results of this argon-ion pumped cw OPO are presented in section V. 6. The OPO operated with a minimum pump power threshold of $P_p^{th} \approx 115$ mW incident on the OPO resonator. By altering the temperature of the LBO crystal between $T_{xtal} \approx 20$ and 86 °C, the output frequencies of the OPO could be varied coarsely under temperature-tuned type II non-critical phase-matching, over a frequency bandwidth of $\Delta\nu_s + \Delta\nu_i \approx 20$ THz. The signal frequency could be tuned coarsely from $\nu_s \approx 607$ to 598 THz in the blue / green spectral region, and corresponding to wavelengths from $\lambda_s \approx 502$ to 494 nm respectively. The idler frequency could be tuned coarsely from $\nu_i \approx 227$ to 217 THz, and corresponding to wavelengths from $\lambda_i \approx 1.32$ to 1.38 μm respectively. Total, peak external conversion efficiencies of $\eta_{ext} \approx 9\%$ were obtained, when operating at approximately five times above the pump power threshold.

Similar to the method employed to examine the amplitude and frequency properties of the OPO in chapter IV, by scanning the length of the OPO cavity over nanometre ranges, the mode-selection characteristics of this

OPO were evaluated. Single signal and idler frequency mode-pairs corresponded to discrete cavity length positions which were separated by $\Delta L_{hop} \approx 6$ nm. This allowed for amplitude-stable operation of the OPO on single-frequency mode-pairs, by employing closed-loop servo-control on the length of the single-cavity OPO. Through this method, amplitude-stable, single-frequency mode-pairs were held on resonance for periods of $\Delta t \approx 10$ s seconds.

Finally, in section V. 7, the important results are considered with respect to further improvements in the design of the optical resonator that would allow for smooth frequency tuning of the signal and idler frequencies. This led to the design of the dual-cavity OPO resonator [10], which is described experimentally in chapter VI of this thesis.

V. 2 Single-frequency pump source operating at 824 THz.

In this section, the operating characteristics of the source of pump frequency for the type II phase-matched OPO are considered in detail. The argon-ion laser, discussed in the previous chapter, was used again as the source of input pump radiation. The steps taken to provide narrow-linewidth, single-frequency, and frequency-stable output radiation are outlined, and the ensuing frequency jitter / linewidth of the pump source is measured and discussed. Once again, the limiting factors on the level of pump frequency stability are addressed.

The laser pump source for this OPO was selected to fulfil several criteria, as discussed in more general terms in chapter III. The specific criteria for the pump source for this cw OPO included continuous-wave output, single longitudinal mode operation, high cw power output, and operation in the ultra-violet spectral region, corresponding to an operating frequency between $750 < \nu_p < 1000$ THz.

Single longitudinal mode operation was required to allow for the possibility of amplitude and frequency stable operation of the OPO outputs. High power radiation at the Watt-level was required to operate the doubly-resonant OPO reliably and efficiently above threshold. Frequency operation at $\nu_p \approx 800$ THz was required to operate an OPO that could be phase-matched to provide signal and idler frequencies in the visible and near infra-red spectral regions, respectively. This provided widely spaced signal and idler frequency

pairs, and opened up the possibility of studying in detail a cw OPO that operated with outputs that were significantly removed from frequency-degeneracy, contrasting the properties of the near frequency-degenerate type I phase-matched cw OPO arrangement, described in chapter IV.

Presently, there are a limited number of cw laser pump sources that can be considered for use as the pump source for such a cw OPO. These include high-power gas lasers that can be forced to operate efficiently on single transition lines [11 - 13], or near infra-red solid-state lasers when frequency up-converted into the ultra-violet spectral region [14 - 16].

In recent years, engineers have steadily enhanced the performance of rare-gas ion lasers operating in the ultra-violet spectral region [17]. Lifetime, durability, and output powers have improved, while costs have been reduced and shorter ultra-violet wavelengths made available. The most suitable gas laser is the argon-ion laser, which has several lasing transition lines in the ultra-violet spectral region [12]. The highest power transition lines occur at frequencies of 825 THz (363.8 nm) and 855 THz (351 nm). Other ion lasers that have outputs in the ultra-violet spectral region include krypton-ion [18] and neon-ion [19] lasers. The three krypton-ion transition lines between 890 THz (337 nm) and 843 THz (356 nm) are used regularly with a combined cw multi-mode power of ≈ 2 W to pump dye lasers. Neon-ion lasers can emit ≈ 1 W cw multi-mode power, divided among three transition lines between 904 THz (332 nm) and 825 THz (339 nm). However, argon-ion lasers, operating in the ultra-violet spectral region, are the standard pump source for many tunable dye lasers, with over 7 W multi-line power distributed between 898 THz (334 nm) and 825 THz (363.8 nm).

Suitable solid-state lasers include Ti:sapphire lasers [20] or high-power phase-locked diode-laser arrays [21], frequency-doubled with crystals of LBO [16, 22] or KNbO_3 [23, 24], and whose operating frequency can be selected from a wide range, as determined by the bandwidth of the laser source. It is worthwhile considering the suitability of diode-laser-pumped solid-state Nd-based lasers, frequency-tripled into the ultra-violet spectral region. Although this method has been employed often to provide ultra-violet pump frequencies from nanosecond duration *Q*-switched laser sources [25], and these have been used effectively to pump pulsed OPOs [26], to date, there has been no experimental realization of this frequency-conversion process in the cw regime. This is a consequence of the requirement to enhance both the

fundamental and the second-harmonic frequencies in an external doubly-resonant enhancement arrangement, to obtain significant cw conversion efficiencies. Presently, the highest cw power levels in the ultra-violet spectral region are provided by frequency-doubling argon-ion lasers using the nonlinear material BBO [27, 28]. It is likely that the more widespread generation of the fourth frequency-harmonic [14] from diode-laser-pumped Nd-based lasers will precede third-harmonic generation techniques. Frequency quadrupling involves resonant enhancement of only the second-harmonic wave, avoiding the undesirable complications of doubly-resonant enhancement that would be present when frequency-tripling.

The pump source selected for the cw OPO was an argon-ion laser which operated at a frequency of $\nu_p = 824$ THz (363.8 nm). It was selected as the most convenient and highest cw single-frequency power laser source currently available in the ultra-violet spectral region. The argon-ion laser source used was the same large-frame *Spectra-Physics* model 2045-E that was purchased to provide the source of pump radiation for the OPO that was described in chapter IV. The main difference in the two resonator geometries involved the use of wavelength-selective optics to force lasing on the desired transition, and a solid etalon for increased frequency stability.

The *Spectra-Physics* model 2045-E argon-ion laser was configured as a linear, standing-wave resonator; figure V. 1.

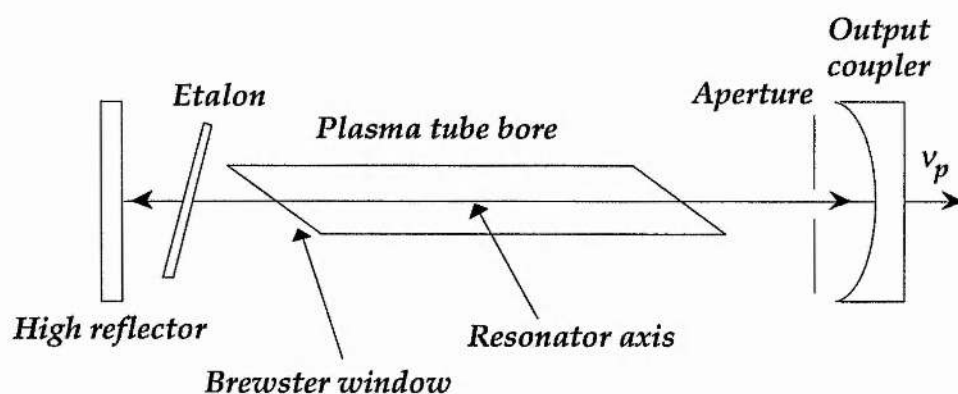


Figure V. 1.

Schematic representation of the argon-ion laser resonator, used to provide high-power, narrow-linewidth, single-frequency radiation in the ultra-violet spectral region, at a frequency of $\nu_p = 824$ THz.

Cavity mirrors were selected that would allow for oscillation only at the frequency $\nu_p = 824$ THz (363.8 nm), and suppress oscillation of those transition lines close to this frequency, and in particular the high-gain transition line at $\nu_p = 855$ THz (351 nm) [12]. This resonator configuration differed from that described in chapter IV by the absence of a dispersive prism, and the use of wavelength-selective optics. In addition to suppressing undesired lasing transitions, wavelength selective optics contribute also to an increase in the passive stability of the resonator [29]. By using these optics, the temperature and vibration sensitivity associated with using a prism for wavelength selection is reduced.

For a typical large-frame argon-ion laser, operating on a single transition line at a frequency of $\nu_p = 824$ THz, the frequency gain-bandwidth is significantly greater than the axial mode spacing of the resonator. Therefore, similar to the spectral output of this laser operating in the visible spectral region, then without the use of frequency-selective components, the output consisted of a number of longitudinal modes with random phase and amplitude distribution. To reduce the linewidth of the laser output to a single-frequency, an etalon was incorporated within the cavity to select just one of the axial modes under the gain profile: the etalon specifications are similar to those discussed in chapter IV for operation at 514.5 nm.

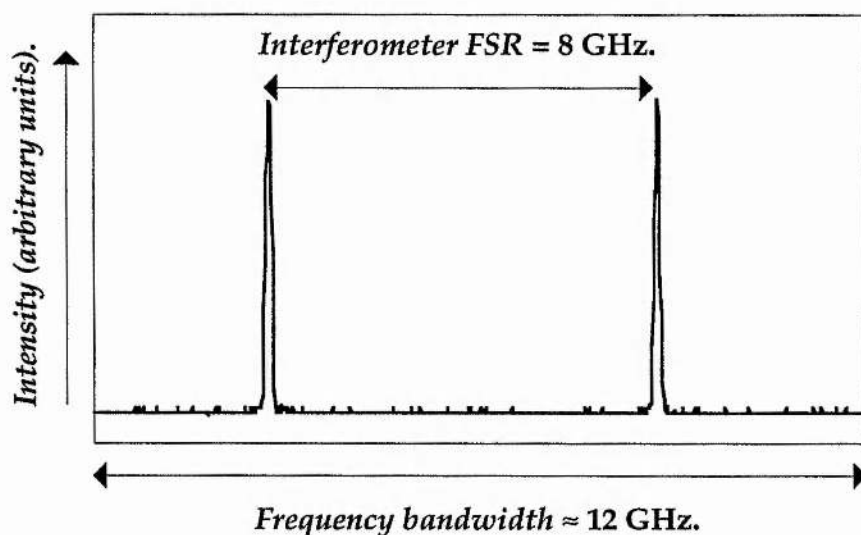


Figure V. 2.

Single-frequency operation of the argon-ion laser operating at a frequency of $\nu_p = 824$ THz, corresponding to a wavelength of $\lambda_p = 363.8$ nm, used as the pump source for the cw OPO.

Single-frequency operation of the argon-ion laser was monitored externally on a scanning confocal *Fabry-Perot* interferometer of free spectral range $FSR_{int} = 8$ GHz. A trace of the free-running, single-frequency operation of the laser is shown in figure V. 2. Typically, single-frequency power levels in excess of $P_p \approx 1.5$ W could be achieved in this manner, representing an efficiency of ≈ 80 % from multi-mode to single-mode operation. With the argon-ion laser operating free-running on a single longitudinal mode, the short-term ($\Delta t \approx 1$ second) frequency-jitter (FWHM) was measured to be $\Delta\nu_{p-stab} \approx \pm 15$ MHz.

To decrease the linewidth / frequency-jitter of the pump frequency, the pump source was actively stabilized to the external etalon. Figure IV. 3 is a block diagram of the active system used to reduce the frequency jitter [29 - 31]. The system was based on a piezo-electric actuator that controlled the optical cavity length of the laser in the 10 Hz to 1 kHz range. The frequency discriminator used to provide the jitter correction signal was the electrically tunable confocal interferometer, described above. Frequency discrimination was provided via slope detection on the side of the interferometer transmission peak.

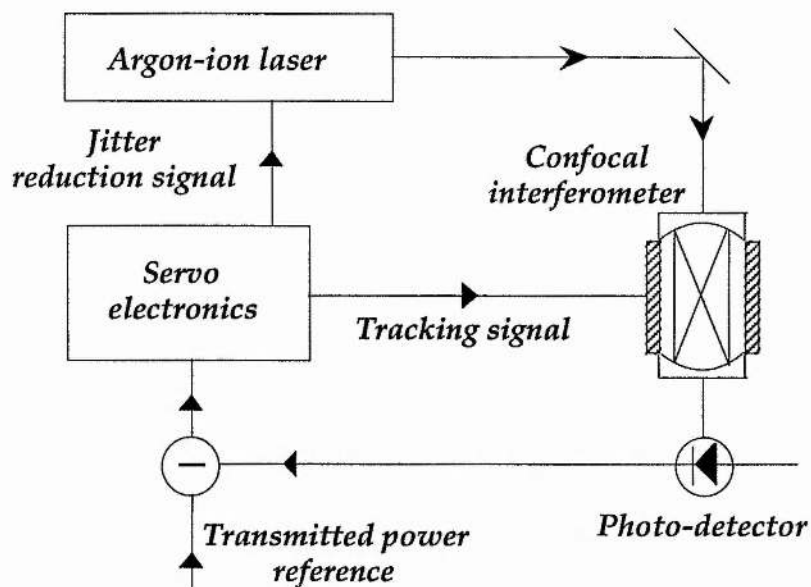


Figure V. 3
Block diagram of the system for active jitter reduction of the single-frequency operation of the argon-ion laser.

The interferometer was maintained at constant average transmitted power by feedback to the piezo-electric interferometer spacer. Thus, the discriminator stayed tuned to the laser frequency. (The interferometer was not ratio-detected, so its minimum frequency noise was limited by amplitude-modulated noise on the laser [29 - 31].)

The piezo-electric actuator used within the laser cavity performed two functions in conjunction with the jitter reduction. First, it was a special tri-component actuator which provided angular adjustment of the mirror without cavity length translation. This capability was used in conjunction with a quadrant cell photo-detector to hold the output beam position fixed [29 - 31]. Second, the cavity length translation capability was used in conjunction with the temperature dithered intra-cavity etalon loop to lock the cavity length to the centre of the etalon passband. This eliminated mode-hops and provided good long term stability based upon the intra-cavity temperature stabilized etalon. By using the active feedback system, the frequency jitter of the argon-ion laser was reduced by a factor of approximately five to a level of $\Delta\nu_{p-stab} \approx \pm 3$ MHz (FWHM).

The important characteristics of the argon-ion laser, used as the source of input pump frequency for the cw OPO, are summarized in table V. 1. The linewidths are displayed for the cases of both free-running and actively-stabilized operation. For the remainder of this chapter, it is assumed that the pump laser is operating with the jitter reduction servo-control.

Table V. 1
Characteristics of the input pump frequency.

<i>Pump source</i>		<i>Argon-ion laser</i>
<i>Frequency</i>	ν_p	824 THz
<i>Wavelength</i>	λ_p	363.8 nm
<i>Power</i>	P_p	≈ 1.5 W
<i>Jitter (≈ 1 second)</i>	$\Delta\nu_{p-stab}$	$\approx \pm 15$ MHz (<i>unlocked</i>)
		$\approx \pm 3$ MHz (<i>locked</i>)

V. 3 Optical parametric oscillator design.

In this section, there is a description of the design of the OPO resonator. In particular, the crystal properties are examined that would allow for the generation of widely spaced signal and idler frequencies from a cw OPO, operating in the green and near-infra-red spectral regions, respectively. The resonator components were analysed with a view to obtaining low pump power thresholds, wide (coarse) frequency tuning, stable OPO operation on a single signal and idler frequency mode-pair, and significant values for the external conversion efficiency.

The nonlinear material chosen for the OPO was LBO [32]. This material was selected for its low absorption / scattering losses in the ultra-violet, visible and near infra-red spectral regions [32], non-critical phase-matching for pump sources operating in the ultra-violet spectral region [3 - 5], and its high optical damage threshold [33]. In particular, LBO can be phase-matched in the type II geometry at room-temperature, and this provides signal and idler frequencies that are widely removed from frequency-degeneracy. (This important feature would allow for the study of significantly different resonator designs, opening up the prospect for smooth frequency tuning from a cw OPO. This subject is discussed in more detail in chapter VI of the thesis.)

When pumped at a frequency of $\nu_p \approx 820$ THz, LBO can be temperature-tuned under type II non-critical phase-matching, with $\phi = 90^\circ$, and $\theta = 0^\circ$, as discussed in chapter III. The pump and idler fields are polarized along the crystal x -axis, and the signal is polarized along the crystal y -axis, as displayed in figure V. 4; $o \rightarrow e+o$. The crystal was cut with plane-parallel, polished input and output faces. These faces were coated to be anti-reflecting at the pump, signal and idler frequencies (triple anti-reflection coating). The single-pass power transmission losses, including reflection loss from the anti-reflection coatings and absorption / scattering in the material, were specified to be $\beta_{s,s-p} \approx \beta_{i,s-p} < 0.25\%$ at 598 and 227 THz (signal and idler frequencies respectively) and $\beta_{p,s-p} < 2\%$ at 824 THz (pump frequency).

The crystal was placed within a temperature-controlled oven, similar in design to the oven described in chapter IV, to specify the exact phase-matching temperatures, and surrounded by two cavity mirrors to form a low loss, single-cavity resonator for the signal and idler fields. In addition, the

mirrors were selected to satisfy cavity stability and confocal focusing of the three waves within the gain medium.

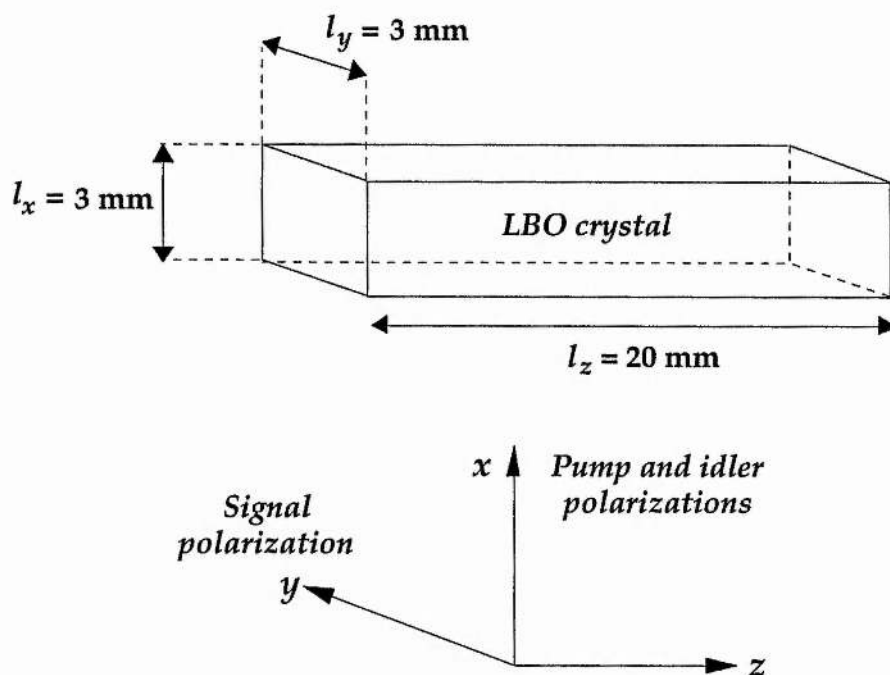


Figure V. 4.

Crystal cut for the LBO crystal, and dimensions along the three principal optical axes. Propagation is along the z principal optical axis.

To satisfy confocal focusing requirements within the nonlinear material of length $l = 20 \text{ mm}$, the resonator provided spot sizes of $W_s \approx 30.6 \mu\text{m}$, $W_i \approx 52.7 \mu\text{m}$, and $W_p \approx 26.4 \mu\text{m}$, for the signal, idler, and pump fields, respectively, and these were located at the centre of the nonlinear crystal. The cavity geometry is illustrated schematically in figure V. 5. The inner surfaces of the cavity mirrors were fabricated to 15 mm radius of curvature (ROC), and located at a distance of $\approx 6.5 \text{ mm}$ from the crystal faces, forming a symmetric resonator. Once again, the outer surfaces were curved to 20 mm radius of curvature to reduce the effects of the input mirror substrate on the focused Gaussian pump beam.

The inner surfaces of the cavity mirrors were coated to provide high reflectivity for the signal and idler frequencies at around room-temperature ($T_{xtal} \approx 20 \text{ }^\circ\text{C}$), with $R_s \approx R_i > 99.7 \%$ at $\nu_s \approx 598$ and $\nu_i \approx 227 \text{ THz}$, respectively,

and corresponding to signal and idler wavelengths of $\lambda_s \approx 502$ and $\lambda_i \approx 1320$ nm, respectively. In addition, partial reflectivity at the pump frequency of $\nu_p \approx 824$ THz was specified to be $R_p \approx 55\%$. The effects of the pump reflectivity, and the corresponding finesse of the OPO cavity at the pump frequency, are considered in more detail in section V. 4.

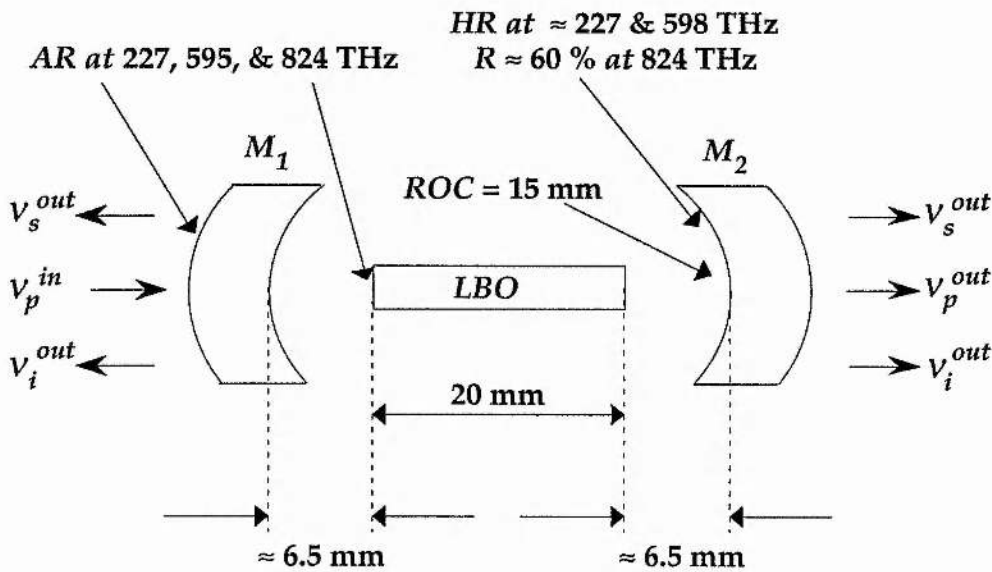


Figure V. 5. Schematic representation of the symmetric, near-confocal resonator geometry, including the two cavity mirrors and the nonlinear material, forming a single-cavity, doubly-resonant OPO. ROC: radius-of-curvature; HR: highly-reflecting; AR: anti-reflecting.

To provide for a high degree of passive stability in the design of the OPO resonator, the nonlinear crystal and cavity mirrors were held within a highly-stable resonator configuration. This cavity design is illustrated schematically in figure V. 6. Such a cavity was constructed to increase the level of passive stability over the resonator that was used for the OPO in chapter IV. In that case, the cavity mirrors were held in separate mounts on the optical bench. The inclusion of length-determining (invar-based) support was considered essential if phase-matching geometries were to be investigated that could allow for stable OPO operation. (In particular, see reference [7] for a description of ultra-stable cw OPO cavities.)

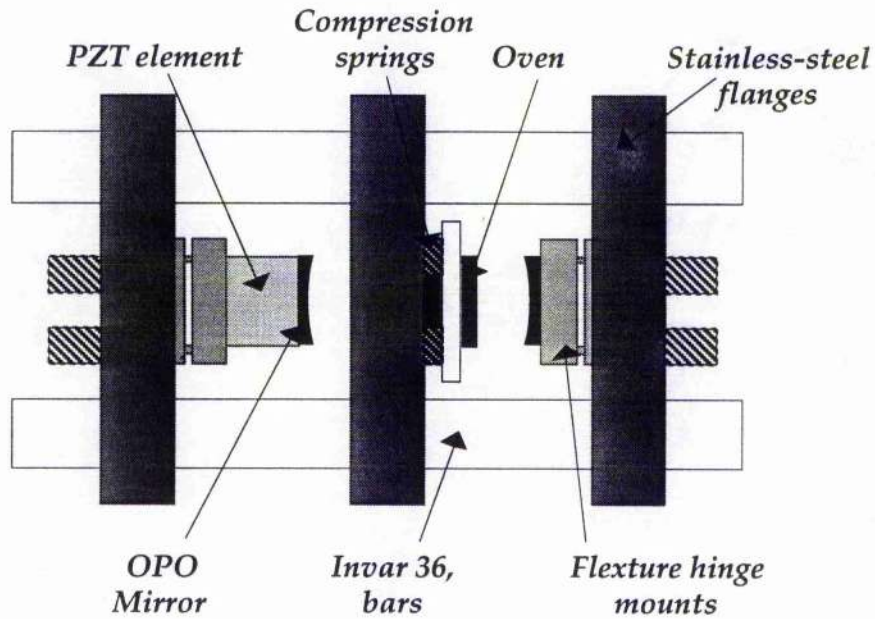


Figure V. 6.

Resonator design for an increased level of passive stability, with the cavity length determined by low-expansion invar bars. The short-term cavity length perturbations were reduced by using highly-stable mounts for the optical components, and effective isolation from the environment through the use of a lead-based, acoustic-damping, enclosure. PZT: piezo-electric transducer.

The design incorporated three low-expansion invar rods as the length-determining members and massive stainless-steel flanges to house the mirror mounts and the crystal oven. The mirror mounts were of a commercial design (*Photon-Control micropoint 25*) based on flexure-hinges with micrometer drives. The whole assembly was housed within an acoustic enclosure lined with a foam / lead / foam sandwich. Air spaces within the cavity were further isolated from convection currents. The mirrors were mounted on high-modulus, piezo-electric ceramics to enable active control of the cavity length.

V. 4 Pump frequency and cavity length requirements.

In this section, there is an analysis of the stability requirements of the pump frequency and the OPO cavity length to maintain stable OPO operation on a single signal and idler frequency mode-pair. Additional parameters that will affect the operation of the OPO are considered, including in particular the effects due to partial resonance of the OPO cavity at the pump frequency.

The requirements on the stability of the pump frequency and the cavity length to maintain amplitude and frequency stable OPO operation in a single-cavity OPO design were shown in chapter II to be highly dependent on the mis-match in the free spectral ranges of the signal and idler fields within the OPO [9]. Therefore, the type II phase-matching geometry, where the signal and idler fields are polarized along orthogonal axes of the birefringent nonlinear material, offers advantages over type I phase-matched geometries [1, 6 - 8, 34, 35].

Once again, the computer program was used to predict the tolerance of the OPO output to perturbations / detunings in the pump frequency and the OPO cavity length [9]. The input data used for the modelling is presented in table V. 2.

Table V. 2
Input data used for the computer model.

<i>Phase-matching</i>		<i>Type II</i>
<i>Pump frequency</i>	ν_p	824 THz
<i>Signal frequency</i>	ν_s	≈ 598 THz
<i>Idler frequency</i>	ν_i	≈ 227 THz
<i>Temperature</i>	T_{xtal}	20°C
<i>Crystal length</i>	l	20 mm
<i>OPO finesses</i>	F_s, F_i	≈ 400
<i>Mirror separation</i>	L	33 mm
<i>FSR mis-match</i>	ΔFSR	2.1 %

Figure V. 7 illustrates graphically the effects of pump frequency and cavity length detunings on the selection of the lowest threshold signal and idler frequency mode-pairs, based on the data displayed in table V. 2.

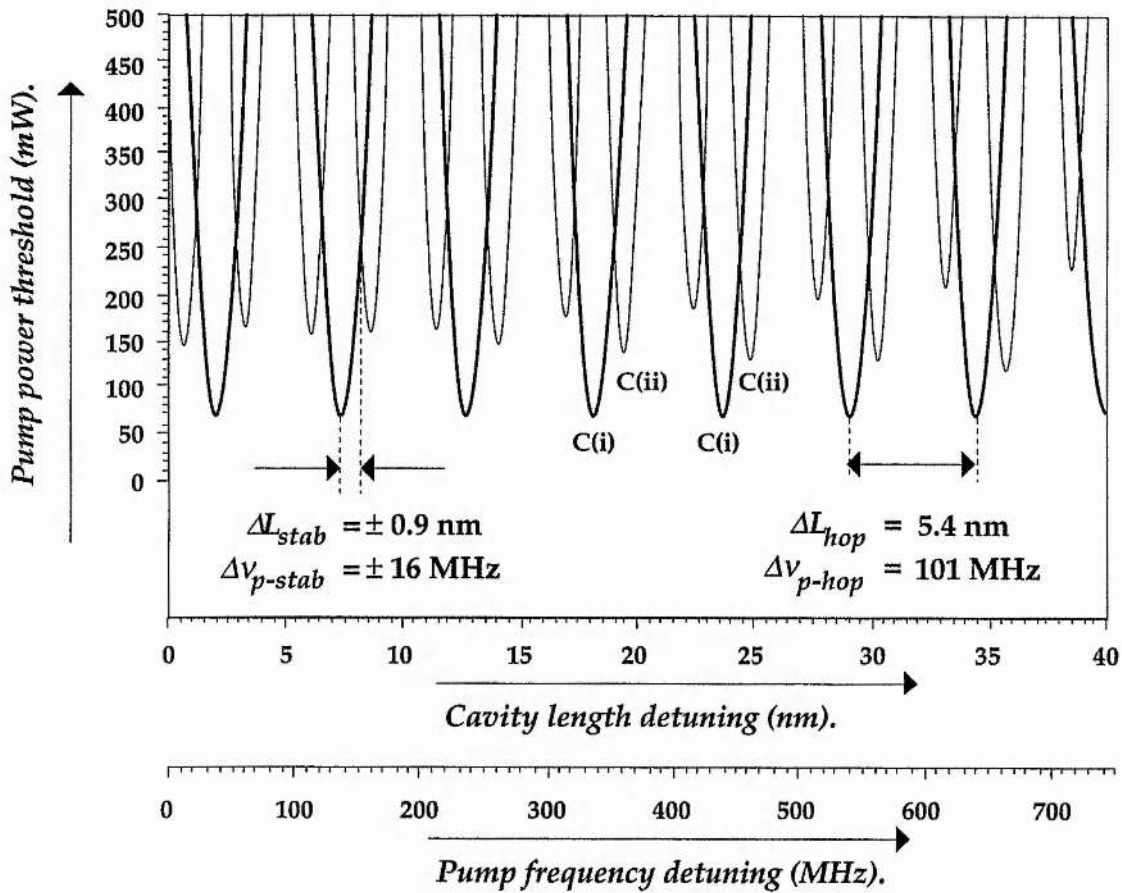


Figure V. 7.

The effect on the mode selection of the output of the OPO for a pump frequency detuning of $\Delta \nu_p = 740 \text{ MHz}$, and for a cavity length detuning of $\Delta L = 40 \text{ nm}$. C(i) and C(ii); adjacent mode-clusters.

Figure V. 7 shows that the pump frequency must be stable to within $\Delta \nu_{p-stab} \approx \pm 16 \text{ MHz}$, and the cavity length to within $\Delta L_{stab} \approx \pm 0.9 \text{ nm}$, to maintain operation on a single signal and idler frequency mode-pair. Mode-hops between adjacent mode-pairs within the same cluster (bold-type parabolas in figure V. 7) are predicted to occur for pump frequency detunings of $\Delta \nu_{p-hop} \approx 101 \text{ MHz}$, or cavity length detunings of $\Delta L_{hop} \approx 5.4 \text{ nm}$.

It is revealing to contrast this graph with figures IV. 10 and IV. 11 in chapter IV, for the effects of detunings on the type I phase-matched, near frequency-degenerate OPO, which displayed a required pump frequency stability of $\Delta v_{p-stab} \approx \pm 170$ kHz, and a cavity length stability of $\Delta L_{stab} \approx \pm 10$ pm, to maintain oscillation on the same signal and idler single-frequency mode-pair. In particular, the type I phase-matched OPO was predicted, and shown, to remain operational irrespective of the detunings (as long as the intra-cavity pump field was above threshold). The increased modulation in the output of the OPO in the type II phase-matching geometry, as predicted by figure V. 7, implies that, for a fixed pump frequency, the OPO will operate only at discrete values of the cavity length, and that there will exist a significant range of cavity length values for which a low threshold mode-pair does not exist [7 - 9]. Therefore, the type II phase-matching geometry has the potential to provide distinct on-off behaviour, when operating just above threshold, that could be exploited for amplitude stable OPO operation on a single-frequency mode-pair.

In this phase-matching geometry in LBO, the stability criteria can be further estimated by using the equations that were derived in chapter II. The dispersion terms in the derivation of the free spectral ranges are neglected, since the mis-match in the signal and idler free spectral ranges is considerable. Within such a doubly-resonant, single-cavity OPO, the cavity length and pump frequency requirements were shown to be as follows:

$$\Delta L_{stab} \approx \pm \frac{c}{2v_p F} , \quad [V. 1]$$

$$\Delta v_{p-stab} \approx \pm \frac{FSR}{F} , \quad [V. 2]$$

These equations predict that the pump frequency should be stable to within $\Delta v_{p-stab} \approx \pm 8.3$ MHz, and the cavity length to within $\Delta L_{stab} \approx \pm 0.45$ nm. These values differ slightly from figure V. 7 because equations V. 1 and V. 2 assume that when the threshold increases by a factor of two, the OPO stops working. Figure V. 7 takes the stability requirements to be when the OPO hops to an adjacent mode-pair, irrespective of pump power threshold. Again, stable OPO operation is suggested, given the frequency-stabilized pump laser used, and the stable OPO cavity arrangement adopted. Consider the cavity length detuning predicted to cause the output of the OPO to hop between

adjacent mode-pairs within the same cluster. This was shown in chapter II to correspond to detunings of

$$\Delta L_{hop} \approx \frac{c}{2v_p} \frac{\Delta n l}{(\bar{n}l + L)}, \quad [V. 3]$$

and this implies discrete signal and idler mode-pairs every $\Delta L_{hop} \approx 4$ nm.

Given that the stability of the frequency-stabilized pump source was within the level of the minimum stability requirements, it was realistic to assume that servo-control feedback on the cavity length of the OPO would be adequate to maintain amplitude-stable operation of the OPO on a single-frequency mode-pair.

*Table V. 3
Parameter values for threshold analysis.*

<i>Pump frequency</i>	v_p	824 THz
<i>Pump ref. index</i>	n_p	1.60
<i>Crystal length</i>	l	20 mm
<i>Nonlinear coefficient</i>	d_{eff}	-0.76 pm/V
<i>Degeneracy factor</i>	δ	0.45
<i>Signal/idler finesse</i>	F_s, F_i	400
<i>Pump enhancement</i>	E_{p-max}	2.2
<i>Measured enh'ment</i>	E_p	1.6

The next important consideration for the pump source involved predicting the pump power threshold. For this, the expression derived for a pump enhanced doubly-resonant OPO (equation IV. 6) was used, assuming that the pump field was held on resonance and that the optimum phase-relationship was maintained between the three waves on reflection. Table V. 3 lists the values that were used within the threshold equation. The finesse of the

signal and idler fields were estimated from the expected cavity losses, as given by the reflection and transmission curves from the coating manufacturers. From these values, a threshold of $P_p^{th} \approx 28.8$ mW was predicted for the OPO. Once again, this value was within the level of single-frequency power available from the argon-ion pump laser.

The effects of pump resonance are now considered. Since the reflectivity of the OPO mirrors at the pump frequency were almost identical to those mirrors used in chapter IV, similar pump-resonance effects were predicted.

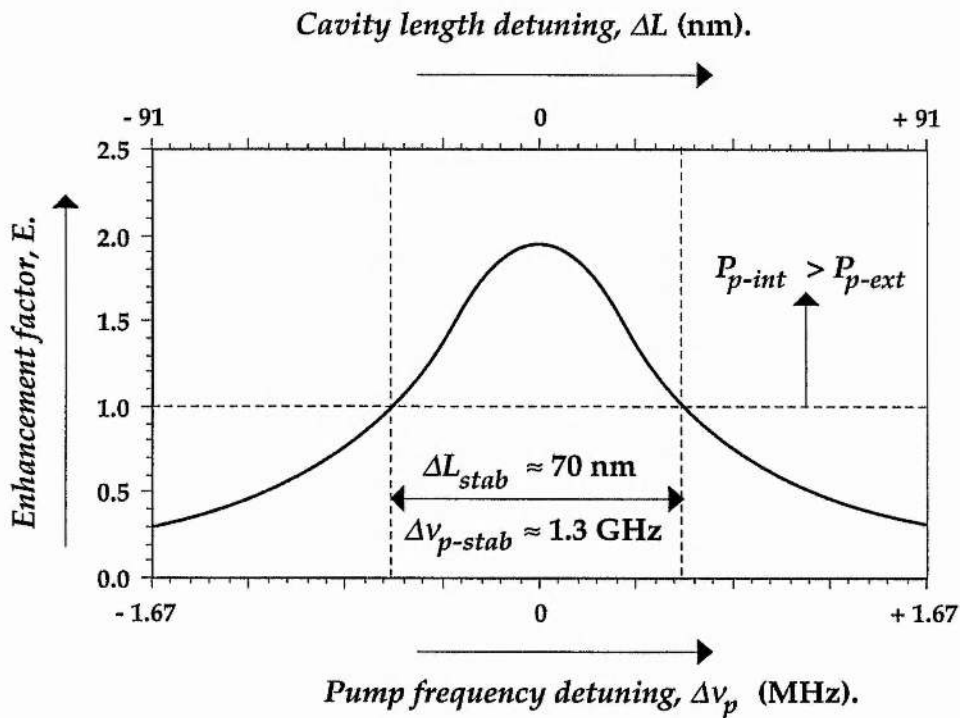


Figure V. 8.

Theoretical variation of the intra-cavity pump field for detunings in the pump frequency and OPO cavity length, assuming an intra-cavity, parasitic, round-trip power loss of $\beta_{p,r-t} \approx 5\%$, and a pump finesse of $F_p \approx 5.2$.

The variation of the pump field within the resonator is shown in figure V. 8 for pump frequency and cavity length detunings, and assuming an intra-cavity pump field parasitic loss of $\beta_{p,r-t} \approx 5\%$.

Figure V. 8 predicts that the intra-cavity pump field should remain at a near-constant level, once the pump field is tuned close to exact pump-field resonance. Therefore, as expected, the cavity length requirements were guided primarily by the OPO double-resonance condition. Assuming that the OPO cavity operated close to a pump field resonance, the cavity length requirements of the OPO to maintain single mode-pair operation were unaltered by the additional resonance condition imposed by the reflectivity of the cavity mirrors at the pump frequency. (However, the effects of pump field resonance played a significant role in further operation of the OPO, including smooth frequency tuning of the OPO outputs. These effects are evaluated in chapter VI.)

In summary, table V. 4 displays the expected requirements on the pump frequency and the OPO cavity length to operate the OPO above threshold and further, with stable operation on a single signal and idler frequency mode-pair.

*Table V. 4
Requirements on pump frequency and cavity length.*

Signal and idler frequency double-resonance.

<i>Pump frequency</i>	Δv_{p-stab}	$\approx \pm 3 \text{ MHz}$
<i>Cavity length</i>	ΔL_{stab}	$\approx \pm 0.2 \text{ nm}$

Pump frequency resonance.

<i>Pump frequency</i>	Δv_{p-stab}	$\approx \pm 0.65 \text{ GHz}$
<i>Cavity length</i>	ΔL_{stab}	$\approx \pm 35 \text{ nm}$

Pump power threshold.

<i>Pump frequency</i>	P_{p-th}^{in}	$\approx 29 \text{ mW}$
-----------------------	-----------------	-------------------------

V. 5 Experimental arrangement.

In this section, the apparatus that was used to operate the OPO is described. The set-up was similar to the arrangement outlined in chapter IV. In particular, both experimental arrangements used linear, standing-wave resonators for both the source of pump frequency and the OPO cavity. The experimental arrangement for the ultra-violet pumped LBO OPO is illustrated schematically in figure V. 9.

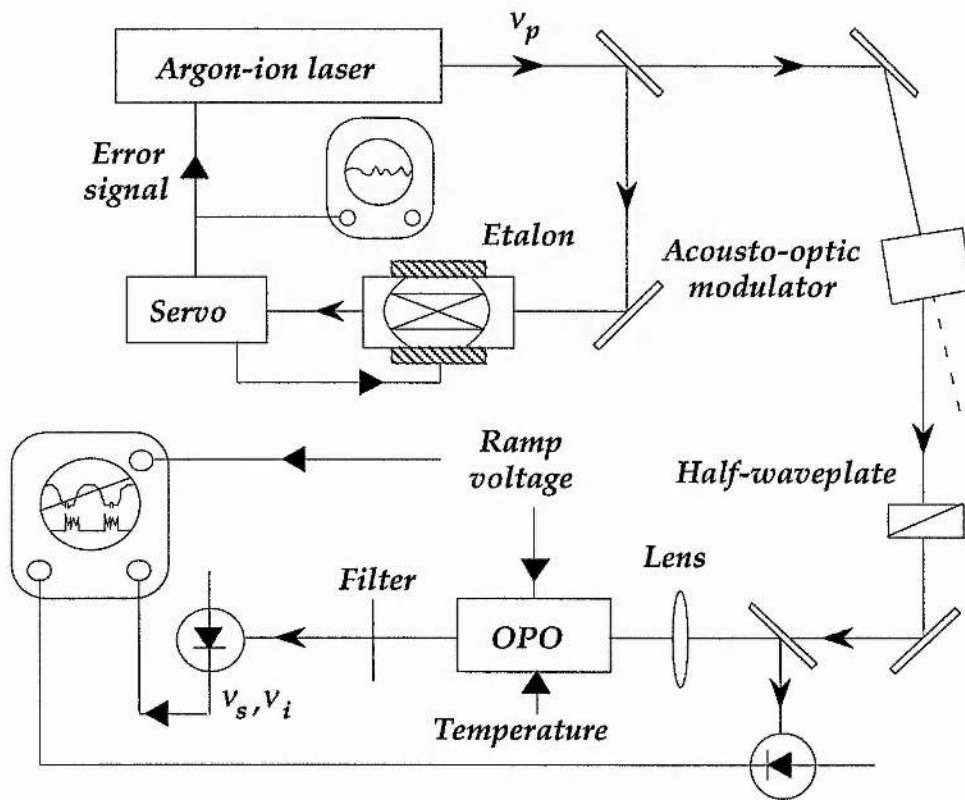


Figure V. 9.

Experimental apparatus used to couple pump radiation from the single-frequency argon-ion laser into the OPO cavity and to operate the OPO above threshold.

The use of a linear, standing-wave, on-axis OPO resonator, coupled with a linear, standing-wave pump laser source, required the use of effective isolation of the pump source from back-reflections and back-conversion from the OPO cavity. The method used to provide this in chapter IV, when the

argon-ion laser was operating in the green spectral region, involved the use of a *Faraday* isolator. This method of isolation could not be used for the arrangement described in this chapter due to the lack of a suitable material that could combine the properties of high transmission and a considerable *Faraday* effect in the ultra-violet spectral region. Therefore, another method of pump laser isolation was required in this experiment. The technique that was employed involved the use of an acousto-optic modulator to frequency shift the radiation from the pump laser [36]. The pump frequency was shifted by $\Delta\nu = 70$ MHz by the acousto-optic modulator for forward and backward travelling pump waves [37]. Therefore, any pump radiation that returned on-axis to the laser resonator was shifted by $2\Delta\nu = 140$ MHz, chosen specifically to avoid any axial mode resonances of the argon-ion cavity (recall that the free spectral range of the argon-ion laser was $FSR_p \approx 84$ MHz [2]).

The mode-matching of the pump beam into the OPO resonator is considered now. The argon-ion output beam had to be transformed by at least one lens to fulfil the required beam parameters at the input mirror of the OPO, and therefore to achieve the desired focusing of the pump wave. This analysis follows the equations presented in chapter II, for the propagation and transformation of Gaussian beams. The argon-ion laser output operating in the ultra-violet spectral region had the following beam parameters [2]; full angle divergence at $1/e^2$ power points

$$2\theta_p = \frac{2\lambda_p}{n\pi W_{p,laser}} = 0.5 \text{ mrad.} \quad [\text{V. 4}]$$

This implied an effective waist size for the pump source of $W_{p,laser} \approx 463 \mu\text{m}$. The pump mode was matched into the OPO resonator to a spot size of $W_{p,OPO} \approx 26.4 \mu\text{m}$, by using one focusing lens.

Figure V. 10 displays the required locations of the waists of the pump laser and the OPO cavity, relative to the lens, for different focal length values. From this graph, a single lens of focal length $f = 250$ mm was selected. The main consideration was again the physical length of the argon-ion laser, with the waist located at a distance of ≈ 2 m from the argon-ion laser output plane. Less important were the changes in the free-space optical paths due to propagation through the ancillary optical components.

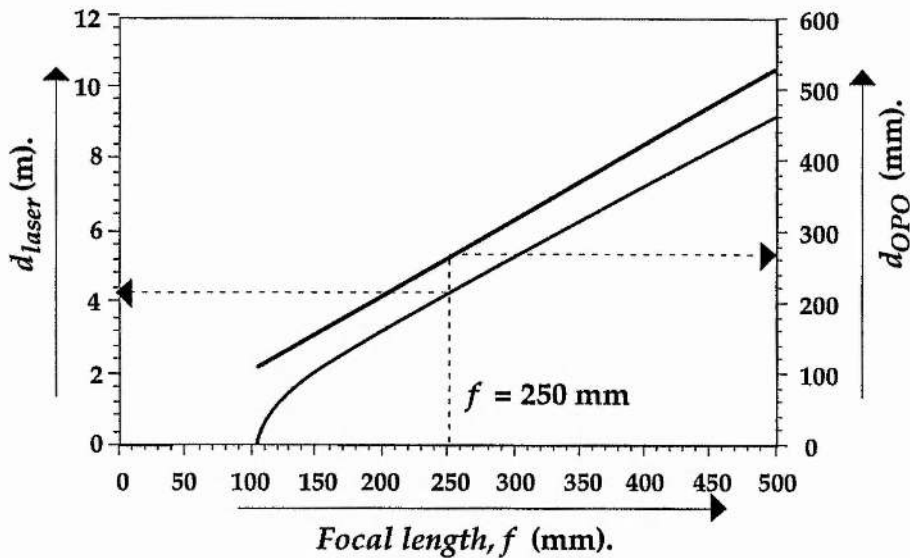


Figure V. 10.

Theoretical locations of the input and output waists for different values of the focal length of the single lens.

V. 6 Results and discussion.

This section summarizes the key results of the argon-ion pumped, type II phase-matched, cw OPO, operating near room-temperature. The amplitude and frequency characteristics of the OPO were investigated by scanning the cavity length of the OPO, and examining the corresponding changes in the intensity of the OPO outputs. From this analysis, precise values were inferred for the stability requirements on the cavity length to maintain single-frequency operation, and to hop between adjacent mode-pairs of the OPO cavity. The effects of pump frequency resonance were studied, and shown also to be in good agreement with the analysis of section V. 5. Finally, by applying servo-control feedback to the cavity length of the OPO, single-frequency signal and idler mode-pairs were held on resonance for periods of $\Delta t \approx 10$ s seconds.

With the arrangement described in the previous section, the OPO operated with a minimum pump power threshold of $P_p^{th} \approx 115$ mW. Figure V. 11 displays the power characteristics of the OPO. The OPO power was measured as the peak values of the OPO output from the exit cavity mirror. The total external power was assumed to be due to equal power levels being emitted from both of the cavity mirrors. (In practice, and

without cavity length control, the average power detected was of the order of several-mW.) Figure V. 11 displays the power characteristics of the OPO for incident pump powers of up to $P_p \approx 1$ W.

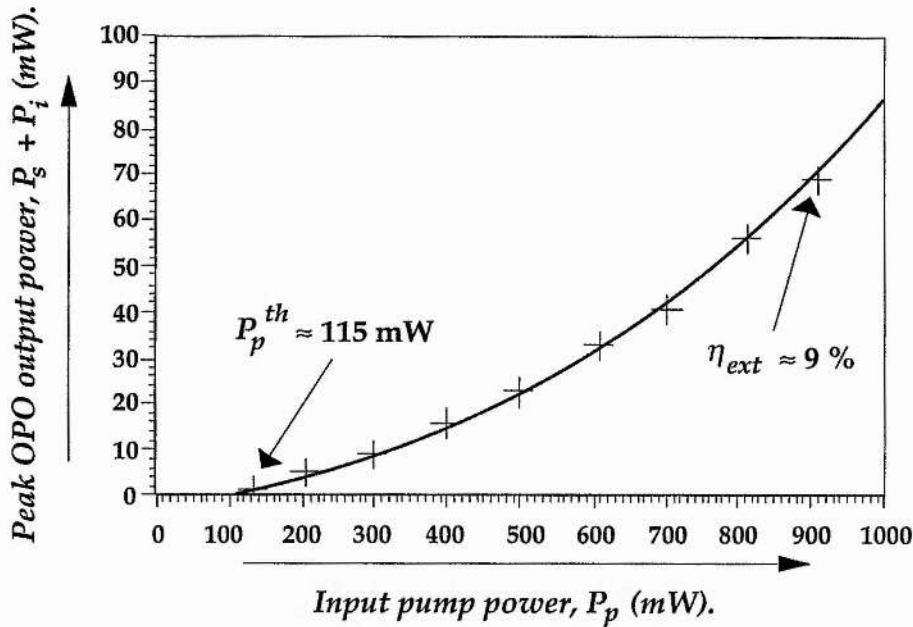


Figure V. 11.

Input and output powers for the OPO, showing a pump power threshold of $P_p^{th} \approx 115$ mW and an total, peak external conversion efficiency of $\eta_{ext} \approx 9\%$.

The experimental value for the pump power threshold differed significantly from the theoretical value. This was attributed to imperfect mode-coupling and to the uncertainties in the exact cavity losses (finesses) for the resonant fields and the nonlinear coefficients. (Recall that the finesses were estimated from the transmission curves obtained from the coating manufacturers.)

To assess the operation of the single-cavity, doubly-resonant OPO with respect to amplitude and frequency stability, the cavity length of the OPO was ramped over nanometre ranges, by applying a voltage to a piezo-electric element that controlled the position of one of the cavity mirrors. By using this technique, both the pump and the OPO resonance conditions could be evaluated. The intensity variations of the transmitted pump field, along with the OPO output, are displayed in figure V. 12.

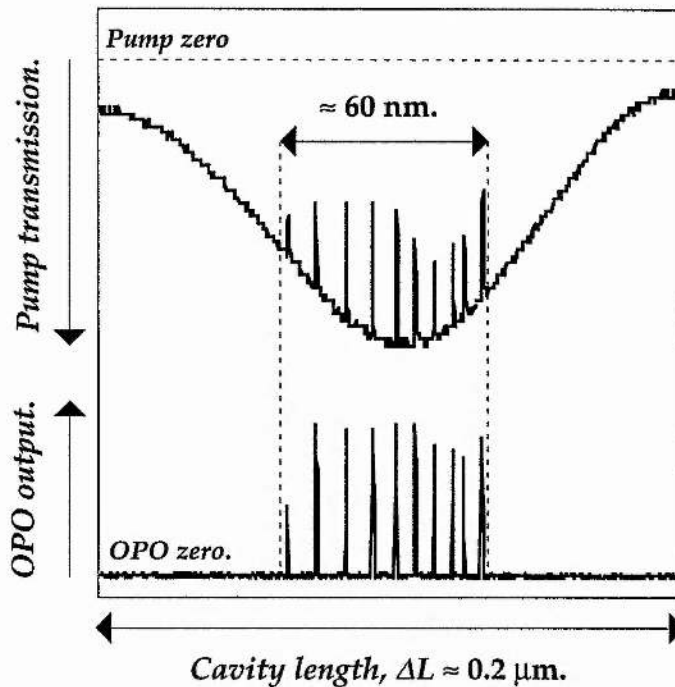


Figure V. 12.

Variations in the intensity of the transmitted pump field and the OPO output as the cavity length is detuned through $\Delta L \approx 0.2 \mu\text{m}$. Single-frequency signal and idler mode-pairs are shown to correspond to discrete positions of the OPO cavity length. The OPO operated over a total cavity length detuning of $\Delta L \approx 60 \text{ nm}$, as dictated by the resonance conditions at the pump frequency.

This figure displays cavity length detuning in a type II phase-matched single-cavity, doubly-resonant OPO with a partially-resonant pump field. The effect of the partial pump resonance is shown in the upper trace. The intra-cavity field is sufficient to overcome the threshold of the OPO only when the cavity length corresponds to near pump resonance. (The assumption is made that, over the time of the cavity length scan, the pump frequency stability was sufficient to assume a fixed frequency pump source.) The allowable cavity length detuning, over which sufficient pump radiation is coupled into the OPO cavity, is $\Delta L \approx 60 \text{ nm}$. This is in good agreement with the pump resonance analysis which was presented in the previous section, and assumed OPO operation for enhancement factors of greater than unity.

A further property that could be inferred from the cavity length scans was the quality of the mode-matching of the pump radiation into the OPO

cavity. This was achieved by measuring the level of the transmitted pump field, when exactly on and off pump resonance. When the OPO operated below threshold, and therefore contributed no pump depletion or additional internal pump loss, approximately 70 % of the incident pump field was transmitted through the OPO cavity on resonance. This represents an intra-cavity circulating pump power of $E_p \approx 1.6$ times the incident power. This is lower than the expected value of $E_p \approx 2.2$, and can be attributed to imperfect mode-matching. Another sign of imperfect mode-matching is that, when exactly off pump resonance, the transmitted pump field is significantly above the pump base-line in figure V. 12.

Figure V. 12 illustrates that the OPO output corresponded to discrete values of the OPO cavity length. These effects are displayed in more detail in figure V. 13.

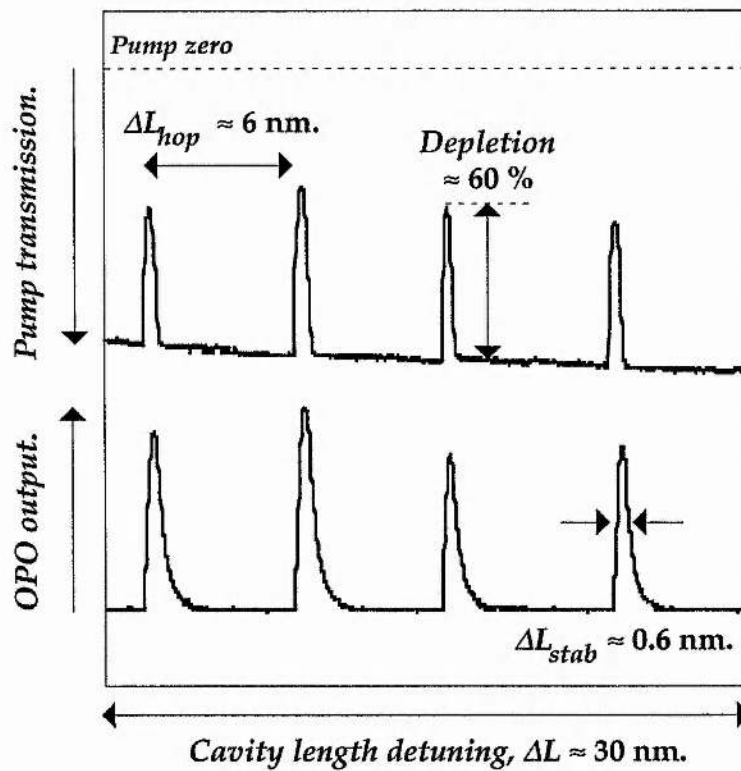


Figure V. 13.

Cavity length scanning of the single-cavity, doubly-resonant OPO over a cavity length detuning of $\Delta L \approx 30$ nm, illustrating discrete values for the pump depletion / OPO operation, and the cavity length tolerances for operation on a single-frequency mode-pair, and to hop to an adjacent OPO mode-pair within the same cluster.

Figure V. 13 indicates hopping of the OPO output between adjacent mode-pairs within the same cluster, and separated by cavity length spacings of $\Delta L_{hop} \approx 6$ nm. This value was in good agreement with the modelling of section VI. 4. In addition, the cavity length stability range was estimated to be $\Delta L_{stab} \approx 0.6$ nm, to maintain operation on a single signal and idler mode-pair. (Note that there is a significant proportion of the cavity length for which there is insufficient overlap of the signal and idler mode resonances to overcome threshold, even when the pump field is near exact resonance.) Pump depletions of ≈ 60 % are also implied from figure V. 13, verifying that the OPO cavity was under-coupled (the external conversion efficiency was sub-10 %).

Therefore, the cavity length conditions, as described above, could allow for amplitude stable OPO operation, by holding the cavity length fixed to within $\Delta L_{stab} \approx 0.6$ nm, and assuming that the short-term stability of the pump frequency was adequate, and could therefore be neglected. Servo-control feedback on the cavity length of the OPO was applied to achieve amplitude stable operation. This was provided by stabilizing the output intensity of the OPO to maintain operation on a single signal and idler frequency mode-pair, as shown schematically in figure V. 14.

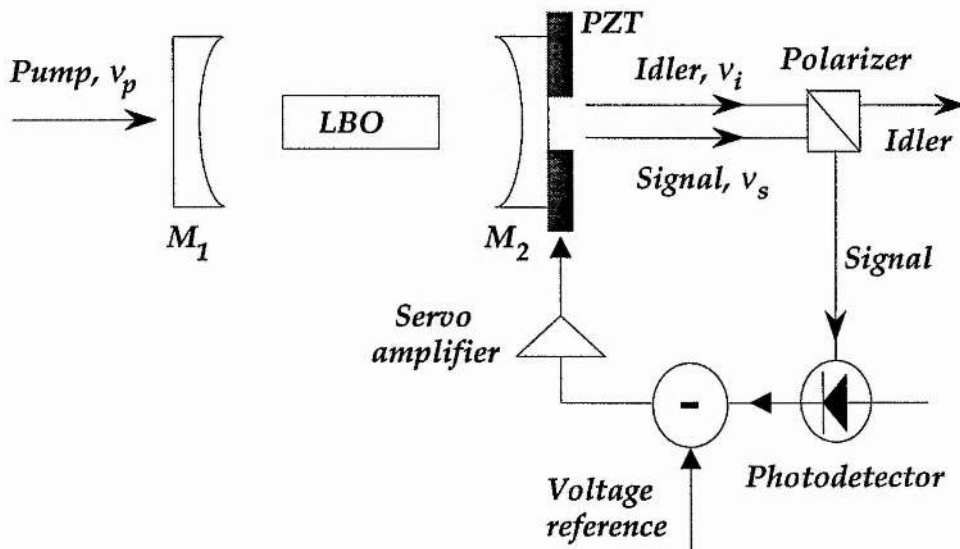


Figure V. 14.

Block diagram of the servo-control feedback loop to maintain the output of the OPO on a single-frequency signal and idler frequency mode-pair.

The servo-control feedback method employed was analogous to side-of-fringe locking. The cavity length of the OPO was detuned slightly off a power maximum and the signal frequency output was monitored on a photo-diode. The output from this photo-diode was compared to a reference voltage and the difference voltage was taken to form the error-signal for the servo-loop. This error-signal was integrated and fed via a high-voltage amplifier to the piezo-electric element that controlled the OPO cavity length. In this way, the cavity length was adjusted continuously to hold the power output from the OPO constant, and to maintain the OPO operating on the same single-frequency mode-pair. The bandwidth of the servo-loop was limited by the first mechanical resonance of the piezo-electric element to approximately ≈ 2 kHz. (This locking method has been used by other workers to stabilize the output of type II phase-matched doubly-resonant cw OPOs [34].) Given the frequency instability of the pump source, it was the amplitude and not the frequency of the OPO that was maintained constant. To achieve frequency stability of the OPO outputs, one of the outputs (e.g. the signal frequency) would have had to be locked to a stable external etalon, or to an external frequency reference. This frequency reference could take the form of an atomic transition or a microwave frequency standard [6, 7].

Analysing interferometers with significantly different free spectral ranges were employed to verify unambiguously that the output of the OPO was confined to a single signal and idler frequency mode-pair. Figure V. 15 displays single-frequency operation, as viewed on a plane-parallel interferometer of free spectral range $FSR_{int} \approx 3$ GHz.

In addition, a second photo-diode was used to monitor the power output from the OPO. The power output showed 20 - 30 % amplitude fluctuations on time-scales of the order of a few milliseconds. This was a direct result of the short-term frequency-jitter in the pump frequency, and the imperfect correction made to the OPO cavity length on these timescales, due to limitations of the servo-control bandwidth. Generally, it was found possible by this servo-control technique to maintain oscillation on the same single-frequency mode-pair for time periods of the order of a few 10s seconds.

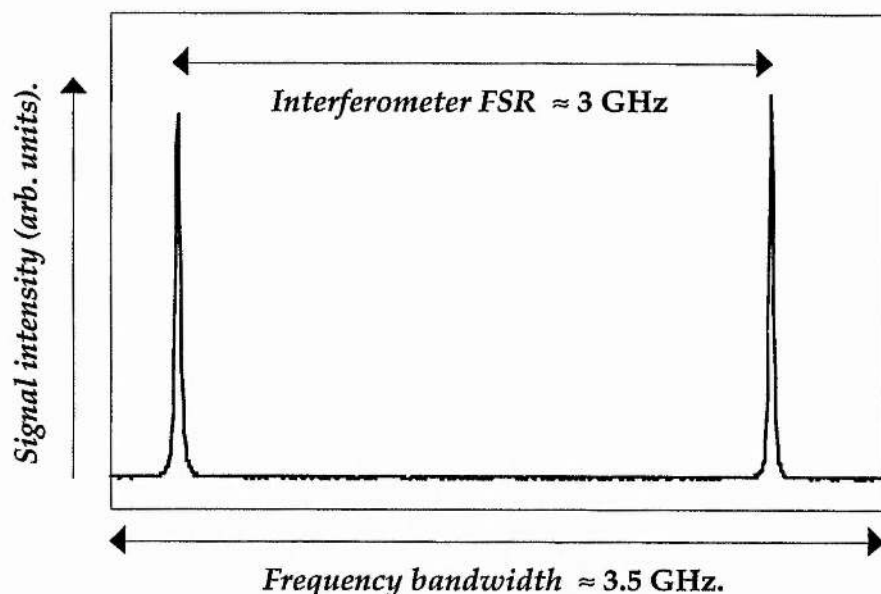


Figure V. 15.

Single-frequency operation of the signal frequency output from the OPO, as monitored on a scanning plane-parallel interferometer of free spectral range 3 GHz.

Temperature-tuning of the non-critical phase-matching geometry allowed for wide (coarse) frequency tuning of the signal and idler frequencies. The output frequencies of the OPO were varied coarsely by changing the precise temperature of the LBO crystal. The extent of the frequency tuning was limited by the bandwidth of the optical coatings within the OPO resonator to maintain high-finesse fields for both the signal and idler frequencies. By varying the temperature from $T_{xtal} \approx 20$ to ≈ 86 °C, the OPO could be tuned coarsely over a total frequency bandwidth of $\Delta\nu = \Delta\nu_s + \Delta\nu_i \approx 20$ THz. The signal frequency was tuned in the green / blue spectral region from $\nu_s \approx 598$ to 607 THz, and corresponding to wavelengths from $\lambda_s \approx 502$ to 494 nm, respectively. The idler frequency was tuned in the near infra-red spectral region from $\nu_i \approx 227$ to 217 THz, and corresponding to wavelengths from $\lambda_i \approx 1.32$ to 1.38 μm , respectively. The tuning rate in this phase-matching geometry corresponded to ≈ 150 GHz/°C, and was in agreement with the findings of other workers [3 - 5]. (It is reasonable to assume that, since the coatings were specified to be optimum at room-temperature, a similar range of tuning would be possible for lower temperatures. This feature would have required cooling the nonlinear medium, and was not investigated.)

Although the driving motivation behind this work was to operate the OPO with amplitude-stable signal and idler outputs, it is worth considering further the temperature dependence of these outputs. As discussed in chapter III, the type II phase-matching geometry offers less sensitivity in the output frequencies to small changes in the phase-matching temperature than equivalent type I phase-matched geometries. Therefore, the tuning rate of $\approx 150 \text{ GHz}/^\circ\text{C}$, reported in this chapter, represents the least sensitive LBO OPO arrangement, with regard to temperature perturbations. To obtain stable, free-running operation from this phase-matching geometry, with, for example, MHz-level stability, sub-mK temperature control would be necessary. This emphasizes further the need for cavity length control, and fine pump frequency tuning, to compensate for temperature drifts. When compared to KTP in the type II phase-matching geometry, with a reported tuning rate of $\approx 300 \text{ MHz}/^\circ\text{C}$ [7], LBO must be regarded as an inferior choice of nonlinear medium if phase-matching in KTP exists for the chosen pump / phase-matching arrangement. Again, this points towards the immediate use of LBO only in phase-matching geometries that cannot be accessed by using other nonlinear materials.

The main results from this argon-ion pumped type II cw OPO are summarized in table V. 5.

*Table V. 5
Operating characteristics of the cw OPO.*

<i>Pump power threshold</i>	P_p^{th}	$\approx 115 \text{ mW}$
<i>External efficiency</i>	η_{ext}	$\approx 9 \%$
<i>Signal frequency tuning</i>	$\Delta\nu_s$	598 - 607 THz
<i>Idler frequency tuning</i>	$\Delta\nu_i$	227 - 217 THz
<i>Coarse tuning rate</i>	$\Delta\nu$	150 GHz/ $^\circ\text{C}$

V. 7 Conclusions.

The performance of the argon-ion pumped non-degenerate type II phase-matched LBO cw OPO has displayed many of the characteristics that were predicted from theory and modelling. The requirements on the stability of the pump frequency were relaxed by operating the OPO under type II phase-matching, in which there was a significant mis-match in the free spectral ranges of the signal and idler fields within the resonator. The stability of the pump source was found to be adequate to operate the OPO reliably on single signal and idler frequency mode-pairs. Amplitude-stable operation of the OPO on single signal and idler frequency mode-pairs was obtained for periods of ≈ 10 s seconds.

Critical to the reliable operation of the OPO was the passive stability of the OPO resonator. The highly-stable, invar-based, cavity design enabled the use of servo-control feedback to provide the desired amplitude-stable outputs. To achieve frequency control of the OPO outputs, the absolute frequency of the pump source should be stabilized to kHz-levels. The OPO frequencies could then be referenced to frequency standards within measurable frequency locking bandwidths, or by locking to stable external etalons. When amplitude and frequency stabilization schemes are employed together, such an OPO has the potential to serve as a practical frequency divider [6, 7, 38].

The constraints of the single-cavity OPO again prevented further study of this phase-matching geometry. Frequency tuning of the OPO outputs can only be possible by tuning the precise frequency of the pump source and correcting by length changes of a single cavity OPO, or by separating internally the signal and idler fields and resonating these in discrete cavities. This latter method describes the dual-cavity oscillator approach [10]. The non-degenerate frequencies involved in this type II phase-matching geometry provide an ideal opportunity to decouple efficiently the OPO resonances, and this method is described in the following chapter which contains experimental results from the first demonstration of such a dual-cavity, doubly resonant cw OPO.

The signal and idler frequencies were tuned coarsely over extensive frequency bandwidths in the green and near infra-red spectral regions. In the present geometry, these frequencies are in a ratio of $\approx 2.6:1$. By increasing further the phase-matching temperature of the LBO crystal to $T_{xtal} \approx 175^\circ\text{C}$, the frequencies would be in a 3:1 frequency ratio. Therefore, this phase-

matching geometry in LBO offers the possibility of exact 3:1 frequency division. If this configuration was to be realized experimentally, it would be necessary to detect the point of exact 3:1 signal:idler operation, which is not a problem at frequency degeneracy where the signal and idler frequencies are equal [38].

There are several possible solutions to this problem, as discussed in reference [38] and in the final section of the previous chapter. If the pump source for the OPO is the second harmonic frequency of some master laser, then this laser frequency (possibly frequency offset) and the idler frequency could be summed to yield a frequency near the signal frequency. The sum frequency output will be coherent with the OPO signal wave only when the signal and idler frequencies are exactly in the ratio 3:1. The sum of the pump frequency and the idler frequency could also be optically fed-back to injection lock the phase of the signal frequency, or the pump frequency could be deeply phase-modulated and mixed with both the signal and the idler frequencies. This would alternatively sum the pump frequency with the idler frequency to yield the signal frequency, and subtract the pump frequency from the signal frequency to yield the idler frequency, as the phase is varied, and it would produce an amplitude-modulated output only when the exact 3:1 condition was met. If no master laser at half the pump frequency was available, the idler frequency could be frequency-tripled and compared with the signal frequency, which is the technique required to lock an OPO to the 2:1 signal:idler frequency operating point, where the idler frequency can be frequency doubled and compared with the signal frequency.

In summary, type II phase-matched geometries offer significant advantages over type I phase-matched geometries, with regard to the requirements on the pump frequency and OPO cavity length stability. When further type II phase-matching geometries become available in newly developed nonlinear materials (e.g. KTA [39] and CTA [40]), and different pump sources become available for these OPOs, then such OPOs may form practical devices for the generation of highly-stable signal and idler frequency radiation.

References.

1. F. G. Colville, M. J. Padgett, A. J. Henderson, J. Zhang, & M. H. Dunn,
"Continuous-wave parametric oscillator pumped in the ultra-violet,"
Opt. Lett. **18**, 1065 (1993).
2. Model 2040E and 2045E; High power ion laser,
Spectra-Physics laser products division, CA 94039-7013, USA.
Instruction manual, part no. 0000-210A, Rev. A, October 1990.
3. F. Hanson & D. Dick,
"Blue parametric generation from temperature-tuned LiB_3O_5 ,"
Opt. Lett. **16**, 205 (1991).
4. M. Ebrahimzadeh & M. H. Dunn,
"A visible optical parametric oscillator pumped by an excimer laser,"
in *Conference on Lasers and Electro-Optics*, Vol. 5 of OSA 1988 Technical Digest Series
(Optical Society of America, Washington, D. C., 1988), paper CPD 30.
5. Y. Cui, M. H. Dunn, C. J. Norrie, W. Sibbett, Y. Tang, & J. A. C. Terry,
"All-solid-state optical parametric oscillator for the visible,"
Opt. Lett. **17**, 646 (1992).
Y. Tang, Y. Cui, & M. H. Dunn,
"Lithium triborate optical parametric oscillator pumped at 266 nm,"
Opt. Lett. **17**, 192 (1992).
6. D. Lee & N. C. Wong,
"Tunable optical frequency division using a phase-locked optical parametric
oscillator,"
Opt. Lett. **17**, 13 (1992).
7. D. Lee & N. C. Wong,
"Stabilization and tuning of a doubly-resonant optical parametric oscillator,"
J. Opt. Soc. Am. B **10**, 1659 (1993).
8. T. Debuisschert, A. Sizmann, E. Giacobino, & C. Fabre,
"Type-II continuous-wave optical parametric oscillators: oscillation and frequency-
tuning characteristics,"
J. Opt. Soc. Am. B **10**, 1668 (1993).
9. M. J. Padgett, F. G. Colville, & M. H. Dunn,
"Mode selection in doubly-resonant optical parametric oscillators,"
In press, *IEEE J. Quant. Electron.*
10. F. G. Colville, M. J. Padgett, & M. H. Dunn,
"Continuous-wave, dual-cavity, doubly-resonant, optical parametric oscillator,"
Appl. Phys. Lett. **64**, 1490 (1994).
11. W. B. Bridges & A. N. Chesler,
"Visible and UV laser oscillation at 118 wavelengths in ionized neon, argon, krypton,
xenon, oxygen and other gases,"
Appl. Opt. **4**, 573 (1965).
P. K. Cheo & H. G. Cooper,
"Ultraviolet ion laser transitions between 2300 and 4000 Å,"
J. Appl. Phys. **36**, 1862 (1965).
12. J. R. Fendley,
"L-1 - Continuous UV lasers,"
IEEE J. Quant. Electron. QE-4, 627 (1968).
13. H. R. Luthi, W. Seelig, & J. Steinger,
"Power enhancement of continuous ultraviolet lasers,"
Appl. Phys. Lett. **31**, 670 (1977).
14. L. Y. Liu, M. Oka, W. Wiechmann, & S. Kubota,
"Longitudinally diode-pumped continuous-wave 3.5-W green laser,"
Opt. Lett. **19**, 189 (1994).

15. C. S. Adams & A. I. Ferguson,
"Tunable narrow linewidth ultra-violet light generation by frequency doubling of a ring Ti:sapphire laser using lithium tri-borate in an external enhancement cavity,"
Opt. Comm. **90**, 89 (1992).
16. S. Bourzeix, M. D. Plimmer, F. Nez, L. Julien, & F. Biraben,
"Efficient frequency doubling of a continuous wave titanium:sapphire laser in an external enhancement cavity,"
Opt. Comm. **99**, 89 (1993).
17. *Laser focus world*,
"Ion lasers deliver power at visible and UV wavelengths,"
p97, December 1992.
18. K. Banse, G. Herziger, G. Schafer, & W. Seelig,
"Continuous UV-laser power in the watt range,"
Phys. Lett. **27A**, 682 (1968).
19. H. R. Luthi & J. Steinger,
"Continuous operation of a high power neon ion laser,"
Opt. Comm. **27**, 435 (1978).
20. T. L. Boyd & H. J. Kimble,
"Frequency stabilization of a continuous-wave Ti:sapphire laser,"
Opt. Lett. **16**, 808 (1991).
21. W. Wang, K. Nakagawa, S. Sayama, & M. Ohtsu,
"Coherent addition of injection-locked high-power AlGaAs diode lasers,"
Opt. Lett. **17**, 1593 (1992).
- R. Waarts, R. Parke, D. Nam, D. Welch, D. Mehuys, R. Lang, S. O'Brien, & D. Scifres,
"Second-harmonic generation with high-power coherent monolithic GaAs master oscillator power amplifier,"
in *Conference on Lasers and Electro-Optics*, Vol. 10 of OSA 1993 Technical Digest Series (Optical Society of America, Washington, D. C., 1993), paper CWC 2.
22. Da-Wun Chen & J. T. Lin,
"Temperature-tuned phase-matching properties of LiB₃O₅ for Ti:sapphire laser frequency doubling,"
IEEE J. Quant. Electron. **QE-29**, 307 (1993).
- G. A. Skripko, S. G. Bartoshevich, I. V. Mikhnyuk, & I. G. Tarazevich,
"LiB₃O₅: a highly efficient frequency converter for Ti:sapphire lasers,"
Opt. Lett. **16**, 1726 (1991).
23. P. Gunter, P. M. Asbeck, & S. K. Kurtz,
"Second-harmonic generation with Ga_{1-x}Al_xAs lasers and KNbO₃ crystals,"
Appl. Phys. Lett. **35**, 461 (1979).
- W. J. Kozlovsky, W. Lenth, E. E. Latta, A. Moser, & G. L. Bona,
"Generation of 41 mW of blue radiation by frequency doubling of a GaAlAs diode laser,"
Appl. Phys. Lett. **56**, 2291 (1990).
- D. W. Nam & R. G. Waarts,
"Advanced laser diodes bring compact blue-green sources to light,"
Laser Focus World, p49 (August 1994).
24. E. S. Polzik & H. J. Kimble,
"Frequency doubling with KNbO₃ in an external cavity,"
Opt. Lett. **16**, 1400 (1991).
25. B. Wu, N. Chen, C. Chen, D. Deng, & Z. Xu,
"Highly efficient ultraviolet generation at 355 nm in LiB₃O₅,"
Opt. Lett. **14**, 1080 (1989).
26. Y. Wang, Z. Xu, D. Deng, W. Zheng, B. Wu, & C. Chen,
"Visible optical parametric oscillation in LiB₃O₅,"
Appl Phys. Lett. **59**, 531 (1991).
27. Y. Taira,
"Continuous 6-watt coherent deep UV generation using a resonant doubling technique,"
in *Conference on Lasers and Electro-Optics*, Vol. 10 of OSA 1993 Technical Digest Series (Optical Society of America, Washington, D. C., 1993), paper CFL 3.

28. S. Owa, Y. Taira, & S. S. Kano,
 "Efficient second-harmonic generation using an external cavity for cw ultra-violet radiation,"
 in *Conference on Lasers and Electro-Optics*, Vol. 10 of OSA 1993 Technical Digest Series (Optical Society of America, Washington, D. C., 1993), paper CFL 4.
29. J. Eckstrand, S. C. Guggenheimer, & D. L. Wright,
 "Active single-frequency stabilization of an argon-ion laser,"
 in *Conference on Lasers and Electro-Optics*, Vol. 9 of OSA 1992 Technical Digest Series (Optical Society of America, Washington, D. C., 1992), paper CPC 4.
30. S. C. Guggenheimer & D. L. Wright,
 "Controlling the propagation axes of an ion laser,"
Rev. Sci. I. **62**, 2389 (1991).
31. *Laser focus world*,
 "Servo actively reduces jitter in single-frequency ion lasers,"
 Vol. 29, 3, 16 (1993).
32. C. Chen, Y. Wu, A. Jiang, B. Wu, G. You, R. Li, & S. Lin,
 "New nonlinear-optical crystal: LiB_3O_5 ,"
J. Opt. Soc. Am. B **6**, 616 (1989).
33. S. T. Yang, C. C. Pohalski, E. K. Gustafson, R. L. Byer, R. S. Feigelson, R. J. Raymakers, & R. K. Route,
 "6.5-W, 532-nm radiation by cw resonant external-cavity second-harmonic generation of an 18-W Nd:YAG laser in LiB_3O_5 ,"
Opt. Lett. **16**, 1493 (1991).
34. T. Debuisschert, S. Reynaud, A. Heidmann, E. Giacobino, & C. Fabre,
 "Observation of large quantum noise reduction using an optical parametric oscillator,"
Quant. Opt. **1**, 3 (1989).
 S. Reynaud, C. Fabre, & E. Giacobino,
 "Quantum fluctuations in a two-mode parametric oscillator,"
J. Opt. Soc. Am B **4**, 1520 (1987).
 A. Heidmann, R. J. Horowicz, S. Reynaud, E. Giacobino, & C. Fabre,
 "Observation of quantum noise reduction on twin laser beams,"
Phys. Rev. Lett. **59**, 2555 (1987).
35. P. Grangier, R. E. Slusher, B. Yurke, & A. LaPorta,
 "Squeezed-light-enhanced polarization interferometer,"
Phys. Rev. Lett. **59**, 2153 (1987).
36. R. G. Smith,
 "Use of the acousto-optic light deflector as an optical isolator,"
IEEE J. Quant. Electron. **9**, 545 (1973).
37. Acousto-optic modulator,
 Model ASM-702-8 instruction manual,
InterAction Corp., IL 60104, USA.
38. C. D. Nabors, S. T. Yang, T. Day, & R. L. Byer,
 "Coherence properties of a doubly-resonant monolithic optical parametric oscillator,"
J. Opt. Soc. Am. B **7**, 815 (1990).
39. P. E. Powers, S. Ramakrishna, C. L. Tang, & L. K. Cheng,
 "Optical parametric oscillation with KTiOAsO_4 ,"
Opt. Lett. **18**, 1171 (1993).
 L. K. Cheng, L.-T. Cheng, J. D. Bierlein, F. C. Zumsteg, & A. A. Ballman,
 "Properties of doped and undoped crystals of single domain KTiOAsO_4 ,"
Appl. Phys. Lett. **62**, 346 (1993).
40. P. E. Powers, C. L. Tang, & L. K. Cheng,
 "High-repetition-rate femtosecond optical parametric oscillator based CsTiOAsO_4 ,"
Opt. Lett. **19**, 37 (1994).

Chapter VI.

Dual-Cavity, Doubly-Resonant Oscillator with Separate Signal and Idler Cavity Length Control.

Contents.	Page.	
VI. 1	Introduction.	253
VI. 2	Optical parametric oscillator design.	255
VI. 3	Pump frequency and cavity length requirements.	258
VI. 4	Results and discussion.	260
VI. 5	Conclusions.	267
	References.	270

VI. 1 Introduction.

Up until now, the continuous-wave (cw) optical parametric oscillators (OPOs) described within this thesis (chapters IV and V) have relied upon the use of two-mirror, single-cavity designs to resonate the signal and idler fields [1, 2]. However, as discussed extensively in chapter II, and consistently throughout the text, this common two-mirror cavity geometry represents a significant drawback in the design of doubly-resonant cw OPOs, in which the same two mirrors must satisfy simultaneously mode coincidences for both the resonant fields.

The concept of using dual optical cavities within a common resonator arrangement, for improved frequency control, dates back to the 1960s. Dual-cavity resonators were once considered highly appropriate for achieving single-frequency operation from argon-ion lasers. Such Fox-Smith interferometer designs exploited a folded optical cavity, through use of an intra-cavity beam-splitter, to provide frequency selection from a master cavity that contained the gain medium of the laser [3 - 5]. Further examples of dual-cavity resonators are included in references [6] to [8]. Within pulsed OPO geometries, the addition of further optical cavities have been particularly effective in reducing the linewidth of the OPO outputs [9, 10]. Long before the demonstration of the first cw OPOs [11, 12], the benefits of separate cavity

length control for the signal and idler frequencies were recognized [13]. This concept has also been discussed briefly in more recent papers, but without addressing specifically the experimental realization of such a resonator design [2, 14 - 16].

This chapter describes the operating characteristics of the first cw OPO that used a dual-cavity resonator design to separate internally the signal and idler fields within a doubly-resonant cw OPO [17 - 19]. The OPO used the same pump source as the OPO described in the previous chapter, and operated at a frequency of $\nu_p = 824$ THz, corresponding to a pump wavelength of $\lambda_p = 363.8$ nm. The OPO used the same nonlinear crystal, lithium triborate (LBO), operating specifically at room temperature in the type II phase-matching geometry, described in chapter V. However, the OPO described in this chapter incorporated an intra-cavity beam-splitter to separate internally the optical paths of the resonant signal and idler fields, in such a way that the two frequencies could resonate with independent cavity length control.

The design of the OPO cavity is outlined in section VI. 2. The beam-splitter was coated to provide high-reflectivity for the signal frequency and high-transmission for the idler frequency, and was placed within the resonator at Brewster's angle to exploit the orthogonal polarizations of the type II phase-matched OPO. The efficient formation of the dual-cavity OPO depended critically on the ability to maintain two high finesse resonators for the signal and the idler frequencies, in the presence of additional intra-cavity components. A cavity design was constructed to provide a comparable degree of passive stability to the highly-stable, single-cavity, OPO that was described in chapter V. This method involved fixing the nonlinear crystal, the beam-splitter, and the three cavity mirrors on a single length-determining base-plate.

The mode-selection properties of the output frequencies of this OPO are discussed in section VI. 3. The cavity length and pump frequency stability requirements were similar to the single-cavity design, to hold a single signal and idler frequency mode-pair on resonance. However, the dual-cavity design allowed for smooth, continuous tuning of the output frequencies by scanning the optical length of one cavity, and applying servo-control feedback to the other cavity length, to maintain the double-resonance condition. The level of smooth frequency tuning from the OPO is discussed with respect to

the pump resonance effects which were maintained within the idler cavity of the dual-cavity OPO, and considering the limitations of the fixed frequency pump source provided by the argon-ion laser.

The results of the dual-cavity OPO are presented in section VI. 4. The three mirror dual-cavity design operated with a minimum pump power threshold of $P_p^{th} \approx 200$ mW. While the double-resonance condition for the signal and idler frequencies was fulfilled, the OPO could be tuned smoothly over a frequency bandwidth of $\Delta\nu_s \approx \Delta\nu_i \approx 0.4$ GHz, by deliberately scanning the cavity length of the idler frequency, and relying upon the signal cavity servo-control feedback loop to maintain double-resonance.

Finally, in section VI. 5, the important results are considered with respect to improvements in the stability of the pump frequency, and a relaxation of the pump field finesse within the OPO resonator. Cavity designs are discussed that could eliminate all effects of pump resonance, while maintaining low pump power thresholds. In addition, applications of the dual-cavity resonator to optical frequency metrology schemes are outlined in detail.

VI. 2 Optical parametric oscillator design.

In this section, there is a description of the design of the OPO resonator. In particular, the resonator geometry is examined, allowing for the efficient decoupling of the resonant fields of the signal and idler frequencies within the OPO resonator. The intra-cavity components were analysed with a view to obtaining pump power thresholds at the mW-level, stable OPO operation on a single signal and idler frequency mode-pair, and smooth frequency tuning of the OPO outputs in the presence of a fixed frequency pump source.

To provide efficient spatial separation within the OPO resonator, the beam-splitter must contribute minimal additional parasitic losses for both the signal and idler fields, thus maintaining the high finesse required for double-resonance and low values of the pump power threshold. Discrimination between the two intra-cavity fields was provided by the type II phase-matching geometry, and the non-degenerate frequencies of the signal and idler waves associated with the phase-matching geometry. The type II phase-matching geometry with orthogonally-polarized signal and idler fields allowed for polarization separation. Frequency non-degeneracy with a

significant frequency mis-match in the signal and idler frequencies allowed for dichroic-coating separation. These two attributes were combined effectively in the design of the intra-cavity beam-splitter.

The cavity design is illustrated schematically in figure VI. 1. The beam-splitter was inserted into the resonator on one side of the nonlinear crystal, and a third mirror was added to form a second independent optical resonator. The cavity mirrors used were all identical to those described in chapter V for the single-cavity resonator design.

It is important to realize that the coating requirements on the cavity mirrors can be reduced substantially by forming a dual-cavity resonator, due to the spatial separation from the beam-splitter. Although mirrors M_2 and M_3 used in this experiment, as shown in figure VI. 1, were highly-reflecting at both the signal and idler frequencies, the coating requirements were relaxed in principle. The mirror M_2 only had the requirement to be highly-reflecting at the idler frequency, and the mirror M_3 only had the requirement to be highly-reflecting at the signal frequency. This factor is discussed in section VI. 5 with respect to further phase-matching geometries in cw OPOs within optical frequency division schemes.

The Brewster-angled beam-splitter was fabricated from the material herasil, with a refractive index of $n_{b-s} \approx 1.54$, and inserted into the cavity at an incident angle of $\theta_i \approx 57^\circ$. The beam-splitter was coated to provide $T_i \geq 99.7\%$ transmission for the p -polarized idler wave at a frequency of $\nu_i = 227$ THz, and $R_s \geq 99.7\%$ reflection for the s -polarized signal wave at a frequency of $\nu_s = 598$ THz. In addition, the beam-splitter provided $T_p \geq 97\%$ transmission for the p -polarized pump wave at a frequency of $\nu_p = 824$ THz. The pump transmission of the beam-splitter retained the partial pump resonance that was described in the design of the single-cavity OPO resonator in chapter V.

Given that the intra-cavity parasitic losses would be increased, due to the additional surfaces encountered by the resonant fields on a round-trip of the OPO cavity, the enhanced pump field and double-pass interaction due to the pump resonant effects, were considered essential, given the available pump power from the argon-ion laser.

Before studying the frequency properties of the output of the OPO, the passive stability must be at a level where the OPO can maintain short-term

free-running operation on single signal and idler frequency mode-pairs, similar to the requirements on the single-cavity design of chapter V.

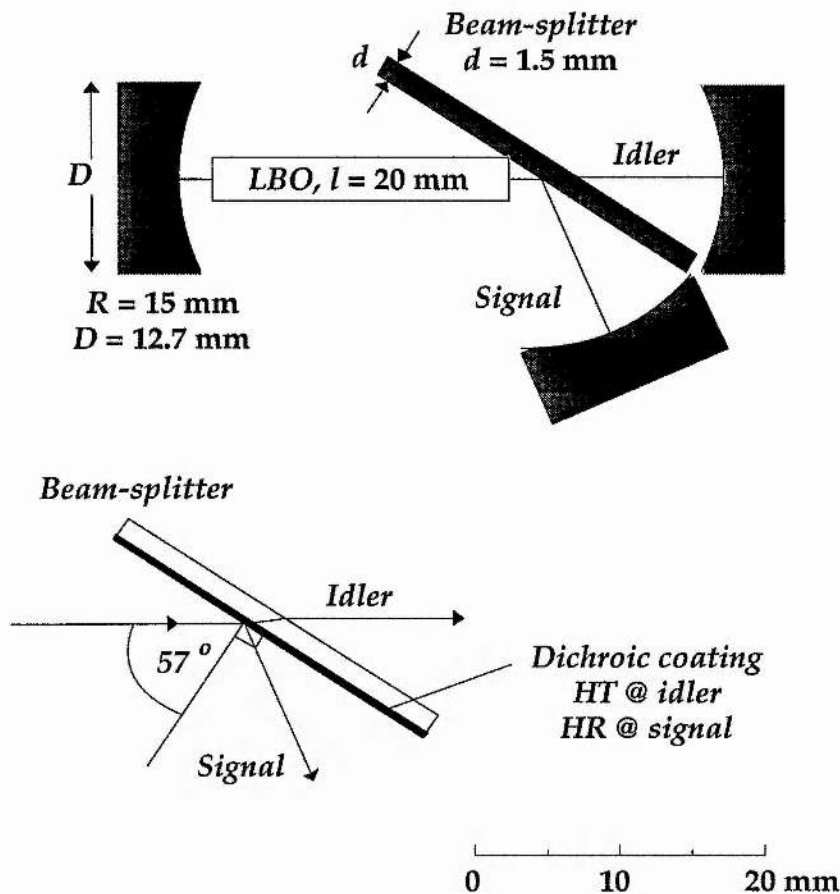


Figure VI. 1.

Schematic representation of the dual-cavity resonator design, illustrating the power reflection and transmission coefficients of the beam-splitter substrate for the three intra-cavity fields. R: radius-of-curvature; D, d: diameters; HT: highly-transmitting; HR: highly-reflecting.

Critical to the passive stability of the dual-cavity OPO was fixing the beam-splitter plate and the LBO crystal on a single block without angular / translational adjustment, and relying upon external pump-beam alignment for exact on-axis propagation along the z-principal optical axis of the LBO material. Cavity alignment was provided by micrometer control on the three flexure-hinged mirror mounts. The cavity components were

attached to a single length-determining base-plate, and surrounded by extensive mechanical and acoustic isolation to increase the passive stability of the two resonators. The base-plate was itself fixed to a substantial granite base, which sat in a sand tray to eliminate further vibrations from the optical bench. (In this way, the mechanical and acoustic disturbances were considerably reduced over a previously constructed equivalent cavity design that used separate, discrete mounting for the five resonator components, and which is illustrated inside the front cover of the thesis.)

To illustrate the compact size of the dual-cavity resonator, the size of the cavity components used in the experiment are shown in the scale diagram of figure IV. 1. The mirrors are all of 15 mm radius of curvature, with a diameter of 12.7 mm, and have the same dielectric reflectivity profile as the mirrors used for the single-cavity device of chapter V. All three mirrors had piezo-electric components controlling the precise lengths of the two optical cavities.

As mentioned previously, the pump frequency and phase-matching specifications were the same as the cw OPO that was outlined in chapter V. Therefore, the experimental arrangement, with respect to the isolation of the pump source and the mode-matching of the pump beam into the OPO resonator, were identical to that of the previous chapter.

VI. 3. Pump frequency and cavity length requirements.

In this section, there is an analysis of the requirements of the pump frequency and the OPO cavity length to maintain operation on a single-frequency mode-pair, and further, to generate smooth frequency tuning from the dual-cavity resonator. Frequency and amplitude stabilization methods are addressed that take advantage of the additional degree of freedom provided by the dual-cavity resonator.

The stability requirements to maintain operation on a single signal and idler frequency mode-pair were assumed to be similar to those of the single-cavity device of chapter V. This is because the pump frequency and the phase-matching geometry are identical in the single- and dual-cavity resonator designs. The mis-match in the free spectral ranges takes on a new significance in the dual-cavity resonator. Dual-cavity resonators were analysed in detail in chapter II. In general, the lengths of the two cavities and

the finesses of the signal and idler fields can be considerably different, when compared to single-cavity OPO designs. The control of the free spectral ranges of the signal and idler fields was shown to provide one method of relaxing the pump frequency and the cavity length requirements to maintain single-frequency mode-pair operation.

In this dual-cavity arrangement, the cavity lengths and the finesses for the signal and idler fields were similar to the single-cavity design, by virtue of using the same cavity mirrors in both designs. Since the mis-match in the free spectral ranges was at a level that had allowed for stable single mode-pair operation in the single-cavity design, no further allowances were made in the dual-cavity OPO. (This could have been provided by increasing the length of one of the two cavity arms, while decreasing the finesse of this cavity to further reduce the stability requirements, as discussed in chapter II and in reference [19].)

Therefore, the effects of detuning the pump frequency or the cavity length on the mode-selection of the OPO were assumed to be comparable to the modelling of the previous chapter. Specifically, the effects of cavity length detuning are complicated by the separate cavity lengths of the signal and idler fields. When the two fields are resonant within the same common cavity, the effects of cavity length detunings can be interpreted as a combination of the frequency shifts of the two resonant fields, and of the shift in the overlap of the resonance peaks with respect to each other. Therefore, within the dual-cavity design, when one of the cavity lengths is fixed, then the level of detuning of the other cavity length is required to be a combination of the two relative shifts in the resonance peaks of the single-cavity design.

Consider now the combined effects of pump frequency and cavity length perturbations. For the single-cavity OPO design, the cavity length requirements were valid only when the pump frequency requirements were within the minimum levels that could maintain single-frequency mode-pair operation. Therefore, the pump frequency requirements can be regarded as the most critical in stable OPO operation in a single-cavity resonator design. However, in the dual-cavity OPO design, the freedom from forming separate optical cavities eliminates this constraint, and opens up the possibility for using a wider selection of pump sources for cw OPOs.

The analysis of chapter II is applied now to the cavity design of the OPO described in this chapter. Recall equation II.146 that relates the frequency

instabilities of the pump frequency, and the required detunings of the signal and idler cavity lengths:

$$\Delta\nu_p \approx \Delta L_s \left(-\frac{2\nu_s FSR_s}{c} \right) + \Delta L_i \left(-\frac{2\nu_i FSR_i}{c} \right). \quad [\text{VI. 1}]$$

For the dual-cavity OPO, with separate optical lengths for the signal and idler fields, this equation consists of three parameters that can be controlled individually. Moreover, with sufficient servo-feedback on one of these parameters, perturbations in the other two can be eliminated to retain single-frequency mode-pair operation. Therefore, the constraints on the pump frequency can be lifted by independent cavity length control from the dual-cavity resonator, as discussed above.

It follows from equation VI. 1 that the above method can be used also to generate smooth frequency tuning from an OPO. There are two different techniques that can be used for this. First, by holding the frequency, or cavity length, of one of the two OPO frequencies constant, the pump frequency can be tuned as long as the other OPO cavity length maintains the double-resonance condition. Second, by holding the pump frequency constant, one of the OPO cavity lengths can be tuned as long as the other cavity length maintains the double-resonance condition. In the experimental set-up, there was no convenient method for scanning accurately the frequency of the pump laser. Therefore, the second tuning method, as outlined above, became the only option to generate smooth frequency tuning from the dual-cavity OPO.

VI. 4 Results and discussion.

The reflectivity of the cavity components for the input pump wave were used again to assist the optical alignment of the two OPO cavities. First, the pump field was resonated appropriately in the idler cavity of the OPO. This ensured that the idler frequency cavity was aligned perfectly. Second, the signal frequency cavity was aligned from a weak interference pattern resulting from the residual reflections from the Brewster-plate for the counter propagating waves of the resonant pump field.

The dual-cavity OPO was operated with a minimum pump power threshold of $P_p^{th} \approx 200$ mW. Therefore, the additional losses experienced by the OPO intra-cavity fields did not affect significantly the threshold of the OPO. The increase in the pump power threshold over the single-cavity OPO corresponded to an increase in the product of the round-trip cavity power losses of $\approx 30\%$, assuming identical mode-matching in the single- and dual-cavity resonators. The product of the losses is considered above, since it was not possible to evaluate precisely the individual increases in the parasitic losses due to the separate signal and idler fields. More importantly, this particular power level (≈ 200 mW) implied that the OPO could be operated reliably and consistently at levels of two to three times above pump power threshold, when using the argon-ion laser as the pump source. Therefore, the frequency tuning properties could be examined adequately from this dual-cavity resonator design.

Before attempting to provide smooth frequency tuning, it was essential to ensure that the cavity stability was of an acceptable standard. The cavity arrangement for locking the dual-cavity OPO is shown schematically in figure VI. 2.

All three cavity mirrors were mounted so as to have piezo-electric control. Although, in principle, fine adjustment should only be required on one of the independent cavity arms, it was found highly advantageous to have more freedom to allow for smooth frequency tuning in this dual-cavity arrangement. One of the drawbacks of this dual-cavity resonator was the dependence of the pump frequency resonance condition to the idler frequency cavity length. Therefore, the piezo-electric control of the idler cavity length was used to ensure that the OPO operated near to exact pump field resonance, ensuring sufficient pump field radiation within the cavity to overcome threshold. Manual control of the voltage level to the piezo-electric element that controlled the position of the idler cavity mirror, brought the pump field near resonance. Thereafter, the voltage level to the signal cavity was fine-tuned to achieve a near-coincidence of signal and idler resonances, and so attain oscillation.

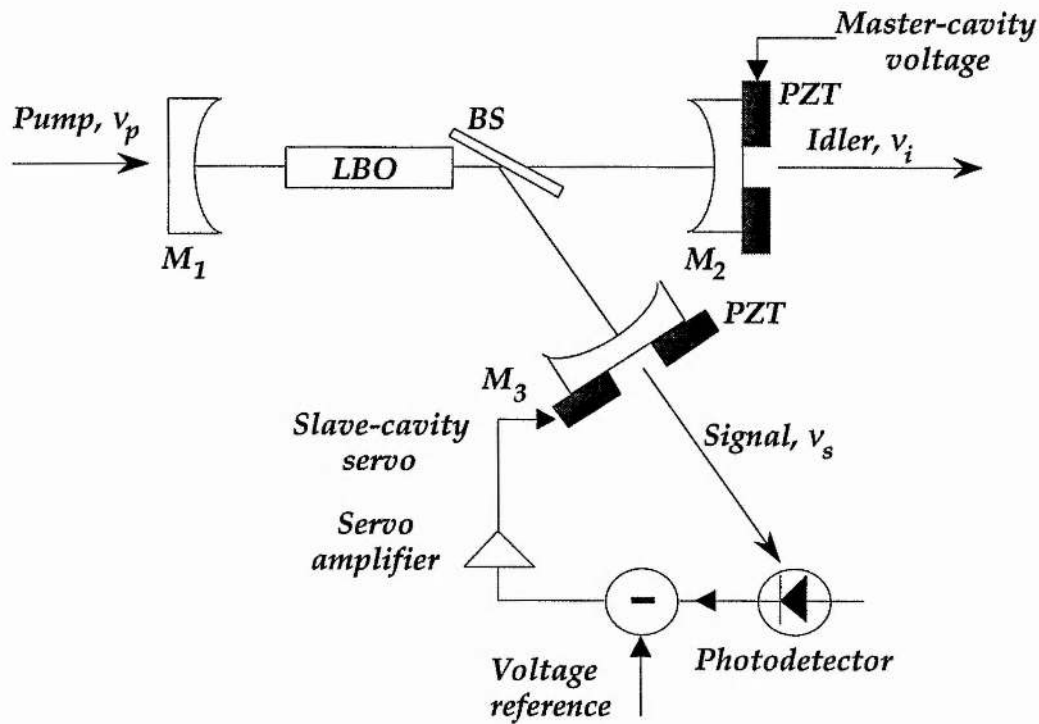


Figure VI. 2.

Schematic representation of the dual-cavity resonator design, illustrating the independent cavity length control and the feedback servo-loop used to provide smooth frequency tuning.

Without further manual control of the voltage levels, the OPO would either switch off, or hop to a different mode-pair, provided that the pump power was sufficient to maintain threshold. The free-running intensity variations of the OPO output are shown in figure VI. 3, for a time period of $\Delta t \approx 50$ seconds. The mode-hops were a consequence of the long-term frequency drift in the pump source, from thermal expansion effects of the OPO mounts causing cavity length drifts, and from mK variations in the temperature of the nonlinear crystal. Free-running, single-frequency operation was provided for time periods of up to $\Delta t \approx 20$ seconds. The intensity is shown to vary as the OPO hops from one mode-pair to another. Eventually, the cavity length / pump frequency has changed to such a degree that insufficient pump radiation can be coupled into the cavity to reach threshold.

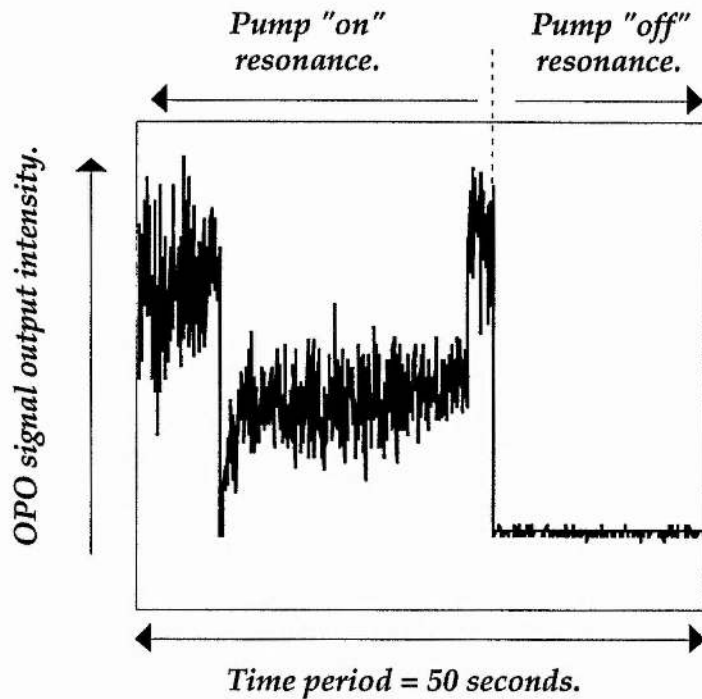


Figure VI. 3.

Free running intensity fluctuations from the dual-cavity OPO, illustrating the effects of the partial pump field resonance within the idler frequency cavity. While the pump field within the resonator is sufficient to overcome threshold, the OPO hops between different signal and idler frequency mode-pairs.

One of the outputs of the dual-cavity resonator (in this case the signal frequency) was monitored externally on an ultra-stable, low-expansion, scanning confocal interferometer of free spectral range $FSR_{int} = 2$ GHz. A trace illustrating free-running, single-frequency, operation is shown in figure VI. 4.

At this level of passive stability within the dual-cavity resonator, with fixed frequency single mode-pairs remaining on resonance for time periods of $\Delta t \approx 10$ s seconds, the servo-control feedback could be applied easily to provide amplitude-stable, smooth frequency tuning from the OPO.

The method employed for the servo-locking is displayed in the resonator design, as illustrated by figure VI. 2. When the pump field operated near pump resonance, and the signal and idler fields were adjusted to fulfil the condition of simultaneous resonance, the intensity of the output signal

field was monitored on a photo-diode. The level of the photo-diode was compared to a reference voltage, and the difference voltage was taken to form the error-signal. This error-signal was then integrated and fed through a high-voltage amplifier to the piezo-electric element that controlled the length of the signal cavity. This method provided amplitude-stable operation of individual signal and idler frequency mode-pairs.

As discussed in the previous section, to generate smooth frequency tuning, two frequency (cavity length) parameters must be adjusted simultaneously. Given the fixed frequency pump source, these two parameters were the two different cavity lengths / frequencies of the dual-cavity resonator. By manually adjusting the voltage level to the piezo-electric elements that controlled the length of the idler cavity, and relying upon the signal cavity servo-loop to maintain the double-resonance condition, smooth frequency tuning was provided by the dual-cavity OPO. Through this method, up to $\Delta\nu_s \approx 0.4$ GHz tuning from the signal frequency was measured consistently by observing the frequency shift of the single-frequency trace on the stable monitoring interferometer.

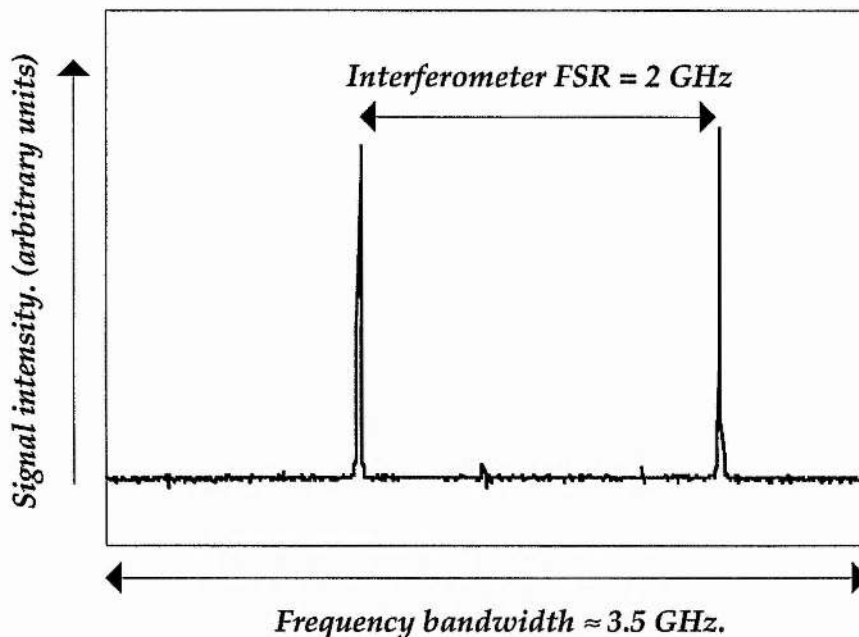


Figure VI. 4.

Free-running, signal wave, single-frequency operation, as monitored on a scanning interferometer of free spectral range $FSR_{int} = 2$ GHz. Single-frequency mode-pairs were observed for $\Delta t \approx 10$ s seconds.

Although accurate and stable diagnostics were used to monitor only the tuning of the signal frequency, it is reasonable to infer that this level of tuning was provided also by the idler frequency. This is because the scanning method used was restricted to time periods of $\Delta t \approx 10$ seconds, over which the pump frequency drift was measured to be $\Delta \nu_p \approx 20$ MHz, and the cavity-length expansion of the monitoring external etalon was considered negligible. Therefore, the range of idler frequency tuning was calculated simply from the conservation of energy relation when using a fixed frequency pump source.

The range of smooth frequency tuning of the signal and idler fields was restricted by the effects of the weak pump field resonance within the idler frequency branch of the dual-cavity resonator. The smooth tuning method outlined above involved changing initially the optical length of the idler frequency. However, in addition to altering the resonant frequency of the idler wave, the resonance condition of the pump field is affected simultaneously. The idler cavity length could only be tuned so long as the pump field was maintained near pump field resonance.

It was shown in chapter V that the pump field was sufficient to overcome OPO threshold for cavity length detunings of the order of $\Delta L_i \approx 60$ nm. This value was taken as the equivalent idler frequency detuning allowed in the dual-cavity OPO before insufficient pump power was coupled into the resonator. Therefore, this figure was used to calculate the change in the idler frequency permitted from manual tuning. The idler frequency cavity length was measured to be $L_i \approx 35$ mm. Therefore, the free spectral range of the idler frequency cavity was $FSR_i \approx 3.5$ GHz. When the idler frequency cavity length was detuned through $\Delta L_i \approx 60$ nm, the resonant frequency alters by $\Delta \nu_i \approx 0.3$ GHz, in good agreement with the values measured in practise.

The level of smooth frequency tuning from a dual-cavity oscillator, with the pump field resonant within the idler frequency cavity was derived in chapter II as follows:

$$|\Delta \nu_{s-max}| = |\Delta \nu_{i-max}| \approx \frac{FSR_i}{F_p} \frac{\nu_s}{\nu_p}, \quad [VI. 2]$$

and this implies smooth frequency tuning of $\Delta \nu_{s,i} \approx 0.2$ GHz. Again, this value is in good agreement with the experimental observation.

Effects of pump field resonance when using a fixed frequency pump source have been shown to be a limiting factor on the allowable smooth frequency tuning from a dual-cavity OPO. To open up the possibility of greater levels of smooth frequency tuning, it would be necessary to remove this constraint completely. There are several different methods that could be used to obtain this, while maintaining high finesse signal and idler frequencies and low pump power thresholds. One such method involves taking advantage of the reduced coating specifications of independent signal and idler frequency cavities. Consider the proposed four mirror OPO cavity design, as shown in figure VI. 5.

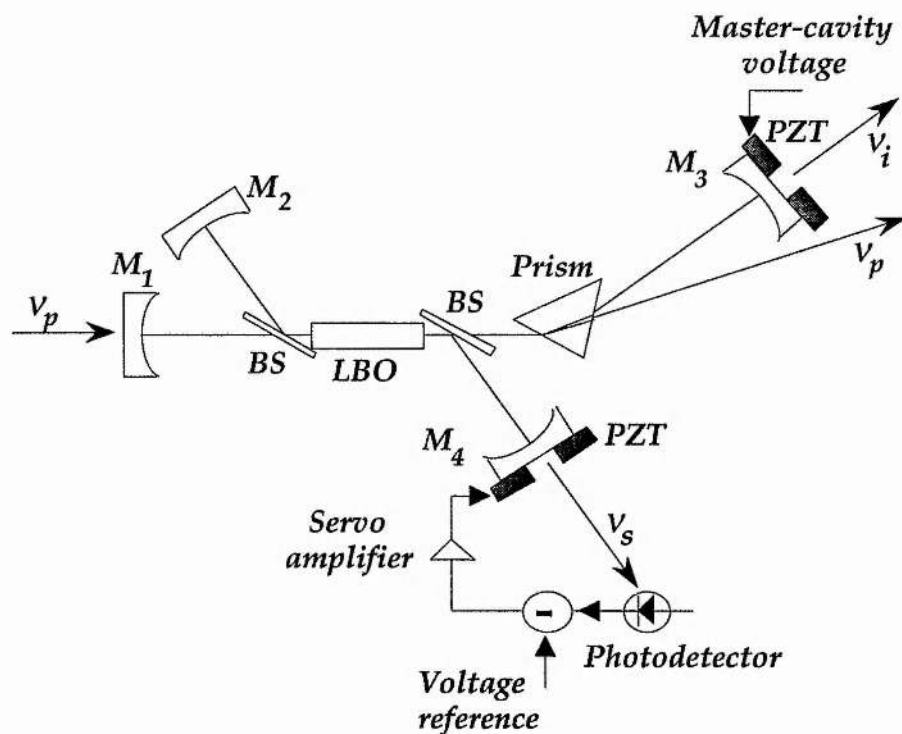


Figure VI. 5.
Proposed schematic representation of an ideal dual-cavity OPO resonator, with reduced coating requirements for the pump, signal and idler frequencies. Pump resonance effects, which are impossible to avoid completely in linear cavity designs, are eliminated in this arrangement.

Within this resonator, the two intra-cavity beam-splitters could separate totally the signal and idler fields. The signal field could be brought to resonance between the cavity mirrors M_2 and M_4 . The idler frequency could be brought to resonance between mirrors M_1 and M_3 . Therefore, separate dielectric reflectivity profiles could be deposited on mirror substrates for the signal and idler frequencies. In addition, the effects of pump field resonance could be eliminated completely by decoupling efficiently the pump wave by use of an intra-cavity prism. It could be expected that the prism would contribute negligible loss for the idler frequency. The only constraint on the OPO mirrors for the pump field would be that the input mirror M_1 is highly-transmitting at the pump frequency. If this additional constraint is problematic, then the pump field could be coupled into the OPO resonator through the use of a second intra-cavity prism. If this dual-cavity resonator could be constructed, then smooth tuning should be possible over ranges that could approach theoretically the entire phase-matching bandwidth. In practise, the smooth frequency tuning would be limited by the allowable cavity length translation from piezo-electric stacks controlling the length of the cavity mirrors. However, if the crystal temperature is controlled with sufficient accuracy, then this could be used in conjunction with cavity length control for increased levels of frequency tuning.

VI.4 Conclusions.

In this chapter, the dual-cavity, doubly-resonant cw OPO has been analysed theoretically and investigated experimentally. The type II phase-matching geometry in LBO, when pumped in the ultra-violet spectral region, combined with widely spaced, non-degenerate signal and idler frequencies, has allowed for the efficient intra-cavity separation of the signal and idler fields. By inserting a beam-splitter into the cavity, and adding a third cavity mirror, the pump power threshold was maintained at a level that allowed for reliable and consistent operation at levels of two to three times above the pump power threshold of $P_p^{th} \approx 200$ mW.

A high degree of passive stability of the dual-cavity OPO was provided by taking great care to isolate the resonator from acoustic and mechanical vibrations in the laboratory environment. This led to the free-running operation of single signal and idler frequency mode-pairs over time periods of $\Delta t \approx 10$ s seconds. At this level, the servo-control electronics were effective in

producing smooth frequency tuning of the signal and idler frequency mode-pairs. By manually adjusting the precise length of the idler frequency cavity, the signal frequency cavity length was locked to maintain double-resonance over tuning ranges of $\Delta\nu_s \approx \Delta\nu_i \approx 0.4$ GHz.

The smooth tuning range of this dual-cavity OPO was shown to be limited by the effects of the pump field resonance within the idler frequency cavity. The level of smooth frequency tuning was shown to be in good agreement with the modelling presented. Further levels of smooth frequency tuning were discussed that involved the elimination of pump resonance effects within the OPO cavity.

The dual-cavity, doubly-resonant OPO will find use in methods of optical frequency division that require smooth frequency tuning ranges at the GHz-level [20, 21]. In addition, the reduced coating requirements will be highly advantageous in frequency division methods that involve integral ratios of the pump, signal and idler frequencies, and the subsequent difficulties of maintaining high coating specifications at all three frequencies.

Following the publications that described this experiment [17 - 19], subsequent demonstrations of dual-cavity resonators have been provided by other groups [22, 23]. Once again, type II phase-matching provided for spatial frequency separation of the resonant fields. However, in these cases, the nonlinear material used for the OPOs was type II phase-matched KTP, and the pump sources were a frequency-stable krypton-ion laser operating in the green spectral region [22], case (a), and a Ti:sapphire laser operating in the near infra-red spectral region [13], case (b).

These cavity designs were extensions of single-cavity resonators, in which the effects of pump field resonance have already been shown to be negligible [24]. The experimental layouts are illustrated in figure VI. 6.

In case (a), illustrated in figure IV. 6 (a), the signal and idler fields are split in a manner similar to the LBO dual-cavity OPO of this chapter. However, all of the cavity mirrors were nominally highly-transmitting at the pump frequency, allowing for single-pass pump field interaction. This implied that the OPO could oscillate for all cavity length positions, so long as the double-resonance condition was maintained. Smooth frequency tuning was displayed over $\Delta\nu_s \approx \Delta\nu_i \approx 0.9$ GHz. The limit to smooth frequency tuning was attributed to the effects of weak pump resonance of the pump

field, which caused a dephasing of the pump frequency with respect to the signal and idler frequencies. Again, this points towards complete non-resonance of the pump field, and the prism coupling method proposed in figure VI. 5.

The realization of the dual-cavity oscillator has prompted considerable interest in cw OPOs, for both scientific [16] and commercial applications. One of the remaining challenges is the formation of a dual-cavity cw OPO, within type I phase-matched geometries. This is likely to incorporate prism separation of the two parallel-polarized resonant fields of the OPO. When such an experiment has been demonstrated, cw OPOs will be in a position to provide smooth frequency tuning over GHz-levels, and coarse frequency tuning over hundreds of THz.

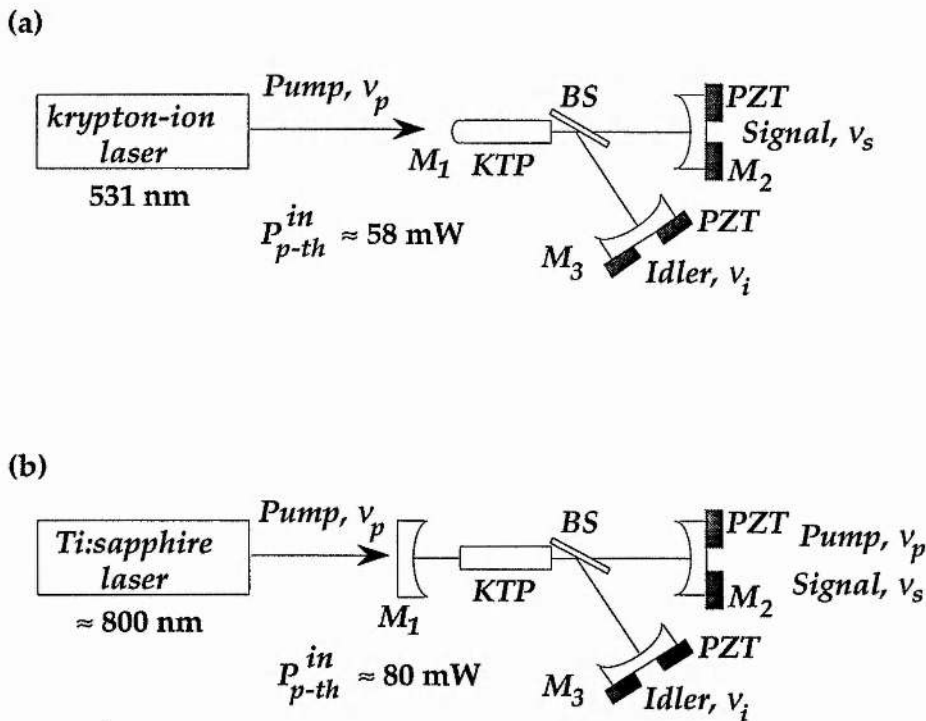


Figure IV. 6. Schematic representations of the subsequent experimental demonstrations of the dual-cavity resonators (from references [22] and [23], for cases (a) and (b), respectively). The approach adopted in case (a) is similar to the dual-cavity OPO, discussed in this chapter. In case (b), the pump field is resonated strongly within one of the cavities.

Finally, it is revealing to compare these dual-cavity OPOs to the recent singly-resonant oscillator, as described in reference [25]. The only cw singly-resonant oscillator constructed to date has operated with a pump power threshold at the multi-Watt level, and has provided smooth frequency tuning of the OPO outputs over a few hundred MHz [25]. The most attractive property of a cw singly-resonant oscillator is the high conversion efficiency that can be provided for the non-resonant OPO frequency, with the possibility of multi-Watt, free-running, tunable radiation. As cw pump sources become available with output powers of tens of Watts, and nonlinear materials are developed that can combine the properties of high damage thresholds with high effective nonlinear coefficients, cw singly-resonant oscillators will provide an attractive means of high power, high spectral quality radiation. Within the context of cw OPOs, such radiation may allow for serial OPO configurations, in which the output of one OPO is used as the pump source for further OPO stages. This will hasten the realization of referencable frequency chains over considerable spectral bandwidths [21].

References.

1. F. G. Colville, A. J. Henderson, M. J. Padgett, J. Zhang, & M. H. Dunn, "Continuous-wave parametric oscillation in lithium triborate," *Opt. Lett.* **18**, 205 (1993).
2. F. G. Colville, M. J. Padgett, A. J. Henderson, J. Zhang, & M. H. Dunn, "Continuous-wave parametric oscillator pumped in the ultra-violet," *Opt. Lett.* **18**, 1065 (1993).
3. A. G. Fox,
US Patent 3504299.
4. P. W. Smith,
"Stabilized, single-frequency output from a long laser cavity,"
IEEE J. Quant. Electron. QE-1, 343 (1965).
"On the stabilization of a high-power single-frequency laser,"
IEEE J. Quant. Electron. QE-2, 666 (1966).
5. C. J. Johnson,
"Stabilization of a composite-cavity single-frequency laser,"
IEEE J. Quant. Electron. QE-4, 699 (1968).
W. W. Rigrod,
"Selectivity of open-ended interferometric resonators,"
IEEE J. Quant. Electron. QE-6, 9 (1970).
6. J. Salzman, J. S. Osinski, R. Bhat, K. Cummings, & L. Harriot,
"Cross coupled cavity semiconductor laser,"
Appl. Phys. Lett. **52**, 767 (1988).
7. I. H. Mitchell & C. B. Wheeler,
"The coupled-cavity laser interferometer with rationally related cavity lengths,"
J. Phys. E. Sci. Instrum. **21**, 696 (1988).

8. K. Y. Liou, C. A. Burrus, & F. Bosch,
"Graded-index-rod external coupled-cavity laser with backface output-monitor-stabilized single-frequency operation,"
J. Lightwave Tech. **3**, 985 (1985).
9. R. L. Byer, R. L. Herbst, & R. N. Fleming,
"A broadly tunable IR source,"
in "Laser Spectroscopy" (S. Haroche, J. C. Pebay-Peyroula, T. W. Hansch, & S. E. Harris, Eds.), Springer-Verlag, Berlin, 207 (1975).
10. J. Pinard & J. F. Young,
"Interferometric stabilization of an optical parametric oscillator,"
Opt. Comm. **4**, 425 (1972).
11. R. G. Smith, J. E. Geusic, H. J. Levinstein, J. J. Rubin, S. Singh, & L. G. Van Uitert,
"Continuous optical parametric oscillation in $Ba_2NaNb_5O_{15}$,"
Appl. Phys. Lett. **12**, 308 (1968).
12. R. L. Byer, M. K. Oshman, J. F. Young, & S. E. Harris,
"Visible cw parametric oscillator,"
Appl. Phys. Lett. **13**, 109 (1968).
13. G. D. Boyd & A. Ashkin,
"Theory of parametric oscillator threshold with single-mode optical masers and observation of amplification in $LiNbO_3$,"
Phys. Rev. **146**, 187 (1966).
14. J. Falk,
"Instabilities in the doubly resonant parametric oscillator: a theoretical analysis,"
IEEE J. Quant. Electron. **QE-7**, 230 (1971).
15. R. C. Eckardt, C. D. Nabors, W. J. Kozlovsky, & R. L. Byer,
"Optical parametric oscillator frequency tuning and control,"
J. Opt. Soc. Am. B **8**, 648 (1991).
16. N. C. Wong,
"Gravity-wave detection via an optical parametric oscillator,"
Phys. Rev. A **45**, 3176 (1992).
17. F. G. Colville, M. J. Padgett, & M. H. Dunn,
"Continuous-wave, dual-cavity, doubly-resonant, optical parametric oscillator,"
Appl. Phys. Lett. **64**, 1490 (1994).
F. G. Colville, M. H. Dunn, P. Gill, M. J. Padgett, & W. Sibbett,
International patent application no. 9309031.4,
filed with the British Technology Group Ltd. 1994.
18. F. G. Colville, M. J. Padgett, & M. H. Dunn,
"Continuous-wave, dual-cavity, doubly-resonant, optical parametric oscillator,"
in *Digest of Topical Meeting on Advanced Solid-State Lasers*, paper AWA3 (1994).
19. F. G. Colville, M. J. Padgett, & M. H. Dunn,
"Smooth frequency tuning from optical parametric oscillators: the transition from single- to dual-cavity oscillators,"
in *Proceedings of Topical Meeting on Advanced Solid-State Lasers*, (1994).
20. N. C. Wong,
"Optical frequency division using an optical parametric oscillator,"
Opt. Lett. **15**, 1129 (1990).
21. N. C. Wong,
"Optical frequency counting from the UV to the near IR,"
Opt. Lett. **17**, 1155 (1992).
22. D. Lee & N. C. Wong,
"Tuning characteristics of a cw dual-cavity KTP optical parametric oscillator,"
in *Conference on Lasers and Electro-Optics*, Vol. 8 of OSA 1994 Technical Digest Series (Optical Society of America, Washington, D. C., 1994), paper CWE 5.

23. R. Knappe, J. Barschke, C. Becher, B. Beier, M. Scheidt, K.-J. Boller, & R. Wallenstein,
"Injection-locked high power diode arrays and their application as pump sources for blue and green Nd:YAB lasers, monolithic Nd:YAG ring lasers, and cw KTP optical parametric oscillators,"
in *Conference on Lasers and Electro-Optics*, Vol. 8 of OSA 1994 Technical Digest Series (Optical Society of America, Washington, D. C., 1994), paper CThL 4.
24. D. Lee & N. C. Wong,
"Stabilization and tuning of a doubly-resonant optical parametric oscillator,"
J. Opt. Soc. Am. B **10**, 1659 (1993).
25. S. T. Yang, R. C. Eckardt, & R. L. Byer,
"Continuous-wave singly resonant optical parametric oscillator pumped by a single-frequency resonantly doubled Nd:YAG laser,"
Opt. Lett. **18**, 971 (1993).
"1.9-W cw ring-cavity KTP singly resonant optical parametric oscillator,"
Opt. Lett. **19**, 475 (1994).

Chapter VII.

Multiple Parameter Tuning through use of a Frequency-Tunable Titanium:Sapphire Laser.

Contents.	Page.	
VII. 1	Introduction.	273
VII. 2	Widely tunable, single-frequency pump source.	278
VII. 3	Optical parametric oscillator design.	280
VII. 4	Pump frequency and cavity length requirements.	284
VII. 5	Experimental arrangement.	287
VII. 6	Results and discussion.	288
VII. 7	Conclusions.	290
	References.	293

VII. 1 Introduction.

The three previous chapters have been concerned with the operation of cw OPOs which have used, as the sources of input pump frequency, lasers whose ranges of operating frequencies were severely limited by the narrow gain-bandwidth associated with specific lasing transitions in these lasers [1 - 3]. For the two argon-ion laser transitions used, the frequency bandwidths over which the power output from the lasers remain within approximately 50 % of that available at line-centre are $\Delta\nu_{g-b} \approx 3$ GHz and $\Delta\nu_{g-b} \approx 1$ GHz, for the lasing transitions at $\nu_p = 583$ THz (514.5 nm) and $\nu_p = 824$ THz (363.8 nm), respectively [4, 5]. The result of this was that the sum of the OPO output frequencies was confined to this limited pump frequency bandwidth. Therefore, the OPOs could generate only specific signal and idler frequency mode-pairs that were defined by the near-fixed pump frequencies. In these cases, the only free parameter in the down-conversion process was the frequency difference between the signal and idler frequencies (as defined by the phase-matching temperatures of the nonlinear materials). Moreover, all demonstrations of cw OPOs, prior to this experiment, had used fixed-frequency sources of input radiation [6].

One method of increasing substantially the range of signal and idler frequencies covered is to use a source of pump frequency that can be selected from over wider frequency bandwidths. To achieve this, different sources of pump frequency must be employed other than gas lasers [1, 3, 7 - 8] (or diode-laser-pumped solid-state Nd-based lasers and their frequency-harmonics [9, 10]). Pump frequency tuning allows for freedom in selecting the sum frequency of the signal and idler frequencies. Therefore, in this case, the OPO based system has two independent tuning parameters: the sum and difference frequencies of the down-converted signal and idler frequencies [11].

Such increased pump frequency bandwidths are available from so-called tunable laser sources. Tunable pump lasers were a main concern of chapter III, and a variety of pump sources were outlined that could operate in different spectral regions. To summarize these findings, only three sources can be considered at the moment. These are dye lasers, vibronic solid-state laser gain media, and single-frequency, narrow-linewidth semiconductor diode lasers.

Despite the capability of generating high power and narrow-linewidth single-frequency radiation, dye lasers have never been applied as the pump sources for cw OPOs. However, their widespread availability has been utilized effectively when used as pump sources for OPOs operating in the pulsed mode [12 - 14]. Through this method, the advantages of combining pump frequency tuning with OPO frequency tuning have been demonstrated. With the current emphasis being shifted in the research front away from the use of dye lasers in the laboratory, it is unlikely that they will find a use in the future as pump sources for cw OPOs, although in principle they still offer a viable source of pump frequency radiation for many laboratory-based experiments, where the main concern is to investigate the properties of the OPO cavity rather than the characteristics of the pump source.

The emergence of vibronic laser gain media in the past decade [15], and in particular the widespread use of titanium doped sapphire (Ti:sapphire) lasers [16 - 18], on both the research and commercial fronts, has made them an ideal choice of pump laser for the next generation of cw OPOs. The solid-state lasing medium, and the ability of these lasers to be pumped directly by solid-state laser sources, either from frequency-doubled diode laser pumped Nd-based lasers [19] or directly from diode lasers, has allowed for frequency-stable devices that are compact, portable, efficient, and relatively easy to operate.

The frequency coverage of these lasers extends over a wide bandwidth in the visible and near infra-red spectral regions, and this can allow for OPO down-conversion throughout the near infra-red spectral region, and within detectable frequency bandwidths of stable infra-red frequency standards.

In the longer term, it is likely that phase-locked diode-laser arrays, operating with high power and frequency-stable narrow-linewidth radiation, will find an application as the pump source for cw OPOs [20]. The inherently compact design, and the capability for scaling up the power levels available [21], make this choice of widely tunable radiation an excellent pump source for OPOs to down-convert visible radiation to regions where diode-lasers are currently unavailable. Whereas, at present, diode-lasers appear to be the preferred source of frequency-tunable cw radiation for frequencies greater than $\nu \approx 150$ THz, lower frequencies derived from diode lasers could be provided by OPO down-conversion techniques.

This chapter describes the use of a widely tunable single-frequency pump source, operating in the near infra-red spectral region, that was used to pump a cw lithium triborate (LBO) OPO [22]. The source of pump frequency was a Ti:sapphire laser, that was pumped by an argon-ion laser, configured to deliver multi-line pumping radiation. The precise pump frequency of the free-running Ti:sapphire laser was found to display a short-term frequency jitter / linewidth of $\Delta\nu_{p-stab} \approx \pm 15$ MHz. The exact pump frequency for the OPO could be chosen coarsely from a frequency bandwidth ranging from $\nu_p \approx 370$ to 385 THz, and corresponding to free-space pump wavelengths from $\lambda_p \approx 810$ to 780 nm, respectively.

The LBO OPO was chosen to operate under the conditions of type I non-critical phase-matching, with the signal and idler frequencies temperature-tunable around the point of frequency-degeneracy (i.e. similar to the phase-matching geometry in chapter IV). The OPO was tuned coarsely over a total frequency bandwidth of $\Delta\nu = \Delta\nu_s + \Delta\nu_i \approx 24$ THz, centred at a frequency of $\nu_s \approx \nu_i \approx 188$ THz, and corresponding to a wavelength of $\lambda_s \approx \lambda_i \approx 1.6$ μm .

In section VII. 2, there is a description of the argon-ion laser pumped Ti:sapphire laser which was used as the pump source for the cw OPO. The argon-ion laser operated with multi-line, multi-mode output, covering several lasing transition lines between $\nu \approx 560$ and 650 THz, with the majority of the power concentrated on the high-gain transition lines at

$\nu \approx 615$ THz (488 nm) and 583 THz (514.5 nm) [23]. The Ti:sapphire laser was a commercial design, configured as a travelling-wave, ring-cavity geometry, with single-frequency output powers in excess of $P_p \approx 1$ W [24]. The output of the Ti:sapphire laser could be tuned coarsely, while maintaining single-frequency output power at the Watt-level, between $\nu_p \approx 350$ and 400 THz, corresponding to free-space pump wavelengths between $\lambda_p \approx 750$ and 850 nm, respectively. The Ti:sapphire laser operated free-running and without any active stabilization, and had a measured short-term frequency jitter (FWHM) of $\Delta\nu_{p-stab} \approx \pm 15$ MHz.

The design of the OPO resonator is described in section VII. 3. The nonlinear crystal chosen for the OPO was LBO, cut for propagation along the x -principal optical axis, to satisfy type I non-critical phase-matching. The crystal was placed at the intra-cavity focus of a near concentric resonator, and heated to the desired phase-matching temperatures of $T_{xtal} \approx 130$ to 180 °C. The two OPO mirrors that formed the standing-wave, linear resonator were coated to be highly-reflecting over the spectral region between $\nu \approx 200$ THz (1.5 μm) and 175 THz (1.7 μm), with a centre frequency of $\nu \approx 187$ THz (1.6 μm), and anti-reflecting for pump frequencies between $\nu_p \approx 390$ THz (770 nm) and 360 THz (830 nm). The faces of the plane-parallel polished nonlinear crystal were coated to be anti-reflecting at both the pump frequency and the OPO outputs near the frequency-degeneracy point. Therefore, the single-cavity, doubly-resonant OPO formed a high finesse cavity for the resonant signal and idler frequencies, while allowing for single-pass, near-non-resonant, pump field interaction within the gain medium.

The OPO operated under the conditions of type I non-critical phase-matching, and with signal and idler frequencies near to frequency-degeneracy. This phase-matching geometry was analysed in chapter IV, where the pump source was the argon-ion laser operating at a frequency of $\nu_p = 583$ THz (514.5 nm). Since the Ti:sapphire laser operated free-running with a short-term frequency jitter of the same magnitude as the argon-ion laser, the expected mode properties of the OPO are similar to those, as outlined in chapter IV. Stable OPO operation would have required a pump frequency stability of $\Delta\nu_{p-stab} \leq 0.48$ MHz, and an OPO cavity length stability of $\Delta L \leq 25$ pm, to maintain operation on a single signal and idler frequency mode-pair. The requirements for stable OPO operation from an OPO that uses LBO as the nonlinear gain medium and a Ti:sapphire laser as the source of pump frequency, are analysed fully in section VII. 4.

The experimental arrangement is described in section VII. 5. The pump source was isolated from the single-cavity, standing-wave, linear OPO resonator by the use of a *Faraday* isolator that provided greater than ≈ 30 dB attenuation. This ensured free-running operation of the Ti:sapphire laser, and eliminated feedback of pump radiation from the OPO cavity into the counter-propagating direction of the Ti:sapphire ring laser. A single focusing lens of focal length $f = 88.5$ mm was used to mode-match the pump radiation into the OPO cavity. The output of the Ti:sapphire pump source was focused to a spot size of $W_{p,OPO} \approx 40 \mu\text{m}$ ($1/e$ electric-field radius), at the centre of the OPO gain medium, to satisfy the conditions of confocal focusing.

The experimental results from the Ti:sapphire pumped OPO are presented in section VII. 6. The single-pass, doubly-resonant OPO operated with a minimum pump power threshold of $P_p^{th} \approx 360$ mW. When operating at pump power levels of two times above threshold, pump depletions of $\approx 40\%$ and external conversion efficiencies of $\eta_{ext} \approx 4\%$, were measured. Since the stability requirements of the pump laser were outwith the minimum level for stable OPO operation, the fine frequency tuning properties of the OPO were not examined. However, the extensive coarse frequency tuning of the OPO was investigated by varying the precise frequency of the pump source, and adjusting the phase-matching temperature of the LBO crystal to achieve a wide range of signal and idler output frequencies. By varying the frequency of the pump source between $\nu_p \approx 385$ THz (780 nm) and 370 THz (810 nm), the OPO could be tuned coarsely over a frequency bandwidth of $\Delta\nu = \Delta\nu_s + \Delta\nu_i \approx 24$ THz, corresponding to signal and idler frequencies between $\nu \approx 201$ THz (1.49 μm) and 175 THz (1.71 μm). The range of the OPO outputs was limited primarily by the bandwidth of the optical coatings within the OPO cavity, and to a lesser extent, by the reduced pump powers available when operating outwith the range of pump frequencies, as stated above.

Finally, the conclusions of this chapter are outlined in section VII. 7. In particular, the applications of the Ti:sapphire laser for use within low threshold, frequency-stable cw OPOs, is discussed in detail. Improvements in the linewidth of the pump source are considered with respect to using LBO in the type I phase-matched geometry. More generally, the use of other nonlinear crystals in type II phase-matched geometries with such a frequency tunable pump source, is addressed [11, 20, 25].

VII. 2 Widely tunable single-frequency pump source.

This section describes the operating characteristics of the pump source for the cw LBO OPO. The Ti:sapphire laser was optically pumped by multi-line radiation from the large-frame argon-ion laser [23] that was used directly as the pump source for the cw OPOs that were discussed in chapters IV to VI of this thesis.

The argon-ion laser was configured as a linear, two-mirror, standing-wave cavity, with no intra-cavity frequency-selective elements. The cavity mirrors were highly-reflecting over a wide frequency bandwidth ($\Delta\lambda \approx 70$ nm) that encompassed several lasing transitions between $\lambda \approx 460$ to 530 nm. Therefore, the output of the argon-ion laser consisted of multi-mode and multi-line radiation in a diffraction-limited TEM₀₀, lowest order Gaussian beam. The power output was restricted to a maximum of $P_p \approx 10$ W for this experiment, although multi-line powers in excess of $P_p \approx 20$ W were available from the laser.

The Ti:sapphire laser was a modified, commercially-available product manufactured by *Schwartz Electro-Optics (Titan CW-Series)* [24, 25]. The pumping arrangement and cavity geometry are illustrated in figure VII. 1. The four-mirror, figure-eight, cavity included a Brewster-cut gain element, a multi-plate birefringent filter for broad (coarse) tuning, an optical diode to ensure unidirectional oscillation, and an etalon to maintain single-frequency operation at high power levels. The fold angle common to the two crossing legs of the resonator was designed for astigmatic compensation. The laser was longitudinally pumped by the cw argon-ion laser that was linearly polarized in the plane of the cavity. The half-waveplate was used to achieve the desired orientation of the pump polarization.

The Ti:sapphire laser resonator included 100 mm radius-of-curvature mirrors surrounding the 7.45 mm Ti:sapphire crystal, forming a spot size at the centre of the crystal of $W_{p,laser} \approx 25$ μm . (This crystal length matches the confocal parameter of the cavity.) For an input pump power from the argon-ion laser of $P_p \approx 10$ W, the Ti:sapphire laser delivered single-frequency output powers in excess of $P_p^{in} \approx 1$ W over the spectral region from $\nu_p \approx 390$ THz (770 nm) to 361 THz (830 nm).

Single-frequency operation of the Ti:sapphire laser was monitored by an external scanning confocal interferometer of free spectral range

$FSR_{int} \approx 5$ GHz, as displayed in figure VII. 2. In addition, this stable etalon was used to estimate the short-term frequency jitter, by evaluating the intensity variations of the transmitted pump field through the etalon. In this manner, the short-term, free-running, frequency jitter was estimated to be $\Delta\nu_{p-stab} \approx \pm 15$ MHz. This was attributed to mechanical and acoustic induced effects on the intra-cavity components (in particular the four cavity mirrors). These effects were reduced to a level of $\Delta\nu_{p-stab} \approx \pm 5$ MHz, by enclosing the laser cavity within a lead / foam / lead arrangement.

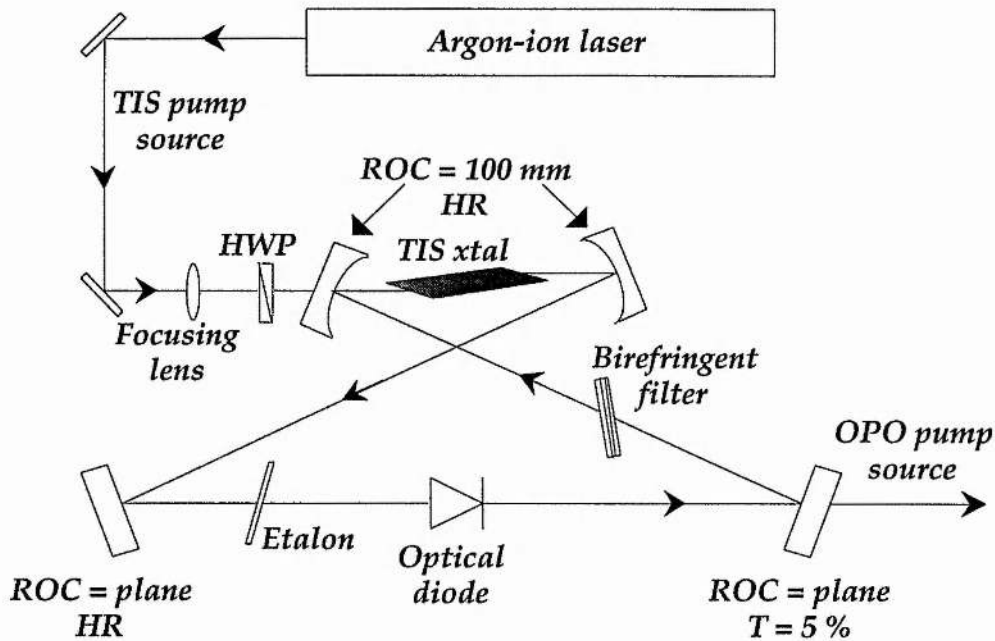


Figure VII. 1.

Schematic representation of the argon-ion laser pumped Ti:sapphire laser, used as the pump source for the cw OPO. The Ti:sapphire laser was configured as a travelling-wave, ring cavity oscillator, with single-frequency output powers at the Watt-level. TIS: Ti:sapphire; ROC: radius of curvature; HR: high-reflector; HWP: half-waveplate (for argon-ion radiation).

Given the phase-matching geometry that had been selected for the OPO arrangement (i.e. type I phase-matching near frequency-degeneracy), it was decided to proceed no further with the frequency stability of the Ti:sapphire laser. To obtain the desired stability at sub-100 kHz, active stabilization

schemes would have been required, in addition to a complete re-construction of the Ti:sapphire resonator design. While this was not adopted, it is worthwhile recalling that other commercially-available Ti:sapphire lasers can deliver single-frequency radiation with linewidths of sub-50 kHz [27], and that a number of frequency-stable Ti:sapphire lasers have been reported [16 - 18], as expected from a solid-state laser gain medium.

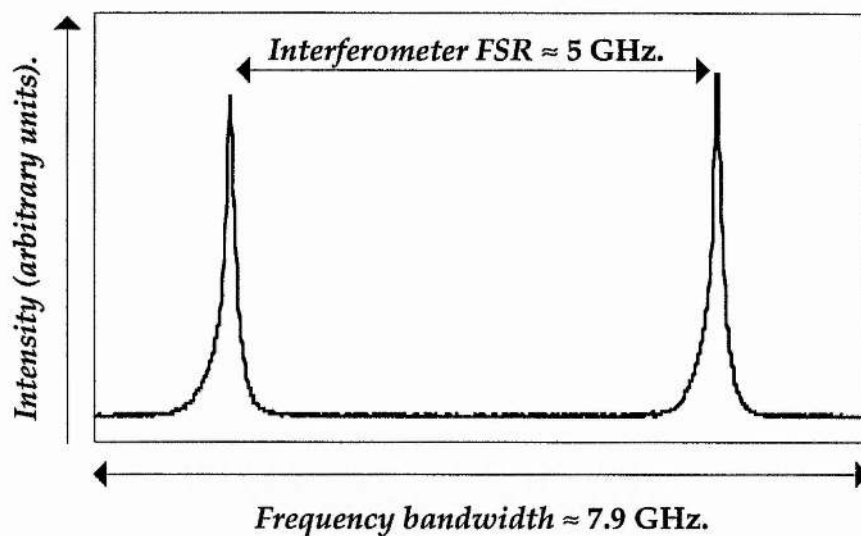


Figure VII. 2.

Single-frequency operation of the argon-ion pumped Ti:sapphire laser, used as the pump source for the LBO OPO, and monitored on a scanning confocal interferometer of free spectral range $FSR_{int} \approx 5$ GHz.

The important characteristics of the pump source for the OPO are summarized in table VII. 1.

VII. 3 Optical parametric oscillator design.

This section discusses the design of the OPO resonator. In particular, there is an overview of the nonlinear material selection, when using the Ti:sapphire laser directly as the pump source for a cw OPO. The two mirror, linear, standing-wave, OPO cavity that provides a high finesse resonator for the doubly-resonant signal and idler frequencies is analysed. Mirrors were

positioned again to allow for the use of confocal focusing of the three fields over the length of the gain medium.

Table VII. 1
Characteristics of the input pump frequency.

<i>Pump source</i>		<i>Ti:sapphire laser</i>
<i>Frequencies</i>	ν_p	400 - 350 THz *
<i>Wavelengths</i>	λ_p	750 - 850 nm *
<i>Power</i>	P_p	> 1 W
<i>Jitter (≈ 1 second)</i>	$\Delta\nu_{p-stab}$	$\approx \pm 5 - 15$ MHz

**defined by current set of mirrors.*

A nonlinear material was required that could be phase-matched under the conditions of non-critical phase-matching, when using the Ti:sapphire laser as the pump source. At the time of this experiment, two different materials were considered for this; LBO and KTP. Of these, the nonlinear material KTP has been used frequently in the type II non-critical phase-matched geometry with pulsed pump sources operating in the near infra-red spectral region [28, 29]. In this geometry, the OPO can be operated with signal and idler frequencies significantly removed from frequency-degeneracy. For a pump source operating at a frequency of $\nu_p \approx 375$ THz, corresponding to a free-space wavelength of $\lambda_p \approx 800$ nm, non-critically phase-matched signal and idler frequencies are typically in the ratio $\approx 2:1$; see chapter III. Complications arise when forming a doubly-resonant cw OPO in this arrangement. This is caused by the reduced transmission of KTP beyond wavelengths of 107 THz (2.8 μ m). Therefore, it is difficult to form a high-resonant cavity for the idler frequency, and this precludes the use of a conventional doubly-resonant oscillator. With the power levels required for singly-resonant operation two orders of magnitude higher than those currently available from Ti:sapphire lasers, the use of non-critically phase-matched KTP remains problematic for cw OPO operation, unless the pump

field is enhanced within the OPO resonator [20]. This problem is not encountered in pulsed experiments, where the peak pump powers available enable the relatively straight-forward construction of singly-resonant OPOs [28, 29]. In this case, resonance at the idler frequency can be discarded for signal frequency single-resonance. The emergence of variants of KTP, including KTA and CTA, may offer advantages for such a cw phase-matching geometry, with extended transmission out to wavelengths near $\lambda \approx 3.7 \mu\text{m}$ [30, 31], discussed in detail in chapter III.

While the above assessment appears to eliminate the use of KTP with the Ti:sapphire laser as the pump source, it should be recalled that the low walk-off in critically phase-matched KTP has allowed for the construction of doubly-resonant cw OPOs, pumped by sources in the green spectral region, and operating near frequency-degeneracy [7, 8]. Therefore, KTP may yet prove to be a useful material for cw use with the Ti:sapphire laser as the pump source within a critically phase-matched OPO geometry. (This possibility is discussed further in the final section of this chapter.)

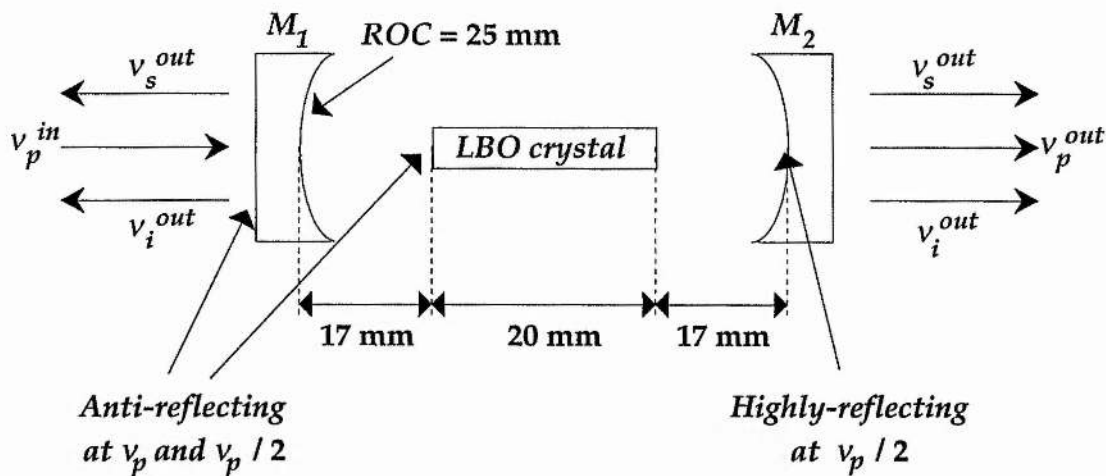


Figure VII. 3.

Schematic representation of the single-cavity, doubly-resonant OPO. The linear, standing-wave resonator formed a high finesse cavity for the signal and idler frequencies, centred at $\nu \approx 187 \text{ THz}$. The cavity mirrors were anti-reflecting for Ti:sapphire pump frequencies, allowing for near-single-pass pump interaction. Mirrors M_1 and M_2 were identical. ROC: radius of curvature.

The other nonlinear material considered was LBO. In chapter III, the temperature tuning properties of LBO in the 1 to 2 μm spectral region ($\nu \approx 300$ to 700 THz) were discussed in detail. In particular, when a widely tunable pump source is utilized, LBO can be temperature-tuned under the conditions of type I non-critical phase-matching to provide radiation over the whole of the 1 to 2 μm spectral region [32]. Further, the crystal temperatures required are restricted to near room-temperature, assisting simple experimental OPO designs. The significant drawback to this down-conversion process is the use of LBO in the type I phase-matching geometry, with the signal and idler frequencies polarized along the same resonator axis, and the resulting difficulty in forming a dual-cavity oscillator with separate signal and idler cavity length control.

Therefore, LBO was selected as the gain medium for the Ti:sapphire pumped cw OPO. To simplify the cavity design, with respect to optical coatings, operation at, and around, frequency-degeneracy was selected. The two-mirror, single-cavity, doubly-resonant OPO is illustrated in figure VII. 3. The LBO crystal was cut for propagation along the x -axis ($\theta = 90^\circ$, $\phi = 0^\circ$), with dimensions of 3, 3, and 20 mm, along the y , z , and x principal optical axes, respectively. The pump wave was polarized along the y -axis, and the generated signal and idler waves were polarized along the z -axis; $e \rightarrow o+o$.

The crystal had anti-reflection coatings applied to its faces for both the pump frequency at $\nu_p \approx 375$ THz (0.8 μm), and near-degenerate OPO frequencies at $\nu_s \approx \nu_i \approx 187$ THz (1.6 μm). The single-pass transmission loss of the crystal was specified to be $\beta_{p,s-p} < 1\%$ at $\nu_p \approx 375$ THz, and $\beta_{s,i,s-p} < 0.25\%$ at $\nu_s \approx \nu_i \approx 187$ THz. The crystal was placed at the intracavity focus of a linear, near-concentric resonator, formed by two mirrors of 25 mm radius-of-curvature. These mirrors were located at a distance of ≈ 17 mm from the crystal faces, and coated to be highly-reflecting ($R > 99.7\%$) at $\nu \approx 187$ THz, forming a high-finesse ($F \approx 400$), low-loss resonator for the signal and idler fields. In addition, these mirrors were nominally high-transmitting for the pump frequencies, thus ensuring near-single-pass, non-resonant pump interaction. The pump beam was focused to a spot size ($1/e$ electric-field radius) of $W_{p-OPO} \approx 40$ μm , at the centre of the nonlinear material.

The confocal parameters of the OPO waves were set equal to the crystal length. The linear standing-wave cavity provided spot sizes of

$W_s \approx W_i \approx 56 \mu\text{m}$ for the OPO frequencies, maximising the spatial mode overlap between the pump and the OPO waves, lowering the threshold to a level compatible with the cw pump source. The LBO crystal was enclosed within a temperature-controlled oven to reach the desired non-critical phase-matching temperatures.

VII. 4. Pump frequency and cavity length requirements.

The requirements on the pump frequency and the cavity length are similar to those outlined in chapter IV for the type I phase-matching geometry in LBO near frequency-degeneracy. The computer model was used again to examine this phase-matching geometry [33]. The input data are summarized in table VII. 2.

Table VII. 2
Input data used for the computer model.

<i>Phase-matching</i>		<i>Type I</i>
<i>Pump frequency</i>	ν_p	375 THz
<i>Signal frequency</i>	ν_s	184 THz
<i>Idler frequency</i>	ν_i	191 THz
<i>Temperature</i>	T_{xtal}	150°C
<i>Crystal length</i>	l	20 mm
<i>OPO finesses</i>	F_s, F_i	≈ 400
<i>Mirror separation</i>	L	54 mm
<i>FSR mis-match</i>	ΔFSR	0.02 %

The requirements specific to this Ti:sapphire / LBO experiment are displayed in figure VII. 4, and differ from the analyses of chapter IV, in the values for the three frequencies, the OPO cavity length, and the sub-harmonic finesses.

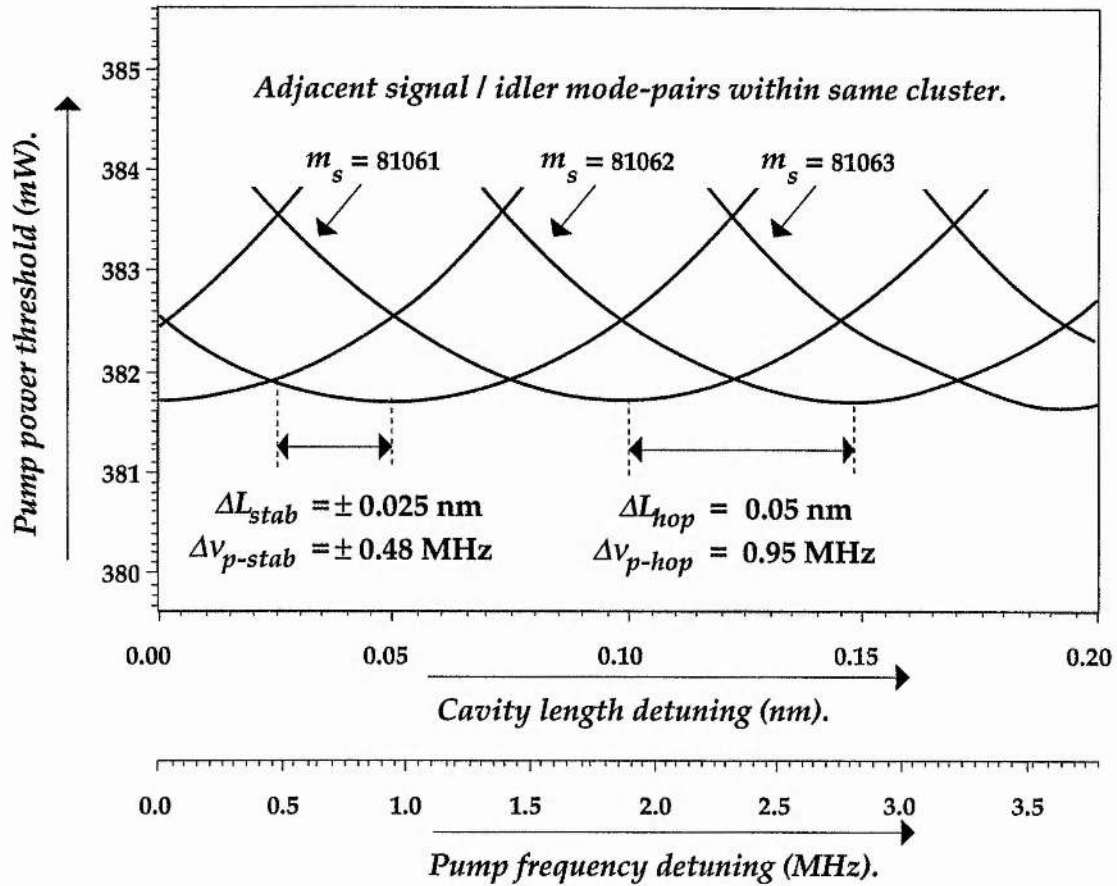


Figure VII. 4.

Modelling of the requirements on the pump frequency and the OPO cavity length to maintain operation on a single signal and idler frequency mode-pair.

Figure VII. 4 indicates that the pump frequency should be held stable to within $\Delta v_{p-stab} \approx 0.48 \text{ MHz}$, and the OPO cavity length to within $\Delta L_{stab} \approx 0.025 \text{ nm}$ to hold the OPO output on the same signal and idler frequency mode-pair. Again, these specifications highlight the severe tolerances of a single-cavity, doubly-resonant OPO with type I phase-matching near frequency-degeneracy.

The frequency instability of the pump source used for the experiment implied that frequency or amplitude stable operation of the OPO outputs would not be possible. Indeed, the pump frequency stability is nearly two orders of magnitude outwith the minimum requirements for stable OPO operation. Therefore, no effort was taken to investigate the fine frequency

properties of the OPO. Instead, other factors were examined that allowed for wide frequency tuning through the use of coarse frequency tuning of the pump source, combined with coarse frequency tuning of the OPO outputs, by altering the precise phase-matching temperature of the LBO crystal.

To estimate the pump power threshold required for the OPO, the expression for a linear, standing-wave cavity with a single-pass, non-resonant, pump interaction, is recalled. For the case of near-equal signal and idler frequencies and finesses, the threshold can be written as follows:

$$\left(P_p^{in}\right)_{th-min} = \frac{n_p^2 \epsilon_0 c^4}{2F_s F_i l |d_{eff}|^2 v_p^3} \quad [VII. 1]$$

The values used within this threshold expression are collected in table VII. 3

Table VII. 3
Parameter values for threshold analysis.

<i>Pump frequency</i>	v_p	375 THz
<i>Pump ref. index</i>	n_p	1.60
<i>Crystal length</i>	l	20 mm
<i>Nonlinear coefficient</i>	d_{eff}	1.24 pm/V
<i>Degeneracy factor</i>	δ	1
<i>Signal/idler finesse</i>	F_s, F_i	400

From table VII. 3, a pump power threshold of $P_{p-th}^{in} = 354$ mW is predicted for the OPO, assuming confocal focusing and perfect spatial mode overlap between the three waves over the length of the gain medium. Table VII. 4 displays the expected requirements on the pump source and the OPO cavity length to operate the OPO above threshold, and with stable operation on a single signal and idler frequency mode-pair.

Table VII. 4

Requirements on pump frequency and cavity length.

Signal and idler frequency double-resonance.

Pump frequency	$\Delta\nu_{p-stab}$	$\approx \pm 0.48$ MHz
Cavity length	ΔL_{stab}	$\approx \pm 25$ pm

Pump power threshold.

Ti:sapphire power	P_{p-th}^{in}	354 mW
-------------------	-----------------	--------

VII. 5. Experimental arrangement.

This section describes the experimental arrangement of the Ti:sapphire pumped cw LBO OPO [22]. The pumping radiation was mode-matched into the OPO cavity by use of a single focusing lens of focal length $f = 88.5$ mm. A *Faraday* isolator with > 30 dB attenuation was used to maintain free-running operation of the Ti:sapphire laser. A half-waveplate ensured the correct orientation of the pump radiation in the OPO gain medium. This layout is illustrated schematically in figure VII. 5.

The signal and idler frequencies were separated from the transmitted pump field through the use of filters and polarizers, and the combined OPO output was monitored on a photo-diode / monochromator arrangement, for OPO power and wavelength measurements.

Although optical feedback was not expected to affect the free-running performance of the pump laser, it can occur due to coupling into a counter-propagating mode of the ring cavity. Extremely small coupling between the forward and reverse modes can produce a significant feedback effect. However, it is important to realise again that a ring cavity OPO geometry would reduce feedback effects into the Ti:sapphire laser cavity; see the OPO resonators described in references [34] and [35].

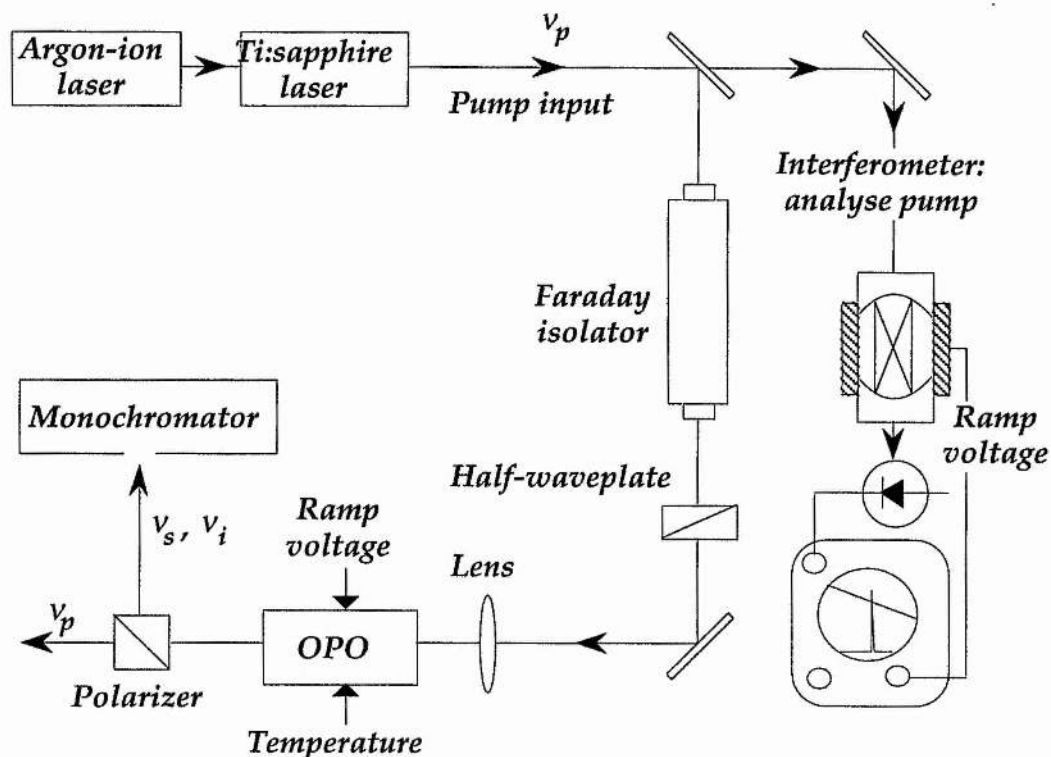


Figure VII. 5.

Schematic representation of the Ti:sapphire pumped LBO OPO. A single focusing lens mode-matched the pump radiation into the OPO cavity. A *Faraday* isolator was used to prevent back-reflections and back-conversion from entering the counter-propagating direction of the travelling-wave pump laser.

VII. 6. Results and discussion.

The OPO operated with a minimum pump power threshold of $P_{p-th}^{in} \approx 360$ mW, in reasonable agreement with the analysis of section VII. 4, considering the uncertainties in the quality of the optical coatings (OPO cavity finesses). With single-frequency pump powers at the Watt-level available from the pump source, the OPO was operated reliably at two to three times above threshold. (By reducing the requirements on the optical coatings, through for example monolithic [10] / semi-monolithic [7] crystal fabrication, longer crystal samples [36], or by double-passing the pump field through the OPO gain medium [7], lower thresholds should be possible without the need for undesirable pump-enhanced resonance effects [20].)

When pumping at two times above threshold, pump depletions of $\approx 40\%$ and peak output powers (signal + idler) of $P_s^{out} + P_i^{out} \approx 30\text{ mW}$ were obtained consistently. (No attempt was made to separate externally the near degenerate signal and idler frequencies.)

As discussed previously, the fine frequency tuning properties of this particular type I phase-matching geometry were not studied. Instead, the effects of multiple parameter tuning were analysed by combining pump frequency tuning and the OPO phase-matching temperatures. Two different modes of coarse frequency tuning can be investigated within the present arrangement. First, by operating the Ti:sapphire laser at a fixed frequency, the OPO could be temperature-tuned under non-critical phase-matching to provide signal and idler frequency mode-pairs around degeneracy. Second, by maintaining the LBO crystal at a constant temperature, the pump frequency could be tuned to generate further signal and idler frequency mode-pairs.

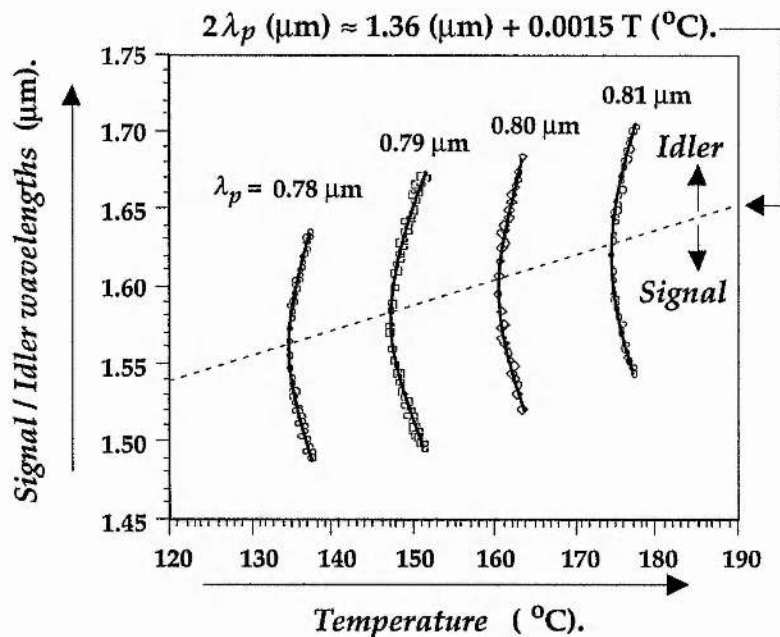


Figure VII. 6.

OPO temperature tuning under non-critical phase-matching for four specific pump wavelengths. The dashed line illustrates the near-linear relationship between temperature and degenerate OPO operation for these operating wavelengths.

The procedure used was the first method outlined above. By varying the frequency of the pump laser and heating the LBO crystal to the appropriate phase-matching temperatures, the OPO was tuned from $\nu \approx 201$ to 175 THz ($\lambda \approx 1.49$ to 1.71 μm). The tuning curves for four specific pump wavelengths are displayed in figure VII. 6. Typically, tuning over $\Delta\nu \approx 20$ THz was obtained for a temperature change of $\Delta T_{\text{xtal}} \approx 4$ °C. This range was limited only by the bandwidth of the optical coatings. (By selecting different crystal / mirror coatings, further tuning ranges over the whole of the 1 - 2 μm spectral region could be accessed readily [32].)

VII. 7. Conclusions.

A widely tunable cw OPO in the 1.5 - 1.7 μm spectral region has been presented. Multiple parameter tuning has been used, allowing for the control of the sum and difference of the signal and idler frequencies. The sum frequency was set by the precise frequency of the Ti:sapphire laser: the difference frequency was set by the phase-matching temperature of the LBO crystal.

Given the available frequency coverage of a Ti:sapphire laser, and the transparency of the LBO crystal (as far as 2.6 μm), tuning should be possible over wider spectral bandwidths. Therefore, the use of LBO in the type I non-critical phase-matching geometry offers the possibility of wide, coarse frequency tuning from a cw laser pump source, tunable in the near infra-red spectral region. However, unless dual-cavity designs can be incorporated within these OPOs, this down-conversion process will remain particularly ineffective.

In the absence of alternative nonlinear media, some applications of this down-conversion process are considered. First, assume a Ti:sapphire laser operating at $\nu_p \approx 354$ THz ($\lambda_p \approx 848$ nm), and acting as the pump source for a near frequency degenerate OPO. By locking the signal and idler frequencies at exact frequency degeneracy (self phase-locking technique [10]) or offset-locked with a stable, known frequency difference [7], the OPO outputs will operate at $\nu_{s,i} \approx 177$ THz ($\lambda_{s,i} \approx 1.7$ μm). Exact frequency referencing can be provided by locking either, or both, the signal and idler frequencies, to the frequency doubled output of a methane-stabilized He:Ne laser operating at

$\nu_{ref.} \approx 88$ THz ($3.39 \mu\text{m}$). This proposed experiment is outlined in figure VII. 7, and discussed briefly in reference [37].

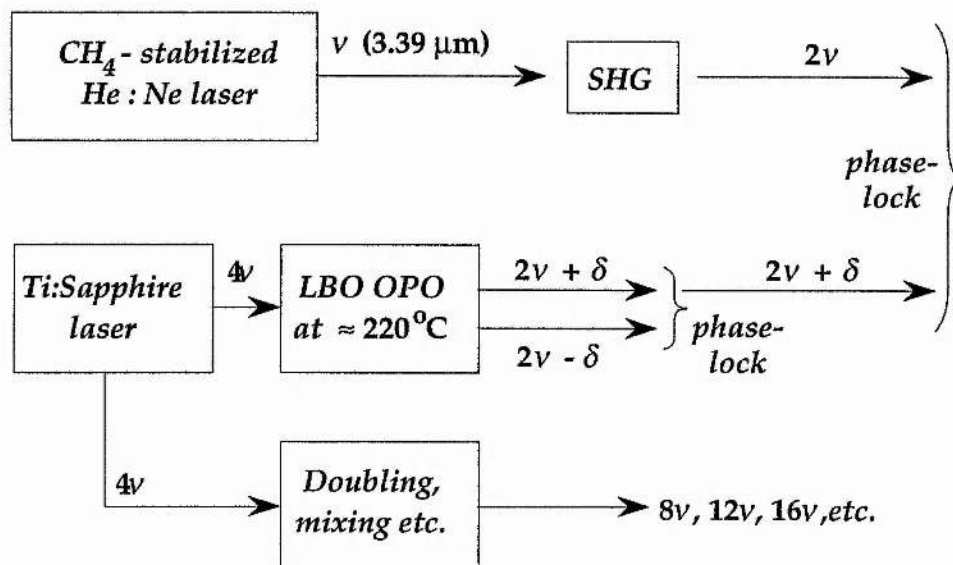


Figure VII. 7.

Proposed experiment utilizing a Ti:sapphire pumped LBO OPO, and a methane-stabilized He:Ne laser, to generate visible frequency harmonics of the stable infra-red frequency standard. δ : microwave frequency difference; SHG: second harmonic generation.

Through this method, it would be possible to generate visible frequency harmonics of the stable infra-red He:Ne laser, by frequency converting an output of the Ti:sapphire laser to generate higher frequencies.

Another application would be to reference a pump source at $\nu_{ref.} \approx 0.78 \mu\text{m}$ to an absorption line in rubidium, and to use this pump source to pump an OPO with signal and idler output frequencies near frequency-degeneracy, that could link diode laser sources in the visible and near infra-red spectral regions [38]. Alternatively, the pump frequency could be summed with the degenerate OPO output to yield a frequency around $\nu_{ref.} \approx 600$ THz that could be referenced to an absorption line in iodine [39].

If LBO was to be replaced with KTP or KTA, in some critically phase-matched geometry, then further options would become available. For example, an idler frequency output from a cw OPO could be located directly at $\nu_i \approx 88$ THz and beat against a methane-stabilized He:Ne laser. The signal and idler frequency outputs could be locked in a 3:1 frequency ratio, locating the pump frequency at the fourth frequency harmonic of the infra-red frequency standard. Again, further frequency harmonics could be generated through additional nonlinear frequency conversion processes. As discussed in chapter III, CTA offers the ideal properties to replace LBO within the context of the phase-matching geometry described in this chapter. Operation near frequency degeneracy should be possible in the type II phase-matching geometry, when using the Ti:sapphire laser as the pump source. Lower thresholds and smooth frequency tuning could be expected from such a device.

Finally, consider a Ti:sapphire laser operating at $\nu \approx 297$ THz ($1.01 \mu\text{m}$). By frequency doubling this radiation to $\nu \approx 594$ THz (505 nm), and using this radiation to pump an OPO with signal and idler frequencies in an exact 3:1 frequency ratio, then the idler frequency would be $\nu \approx 148$ THz ($\approx 2.02 \mu\text{m}$), and could be referenced to a holmium-based laser transition (see section IV. 7). In this geometry, the signal frequency would be located at $\nu_{ref.} \approx 445$ THz, and could be used to drive the clock transition of the strontium ion. Therefore, this method would provide a link between a visible ion trap and the near infra-red spectral region, with the possibility of using the power available from a holmium-based laser for further OPO stages (e. g. by using AgGaSe_2 or AgGaS_2) to generate lower frequencies that could then be referenced to a harmonic of a stable CO_2 laser at a frequency of $\nu_{ref.} \approx 28$ THz ($\lambda \approx 10.6 \mu\text{m}$) [40].

In summary, the experiment described in this chapter illustrates the advantages of using tunable pump radiation, compared to fixed frequency pump sources. Each of the above-proposed schemes takes advantage of the freedom in selecting the sum of the signal and idler frequencies, and these experiments form the thrust of present research involving the use of OPOs within high precision optical frequency metrology. The development of new tunable pump sources and nonlinear materials will hasten the realization of these experiments.

References.

1. F. G. Colville, A. J. Henderson, M. J. Padgett, J. Zhang, & M. H. Dunn,
"Continuous-wave parametric oscillation in lithium triborate,"
Opt. Lett. **18**, 205 (1993).
2. F. G. Colville, M. J. Padgett, A. J. Henderson, J. Zhang, & M. H. Dunn,
"Continuous-wave parametric oscillator pumped in the ultra-violet,"
Opt. Lett. **18**, 1065 (1993).
3. F. G. Colville, M. J. Padgett, & M. H. Dunn,
"Continuous-wave, dual-cavity, doubly-resonant, optical parametric oscillator,"
Appl. Phys. Lett. **64**, 1490 (1994).
"Smooth frequency tuning from optical parametric oscillators: the transition from
single- to dual-cavity oscillators,"
in *Proceedings of Topical Meeting on Advanced Solid-State Lasers*, (1994).
4. I. Gorog, & F. W. Spong,
"An approximate linewidth determination method and the magnetic-field-tunable
stable spectrum of the argon laser,"
IEEE J. Quant. Electron. QE-3, 691 (1967).
5. H. R. Luthi, W. Seelig, & J. Steinger,
"Power enhancement of continuous ultraviolet lasers,"
Appl. Phys. Lett. **31**, 670 (1977).
6. See table I. 1 in chapter I of this thesis,
References [24] to [59].
7. D. Lee & N. C. Wong,
"Tunable optical frequency division using a phase-locked optical parametric
oscillator,"
Opt. Lett. **17**, 13 (1992).
"Stabilization and tuning of a doubly-resonant optical parametric oscillator,"
J. Opt. Soc. Am. B **10**, 1659 (1993).
8. T. Debuisschert, S. Reynaud, A. Heidmann, E. Giacobino, & C. Fabre,
"Observation of large quantum noise reduction using an optical parametric oscillator,"
Quant. Opt. **1**, 3 (1989).
S. Reynaud, C. Fabre, & E. Giacobino,
"Quantum fluctuations in a two-mode parametric oscillator,"
J. Opt. Soc. Am B **4**, 1520 (1987).
A. Heidmann, R. J. Horowicz, S. Reynaud, E. Giacobino, & C. Fabre,
"Observation of quantum noise reduction on twin laser beams,"
Phys. Rev. Lett. **59**, 2555 (1987).
9. L.-A. Wu, H. J. Kimble, J. L. Hall, & H. Wu,
"Generation of squeezed states by parametric down conversion,"
Phys. Rev. Lett. **57**, 2520 (1986).
10. C. D. Nabors, S. T. Yang, T. Day, & R. L. Byer,
"Coherence properties of a doubly-resonant monolithic optical parametric oscillator,"
J. Opt. Soc. Am. B **7**, 815 (1990).
11. N. C. Wong,
"Optical frequency division using an optical parametric oscillator,"
Opt. Lett. **15**, 1129 (1990).
12. R. W. Wallace,
"Rapidly tunable dye-laser-pumped parametric oscillator,"
IEEE J. Quant. Electron. QE-8, 820 (1972).
13. *Laser Focus World*,
"Extending the tunability spectrum,"
November 1970, p42.
14. D. C. Edelstein, E. S. Wachman, & C. L. Tang,
"Broadly tunable high repetition rate femtosecond optical parametric oscillator,"
Appl. Phys. Lett. **54**, 1729 (1989).

15. P. F. Moulton,
"Spectroscopic and laser characteristics of Ti:Al₂O₃,"
J. Opt. Soc. Am. B 3, 125 (1986).
- B. B. Snavely,
in "Dye Lasers" (F. P. Schafer Ed.) Springer-Verlag, p86 (1973).
16. T. L. Boyd & H. J. Kimble,
"Frequency stabilization of a continuous-wave Ti:sapphire laser,"
Opt. Lett. 16, 808 (1991).
17. S. Bourzeix, M. D. Plimmer, F. Nez, L. Julien, & F. Biraben,
"Efficient frequency doubling of a continuous wave titanium:sapphire laser in an external enhancement cavity,"
Opt. Comm. 99, 89 (1993).
18. C. S. Adams & A. I. Ferguson,
"Tunable narrow linewidth ultra-violet light generation by frequency doubling of a ring Ti:sapphire laser using lithium triborate in an external enhancement cavity,"
Opt. Comm. 90, 89 (1992).
19. G. T. Maker & A. I. Ferguson,
"Ti:sapphire laser pumped by a frequency-doubled diode-pumped Nd:YLF laser,"
Opt. Lett. 15, 375 (1990).
- T. R. Steele, D. C. Gerstenberger, A. Drobshoff, & R. W. Wallace,
"Broadly tunable high-power operation of an all-solid-state titanium-doped sapphire laser system,"
Opt. Lett. 16, 399 (1991).
20. R. Knappe, J. Barschke, C. Becher, B. Beier, M. Scheidt, K.-J. Boller, & R. Wallenstein,
"Injection-locked high power diode arrays and their application as pump sources for blue and green Nd:YAB lasers, monolithic Nd:YAG ring lasers, and cw KTP optical parametric oscillators,"
in *Conference on Lasers and Electro-Optics*, Vol. 8 of OSA 1994 Technical Digest Series (Optical Society of America, Washington, D. C., 1994), paper CThL 4.
21. W. Wang, K. Nakagawa, S. Sayama, & M. Ohtsu,
"Coherent addition of injection-locked high-power AlGaAs diode lasers,"
Opt. Lett. 17, 1593 (1992).
22. F. G. Colville, M. Ebrahimzadeh, W. Sibbett, & M. H. Dunn,
"Continuous-wave LiB₃O₅ optical parametric oscillator pumped by a tunable Ti:sapphire laser,"
Appl. Phys. Lett. 64, 1765 (1994).
in *Conference on Lasers and Electro-Optics*, Vol. 8 of OSA 1994 Technical Digest Series (Optical Society of America, Washington, D. C., 1994), paper CTuK19.
23. Model 2040E and 2045E; High power ion laser,
Spectra-Physics laser products division, CA 94039-7013, USA.
Instruction manual, part no. 0000-210A, Rev. A, October 1990.
24. Titan-CW series; Ti:sapphire tunable lasers,
Schwartz Electro-Optics Inc. laser products division, FL 32804, USA.
25. N. C. Wong,
"Optical frequency counting from the UV to the near IR,"
Opt. Lett. 17, 1155 (1992).
26. J. Harrison, A. Finch, D. M. Rines, G. A. Rines, & P. F. Moulton,
"Low-threshold, cw, all-solid-state Ti:Al₂O₃ laser,"
Opt. Lett. 16, 581 (1991).
27. MBR110 single frequency Ti:sapphire laser,
Microlase optical systems Ltd., Glasgow, UK.
28. C. L. Tang, P. E. Powers, & R. J. Ellingson,
"Optical parametric processes and broadly tunable femtosecond sources,"
Appl. Phys. B 58, 243 (1994).
29. J. M. Dudley, D. T. Reid, M. Ebrahimzadeh, & W. Sibbett,
"Characteristics of a noncritically phasematched Ti:sapphire pumped femtosecond optical parametric oscillator,"
Opt. Comm. 104, 419 (1994).

30. L. K. Cheng, L.-T. Cheng, J. D. Bierlein, & F. C. Zumsteg,
"Properties of doped and undoped crystals of single domain KTiOAsO_4 ,"
Appl. Phys. Lett. **62**, 346 (1993).
31. P. E. Powers, S. Ramakrishna, C. L. Tang, & L. K. Cheng,
"Optical parametric oscillation with KTiOAsO_4 ,"
Opt. Lett. **18**, 1171 (1993).
32. J. D. Kafka, M. L. Watts, & J. W. Pieterse,
in *Conference on Lasers and Electro-Optics*, Vol. 11 of OSA 1993 Technical Digest Series
(Optical Society of America, Washington, D. C., 1993), paper CPD32.
33. M. J. Padgett, F. G. Colville, & M. H. Dunn,
"Mode selection in doubly-resonant optical parametric oscillators,"
In press, *IEEE J. Quant. Electron.*
34. S. T. Yang, R. C. Eckardt, & R. L. Byer,
"Continuous-wave singly resonant optical parametric oscillator pumped by a single-
frequency resonantly doubled Nd:YAG laser,"
Opt. Lett. **18**, 971 (1993).
"Power and spectral characteristics of continuous wave parametric oscillators: the
doubly to singly resonant transition,"
J. Opt. Soc. Am. B **10**, 1684 (1993).
"1.9-W cw ring-cavity KTP singly resonant optical parametric oscillator,"
Opt. Lett. **19**, 475 (1994).
35. E. S. Polzik, J. Carri, & H. J. Kimble,
"Spectroscopy with squeezed light,"
Phys. Rev. Lett. **68**, 3020 (1992).
36. Growth samples of up to 30 mm are now available in lithium triborate.
37. A. Bell, E. Riis, & A. I. Ferguson,
"Frequency metrology using Ti:sapphire lasers,"
at the Eleventh UK National Quantum Electronics Conference, paper 11, 1993.
38. W. Wang, K. Nakagawa, Y. Toda, & M. Ohtsu,
"1.5 μm diode laser-based nonlinear frequency conversions by using potassium titanyl
phosphate,"
Appl. Phys. Lett. **61**, 1886 (1992).
W. Wang & M. Ohtsu,
"Continuous-wave optical parametric amplifier that uses a diode laser for a wideband
coherent optical frequency sweep generator,"
Opt. Lett. **18**, 876 (1993).
"Frequency-tunable sum- and difference-frequency generation by using two diode lasers
in a KTP crystal,"
Opt. Comm. **102**, 304 (1993).
39. A. Arie, S. Schiller, E. K. Gustafson, & R. L. Byer,
"Absolute frequency stabilization of diode-laser-pumped Nd:YAG lasers to hyperfine
transitions in molecular iodine,"
Opt. Lett. **17**, 1204 (1992).
40. O. Acef, J. J. Zondy, M. Abed, D. G. Rovera, A. H. Gerard, A. Clairon, Ph. Laurent,
Y. Millerioux, & P. Juncar,
"A CO_2 to visible optical frequency synthesis chain: accurate measurement of the
473 THz HeNe/ I_2 laser,"
Opt. Comm. **97**, 29 (1993).

Chapter VIII.

Conclusions.

This chapter summarizes the work presented in the thesis, and draws conclusions from the modelling and subsequent experiments undertaken. Other groups have also made considerable progress developing cw OPOs, and the relevance of this thesis in particular is discussed within the general context of current cw OPO research. Finally, the present limitations of cw OPOs as practical optical frequency dividers are discussed and compared to the implementation of alternative nonlinear optical techniques, in particular difference frequency mixing.

First, consider the main conclusions that can be taken from the modelling of the operation of cw OPOs. The analysis of the pump power thresholds showed that the double-resonance condition, as opposed to that of single-resonance, must be maintained to operate cw OPOs reliably above threshold with low input pump powers. This is because the pump powers required for singly-resonant operation are too far above those presently available from commonly-used narrow-linewidth laser sources, and so it would seem that the prospect for cw singly-resonant oscillators is not particularly promising. Nevertheless, this must not be seen as a limiting factor in the ability to generate narrow-linewidth, frequency-stable, and frequency-tunable radiation from cw OPOs in general, because other forms of OPO resonators can combine this smooth frequency tuning of singly-resonant oscillators with the added advantage of low pump power thresholds. In addition to lowering the pump power thresholds to the mW-level, the doubly-resonant condition narrows the linewidth of the signal and idler frequencies significantly. Ironically, it is this inaccessibility of high singly-resonant pump power thresholds which has been an important factor in hastening progress in doubly-resonant cw OPOs with regard to frequency-stability and smooth frequency tuning.

The analysis of the mode-selection properties in doubly-resonant oscillators highlighted a number of critical factors with regard to the design of the optical resonators and the selection of phase-matching geometries. The signal and idler fields within doubly-resonant oscillators can be brought to

resonance either within a common cavity arrangement (single-cavity) or in separate cavities in which the gain element is located within a common part of these cavities (dual-cavity).

Mode-selection properties within the single-cavity resonator were studied to assess the requirements with regard to amplitude-stable single mode-pair operation. In this context, the phase-matching geometry selected is the deciding factor. Amplitude-stable operation is easier to obtain when employing either type II phase-matching geometries or type I phase-matching geometries in which the signal and idler frequencies are significantly removed from frequency-degeneracy. This is a consequence of the increased mis-match in the free spectral ranges of the signal and idler fields provided within these geometries. However, the limiting factor for single-cavity OPOs is their inability to provide smooth frequency tuning of the signal and idler outputs in the presence of a fixed frequency pump source.

Dual-cavity oscillators were studied to allow for smooth frequency tuning of the OPO outputs irrespective of the nature of the pump source (fixed or tunable pump frequency). The independent control of the signal and idler cavity lengths (frequencies) allows for smooth frequency tuning when servo-control feedback is applied to one of the two cavity lengths. When this is accomplished, continuous frequency tuning is possible over the entire phase-matching bandwidth of the OPO. This frequency tuning range can be compared to that available from the aforementioned singly-resonant oscillators which operate on the cavity mode frequency nearest the centre of the parametric gain profile. Therefore, in contrast to dual-cavity oscillators, singly-resonant oscillators are prone to mode-hops when tuned through half a free spectral range of the OPO resonator.

In addition to providing relaxed stability requirements within a single-cavity geometry, type II phase-matching geometries were shown to be ideal to allow for the transition from single- to dual-cavity resonators. Quite simply, this is because, within type II phase-matching geometries, the signal and idler fields are polarized along orthogonal axes of the optical resonator, and polarization separation can be implemented efficiently to decouple spatially the signal and idler paths to allow for discrete cavity length control. Therefore, type II phase-matching is preferable to type I phase-matching in both single- and dual-cavity resonators.

Pump sources were identified that would be suitable for pumping cw OPOs within frequency division schemes where in general, the three frequencies (pump, signal and idler) must be referenced to known frequency sources. Therefore, the ability to tune systematically the precise frequency of the pump source (signal and idler sum frequency) close to a referenced frequency source (e.g. an ion trap in the visible spectral region) can be a critical factor. In this context, tunable lasers offer significant advantages over fixed frequency sources as the pump sources for cw OPOs, either through their fundamental operating frequencies or their frequency harmonics. When considering widely-tunable, high-power, and narrow-linewidth pump sources that are commonly available within research laboratories and industrial centres, the Ti:sapphire laser is the most appropriate source. However, the current development of new widely-tunable and inherently narrow-linewidth laser sources offer particular advantages with regard to direct diode-pumping and portability, and may eventually become the preferred pump sources for cw OPOs.

Compared to the increasing availability of useful pump sources for cw OPOs, the topic of nonlinear material selection is not so encouraging. Non-critical phase-matching geometries were considered when using currently-available materials to provide integral-related ratios of pump, signal, and idler frequencies. In general, the high order integral-related outputs required for optical frequency dividers are possible only when using nonlinear materials whose birefringence is particularly sensitive to small variations in crystal temperature. While temperature tuning can be used to generate widely tunable OPO frequencies from a fixed frequency pump and while maintaining non-critical phase-matching, it can present severe problems when aiming to generate highly-stable OPO frequencies. Within any particular phase-matching geometry, it is important to evaluate the effects of mK temperature perturbations. Conversely, materials whose birefringence has a low temperature dependence, can take advantage of this feature by exploiting temperature control as a tuning parameter to generate smooth frequency tuning. Another desirable attribute of nonlinear materials is electro-optic tuning which can also assist fine frequency control. At present, the type II phase-matching geometries of KTP, CTA, and KTA are unique in combining low temperature sensitivity, type II phase-matching, and electro-optic tuning. However, these materials offer limited choice in the selection of signal and idler frequency ratios, and any application will probably be unique to a particular material and pump frequency combination. However, the

addition of certain dopants during crystal growth may be all that is required to alter the phase-matching characteristics to produce the desired signal and idler frequencies.

A more worrying situation at the moment is the absence of high quality nonlinear optical materials in the mid to far infra-red spectral regions. The nonlinear materials that were initially assessed in the thesis have transparency ranges confined to the near infra-red spectral region; generally at wavelengths shorter than $\lambda \approx 3 - 4 \mu\text{m}$. This provides a serious limitation within the context of optical frequency dividers because referenceable frequency standards (perhaps the CH_4 - stabilized He:Ne laser at $\lambda = 3.39 \mu\text{m}$, but more desirably, the OsO_4 - stabilized CO_2 laser at $\lambda = 10.6 \mu\text{m}$) operate in spectral regions currently outwith the range of these commercially available, high quality nonlinear materials. This eliminates, at present, the use of OPOs to link these referenceable frequencies with visible optical frequency standards. Therefore, the design of frequency synthesis chains may have to rely more heavily on relatively inefficient single-pass up-conversion stages (from $\lambda = 10.6 \mu\text{m}$) to link the far infra-red to the visible spectral region.

As discussed above, in the short-term, the difficulties associated with forming mid infra-red cw OPOs dictate that other forms of frequency conversion from the visible to the mid infra-red spectral region will probably dominate. In particular, difference frequency mixing techniques may allow for this transition. There are several advantages when using difference frequency mixing arrangements compared to optical parametric oscillators. By using two highly intense input fields (pump and signal frequencies) adequate output power levels (at the idler frequency) can be generated, without the need for any cavity resonance conditions. Therefore, the amplitude and frequency characteristics of the output are stable, similar to single-pass second harmonic generation configurations. Having eliminated the requirement for an optical cavity in difference frequency mixing, some critical OPO conditions are immediately relaxed. These include the following: low absorption within the gain medium that is essential for high finesse fields within an optical cavity; tightly focused spot sizes required for high parametric gain and which can cause crystal damage; complicated mirror and crystal coatings. When these factors are addressed, difference frequency mixing becomes an effective method of generating lower frequencies from the visible spectral region to the mid / far infra-red, even when using

currently available nonlinear materials which have been considered inappropriate for OPO use.

The experimental OPO configurations analysed within the thesis were chosen to complement the prior modelling of these devices. In particular, each experiment was designed to yield information on individual aspects of the modelling requirements of OPO-based systems. Such aspects include the following: the use of pump sources that operate in the ultra-violet, visible and near infra-red spectral regions; the benefits of widely tunable sources of pump radiation; the use of non-critical phase-matching geometries in LBO for each of the above pump sources; operation of cw OPOs near frequency-degeneracy and also with signal and idler frequencies in a near integral-related ratio; the comparison of type I and type II phase-matching geometries; the investigation of methods for maintaining single signal and idler mode-pairs on resonance within a single-cavity OPO with a fixed frequency pump source; the development of a dual-cavity resonator to allow for smooth frequency tuning with a fixed frequency pump source. Each of these aims was fulfilled within the course of these studies.

Within each experiment, the choice of pump laser was dictated ultimately by the availability of laser sources within the laboratory. The argon-ion laser used was not intended to represent a viable source for pumping cw OPOs, but was selected as a convenient source of high-power single-frequency radiation when operating in either the visible or ultra-violet spectral region. To this extent, it fulfilled its purpose by providing sufficient single-frequency power levels to enable operating the cw OPOs at \approx three times above threshold, and therefore to gain information on the characteristics of the OPO devices. Further, when operating with multi-line radiation, the argon-ion laser proved to be essential as the pump source for the single-frequency Ti:sapphire laser, used as the other OPO pump source. The argon-ion laser simulated the power levels that could be provided from all-solid-state sources of tunable radiation, when frequency up-converted to the visible or ultra-violet spectral regions. However, the frequency stability of the commercial product used ($\Delta\nu_p \approx \pm$ MHz) was not at the level commonly achieved when using all-solid-state sources (typically $\Delta\nu_p \approx \pm$ kHz), and this proved to be the limiting factor on the performance of the OPO pump sources.

The Ti:sapphire laser (limited again in stability at the level of $\Delta\nu_p \approx \pm\text{MHz}$) provided a convenient source of widely tunable radiation, and allowed for the sum frequency of the signal and idler frequencies to be chosen from a wide frequency bandwidth. The range of available sum frequencies was limited by the bandwidth of the optical coatings on the components within the Ti:sapphire laser.

Both type I and type II non-critical phase-matching geometries were realized with the nonlinear material LBO. The type I phase-matching geometries were operated at elevated temperatures (dependent on the exact input pump frequency), and near to frequency degeneracy. The type II phase-matching geometry was operated at room-temperature and with signal and idler frequencies in a near 3:1 frequency ratio. Given the range of pump frequencies selected for the type I phase-matching geometry (argon-ion laser and Ti:sapphire laser in the visible and near infra-red spectral regions, respectively), the crystal temperatures required for type I non-critical phase-matching were considerably higher than room-temperature. Therefore, OPO operation near frequency-degeneracy was selected to reduce the requirements on the optical coatings and in particular the nonlinear material, when operating at these high temperatures. In these conditions, the strongly anisotropic thermal expansion of LBO requires a high degree of care in selecting the match of the nonlinear crystal and the coating material. (Two further proposed cw OPO experiments involving the use of LBO at elevated temperatures, not discussed in the thesis, were unsuccessful due to coating failure at temperatures above $T_{xtal} \approx 100^\circ\text{C}$. However, unlike the above dual-anti-reflecting coatings, the coatings applied to these crystals were complicated triple-anti-reflecting coatings, and in one case, the LBO crystal was curved to a radius-of-curvature of $ROC = 20\text{ mm}$.) The type II phase-matching geometry, operating at room-temperature, allowed for a more complicated coating specification, and could be tuned over the entire bandwidth of the coatings, which involved raising the crystal temperature to only $T_{xtal} \approx 86^\circ\text{C}$.

The mode-selection properties from both the type I and type II phase-matched geometries were assessed by ramping the OPO cavity lengths over nanometer ranges, and observing the intensity variations of the OPO outputs and the depleted pump field. Within the type I geometry near frequency-degeneracy, the free spectral ranges of the signal and idler fields were almost identical, and this prevented OPO operation on a single signal / idler

frequency mode-pair. When the type II phase-matching geometry was employed, the mis-match in the free spectral ranges was substantially increased, and signal / idler frequency mode-pairs corresponded to discrete positions of the cavity length, in agreement with theory. This allowed for amplitude-stable operation of the OPO, given adequate pump frequency stability, a high degree of passive stability within the OPO cavity, and with servo-control feedback determining the length of the single-cavity OPO to maintain the double resonance condition.

By exploiting the orthogonal polarizations of the type II phase-matched geometry and the mis-match in the signal and idler frequencies, a dichroic-coated polarizing beam-splitter was incorporated within the resonator, and separate cavity mirrors were used to resonate the signal and idler fields within independently controlled optical cavity lengths. The dual-cavity oscillator allowed for smooth frequency tuning of the signal and idler frequencies, by manually adjusting the voltage to a piezo-electric transducer controlling the optical length of the idler cavity, and relying upon servo-control feedback to the signal cavity length, to maintain the double-resonance condition. Again, the passive stability of the OPO cavity was critical to the reliable operation of the device, with the servo-control feedback effective only when the OPO maintained free running operation on single-frequency mode-pairs over time periods of the order $\Delta t \approx 10$ s seconds. The range of smooth frequency tuning was limited by a weak pump resonance within one of the resonant OPO cavities (in this case, the idler cavity), which caused the intra-cavity field to drop below threshold when the idler cavity length was tuned off pump resonance.

Pump resonance effects were discussed frequently throughout the thesis. In general, they add only to the complexity of the devices. Since the pump power thresholds for doubly-resonant oscillators are well within the range of most cw single-frequency lasers, this eliminates the requirement of enhancing the pump field within the OPO cavity to reduce further the threshold. In addition, for almost all high-resolution experiments within quantum optics, cw power levels at the μ W-level are adequate. This is particularly true at a time when the quantum efficiencies and bandwidths of detectors are extremely high. Therefore, whenever possible, pump resonance effects should be eliminated within cw OPOs. However, there are two cases for which a high pump resonance can be utilized: First; within squeezed states of light experiments, where the objective is to detect equal numbers of signal

and idler photons generated within the OPO cavity. These experiments demand that the useful output coupling of both fields is significantly higher than the intra-cavity parasitic losses. Therefore, when the output coupling is specified at, for example, $\approx 5\%$ for both the signal and idler fields, then the threshold increases substantially above most cw laser sources. Now, pump enhancement techniques can be utilized to return the OPO threshold to the mW-level. Second; within cascaded (serial) OPO stages where high external conversion efficiencies are required. In this case, the higher OPO output powers can be obtained by sacrificing one OPO resonance constraint for that of the pump frequency within the OPO cavity, thus forming a pump-enhanced singly-resonant oscillator. However, the practical design of such systems places extremely high specifications on the coatings at the pump frequency, in order to attain high enhancement factors. In general, practical pump-enhanced systems will operate with pump power thresholds that are an order of magnitude higher than straight-forward doubly-resonant oscillators. This is because the signal and idler fields (as generated within the OPO cavity) can always be chosen to be significantly greater than those possible for an enhanced intra-cavity pump field which is critically dependent on the balance (impedance) of the intra-cavity loss to the input coupling parameter.

During the course of these studies, several important experiments were reported by other groups in the field of cw OPOs. These are now considered, and related to the progress made within the thesis.

The first cw singly-resonant oscillator has been reported in reference [1]. The material used for this was KTP in the type II non-critical phase-matching geometry. The pump power threshold, with a single-pass pump field, was $P_{p-th} = 4.3\text{ W}$, and this was provided by the second harmonic frequency of a lamp-pumped Nd:YAG laser. As expected, the OPO operated free-running on a single-frequency mode-pair, and could be tuned smoothly in frequency over a range defined by the resonant cavity free spectral range ($\Delta\nu \approx 0.55\text{ GHz}$). However, at present, such a system cannot be extended to other nonlinear materials or other pump sources. This is a consequence of the threshold level reported in this experiment. To obtain multi-watt pump power levels in the green spectral region for the above experiment, two lamp-pumped Nd:YAG laser heads were incorporated into one laser system that provided $P_p \approx 24\text{ W}$ cw single-frequency power at the fundamental wavelength of $\lambda = 1.064\text{ }\mu\text{m}$. The lack of pump sources producing cw single-frequency output powers at this level represents the first limitation of cw singly-resonant oscillators. To

operate an equivalent cw OPO pumped at $\lambda = 1.064 \mu\text{m}$ would require a cw single-frequency pump power source that produced $P_p \approx 35 \text{ W}$. The high power levels also represent a problem with regard to focused power densities and material damage; the nonlinear materials with higher effective nonlinear coefficients have low damage intensities (MgO:LiNbO₃ and KNbO₃); the material with the highest cw damage threshold, LBO, has a significantly lower effective nonlinear coefficient, and would require power levels an order of magnitude greater than the KTP based device, described above. Therefore, currently-available pump sources and nonlinear materials dictate that truly singly-resonant cw OPOs will be few in number.

More significant advances have been made by other groups when using type II phase-matched geometries with low threshold, doubly-resonant oscillators. Specifically, type II phase-matched geometries are now widely recognized as critical to the development of cw OPOs [2 - 5]. A highly stable KTP OPO, described in reference [6], has been used to generate a cw 3 THz span wideband optical frequency comb, by using the idler frequency output of the OPO as the input for a LiNbO₃ phase-velocity-matched modulator. The frequency comb was utilized to lock the signal-idler difference frequency at $\Delta\nu = 665 \text{ GHz}$. In such a scheme, the output of the doubly-resonant oscillator can be phase-locked to a microwave source beyond the bandwidth of detector systems. Such an experiment allows the OPO to be tuned systematically over a range of several-THz with the precision of a microwave synthesizer, and will be critical within an OPO-based optical frequency counting system, as outlined in reference [7].

Following the success of the dual-cavity oscillator described in this thesis, subsequent demonstrations of other dual-cavity OPOs in type II phase-matched geometries have confirmed the suitability of this technique for providing improved frequency control in doubly-resonant OPOs [4, 5]. The dual-cavity resonator will play a fundamental role in any future application of cw OPOs. However, to date, all dual-cavity OPOs have relied upon polarization splitting of the intra-cavity fields allowed within type II phase-matched geometries. The realization of a dual-cavity oscillator within a type I phase-matching arrangement will enable new nonlinear materials, that can only provide type I non-critical phase-matching, to be used to generate high-precision, frequency tunable OPO radiation. Such intra-cavity separation is likely to be provided from low loss beam-splitters or prisms.

A further development has been the application of a single-frequency diode-laser as the direct pump source for a cw OPO [5]. The nonlinear material used was, once again, type II phase-matched KTP and the OPO outputs were tunable in the near infra-red spectral region. The emergence of widely-tunable and narrow-linewidth diode lasers throughout the visible spectral region will prove essential for the incorporation of cw OPOs within diode-laser based frequency chains, spanning the optical spectrum.

In contrast to most texts on OPOs in which the widely-tunable aspect of their performance is promoted as their most desirable attribute, this thesis has chosen to address particular issues for which tunable radiation is but one of several priorities. When considering specifically the role of cw OPOs with regard to generating widely-tunable cw radiation, it is important to evaluate the availability of other more convenient sources and current research trends, both of which point towards the use of single-frequency diode lasers as the preferred sources of tunable cw radiation.

Another topic discussed exclusively in this text has been the use of birefringence to offset material dispersion, thereby providing equal phase-velocities for the three waves. However, recently, the technique of using guided wave and periodic structures has attracted considerable interest. In this case, phase-matching is achieved by introducing a periodicity in the structure that modifies the propagation constants or the sign of the nonlinear coefficients: quasi-phase-matching. This allows for new phase-matching geometries with large nonlinearities, and can overcome some of the limitations inherent to birefringent phase-matching. This method could be important for manipulating currently available nonlinear materials (in particular LiNbO_3) for use with cw lasers out to $\approx 4 \mu\text{m}$. However, in the short term, quasi-phase-matching may prove more advantageous for single-pass difference frequency mixing [8].

CW OPOs are now under development at half a dozen research laboratories around the world, and this number will probably increase within the next few years. New nonlinear materials are urgently required before cw OPOs can provide integer related pump, signal, and idler frequencies, that will make them suitable to be incorporated directly as practical optical frequency dividers. When this happens, cw OPOs will form indispensable components within optical frequency metrology schemes.

References.

1. S. T. Yang, R. C. Eckardt, & R. L. Byer,
"1.9-W cw ring-cavity KTP singly resonant optical parametric oscillator,"
Opt. Lett. **19**, 475 (1993).
2. L. R. Brothers, D. Lee & N. C. Wong,
"Terahertz optical frequency comb generation and phase locking of an optical
parametric oscillator at 665 GHz,"
Opt. Lett. **19**, 245 (1994).
3. T. Debuisschert, A. Sizmann, E. Giacobino, & C. Fabre,
"Type-II continuous-wave optical parametric oscillators: oscillation and frequency-
tuning characteristics,"
J. Opt. Soc. Am. B **10**, 1668 (1993).
4. D. Lee & N. C. Wong,
"Tuning characteristics of a cw dual-cavity KTP optical parametric oscillator,"
in *Conference on Lasers and Electro-Optics*, Vol. 8 of OSA 1994 Technical Digest Series
(Optical Society of America, Washington, D. C., 1994), paper CWE 5.
5. R. Knappe, J. Barschke, C. Becher, B. Beier, M. Scheidt, K.-J. Boller, & R. Wallenstein,
"Injection-locked high power diode arrays and their application as pump sources for
blue and green Nd:YAB lasers, monolithic Nd:YAG ring lasers, and cw KTP optical
parametric oscillators,"
in *Conference on Lasers and Electro-Optics*, Vol. 8 of OSA 1994 Technical Digest Series
(Optical Society of America, Washington, D. C., 1994), paper CThL 4.
6. D. Lee & N. C. Wong,
"Stabilization and tuning of a doubly-resonant optical parametric oscillator,"
J. Opt. Soc. Am. B **10**, 1659 (1993).
7. N. C. Wong,
"Optical frequency counting from the UV to the near IR,"
Opt. Lett. **17**, 1155 (1992).
8. S. Sanders, D. W. Nam, R. J. Lang, M. L. Bortz, & M. M. Fejer,
"Generation of 3.0 μm radiation by quasi-phasematched difference frequency mixing of
near IR laser diode wavelengths in LiNbO_3 waveguides,"
in *Conference on Lasers and Electro-Optics*, Vol. 8 of OSA 1994 Technical Digest Series
(Optical Society of America, Washington, D. C., 1994), paper CThD 4.

Acknowledgements.

The work carried out over the past four years could not have been possible without the assistance of several people.

I am grateful to Malcolm Dunn for securing the initial funding for the cw OPO research programme in collaboration with Patrick Gill at the National Physical Laboratory. I appreciate their continued support and encouragement over the course of the contract.

I owe particular thanks to Miles Padgett for his voluntary enthusiasm, commitment, and perseverance. Although not always appreciated to begin with, his constructive advice and criticism has been the single most important factor in hastening some of the cw OPO achievements over the past three years, many of which are discussed within the thesis.

I am grateful for the suggestions of both Wilson Sibbett and David Hanna regarding improvements to the layout and content of the thesis.

The efficiency and friendliness of the administrative and domestic staff within the department allowed for a pleasant and effective environment in which to study. I would like to thank all the cleaners, secretaries, librarians, and workshop technicians for their support and assistance.

Bearing in mind that the construction of OPOs will always be considerably easier than building a reliable laser source, I would like to thank the *Spectra-Physics* engineers for maintaining the trouble-free operation of the argon-ion laser.

Further departmental credits for both cw-laser and OPO performance characteristics are given to Nigel, Sara, Callum, Hong, Bruce, and Majid, to whom all the queries within the thesis should be directed. For being in the same Ph.D boat (often sinking), and knowing how it feels: Cameron, Christian, Angus, Neil, Fiona, Jorma, Jason, Zhang etc...

Finally, to the one that is to me quite simply the best; for joint suffering throughout the thesis writing, for contributing to the grammar/layout of the thesis, for having an endless supply of love, and for placing her trust in the future: many thanks Miss H. Bunch.

Glossary of Symbols.

The following list of symbols does not include all the varieties formed by adding suffices, nor does it include all the cases where a symbol is used as a measure of physical dimensions. The subscripts p , s , and i refer to the pump, signal, and idler frequencies respectively. The subscripts $stab$ and hop refer to the requirements, on the relevant parameters, to maintain single signal / idler mode-pair operation.

b	confocal parameter, dispersive constant.
c	velocity of light.
d	diameter, distance, nonlinear coefficient.
d_{eff}	effective nonlinear coefficient.
f	focal length.
f_c	characteristic focal length.
h	Planck's constant.
\bar{h}_m	reduction factor.
k	wave-vector magnitude.
l	crystal length.
m	longitudinal mode number.
n	refractive index.
\bar{n}	average of signal / idler refractive indices, average thermal photon number.
r	field amplitude reflection, radial distance.
t	field amplitude transmission.
A	field amplitude.
B	double refraction parameter.
E	field enhancement factor, electro-magnetic field.
F	finesse.
I	current, photon flow, intensity.
I_{dam}	damage threshold intensity.
L	cavity length.
M	cavity mirror, spatial coupling factor.
M_{cl}	number of modes between clusters.
N	photon number.
N_{cl}	number of modes within a cluster.
P	polarization, power.

R	power coefficient of reflection, radius of curvature, quantum noise reduction factor.
T	power coefficient of transmission, temperature.
W	Gaussian beam radius.
ΔI	signal / idler intensity difference.
ΔL	cavity length detuning.
ΔT	temperature detuning.
AR	anti-reflecting.
BS	beam-splitter.
FSR	free spectral range.
FSR_{int}	interferometer free spectral range.
HR	highly-reflecting.
ROC	radius of curvature.
ΔFSR	mis-match in signal and idler free spectral ranges.
$ \alpha ^2$	normalized photon flow.
β	power loss, intra-cavity parasitic power loss.
χ	coupling coefficient.
χ_s	electrical susceptibility.
δ	difference frequency, phase-shift, degeneracy factor,
ϵ_0	permittivity of free space.
ϕ	angle to crystallographic axis.
φ	linear phase-shift.
γ	field loss / transmission coefficient, field decay rate.
η_{ext}	external conversion efficiency.
κ	coupling coefficient.
λ	light wavelength.
μ	absorption / loss coefficient.
μ_0	permeability of free space.
ν	frequency.
ν_{ref}	reference frequency.
θ	angle to crystallographic axis, phase-shift, full angle divergence.
ρ	absorption coefficient, resistivity, Poynting vector walk-off.
σ	pumping level.
Δ	relative round-trip detuning.
$\Delta\nu$	frequency detuning / mis-match.
$\Delta\nu_{g-b}$	gain bandwidth.
$\delta\varphi$	phase-detuning.

Appendix.

- I An approximate value to the walk-off allowed in continuous-wave optical parametric oscillators.

- II Listing of mode-selection computer program.

- III Publications & conference proceedings.

Appendix I.

An approximate value to the walk-off allowed in continuous-wave optical parametric oscillators.

The analysis of this thesis has dealt specifically with non-critical phase-matching geometries in which the effects of Poynting vector walk-off are absent.

In general, for critically phase-matched geometries, and when focusing to small spot sizes that satisfy confocal focusing, the pump power threshold is increased substantially. However, it is important to determine exactly at what point walk-off causes the pump power threshold to increase to a value outwith the reach of cw laser sources.

The pump power threshold is assumed to be directly proportional to the reduction factor, $\bar{h}_m(B, \xi)$, as defined in reference [1]; i.e.

$$P_{p-th}^{in} \propto \bar{h}_m(B, \xi) . \quad [A. 1]$$

For cw laser sources, the point at which the threshold is increased by one order of magnitude is taken as the critical limit for cw doubly-resonant oscillation. Therefore, this represents a reduction factor of

$$\bar{h}_m(B, \xi) \approx 0.1 . \quad [A. 2]$$

To simulate the focusing conditions considered within this thesis, equal confocal parameters are maintained in this analysis. However, at the reduction level as given by equation [A. 2], confocal focusing still corresponds to near-optimum focusing conditions. Therefore

$$\xi = \frac{L}{b} = 1 , \quad [A. 3]$$

where all the terms have their usual meanings. Now consider figure A. 1 which displays the gain reduction factor $\bar{h}_m(B, \xi)$, plotted against ξ , for different values of the double-refraction parameter, B , which is defined as [1]

$$B = \frac{\rho}{2} \sqrt{\frac{\pi L n_p}{\lambda_p}}, \quad [\text{A. 4}]$$

where ρ is the radian angle of Poynting vector walk-off (angle between the energy propagation direction and the wave-vector direction). It takes on the value of zero for non-critical phase-matching, and has a finite value in critically phase-matched geometries. The other terms have their usual meanings.

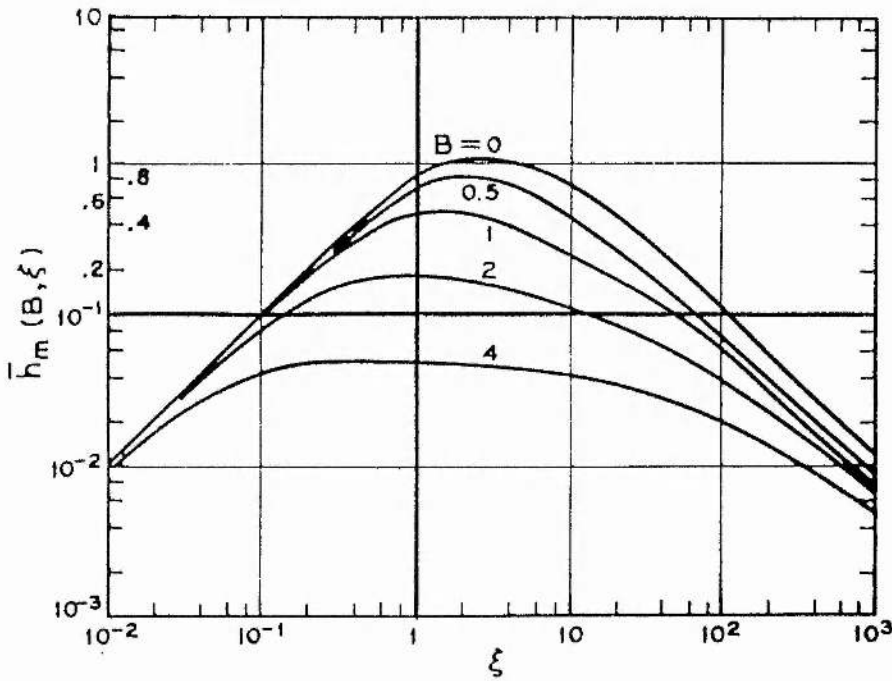


Figure A. 1.

Gain reduction factor (y-axis) against the focusing parameter (x-axis), for different values of the double-refraction parameter, in doubly-resonant optical parametric oscillators (from reference [1]).

From figure A. 1, and assuming confocal focusing (vertical line), gain reductions by a factor of ten (horizontal line) occur for a double-refraction parameter of approximately

$$B \approx 3 . \quad [A. 5]$$

Combining equations [A. 4] and [A. 5] yields the radian walk-off angle that causes an increase in threshold by one order of magnitude as

$$\rho \approx 6 \sqrt{\frac{\lambda_p}{\pi L n_p}} = 6 \sqrt{\frac{2}{k_p L}} . \quad [A. 6]$$

For example, consider a pump wavelength at $\lambda_p \approx 0.5 \mu\text{m}$, a crystal length of $L \approx 20 \text{ mm}$, and a pump refractive index in the nonlinear medium of $n_p \approx 1.6$. This provides a cw walk-off limit of $\rho \approx 0.0134 \text{ rads} \approx 0.77^\circ$.

Reference.

1. G. D. Boyd & D. A. Kleinman,
"Parametric interaction of focused Gaussian light beams,"
J. Appl. Phys. 39, 3597 (1968).

Appendix II.

Listing of mode-selection computer program.

```
OPEN "Cavity length = 30mm" FOR OUTPUT AS #1
cav0#=.030
GOSUB prog
CLOSE #1
```

```
END
```

```
outputinfo:
```

```
WINDOW 5
```

```
PRINT:PRINT:PRINT
```

```
PRINT "Calculation of parametric gain in a single-cavity doubly-resonant OPO"
```

```
PRINT
```

```
PRINT "Copyright: M. J. Padgett, F. G. Colville, & M. H. Dunn, Dept. of Physics & Astronomy,  
University of St. Andrews, Fife, Scotland, April 1994, Version 4.6"
```

```
PRINT
```

```
PRINT "Nonlinear material: LBO"
```

```
PRINT "Type II, non-critical phase-matching, optimized for 825 THz pump input"
```

```
PRINT
```

```
PRINT "Form of data input as follows"
```

```
PRINT "Frequencies: Hz"
```

```
PRINT "Temperature: °C"
```

```
PRINT "Crystal and cavity lengths: m"
```

```
PRINT "Press <return> to get default values"
```

```
RETURN
```

```
fileheader:
```

```
PRINT #1,CHR$(9);
```

```
PRINT #1,T#;
```

```
PRINT #1,CHR$(9);
```

```
PRINT #1,CHR$(9);
```

```
PRINT #1,cav0#;
```

```
PRINT #1,CHR$(9);
```

```
PRINT #1,CHR$(9);
```

```
PRINT #1,Lp#;
```

```
PRINT #1,CHR$(9);
```

```
PRINT #1,CHR$(9);
```

```
PRINT #1,Lsnpm#;
```

```
PRINT #1,CHR$(9)
```

```
RETURN
```

```
prog:
```

```
REM Program to calculate parametric gain for single-cavity doubly-resonant OPO signal and  
idler mode-pairs
```

```
REM M. J. Padgett, F. G. Colville, & M. H. Dunn; April 1992
```

```
DIM STATIC pthresh$(12,15)
```

```
GOSUB constants
```

```
GOSUB setwindows
```

```
Wp#=8246200000000000#:cry#=.02:finesse&=500
```

```
Winc#=10000000000#:moderange&=1000:T#=20
```

```
cavinc#=5E-11:cavrange#=5E-08
```

```
cav#=cav0#-cavrange#
```

```
GOSUB outputvariables
```

```
GOSUB findphasematch
```

```
GOSUB outputphasematch
```

```
GOSUB fileheader
```

```
WHILE cav#<cav0#+cavrange#
```

```
Lp#=3000000000000000#/Wp#
```

```
GOSUB outputvariables
```

```

REM GOSUB findphasematch
GOSUB outputphasematch
GOSUB findcentremode
GOSUB startmodeno
GOSUB findpmin
REM GOSUB outputcentremode
GOSUB initpthresh
GOSUB searchmodes
GOSUB rankmodes
REM GOSUB outputmodelosses
GOSUB writefile
cav#=cav#+cavinc#
WEND
RETURN

```

writefile:

```

Length=(cav#-cav0#)*1E+09
PRINT #1,USING"###.#####";Length;
PRINT #1,CHR$(9);
FOR n=1 TO 5
PRINT #1,;pthresh#(1,n);
PRINT #1,CHR$(9);
PRINT #1,USING"#####";pthresh#(12,n);
PRINT #1,CHR$(9);
NEXT
PRINT #1,CHR$(9)
RETURN

```

setwindows:

```

WINDOW 1,"Input parameters",(5,50)-(490,325),7
WINDOW 2,"Phase-matching condition",(5,70)-(490,325),7
WINDOW 3,"Signal mode at centre of phase-match",(5,90)-(490,325),7
WINDOW 4,"15 lowest loss modes",(5,50)-(490,325),7
WINDOW 5,"Set up info",(5,50)-(490,325),7
WINDOW 6,"Mode details",(5,50)-(490,340),7
RETURN

```

searchmodes:

```

WINDOW 4
PRINT"Searching for mode clusters"
nsguess#=nspm#
jumpmode&=0
ms&=msstart&
WHILE ms&<msfinish&
ms&=ms&+jumpmode&
n#=nsguess#:m&=ms&
GOSUB Wsmodecalc
Ws#=W#:Ls#=L#:ns#=n#
nsguess#=ns#
Wiguess#=Wp#-Ws#
Liguess#=3000000000000000#/Wiguess#
L#=Liguess#
GOSUB nxcalc
niguess#=n#
n#=niguess#:L#=Liguess#
GOSUB mcalc
mi&=m&
n#=niguess#:m&=mi&

```

```

GOSUB Wimodecalc
Wi#=W#:Li#=L#:ni#=n#
niguess=ni#
dW#=Wp#-Wi#-Ws#
REM PRINT ms&,dW#
jumpmode&=INT(ABS(dW#/4E+08)+1)
IF ABS(dW#) >100000000# THEN GOTO loopend
Ws#=Ws#+dW#/2
Wi#=Wi#+dW#/2
Ls#=3000000000000000#/Ws#
Li#=3000000000000000#/Wi#
L#=Ls#
GOSUB nycalc
ns#=n#
L#=Li#
GOSUB nxcalc
ni#=n#
GOSUB dkcalc
GOSUB dklosscalc
GOSUB flosscalc
pthresh#=(3.1415/finesse&)^2*floss#/dkloss#
REM GOSUB outputmodedetails
GOSUB assessmode
loopend:
WEND
RETURN

dklosscalc:
IF dk#=0 THEN dkloss#=1 ELSE dkloss#=(SIN(dk#*cry#/2)/(dk#*cry#/2))^2
RETURN

flosscalc:
FSR#=c#/(2*(cry#*((ni#+ns#)/2)+cav#-cry#))
floss#=1+(finesse&*dW#/FSR#)^2
RETURN

assessmode:
REM PRINT"assessmode"
IF pthresh# < pthresh#(12,15) THEN GOSUB replacemode
RETURN

replacemode:
REM PRINT"replace mode"
GOSUB arrayload15
FOR n=1 TO 14
IF pthresh#(12,15) < pthresh#(12,n) THEN GOSUB swapmode15
NEXT n
RETURN

swapmode15:
FOR m=1 TO 12
temp#=pthresh#(m,15)
pthresh#(m,15)=pthresh#(m,n)
pthresh#(m,n)=temp#
NEXT m
RETURN

```

```
reordermodes:
FOR m=1 TO 12
temp#=pthresh#(m,n+1)
pthresh#(m,n+1)=pthresh#(m,n)
pthresh#(m,n)= temp#
NEXT m
RETURN
```

```
rankmodes:
PRINT "rankmodes"
FOR P=1 TO 14
FOR n=1 TO 14
IF pthresh#(12,n+1) < pthresh#(12,n) THEN GOSUB reordermodes
NEXT n
NEXT P
RETURN
```

```
arrayload15:
pthresh#(1,15)=ms&
pthresh#(2,15)=Ws#
pthresh#(3,15)=Ls#
pthresh#(4,15)=mi&
pthresh#(5,15)=Wi#
pthresh#(6,15)=Li#
pthresh#(7,15)=dW#
pthresh#(8,15)=ms&+mi&
pthresh#(9,15)=dk#
pthresh#(10,15)=dkloss#
pthresh#(11,15)=floss#
pthresh#(12,15)=pthresh#
RETURN
```

```
outputmodedetails:
PRINT "mode cluster"
PRINT "ms= "ms&
PRINT "Ws= "Ws#
PRINT "mi= "mi&
PRINT "Wi= "Wi#
PRINT "mi+ms= "mi&+ms&
PRINT "∂W= "dW#
PRINT "∂k= "dk#
PRINT "∂kloss= "dkloss#
PRINT "floss= "floss#
PRINT "pthresh= "pthresh#
RETURN
```

```
initpthresh:
FOR n=1 TO 15
pthresh#(12,n)=1
NEXT n
RETURN
```

```
outputmodelosses:
WINDOW 4
PRINT:PRINT:PRINT
PRINT " ";
PRINT"ms";PRINT" ";PRINT"Ws";
PRINT" ";
```

```

PRINT"mi";PRINT" ";PRINT"Wi";
PRINT" ";
PRINT"pthresh"
FOR n=1 TO 15
PRINT USING "#####";pthresh#(1,n);PRINT" ";
PRINT USING "##.#####^";pthresh#(2,n);PRINT" ";
PRINT USING "#####";pthresh#(4,n);PRINT" ";
PRINT USING "##.#####^";pthresh#(5,n);PRINT" ";
PRINT USING "##.#####";pthresh#(12,n)
NEXT n
RETURN

```

```

constants:
c#=3E+08
RETURN

```

```

collectvariables:
WINDOW 1
INPUT"Pump centre frequency? ",D#
IF D#>0 THEN P#=D#
INPUT"Pump detuning? ",D#
IF D#<>0 THEN dp#=D#
INPUT"Temperature? ",D#
IF D#>0 THEN T#=D#
INPUT"Cavity length? ",D#
IF D#>0 THEN cav#=D#
INPUT"Crystal length? ",D#
IF D#>0 THEN cry#=D#
INPUT"Finesse? ",D&
IF D&>0 THEN finesse&=D&
INPUT"Moderange? ",D&
IF D&>0 THEN moderange&=D&
RETURN

```

```

outputvariables:
WINDOW 1
REM PRINT:PRINT:PRINT
REM PRINT "Pump frequency = "Wp#
REM PRINT "Pump wavelength = "Lp#
REM PRINT
PRINT "Temperature = "T#
PRINT
PRINT "Cavity length = "cav#
PRINT "Crystal length = "cry#
REM PRINT
REM PRINT "Cavity finesse = "finesse&
REM PRINT
REM PRINT "Mode range = "moderange&
RETURN

```

```

findphasematch:
WINDOW 2
Lp#=3000000000000000#/Wp#
Ws1#=1.145*Wp#/2
Wi1#=Wp#-Ws1#
Ls1#=3000000000000000#/Ws1#
Li1#=3000000000000000#/Wi1#
L#=-Ls1#

```

```

GOSUB nycalc
ns1#=n#
L#=Li1#
GOSUB nxcalc
ni1#=n#
L#=Lp#
GOSUB nxcalc
np#=n#
Ws#=Ws1#:ns#=ns1#:Wi#=Wi1#:ni#=ni1#
GOSUB dkcalc
dk1#=dk#
Ws2#=Ws1#-Winc#
Wi2#=Wp#-Ws2#
Ls2#=3000000000000000#/Ws2#
Li2#=3000000000000000#/Wi2#
L#=Ls2#
GOSUB nycalc
ns2#=n#
L#=Li2#
GOSUB nxcalc
ni2#=n#
Ws#=Ws2#:ns#=ns2#:Wi#=Wi2#:ni#=ni2#
GOSUB dkcalc
dk2#=dk#
WHILE dk1#*dk2#>0
dk1#=dk2#
Ws2#=Ws2#-Winc#
Wi2#=Wp#-Ws2#
Ls2#=3000000000000000#/Ws2#
Li2#=3000000000000000#/Wi2#
L#=Ls2#
GOSUB nycalc
ns2#=n#
L#=Li2#
GOSUB nxcalc
ni2#=n#
Ws#=Ws2#:ns#=ns2#:Wi#=Wi2#:ni#=ni2#
GOSUB dkcalc
PRINT dk#
dk2#=dk#
WEND
Wsnpm#=Ws2#:Winpm#=Wi2#:nsnpm#=ns2#:ninpm#=ni2#:dknpm#=dk2#
Lsnpm#=Ls2#:Linpm#=Li2#
RETURN

```

outputphasematch:

```

WINDOW 2
REM PRINT:PRINT:PRINT
REM PRINT "Pump frequency = "Wp#
PRINT "Pump wavelength = "Lp#
PRINT "Pump refractive index = "np#
PRINT "Temperature = "T#
PRINT
REM PRINT "Nominal phase-matched signal frequency = "Wsnpm#
PRINT "Nominal phase-matched signal wavelength = "Lsnpm#
PRINT "Signal refractive index = "nsnpm#
REM PRINT
REM PRINT "Nominal phase-matched idler frequency = "Winpm#

```

```
PRINT "Nominal phase-matched idler wavelength = "Linpm#
PRINT "Idler refractive index = "ninpm#
REM PRINT
REM PRINT "dk= "dknprm#
RETURN
```

```
findpmin:
pmin#=(3.1415/finesse&)^2
RETURN
```

```
findcentremode:
n#=nsnpm#:L#=Lsnpm#
GOSUB mcalc
mspm&=m&
GOSUB Wsmodecalc
Wspm#=W#:Lspm#=L#:nspm#=n#
Witpm#=Wp#-Wspm#
Litpm#=3000000000000000#/Witpm#
L#=Litpm#
GOSUB nxcalc
nitpm#=n#
GOSUB mcalc
mi&=m&
GOSUB Wimodecalc
Wipm#=W#:Lipm#=L#:nipm#=n#
dW#=Wp#-Wspm#-Wipm#
Wspm#=(Wspm#+dW#)/2
Wipm#=(Wipm#+dW#)/2
Lspm#=3000000000000000#/Wspm#
Lipm#=(3000000000000000#/Wipm#)
L#=Lspm#
GOSUB nycalc
ns#=n#
L#=Lipm#
GOSUB nxcalc
ni#=n#
Ws#=Wspm#:Wi#=Wipm#
GOSUB dkcalc
dkpm#=dk#
RETURN
```

```
mcalc:
m&=INT((2000000#*((cav#-cry#)+(cry#*n#))/L#)+.5)
RETURN
```

```
startmodeno:
msstart&=mspm&-moderange&
msfinish&=mspm&+moderange&
n#=nstpm#:m&=msstart&
GOSUB Wsmodecalc
Wsstart#=W#:Lsstart#=L#:nsstart#=n#
Wistart#=Wp#-Wsstart#
Listart#=3000000000000000#/Wistart#
L#=Listart#
GOSUB nxcalc
nistart#=n#
Ws#=Wsstart#:ns#=nsstart#:Wi#=Wistart#:ni#=nistart#
GOSUB dkcalc
```

```

dkstart#=dk#
n#=#nstpm#:m&=#msfinish&
GOSUB Wsmodecalc
Wsfinish#=W#:Lsfinish#=L#:nsfinish#=n#
Wifinish#=Wp#-Wsfinish#
Lifinish#=3000000000000000#/Wifinish#
L#=#Lifinish#
GOSUB nxcalc
nifinish#=n#
Ws#=#Wsfinish#:ns#=#nsfinish#:Wi#=#Wifinish#:ni#=#nifinish#
GOSUB dkcalc
dkfinish#=dk#
RETURN
outputcentremode:
WINDOW 3
PRINT:PRINT:PRINT
PRINT "Phase-matched signal mode number = "mspm&
PRINT "Phase-matched signal frequency = "Wspm#
PRINT "Phase-matched signal wavelength = "Lspm#
PRINT "Refractive index at signal frequency = "nspm#
PRINT "dk at phase-matched mode = " dkpm#
PRINT
PRINT "Start signal mode number = "msstart&
PRINT "dk at start = "dkstart#
PRINT "Finish signal mode number = "msfinish&
PRINT "dk at finish = "dkfinish#
PRINT
PRINT "Minimum parametric gain = "pmin#
RETURN

```

```

Wimodecalc:
L1#=#(2000000#*((cav#-cry#)+(cry#*n#)))/m&
W1#=#3000000000000000#/L1#
L#=#L1#
GOSUB nxcalc
L2#=#(2000000#*((cav#-cry#)+(cry#*n#)))/m&
W2#=#3000000000000000#/L2#
WHILE ABS(W1#-W2#) > 1#
W1#=#W2#
L#=#L2#
GOSUB nxcalc
L2#=#(2000000#*((cav#-cry#)+(cry#*n#)))/m&
W2#=#3000000000000000#/L2#
WEND
W#=#W2#:L#=#L2#
RETURN

```

```

Wsmodecalc:
L1#=#(2000000#*((cav#-cry#)+(cry#*n#)))/m&
W1#=#3000000000000000#/L1#
L#=#L1#
GOSUB nycalc
L2#=#(2000000#*((cav#-cry#)+(cry#*n#)))/m&
W2#=#3000000000000000#/L2#
WHILE ABS(W1#-W2#) > 1#
W1#=#W2#
L#=#L2#
GOSUB nycalc

```

```
L2#=(2000000#*((cav#-cry#)+(cry#*n#)))/m&
W2#=3000000000000000#/L2#
WEND
W#=W2#:L#=L2#
RETURN
```

```
nycalc:
n#=2.53969+(.01249/(L#^2-.01339))-(.02029*L#^2)
n#=SQR(n#)
n#=n#-(.0000136#*(T#-20))
RETURN
```

```
nxcalc:
n#=2.45316+(.0115/(L#^2-.01058))-(.01123*L#^2)
n#=SQR(n#)
n#=n#-(.000001#*(T#-20))
RETURN
```

```
nzcalc:
n#=2.58515+(.01412/(L#^2-.00467))-(.0179132*L#^2)-(0.000417214#*L#^4)+(7.651830000000001D-
06*L#^6)
n#=SQR(n#)
n#=n#-((.0000061#-.0000021#*L#)*(T#-20))
RETURN
```

```
dkcalc:
dk#=2*3.1415*((np#*Wp#)-(ns#*Ws#)-(ni#*Wi#))/c#
RETURN
```

Appendix III.

Publications.

F. G. Colville, A. J. Henderson, M. J. Padgett, J. Zhang, & M. H. Dunn,

"Continuous-wave parametric oscillation in lithium triborate,"

Opt. Lett. **18**, 205 (1993).

F. G. Colville, M. J. Padgett, A. J. Henderson, J. Zhang, & M. H. Dunn,

"Continuous-wave parametric oscillator pumped in the ultra-violet,"

Opt. Lett. **18**, 1065 (1993).

F. G. Colville, M. J. Padgett, & M. H. Dunn,

"Continuous-wave, dual-cavity, doubly-resonant optical parametric oscillator,"

Appl. Phys. Lett. **64**, 1490 (1994).

F. G. Colville, M. Ebrahimzadeh, W. Sibbett, & M. H. Dunn,

"Continuous-wave LiB_3O_5 optical parametric oscillator pumped by a tunable Ti:sapphire laser,"

Appl. Phys. Lett. **64**, 1765 (1994).

M. J. Padgett, F. G. Colville, & M. H. Dunn,

"Mode selection in doubly resonant optical parametric oscillators,"

IEEE J. Quantum Electron. **QE-30**, (1994).

A. J. Henderson, M. J. Padgett, F. G. Colville, J. Zhang, & M. H. Dunn,

"Doubly-resonant optical parametric oscillators: tuning behaviour and stability requirements,"

Submitted to Opt. Comm., 1994.

T. R. Stevenson, F. G. Colville, M. H. Dunn, & M. J. Padgett.

"Doubly-resonant optical parametric oscillator formed by index-matching cavity mirrors directly onto an uncoated LiB_3O_5 crystal,"

Submitted to Opt. Lett., 1994.

M. H. Dunn, F. G. Colville, A. J. Henderson, M. J. Padgett, & G. Robertson.

"Continuous frequency tuning of optical parametric oscillators,"

Submitted to J. Opt. Soc. Amer. B, 1994.

Conference proceedings.

F. G. Colville, M. J. Padgett, A. J. Henderson, J. Zhang, & M. H. Dunn,
"Continuous-wave optical parametric oscillator pumped in the ultra-violet,"
in *Conference on Lasers and Electro-Optics*, OSA 1993 Tech. Digest Series, paper CPD15.

F. G. Colville, M. J. Padgett, A. J. Henderson, J. Zhang, & M. H. Dunn,
"Continuous-wave lithium triborate optical parametric oscillators,"
in *Technical Digest of Papers*, at the Eleventh UK National Quantum Electron. Conf., paper 4.

F. G. Colville, M. J. Padgett, and M. H. Dunn,
"Continuous-wave, dual-cavity, doubly-resonant optical parametric oscillators,"
in *Digest on Advanced Solid-State Lasers*, OSA 1994 Tech. Digest Series, paper AWA3.

F. G. Colville, M. J. Padgett, & M. H. Dunn,
"Smooth frequency tuning from optical parametric oscillators: the transition from single- to dual-cavity resonators,"
in *Advanced Solid-State Lasers*, T. Y. Fan & B. H. T. Chai, eds., Vol. 20 of OSA Proceedings Series (Opt. Soc. of America, Washington, D. C., 1994) pp 438 - 442.

F. G. Colville, M. Ebrahimzadeh, W. Sibbett, & M. H. Dunn,
"Continuous-wave LiB_3O_5 optical parametric oscillator pumped by a tunable Ti:sapphire laser,"
in *Conference on Lasers and Electro-Optics*, OSA 1994 Tech. Digest Series, paper CTuK19.

M. Ebrahimzadeh, D. T. Reid, F. G. Colville, W. Sibbett, & M. H. Dunn,
"Continuous-wave and femtosecond optical parametric oscillators of LBO and KTP pumped by tunable Ti:sapphire lasers,"
at *Institute of Physics Annual Congress, Advances in Solid-State Lasers*, paper 5 (1994).

T. R. Stevenson, F. G. Colville, M. H. Dunn, & M. J. Padgett.
"Doubly-resonant optical parametric oscillator formed by index-matching cavity mirrors directly onto an uncoated LiB_3O_5 crystal,"
submitted to *Conference on Lasers and Electro-Optics*, OSA 1995 Tech. Digest Series.

Continuous-wave parametric oscillation in lithium triborate

Finlay G. Colville, Angus J. Henderson, Miles J. Padgett, Jun Zhang, and Malcolm H. Dunn

J. F. Allen Physics Research Laboratories, Department of Physics and Astronomy, University of St. Andrews, North Haugh, St. Andrews, Fife KY16 9SS, UK

Received September 9, 1992

We demonstrate a continuous-wave optical parametric oscillator that uses lithium triborate as the nonlinear material in a temperature-tuned noncritical phase-matched type I geometry. Pumped at 514.5 nm, the triply resonant oscillator has a threshold of 50 mW. We obtain peak output powers of 90 mW corresponding to a 10% external conversion efficiency and measure a tuning range of 0.966 to 1.105 μm , limited by the bandwidth of the mirrors. Operating the optical parametric oscillator both at and away from degeneracy, we observe rapid changes in output power as a function of cavity length owing to competition between signal and idler mode pairs.

Experiments on cw optical parametric oscillators (OPO's) began in the late 1960's and used crystals of $\text{Ba}_2\text{NaNb}_5\text{O}_{15}$ (Ref. 1) and LiNbO_3 (Ref. 2) as the nonlinear materials. During the 1980's, attention switched to the newly developed crystals of $\text{MgO}:\text{LiNbO}_3$ (Ref. 3) or KTP (Ref. 4) and their implementation within various novel geometries, including a diode-pumped monolithic ring.³ In this Letter we report what is to our knowledge the first demonstration of LiB_3O_5 (LBO) as the nonlinear material in a cw OPO. LBO has several advantages over previously used materials,⁵ offering a higher damage threshold and a wider optical transparency that extends into the UV. These properties, along with the possibility of temperature-tuned noncritical phase matching, make LBO a promising choice for cw OPO applications.

A critical parameter in the design of all OPO's is the pump power required to reach threshold. The threshold pump power is proportional to the losses at signal, idler, and pump wavelengths.⁶ For pulsed operation it is usually sufficient for the OPO cavity to be resonant at either the signal or the idler wavelength (i.e., low loss for signal or idler). Such devices are described as singly resonant oscillators. However, to reduce the threshold to a level compatible with cw operation, it is usually necessary to make the OPO cavity resonant at both signal and idler wavelengths (i.e., low loss at signal and idler). This is called a doubly resonant oscillator (DRO). A further reduction in threshold can be achieved by making the OPO cavity resonant at all three wavelengths, i.e., making it a triply resonant oscillator (TRO). The transition from DRO to TRO is somewhat complex, since the efficient conversion of the pump itself represents a source of loss at the pump wavelength. In addition, a high cavity finesse at the pump wavelength can make it difficult to couple the pump energy into the cavity efficiently owing to stringent mode-matching requirements.

In DRO's the output wavelengths of signal and idler fields are overconstrained, since, in addition to satisfying the requirement for energy conservation (i.e., $\omega_i + \omega_s = \omega_p$), the lowest overall loss is attained

when the signal and idler frequencies match those of a cavity mode and also satisfy the phase-matching condition.⁷ For a cavity common to signal and idler fields, it is difficult to satisfy all these conditions simultaneously, and the lowest loss is achieved at a compromise between detuning of the signal and idler frequencies away from the cavity modes and the phase-matched condition. As the cavity length or the pump frequency is scanned, the overall loss (and hence output power) is modulated as the output of the OPO hops from one signal and idler mode pair to the next. Many such mode hops occur within the free spectral range of the OPO cavity, and the exact behavior depends critically on the mismatch between the free spectral ranges for signal and idler fields.⁸ TRO's display an additional complexity in that the pump field also has to be held on a resonance of the OPO cavity. Despite this, we have chosen to resonate the pump field weakly because by doing so it is possible to assess the cavity alignment and the mode matching of the pump beam into the cavity.

Our experimental setup is shown in Fig. 1. The LBO crystal is cut for type I noncritical phase matching ($\theta = 90^\circ$, $\phi = 0^\circ$), with dimensions of 3, 3, and 20 mm along the y , z , and x principal optical

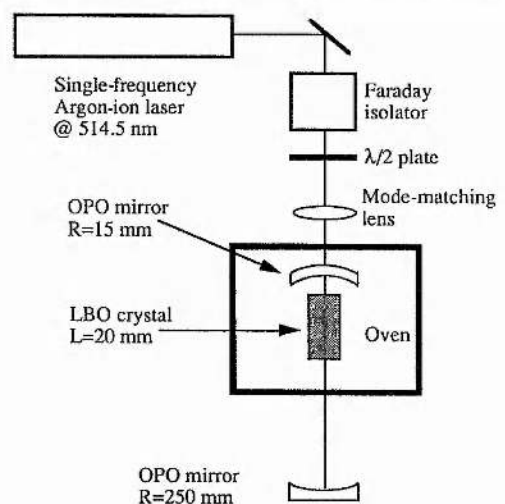


Fig. 1. Schematic of the experimental setup.

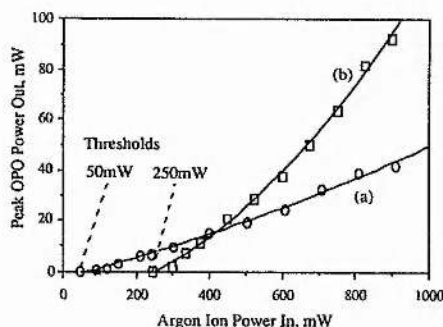


Fig. 2. Peak OPO output power (idler plus signal) as a function of input pump power for the high reflector [curve (a)] and the output coupler [curve (b)].

axes, respectively, and placed inside a temperature-controlled oven to achieve the desired phase matching. The crystal has a dual antireflection coating applied to each face for the pump wavelength at 514.5 nm and for the OPO idler-signal operation around the degenerate wavelength of 1.029 μm . This design maximizes the effective nonlinear coefficient to be $d_{\text{eff}} = 1.24 \text{ pm/V}$ and provides the lowest possible value of threshold for the OPO. The pump source is a commercial cw argon-ion laser, operating at 514.5 nm on a single longitudinal mode. A Faraday isolator is used to prevent backreflections and backconversion from interacting with the single-longitudinal-mode operation of the argon-ion laser, and a 150-mm focal-length lens is used to mode match the pump beam into the OPO cavity. The OPO cavity is formed by a 15-mm-curvature input mirror located inside the oven, approximately 7 mm from the crystal, and an external 250-mm-curvature output mirror, with a mirror separation of approximately 270 mm. This cavity design allows space inside the resonator for any required additional optics while forming a waist size for the signal and idler fields of 45 μm ($1/e$ electric-field radius) at the center of the 20-mm crystal, with a Boyd-Kleinman focusing factor $h(B=0, \xi=1) \approx 1.9$. A focusing parameter of $\xi=1$ corresponds to confocal focusing. In addition, the input coupling mirror is designed with its rear surface concentric with the front, therefore greatly reducing the focusing effects of the substrate on the input beam and thus easing alignment. The external mirror is chosen to be either a similar high reflector or an output coupler that is 0.5% transmitting at 1.029 μm . All mirrors have reflectivities of 60% at the pump wavelength of 514.5 nm.

The OPO cavity is hence strongly resonant at signal and idler wavelengths and weakly resonant at the pump wavelength, with a measured finesse at 514.5 nm of 6.0 (as expected from the mirror reflectivities). We have found that poor impedance and mode matching limits the coupling efficiency of the pump beam into the OPO cavity to 45%. Allowing for the resonant enhancement of the pump field, the intracavity field strength is approximately equal to the incident power, and therefore we use the expression for a DRO to predict the required pump power to reach threshold.

The pump threshold power for a DRO at degeneracy, with a unity Boyd-Kleinman focusing parameter is given by¹⁰

$$P_p^{\text{th}} = \frac{\beta^2 c n_p^2 \epsilon_0 \lambda_p^3}{8\pi^2 d_{\text{eff}}^2 L}, \quad (1)$$

where β is the round-trip power loss at degeneracy of signal or idler fields, c is the velocity of light in free space, n_p is the refractive index of the medium at the pump wavelength, ϵ_0 is the permittivity of free space, d_{eff} is the effective nonlinear coefficient, and L is the crystal length.

By using a Nd:YAG laser to measure the degradation in finesse of a high- Q cavity on insertion of the crystal, we deduce the round-trip crystal losses to be $\sim 0.4\%$. Allowing for parasitic mirror loss (0.05% per mirror), the above equation predicts pump power thresholds of 20 mW for the high reflector and 50 mW for the output coupler. The measured thresholds are 50 and 250 mW, respectively, values that are significantly higher than predicted theoretically. At this stage we believe that this may be due to poor temperature uniformity within the oven, which reduces the effective length of the crystal.

Figure 2 shows the measured output power from the OPO when it is slightly detuned from degeneracy for incident pump powers of as much as 900 mW. At present, the passive stability of our cavity is insufficient to maintain the OPO on a single signal

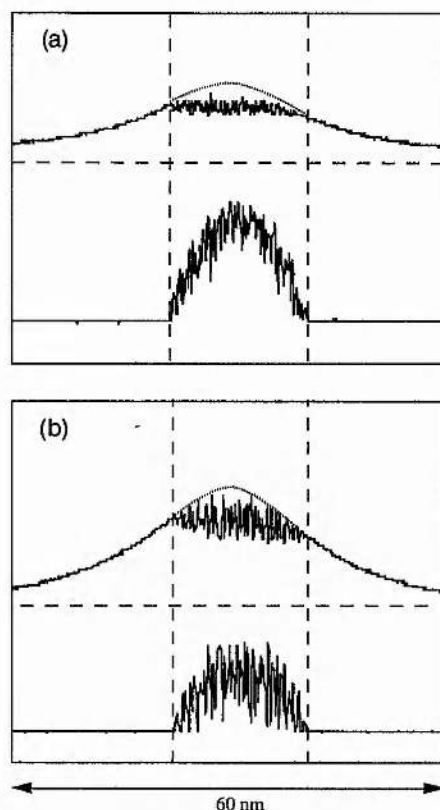


Fig. 3. Pump transmission and OPO output as a function of cavity length, tuned (a) very close to and (b) slightly removed from degeneracy, for a pump power of 500 mW. The upper traces show the pump depletion, and the lower traces show the OPO operation.

and idler mode pair. The cavity length is scanned by using a piezoelectric-mounted output mirror, and the OPO hops between adjacent signal and idler mode pairs. The OPO output and pump depletion are recorded by using a photodiode and a fast storage oscilloscope. In the region of a pump resonance, the OPO is above threshold, and analysis of the OPO output shows that the peak power is approximately twice the average output power. Figures 3(a) and 3(b) display the pump depletion and OPO output with 500-mW incident pump power when the OPO is tuned (a) close to and (b) slightly removed from degeneracy.

For an incident pump power of 900 mW and the output coupler mirror, an average output power of 46 mW is obtained, which corresponds to a peak power of approximately 90 mW and a maximum external conversion efficiency of 10%. Degenerate operation of the oscillator is obtained at approximately 183 °C, and tuning from 0.966 to 1.105 μm is possible for a 3 °C temperature shift. This is limited only by the bandwidth of the mirror and crystal coatings. The degenerate phase-matching temperature is in agreement with results from reported second-harmonic generation¹¹ with LBO as the doubling material.

Figure 3 shows pump depletion and OPO output as a function of cavity length for both degenerate and nondegenerate operation. The rapid modulation of the OPO output is a result of the competition between neighboring signal and idler mode pairs. Subnanometer changes in cavity length may cause the output of the OPO to hop to the $n_s \pm 1$ and $n_i \mp 1$ modes, where n_s and n_i are the mode numbers of the signal and idler modes, respectively. By starting from a condition of perfect coincidence of both signal and idler frequencies with the cavity modes, a change in the length of the cavity causes a detuning of the cavity modes away from the signal and idler frequencies and hence an increase in the overall loss. For degenerate operation, the free spectral ranges for signal and idler modes are equal, and a small change in cavity length causes a mode hop to an adjacent mode pair, and hence the low-loss condition is maintained. Away from degeneracy, the free spectral ranges are slightly mismatched and a larger change in cavity length is required to select the adjacent mode pair. It follows that the maximum detuning between the signal and idler fields from the nearest cavity modes, before a mode hop, increases with the mismatch in the free spectral ranges and therefore with the detuning away from degeneracy. Consequently, Fig. 3(b) (nondegenerate) shows a greater modulation in output power than Fig. 3(a) (degenerate).

In conclusion, we have demonstrated a low-threshold (50 mW), high-external-efficiency (10%) cw LBO OPO with output powers as high as 90 mW for 900 mW of 514.5-nm pump input. The OPO is tunable from 0.966 to 1.105 μm for a 3 °C temperature shift. In addition, we have observed

the rapid fluctuations in output power owing to changes in cavity length that cause mode hopping between adjacent signal and idler mode pairs.

Given the transparency range of LBO from 160 nm to 2.6 μm ,⁵ a temperature-tuned, noncritical phase-matching, type I geometry OPO of this kind, when pumped by a green cw single-longitudinal-mode source, should give cw output at any signal-idler pair from approximately 670 nm to 2.6 μm . In addition to the argon-ion laser, possible pump sources include a frequency-doubled diode-pumped solid-state laser (e.g., Nd:YAG or Nd:YLF). We are currently investigating this tuning range with a particular interest in developing OPO's that operate with signal-to-idler ratios of 2:1 and 3:1, thus acting as optical frequency dividers.

The low threshold powers that we have obtained suggest two extensions to this study. First, it may be possible to make a singly resonant oscillator cw OPO that typically would require ~ 100 times more pump power, i.e., ~ 5 W, which can be obtained from an argon-ion laser. Second, currently available UV cw lasers have sufficient power output to pump a LBO OPO above threshold. This could be achieved by using a UV line from an argon-ion laser or a frequency-tripled diode-pumped Nd:YAG laser. With a type II geometry, this would give continuous tuning throughout the visible spectrum and beyond.

Malcolm H. Dunn gratefully acknowledges the financial support of a Royal Society Leverhulme Trust Senior Research Fellowship. This research is supported by a contract with the National Physical Laboratory, Teddington, UK.

References

1. R. G. Smith, J. E. Geusic, H. J. Levinstein, J. J. Rubin, S. Singh, and L. G. Van Uitert, *Appl. Phys. Lett.* **12**, 308 (1968).
2. R. L. Byer, A. Kovrigin, and J. F. Young, *Appl. Phys. Lett.* **15**, 136 (1969).
3. C. D. Nabors, R. C. Eckardt, W. J. Kozlovsky, and R. L. Byer, *Opt. Lett.* **14**, 1134 (1989).
4. A. Heidmann, R. J. Herowicz, S. Reynaud, E. Giacobino, C. Fabre, and G. Camy, *Phys. Rev. Lett.* **59**, 2555 (1987).
5. C. Chen, Y. Wu, A. Jiang, B. Wu, G. You, R. Li, and S. Lin, *J. Opt. Soc. Am. B* **6**, 616 (1989).
6. R. Fisher and L. A. Kulevskii, *Sov. J. Quantum Electron.* **7**, 135 (1977).
7. R. C. Eckardt, C. D. Nabors, W. J. Kozlovsky, and R. L. Byer, *J. Opt. Soc. Am. B* **8**, 646 (1991).
8. M. Padgett and M. H. Dunn, "Mode selection in doubly resonant optical parametric oscillators," *IEEE J. Quantum Electron.* (to be published).
9. G. D. Boyd and D. A. Kleinman, *J. Appl. Phys.* **39**, 3597 (1968).
10. S. E. Harris, *Proc. IEEE* **57**, 2096 (1969).
11. T. Ukachi, R. J. Lane, W. R. Bosenberg, and C. L. Tang, *Appl. Phys. Lett.* **57**, 980 (1990).

Continuous-wave parametric oscillator pumped in the ultraviolet

F. G. Colville, M. J. Padgett, A. J. Henderson, J. Zhang, and M. H. Dunn

J. F. Allen Physics Research Laboratories, Department of Physics and Astronomy, University of St. Andrews, North Haugh, St. Andrews, Fife KY16 9SS, Scotland

Received March 18, 1993

We demonstrate what is to our knowledge the first continuous-wave optical parametric oscillator pumped by an ultraviolet source. An argon-ion laser operating at 364 nm is used to pump the nonlinear material lithium triborate, which generates tunable radiation in the blue-green and near-infrared spectral regions. With the cavity stabilized to stay on a single-frequency mode pair, we measure a threshold of 115 mW and a maximum output power of 103 mW. By use of a noncritical phase-matched, type II geometry, tuning ranges from 502 to 494 nm (signal) and 1.32 to 1.38 μm (idler) are observed.

Continuous-wave optical parametric oscillators (OPO's) have been recognized for 30 years as potential sources for generating widely tunable single-frequency visible radiation. The first cw OPO's used either $\text{Ba}_2\text{NaNb}_5\text{O}_{15}$ or LiNbO_3 as the nonlinear material, pumped by argon-ion lasers operating in the blue-green spectral region at 488–514.5 nm or frequency-doubled Nd:YAG lasers at 532 nm. The output from these OPO's was highly erratic, and for many years other sources of tunable radiation were preferred, despite the potential of OPO's for narrow-linewidth output over an extensive tuning range.¹ Researchers studying squeezed states of light² renewed interest in cw OPO's by extending their operation to recently available materials with improved optical quality (KTP and $\text{MgO}:\text{LiNbO}_3$). By use of stable pump sources, cw OPO's finally provided reliable single mode-pair selection.³ However, the pump wavelengths have remained within the aforementioned blue-green spectral region. Currently, cw OPO's are regarded as promising devices for optical frequency division,⁴ which requires OPO's to operate with pump sources extending from the UV to the infrared and at widely spaced signal-idler wavelengths.

Pump sources in the blue-green spectral region have been favored partly because the threshold pump power scales as the third power of the pump wavelength (i.e., $P_p^{\text{th}} \propto \lambda_p^3$).¹ For example, by frequency doubling of a Nd:YAG laser, the threshold is reduced by a factor of 8 and the threshold pump power for a cw OPO becomes within reach of the single-frequency power available. However, when one uses a pump source at $\approx 0.5 \mu\text{m}$, the OPO tuning range is confined to the red end of the visible spectrum and the near infrared. For the entire visible region to be accessed from the OPO, it is essential that the OPO be pumped with a UV source. Also, the shorter pump wavelength can significantly reduce the threshold. Therefore the nonlinear crystal for such as OPO must have wide optical transparency that encompasses the UV pump wavelength and the two OPO wavelengths. To date, the lack of a suitable nonlinear material with

an optical transparency extending into the UV has prevented progress in visible cw OPO's.

The development of the borate family of nonlinear crystals, and in particular lithium triborate⁵ (LBO), has led to renewed interest in tunable visible output. LBO has all the properties required for cw OPO's, including wide optical transparency (160 nm to 2.6 μm), moderate nonlinear coefficients ($>1 \text{ pm/V}$), and a high optical damage threshold [$>10 \text{ MW/cm}^2$ (Ref. 6)]. Recently we demonstrated what is to our knowledge the first cw operation of an OPO using LBO as the nonlinear medium. This OPO was pumped by a single-frequency argon-ion laser operating at 514.5 nm.⁷ The configuration exploited the type I noncritical phase-matching geometry and demonstrated the potential of LBO for cw OPO applications.

In this Letter we describe what is to our knowledge the first UV-pumped cw OPO. Pumping the OPO at 364 nm by a single-frequency argon-ion laser and using LBO as the nonlinear crystal, we demonstrate a threshold of 115 mW and a maximum external conversion efficiency of 9.4%. Despite the use of a free-running gas laser as the pump source, the advantages of nondegenerate operation permit stable single mode-pair operation of the OPO. As the crystal temperature is varied from 18 to 86 °C, tuning is from 502 to 494 nm (signal) and 1.32 to 1.38 μm (idler).

Figure 1 displays a schematic of the experimental arrangement used in the present studies. The pump source is a commercial cw argon-ion laser (Spectra-Physics 2045-E) operating at 364 nm on a single longitudinal mode. An acousto-optic (A-O) modulator prevents feedback of the pump wave into the cavity mode, which can perturb the single-frequency laser operation. A 225-mm focal-length lens mode matches the pump beam into the OPO cavity. The LBO crystal is cut for type II noncritical phase matching ($\theta = 0^\circ$, $\phi = 90^\circ$), with dimensions of 3, 3, and 20 mm along the x , y , and z principal optical axes, respectively. For this type II geometry at room temperature and a pump source at 364 nm, the Sell-

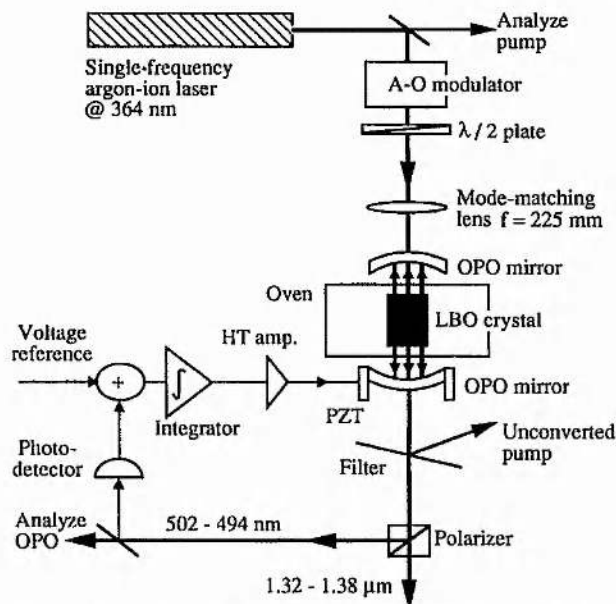


Fig. 1. Schematic of the experimental setup. HT amp., high-tension amplifier; PZT, piezoelectric transducer.

meier equations for LBO⁸ predict signal and idler wavelengths of 502 nm and 1.32 μm , respectively. Although the lowest thresholds are obtained by direct deposit of dielectric mirrors upon spherically curved crystal faces,³ we formed the resonator with external cavity mirrors. This is due to concerns regarding coating and polishing quality for what is a novel material for cw OPO's. However, such an approach will permit frequency-selective schemes involving intracavity components.

To ensure low losses, high demands are placed on the quality of the coatings for all three wavelengths. The crystal has a triple antireflection coating applied to both faces, specified to be >99.7% transmitting at the OPO wavelengths and >97% transmitting at the pump wavelength. The OPO cavity is formed by two 15-mm-curvature mirrors separated by ≈ 22 mm, placed symmetrically about the crystal, which is held in an oven to permit noncritical phase-matched tuning at elevated temperatures. The OPO employs a linear, standing-wave cavity with waist sizes for the signal and idler fields of ≈ 32 and ≈ 51 μm , respectively ($1/e$ electric-field radius), at the center of the crystal, with a Boyd-Kleinman focusing factor h ($B = 0$, $\xi = 1$) ≈ 1 .⁹ (A focusing parameter of $\xi = 1$ corresponds to confocal focusing.)

The OPO mirrors were specified to be $\approx 55\%$ reflecting at the pump wavelength and >99.7% reflecting at both 502 nm and 1.32 μm . The OPO cavity is strongly resonant at the OPO wavelengths and weakly resonant at the pump (finesse at the pump ≈ 5.2). Although the cavity becomes overconstrained by having to resonate all three wavelengths simultaneously, alignment is simplified by use of the pump resonance as a reference. In principle, resonating the pump field reduces the threshold of the OPO. However, for full benefit to be obtained, the dephasing of the three waves on the return pass must not diminish the gain obtained during the forward pass. We observed that $\approx 70\%$ of the incident pump

power was transmitted by the cavity on resonance below threshold, corresponding to a circulating field enhancement of ≈ 1.6 . This is less than the value, 2.2, expected from the mirror reflectivities, probably owing to imperfect mode matching. We have chosen to use the expression for a doubly resonant oscillator, with a double-pass field-enhanced pump, to predict the threshold pump power. Assuming a unity Boyd-Kleinman focusing parameter and that optimum relative phase shifts are maintained among the three waves on the return pass, the minimum threshold pump power is given by^{1,10}

$$P_p^{\text{th}} = \frac{\alpha_s \alpha_i n_p^2 c \epsilon_0 \lambda_p^3}{8\pi^2 d_{\text{eff}}^2 L (1 - \delta^2)^2 (1 + r_p)^2 \eta_p},$$

where α_s and α_i are the round-trip power losses of the signal and idler fields, respectively, c is the velocity of light in free space, n_p is the refractive index of the medium at the pump wavelength, ϵ_0 is the permittivity of free space, d_{eff} is the effective nonlinear coefficient, L is the crystal length, δ is the degeneracy factor,¹ r_p is the electric-field reflectivity of the output cavity mirror at the pump frequency (a value of 0.74), and η_p is the measured pump field enhancement ratio on resonance (a value of 1.6).

From the coating and crystal specifications, we estimate the round-trip power losses to be $\approx 2\%$ at both OPO wavelengths. If we take $d_{\text{eff}} = -1.15$ pm/V, the above equation predicts a threshold pump power of ≈ 20 mW. The experimental threshold is found to be 115 mW. This discrepancy can be accounted for by the uncertainty in the cavity losses, phase changes, beam degradation that is due to intermediate optics, and imperfect mode matching.

Using a piezoelectric-mounted mirror, we studied the OPO output and the transmitted pump as a function of cavity length. In the region of a pump resonance, when the circulating field intensity is above threshold, the OPO oscillates, and a corresponding

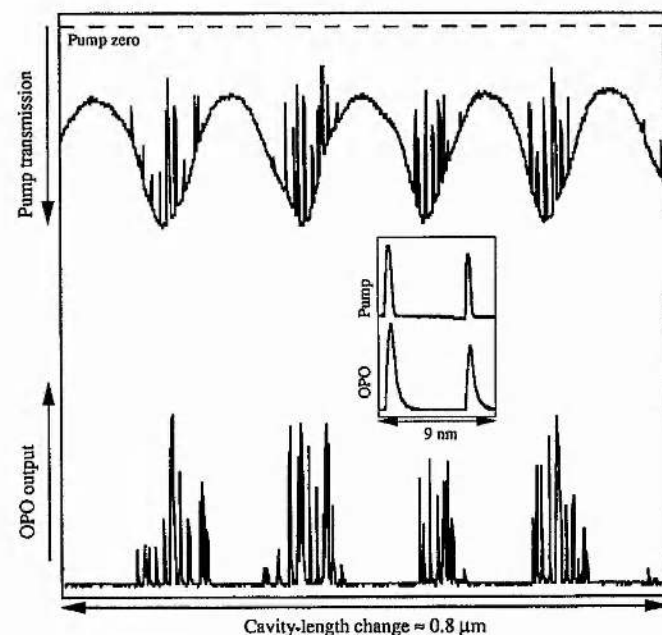


Fig. 2. Pump transmission and OPO output as a function of cavity length.

reduction in the transmitted pump is observed (see Fig. 2). The modulation of the OPO output is due to competition between different signal and idler mode pairs, characteristic of doubly resonant oscillators, and is caused by attempting to resonate simultaneously two frequencies in the same dispersive optical cavity.¹¹ Small changes in the cavity length or the pump frequency cause a mode hop to an adjacent mode pair or cluster (inset of Fig. 2). We observe hopping at cavity-length changes of between 5–7 nm. For a signal–idler mode pair at 502 and 1320 nm, the free spectral ranges are mismatched by $\approx 3\%$, and for these conditions the measured length change is consistent with hopping to an adjacent mode pair in the same cluster.

All demonstrations of single-frequency output from cw OPO's have been for near-degenerate OPO's, which can require high degrees of stability on both the pump and OPO resonator lengths.¹¹ By selection of frequencies whose cavity free spectral ranges are mismatched to a large extent, the stability requirements are substantially relaxed.¹² In this experiment such a mismatch enables us to obtain stable single-frequency output despite a relatively unstable pump source ($\approx \pm 10$ MHz). The dc voltage from a photodetector monitoring the signal output is compared with a reference voltage, and the difference is used to servo control the OPO cavity length (see Fig. 1). This arrangement enabled us to hold the OPO on a single peak in the power output variation with cavity length (inset of Fig. 2). Under this condition, the signal wave was monitored with a scanning interferometer and seen to be single frequency.

A maximum of 103-mW total OPO output (signal plus idler) was achieved for an incident pump power of 1.1 W (external conversion efficiency of 9.4%). By increasing the ratio of useful to parasitic losses, one can obtain higher slope efficiencies but at the expense of higher thresholds. Tuning is from 502 to 494 nm and 1.32 to 1.38 μm , at rates of -0.12 nm/ $^{\circ}\text{C}$ (signal) and $+0.88$ nm/ $^{\circ}\text{C}$ (idler), over the range 18 to 86 $^{\circ}\text{C}$, limited by the bandwidth of the coatings. By varying the crystal temperature from -30 to $+450$ $^{\circ}\text{C}$, we anticipate tuning ranges from 507 to 449 nm (signal) and 1.28 to 1.70 μm (idler). At ≈ 175 $^{\circ}\text{C}$, the two OPO frequencies would be in an exact 3:1 ratio.

In conclusion, we have demonstrated what is to our knowledge the first cw OPO pumped by a UV source. This experiment represents a step toward extending the range of frequencies provided from cw OPO's. We obtain a threshold of 115 mW, a maximum external conversion efficiency of 9.4%, and tuning over

8 nm in the visible and 60 nm in the infrared spectral regions. The 494-nm signal wavelength is to our knowledge the lowest ever generated by a cw OPO [the previous low was 640 nm (Ref. 13)]. The large mismatch in free spectral ranges has permitted stable operation of the OPO on a single frequency.

The argon-ion pump wavelength at 364 nm was selected because of its proximity to frequency-tripled diode-pumped all-solid-state laser sources (Nd:YAG at 355 nm or Nd:YLF at 349 nm). We aim to replace the argon-ion laser with one of these sources, which should result in an all-solid-state cw visible OPO. Further, by frequency quadrupling the radiation from an all-solid-state source and using the type II noncritical phase-matched geometry, we can produce tunable cw radiation near ≈ 300 nm. In the short term, we plan to construct further OPO's operating with frequencies in exact 3:1 ratios, as a step toward the parallel OPO scheme⁴ for optical frequency division.

M. H. Dunn gratefully acknowledges the financial support of a Royal Society Leverhulme Trust Senior Research Fellowship. This research program is supported by a contract with the National Physical Laboratory, Teddington, UK.

References

1. R. G. Smith, in *Lasers: A Series of Advances*, A. K. Levine and A. J. DeMaria, eds. (Dekker, New York, 1976), Vol. 4, p. 189.
2. L. Wu, M. Xiao, and H. J. Kimble, *J. Opt. Soc. Am. B* **4**, 1465 (1987).
3. C. D. Nabors, R. C. Eckardt, W. J. Kozlovsky, and R. L. Byer, *Opt. Lett.* **14**, 1134 (1989).
4. N. C. Wong, *Opt. Lett.* **17**, 1155 (1992).
5. C. Chen, Y. Wu, A. Jiang, B. Wu, G. You, R. Li, and S. Lin, *J. Opt. Soc. Am. B* **6**, 616 (1989).
6. S. T. Yang, C. C. Pohalski, E. K. Gustafson, R. L. Byer, R. S. Feigelson, R. J. Raymakers, and R. K. Route, *Opt. Lett.* **16**, 1493 (1991).
7. F. G. Colville, A. J. Henderson, M. J. Padgett, J. Zhang, and M. H. Dunn, *Opt. Lett.* **18**, 205 (1993).
8. S. Lin, J. Y. Huang, J. Ling, C. Chen, and Y. R. Shen, *Appl. Phys. Lett.* **59**, 1541 (1991).
9. G. D. Boyd and D. A. Kleinman, *J. Appl. Phys.* **39**, 3597 (1968).
10. J. E. Bjorkholm, A. Ashkin, and R. G. Smith, *IEEE J. Quantum Electron.* **QE-6**, 797 (1970).
11. R. C. Eckardt, C. D. Nabors, W. J. Kozlovsky, and R. L. Byer, *J. Opt. Soc. Am. B* **8**, 646 (1991).
12. M. J. Padgett, F. G. Colville, and M. H. Dunn, "Mode selection in doubly resonant optical parametric oscillators," *IEEE J. Quantum Electron.* (to be published).
13. C. Lawrence and F. Tittel, *J. Appl. Phys.* **42**, 2137 (1971).

Continuous-wave, dual-cavity, doubly resonant, optical parametric oscillator

F. G. Colville, M. J. Padgett, and M. H. Dunn

J. F. Allen Physics Research Laboratories, Department of Physics and Astronomy, University of St. Andrews, Fife, KY16 9SS, Scotland

(Received 25 August 1993; accepted for publication 28 December 1993)

We have demonstrated a continuous-wave optical parametric oscillator that uses separate optical cavities to resonate independently the nondegenerate signal and idler frequencies. The three-mirror cavity utilizes the type II phase-matching geometry in lithium triborate, with the orthogonally polarized signal and idler fields separated by an intracavity, dichroic-coated, Brewster-angled beam splitter. This dual-cavity oscillator can overcome mode and cluster hopping effects, which are characteristic of doubly resonant, continuous-wave optical parametric oscillators. We measure a pump power threshold of ≈ 200 mW and smooth tuning over ≈ 0.4 GHz. The tuning range is limited by pump resonance effects within the idler cavity.

Optical parametric oscillators (OPOs) are now widely regarded as practical devices for the generation of coherent radiation that is continuously tunable over exceptionally large spectral ranges.¹ In particular, continuous-wave (cw) operation of OPOs promises, in addition to extensive and continuous spectral coverage, the generation of narrow-linewidth and frequency-stable output.² Recently, there have been a number of proposals to apply cw OPOs to specific present-day challenges, including optical frequency division,³ wavelength division multiplexing,⁴ and gravitational wave detection.⁵ These proposals take advantage of the unique coherence properties of cw OPOs.⁶ Typically, the phase diffusion linewidth is in the mHz range, and the linewidths of the coherent, subharmonic OPO outputs are limited essentially by the input pump linewidth. Indeed, cw OPOs have been applied successfully to generate strongly correlated twin beams whose intensity correlation falls below the usual shot-noise level.⁷

To date, cw OPOs have operated with pump sources in the ultraviolet and blue/green spectral regions, and have been tuned over specific ranges between ≈ 0.5 and $2 \mu\text{m}$ by using a variety of nonlinear materials.^{2,7-14} As the optical quality of these nonlinear materials continues to improve, and developments in solid-state lasers increase the power and the spectral purity of available pump sources, cw OPOs providing the appropriate wavelength coverage and spectral quality to satisfy the above applications could become feasible. Presently, in addition to the need for extended spectral coverage, considerable work is required to increase substantially the range of smooth, continuous tuning from cw OPOs.

To operate cw OPOs with pump power thresholds at the mW level, it is essential to resonate both the signal and idler frequencies within the optical cavity. Indeed, such single-cavity doubly resonant OPOs (DROs), in which both the signal and idler fields are resonated by two common mirrors, have provided routinely sub-100 mW pump power thresholds. However, the constraints of maintaining two discrete frequencies simultaneously on resonance within a single cavity, has prevented the widespread use of cw OPOs. Perturbations in the pump frequency (\approx MHz) or the OPO cavity length (\approx nm) can cause mode and cluster hopping effects.¹³

Smooth tuning over GHz levels becomes easier by removing the necessity to resonate different optical fields within the same two-mirror cavity. This can be achieved by forming a singly resonant oscillator (SRO) where only one of the signal or idler fields is resonant. Often this method is applied with high peak-power pulsed pump sources. However, SRO thresholds are typically a factor of $\approx 10^3$ or more higher than DRO thresholds.¹⁴ Therefore, SRO thresholds are difficult to reach with cw pump sources. The attractive low threshold of the DRO can be combined with the prospect of smooth tuning by separating internally the signal and idler fields, and resonating the signal and idler frequencies in different optical cavities. This is the dual-cavity OPO, and we describe in this letter what we believe to be the first reported device of its kind.

The dual-cavity OPO uses the same pump source and nonlinear crystal as the single-cavity, two-mirror device that we described in Ref. 12. To summarize, the pump source is a single-frequency argon-ion laser operating at 364 nm and stabilized to an external etalon. We measure the short-term residual frequency fluctuations to be $\approx \pm 3$ MHz. The nonlinear crystal is lithium triborate (LBO), cut parallel to the z axis for noncritical phase matching ($\theta=0^\circ$, $\phi=90^\circ$), with dimensions of 3, 3, and 20 mm along the x , y , and z principal axes, respectively. The plane-parallel polished crystal faces have triple antireflection coatings deposited for the pump, at 364 nm, and the OPO frequencies. For room-temperature operation, the pump, at 364 nm, gives rise to signal and idler wavelengths at 502 and 1320 nm, respectively. In the single-cavity device, the OPO cavity is formed by two 15-mm-curvature mirrors that are highly reflecting at the OPO frequencies, and $\approx 55\%$ reflecting at the pump frequency, and situated within ≈ 5 mm of the crystal faces. Therefore, this single-cavity OPO is strongly resonant for the signal and idler frequencies (finesse of each ≈ 300), and weakly resonant at the pump frequency (finesse ≈ 5). The OPO operates with a threshold of 115 mW, and is temperature-tunable (20–85 °C) under noncritical phase-matching from 502 to 494 nm (signal) and 1.32 to 1.38 μm (idler), limited by the bandwidth of the coatings. By applying servocontrol on the length of the single cavity, the OPO can

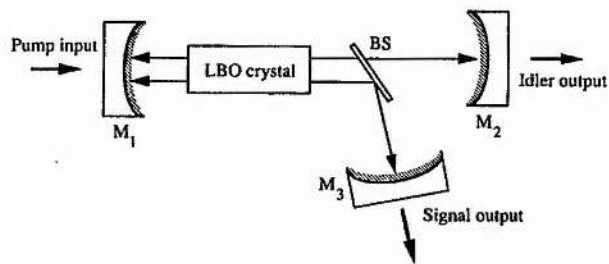


FIG. 1. Schematic representation of the dual-cavity, doubly resonant, optical parametric oscillator. The two OPO frequencies are separated internally by the beam splitter (BS). The idler and signal frequencies resonate between mirrors M_1 and M_2 , and M_1 and M_3 , respectively.

maintain operation on a single-frequency mode pair. Smooth tuning is prevented by the constraints of simultaneous resonance of two frequencies within a single cavity.

To form the dual-cavity OPO, a dichroic-coated, Brewster-angled beam splitter is inserted into the cavity to separate the signal and idler fields, and a third mirror is added to form a new resonator. Critical to the efficient operation of this dual-cavity OPO is the type II phase-matching geometry and the nondegenerate OPO frequencies. Type II phase matching provides orthogonally polarized signal and idler fields, allowing polarization decoupling; nondegeneracy allows effective dichroic-coating separation. The Brewster-angled beam splitter was coated to be $>99.7\%$ transmitting for the p -polarized idler wave at $\approx 1.32 \mu\text{m}$, and $>99.7\%$ reflecting for the s -polarized signal wave at $\approx 502 \text{ nm}$. In addition, the $>97\%$ transmission of this beam splitter for the p -polarized pump wave allowed the weak pump resonance to be maintained. This ensured that sufficient pump power was coupled effectively into the resonator to overcome threshold. A schematic of the cavity is displayed in Fig. 1, illustrating the separate optical cavities within the three-mirror arrangement. Threshold for the dual-cavity OPO was found to be $\approx 200 \text{ mW}$, indicating low round-trip power losses for both the OPO fields, even in the presence of the additional intra-cavity component.

Before applying any servocontrol feedback, it is important to ensure sufficient passive stability within the five-element resonator to maintain free-running single-frequency mode-pair operation. Critical to this was fixing the beam-splitter plate and the LBO crystal on a single block, and relying upon external pump-beam alignment for exact on-axis propagation. Cavity alignment was provided by micrometer control on the three flexure-hinged mirror mounts. The cavity components were attached to a single length-determining base plate, and surrounded by mechanical and acoustic isolation. Despite relatively poor short-term stability of the pump source, the OPO reliably held single-frequency mode-pair operation for periods of $\approx 20 \text{ s}$ (see Fig. 2). Therefore, the transition from a single to a dual-cavity configuration did not significantly degrade the passive stability of the OPO. To retain single-frequency operation, we are now able to adjust one of the cavity lengths to correct for length fluctuations in the other, or for perturbations in the pump frequency, thereby maintaining dual resonance for both the signal and idler fields. In addition, if one of the cavities is

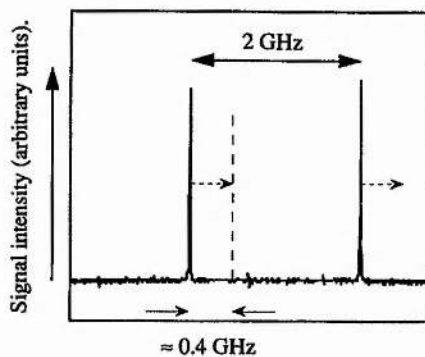


FIG. 2. Signal wave single-frequency trace, as monitored on a scanning interferometer of free spectral range 2 GHz.

servolocked, so as to follow the other, smooth tuning can be achieved by scanning this latter cavity.

As discussed, the pump is weakly resonant within the idler cavity. This resonance, although weak, provides an upper limit to the tuning possible from this particular dual-cavity OPO, which operates with a fixed nontunable pump frequency. When the pump is off resonance, insufficient pump radiation is coupled into the OPO, and threshold cannot be overcome. Specifically, the range over which the circulating pump field is sufficient to overcome threshold can be estimated by scanning the length of the pump-resonant cavity, and observing the range over which the OPO fluctuates between on and off. Figure 3 is such a pump resonance trace, similar to Fig. 2 in Ref. 12. From this trace, we measure a range of idler cavity lengths of $\approx 60 \text{ nm}$, over which tuning will be possible in our dual-cavity OPO. This cavity length shift for an idler frequency, corresponding to a wavelength of $1.32 \mu\text{m}$, implies an OPO frequency tuning range of $\approx \frac{1}{11}$ of the idler cavity free spectral range of $\approx 3.5 \text{ GHz}$. Therefore, by fine tuning the idler cavity length over 60 nm and servocontrolling the length of the signal cavity to maintain double resonance, we predict a smooth and continuous tuning range of $\approx 0.3 \text{ GHz}$. In practice, we have been able to demonstrate smooth tuning ranges of $\approx 0.4 \text{ GHz}$, limited, as expected, by the width of the pump resonance.

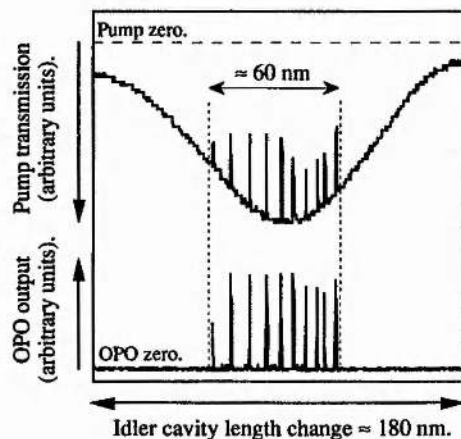


FIG. 3. Pump frequency resonance, showing the fraction of the cavity length available for smooth frequency tuning.

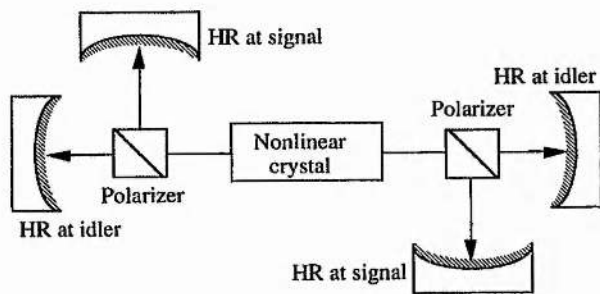


FIG. 4. Proposal for type II phase-matched DROs, in which coating specifications are considerably reduced. HR; high reflector.

Usually, pump resonance is eliminated by specifying the input coupling mirror (M_1 in Fig. 1) to be highly transmitting at the pump frequency, and relying upon sufficient single or double-pass parametric gain to reach threshold. However, since the main purpose of the input mirror is to be highly reflecting at the two OPO frequencies, it can be difficult to achieve any additional coating constraint without degrading reflectivity at one or both of the OPO frequencies. The problem of mirror coatings has led to almost exclusive use of cw OPOs that operate at, or very close to, frequency degeneracy, with more manageable dual-wavelength demands.

We propose a cavity geometry that greatly simplifies the coating specifications of type II phase-matched DROs, and further highlights the benefits of spatial separation within OPO cavities. If a second polarizer is placed within the cavity, and a fourth mirror added, the signal and idler fields will now resonate with their own pair of cavity mirrors (Fig. 4). Now, separate reflectivity coatings can be applied to cavity mirrors, important for optical frequency division, where OPO frequencies may be exact integral multiples of the pump frequency.

In conclusion, we have demonstrated a dual-cavity OPO which resonates the two nondegenerate OPO frequencies in separate cavities. The low threshold obtained allows its ap-

plication to OPOs pumped by that selection of pump sources that can presently provide >200 mW power output. The separate cavity-length control greatly aids frequency tuning. By fine tuning the idler cavity length, and servo-controlling the signal cavity length to maintain double resonance, we could tune the OPO over ≈ 0.4 GHz. In the absence of pump resonance, tuning should be possible over far greater ranges. Cavity lengths can be selected to provide frequency tuning that will only be limited by the allowable cavity-length translation from, for example, PZT, electro-optic, or temperature servo-control. In the short term, we are planning to extend operation to the four-mirror geometry, which will reduce the dependence on the pump frequency resonance. The suitability of the dual cavity to optical frequency division methods should assist progress toward OPO cavity designs that can provide the high specification required at all three frequencies.

This research is supported by a contract with the National Physical Laboratory, Teddington, U.K.

- ¹For reviews of cw OPOs, see R. L. Byer in *Treatise in Quantum Electronics*, edited by H. Rabin and C. L. Tang (Academic, New York, 1973), pp. 587–702, or the special edition of *J. Opt. Soc. Am. B* **10**, 1659 (1993).
- ²C. D. Nabors, S. T. Yang, T. Day, and R. L. Byer, *J. Opt. Soc. Am. B* **7**, 815 (1990).
- ³N. C. Wong, *Opt. Lett.* **15**, 1129 (1990).
- ⁴N. C. Wong, *IEEE Photon. Tech. Lett.* **4**, 1166 (1992).
- ⁵N. C. Wong, *Phys. Rev. A* **45**, 3176 (1992).
- ⁶R. Graham and H. Haken, *Z. Phys.* **210**, 276 (1968).
- ⁷A. Heidmann, R. J. Horowicz, S. Reynaud, E. Giacobino, C. Fabre, and G. Camy, *Phys. Rev. Lett.* **59**, 2555 (1987).
- ⁸R. G. Smith, J. E. Geusic, H. J. Levinstein, J. J. Rubin, S. Singh, and L. G. Van Uitert, *Appl. Phys. Lett.* **12**, 308 (1968).
- ⁹R. L. Byer, A. Kovrigin, and J. F. Young, *Appl. Phys. Lett.* **15**, 136 (1969).
- ¹⁰C. Laurence and F. Tittel, *J. Appl. Phys.* **42**, 2137 (1971).
- ¹¹R. G. Smith, *IEEE J. Quantum Electron.* **QE-9**, 530 (1973).
- ¹²F. G. Colville, M. J. Padgett, A. J. Henderson, J. Zhang, and M. H. Dunn, *Opt. Lett.* **18**, 1065 (1993).
- ¹³R. C. Eckardt, C. D. Nabors, W. J. Kozlovsky, and R. L. Byer, *J. Opt. Soc. Am. B* **8**, 646 (1991).
- ¹⁴S. T. Yang, R. C. Eckardt, and R. L. Byer, *Opt. Lett.* **18**, 971 (1993).

Continuous-wave LiB_3O_5 optical parametric oscillator pumped by a tunable Ti:sapphire laser

F. G. Colville, M. Ebrahimzadeh, W. Sibbett, and M. H. Dunn

J. F. Allen Physics Research Laboratories, Department of Physics and Astronomy, University of St. Andrews, North Haugh, St. Andrews, Fife KY16 9SS, Scotland

(Received 25 October 1993; accepted for publication 10 January 1994)

We have demonstrated a continuous-wave optical parametric oscillator that uses lithium triborate as the nonlinear material and a tunable Ti:sapphire laser as the pump source. By exploiting type I noncritical phase matching and a combination of temperature and pump frequency tuning, we have generated widely tunable radiation from 1.49 to 1.70 μm , limited by the bandwidth of the optical coatings. Total output powers of 30 mW and pump depletions of 40% have been obtained at two times the oscillation threshold of 360 mW. We discuss the application of this nonlinear frequency conversion process to several recently proposed experiments.

Continuous-wave (cw) optical parametric oscillators (OPOs) can provide highly coherent radiation, tunable over extensive spectral regions, and can operate efficiently and reliably with pump power thresholds at the mW level. They can generate frequency outputs that almost exactly reproduce the statistical properties of the pump source.¹ Recently, there has been considerable progress in the development of cw OPOs. By using a highly stable, monolithic $\text{MgO}:\text{LiNbO}_3$ OPO resonator, self-phase-locking at exact frequency degeneracy has been demonstrated by Nabors *et al.*² Tunable optical frequency division has been proposed by Wong,³ and subsequently demonstrated by Lee and Wong in a KTP OPO.⁴ Progress towards smooth frequency tuning has been provided by Yang *et al.* with the demonstration of the first cw singly resonant OPO,⁵ and by Colville *et al.* in the form of a dual-cavity, doubly resonant LBO OPO with independent signal and idler cavity-length control.⁶ cw OPOs have also been applied to generate nonclassical states of light, delivering twin beams whose intensity correlation falls below the shot-noise limit.⁷

These experiments have led to the development of frequency- and amplitude-stable devices, resulting in proposals to apply cw OPOs for a multichannel coherent optical communication system,⁸ as a gravitational-wave detector,⁹ and for an optical frequency comb generator.^{10,11} Many of these require the combination of tunable pump sources operating $\sim 0.8 \mu\text{m}$ and cw OPOs operating in the near-infrared spectral region. However, with the exception of Ref. 6, cw OPOs remain particularly limited in their frequency coverage, having operated mainly with fixed-frequency pump sources with wavelengths of $\approx 0.5 \mu\text{m}$ and tuning around frequency degeneracy ($\approx 1 \mu\text{m}$). To provide frequency tuning over wider spectral regions, it is highly advantageous to use a pump source whose operating frequency can itself be chosen to satisfy specific applications. Such multiple-parameter tuning is essential for reaching any frequency pair in the OPO phase-matching bandwidth. Therefore, the combination of a tunable pump source and a widely tunable cw OPO can potentially offer narrow-linewidth radiation over an unprecedented spectral range.

In this letter, we describe a widely tunable cw OPO which uses LiB_3O_5 (LBO) as the nonlinear material, and a

tunable laser as the pump source. Furthermore, we have operated the OPO in the 1.6 μm spectral region resulting in frequency coverage of 25 THz, from 1.49 to 1.70 μm , limited only by the bandwidth of the optical coatings. In particular, we explain the choice of the pump laser, nonlinear material, and the phase-matching geometry.

The configuration of the cw Ti:sapphire pumped OPO is depicted in Fig. 1. The pump source is a commercially available, cw Ti:sapphire laser (Schwartz Electro-Optics, Titan), which is configured in a unidirectional ring cavity and delivers single-frequency output power of $\approx 1 \text{ W}$ at $\approx 0.8 \mu\text{m}$ for $\approx 9 \text{ W}$ argon-ion input pump power. Without active stabilization, the frequency stability of the Ti:sapphire laser is at best $\approx \pm 5 \text{ MHz}$, although under normal laboratory conditions, a passive stability of $\approx \pm 15 \text{ MHz}$ is more representative. For the OPO gain medium, we chose lithium triborate (LBO).¹² LBO is one of several new nonlinear materials grown to high optical quality, and is commonly used in OPOs with high peak power, pulsed pump sources, providing extensive wavelength coverage from the ultraviolet through to its infrared transmission cutoff at $\approx 2.6 \mu\text{m}$. It was selected for its high damage threshold, low losses at 0.8 and 1.6 μm , moderate nonlinear coefficients, and most importantly, for temperature-tuned noncritical phase matching (NCPM) at the operating frequencies.

For cw OPOs, it is imperative to ensure that intracavity losses are reduced to a minimum. Consequently, degradation in the conversion efficiency from the effect of walkoff in

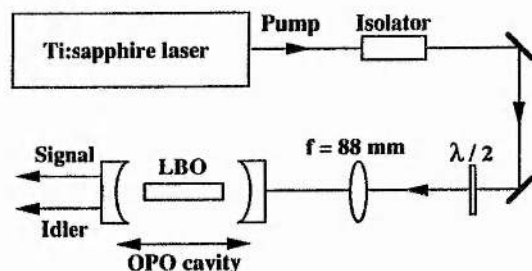


FIG. 1. Schematic representation of the experimental setup.

critical phase matching must be avoided when possible. In most cases, this dictates the use of NCPM, although the low walkoff in type II phase-matched KTP has permitted propagation at an angle of 25° from a principal axis.⁴ The lack of NCPM at frequency degeneracy in KTP^{13,14} and MgO:LiNbO₃ for pump sources at $\approx 0.8 \mu\text{m}$, has prompted the selection of LBO. When pumped at $\approx 0.8 \mu\text{m}$, the type I NCPM geometry of LBO can be temperature tuned, generating parallel-polarized signal and idler OPO frequencies. When operated near degeneracy, wide frequency tuning is possible for small variations in the crystal temperature.

The LBO crystal used in the experiment is cut for propagation along the x -axis ($\theta=90^\circ$, $\phi=0^\circ$), with dimensions of 3, 3, and 20 mm, along the y , z , and x principal optical axes, respectively. The pump wave is polarized along the y -axis and the generated signal/idler waves are polarized along the z -axis. The crystal has antireflection coatings applied to its faces for both the pump wavelength at $\approx 0.8 \mu\text{m}$, and near-degenerate OPO wavelengths $\sim 1.6 \mu\text{m}$. The single-pass transmission loss of the crystal is specified to be $<1\%$ at $0.8 \mu\text{m}$ and $<0.25\%$ at $1.6 \mu\text{m}$. The crystal is placed at the intracavity focus of a linear, near-concentric resonator, formed by two mirrors of 25 mm radius of curvature. These mirrors are located at ~ 17 mm from the crystal faces, and coated to be highly reflecting ($R>99.7\%$) at $\sim 1.6 \mu\text{m}$, forming a high finesse, low loss resonator for the signal and idler frequencies. In addition, these mirrors are highly transmitting for the pump frequencies, thus ensuring single pass, nonresonant, pump interaction. The pump beam is focused to a spot size ($1/e$ electric field radius) of $\approx 40 \mu\text{m}$, at the center of the nonlinear material. A Faraday isolator is located between the Ti:sapphire laser and the OPO cavity to prevent feedback into the pump laser.

We set the confocal parameters of the OPO waves equal to the crystal length. The linear, standing-wave cavity provides spot sizes of $\approx 56 \mu\text{m}$ for the OPO frequencies, maximizing the spatial mode overlap between the pump and the OPO waves, and further lowering the threshold to a level compatible with the cw pump source. The LBO crystal is enclosed within a temperature-controlled oven and heated to temperatures between ≈ 130 and $\approx 185^\circ\text{C}$, to satisfy NCPM.

Two different modes of tuning can be investigated with the present arrangement. First, by operating the Ti:sapphire laser at a fixed frequency, the OPO can be temperature-tuned under NCPM to provide signal and idler frequency pairs around degeneracy. Second, by maintaining the LBO crystal at a constant temperature, the pump frequency can be tuned to generate further signal and idler pairs. By varying the frequency of the pump laser and heating the LBO crystal to the appropriate phase-matching temperatures, the OPO could be tuned from 1.49 to $1.70 \mu\text{m}$. The tuning curves for four specific pump wavelengths are displayed in Fig. 2. Typically, tuning over >20 THz could be obtained for a temperature change of $\approx 4^\circ\text{C}$. This range is limited only by the bandwidth of the present optical coatings. By selecting different crystal/mirror coatings, further tuning ranges over the whole of the $1\text{--}2 \mu\text{m}$ spectral region can be accessed readily.

The threshold for the OPO was found to be 360 mW. Assuming an effective nonlinear coefficient of 1.2 pm/V for

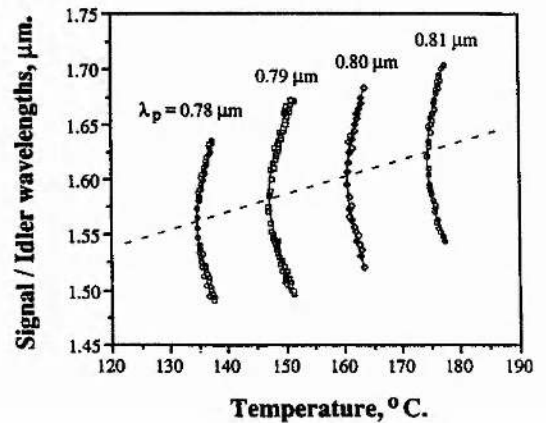


FIG. 2. OPO temperature tuning under noncritical phase matching for four specific pump wavelengths. The dashed line illustrates the near-linear relationship between temperature and degenerate OPO operation for these operating wavelengths.

LBO¹² and optimum mode-matching of the pump beam into the resonator, this threshold value implies round-trip signal/idler power losses of $\approx 1.6\%$, or a cavity finesse of ≈ 400 at $1.6 \mu\text{m}$. By reducing the requirements on optical coatings, through for example monolithic crystal fabrication,² longer crystal samples, or by double passing the pump wave through the gain medium,⁴ lower thresholds should be possible. Pump depletions of up to $\approx 40\%$ and peak output powers (signal+idler) of ≈ 30 mW were obtained when operating at around two times the operating threshold, consistent over most of the spectral coverage.

In doubly resonant OPOs, small perturbations in the pump frequency ($\approx \text{MHz}$) or the cavity length ($\approx \text{nm}$) cause large power fluctuations in the OPO, with mode and cluster hopping. The frequency tuning characteristics of the type I phase-matching geometry around frequency-degeneracy have been studied extensively by Eckardt *et al.*¹⁵ In particular, a single mode-pair output from the OPO demands the use of pump lasers stabilized to kHz levels, and sub-nm OPO cavity-length control. Since the principal objective of this letter is to highlight the range of coarse tuning under NCPM, no attempt has been made to operate the OPO on a single signal/idler mode pair, and to date both the pump source and the OPO cavity length have been operated passively without any servocontrol. Therefore the OPO output is subject to mode and cluster hopping. However, by using a stable pump source and OPO cavity, and in keeping with the results from other workers,^{2,15} we would expect the OPO to operate reliably on a single signal and idler mode pair. (Presently, commercial Ti:sapphire lasers can achieve frequency stabilities within ≈ 50 kHz.) Smooth frequency tuning would then require simultaneous adjustment of the OPO cavity length and fine tuning of the pump frequency to maintain the double-resonance condition.

The cavity length or pump-frequency detuning required to cause a mode hop is dependent on the mismatch in the free-spectral ranges of the signal and idler fields.¹⁵ Therefore, to obtain single signal/idler mode-pair operation near frequency degeneracy, type II phase matching is preferable to type I phase matching. This is because the signal and idler

fields in type II phase matching are polarized along orthogonal axes of the birefringent crystal. Hence, even at exact frequency degeneracy, the refractive indices, and consequently the free-spectral ranges, for the signal and idler fields are different. This mismatch in the free-spectral ranges of the signal and idler fields reduces the sensitivity to mode and cluster hopping in the output of the OPO. These characteristics have been studied recently by Debuisschert *et al.*¹⁶ and Lee and Wong.¹⁷ A further benefit of type II phase matching is the possibility of polarization splitting to form separate resonant cavities for the signal and idler fields.⁶ Therefore, the proposed use of type II phase-matched KTP¹⁰ as an alternative to LBO for frequency down-conversion to the 1.5 μm spectral region would be beneficial if the increase in threshold due to walkoff losses caused by propagation at an angle of $>50^\circ$ from a principal axis, can be overcome.

The nonlinear frequency conversion process described in this letter is highly suitable as a precision frequency-tunable source. By operating the Ti:sapphire laser at $\approx 0.85 \mu\text{m}$, the down-converted subharmonic from a degenerate LBO OPO could be phase locked to the frequency-doubled output of a CH_4 -stabilized He:Ne laser (3.39 μm), resulting in visible integral harmonics of the stable infrared frequency standard. A similar OPO could also be used as a frequency link between the 1.5 μm region and the 0.78 μm region, where a rubidium absorption line could be used as a frequency standard to lock the visible laser frequency.¹⁸ Alternatively, the sum frequency of a pump source operating at $\approx 0.8 \mu\text{m}$ and its frequency subharmonic could be referenced to an iodine absorption at $\approx 0.5 \mu\text{m}$.¹⁹

In summary, we have demonstrated coarse frequency tuning over 25 THz by combining a tunable pump source with a temperature-tunable cw LBO OPO operating under type I NCPM. The spectral region that we have highlighted

is important for a number of applications from optical frequency metrology to optical communications. Further improvements in the stability of the pump laser and design of the OPO resonator should reduce the threshold and provide amplitude and frequency stable OPO outputs in the 1–2 μm spectral region.

The authors would like to thank M. J. Padgett and S. Shepherd for helpful discussions. F. G. Colville acknowledges financial support from the National Physical Laboratory, Teddington, UK. M. Ebrahimzadeh is a Royal Society Research Fellow.

¹R. Graham and H. Haken, *Z. Phys.* **210**, 276 (1968).

²C. D. Nabors, S. T. Yang, T. Day, and R. L. Byer, *J. Opt. Soc. Am. B* **7**, 815 (1990).

³N. C. Wong, *Opt. Lett.* **15**, 1129 (1990).

⁴D. Lee and N. C. Wong, *Opt. Lett.* **17**, 13 (1992).

⁵S. T. Yang, R. C. Eckardt, and R. L. Byer, *Opt. Lett.* **18**, 971 (1993).

⁶F. G. Colville, M. J. Padgett, and M. H. Dunn, *Appl. Phys. Lett.* **64**, 1490 (1994).

⁷A. Heidmann, R. J. Horowicz, S. Reynaud, E. Giacobino, C. Fabre, and G. Camy, *Phys. Rev. Lett.* **59**, 2555 (1987).

⁸N. C. Wong, *IEEE Photon. Technol. Lett.* **4**, 1166 (1992).

⁹N. C. Wong, *Phys. Rev. A* **45**, 3176 (1992).

¹⁰W. Wang and M. Ohtsu, *Opt. Lett.* **18**, 876 (1993).

¹¹N. C. Wong, *Opt. Lett.* **17**, 1155 (1992).

¹²C. Chen, Y. Wu, A. Jiang, B. Wu, G. You, R. Li, and S. Lin, *J. Opt. Soc. Am. B* **6**, 616 (1989).

¹³W. Wang, K. Nakagawa, Y. Toda, and M. Ohtsu, *Appl. Phys. Lett.* **61**, 1886 (1992).

¹⁴W. Wang and M. Ohtsu, *Opt. Commun.* **102**, 304 (1993).

¹⁵R. C. Eckardt, C. D. Nabors, W. J. Kozlovsky, and R. L. Byer, *J. Opt. Soc. Am. B* **8**, 646 (1991).

¹⁶T. Debuisschert, A. Sizmann, E. Giacobino, and C. Fabre, *J. Opt. Soc. Am. B* **10**, 1668 (1993).

¹⁷D. Lee and N. C. Wong, *J. Opt. Soc. Am. B* **10**, 1649 (1993).

¹⁸H. Furuta and M. Ohtsu, *Appl. Opt.* **28**, 3737 (1989).

¹⁹A. Aric, S. Schiller, E. K. Gustafson, and R. L. Byer, *Opt. Lett.* **17**, 1204 (1992).

Smooth Frequency Tuning from Optical Parametric Oscillators: The Transition from Single- to Dual-Cavity Oscillators

F. G. Colville, M. J. Padgett, and M. H. Dunn

*J. F. Allen Physics Research Laboratories, Department of Physics and Astronomy,
University of St. Andrews, North Haugh, St. Andrews, Fife KY16 9SS, Scotland, United Kingdom*

Abstract

We analyse the frequency tuning properties of single- and dual-cavity doubly-resonant optical parametric oscillators. Comparison is made to experimental configurations that use lithium triborate continuous-wave optical parametric oscillators, pumped by a single-frequency argon-ion laser. We compare single- and dual-cavity resonators that use type II phase-matching at room-temperature with non-degenerate frequencies.

Introduction

The use of continuous-wave (cw) optical parametric oscillators (OPOs) as sources of tunable radiation over extended frequency ranges suffered a set-back when the first cw OPOs revealed undesirable tuning characteristics. Recently, difficulties associated with stabilizing cw OPOs have been overcome [1,2]. However, issues such as mode-selection and frequency-stability need to be addressed further if reliable systems are to be obtained. Applications, such as high-resolution spectroscopy and frequency division, require sources of continuously-tunable single-frequency radiation. OPO tuning properties are affected by the type of phase-matching employed and how far removed from frequency-degeneracy the OPO is phase-matched. The choice of OPO material, the resonator design, and the tuning elements, are also critical decisions.

Firstly, we describe the OPOs that were realized experimentally. We derive expressions for the requirements to maintain amplitude-stable single mode-pair operation; and to generate smooth frequency tuning. We compare the experimental results to a simplified theory. Finally, we summarize the key results of these studies.

Pump source and nonlinear crystal

The pump source used was an argon-ion laser which was selected as a convenient source of high-power single-frequency radiation, when operating in the ultra-violet spectral region at 363.8 nm, and was actively-stabilized to an external etalon, with a stability of $\approx \pm 3$ MHz.

The nonlinear crystal, lithium triborate (LiB_3O_5 ; LBO), was selected for its high damage threshold, moderate nonlinear coefficients, and wide transparency. Previously, the use of LBO within OPOs had been confined to devices that used pulsed pump sources operating in the ultra-violet, green or near-infra-red regions. In each of these regions, non-critical phase-matching (NCPM) geometries have been identified, and wide OPO temperature-tuning has been generated. These desirable NCPM geometries suggest LBO as a suitable crystal for use within cw OPOs [3-6].

Pumped at 363.8 nm, LBO can be temperature-tuned under type II NCPM [4], and operated at room-temperature. Figure 1 illustrates this phase-matching geometry in LBO, with the temperature-tuning possible. The frequency bandwidth of the output of the OPO was limited by the narrow-band coatings on the crystal faces and cavity-mirrors.

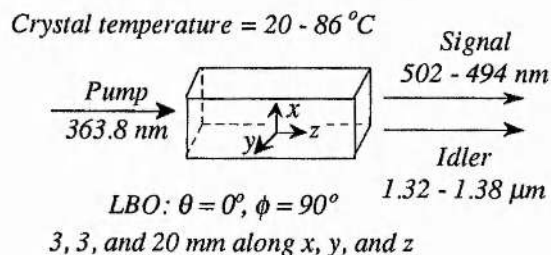


Figure 1. Type II NCPM and tuning in LBO.

Modelling and results

Introduction

In optical parametric down-conversion, an input pump wave at frequency ν_p is converted into two outputs; the signal and idler, at frequencies ν_s and ν_i . These frequencies obey the energy conservation relation, $\nu_p = \nu_s + \nu_i$. To form the OPO, resonance is provided by feedback at cavity mirrors for either, or both, the signal and idler. A device with feedback at one of the signal or idler is referred to as a singly-resonant OPO (SRO), in which the exact frequency of the resonant field is that of the cavity mode closest to the optimum phase-matching condition. The frequency of the non-resonant field is dictated merely by energy conservation.

CW OPOs are configured routinely as doubly-resonant OPOs (DROs), in which both the signal and idler are brought to resonance simultaneously. This results in significantly lower pump power thresholds compared to SRO devices. However, four conditions must be satisfied simultaneously; energy-conservation, phase-matching, and cavity resonances for the signal and idler. This introduces complications in the tuning [7].

Mode frequencies and tuning rates

We analyse two different DRO configurations. Figure 2(a) illustrates the single-cavity DRO, where the two OPO frequencies are resonant within a common cavity. The dual-cavity DRO is shown in figure 2(b), where an additional component separates spatially the signal and idler fields, and a third mirror forms a second resonator.

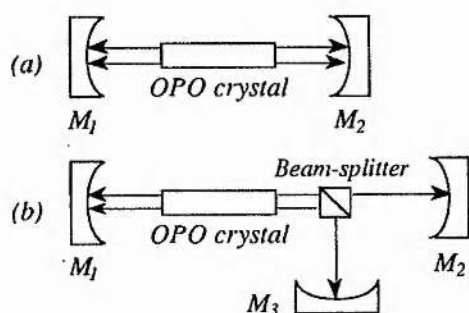


Figure 2. Single- (a) and dual-cavity (b) DROs.

We denote the signal (idler) cavity-length by $L_{s(i)}$, and the length of the OPO crystal by l . The resonance condition for the signal (idler) is

$$\nu_{s(i)} = \frac{m_{s(i)}c}{2(L_{s(i)} + (n_{s(i)} - 1)l)}, \quad (1)$$

where $m_{s(i)}$ is the longitudinal mode number of the signal (idler), $n_{s(i)}$ is the refractive index of the signal (idler) within the nonlinear material, and c is

the velocity of light. A change in the length of the signal (idler) cavity of $\Delta L_{s(i)}$ causes the resonant frequency of the signal (idler) field to change by $\Delta \nu_{s(i)}$ and such that

$$\Delta \nu_{s(i)} = \frac{-\Delta L_{s(i)} \nu_{s(i)}}{L_{s(i)} + (n_{s(i)} - 1)l}. \quad (2)$$

To calculate, to good approximation, numerical values for the tuning rates, dispersion terms are ignored and equation [2] becomes

$$\Delta \nu_{s(i)} \approx \frac{-2\Delta L_{s(i)} \nu_{s(i)} FSR_{s(i)}}{c}, \quad (3)$$

where $FSR_{s(i)}$ is the free spectral range of the signal (idler) cavity.

Mode hopping

Pairs of signal and idler modes that satisfy energy conservation are termed mode-pairs. Within the phase-matching bandwidth, there are several mode-pairs for which the signal and idler lie close enough to the cavity modes for the OPO to oscillate. Changes in either the cavity mode frequencies or the pump-frequency cause the OPO output to switch from one mode-pair to another. Depending on the mis-match in the FSR s of the signal and idler, and in their finesses, the new mode-pair is either adjacent to the original (mode-hop), or many mode-pairs removed (cluster-hop) [7].

The mis-match in the FSR s dictates the level of cavity-length/pump-frequency detuning required to cause a hop to an adjacent mode-pair. Assuming that the original mode-pair is exactly on resonance, then by changing the cavity mode frequencies by a total amount equal to the mis-match in the FSR s, a mode-hop will occur. Therefore, the condition for a mode-hop is given by

$$\Delta FSR \approx \frac{2(\Delta L_s \nu_s FSR_s + \Delta L_i \nu_i FSR_i)}{c}, \quad (4)$$

where ΔFSR is the mis-match in the FSR s.

For a single-cavity OPO with approximately equal cavity lengths for the signal and idler, we consider the FSR s of the signal and idler, as inserted on the right hand side of equation [4], to be approximately equal; i.e. $L_s \approx L_i \approx L$ and hence $FSR_s \approx FSR_i \approx FSR$. Now, for the case of similar cavity finesses for the signal and idler, and by substituting $\Delta L_s = \Delta L_i = \Delta L_{hop}$ into equation [4], the cavity-length detuning for a mode-hop is

$$\Delta L_{hop} \approx \frac{\Delta FSR}{2FSR} \lambda_p, \quad (5)$$

where λ_p is the free-space pump wavelength. This expression can be written in terms of the refractive indices of the signal and idler frequencies within the nonlinear crystal; i.e.

$$\Delta L_{hop} \approx \frac{\lambda_p}{2} \frac{|n_s - n_i|l}{(L + (\bar{n} - 1)l)}, \quad (6)$$

where \bar{n} is the average refractive index.

The second parameter that affects the tuning behaviour of the OPO is the pump-frequency. The detuning required to cause a mode-hop is given by

$$\Delta v_{p-hop} = \Delta FSR \quad (7)$$

Pump power threshold

The pump power threshold is dependent on the degree to which the resonance conditions for the signal and idler modes are satisfied and can be understood in terms of figure 3, in which the linear scales for the signal and idler are reversed.

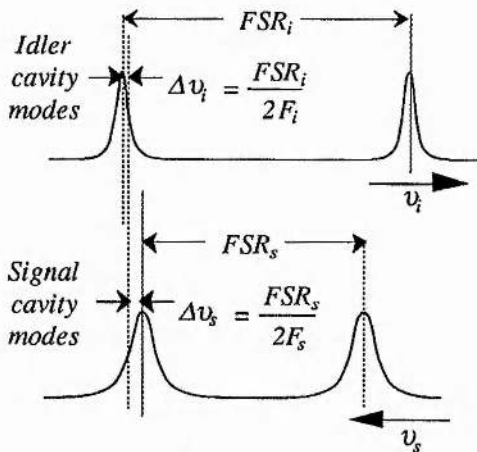


Figure 3. Detuning of the cavity modes.

This figure is used to derive expressions that predict the tolerances to fluctuations in the cavity-length or pump-frequency on a single mode-pair. The maximum detuning, Δv , while maintaining operation on a single mode-pair, is given by

$$\Delta v = \Delta v_s + \Delta v_i \leq \frac{FSR_s}{2F_s} + \frac{FSR_i}{2F_i} \quad (8)$$

We equate the above expression to equation [15] in reference [7] which derives the standard expression for the DRO threshold; i.e.

$$P_{th} \propto 1 + \left(\frac{2(\Delta v_s + \Delta v_i)F_s F_i}{F_i FSR_s + F_s FSR_i} \right) \quad (9)$$

Equation [8] is related to the second term of equation [9], and corresponds to the detuning that doubles the threshold.

Cavity-length detuning

We take the point where the threshold, P_{th} doubles as an indication of the range over which the OPO operates on a single mode. Equation [8] becomes

$$\left| \frac{4}{c} (\Delta L_s v_s FSR_s + \Delta L_i v_i FSR_i) \right| \leq \frac{FSR_s}{F_s} + \frac{FSR_i}{F_i} \quad (10)$$

For a single-cavity OPO, where $\Delta L_s = \Delta L_i = \Delta L$, and with similar finesses for the signal and idler, i.e. $F_s \approx F_i \approx F$, the cavity-length stability is

$$\Delta L_{stab} \approx \pm \frac{\lambda_p}{2F} \quad (11)$$

For a dual-cavity, the FSR of the signal may differ significantly from that of the idler field. Then, assuming both cavities are subject to the same cavity-length change and have comparable finesses, the cavity-length stabilities are

$$\Delta L_{stab} \approx \pm \frac{\lambda_p}{4F_{s(i)}} \text{ for } FSR_{s(i)} \gg FSR_{i(s)} \quad (12)$$

Pump-frequency detuning

For fixed cavity-lengths, an indication as to the pump-frequency detuning allowed, while maintaining operation on a single mode-pair, is

$$|\Delta v_p| \leq \frac{FSR_s}{2F_s} + \frac{FSR_i}{2F_i} \quad (13)$$

For a single-cavity DRO, where $FSR_s \approx FSR_i \approx FSR$, and with similar finesses for the signal and idler, i.e. $F_s \approx F_i \approx F$, the stability requirement on the pump-frequency is

$$\Delta v_{p-stab} \approx \pm \frac{FSR}{F} \quad (14)$$

For a dual-cavity DRO, the FSR s and/or the finesses of the signal and idler may differ significantly. For unequal finesses and unequal FSR s, the stability conditions are

$$\Delta v_{p-stab} \approx \pm \frac{FSR_{s(i)}}{2F_{s(i)}} \text{ for } FSR_{s(i)} \gg FSR_{i(s)} \quad (15)$$

Single-cavity amplitude-stable operation

Multiple-parameter tuning allows for smooth frequency tuning of the OPO. For perturbations in the pump-frequency, then to maintain double-resonance, the signal and idler lengths must change accordingly. Therefore, the following expression must now be satisfied;

$$\Delta v_p = \Delta v_s + \Delta v_i \approx - \frac{2(\Delta L_s v_s FSR_s + \Delta L_i v_i FSR_i)}{c} \quad (16)$$

A servo-lock applied to either the signal or the idler cavity-length which holds the OPO output power at a constant level, will maintain the OPO on a single mode-pair above threshold, correcting at the same time for both cavity-length and pump-frequency perturbations.

For a single-cavity DRO, with $FSR_s \approx FSR_i \approx FSR$, and with similar finesses for the signal and idler, equation [16] becomes

$$\Delta v_p \approx -2\Delta L \left(\frac{FSR}{\lambda_p} \right) \quad (17)$$

Smooth frequency tuning can be obtained by changing the cavity-length by ΔL while controlling simultaneously the pump-frequency to maintain the double-resonance condition.

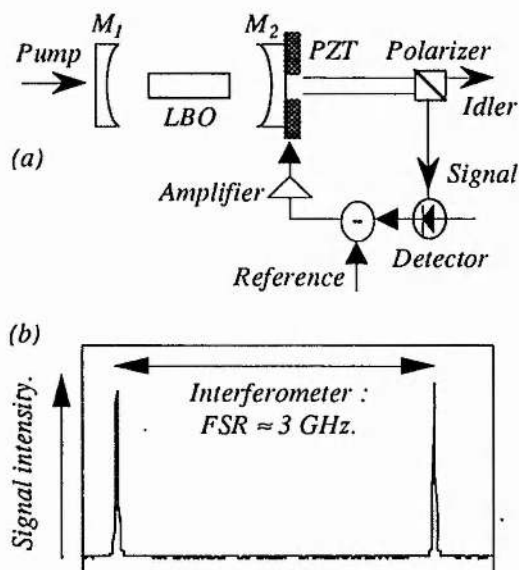


Figure 4. Single-cavity servo-lock (a), and signal-wave single-frequency operation (b).

We stabilized the output of a single-cavity DRO to maintain operation on a single mode-pair by using a simple intensity-lock, as illustrated in figure 4(a). The DRO was locked to the side of a resonance mode, maintaining operation on a single mode-pair; see figure 4(b).

For a fixed pump-frequency, and by simply changing the common cavity-length, a single-cavity DRO cannot be used to tune continuously the DRO outputs. To provide this, it is essential to have independent control of the signal and idler cavity-lengths. There have been two methods reported for achieving this [2,5]. The first method used a single-cavity DRO [2] with type II phase-matching. A tunable birefringent element, placed within a single-cavity, can be used to adjust the individual signal and idler cavity-lengths. The second method, which we have pursued, is to use a dual-cavity DRO [5].

Dual-cavity smooth frequency tuning

For type II phase-matching geometries, a polarizing beam-splitter can separate the signal and idler into different cavities. For the non-degenerate type II phase-matching in LBO, we used a coating-enhanced, polarizing beam-splitter to allow for the transition between single- and dual-cavity operation. The intra-cavity beam-splitter was inserted into the cavity at Brewster's angle, and coated to provide $> 99.7\%$ transmission for the p -polarized idler wave and $> 99.7\%$ reflectivity for

the s -polarized signal wave. In addition, $> 97\%$ transmission was provided for the p -polarized pump wave.

Controlling the signal and idler cavity frequencies allows for smooth tuning of the OPO without the need for a tunable pump-frequency.

We express the relation between the two cavity-length detunings, ΔL_s and ΔL_i , to provide smooth-tuning from a dual-cavity DRO operating with a fixed frequency pump source as

$$\Delta L_s = \Delta L_i \frac{FSR_i v_i}{FSR_s v_s} \quad (18)$$

One cavity is controlled to provide fine adjustment of the output frequency (master-cavity); the other cavity (slave-cavity) is servo-locked to maintain constant output power.

In our dual-cavity DRO, we employed servo-control on the length of the signal cavity to maintain double-resonance; figure 5(a). Smooth tuning is achieved by scanning the length of the idler cavity, and relying on the signal cavity-servo to maintain double-resonance. Figure 5(b) shows a trace of the locked signal single-frequency.

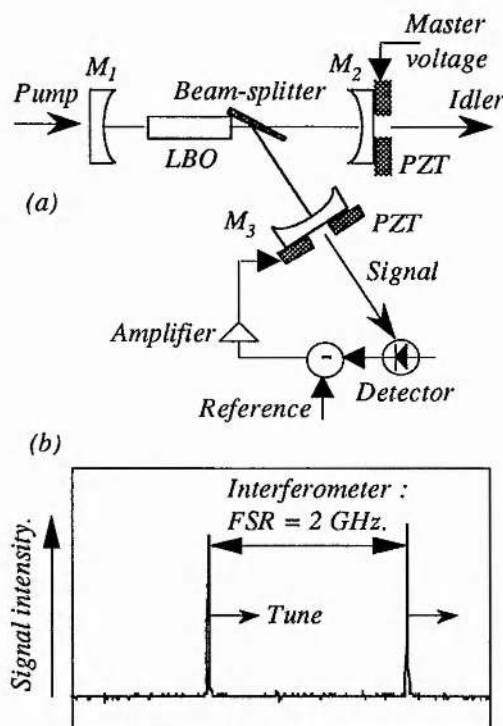


Figure 5. Dual-cavity servo-lock (a), and signal-wave single-frequency operation (b).

For this first dual-cavity demonstration, the influence of a partially resonant pump field within the OPO cavity restricted the allowable tuning range. In addition to being highly-reflecting at the signal and idler, the mirrors were $\approx 55\%$ reflecting at the pump. This introduced a weak resonance at

the pump frequency, with a pump finesse, $F_p \approx 5$. This dependence of an OPO cavity-length to the pump-frequency placed an upper limit to which the idler cavity could be scanned in length/frequency, before the pump field dropped below threshold.

To predict the level of smooth frequency tuning from our dual-cavity, we assume again, when at perfect resonance for the signal and idler, the OPO is operating at \approx two times threshold. For a resonant pump field within the idler (signal) cavity of the OPO, the range over which the idler (signal) cavity-length can be scanned, while maintaining an OPO output, is

$$\Delta L_i \approx \frac{\lambda_p}{2F_{p-idler(signal)}}, \quad (19)$$

where $F_{p-idler(signal)}$ is the finesse of the idler (signal) cavity for the pump frequency. We rewrite equation [19], to express the maximum tuning ranges for the signal and idler, Δv_{s-max} and Δv_{i-max} , when using a fixed frequency pump source, resonant within the idler (signal) cavity, as

$$|\Delta v_{s-max}| = |\Delta v_{i-max}| \approx \frac{FSR_{i(s)}}{F_{p-idler(signal)}} \frac{\lambda_p}{\lambda_{i(s)}}. \quad (20)$$

Therefore, for our dual cavity DRO, we expect the smooth frequency tuning range to be limited to \approx 0.2 GHz. In practise, we could tune the outputs of the dual-cavity OPO through \approx 0.4 GHz.

Conclusions

We have derived simple expressions for the requirements on the stability of the OPO cavity-length, and the pump-frequency, to maintain amplitude-stable, single-frequency mode-pair operation.

To provide stable mode-pair operation, it is essential to have fine-control of the OPO cavity-length to compensate for pump-frequency perturbations. The most appropriate OPO designs for this are monolithic resonators [1], with electric-optic cavity-length control. In our discrete-component single-cavity OPO, this fine-control was provided by piezo-electric feedback to an OPO cavity-mirror [6].

To provide smooth-frequency-tuning for a fixed pump-frequency, it is essential to have independent control of the cavity-lengths of both the signal and idler. The most elegant demonstration of this technique has combined type II phase-

matched KTP with orthogonal length control in a single-cavity [2]. To provide this from our LBO OPO, we proposed the use of a dual-cavity OPO, and further, took advantage of both type II phase-matching and frequency non-degeneracy to provide a first experimental demonstration of this technique [7]. When pump resonance effects are eliminated completely, this tuning method has the possibility of generating smooth frequency tuning at the GHz-level.

Future progress in cw OPOs is likely to take advantage of pump sources whose operating frequency can be selected from a large gain-bandwidth. Presently, the most appropriate laser source for this is a Ti:sapphire laser, and recently we have demonstrated the use of this laser to pump a cw OPO in the 1.5 to 1.7 μm spectral region [8]. When such pump sources are combined with dual-cavity resonators, cw OPOs will become ideal candidates for optical frequency division schemes.

References

1. C. D. Nabors, R. C. Eckardt, W. J. Kozlovsky, and R. L. Byer, "Efficient single-axial-mode operation of a monolithic MgO:LiNbO₃ optical parametric oscillator," *Opt. Lett.* **14**, 1134-1136 (1989).
2. D. Lee and N. C. Wong, "Tunable optical frequency division using a phase-locked optical parametric oscillator," *Opt. Lett.* **17**, 13-15 (1992).
3. F. G. Colville, A. J. Henderson, J. Zhang, M. J. Padgett, and M. H. Dunn "Continuous-wave parametric oscillation in lithium triborate," *Opt. Lett.* **18**, 205-207 (1993).
4. F. G. Colville, M. J. Padgett, A. J. Henderson, J. Zhang, and M. H. Dunn "Continuous-wave parametric oscillator pumped in the ultraviolet," *Opt. Lett.* **18**, 1065-1067 (1993).
5. F. G. Colville, M. J. Padgett, and M. H. Dunn "Continuous-wave, dual-cavity, doubly-resonant optical parametric oscillator," to be published, *Appl. Phys. Lett.* **64** (1994).
6. F. G. Colville, M. Ebrahimzadeh, W. Sibbett, and M. H. Dunn "Continuous-wave LiB₃O₅ optical parametric oscillator pumped by a tunable Ti:sapphire laser," to be published, *Appl. Phys. Lett.* **64** (1994).
7. R. C. Eckardt, C. D. Nabors, W. J. Kozlovsky, and R. L. Byer "Optical parametric oscillator frequency tuning and control," *J. Opt. Soc. Am. B*, **8**, 646-667 (1991).